



AIP
Conference
Proceedings

**International Conference on
Electrical, Electronics, Materials and Applied Science
(ICEEMAS) - 2017**

22nd and 23rd December 2017



Swami Vivekananda Institute of Technology

Ranked amongst top 25 Engineering colleges in Telangana under 2017 - SARVGYAN survey.
Secunderabad, Telangana, India.

www.svit.ac.in | www.iceemas.org | info@svit.ac.in | iceemas@gmail.com

S No	TITLE of The Paper	Page No
1	Engine-Propeller Power Plant Aircraft Community Noise Reduction Key Methods	1
2	Isolation, Biomass Estimation and Characterization of the Biofuel Potential of Diatom Navicula Sphaerophora	9
3	Analysis of bulk arrival queueing system with batch size dependent service and working vacation	16
4	A Comparative Study on the Luminescence Properties of Ce ³⁺ /Tb ³⁺ -Doped Gd ₃ O ₃ Based Host Nanomaterials	22
5	Effect of Length to Thickness Ratio on Free Vibration Analysis of Thick Fiber Reinforced Plastic Skew Cross Ply Lamine with Circular Cutout	26
6	Impact on Sediments and Water by Release of Copper from Chalcopyrite Bearing Rock due to Acidic Mine Drainage	32
7	World Of Intelligence Defense Object Detection - Machine Learning (Artificial Intelligence)	40
8	Geopolitical model of investment power station construction project implementation	47
9	Solar Panel Cleaning Robot	57
10	Mathematical Modelling and Numerical simulation of Forces in milling process	67
11	A Review on Mechanical Properties of Magnesium Based Nano Composites	73
12	Treatability Study of the Effluent Containing Reactive Blue 21 Dye by Ozonation and the Mass Transfer Study of Ozone	79
13	Performance of Dual Inverter Fed Open end winding Induction Motor Drive Using Carrier Shift PWM Techniques	86
14	Denoising and Segmentation of the Retinal Layers in Optical Coherence Tomography Images	95
15	A Survey on Blood Group Determination	104
16	GUI Implementation of Image Encryption and Decryption using Open CV Python Script on Secured TFTP Protocol	110
17	Experimental Investigation on Stability and Dielectric break down strength of Transformer oil based nanofluids	118
18	Performance and Analysis of MAC Protocols Based on Application	124
19	An Efficient Collaborative Approach For Black Hole Attack Discovery And Mitigating Its Impact In Manet	130
20	Dates Fruits Classification Using Svm	136
21	Adsorbent Material Based on Passion-fruit Waste to Remove Lead (Pb), Chromium (Cr) and Copper (Cu) from Metalcontaminated Waters	142
22	AC And DC Conductivity Due To Hopping Mechanism In Double Ion Doped Ceramics	146

23	Efficient Finite Element Modelling for the Investigation of the Dynamic Behaviour of a Structure with Bolted Joints	155	42
24	Optimization and development of Solar power system under diffused sunlight condition in rural areas with Super capacitor integration	161	43
25	Performance Analyses of Z-source and Quasi Z-source Inverter for Photovoltaic Applications	167	44
26	Investigation of Needleless Electrospun PAN Nanofiber Mats	174	45
27	Dynamic Analysis of I Cross Beam Section Dissimilar Plate Joined by TIG Welding	181	46
28	The Effective use of Virtualization for Selection of Data Centers in a Cloud Computing Environment	188	47
29	Determination of accuracy of winding deformation method using kNN based classifier used for 3 MVA transformer	196	48
30	Review on Factors Affecting the Performance of Pulse Detonation Engine	207	49
31	Adoption of the Hash Algorithm in a Conceptual Model for the Civil Registry of Ecuador	214	50
32	Examinations of the Effect of Flame Retardants on Thermal and Mechanical Properties and the Structure of Polybutylene Terephthalate	223	51
33	Individual Prognosis Of Quality Indicators Of Space Equipment Elements	233	52
34	Algorithm Of Development Of Measures Of Complex Protection OE S From ESD	240	53
35	Study on Effect of Mixing Mechanism by the Transverse Gaseous Injection Flow in Scramjet Engine with Variable Parameters	248	54
36	Prediction of Customer Behaviour Analysis Using Classification Algorithms	254	55
37	Optical Network Security using Unipolar Walsh Code	261	56
38	Computer Aided Detection system for Lung Cancer using computer tomography scans	265	57
39	Microstructural investigation of Aluminum-Graphene Nano platelets composites prepared by powder metallurgy	271	58
40	Performance Analysis of Routing Protocols for IoT	277	59
41	A Study on Heterogeneous Photocatalytic Degradation of Various Organic Compounds Using N-TiO ₂ under UV-Light Irradiation	285	60

42	State of the Art Metrics for Aspect Oriented Programming	
43	Intense green emission from Tb ³⁺ -doped TeO ₂ -WO ₃ -GeO ₂ glasses	294
44	Integration of Supercapacitive storage in Renewable Energy system to compare the response of two level and five level inverter with RL type Load	306
45	Method of lungs regional ventilation function assessment on the basis of continuous lung monitoring results using multi-angle electrical impedance tomography	312
46	Research of Robust Feature Detector Efficiency In Case Of Scene Uneven Illumination Changes	317
47	About approximation of Integer Factorization Problem by the combination Fixed-point Iteration Method and Bayesian Rounding for quantum cryptography	322
48	Computationally Efficient Method for Determining Averaged Distribution of Differentials for Pseudo-dynamic substitutions	328
49	Organization Of The Secure Distributed Computing Based On Multi-agent System	333
50	The Optimal Input Optical Pulse Shape for The Self-Phase Modulation Based Chirp Generator	340
51	Assessment of the sensitivity of multi-angle electrical impedance tomography to heterogeneous formations	345
52	Development of the algorithm of measurement data and tomographic section reconstruction results processing for evaluating the respiratory activity of the lungs using the multi-angle electric impedance tomography	350
53	Determination of Bending and Axial Compression Young's Modulus of Cellular Mortar Exposed to High Temperatures	356
54	Implementation of One Dimensional Finite Difference Heat Conduction Method to Quantity Heat Transfer through Lightweight Cellular Mortar	361
55	Experimental Study to Establish Compressive and Flexural Strength of High Performance Concrete (HPC) with Addition of Treated Cocos Nucifera Fibre	367
56	Cocos Nucifera Fiber Strengthen High Performance Concrete: Young's Modulus, Ultrasonic Pulse Velocity and Ductility Properties	373
57	Use Of Treated Domestic Wastewater After Chlorination In Fly Ash Cement Mortar	378
58	Evaluation Of Sulfates Resistance Of Fly Ash Cement Mortar Made With Treated Domestic Wastewater After Chlorination	383
59	Experimental Study And Ignition Fire Risk Mapping On Friction Stir Welding Parameters Of Dissimilar Alloys For The Benefits Of Environment	389
60	Selection of Slot per Pole ratio for a Permanent Magnet Brushless DC Motor	394
61	Design Optimization for Permanent Magnet Machine with Efficient Slot per Pole Ratio	400

Treatability Study of the Effluent Containing Reactive Blue 21 Dye by Ozonation and the Mass Transfer Study of Ozone

Priyadarshini Velpula^{1, a)}, Santosh Ghuge^{2, b)} and Anil K. Saroha^{3, c)}

¹*M.Tech, Dept. of Chem. Engg.-IITD, Delhi. Presently, Asst. Prof., Chem. Engg. Dept., RGUKT-Basar.*

²*Research Scholar, Dept. of Chemical Engineering-IITD, Delhi-110016*

³*Faculty, Dept. of Chemical Engineering-IITD, Delhi-110016.*

^{a)}priya.kmm93@gmail.com

^{b)}sanghuge@yahoo.co.in

^{c)}aksaroha@chemical.iitd.ac.in

Abstract: Ozonation is a chemical treatment process in which ozone reacts with the pollutants present in the effluent by infusion of ozone into the effluent. This study includes the effect of various parameters such as inlet ozone dose, pH of solution and initial concentration of dye on decolorization of dye in terms CRE. The maximum CRE of 98.62% with the reaction rate constant of 0.26 min^{-1} is achieved in 18 minutes of reaction time at inlet ozone dose of 11.5 g/m^3 , solution pH of 11 and 30 mg/L of initial concentration of dye. The presence of radical scavenger (Tertiary Butyl Alcohol) suppressed the CRE from 98.62% to 95.4% at high pH values indicates that the indirect mechanism dominates due to the presence of hydroxyl radicals which are formed by the decomposition of ozone. The diffusive and convective mass transfer coefficients of ozone are calculated as $1.78 \times 10^{-5} \text{ cm}^2/\text{sec}$ and 0.075 min^{-1} . It is observed that the fraction of resistance offered by liquid is very much high compared to gas phase indicates that the ozonation is a liquid phase mass transfer controlled operation.

Keywords: Ozonation, Effluent, Reactive Blue 21 dye, Dye concentration, Color removal, Mass transfer coefficient.

INTRODUCTION

Water is the essential part of life for all the living organisms and also it is very important for many industrial applications. Every day huge amount of waste water is being released from various sources such as industries, agricultural lands and households. Among these, waste water coming from the textile industry is known to contain highly toxic compounds because of the low fixation efficiencies of dyes. Hence there is a serious need for the development of efficient and cost effective treatment processes for to remove such hazardous contaminants. In recent years, advanced oxidation processes (AOPs) are proven to be prominent treatment processes for the textile effluent for decolorization as well as the mineralization [9]. The AOPs includes ozonation, Fenton process, wet-air oxidation and combination of these processes under the presence of UV light and catalyst. Among these, ozonation is one of the effective treatment processes for the dye effluent because of its high oxidizing potential of 2.07 V with high selectivity and reactivity towards the conjugated double bonds of dye molecules, results in the rapid decolorization of dye effluent [4]. In ozonation oxidation of dye molecules takes place in two pathways direct and indirect, which takes place simultaneously during the process [13]. In the direct path way ozone directly reacts on the conjugated double bonds and forms oxidation products, in indirect pathway the formed hydroxyl radicals reacts with these oxidation products and decompose to carbon dioxide, water and inorganic mineral salts [3]. The selectivity of ozone is very less towards the oxidation products such as the organic acids, aldehydes and ketones hence both the decomposition mechanisms are necessary for complete mineralization.

A Study On Heterogeneous Photocatalytic Degradation Of Various Organic Compounds Using N-TiO₂ Under Uv-Light Irradiation

Dhegam Srujana^{1,a)} and Prof. Chinta Sailu^{2,b)}

¹*M.Tech. Department of Chemical Engineering, University College of technology,Osmania University,Hyderabad.
Present Asst.prof.in RGUKT, Basar.*

²*M.Tech, Ph.D. Professor in the Department of Chemical Engineering, University College of technology,Osmania University,Hyderabad*

^{a)} *srujana.dhegam@gmail.com*
^{b)} *csailu@yahoo.com*

Abstract: The aim of this work is to determine the photocatalytic degradation of mixture of four selected organic compounds are Congo Red (CR), Methylene Blue (MB), Diclofenaec (DC), 4-Chlorophenol (4-CP) have been subjected to Photo catalytic degradation by Ultraviolet ($\lambda=254\text{nm}$) radiation in presence of Nitrogen-doped Titanium dioxide (N-TiO₂) catalyst. This paper focused on the enhancement of photo catalysis by modification of TiO₂ employing non-metal ion (Nitrogen) doping. Experiments are conducted with a mixture of equal proportions of organic compounds (CR, MB, DC, and 4-CP) with combined concentrations of 10, 20, 30, 40 and 50 mg/l in water in a batch reactor in presence of N-TiO₂catalyst with UV light ($\lambda=254\text{nm}$). The rate of degradation of each compound is determined by using spectrophotometer. The kinetics of degradation of the selected organic compounds is followed first order rate.

Keywords: Congo Red, Methylene Blue, Diclofenaec, 4-Chlorophenol, UV/N-TiO₂, decolorization, spectrophotometry.

INTRODUCTION

In recent years, problem of wastewater became very important both for the sake of increasing amount and its variety [1, 2]. The presence of toxic organic compounds such as dyes and various phenols in wastewater have been increased [3]. These are being continuously introduced into the aquatic environment through various inputs [2]. The list of trace contaminants or EDCs, resulting from human activities and found in wastewater is long [4-6]. Endocrine Disrupting Compounds are chemicals at some particular concentrations interfere with the endocrine system (or hormone system) in animals including humans. EDCs can block or mimic natural estrogen or natural testosterone, or affect the thyroid function [7]. A wide range of chemicals are EDCs including dyes, pharmaceutical drugs, pesticides, ingredients in cosmetic products and food supplements. Dyes (Congo Red, Methylene Blue (MB)) are commonly used in the textiles, food, cosmetic, and paper industry to impart colour to the products. The effluents from these industries are often discharges into municipal sewage treatment plants or into water resources (like lakes, ponds)[8]. Many pharmaceutical products (Diclofeneac, Ibuprofen) are designed to be biologically active, nowadays their concentrations also has been increased in the environment which have an adverse effect on the ecosystem and human health [9].Phenols like p-chlorophenol (4-CP) a water soluble hazardous material widely used in paper, pharmaceutical and pesticide industries[10]. The removal of organic and inorganic pollutants in water are generally associate with biological [11, 12], chemical [10], physical and physicochemical process or a combination of these. However, these techniques convert non biodegradable matter into sludge, giving rise to a new type of pollution which needs further treatment. As a result of these problems, Advanced Oxidation Processes (AOPs) have been considered as an emerging technology in treating organic chemicals in wastewater. AOPs rely on the hydroxyl radical as the primary mechanism for destruction of organic contaminants. The hydroxyl radicals (HO.) are highly

WATER QUALITY ASSESSMENT OF GODAVARI RIVER AT BASARA REGION

¹BHUKYA RAMAKRISHNA, ²BALLA RANJITH KUMAR, ³KATTA THUKARAM

¹ Assistant Professor, ^{2,3}Student, Civil Engineering Department, RGUKT Basara, Telangana
E-mail: ¹bhukyaramakrishna@gmail.com, ²ranjithballa2@gmail.com, ³kattathukaram297@gmail.com

Abstract - The River Godavari, a holy river known since ancient time, is the second largest river in India. Apart from Ganga and Yamuna, Godavari also holds the special religious importance in India. Spatial variation of the water quality of these holy rivers is difficult to interpret; a monitoring program is often necessary which has responsibility to provide representative and reliable estimation of the river water quality. So systematic study has been carried out to assess the water quality of Godavari River at Basara. Water samples from seven sampling stations were collected and physical and chemical parameters were analyzed by the standard methods. In this study Water Quality was determined on the basis of twelve parameters like P^H , Electrical Conductivity, Alkalinity, Hardness, TDS, TSS, TS, DO, BOD, COD, Fluorides, Nitrates. The pollution level over a period of time is increasing on the river water mainly due to industrial and other waste waters are directly discharge in the river. Hence the present study is aimed to examine the water quality of the Godavari River and to evaluate the impact of such contaminated water.

Keywords - Water quality index, Godavari River, Basara, Physical and Chemical parameters.

I. INTRODUCTION

Water is an important natural resource and precious national assets. It forms the chief constituent of ecological system. Everyone knows that water is essential to continue normal life. We depend on water for more than just for drinking, cooking and personal usage. Big amount of water is often required for industrial and commercial uses such as fisheries, hydropower generation. In some parts of the country, large quantities of water for irrigation are necessary to support agriculture. Water sources may be mainly in the form of rivers, lakes, ground water etc. The availability and quality of water either surface or ground, is getting deteriorated due to some important factors like increasing human activities at the water bodies, sewage discharge, Agricultural effluents, industrialization, urbanization etc. Surface water pollution with chemical, physical and biological contaminants by anthropogenic activities is of great environmental attention all over the world. Rivers play an important role in carrying off municipal and industrial wastewater and run-off from agricultural land. Rivers are one of the most susceptible water bodies to pollutants. Rivers are the main water sources for domestic, industrial and agricultural irrigation purposes in a region. River water quality is one of important factors directly concerning with health of human and living beings. Therefore, it is important to have reliable information on characteristics of water quality for effective pollution control and water resource management.

Industrial effluents those have been continuously thrown into the river is very visible at all major cities. This site is located at Basara Gnana Saraswati temple so water is mainly polluted by the activities of the pilgrims and their bathing, other devotional activities.

The other sources of pollutants include effluents from pioneer distilleries of Dharmabad which is in Nanded district of Maharashtra state. The long-term management of river requires basic understanding of chemical, biological and hydrological characteristics. Since, spatial variation of the water quality is difficult to interpret; a monitoring program is often necessary which has responsibility to provide representative and reliable estimation of the river water quality.

We know single number cannot represent the whole story of water quality of Particular River. There are many other water quality parameters that are not included in finding the index, however, a water quality index based on some very important parameters can provide an indicator of water quality. It is even important that the findings from various tests should be easily communicable to users and policy makers. Water quality index is well-known method as well as one of the most effective tools to expressing water quality that offers a simple, stable, reproducible unit of measure. It, thus, becomes an important parameter for the assessment and management of surfacewater. The general WQI was developed by Brown et al. (1970) and improved by Deininger for the Scottish Development Department (1975). Horton (1965) suggested that the various water quality data could be aggregated into an overall index.

There are various Methods to find water Quality Index such as

1. National Sanitation Foundation (NSF) WQI
2. Canadian Council of Ministers of the Environment (CCME) WQI
3. Weight Arithmetic WQI

In this project we have adopted Weighted Arithmetic method to evaluate WQI considering its flexibility and simplicity.

II. STUDY AREA

The Godavari originates 80 km (50 mi) from the Arabian Sea in the Western Ghats of central India near Nasik in Maharashtra. It flows for 1,465 km (910 mi), first eastwards across the Deccan Plateau then turns southeast, entering the West Godavari district and East Godavari district of Andhra Pradesh, until it splits into two watercourses that widen into a large river delta and flow into the Bay of Bengal.

In our project we have chosen Basara as the reference point along with another six points upstream of Godavari River near Basara temple. We mainly focused on the Saraswati temple at Basara because it is the most visiting place by the pilgrims and also it was polluted by the various materials which are thrown into the river. At Basara Ghats's daily about 1000 pilgrims dip in the river, this count may be goes up to 25000 on some special occasions like Vasantapanchami.

Sample Code	Sample Location	Latitude	Longitude
S1	Triveni Sangamam	77.868	18.814
S2	Kandakurthi	77.888	18.811
S3	Tadbiloli	77.948	18.797
S4	Khosli	76.485	18.396
S5	Basara bridge	77.957	18.863
S6	Basara Ghats	77.961	18.867
S7	Binola	77.953	18.880

Table 1: Sampling Location Co-ordinates

Five Samples were completed upstream of Basara Temple location in order to pollutants mixing pattern before reaching temple area. One sample was collected at downstream of temple location to know if there any self-purification process taking place or not.

III. EXPERIMENTAL DETAILS

3.1 Sample Collection

The water samples were collected from seven sites along the river as given in Table 1. Water samples from the sampling stations were collected in two phases, first time samples were collected in the month of Feb 2017 and second phase collection was carried out in March 2017, by grab sampling method. Parameters were analyzed by the standard methods. The samples were taken in plastic canes and brought to the laboratory with necessary precautions.

3.2 Physico-Chemical analysis

All the samples collected were brought to Environmental Engineering laboratory at RGUKT Basara. They were kept in deep fridge at the

temperature of 0°C-1°C till the further Analysis has taken place. As soon as the samples were brought to the laboratory, samples were tested for PH, Electrical Conductivity, Total Dissolved solids, DO content using water analyzer. BOD (by incubating diluted samples at 25° C for 5 days), COD (by dichromate reflux method using a ferroin indicator), Alkalinity (Titration), Hardness (EDTA Method), TDS (Evaporation method), TSS(filtration through Watman no. 44 filter paper), fluorides(Sparks Spectrophotometric method), Nitrates(Spectrophotometric method) tests were performed.

3.3 Calculation of Weighted Arithmetic WQI

Weighted arithmetic water quality index method classified the water quality according to the degree of purity by using the most commonly measured water quality variables. The method has been widely used by the various scientists and the calculation of WQI was made using the following equation

$$WQI = \frac{\sum WiQi}{\sum Wi}$$

The quality rating scale (Qi) for each parameter is calculated by using this expression

$$Qi = \frac{Vi - Vo}{Si - Vo} \times 100$$

Where,

V_i = Estimated concentration of i^{th} parameter in the analyzed water.

V_o = Ideal value of this parameter in pure water.

$V_o = 0$ (except $P^H = 7$ and $DO = 14.6 \text{ mg/l}$)

S_i = Recommended standard value for i^{th} Parameter.

The unit weight (W_i) for each water quality parameter is calculated by using the following formula

$$Wi = \frac{K}{Si}$$

K = Proportionality constant and can also be calculated by using the following equation.

$$K = \frac{1}{\sum (\frac{1}{Si})}$$

Water Quality Rating according to Weighted Arithmetic method is given in Table 2.

WQI	Status	Possible Usages
0-25	Excellent	Drinking, Irrigation, Industrial
25-50	Good	Domestic, Irrigation, Industrial
51-75	Fair	Irrigation, Industrial
76-100	Poor	Irrigation
101-150	Very Poor	Restricted use for Irrigation
Above 150	Unfit for Drinking	Proper treatment required before usage.

Table 2: Water Quality Rating as per Weight Arithmetic Water Quality Index Method

S.No.	Water Quality Parameter	Standard values	Unit weight
1	P ^H	8.5	0.0910
2	Alkalinity	120	0.0064
3	Hardness	300	0.0026
4	TDS	500	0.0016
5	TSS	500	0.0016
6	TS	500	0.0016
7	EC	300	0.0026
8	DO	5	0.1550
9	BOD	6	0.1290
10	COD	10	0.0773
11	Nitrates	45	0.0172
12	Fluorides	1.5	0.5150

RESULTS AND DISCUSSION

Having successfully collected the samples and performed the physical chemical analysis and values of Water quality index were found, here presenting the results in the form of tables(refer Table 4,5).

Water Quality Parameter	S1	S2	S3	S4	S5	S6	S7
PH	7.83	8.13	8.0	8.08	8.12	7.58	8.13
Alkalinity	274	156	164	148	140	164	156
Hardness	240	170	220	160	275	200	300
TDS	360	210	215	213	208	246	193
TSS	780	1040	280	640	1206	1080	460
TS	1150	1280	510	860	1426	1354	663
EC	729	418	451	438	396	491	386
DO	8.89	7.43	8.32	8.9	8.53	8.2	8.18
BOD	2.0	5.7	4.3	4.7	5.6	8.0	2.6
COD	2.4	16	12	24	27.2	29.2	24
Nitrates	1.93	0.9	0.15	0.83	0.97	0.99	0.13
Fluorides	0.15	1.2	1.6	0.76	0.23	0.98	0.45
WQI	28.60	86.35	91.39	72.32	59.74	89.54	58.60

Table 4: The values of the various parameters for samples collected in Feb 2017

	3	2	2	3	6	7	5
Alkalinity	285	235	163	156	168	174	160
Hardness	170	223	236	189	239	210	298
TDS	368	220	315	180	320	265	200
TSS	970	1230	1089	746	1376	1298	673
TS	1456	1678	1089	746	1376	1298	673
EC	297	329	304	257	432	453	203
DO	7.67	6.54	7.98	8.67	8.23	8.65	7.89
BOD	4.2	6.0	7.8	5.6	5.71	8.31	3.5
COD	5.7	23	23.5	25.7	26.5	30.5	26
Nitrates	3.76	0.91	0.25	1.2	1.1	1.08	0.19
Fluorides	0.34	1.12	1.45	0.57	0.87	1.09	0.99
WQI	44.82	94.03	104.33	70.33	84.92	95.65	83.06

Table 4: The values of the various parameters for samples collected in March 2017

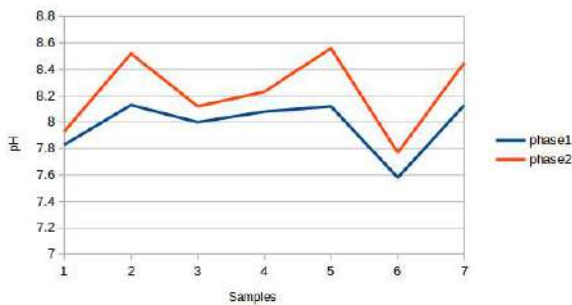


Figure 1: PH Variation along the river length

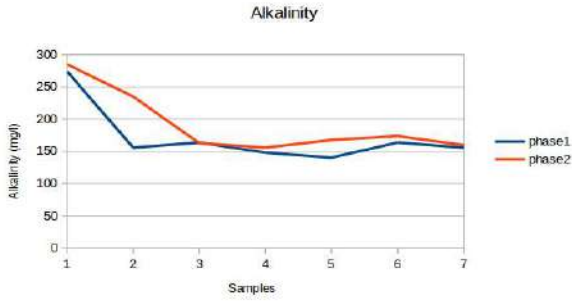


Figure 2: Alkalinity Variation along the river length

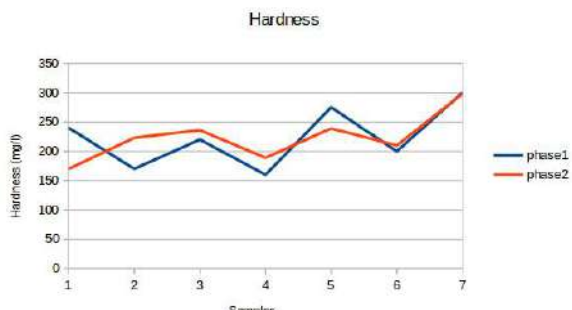


Figure 3: Hardness Variation along the river length

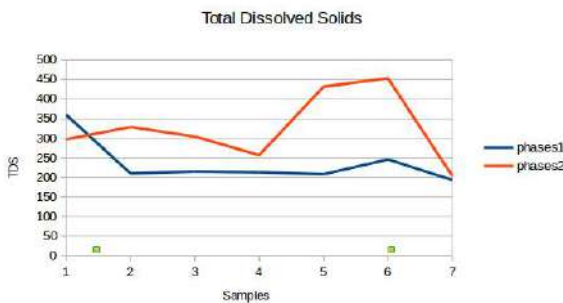


Figure 4:TDS Variation along the river length

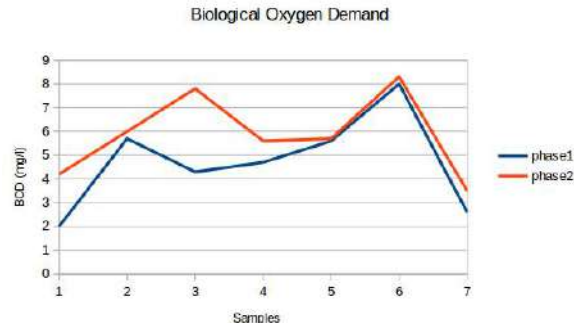


Figure 9:BOD Variation along the river length

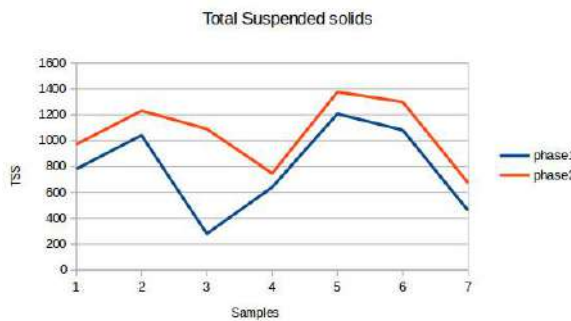


Figure 5:TSS Variation along the river length

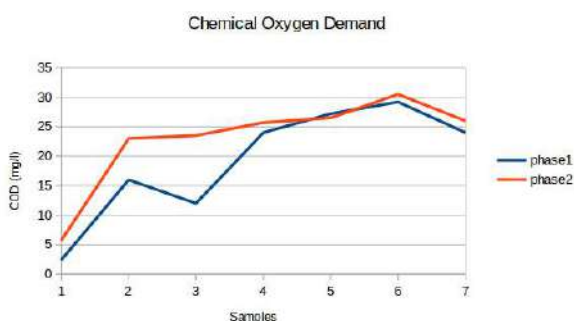


Figure 10:COD Variation along the river length

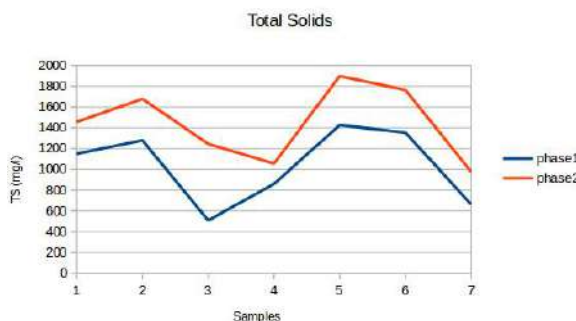


Figure 6:TS Variation along the river length

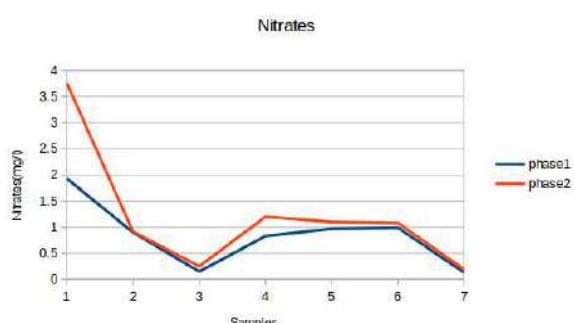


Figure 11:Nitrates Variation along the river length

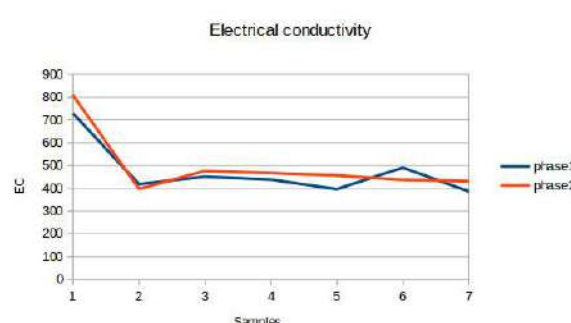


Figure 7:EC Variation along the river length

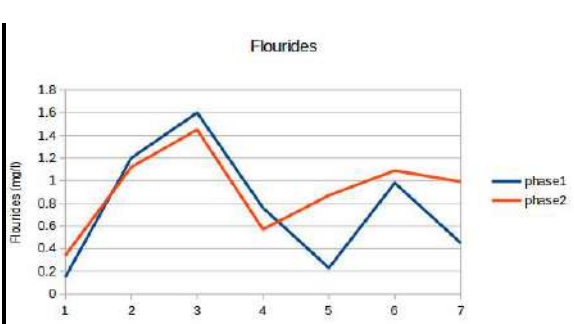


Figure 12:Fluorides Variation along the river length

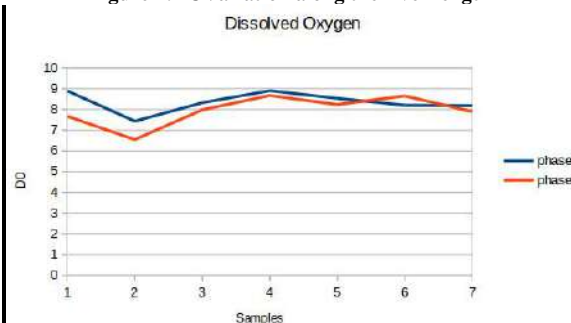


Figure 8:DO Variation along the river length

SUMMARY AND CONCLUSION

The results obtained from analysis of water samples of river Godavari are shown in table 4 and table 5. The reported values of water samples collected in two phases at different areas along the stretch of Godavari river. The results indicate that the quality of water varies considerably from location to location. A summary of the findings is given below.

Major portion of water samples showed slight basic nature with in the permissible limits of drinking water standards except samples S1 and S5 collected in phase-2. The conductivity of water is affected by the suspended impurities and also depends upon the amount of ions in the water. The highest conductivity 729 μ siemen/cm of the Godavari water was observed at Trivenisangamam (S1) during phase-1 collection. Minimum conductivity 209 μ siemen/cm was observed at Binola (S7). Total solids may affect water quality. Water with high total solids generally is of inferior pot ability. Total dissolved solids were observed maximum 368 mg/l and minimum 180 mg/l in. Total suspended solids were recorded maximum 1376 mg/l in sample S5. The sample from S5 and S6 showed

nearly same values but the samples from Basara Bridge (S5) showed light high concentrations of TSS compared samples from Basara Ghats (S6) area. Godavari water contained high dissolved oxygen during Phase-1, followed by a gradual decrease to its lowest values during Phase-2. The higher concentrations of dissolved oxygen during Phase-1 were probably due to low water temperature, relatively low solids concentration. The maximum 8.9 mg/l oxygen content of water was recorded at Kosli (S4) and minimum 6.54 mg/l in Kondakurti sample (S2). BOD has ranged from 2 mg/l to 8.31mg/l. Highest BOD concentration is observed at Basara Ghats region this is probably due to leaving the biodegradable materials from temple such as flowers, leaves and bathing. Nitrates content was found with in the permissible limits. At some locations Fluoride content is was much less than permissible limit and at Tadibiloli (S3) it is slightly higher than standard value.

The WQI value for present samples range from 28.60 to 104.3. Major portion of the sample are showing water quality in the range of poor to very poor. Only one sample exceeded the standard for drinking water remaining all are suitable for drinking water if proper treatment is given.

ACKNOWLEDGMENTS

We would like to express our sincere thanks to **Mrs. Shanti Jagadeeshwari**, Head of the Department, Civil Engineering, RGUKT Basara for giving us permission to use Environmental Laboratory.

REFERENCES

- [1] V.Bawa kalpana and V.B. Gaikawad, "Water Quality Assessment of Godavari river at Nasik,india: Impact of sewage and industrial wastewater".Universal Journal of Environmental Research and Technology 2013 Volume 3, Issue 4: 452- 457
- [2] C.R. Ramakrishnaiah, C.Sadashivaiah ,G.Rajanna, "Assessment of water Quality Index for groundwater in Tumkur Taluk, Karnataka", ISSN: 0973-4945 E-Journal of Chemistry 2009, 6(2), 523-530..
- [3] Dhirendra, M.J., Alok Kumar, and Namita Agrawal.(2009). "Studies on Physicochemical parameters to assess the Water Quality of river Ganga for drinking purpose in Haridwar district", Rasayan J. Chem. 2: 195-203.
- [4] Khan, A.M., V. Srinivasarao, Y.L.N. Murthy, et al, 2008, "Assessment of water quality of Godavari River at Nanded, Maharashtra and Rajamundry, Andhra Pradesh",Journal ofChemistry and Environment 12(1):65-68.
- [5] Manjusha Bohr et al. "Water Quality Assessment of the River Godavari, At Ramkund,Nashik, (Maharashtra), India". International Journal Of Engineering And Science. Issn: 2278-4721, Vol. 2, Issue 2 (January 2013), Pp 64-68
- [6] Ruby Pandey et al. "Assessment of Physico-Chemical Parameters of River Ganga atAllahabad With Respect To WQI", International Journal of Innovative Research in Science, Engineering and Technology, ISSN: 2319-8753, vol 3,Issue 9, September 2014.
- [7] Pushpa Rani et al., "Studies in determination of some parameters of 'Ganga' river water, Kanwar Mela 2013, Haridwar", Journal of innovative biology,ISSN: 2348-6473,June 2014 Vol. 1, Issue 2, P. 122-125.
- [8] Water Quality Status of Water Bodies of Maharashtra with Recourse to Analytical/Statistical Tools(2007-2011), Maharashtra Pollution Control Board (MPCB), 4-23 to 4-31.
- [9] Comprehensive Study of Polluted River Stretches and Preparation of Action Plan of River Godavari from Nasik D/S to Paithan, Maharashtra Pollution Control Board (MPCB),
- [10] APHA, AWWA, WPCF (1989): Standard Methods for the examination of water and Waste Water, 17th Ed (Clescerina, L.S. Eds., Trussell, R.R., Greenberg, A.E.), APHA, Washington D.C. U.S.A.
- [11] Thesis submitted by Prakash, "Water Quality Study on Rivers in SARAWAK". University of Malaysia Sarawak 2005
- [12] Singh, V.K., Singh, K.P. and Mohan, D. "Status of heavy metals in water and bed Sediments of river Gomati – A tributary of the Ganga river", India, Environmental Monitoring and Assessment, 105: 43-67.
- [13] Raut, K.S., Shinde, S.E., Pathan, T.S. and Sonawane, D.C. "Seasonal Variation in physico -chemical characteristics of Ravi rivar" , ISSN 2224-3577 International Journal of Science and Technology, Volume 2 No.5 May 2012
- [14] Kumar, Rita. N., RajalSolanki and Nirmal Kumar J.I. "An Assessment of Seasonal Variation and Water Quality Index of Sabarmati River and Kharicut Canal at Ahmedabad, Gujarat", Electronic Journal of Environment, Agriculture and Food Chemistry10 (8), 2771-278
- [15] BIS (1991): Bureau of Indian Standards, Indian Standard Specification for Drinking water IS10500: 2-4
- [16] W.H.O., 1984. WHO Guidelines for Drinking Water, Geneva, Switzerland. Vol.1



Proceedings of

**5th NATIONAL CONFERENCE
on
Water, Environment & Society
(NCWES - 2018)**

**4th - 6th June, 2018
Hyderabad, India**



Editor : Dr. M.V.S.S. Giridhar

Organized by

CENTRE FOR WATER RESOURCES
Institute of Science and Technology
Jawaharlal Nehru Technological University Hyderabad
Kukatpally, Hyderabad - 500 085

Supported by



Proceedings of
5th National Conference
on
Water, Environment & Society
(NCWES - 2018)
4-6 June, 2018
at JNTUH, Hyderabad, India

Chief Patron

Prof. A. Venugopal Reddy

Vice-Chancellor, J.N.T. University Hyderabad

Patron

Dr. A. Govardhan

Rector, J.N.T. University Hyderabad

Chairman

Dr. N. Yadaiah

Registrar, J.N.T. University Hyderabad

Co-Chairperson

Dr. B. Venkateswara Rao

Director, IST, J.N.T. University Hyderabad

Convener

Dr. M. V. S. S. Giridhar

Associate Professor, CWR, IST, J.N.T. University Hyderabad

Organized by

Centre for Water Resources

Institute of Science and Technology

Jawaharlal Nehru Technological University Hyderabad

Kukatpally, Hyderabad - 500 085

Contents

S.No.	Title	Page No.
INAUGURAL KEYNOTE		
1.	Integrated Water Resources Management by Considering Sedimentation in Serially Linked Reservoirs <i>G.K. Viswanadh and M. Visweswararao</i>	(xxix)
KEYNOTES		
2.	Challenges in Drinking Water Supply for Rural Households in India Through Village Distribution Systems Feed from Bulk Water Supply <i>B. Rajeshwar Rao and Shiva Ram Bandari</i>	3
3.	Qualitative Analysis of Rural Water Supply Distribution Network System Using Watergems Model <i>Gopal M. Naik and R. S. M. Manasa</i>	14
4.	Sense of Urgency for Advanced Irrigation Management Practices for High Agricultural Productivity in the Context of Water Variability Due to Global Climate Change, Food Insecurity Due to World Population Explosion and Water Conflicts Due to the Conflicts of Interest of Stakeholders <i>Mohammed Hussain</i>	20
5.	Water Availability in Indian Rivers: Myths & Realities <i>S. Jeevananda Reddy</i>	29
6.	Sustainable Micro-catchment Development by Continuous Contour Trenching Techniques in Dryland Areas <i>R. S. Patode</i>	43
7.	Water and Energy Efficient Technologies to Address Climate Changes in Ganges <i>Krishna Reddy Kakumanu</i>	50
8.	Use And Applicability of General Circulation Models in the Simulation of Climate System <i>Kulkarni Shashikanth</i>	58
9.	Integrated Water Management System Storm Water Treatment Areas with Applicable Best Management Practice <i>Madhu Edara</i>	65
10.	Geoscientific Knowledge for Sustainable Groundwater Management Special Reference to Tannery Belt in India <i>N. C. Mondal</i>	74
11.	Efficacy of Electrical Resistivity Tomography in Delineation of Groundwater Reservoirs - An Over View <i>S. N. Rai</i>	92
12.	Nutraceuticals Potentials of Vegetables Crops <i>Surendra R. Patil</i>	102
13.	Mathematical Models in Hydrology and Water Resources Engineering <i>M. Anjaneya Prasad and P. Sunder Kumar</i>	115

TECHNICAL PAPERS		
14.	Ghogha Rain Water Harvesting Scheme in 82 Villages of Bhavnagar, Gujarat - A Success Story 14 Years After Completion <i>F. R. Sherwani</i>	125
15.	Role of Isotope Techniques in Characterizing Thermal Fluid- Insights from Godavari Valley Geothermal Field, Telengana <i>Sitangshu Chatterjee and U.K. Sinha</i>	135
16.	Rural Sanitation: A Case Study of Yarikoppa Village <i>Munnoli P M, Mulla S A, Dafedar M, Madivalar P and Reddy G</i>	141
17.	Rural Sanitation for Sustainable Development: A Review <i>Munnoli P M, Mulla S A, Dafedar M, Madivalar P and Reddy G</i>	145
18.	Water Supply and Sanitation Appliances to Save Water: A Review <i>Munnoli P M, Hubli Kiran, Beedimani Priyanka, Aishwarya and Karale Suneel</i>	151
19.	Inferring Dominant Mangrove Vegetation Along Salinity Gradient Based on In-Situ Measurements and Remotely Sensed Imagery <i>Kripa M K, Hari Nivas A, Nikhil Lele, Thangaradjou T, Saravan Kumar A, Archana. U. Mankad and T. V. R Murthy</i>	157
20.	Mathematical Model Studies for Optimizing Outfall Location for Hot Water Discharge from Power Plant <i>Payal Chakote, A. K. Singh, L.R. Ranganath and P. R. Dixit</i>	162
21.	Geospatial Technology to Monitor Spatio-Temporal Changes in Icebergs in East Antarctica <i>Mehanaz sherif and Rajashreebothale</i>	168
22.	Waste Water Treatment Using Moringa Oleifera for Balanced Ecosystem <i>T. Mounika and V. Malathi</i>	174
23.	Atmospheric Changes Due to Photo Chemical Smog <i>M. Kavitha Yadav and K. Sai Pradeep</i>	178
24.	Development of Artificial Neural Network to Forecast Air Pollutants in Pune City <i>Shreenivas N. Londhe and Priyanka P. Shinde</i>	183
25.	Application of Genetic Programming to Retrieve the Ground Water Levels <i>P. R. Dixit, Shrushi D. Lohi and P. S. Kulkarni</i>	189
26.	Flood Routing: A Comparison of Theoretical and Data Driven Technique <i>Pradnya Dixit and Sneha Nikalje and S. N. Londhe</i>	195
27.	Removal of Hexavalent Chromium (Cr Vi) in Wastewater by Using Moringa Oleifera (Drumsticks) <i>Ajinkya Gadhav and A. S. Dharnaik</i>	201
28.	Hydrogeology and Drainage Morphometric Study for Groundwater Potential Zones in Joytiba Hill Area in Kolhapur District, Maharashtra, India-Using Remote Sensing and Gis. <i>Gurav Chandrakant and Md. Babar</i>	205
29.	Non-Revenue-Water Assessment and Reduction Strategy in Urban Water Distribution <i>B. Rajasekhar, G. Venkata Ramana and G. K. Viswanadh</i>	211

30.	Neglected Reality of Manual Scavenging - Prohibited Yet Practiced, A Case of Hyderabad <i>Sumskrutha Talupula</i>	219
31.	Flow Characteristics Over Broad Crested Weir and Dam Spillway <i>Bhukya Ramakrishna, CH. Shivakumargoud, SK. Vaheed Jallewar Praveenkumar and Myakala Prasad</i>	226
32.	Trend Analysis of Extreme Temperature Data of India Using Non-Parametric Methods and Empirical Mode Decomposition <i>Anand Vishnu, Drisya S Dharan, Adarsh S, Anuja PK and Govindan Unnithan</i>	232
33.	Estimation of Physico-Chemical Parameters of Groundwater in Aprupa Watershed, Sangola Taluka, Solapur District, Maharashtra -A Case Study <i>Karim C Mujawar and Abhishek Gadade, Ravi Kshetri, Abhay Birajdar, Sham Pawar, Suhas Shingade and Suryakant Patil</i>	239
34.	Reservoir Sedimentation Analysis: A Case Study <i>Zeenat Ara and Mohammad Zakwan</i>	247
35.	Applications of Green Materials for the Preparation of Eco-Friendly Bricks and Pavers <i>J. Kruthika Mehar, K. Pushpa, G. Pushpa, D. Shravya and B. Vamsi Krishna</i>	254
36.	Environmental-Friendly Concrete for Sustainable Construction of the Buildings <i>C. Lakshmi, G. Sai Ram, K. Sravya Sri, Shravan Manda and B. Vamsi Krishna</i>	262
37.	Reconnoitering Hydrochemical Background using Log-Probability Distribution in a Channel Island, Andhra Pradesh <i>N.C. Mondal</i>	271
38.	Study on Ground Water Contamination in and Around Visakhapatnam Industrial Area <i>P. Trinadha Rao</i>	278
39.	Impacts of Solid Waste Dump Site on Ground Water Quality (Leachate) <i>K. Syamala Devi and K. Venkateswara Rao</i>	287
40.	Spatial Variation of Onset and Withdrawal of Monsoon in Akola District of Western Vidarbha Region <i>G. U. Satpute, Shivakumar Anna, S. M. Apturkar and N. G. Patil</i>	299
41.	Optimal Water Management Modelling for Water Supply and Hydropower <i>Shahbaz Sida and Geeta S. Joshi</i>	306
42.	Changes in Land Use Land Cover Using Geospatial Techniques: A Case Study of Koyna River Basin, Maharashtra, India <i>Amarsinh B. Landage and Ashok K. Keshari</i>	313
43.	Groundwater Development through Drainage Line Treatments in Vidarbha Region of Maharashtra <i>M. B. Nagdeve, R. S. Patode, C. B. Pande and R. S. Mali</i>	321
44.	Impact of Conservation Agriculture Treatments on Runoff and Soil Loss in Soybean Crop under Rainfed Condition <i>R. S. Patode, M. B. Nagdeve, V.V. Gabhane, A. B. Turkhede, N. R. Palaspagar and R. S. Mali</i>	326
45.	Hydrological Water Balance Assessment of A Micro-Catchment using Physically based Model <i>R. S. Patode, M. B. Nagdeve, K. Ramamohan Reddy and G. Ravindra Chary</i>	331

46.	Crop Residue Cutting Mechanisms for Direct Drilling in Agriculture Conservation <i>A. K. Kamble, S. H. Thakare, U. R. Badegaonkar and M. B. Nagdeve</i>	336
47.	Bio-Char Production from Agricultural Crop Residue using Horizontal Reactor <i>A. K. Kamble, A. J. Dere and Sandip Gangil</i>	344
48.	Bio-Energy Utilization through Thermo Efficient Biomass Cook Stove for Rural Households <i>A.K. Kamble and M. B. Nagdeve</i>	350
49.	Studies on Biogas Production from Soybean and Cotton Straws Substrate <i>A.K. Kamble, S.B. Kirjat and M. B. Nagdeve</i>	357
50.	Solar Energy Operated Cabinet Dryer for Drying Tomato Slices <i>A. K. Kamble, Ramesh L. Dombale and M. B. Nagdeve</i>	365
51.	Energy Audit of Cotton Crop Production System <i>A.K. Kamble and M. B. Nagdeve</i>	372
52.	Application of GIS and Remote Sensing for Water Conservation Planning and Management of the Purna Watershed in Akola District of Maharashtra <i>C. B. Pande, R. S. Patode, M. B. Nagdeve, K. N. Moharir and M. B. Dongardive</i>	380
53.	Flow Characteristics of Laboratory Flumes in Free and Submerged Flow Conditions <i>Bhukya Ramakrishna, Gaddam Gangadher, Rapolu Sravani, Hechu Swathi and Mudhigonda Chandramouli</i>	386
54.	A Preliminary Study of Water Distribution System In Adhainagar, Hyderabad <i>K. Shimola, P. Venugopal and T. Sai Bharath</i>	393
55.	Assessment of Water Quality for Drinking and Irrigation Purpose in Alladurg Mandal of Medak District, Telangana State, South India <i>Sanda Rajitha, Adimalla Narsimha and Praveen Raj Saxena</i>	399
56.	Pruning: A New Approach for Quality Production in Acid Lime <i>Surendra R. Patil, Mahipal M. Ganvir, Sonali N. Lokhande and Premlata M. Chandan</i>	405
57.	Feasibility of Energy Production from Bio-Degradable Waste <i>T. Kiran Kumar</i>	411
58.	Advanced Spectral Classification Methods for Hyperspectral Data - A Concise Review <i>Veeramallu Satya Sahithi, MVSS Giridhar and I V Murali Krishna</i>	420
59.	Analysis On Green Building (<i>Case Study: GRIET, Hyderabad, India</i>) <i>Akula Prakash and Rathod Ravinder</i>	434
60.	Estimation of Residential Building Using Low Cost Materials <i>Rathod Ravinder, Akula Prakash, M. Govardhan, Ch. Chaitanya Lakshmi and Varala Akhila</i>	444
61.	Laboratory Study of Bituminous Mixes Using Sisal Fiber <i>Kandlagunta Mounika, Akula Prakash and Rathod Ravinder</i>	448
62.	Kinetics and Isotherm Studies on Cationic Dye Adsorption onto Activated Carbon from Sugarcane Bagasse <i>T. V. Nagalakshmi and K. A. Emmanuel</i>	455

FLOW CHARACTERISTICS OVER BROAD CRESTED WEIR AND DAM SPILLWAY

**Bhukya Ramakrishna¹, Ch. Shivakumargoud², SK.Vaheed³
Jallewar Praveenkumar⁴ and Myakala Prasad⁵**

¹Assistant Professor, ²³⁴Student, Civil Engineering Department, RGUKT Basara, Telangana.

¹bhukyaramakrishna@gmail.com, ²shivakumargoudce430@gmail.com,

³myakal.aprasad02@gmail.com, ⁴pk88114@gmail.com

ABSTRACT

A control section is defined as a section in which a fixed relationship exist between the discharge and depth of flow broad crested weirs, spillways are some typical examples of structures which give rise to control sections. The critical depth is also a control point. However when the flow changes from supercritical flow to subcritical flow, A hydraulic jump is usually formed by passing the critical depth as a control point. So in this context laboratory flume experiments are carried out in the hydraulics laboratory to investigate the head-discharge Relationships and computation of coefficient of discharge for different hydraulic structures with different slopes. In additionally our study also carried out on energy dissipation and specific energy computations between upstream and downstream of hydraulic structures. Results of experiment shows that this average value of coefficient of discharge for different types of broad crested weirs(i.e stream lined broad crested weir, sharp cornered broad crested weir, broad crested weir with raised crest) and dam spillway with toe, ski jump and Baffle blocks are 0.38, 0.35, 0.37, 0.80, 0.70 and 0.80 Respectively. The variation of C_d with h/a was linearly Related and there was power Relationship between discharge and head with R^2 ranging from 0.70 to 0.99 for all structures under study. On the other hand, the classification of jumps based on froude number, and sequent depths is studied and favorable conditions for different hydraulic structures are proposed for energy dissipation.

Keywords: Broad crested weir, Dam Spillway, Coefficient of discharge, toe, ski jump, baffle blocks.

INTRODUCTION

Weirs are generally divided into two broad groups, namely, sharp crested weirs and weirs of finite crest length have been used in hydraulic engineering to control flow in open channels and also for flow measurement, For convenience, we shall refer to these weirs simply as broad crested weirs. Rectangular broad-crested weirs, with either a sharp square edged or rounded entrance, are not as easily submerged as sharp- crested weirs. Considerable amount of case with curvilinear flow existing over the entire weir is referred to as a short-crested weir. Flow over a weir of finite crest length with a square upstream edge where the crest length and head are such that the flow separates from the upstream edge and does not reattach to the weir before the flow leaves the weir. In such a case, the finite crest length weir is acting as a sharp-crested weir. Hence finite crest width weirs could be classified as a broad crested, short- crested, or sharp crested weir. Furthermore, in the case of the broad crested weir, if the crest length is much larger than that required to have a short reach of parallel flow then, based on the variation of the discharge coefficient, we have to add another class of weirs known as long crested weirs. These treatments, as we show later, are not as complete as the treatment for sharp-crested weirs and this work attempts to present a reasonably complete treatment of the discharge characteristics of weirs of finite crest length, using as complete a set of reliable data as possible, for free-flow conditions. Dam spillways are also good energy dissipaters, which includes accessories like toe, ski jump and energy dissipating pegs. Therefore, a laboratory study was planned to establish following results.

1. To determine coefficient of discharge, and develop head-discharge relationships for Broad Crested Weir and Dam Spillway etc. with varied slopes of channel.
2. To determine effective energy dissipater and jump characteristics over different hydraulic structures.

Brief Summary of Significant Experimental Investigations

P. P. Dabral et.al.(2014) work includes a glass sided tilting flow channel based laboratory study was carried out to determine the discharge coefficient and head- discharge relationships for hydraulic structures i.e .Broad Crested Weir, Crump Weir, Sluice gate, Radial Gate and Dam Spillway. The average value of Coefficient of Discharge for Broad Crested Weir, Crump Weir, Sluice Gate, Radial Gate and Dam Spillway was found to be 0.44, 0.85, 0.76, 0.82 and 1.03 respectively. Furthermore, the with h/a was linearly related and there was power relationship between Discharge and Head with ranging from 0.80 to 0.99 for all the structures under study. Willi H. Hager.et.al. (1994) study talks about the flow features over the broad crested weir with vertical upstream wall and sharp crested corner are analysed experimentally. Only the long crested weir is considered, for which the discharge coefficient remains practically constant. The broad crested weir is characterized by insensitivity to tail water submergence. Amruthur S. Ramamurthy.et.al.worked on the characteristics of square-edged and round-nosed, rectangular, broad-crested weirs are studied under free-flow and submerged flow conditions. For the square-edged weir, the effect of non hydrostatic distribution of pressure is taken into account in the formulation of the momentum equation. In addition, for the round-nosed weir, new relations are developed to supplement the existing results for square-edged weirs. The flow- reduction factor for a given submergence is dependent on the degree of rounding of the upstream top corner. Gafsi Mostefa.et.al.(2015) on experimental research of hydraulic characteristics of the flow over the dam spillway. It is in this context they have studied the effect of flow rate and the slope of channel on the energy dissipation.

Sadegh Dehdar-behbahani.et.al.(2016) studied the effect of geometries of guide walls on the flow pattern and rating curve of Balaroud dam spillway's (Iran) was simulated using numerical and physical simulation. Gamal M. Abdel Aal.et.al.(2017) study aims to investigate the over-flow with breakers in dam spillways and to evaluate their effect on energy dissipation. Amir Hossein Azimi.et.al. (2009) work presents a critical analysis of free flow over weirs of finite crest length, with square-edged or rounded entrance. They have confirmed the classification of finite crest length weirs and developed empirical correlations for the discharge coefficient.

Experimental Setup and Laboratory accessories

The laboratory experiments were conducted on a glass sided tilting flume with length 5m, width 30cm and height of 45cm which is depicted in Fig.1. It consist of sloping set up ranging from negative 1 in 200 to positive 1 in 200. This entire set up is connected with sensors and the values are recorded through armfield software.



Fig. 1 Tilting flume channel

Our study includes on hydraulic structures i.e broad crested weirs and dam spillway. These two structures further divided into three more cases individually, those are streamlined, sharp cornered and weir with raised crest height. Again in dam spillway experiments were conducted on dam spillway toe, ski jump and baffle blocks.. respectively and their dimensions are tabulated inthe table 1.

Experimental work

Experiments were conducted on broad crested weir with three types and for three different positive slopes, those are 1 in 200, 1 in 500 and zero slope. In the case of dam spillway, experiments were conducted in the same way and for two different slopes i.e. 1 in 500 and zero slope. The computations of Cd are and results were shown in graphs(see fig 2 to 4

Table 1 Dimensions of hydraulic structures

S. No	Hydraulic structure	Dimensions of structures(cm)
1	Streamlined Broad Crested weir	Length = 40 Height = 12 Breadth = 30
2	Sharp cornered Broad Crested weir	Length = 40 Height = 6 Breadth = 30
3	Broad Crested Weir with raised crest	Length = 40 Height = 18 Breadth = 30
4	Dam spillway with Toe, Ski jump and Baffle blocks	Height = 23 Breadth = 30

The coefficient of discharge of broad crested weir was calculated by using the following formula.

$$Cd = \frac{Q}{b \times f_2 g \times H^{3/2}}$$

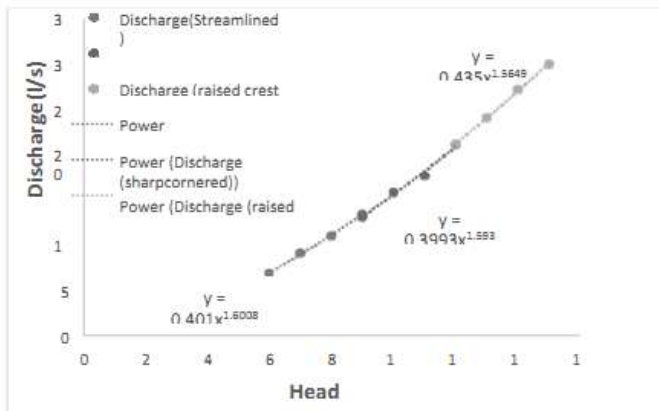


Fig. 2 Discharge Head Curve for 3 Broad Crested Weirs for horizontal slope

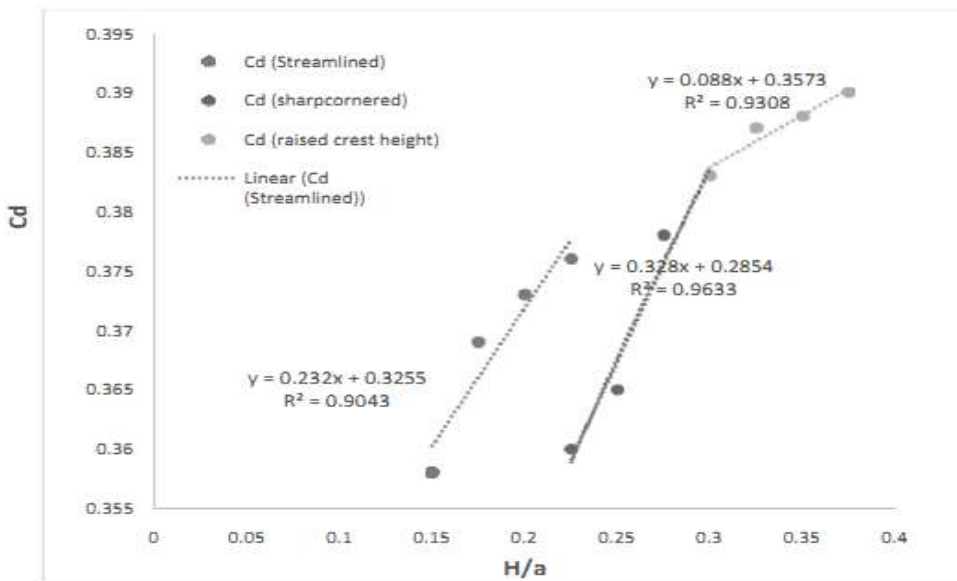


Fig. 3 Variation of Cd with H/a for 3 Broad Crested Weir with horizontal slope

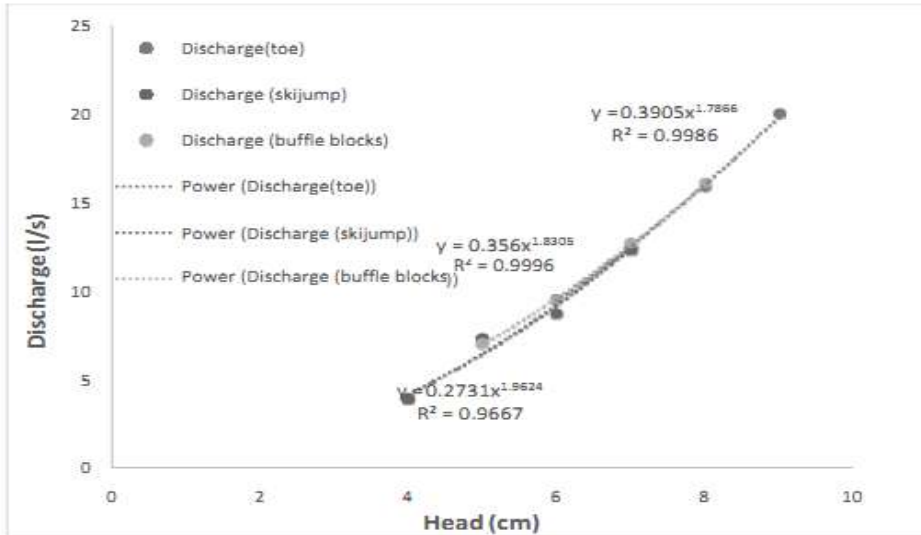


Fig. 4 Discharge Head curve for Dam spillway 3 types for horizontal slope

The coefficient of discharge of dam spillway was calculated by using the following formula.

$$Cd = \frac{Q}{b \times f \cdot 2g \times H^{3/2}}$$

C_d = Coefficient of discharge, Q = rate of discharge in Litre/sec, B = width of channel in cm, g = gravitational acceleration in cm/s^2 , H = head over the weir/spillway.

RESULTS AND DISCUSSION

Coefficient of discharge broad crested weir

The experimental data presents the average values of coefficient of discharge for broad crested weirs of three types with different slopes. It varies in all the cases, the average values of coefficient of discharge for broad crested weir with streamlined body, sharp crested weir and weir with raised crest for horizontal slope are 0.369, 0.370 and 0.387 respectively with R^2 value ranging from 0.75 to 0.99. It is observed that C_d value is nearly same for both streamlined body and sharp cornered weir. This is applicable to only low discharges. For high discharges sharp cornered weir will have less C_d because there may be formation of boundary layer at the upstream edge.

The variation of discharge with head follows power relationship of order ranges from 1.5 to 1.6 for three models for zero slope condition. The variation of C_d with H/a ratio observed to be linear of slope ranging from 0.232 to 0.39 (from graphs). Among all three cases sharp cornered weir observed to be having more slope i.e. 0.39 that means it requires low head comparing to remaining two cases to produce same amount of discharge. Slopes also effects the C_d , it is observed that C_d is increasing with increase in positive slope.

Coefficient of discharge for dam spillway

The experimental data presents the average values of coefficient of discharge for dam spillway of three types with different slopes. It varies in all the cases, the average values of coefficient of discharge for dam spillway with toe, ski jump and with baffle blocks for horizontal slope are 0.787, 0.760 and 0.775 respectively with R^2 value ranging from 0.75 to 0.99. As slope increases C_d value also increases.

The variation of discharge with head follows power relationship of order ranges from 1.78 to 1.96 for three models for zero slope condition. Among all three cases dam spillway with toe that means it requires low head comparing to remaining two cases to produce same amount of discharge.

Specific Energy Computation for broad crested weir

Broad crested weir not only used as a control section but also it is used for energy dissipation. Energy dissipated through the formation of jump. The classification is purely based on Froude number of supercritical flow. Every type of broad crested weir has produced individual type of jumps. For the case of streamlined body, the Froude numbers are in the range of 4.5 to 9 for low heads hence it is classified as steady jump and it is in the range of 2.5 to 4.5 for high discharges hence it is classified as oscillating jump. In the case of weir with sharp cornered edge, the Froude numbers are in the range of 2.5 to 4.5 for low discharges hence it is classified as oscillating jump and it is in the range of 1.7 to 2.5 for high discharges hence it is classified as weak jump. In the case of weir with raised crest height, the Froude numbers are in the range of 4.5 to 9 for low discharges hence it is classified as steady jump and it is in the range of 2.5 to 4.5 for high discharges hence it is classified as oscillating jump.

The jump efficiency is calculated and it was found that for broad crested weir with streamlined body was 70% on an average and for remaining two cases it was very less about 50%. Hence among these three weirs, weir with streamlined body is efficient. Slope also effect the energy dissipation, i.e. as the slope increases the energy dissipation will be more.

Specific energy computations of dam spillway

For the case of spillway with toe, Froude numbers are varying with discharge. In this work for four discharges four different jumps are formed those are oscillating, weak, undular, weak jump. Where as in the case of ski jump mostly the jump formed is weak jump. In the case of spillway with baffle blocks the jump formed is undular jump. This indicates that spillways are weak in dissipation of energy compared to weirs. It is observed that dissipation of energy is entirely depends on head over structure and downstream flow depth. The jump efficiency of spillway with toe was found to be 65% and remaining all are worst in the purpose of dissipation because their flow Froude numbers are less than 1.7.

CONCLUSIONS

- The average values of coefficient of discharge for broad crested weir with streamlined body, sharp cornered body and weir with raised crest height are found to be 0.369, 0.370 and 0.387.
- The average values of coefficient of discharge for dam spillway with toe, ski jump and with baffle blocks are found to be 0.787, 0.760 and 0.775
- For broad crested weir C_d vs H/a plot shows that the variation of C_d with H/a is linear.
- The plot between head and discharge is always follows power relation for both broad crested weir and dam spillway.
- Among the three cases of broad crested weir streamlined body was found to be efficient energy dissipater.
- Among the three types of dam spillway, spillway with toe found to be efficient energy dissipater
- On whole comparison between broad crested weir and dam spillway, broad crested weir found to be good energy dissipater.

REFERENCES

1. Bos, M. G. 1985. Long throated flumes and broad crested weirs, Martinus Nijhoff/Dr W. Junk Publishers, Dordrecht, The Netherlands
2. Chanson, H. (2006). "Minimum specific energy and critical flow conditions in open channels." *J. Irrig. Drain. Eng.*, 132(5), 498–502.
3. Chanson, H., 1995. Discharge measurement of Broad Crested Weir- *Journal of Irrigation and Drainage Engineering (ASCE)*, 121(2):222-224.
4. Gogus, M. and Defne, Z., 2006. Broad-Crested Weirs with Rectangular Compound Cross Sections- *J. Irrigation and Drainage Engineering*, 132(3):272-280.
5. Hager, W. H., 1992. Broad Crusted Weir. *J. Irrigation and Drainage Engineering*, 120(1) Paper no.4385.
6. Hall, G. W.1962. "Analytical determination of the discharge characteristics of broad crested weirs using boundary layer theory." Proc , Institute of Civil Engineers, Vol. 22, Paper No. 6607, ICE, London,177–190.
7. Harrison, A. J. M. 1967. "The streamlined broad-crested weir." *Proc.-Inst. Civ. Eng.*, 38, 657–678.
8. Johnson, M. C. _2000_. "Discharge coefficient analysis for flat-topped and sharp-crested weirs." *J. Irrig. Sci.*, 19.3, 133–137.
9. Johnson, M. C. 2000. "Discharge coefficient analysis for flat-topped and sharp-crested weirs." *Irrig. Sci.*, 19, 133–137.
10. Ramamurthy, A. S., Tim, U. S., and Rao, M. V. J. 1988. "Characteristics of square-edged and round-nosed broad-crested weirs." *J. Irrig.Drain. Eng.*, 114.2, 61–73.
11. Ranga Raju, K. G. 1981_. Flow through open channels, McGraw-Hill,New York.
12. Rao, S. S., and Shukla, M. K. 1971. "Characteristics of flow over weirs of finite crest width." *J. Hydraul. Div., Am. Soc. Civ. Eng.*, 97_11_,1807–1816.
13. Smith, C. D. 1958. "Open channel water measurement with the broadcrested weir." *Bull. Int. Commn Irrig. Drain.*, 46–51.

FLOW CHARACTERISTICS OF LABORATORY FLUMES IN FREE AND SUBMERGED FLOW CONDITIONS

**Bhukya Ramakrishna¹, Gaddam Gangadher², Rapolu Sravani³,
Hechu Swathi⁴ and Mudhigonda Chandramouli⁵**

¹Assistant Professor, ²³⁴⁵Student, Civil Engineering Department, RGUKT Basar, Telangana

¹bhukyaramakrishna@gmail.com, ²ndagangadher@gmail.com, ³swathicivil1557@gmail.com, ⁴sravanisandya111@gmail.com

ABSTRACT

Use of the water resources in an efficient and economical manner, place a vital role in domestic, agricultural and industrial needs are concerned. Measurement of water in an open channel is very much important in collection, distribution, safe delivery of water resources. It is necessary to know how to measure water in open channel. For this purpose the flume which we use are one of the equipment. Flumes will give best results by eliminating major problems like reducing the head loss and removal of sediment. And we can measure accurately by this and in an easy manner also. Free flow is nothing but where the flow in downstream is not affecting the upstream and submerged flow is downstream flow is affecting the upstream flow. With this connection experiments are conducted on laboratory flumes like venturi, Parshall (3"), WSC (2", 45 degrees) on 5m. Tilting Flume. In Venturi and Parshall flume, surface profiles which are drawn along the channel bed shows that the depth of water in upstream is not affected by backwater depth in free flow, where as in submerged flow it was influenced by backwater depth. And drawn the standard profiles for rough estimation of profile in different conditions like Bed slope(-0.005, 0, +0.01), discharge(5l/s, 7l/s, 9l/s, 11l/s), back water depth. The discharge relations in Venturi, Parshell flumes, between actual and theoretical values shows that they are in linear relation. In Parshell flume the channel bed slope, discharge and backwater depth are mutually independent. And in WSC flume, comparison of standard curves in different flow conditions says that, submerged flow is affecting the curve position.

Keywords: Flumes, Free flow, submerged flow, Surface profiles.

INTRODUCTION

The efficient and economical use of water resources is becoming a critical, social concern. Accurate flow measurement is very important for proper and equitable distribution of water among water users. Due to increasing utilization and the value of water, measuring techniques become more important and necessary information concerning the volume of available water is very useful in planning for its future use and distribution. There are several types of flow measurement devices are available those are namely Differential pressure flow meters, Positive displacement flow meter, Electromagnetic flow meters and Open channel flow meters.

Flume is an open channel used for measurement of flow of water. Some varieties of flumes are used in measuring water flow those are Venturi flume, Parshall flume and WSC flume (Washington State College flume). A venturi flume is a critical flow flume where in the critical depth is created by a contraction in width of the channel. Thus the contracted section serves as a control. A venturi flume consists of three sections a converging section, a throat section and diverging section. The flow upstream and downstream of the throat is subcritical and supercritical respectively. Parshall flume is advanced one of the venturi flume it is a standing wave flume. The loss of head for the free flow limit is only about 25 percent of that for the over pour weir. The accuracy of discharge measurements with this flume, under normal operating conditions, is probably within 2 to 5 per cent. The Parshall flume may be operated as a free flow single head device or under submerged flow conditions where two heads are involved. Compare to venturi flume Parshall flume having low head losses. WSC flume noting but a Trapezoidal flume was developed primarily to measure irrigation flows. These flumes having capable of accurately measuring a much wider range of flows than those of the Parshall flume with particular emphasis of low flow sensitivity. It also used for the measuring of Varity types of discharges. The bottom is flat from entrance to exit for better head conservation. These flumes do not require free fall discharge to operate correctly.

There was a lot of work done by eminent personalities on flow measurement by flume. Especially in Parshall flume, an improved version of venturi flume has more applications compared to other types. The WSC flume has wide range of usage for different field conditions.

V. M. CONE, Irrigation Engineer[12] studied the venturi flume he proposed standard discharge curves and tables For best results to use of these the structure can be built as shown in the general plan and gauges should be placed according to that only.

RALPH L. PARSHELL, Irrigation Engineer[6],the free flow it is operated with relatively small head, which is approximately four times that in the flume. And in submerged flow the degree of submergence is also high without much affecting the rate of free flow discharge.

Stock et. Al [11](1955), the Parshall flume, can be operated in free flow or submerged flow where single head or two heads involved respectively. He proposed standard diagrams for determining the loss of head, which is function of throat width, submergence and discharge. He also proposed discharge curves discharge tables for free flow.

Skogerboe et.[9](1966) al says the exact definitions for free and submerged flow. For free flow, submerged flow calibrations he taken upstream head, Upstream head and throat head are taken respectively & by using free flow calibration tables which are given , are used to find out discharge value. Nomo graphs are to obtain the change in water elevation, submergence ratio. Head loss for Parshall flume would be finding out by standard chats which are function of submergence discharge throat width.

Skogerboe et.[10](1965) says that the standard free flow. For submerged flow the equation which is involved is function of acceleration due to gravity, upstream head, throat head, and minimum flow depth occurring in the throat. To get the transitional submergence he equated the free and submerged flow of respective size of flume. The discrepancy between transitional values by plots and computed values are attributed to in accuracies in free flow and submerged flow equations.

Jalam Singh et. Al [2&3] says that there are a lot of work was done beforely on parshell flume till now. And they mainly focused on free flow and sediment ladden flow. Experimental work has been carried out on Parshall flumes and gave coefficient of Parshall flume (K) and exponent (n) were determined through MATLAB programming.

The main objective of "Flow characteristics of laboratory flumes in free and submerged flow conditions" is to define a flow in free or submerged conditions by observing the profiles under a limited conditions of discharge and bed slope of channel. Characteristics of flow includes

1. Determining the discharge through a venturi, Parshall flumes by using head-discharge relationship and comparing those with the standard table, charts, Armfield S6 MKII software in free and submerged flow conditions.
2. Observing the water surface profiles in free flow, submerged flow condition and representing those profiles with respect the channel bed.
3. Plotting the graphs between theoretical

METHODOLOGY

Venturi Flume

In a venturi flume we are finding out the discharge by determining the relationship between upstream head and flow rate of water through a venturi flume and drawing the flow profiles. For that first we have to open the flow control valve and set one flow rate and one bed slope then allow the flow to stabilise, and then measure the depth of the water along the bed of the channel from 1m to 2.5m at every 10cm interval by using hook and point gauge. After this raise the overshot weir then measure reading for every 10cm interval, then again raise the overshot weir and measure the readings along the length of the channel. After this, change the flow rate and again take the readings, same procedure is repeated for different flow rates. By using obtained values we have drawn the flow profiles by taking the distance along x-axis and depth of water along the y-axis. After this we have measured the depth of the water at the upstream side, throat section and at the downstream, by using discharge equation we are finding out the discharge (Q_{the}) , and Q_{act} value directly given by armfield S6 MKII software, graph is plotted for Q_{act} v/s Q_{the} .

$$\text{Discharge Equation: } = \frac{2\sqrt{2Q}}{3\sqrt{3}} \cdot b \cdot H_3^2 \quad \dots\dots(1)$$

Parshall Flume

Parshall flume is the advancement of the venturi flume, in this flume we have observed and studied the water surface profiles in the free flow and submerged flow conditions. Free flow condition means the critical depth occurs in the throat section of a Parshall flume, the discharge is dependent upon only the upstream water, but it is impracticable to install a measuring flume in such a manner that free flow condition always exist. Submerged flow conditions are said to exist in a Parshall flume when the depth of the downstream flow causes the rise in the depth of the upstream flow. For drawing the water surface profiles, we have to set one flow rate and one bed slope, then allow the flow to stabilise. In this case the downstream water does not impose any change in the upstream flow means now the flow is in free flow condition, then measure the depth of the water from 0 to 3m along length of the channel at every 10cm by using hook and point gauge. After this, raise the water level at the downstream side by using the overshot weir and take the water depths for all the intervals. By using these values we had drawn the profiles by taking the distance along x-axis and depth of water along y-axis. By looking at the profiles we can easily identify the formation of the critical depth, and is that profile is under the submergence flow or free flow condition, and ripple formation at the end of the throat section due to downstream flow conditions rise the water level in flume. By knowing the depth of water at the upstream side and downstream side, we can find out the submergence ratio. Submergence ratio is the ratio of depth of downstream water to the depth of upstream water. If the submergence ratio exceeds 50% it will be considered as submergence flow, less than 50% is considered as free flow. We have measured the depth of the water at the upstream side, throat section and downstream side to

find out the discharge in free flow conditions and in submerged flow conditions. After finding the discharge we compared the obtained results with the standard charts and S6 MKII armfield software.

$$\text{Discharge equation in free flow : } Q = 0.992H_a^{1.597} \quad \dots\dots(2)$$

$$\text{Discharge equation in submerged flow: } = -0.953(H_a - H_b)^{0.55}$$

$$\log \frac{H_b}{H_a} 0.0044 \quad \dots\dots(3)$$

Where H_a = Depth of Water in Upstream Sill; H_b = Depth of Water in Throat level Sill

WSC flume

Here we are studying the characteristics of flow of water through a WSC flume and comparing the obtained results with the standard calibration chart. First we have to open the flow control valve and gradually increase the flow rate from 0 to 8lit/sec and after every setting allow flow to stabilise, after that measure the upstream water level, downstream water level and water level at the throat section by using hook and point gauge and also measured the inclined scale reading which is provided on WSC flume after that raise the overshot weir and allow the flow to stabilise then measure the readings. From the flow rate and inclined scale reading on the flume we have to draw the calibration curve and find out the submergence ratio (depth of the water at throat section to upstream depth of water). Finally compare the obtained results with the calibration curve.

RESULTS AND DISCUSSION

Venturi Flume

After installation of venturi flume in tilting flume working section, we put a particular bed slope, discharge then drawn the water surface profile in that condition. Similarly by altering the above conditions we drawn the all surface profile conditions. Example, for a bed slope of 1 in 200 (positive bed slope), at discharge of 3, 5, 7, 9 l/s the water surface profiles are shown below.

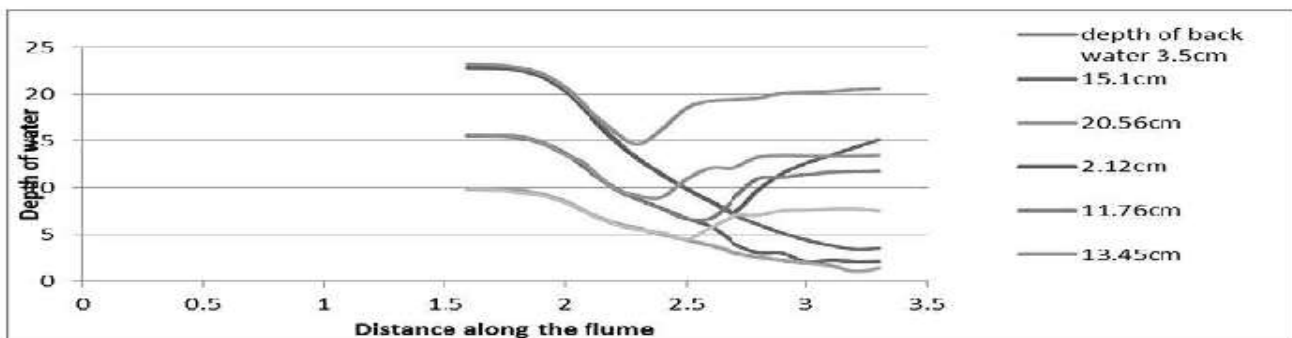


Fig. 1 Flow Profiles In a venturi flume

By observing the flow profiles, we can identify that, increasing depth of back water causes the rise in the water level at the upstream side and also we can find out the discharge for a zero bed slope at a given length of the channel 1.6 to 3.3 m.

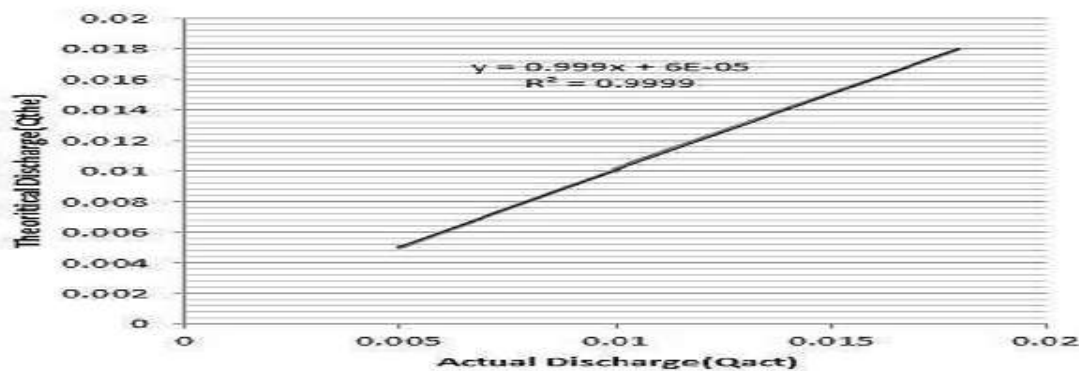


Fig. 2 Discharge Variation of Venturi Flume

The graph plotted as theoretical discharge v/s actual discharge was drawn by taking the values of water depth and substituted these values in the standard discharge equation by this we can get the theoretical discharge, the armfield S6MKII gives the actual discharge values directly, and then actual discharge was taken along the X-axis and theoretical discharge taken along the Y-axis. The resulted graph is linear from the graph we can easily say that the theoretical discharge is approximately equal to the actual discharge.

Parshall Flume

In Parshall Flume profiles are drawn for different bed slope of channel i.e. -0.005, 0, +0.001 and Discharge values of 5l/s, 7l/s, 9l/s, 11l/s and different depth of backwater conditions. From the profiles, at low backwater condition the upstream depth of water cannot affecting. But when this backwater depth is increasing, gradually the upstream water depth in affecting. The first type of flow is called free flow and second flow is called submerged flow. And the flow in between to free and submerged is called as transition submerged flow. And as per Skogerboe et.al [5] (1965), for 3 inch Parshall flume is 56%. The surface profiles which are drawn above, are functions of discharge, bed slope, backwater depth. And the relations between those parameters are discussed below.

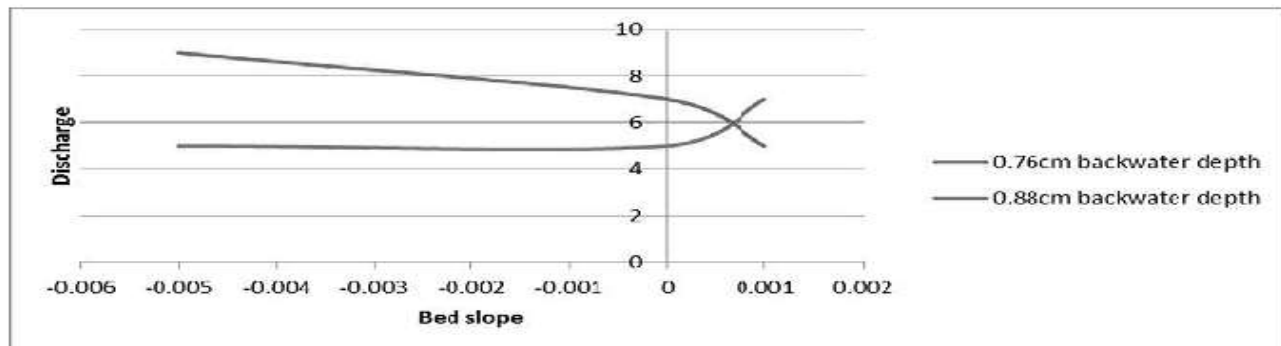


Fig. 3 Discharge variation with respect to channel bed position in Parshall Flume

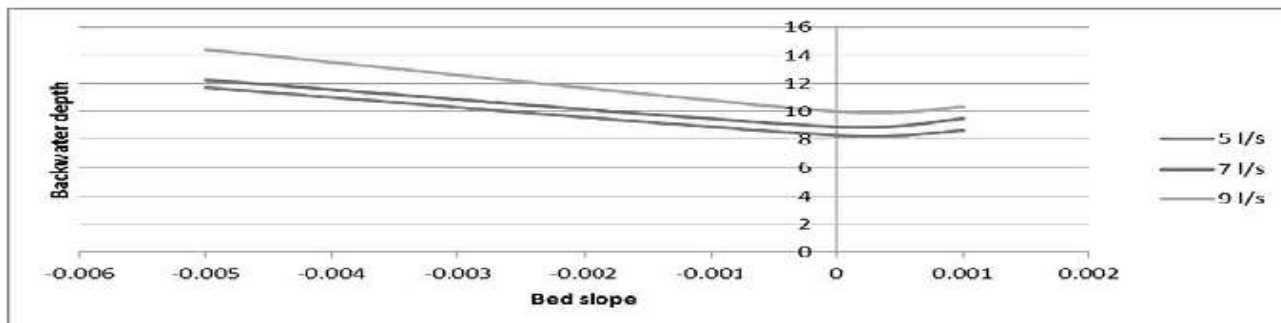


Fig. 4 Backwater variation with respect to Bed slope

From above given set of instructions one can easily find out the surface water profile using below graph

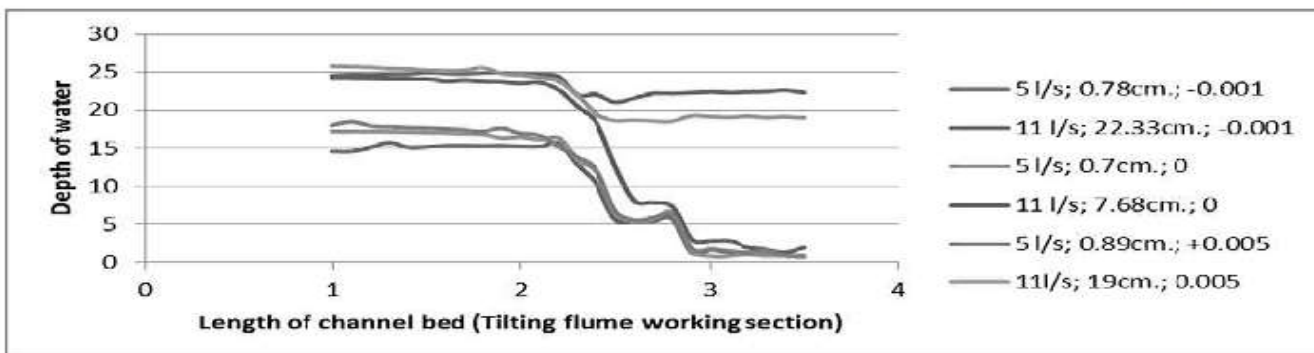


Fig. 5 Standard profiles Of Parshall Flume

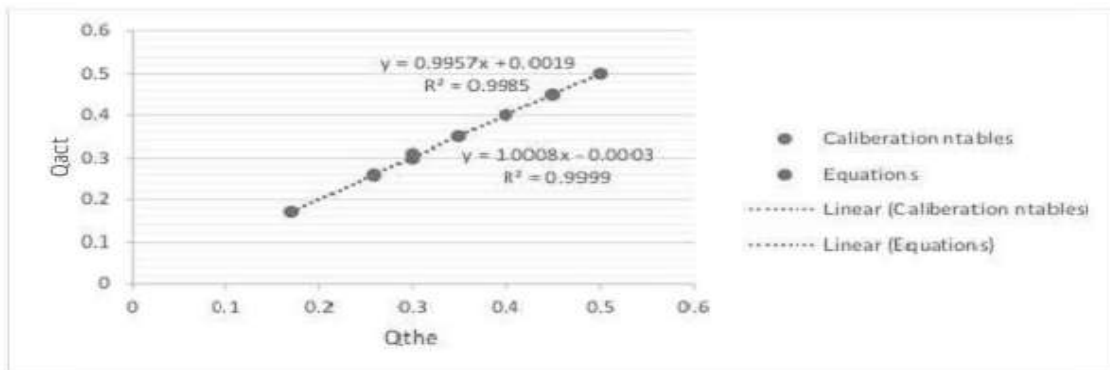


Fig. 6 Coefficient of discharge for Parshall flume

Actual discharge & theoretical discharge are drawn in graph. It clearly says that the slope of 1.1 it is greater than 1, and for Standard equations it is 0.7778, so coefficient of discharge is varying in between 0.7 to 1.

WSC Flume

From the measurements of flow rate and scale reading on the flume, create a Calibration Curve. Compare the scale reading with the upstream water depth at each flow rate. Determine the submergence ratio (depth at the throat y_1 to upstream depth y_0) at which the accuracy of measurement starts to become affected.

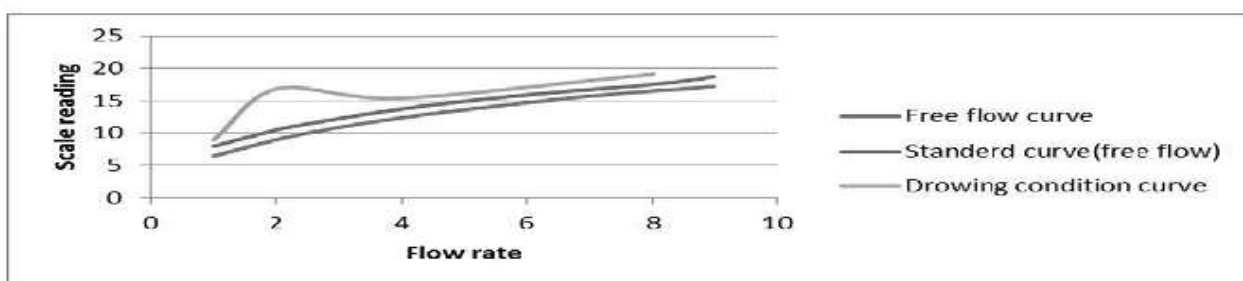


Fig. 7 Comparison of WSC flume Flow calibration curves

Comparing the scale reading with upstream wish at each flow rate there is a slight incrementing the scale reading on the flume. By the calculations of submergence ratio exceeded to the 0.8 there is a slight incrementing the scale reading in the flume. By the increment of scale reading downstream conditions restrict the free flow of water out of the flume due to the increment debris formation, small head losses will occur and flume capacity also decreases. These all conditions are occur at the low flow rate.

SUMMARY AND CONCLUSION

Flow characteristics of Flumes, the objectives of this work is studying the profiles of Venturi, Parshall flumes and discharge relation of Venturi, Parshall and WSC flumes. Studying the surface profiles of Venturi, Parshall flumes shows that, free flow and submerged flow can be identified based on the depth of backwater. i.e backwater depth is influencing the upstream depth of water. If upstream depth of water is not influenced by depth of backwater, it is called as free flow. And In submerged flow upstream depth of water is influenced by depth of backwater. The standard profiles drawn for different conditions like discharge(5l/s, 7l/s, 9l/s, 11l/s), and bed slope(-0.005, 0, 0.01) and backwater depths provides rough estimation of profile under above conditions and the type of flow. From the figures A.1 to

A.10 in APPENDIX-A it is clear that in zero bed slope condition the existence of submerged flow is not at all possible, where as in -0.005, +0.01 bed slope condition both free and submerged flows. The relationship between discharge, bed slope, backwater depth clearly shows that they are mutually dependent. If one parameter changes will affect the other two. Following table clearly shows these relationships.

Table 1 Flow Parameters variation of Parshall flume.

Bed slope	Discharge (Q)	Backwater depth
Initially decreasing and increasing	Increasing	Increasing
Initially constant and increasing	Increasing	Decreasing

Discharge relationships in Venturi, Parshall flume clearly says that the coefficient of discharge values gives to approximately 1, and in WSC flume, comparison of calibration curves in free and submerged flow with standard calibration chart, which was provided by Armfield S6-MKII manual (See APPENDIX-D) says that in submerged flow the curve, in the initial stage getting hump and reached to normal position afterwards, and for free flow it is symmetrical.

REFERENCES

1. Hyatt, M. Leon. 1965. Design, calibration, and evaluation of a trapezoidal measuring flume by model study. M. S. Thesis, Utah State University, Logan, Utah. March.
2. Jalam Singh, H.L.Tiwari, S.K.Mittal , "Flow Characteristic in Parshall Flume – A Review" International Journal of Scientific Engineering and Technology, Volume No.3 Issue No.3, pp : 231–234.
3. Jalam Singh, S.K.Mittal, and 3 H.L.Tiwari, "Parshall Flume Discharge Relation under Free Flow Condition "ISSN 2320-5407 International Journal of Advanced Research(2014), Volume 2, Issue 7,906-915.
4. Parshall, R. L. Measuring Water in Irrigation Channels. Farmers' Bulletin No. 1683, U. S. Dept. of Agriculture, October 1941.
5. Parshall, R. L. Measuring Water in Irrigation Channels With Parshall Flumes and Small Weirs. SCS Circular No. 843, U. S. Dept. of Agriculture. May, 1950.
6. RALPH L. PARSHELL, "THE IMPROVED VENTURI FLUME" Irrigation Engineer, The Colorado Agricultural College, Fort Collins, COLORADO.
7. Robinson, A. R. 1960. Parshall measuring flumes of small sizes, Technical Bulletin 61. Agricultural Experiment Station, Colorado State University, Fort Collins, Colorado. August. [8].Skogerboe, G. V., W. R. Walker, and L. R. Robinson. 1965. Design, operation, and calibration of the Canal "A" submerged rectangular measuring flume. Report PR- WG24-3, Utah Water Rese.arch Laboratory, Utah State University, Logan, Utah.
8. Skogerboe, Gaylord V., Hyatt, M. Leon, England, Joe D., and Johnson, J. Raymond, (1965) "Submerged Parshall Flumes of Small Size", Reports. Paper 79. Utah Water Research Laboratory, Logan, Utah.
9. Skogerboe, Gaylord V., Hyatt, M. Leon, England, Joe D., and Johnson, J. Raymond, (1966) "Measuring Water with Parshall Flumes", Reports. Paper 83. Utah Water Research Laboratory, Logan, Utah.
10. Stock, Eldon M., "Measurement of Irrigation Water" (1955). Reports. Paper 66. Utah Water Research Laboratory, Logan, Utah.
11. V. M. CONE, "THE VENTURI FLUME" Irrigation Engineer, Office of Public Roads and Rural Engineering, United States, Department of Agriculture.
12. Villemonte, J. R. and V. N. Gunaji., "Equation for Submerged Sharp-crested Weirs Found Applicable to 6-inch Parshall Flume." Civil Engineering. June, 1953.



ISSN: 2350-0328

International Journal of Advanced Research in Science, Engineering and Technology

Vol. 5, Issue 12, December 2018

Flow Characteristics of Sharp Crested Weirs

Bhukya Ramakrishna, Shaik Vaheed , P.S.V.Adilakshmi

Assistant Professor, Department of Civil Engineering, RGUKT Basar, Telangana, India,

Assistant Professor, Department of Civil Engineering, RGUKT Basar, Telangana, India,

U.G. student, Department of Civil Engineering, RGUKT Basar, Telangana, India

ABSTRACT - Weirs are commonly used devices in flow measurements. Sharp crested weirs are widely used as discharge measuring device in laboratories, industries and irrigation channels. The main objective of these study is to investigate the flow behaviour of different sharp crested weirs and to obtain the discharge coefficient for different bed slope conditions (Horizontal, and 1in 400,1in 200). Measurement of head over the weir crest is the important aspect in discharge analysis through sharp crested weirs. Width of the weir opening affect the coefficient of discharge and thereby the discharge also. Results of this study shows that the average values of coefficient of discharge for different thin plate weirs (i.e Rectangular weir, V-notch weir, Trapezoidal weir, Sutro weir) 0.697, 0.798, 0.578, 0.598 respectively.

KEYWORDS - Sharp crested weirs, Coefficient of discharge, Head over weir, Weir height.

I. INTRODUCTION

In India open channels in irrigation utilities are used for transportation of water for irrigation purpose. Water supplied to the fields by using open channel, implies that discharge measurement becomes necessary, as the Measurement of discharge in open channels plays a vital role in the equal distribution of water among the users in field and accordingly charging correct amount from them by metering the flow. The measurement of flow in open channels is generally made by means of weirs or sluice gates.

Weir is a standard device for the measurement of flow in open channel. It is an obstruction in the path of flow that causes the liquid to rise behind the weir and then flows over it. By measuring the head of water over the weir the quantity of discharge can be estimated by using well established head-discharge relationship. If the jet of liquid passing over the weir springs free as it leaves the upstream face, the weir is known as sharp crested weir, while broad crested weirs are those which support the falling nappe over its crest, in the longitudinal direction and critical depth occurs over the weir. On the basis of shapes the weirs can be classified as the rectangular, triangular, trapezoidal, parabolic, etc. Sharp crested rectangular weir, V-notch and broad crested weir are most common.

Brief summary of significant experimental investigations: **S.A.Tekade et al.**†(2014) The complete work was carried out in the Water Resources Engineering Laboratory of the Civil Engineering Department at Visvesvaraya National Institute of Technology, Nagpur, India. A rectangular flume 4.2 m long and 1.2 m in width, non tilting type was used in the experiment. Based on the observations carried on discharge measurement by rectangular SCW he concluded that Head-Discharge relationship for SCW is found to be a exponential series. And It can be concluded that as the b/B ratio increases, the head over the notch decreases for the same discharge value.also found thatThe crest height has negligible effect on the discharge characteristics of SCW. **HadiArvanaghi et al.** (2013) According their studies on Rectangular sharp-crested weir is one of the flow measuring tools which are usually used in irrigation and drainage channels. The most essential parameter of discharge equation of this type of weirs is the discharge coefficient. In this study discharge coefficient of the rectangular sharp-crested weir is investigated experimentally and numerically. The results show that the Cd has the fixed value of 0.7 when the following condition is maintained: $H/W > 0.6$, $Fr > 0.2$, $Re > 20000$ Beyond these boundaries, Cd is not constant and it is not recommended to use a unique Cd for different flow conditions. Furthermore in this study the water surface profile. **Rahul Pandey et.al** (2016)studies of Flow Characteristics of Sharp Crested Rectangular Weir and he investigated the flow behaviour of the weirs and obtained the discharge coefficient. So, Now in our study we are going to establish following results to determine coefficient of discharge, and develop

head-discharge relationship for sharp crested weirs (Rectangular, triangular, Trapezoidal, and sutro weir) with varied slopes of channel.

II. EXPERIMENTAL SETUP AND LABORATORY ACCESSORIES

The complete work was carried out in the Water Resources Engineering Laboratory of the Civil Engineering Department at Rajiv Gandhi University Knowledge &Technology, Basar, India. A rectangular flume 5 m long and 30cm in width, 45cm height tilting flume was used in the experiment. It consist of sloping set up ranging from negative 1 in 200 to positive 1 in 200. This entire set up is connected with sensors and the values are recorded through arm field software. The experimental setup is a self contained one having circulating arrangement for the water. A 3 HP pump makes the circulating mechanism work efficiently in the flume. The flume is installed with perplex glass sheets as side walls which make the viewing of the experimental run easy. At the entrance into the channel, flow is regulated by converging vertical plates to prevent vortex motion and thus to control the damp fluctuations at the entry of flume. The water after the weir was then collected into a measuring tank with dimension 4m×3m. A vernier type gauge with accuracy 1mm was used for measuring the bed elevation and water surface elevation. Calibration was done before every run of the experiment to prevent instrumental errors. The depth rod was adjusted accurately to the surface of water to get the value of 'H'. While measuring H it was ensured that the flow in the channel was stable and constant. Discharge is maintained for individual run. Fig 2.1 shows the glass sided tilting flume.



Fig 2.1-Tilting flume channel

In our Study we are going to perform on sharp crested weirs i.e rectangular, triangular, trapezoidal, sutro weir. Following eq. 2.1, 2.2 and 2.3 are required to measure the discharge for

Rectangular sharp crested weir:-

$$Q = \frac{2}{3} C_d b \sqrt{2g} y_c^{3/2} \quad \dots \dots \dots \text{eq. 2.1}$$

Triangular sharp crested weir:-

$$Q = \frac{C}{d} \frac{8}{15} \sqrt{2g} \tan\left(\frac{\theta}{2}\right) \frac{y^{5/2}}{c} \dots \text{eq.2.2}$$

Trapezoidal sharp crested weir:-

$$Q = \frac{2}{3} \cdot \frac{C}{d} \cdot b \sqrt{2g} \cdot y_c^{3/2} + \frac{C}{d} \cdot \frac{8}{15} \sqrt{2g} \tan\left(\frac{\theta}{2}\right) y_c^{5/2} \dots \text{eq.2.3}$$

Sutro weir:-

$$Q = C_0 \left(Y_{\text{datum}} + \frac{2}{3} a \right) \dots \dots \dots \text{eq.2.4}$$

$$C_0 = 2 b C_d (2 g)^{0.5} a^{0.5} \dots \dots \dots \text{eq.2.5}$$

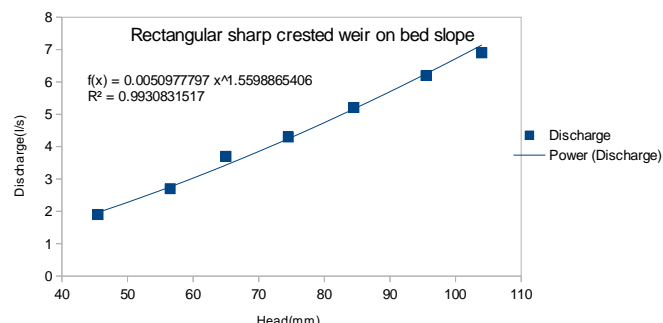
Where C_0 =The proportionality constant, $a=0.030(\text{m})$, $b=0.050(\text{m})$, Y_{datum} = Depth above datum, y_{base} =Depth above base of rectangular weir(m) , y_{origin} =Depth above origin of upper part of weir(m) C_d = Coefficient of discharge, Q = rate of discharge in Litre/sec , B = width of channel in cm g = gravitational acceleration in cm/s^2 , H = head over the weir/spillway

III. RESULTS AND DISCUSSION

Experiment has been done in a laboratory flume with glass made walls. The flume length, width and height are 5, 0.35 and 0.45 m, respectively. Water enters the flume through a stilling system. Then flow passes over the weir and finally flow discharges to the settling basin of the flume. There is a weirs downstream the settling basin which is calibrated to measure the flow rate. Water surface elevation in the flume is measured by a needle type level meter which accuracy is about 0.1 mm For different flow rates and different bed slope conditions (i.e horizontal, 1 in 400). The obtained values were tabulated in following tables.(3.1),(3.2) and discharge-head, Discharge-coefficient of discharge curve for rectangular Sharp crested weir are shown in fig. (3.1),(3.2),(3.3) and (3.4).

Table3.1: Discharge, head, coefficient of discharge of Rectangular Sharp Crested Weir with slope of Horizontal.

Up stream depth (mm)	Head with crest height (mm)	Head over weir (mm)	Flow rate (l/s)	Coefficient of discharge (cd)
130	120.5	45.5	1.9	0.663
140	131.5	56.5	2.7	0.681
150	140	65	3.7	0.695
160	149.5	74.5	4.3	0.716
170	159.5	84.5	5.21	0.716
180	170.5	95.5	6.2	0.714
190	179	104	6.9	0.697


Fig 3.1-Discharge-Head curve Rectangular Sharp crested weir

International Journal of Advanced Research in Science, Engineering and Technology

Vol. 5, Issue 12, December 2018

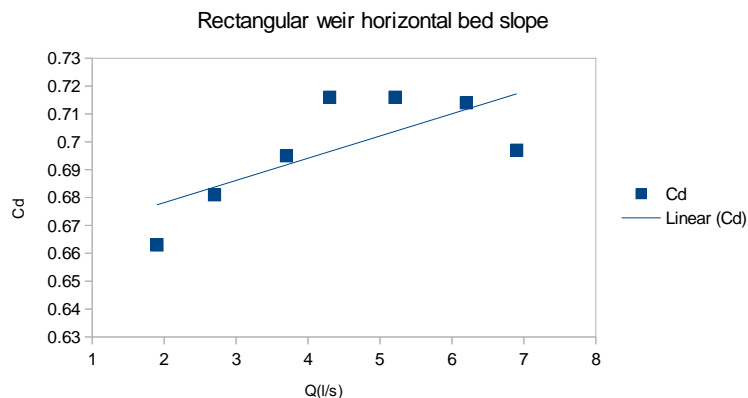


Fig 3.2-Discharge-coefficient of discharge curve for Rectangular weir

Table 3.2:Discharge, head, coefficient of discharge of Rectangular Sharp Crested Weir with slope of 1 in 400

Up stream depth (mm)	Head with crest height (mm)	Head over weir (mm)	Flow rate (l/s)	Coefficient of discharge (cd)
130	124	49	2.5	0.705
140	135	60	3.2	0.71
150	145	70	3.9	0.72
160	150.3	75.3	4.4	0.723
170	163.8	88.8	5.5	0.71
180	175	100	6.4	0.686
190	181.9	106.9	7	0.718

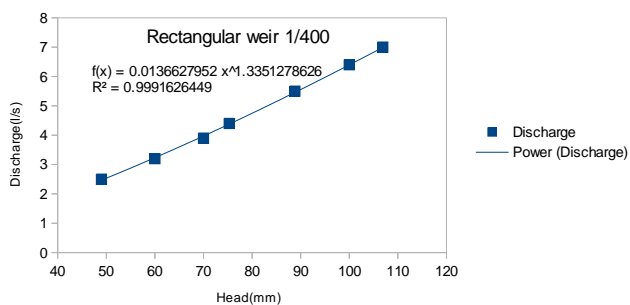


Fig 3.3-Discharge-Head curve for Rectangular weir

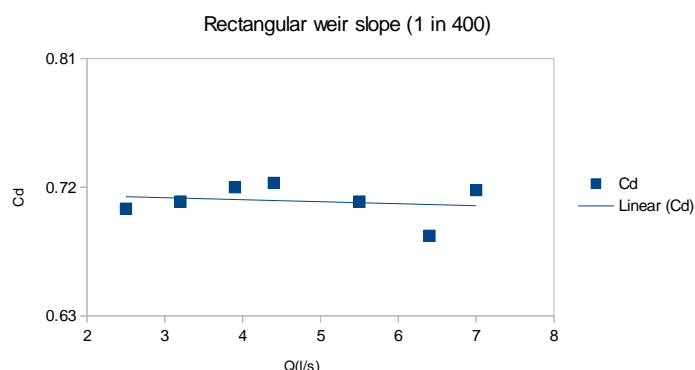


Fig 3.4: Discharge-coefficient of discharge of a rectangular sharp crested weirs

Till now we have conducted for rectangular weir with different bed slope conditions, in the same manner we have performed for the triangular, trapezoidal, sutro weirs. In our experimental study, we have calculated coefficient of discharge for different bed slope conditions i.e horizontal and 1 in 400.and we have observed that the coefficient discharge is got almost same for these bed slope conditions for a particular a sharp crested weirs.

VI: CONCLUSION

Sharp crested weirs is one of the flow measuring tools which are usually used in irrigation and drainage channels. The most essential parameter of discharge equation of this type of weirs is the discharge coefficient. In our study we got average cd values for rectangular, triangular, trapezoidal and sutro weir is 0.697,0.798,0.578,0.598 respectively. Why cd value is more to triangular weir because small contact area so that low frictional stress, low wall surface stress,low drag forces and low surface tension are exist. For other weirs contact area is more so that Cd value is less compare with triangular weir. From the obtained results we concluded that in the practical applications

- For low discharge with high accuracy we can use triangular sharp crested weir to measure the flow.
- For high discharge with considerable accuracy we can use rectangular sharp crested weir to measure the flow.
- For high discharge and less accuracy we can use trapezoidal and sutro sharp crested weirs to measure the flow

REFERENCES

1. Asawa G.L. (2000). " Irrigation Engineering" New Age International (P) limited, publishers. Second Edition.
2. Aydin I., Sakarya A.b., Ger A.M. (2002). "measurement of small discharges in open channels by slit weir", Journal of hydraulics Engineering, ASCE; Vol.128(2): 234-237.
3. Bagheri S., Heidarpour M., (2011). "Characteristics of flow over rectangular sharp crested side weirs", Journal of irrigation and Drainage Engineering, ASCE; Vol.138(6):541-547.
4. Chow V.T.(2002). "Open Channel Hydraulics" Tata McGraw-Hill publication.
5. HadiArvanaghi, NavidNasehiOskue, (2013)." Sharp-Crested Weir Discharge Coefficient ",Journal of Civil Eng. Urban,3(3):87-91
6. Rahul Pandey, Dr.S.K.Mittal and Prof. M.K.Choudhary(2016). "Flow Characteristics of Sharp Crested Rectangular Weir",International Journal of Innovative Science, Engineering&Technology,Vol.3 Issue 3, March 2016.
7. Tekade.S.AandA.D.Vasudeo (2015)."Head Discharge Relationship of Thin Plated Rectangular Sharp Crested Weirs "JAFM, Vol. 9, No. 3, pp. 1231-1235, 2016.
8. RangaRaju, K. G. (2013)." Flow through open channels", Tata McGraw-Hill publications New Delhi Second Edition.
9. Subramanya, k. (2011). "Flow in Open Channels", Tata McGraw-Hill Publication, Third Edition.
10. Vatankhah, A. R. (2010). "Flow measurement using circular sharp-crested weirs", Flow measurement and Instrumentation. Vol. 21(2), 118-122.



Assessment of Aquifer Vulnerability of Nizamabad District, Telangana State, India Using GIS and Drastic Method

B. Ramakrishna^{1(✉)}, P. Rajasekhar², and Shaik Vaheed¹

¹ Civil Engineering Department, RGUKT-Basar, Hyderabad, Telangana, India
bhukyaramakrishna@gmail.com, vaheed.civil@gmail.com

² Civil Engineering Department, Osmania University,
Hyderabad, Telangana, India
prscivilou@gmail.com

Abstract. The precipitation falling on the surface earth, either it runoff over land to the stream or some part of it infiltrates into the ground. The part which moves into the ground either get transplanted by the plants and goes back to the atmosphere or some part of it percolated deep down and contributes water already inside the earth. The water which is existing below the ground surface is commonly called as ground water or subsurface water. Countries like India, most of the people use groundwater for drinking purpose. Due to increase of waste on earth surface which can effect groundwater quality. It can leads to contamination of groundwater. The present study is conducted to assess the groundwater vulnerability and prepare vulnerability map for Nizamabad district, Telangana state using DRASTIC model in ARC GIS 10.4.1 groundwater vulnerability map can be obtained by overlaying seven layers. Such as Depth of water level, Net Recharge, Aquifer Media, Soil Permeability, Topography, Impact of Vadose Zone and Hydraulic conductivity.

Keywords: DRASTIC · GIS · Vulnerability · Groundwater · Hydro geological parameters · Weighted overlay analysis

1 Introduction

Earth is very special because it has much amount of water, the total earth surface covers 71% water. In this 96.5% is salt water that is found in the ocean only just 3.5% of water on the earth is freshwater. In most of this freshwater 68% is glaciers and icecaps. One third is in groundwater and remaining 2% of water is in River, Lakes, Streams and very small amount in atmosphere. From last few decades population is increasing drastically. Due to human activities such as construction of buildings, Industries, Deforestation, Urbanization ground water level is reducing and it is contaminated. The main aim of the study is to evaluate the groundwater vulnerability and prepare vulnerability map. Determine area where groundwater is contaminated. For that area proper management and protection techniques has to follow. This maps are very informative for educating the public. Groundwater vulnerability maps are prepared using standard method. Research and scientist they did lot of work on this and find out so many

variety of method for aquifer vulnerability assessment. Aller et al. (1987) proposed DRASTIC method which is explained in this methodology. According to Al-Zabet et al. (2002) Evaluation of aquifer vulnerability of contamination potential using the DRASTIC method. Muhammad et al. (2014) describes that “Groundwater vulnerability assessment shows an extreme sensitivity to in situ anthropogenic pollutants. A dichotomous assessment of geological and hydrological characteristics makes it possible to determine the vulnerability of groundwater. You-Jailin et al. (2005) describes that “The groundwater pollution in many regions is becoming more and more serious because of over-exploiting and industrial activities”. Lathamani et al. (2015) describes that this investigation was carried out to determine the aquifer vulnerability using DRASTIC method which correlated well with then physicochemical characteristics of groundwater in mysore city. This model was primarily developed by National Water Well Association and U.S. Environmental Protection Agency for different hydrogeologic settings. Henceforth, the model has been modified according to geological or hydro-geological setting such as pesticide DRASTIC, modified DRASTIC, modified pesticide DRASTIC, DRASTIC-LU, DRASTIC-Fm and DRASTIC-AHP by different researchers. DRASTIC model employs hydro-geological data in a Geographical Information System (GIS) environment to compute aquifer vulnerability index. DRASTIC is a shortening of seven physical parameters of hydro-geological which used to define groundwater system and its susceptibility towards pollution. It considers seven parameters, which taken together, provide the acronym such as Depth to groundwater (D), Recharge (R), Aquifer type (A), Soil type (S), Topography (T), Impact of the vadose zone (I), Hydraulic conductivity.

1.1 Study Area

Nizamabad district located in the north - western region in India. The study area is 4288 km² with an average elevation of 395 m above mean sea level. The average annual rainfall in the study area varying from 660 and 1340 mm. Annual average rainfall is 970 mm, the average temperature varying from 24 °C to 40 °C. Location map of nizamabad district is shown in Fig. 1.

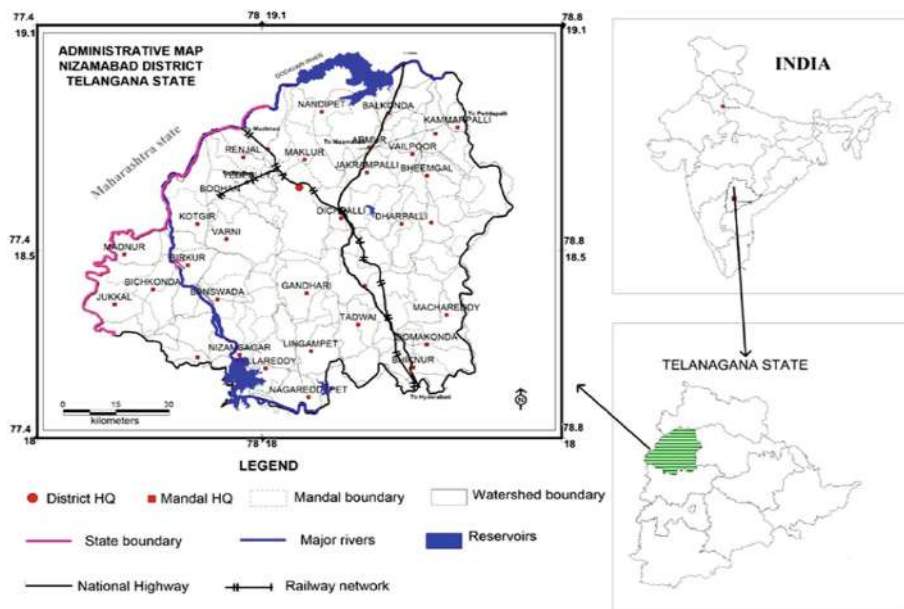


Fig. 1. Location map of nizamabad district

2 Methodology

The present study is to investigate the aquifer vulnerability assessment, DRASTIC model is adopted. DRASTIC means D for Depth to water table, R for Net Recharge, A for Aquifer media, S for Soil media, T for Topography, I for Impact of Vadose zone and finally C for Hydraulic Conductivity, This 7 parameters are overlayed in Geographical Information System and divided into number of units based on rate and weight of each hydrological unit as for Aller et al. (1987). DRASTIC index map is created and this map is reclassified using DRASTIC vulnerability index as shown in Eq. 1.

$$VI = DrDw + RrRw + ArAw + SrSw + TrTw + IrIw + CrCw. \quad (1)$$

In the above Eq. 1, w represents weight, r represents rate. The vulnerability index is weighted sum of rate of all the evaluation factors given by Aller et al. 1987 is shown Table 1 and schematic representation of methodology used in DRASTIC model is shown in Fig. 2.

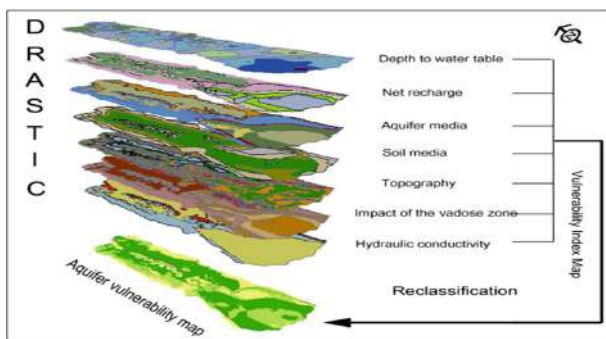
Table 1. DRASTIC parameters ratings and classes (Aller et al. 1987)

Layer	Range	Rating	Typical rating	Weight
Depth to water (m)	0–1.5	10		5
	1.5–4.5	9		
	4.5–9	7		
	9–15	5		
	15–22.5	3		
	22.5–30	2		
	30<	1		
Recharge (mm/y)	254<	9		4
	178–254	8		
	102–178	6		
	51–102	3		
	0–51	1		
Aquifer media	Karst Limestone	9–10	10	3
	Basalt	2–10	9	
	Sand and Gravel	4–9	8	
	Massive Limestone	4–9	6	
	Massive Sandstone	4–9	6	
	Bedded Sandstone, Limestone and Shale Sequences	5–9	6	
	Glacial Till	4–6	5	
	Weathered Metamorphic/Igneous	3–5	4	
	Metamorphic/Igneous	2–5	3	
	Massive Shale	1–3	2	
Soil media	Thin or Absent	10		2
	Gravel	10		
	Sand	9		
	Peat	8		
	Shrinking and/or Aggregate Clay	7		
	Sandy loam	6		
	Loam	5		
	Silty Loam	4		
	Clay Loam	3		
	Muck	2		
	Non shrinking and Non aggregated clay	1		
Topography (%)	0–2	10		5
	2–6	9		
	6–12	5		
	12–18	3		
	18<	1		

(continued)

Table 1. (continued)

Layer	Range	Rating	Typical rating	Weight
Impact of the vadose media	Karst Limestone	8–10	10	5
	Basalt	2–10	9	
	Sand and Gravel	6–9	8	
	Metamorphic/Igneous	2–8	4	
	Sand and Gravel with significant Silt	4–8	6	
	Bedded Sandstone, Limestone and Shale	4–8	6	
	Sandstone	4–8	6	
	Limestone	2–7	6	
	Shale	2–5	3	
	Silt/Clay	2–6	3	
Hydraulic conductivity (m/d)	Confining Layer	1	1	3
	82<	10		
	41–82	8		
	29–41	6		
	12–29	4		
	4–12	2		
	0–4	1		

**Fig. 2.** Schematic representation of methodology

3 Results and Discussion

Depth of water table data is obtained from Central Groundwater Board, Hyderabad. Aquifer media, impact of the vadose zone, hydraulic conductivity data can be taken from National Geographical Research Institute (NGRI), soil media data from the Agricultural Department of Nizamabad, Topography map created the data extracted from Bhuvan Portal and from rainfall data can be taken from Indian Meteorological Department. The collected data was converted in to digital format and inserted into Geographical Information System (GIS) using appropriate latitude and longitude. Based on Aller et al. (1987) Inverse Distance Weighted (IDW) were created by adopting the hundred meter grid interval and value are assigned. Depth to water level, Net Recharge, Aquifer Media, Soil Permeability, Topography Impact of Vadose Zone and Hydraulic Conductivity Index map shown in Figs. 3, 4, 5, 6, 7, 8 and 9 respectively.

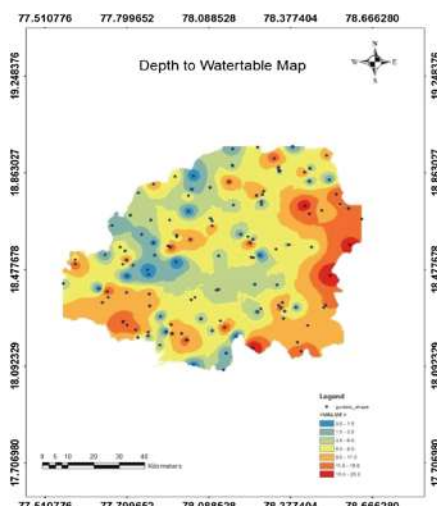


Fig. 3. Depth to watertable

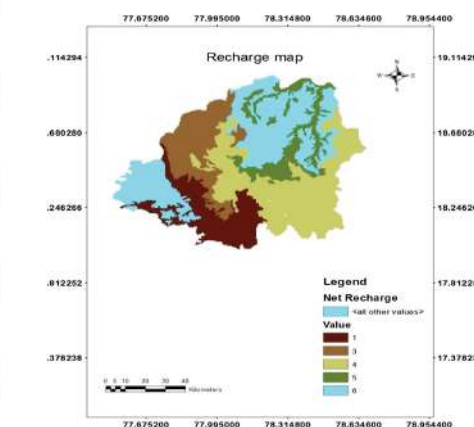


Fig. 4. Net recharge index

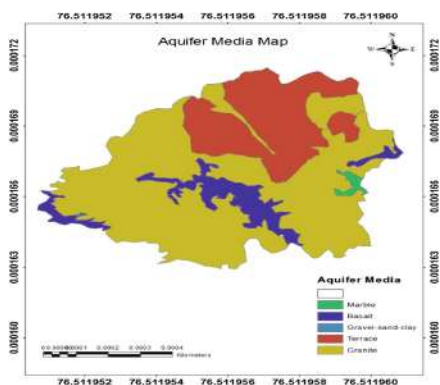


Fig. 5. Aquifer media

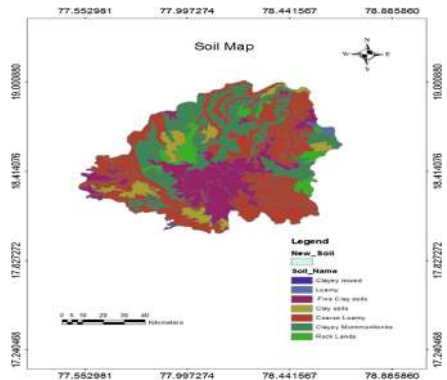


Fig. 6. Soil media

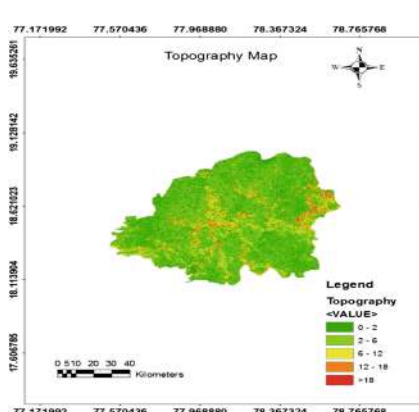


Fig. 7. Topography

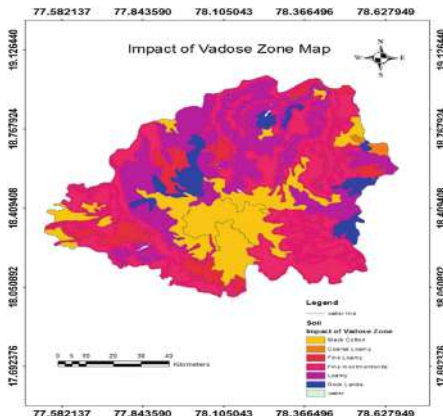


Fig. 8. Vadose zone

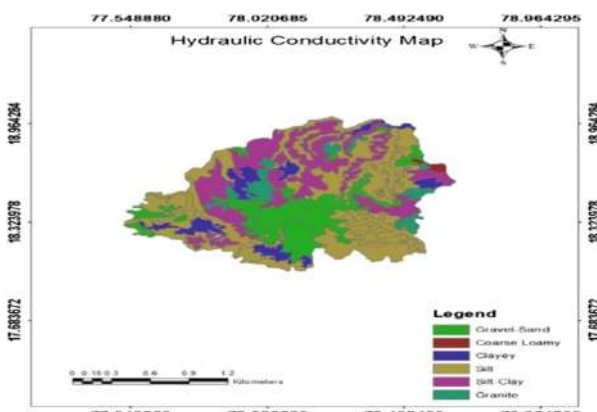


Fig. 9. Hydraulic conductivity

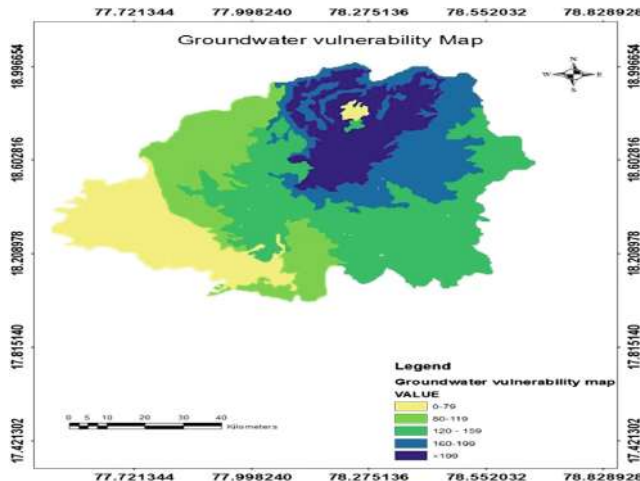


Fig. 10. Vulnerability map

4 Conclusion and Recommendations

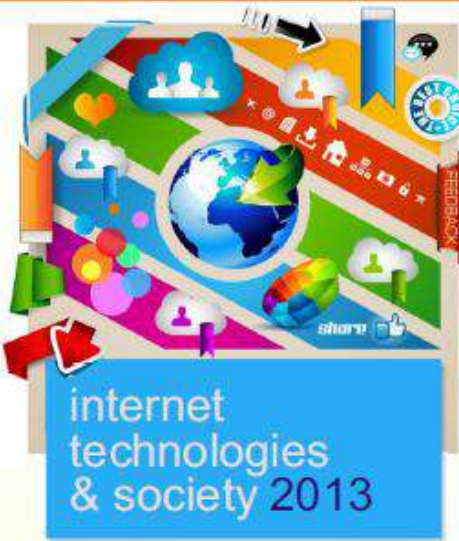
Using ARC GIS 10.4, aquifer assessment vulnerability map was prepared for this study by overlapping 7 parameters. Study area was classified in to five vulnerability zones such as <80 as very low vulnerability, 80–119 as low vulnerability, 120–159 as moderate, 160–199 as high vulnerability and >199 as very high vulnerability. This study revealed that the Nizamabad city is in the medium DRASTIC Index vulnerability zone with the value of 159. The recommendation vulnerability zones of Nizamabad City are obtained according to the indication of Index as shown in Fig. 10. For this area proper management and protection techniques has to be needed.

References

- Aller L, Bennet T, Lehr JH, Petty RJ, Hackett G (1987) DRASTIC: A Standardized System for Evaluating Ground Water Pollution Potential Using Hydrogeologic Settings. US EPA Report 600/287/035, U.S. Environmental Protection Agency
- Al-Zabet T (2002) Evaluation of aquifer vulnerability of contamination potential using the DRASTIC method. Environ Geol 43:203–208
- Babiker IS, Mohamed MA, Hiyama T, Kato K (2005) A GIS-based DRASTIC model for assessing aquifer vulnerability in Kakamigahara Heights, Gifu Prefecture, central Japan. Sci Total Environ 345(1):127–140
- Burow KR, Nolan BT, Rupert MG, Dubrovsky NM (2010) Nitrate in groundwater of the United States, 1991–2003. Environ Sci Technol 44(13):4988–4997
- Erxleben J, Elder K, Davis R (2002) Comparison of spatial interpolation methods for estimating snow distribution in the Colorado Rocky Mountains. Hydrol Process 16(18):3627–3649
- Mehrjardi RT, Jahromi MZ, Mahmoodis Heidari A (2008) Spatial distribution of groundwater quality with geostatistics (case study: Yazd-Ardakan plain). World Appl Sci J 4(1):9–17

- Oliver MA, Webster R (1990) Kriging: a method of interpolation for geographical information systems. *Int J Geograph Inf Syst* 4(3):313–332
- Ramakrishnaiah CR, Sadashivaiah C, Ranganna G (2009) Assessment of water quality index for the groundwater in Tumkur Taluk, Karnataka State, India. *J Chem* 6(2):523–530
- Jamrah A, Al-Futaisi A, Rajmohan N, Al-Yaroubi S (2007) Assessment of groundwater vulnerability in the coastal region of Oman using DRASTIC index method in GIS environment. *Environ Monit Assess* 147(1–3):125–138. <https://doi.org/10.1007/s10661-007-0104-6>
- Javadi S, Kavehkar N, Mousavizadeh MH, Mohammadi K (2010) Modification of DRASTIC model to map groundwater vulnerability to pollution using nitrate measurements in agricultural areas. *J Agric Sci Technol* 13:239–249

INTERNATIONAL CONFERENCE



Kuala Lumpur . Malaysia

29 November to 1 December

PROCEEDINGS

EDITED BY

Piet Kommers, Tomayess Issa,
Nurfadhlina Mohd Sharef and Pedro Isaias



iadis

international association
for development
of the information society

**INTERNATIONAL CONFERENCE
on
INTERNET TECHNOLOGIES
& SOCIETY
(ITS 2013)**

**PROCEEDINGS OF THE
INTERNATIONAL CONFERENCE
on
INTERNET TECHNOLOGIES
& SOCIETY
(ITS 2013)**

KUALA LUMPUR, MALAYSIA

29 NOVEMBER - 1 DECEMBER, 2013

Organised by

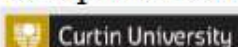


international association for development of the information society

Co-Organised by



Co-Sponsored by



Sponsored by
Curtin Business School

TABLE OF CONTENTS

FOREWORD	ix
PROGRAM COMMITTEE	xiii
KEYNOTE LECTURES	xvii

KEYNOTE PAPER

LEARNING IN THE NETWORKED SOCIETY <i>Piet Kommers</i>	3
--	---

FULL PAPERS

AN APPROACH FOR DEVELOPING ONTOLOGIES USING CONCEPT MAPPING TECHNIQUE COUPLED WITH A TERM EXTRACTION PROCESS <i>Rizwan Iqbal, Masrah Azrifah Azmi Murad, Aida Mustapha and Nurfadhlina Mohd. Sharef</i>	7
A STUDY OF AUSTRALIAN INTERNET SERVICE PROVIDER INDUSTRY STAKEHOLDER COLLABORATION: IMPLICATIONS FOR FUNCTIONAL SERVICE QUALITY PRACTICES <i>Karthik Vilapakkam Nagarajan</i>	15
SOME THINGS I TEND TO OVERLAP EVEN IF NOT NECESSARY. A DISCUSSION ON PIM ARTIFACTS BETWEEN RESEARCHER AND RESEARCH AGENT <i>Monica Pinheiro, Margarida Cardoso, Joaquina Barrulas and Joao Alvaro Carvalho</i>	25
A DISTRIBUTED PRIVACY-PRESERVING MODEL FOR E-SERVICES <i>Wiem Hammami and Lamjed Ben Said</i>	33
HOW PEOPLE DISCLOSE IN FACEBOOK? DIFFERENCES BETWEEN POLISH AND INDONESIAN ON ONLINE DISCLOSURE BEHAVIOUR, NEED FOR POPULARITY, NEED TO BELONG AND SELF-ESTEEM <i>Rahkman Ardi and Dominika Maizon</i>	41

POSTERS

INTELLIGENT E-LEARNING FOR HAZARD PERCEPTION IN EMERGENCY DRIVING	125
<i>Sébastien Tremblay, Simon Banbury, Jean-François Gagnon, Éric Poirier and Christian Hébert</i>	
A FRAMEWORK FOR MINING BEHAVIORS OF PATIENTS BASED ON LENGTH OF STAY IN THE EMERGENCY DEPARTMENT	128
<i>I-Chin Wu, Tzu-Li Chen, Chung-Lun Yang, Ren-Shian Yang and Yen-Yi Feng</i>	
FACE RECOGNITION: A ROBUST APPROACH	131
<i>Supreethi K.P, B Venkat Raman and Swathi Sowmya Bavirthi</i>	

AUTHOR INDEX

FACE RECOGNITION: A ROBUST APPROACH

Supreethi K.P¹, B Venkat Raman² and Swathi Sowmya Bavirthi²

¹Assistant Professor

²Student (M.Tech CS IV Sem)

Department of Computer Science Engineering, College of Engineering, Jawaharlal Nehru Technological University, Hyderabad, Andhra Pradesh, India

ABSTRACT

Face recognition system has drawn attention due to the vast applicability in human-computer interaction and security systems. It has been a significant research area since a few decades. The process aims in giving the identity of a human face for a given image. This can be further applied to identify human faces in video streams also. Designing a face recognition system involves knowledge in the fields of computer vision, pattern recognition, image processing, neuroscience, psychology and machine intelligence. However, faces with different illumination, expression, RST (Rotation, Scale, and Translation) invariance, and pose may be challenging factors for the system. Such factors may also be referred to as uncontrolled environments. The primary design issues for such a system include the execution speed, the size, type of training dataset and reliability of the system under uncontrolled environment. Several algorithms have been implemented for different features of face viz., nose, face, eyes which will work together for recognizing the image.

KEYWORDS

Face detection, face identification, verification, test image, training data set

1. INTRODUCTION

A face recognition system is an application that identifies a person based on the image that has a human face. It takes the image as input either by capturing with a camera or by explicitly taking it as an input file. Face recognition system is being applicable to various systems like human-computer interaction, security systems for authentication of visitors and employees in a company, customs-immigrations, voting systems and law enforcement. Governments of various countries are using face recognition systems as a tool to identify child kidnappers, thieves and other criminals.

A typical face recognition system has five phases [5], they are as follows:

1. Capturing input image,
2. Detecting human face and cropping it,
3. Dimensionality reduction of the cropped face
4. Identifying the face and
5. Verifying the identity of the face.

The paper is organized as follows: a review of different algorithms and techniques used to implement face recognition available in the literature are presented in section 2. Proposed Face recognition technique is presented in section 3, implementation of proposed method is discussed section 3.2 and concluding remarks are given in section 4.

2. RELATED WORK

Various algorithms for face detection, identification and verification have been proposed [5]. In this section, a brief notion of the algorithms in general is presented here under.

International Journal of Recent Technology and Engineering

ISSN : 2277 - 3878

Website: www.ijrte.org

Volume-8 Issue-2S11, SEPTEMBER 2019

Published by:

Blue Eyes Intelligence Engineering and Sciences Publication



	<p>11. Jianzhong Wu, Y. et.al, "Comparison of the development of Smart Grids in China and the United Kingdom", IEEE PES Innovative Smart Grid Technologies Conference Europe (ISGT Europe)-2010.</p> <p>12. KRS Kashyap, B.Dheeraj Reddy, "Ancillary services and stability analysis of distributed generation systems", International Journal of Engineering research and applications, volume 3, Issue 3-May-June-2013.</p> <p>13. Online course at https://nptel.ac.in/syllabus/108101005 on Restructured Power systems (Web), NPTEL.</p> <p>14. Steven Stoft, "Power System Economics: Designing Markets for Electricity", Wiley-IEEE Press-2002.</p> <p>15. https://en.wikipedia.org/wiki/Internet_of_things, accessed on 10 July 2019.</p> <p>16. https://electricenergyonline.com/energy/magazine/1036/article/What-is-between-Grid-of-Things-GoT-and-Internet-of-Things-IoT-is-HoT-Holistically-Orchestrated-Things-.htm, accessed on 12 July 2019.</p> <p>17. Dimitrios Sikeridis, Eirini Eleni Tsipoulopou, Michael Devetsikiotis, Symeon Papavassiliou, "Energy efficient orchestration in wireless powered internet of things infrastructure", IEEE Transactions on Green Communications and Networking, Volume: 3 , Issue: 2 , June 2019.</p> <p>18. Anthony, Rik irons-mclean, Mmarceloyannuzzi, "Orchestrating and automating security for the internet of things", Cisco Press-2018.</p> <p>19. B. Koti Reddy, "Retrofit of MOCB with VCB", International Journal of Research in Engineering, Science and Management, Volume 2, Issue 6-June-2019.</p> <p>20. Dr. M.Khedkar, Dr. G.M.Bhole, "A text book of electric power distribution automation", University Science Press, Laxmi publications-2010.</p>	
	<p>Authors: B Venkat Raman, Nagaratna P Hegde, Nenavath Venkatesh Naik, Allu Siva Kishore Reddy</p> <p>Paper Title: A Deep Learning for the Generation of Textual Story Corresponding to a Sequence of Images</p>	
278.	<p>Abstract: Generating a short story for a sequence of images is much more interesting than generating a single line textual description for an image. Story generation involves relating the meaning of the previous image and the current image and continuing this throughout the sequence of images. This can be helpful for better understanding of the situation. In this paper we present our idea of generating story using a CNN model which is pre-trained on MSCOCO dataset that can detect objects and concepts of language modelling and NLP text pre-processing techniques. We used a custom stories dataset in which we manually labelled every sentence in every story. Number of sentences in the generated story is equal to the number of images. The results are quite accurate in many cases for a small custom stories dataset and the performance is expected to increase with a bigger dataset.</p> <p>Keyword: Image Classification, Convolution Neural Network, Long Short Term Memory, Language Modelling, Text Pre-Processing.</p> <p>References:</p> <ol style="list-style-type: none"> 1. OriolVinyals, AlexanderToshev,SamBengio, DumitruErhan.: Show and Tell: A Neural Image Caption Generator. https://arxiv.org/abs/1411.4555. (2014) 2. Jiang Wang, Yi Yang, Junhua Mao, Zhiheng Huang, Chang Huang, Wei Xu.: CNN-RNN: A Unified Framework for Multi-label Image Classification. https://arxiv.org/abs/1604.04573. (2016) 3. Zachary C. Lipton, John Berkowitz.: A Critical Review of Recurrent Neural Networks for Sequence Learning. https://arxiv.org/abs/1506.00019. (2015) 4. Klaus Greff, Rupesh K. Srivastava, Jan Koutník, Bas R. Steunebrink, Jürgen Schmidhuber.: LSTM: A Search Space Odyssey. https://arxiv.org/abs/1503.04069. (2017) 5. Keiron O'Shea, Ryan Nash.: An Introduction to Convolutional Neural Networks. https://arxiv.org/abs/1511.08458. (2015) 6. M Manojkrishna, M Neelima, M Harshali, M VenuGopalRao.: Image classification using Deep learning. (2018). 7. AshwinBhandare, Maihuli Bhide, PranavGokhale, RohanChandavarkar.: Applications of Convolutional Neural Networks. (2016) 8. Joseph Redmon, Ali Farhadi.: YOLOv3: An Incremental Improvement. https://arxiv.org/abs/1804.02767. (2018) 9. Tsung-Yi Lin, Michael Maire, Serge Belongie, LubomirBourdev, Ross Girshick, James Hays, PietroPerona, DevaRamanan, C. LawrenceZitnick, PiotrDollar.: Microsoft COCO: Common Objects in Context. https://arxiv.org/abs/1405.0312. (2015) 10. YoshuaBengio, RéjeanDucharme, Pascal Vincent, ChristianJauvin.: A Neural Probabilistic Language Model. (2003) 11. Thomas Cherian, AkshayBadola,VineetPadmanabhan.: Multi-cell LSTM Based Neural Language Model. https://arxiv.org/abs/1811.06477. (2018) 12. Jose Camacho-Collados, Mohammad TaherPilehvar.: On the Role of Text Preprocessing in Neural Network Architectures: An Evaluation Study on Text Categorization and Sentiment Analysis. https://arxiv.org/abs/1707.01780. (2018). 	2419- 2422
279.	<p>Authors: BollamPragna, M.RamaBai</p> <p>Paper Title: Spam Detection using NLP Techniques</p> <p>Abstract: Natural Language Processing is a vital field of research having applications in different subjects. Text Classification is a part of NLP where the text is converted into a machine-readable form by performing various methods. Tokenizing, part-of-speech tagging, stemming, chunking are some of the text classification methods. Implementing these methods on our data gives us a classified data on which we will train the model to detect spam and ham messages using Scikit-Learn Classifiers. We proposed a model to solve the issue of classifying messages as spam or ham by experimenting and analyzing the relative strengths of several machine learning algorithms such as K-Nearest Neighbors (KNN), Decision Tree Classifier, Random Forest Classifier, Logistic Regression, SGD Classifier, Multinomial Naive Bayes(NB), Support Vector Machine(SVM) to have a logical comparison of the performance measures of the methods we utilized in this research. The algorithm we proposed achieved an average accuracy of 98.49% with SVM model on 'SMS Spam Collection' dataset.</p> <p>Keyword: K-Nearest Neighbors (KNN), Decision Tree Classifier, Random Forest Classifier, Logistic Regression, SGD Classifier, Multinomial Naive Bayes(NB), Support Vector Machine(SVM)</p> <p>References:</p> <ol style="list-style-type: none"> 1. Navaney, P., Dubey, G., & Rana, A. (2018). "SMS Spam Filtering Using Supervised Machine Learning Algorithms." 2018 8th 	2423- 2426

A Deep Learning for the Generation of Textual Story Corresponding to a Sequence of Images

B Venkat Raman, Nagaratna P Hegde, Nenavath Venkatesh Naik, Allu Siva Kishore Reddy

Abstract Generating a short story for a sequence of images is much more interesting than generating a single line textual description for an image. Story generation involves relating the meaning of the previous image and the current image and continuing this through out the sequence of images. This can be helpful for better understanding of the situation. In this paper we present our idea of generating story using a CNN model which is pre-trained on MSCOCO dataset that can detect objects and concepts of language modelling and NLP text pre-processing techniques. We used a custom stories dataset in which we manually labelled every sentence in every story. Number of sentences in the generated story is equal to the number of images. The results are quite accurate in many cases for a small custom stories dataset and the performance is expected to increase with a bigger dataset.

KeyWords : Image Classification, Convolution Neural Network, Long Short Term Memory, Language Modelling, Text Pre-Processing.

I. INTRODUCTION

Short story generation for sequence of images is the problem in a image caption generator[1,2] because a simple caption generator cannot take sequence of images as input i.e generation of caption for single image only. But our neural story generation is capable of generating a story by understanding the content of each image and by relating those sequence image contents. In these few years many approaches came to generate the captions[1,2] and presented a successful and impressive outcomes but they did not shown an impressive outcome in story generation because most of these techniques are based on RNN(recurrent neural networks) [3].

So we used an advanced network of RNN [3] i.e LSTM(Long Short Term Memory) [4] which is capable of having long term dependency between the words of any sentences. We used CNN(Convolutional Neural Network) [5] to classify the objects which are present in the image. So in our project we give sequence of images as input to the

CNN [5] and it will process those images and classifies them and we assume two labels for each one-hot vector

combination of objects in the image and those labels [2] goes through the LSTM network and generate a textual description as story which is our output.



CNN: Person and Horse

LSTM: a person riding a horse

Story: a person riding a horse and happily sitting on it may be he is going to his home

II. LITERATURE REVIEW

Here we used some already existed concepts for the purpose of Story Generation which are mentioned below.

2.1 Convolutional Neural Network

Rapid advances in computer vision are enabling brand new applications which are producing best results in our daily life by the help Convolutional neural network [5] which is involved in some applications like Image Classification [6], Object Detection, Neural Style Transfer, Face Recognition [7] etc. had used the concept of CNN.

In our Paper, we have used Convolutional Neural Network for the purpose of classifying the objects and tells what type of objects are present in a particular image. In recent years many approaches had came for image classification, all those approaches does the same thing i.e., classifying the object by using CNN.

For objects classification we used yolov3 [8] which is having an incremental development in classifying the objects [6] and it will give much accurate results when we compared to its previous version i.e. yolo,yolov2 and the dataset we used is MSCOCO dataset [9] which is a trained on 80 objects.

Revised Version Manuscript Received on 10 September, 2019.
B Venkat Raman, Research Scholar at Osmania University, Hyderabad and Assistant Professor, CSE, RGUKT, Basar, Telangana, India.
(Email: venkat521@yahoo.co.in)

Nagaratna P Hegde, Professor at Vasavi College Of Engineering, Hyderabad, Telangana, India.
(Email: nagaratnaph@gmail.com)
Nenavath Venkatesh Naik, UG Scholar, Department Of Computer Science & Engineering, RGUKT Basar, Telangana, India.
(Email: venky.b131286@gmail.com)
Allu Siva Kishore Reddy, UG Scholar, Department Of Computer Science & Engineering, RGUKT Basar, Telangana, India.
(Email: kishorerddy8466@gmail.com)

Souvenir

**6th International Conference on
Innovations in
Computer Science & Engineering**

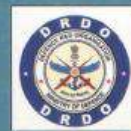
ICICSE-2018

August 17th & 18th, 2018

In collaboration with



Technically Supported by



Editor-in-Chief
Dr. H. S. Saini



Organized by

GNI GURU NANAK INSTITUTIONS

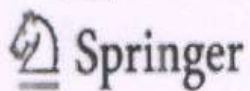
• Engineering • BDS • MDS • Pharmacy • MBA • PGDM

www.gniindia.org

SOUVENIR

**6th International Conference on
Innovations in Computer Science & Engineering
(ICICSE- 2018)**

August 17th & 18th, 2018
in collaboration with
Computer Society of India (CSI)



Editor -In-Chief

Dr. H. S. Saini

Managing Director

Guru Nanak Institutions

Ibrahimpatnam, Hyderabad.

Editor

Dr. Rishi Sayal

Associate Director

Guru Nanak Institutions Technical Campus

Ibrahimpatnam, Hyderabad.

Editor

Dr. A. Govardhan

Rector

Jawaharlal Nehru Technological University

Hyderabad, Telangana, India.

Editor

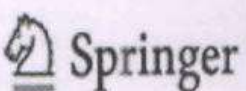
Dr. Rajkumar Buyya

Director, Cloud Computing

The University of Melbourne, Melbourne 3010,

Australia

Technically Supported by



Organised by

GURU NANAK INSTITUTIONS

Engineering • Dental • MBA • MCA • Pharmacy • PGDM

www.gniindia.org

**Souvenir of 6th International Conference on
Innovations in Computer Science & Engineering (ICICSE- 2018)**

Track 3 : Artificial Intelligence / Machine Learning

SLNo.	Paper ID	Title of the Paper	Page No.
38.	13	Electronic Guitar MIDI Controller for Various Musical Instruments using Charlie Plexing Method <i>-Robinson Devasia, Aman Gupta, Sapna Sharma, Saurav Singh and Neeru Rathee</i>	29
39.	35	Music Generation Using Deep Learning Techniques <i>-Somula Ramasubbareddy, D.Saidulu, V.Devasekhar, V.Swathi, Sahaj Singh Maini and K.Govinda</i>	29
40.	45	Development and Investigation of Data Stream Classifier using Lagrangian Interpolation Method <i>-Dr. S. Jayanthi and Dr. J. Mercy Geraldine</i>	30
41.	65	Quron: Basic Representation and Functionality <i>-B Venkat Raman, Nagaratna P Hedge, Dudimetta Mallesh and Bairi Anjaneyulu</i>	31
42.	69	Memorization Approach to Quantum Associative Memory Inspired by a Natural Phenomenon of Brain <i>-B Venkat Raman, K Chandra Shekar, Ranjith Gandhasiri and Sudarshan Gurram</i>	31
43.	77	Supervised Machine Learning Classifier for Email Spam Filtering <i>-Deepika Mallampati, K Chandra Shekar and K Ravikanth</i>	32
44.	85	A Hybrid Feature Selection Approach for Handling a High Dimensional Data <i>-B Venkatesh and J.Anuradha</i>	32
45.	87	Predicting the Entire Static Load Test by Using Generalized Regression Neural Network in the United Arab Emirates <i>-A. K. Alzo'ub and, Farid Ibrahim</i>	33
46.	104	Predicting the risk of readmission of Diabetic Patients using Deep Neural Networks <i>-G Siva Shankar and Dr. K Manikandan</i>	33
47.	105	Reliable Healthcare Monitoring System Using SPOC Framework <i>-P. Ramya, P. Naga Sravanthi and Morampudi Mahesh Kumar</i>	34

(11.47 unread) - veekesh2111 | April 2016 - IJARCE | IJARCE 10.pdf | +

https://ijarce.com/volume-5-issue-4/

International Journal of Advanced Research in Computer and Communication Engineering

A monthly peer-reviewed online and print journal

ISSN Online: 2249-5771
ISSN Print: 2320-540X
Since 2012

Home About Authors Reviewers Topics Peer Review Current Issue Policies Indexing FAQ's Contact

Call for Papers

Vol. 9, Issue 3, March 2020
Paper Submission: 10th March 2020
Author Notifications: within 2 days
Publication in progress

Downloads
Paper Format
Copyright format
[Submit paper to ijarcce@gmail.com](#)

IJARCE Management

Aims and Scope
Call for Papers
Editorial Board
Publication Ethics
Subscription
Librarians
Conference Special Issue

Archives

2020
2019
2018
2017
2016
2015

April 2016

VOLUME 5, ISSUE 4, APRIL 2016

Hybrid Email Spam Detection Method Using Negative Selection and Genetic Algorithms
Mohammad Reza Abdolhanezhad, Touraj Bonakdaram
Abstract: | [PDF](#) | DOI: 10.17148/IJARCE.2016.5401

Antismuggling System for Trees in Forest using Flex Sensor with GSM & Zigbee Network
Prof. Mhaske D.A., Bhabad Vishnu S., Pathare Sagar A.
Abstract: | [PDF](#) | DOI: 10.17148/IJARCE.2016.5402

Palm Print Feature Extraction and Authentication Using 2-D Gabor Filter
Prof. Ajun Nichal, Ms. Supriya Jadhav, Ms. Kaishma Shikalgari, Ms. Poornam Mahamur
Abstract: | [PDF](#) | DOI: 10.17148/IJARCE.2016.5403

Iris Database Compression Using Haar Wavelet Decomposition and Huffman Coding
Alphones Maria, Amlu Anna Joshy, Aneeta Christopher, Anjali B., Ranjitha Rajan
Abstract: | [PDF](#) | DOI: 10.17148/IJARCE.2016.5404

Type here to search

Here in page | [Print](#) | [Highlight](#) | [Match Case](#) | [Match Operators](#) | [Match Whole](#)

https://ijarce.com/volume-5-issue-4/

©VOLUME 5, ISSUE 4, APRIL 2016, ISSN: 2249-5771, DOI: 10.17148/IJARCE.2016.5410

Abstract: | [PDF](#) | DOI: 10.17148/IJARCE.2016.5410

Android Based LAN Monitoring System
Avinash Sasidarhan K., Tushar Nerkar, Kartik Purohit, Harsh Devani, Prof. Amruta Pokhare
Abstract: | [PDF](#) | DOI: 10.17148/IJARCE.2016.5411

Analysis and Comparison of Various Sense Amplifier Topologies for SRAM
Vipul Bhatnagar, Sonali Shrotriya
Abstract: | [PDF](#) | DOI: 10.17148/IJARCE.2016.5412

A Statistical Approach for 3D Hand Gesture Recognition
Venkata Raman B., S. Gupta and Mohammad Akram Pasha
Abstract: | [PDF](#) | DOI: 10.17148/IJARCE.2016.5413

Design and Implementation of FMO/Manchester Encoder using VHDL
D. Durga Prasad, Ch. V. V. S. Srinivas, K. Kiron, A. K. Chaitanya Vorma
Abstract: | [PDF](#) | DOI: 10.17148/IJARCE.2016.5414

A Study on Data Mining Approaches for Agricultural Intelligence
V. Kaleeswaran, Dr. R. Rathipriya
Abstract: | [PDF](#) | DOI: 10.17148/IJARCE.2016.5415

The Security Schemes Implemented In Mobile Ad Hoc Networks
D. Sudha, Dr. A. Vedhivel

A Statistical Approach for 3D Hand Gesture Recognition

Venkat Raman B¹, S Gupta² and Mohammad Akram Pasha³

Lecturer, CSE department, RGUKT Basar, Hyderabad, India¹

Student, CSE department, RGUKT Basar, Hyderabad, India^{2,3}

Abstract: In our daily life, gesture plays most important role and in order to convey data and motions of human being. The process of main aim is Hand gesture recognition can be seen as a way for computers to begin understand human body language , thus building a richer bridge between machines and humans. Current focuses in the field is recognition the hand in whole object and which can be used as a command by user. Many approaches have been made using cameras and computer vision algorithms to interpret sign language . This paper presents a some works on 3D hand gestures motion without using sensors. We first review the how to recognize the hand gesture by using HAAR features . Then, we review the research for 3d hand gesture recognition.

Keywords: Hand detection, hand identification ,motion detection, input image, training data base.

1. INTRODUCTION

Gestures have been one of the important interaction media projected into a classifier which has a capability to in current human -computer interaction(HCI) .HCI is compare and discriminate the features. one of the most popular technique of science . People are trying to make the human life easier by putting their intelligence into machine. As a result almost in everyday we are getting new device which helping our regular life .These application most useful for blind and physically challenged people and not only physically challenged people ,but also for different applications in diversified areas such as aviation, surveying , music directions etc. It is best method to interact with the computer without using sensors and any other devices. Main advantage of this project is very easy to use , natural and initiative [1].

2. HISTORICAL BACKGROUND

The History of hand gesture recognition for computer control started with the invention of glove based control interfaces . Researches realized that gestures inspired by sign language can be used to offer simple commands for a computer interface. This gradually evolved with the development of much accurate accelerometers , infrared cameras and even fiberoptic bend -sensors(optical goniometers).Some of those developments in glove based systems eventually offered the ability to realize computer vision based recognition without any sensors attached to the glove. Over past 25 years, this evolution has resulted in many successful products that offer total wireless connection resistance to the wearer[4].

3. PROPOSED METHOD

3.1 Architecture of the System: The system contains a training data set which contains information about the known hands. Dimension reduction or feature extraction is done both on training [6] data set and input query (test image). The obtained low dimensional feature vector is

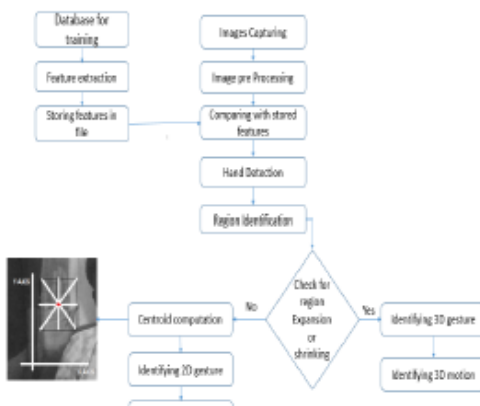


Figure : 1

Images Capturing: Capturing sequence of images from web camera.

Image pre processing: Captured images convert into grayscale to improve performance and resize all images to a fixed size.

Hand Detection: A simple rectangular Haar-like feature can be defined as the difference of the sum of pixels of areas inside the rectangle, which can be at any position and scale within the original image. This modified feature set is called 2-rectangle feature .The values indicate certain characteristics of a particular area of the image. Each feature type can indicate the existence (or absence)

BIOGRAPHIES

Venkat Raman B. is working as teaching faculty in the department of Computer Science and Engineering, Rajiv gandhi University of Knowledge Technologies-Basar, India. His passions include teaching, seminars and conducting workshops. His research interest is in the area of data mining and machine learning.



Samayamantula Gupta is an undergraduate student at Rajiv gandhi University of Knowledge Technologies-Basar, India. His passions include developing innovative software. His research interest is in the area of data mining and machine learning.



Mohammad Akram Pasha is an undergraduate student at Rajiv gandhi University of Knowledge Technologies-Basar, India. His passions include developing innovative software. His research interest is in the area of data mining and machine learning.

https://jarce.com/volume-5-issue-3/

International Journal of Advanced Research in Computer and Communication Engineering
A monthly peer-reviewed online and print journal
ISSN Online: 2231-5391
ISSN Print: 2231-5391
Since 2012

Call for Papers

Vol. 9, Issue 3, March 2020
Paper Submission: 10th March 2020
Author Notifications within 2 days
Publication in progress

Downloads:
Paper Format
Copyright Format
Editor.paper@jarce@gmail.com

JARCE Management

Aims and Scope
Call for Papers
Editorial Board
Publication Ethics
Subscription
Librarian
Conference Special issue

Archives

2020
2019
2018
2017
2016
2015
2014
2013

March 2016

VOLUME 5, ISSUE 3, MARCH 2016

Cloud Computing Intelligent Management by Melioristic Algorithm of Intelligent Water Drop
Mojid Abdous, Touraj Banirostam
Abstract | PDF | DOI: 10.17148/JARCE.2016.5308

Performance Evaluation of Different Multipliers in VLSI using VHDL
M. Aravind Kumar, O. Ranga Rao, M. Dilip, C V Pradeep Kumar Reddy, K.P. Mani
Abstract | PDF | DOI: 10.17148/JARCE.2016.5309

Dynamic Query Form for Relational Database
Priyanka Gupta, Rakesh Kumar Singh, Rambha Agrahari
Abstract | PDF | DOI: 10.17148/JARCE.2016.5310

https://jarce.com/volume-5-issue-3/

Abstract | PDF | DOI: 10.17148/JARCE.2016.5317

Keyword Extraction and Clustering For Document Recommendation in Conversations
Fooja Pandil, Umar Farooq Shahbad, Manpreet Singh, Varsha Gaykhwad, F.S. Ghodichor
Abstract | PDF | DOI: 10.17148/JARCE.2016.5318

A Survey Paper on Data mining Techniques and Challenges in Distributed DICOM
P. Haripriya, R. Parkodi
Abstract | PDF | DOI: 10.17148/JARCE.2016.5319

Efficient Image Classification Using Sum Product Tree Based Parallel Computing Approach Using Large Feature Set
B Venkata Raman, Vaibhav Saikumar and Naresh Ashelli
Abstract | PDF | DOI: 10.17148/JARCE.2016.5320

Text Classification of Crowdsourced Data Using Parallel Computing Nested Baye's Classifier
Venkata Raman B, Rajesh Jakkula and Mahesh Pathiyam
Abstract | PDF | DOI: 10.17148/JARCE.2016.5318

Controlling Mouse Events Using Eye Blink
Sanjay Ganjyalal, William Godad, Neelam Phadnis
Abstract | PDF | DOI: 10.17148/JARCE.2016.5319

Performance Analysis of Hierarchical Location Management Scheme to Locate Mobile Agents
Mamnoon Dabholkar, Suniti Anandwani

Text Classification of CrowdSourced Data Using Parallel Computing Nested Baye's Classifier

Venkat Raman B¹, Rajesh Jakkula² and Mahesh Pathyam³

Lecturer, CSE department, RGUKT Basar, Hyderabad, India¹

Student, CSE department, RGUKT Basar, Hyderabad, India^{2,3}

Abstract: Text classification has drawn attention due to the vast applicability in language identification, spam filtering, genre classification, sentiment analysis, readability assessment, article triage etc. With the goal of classifying crowdsourced data which is gathered from many websites into text classification, Crowd sourced data classification has challenges in getting data from various sources and whatever the data we are getting is huge in amount. Our approach will address challenges to classify the crowdsourced data in parallel computing in which many calculations are carried out simultaneously so that the crowdsourced data will be divided into tree format and calculations will be done simultaneously using nested baye's classifier. Our aim is to classify the algorithms which are obtained using web crawler and will be converted into programmes using nested baye's classifier technique.

Keywords: Web Crawler, Text Classification, Nested Bayes Classifier, Parallel Computing, CrowdSourcing.

INTRODUCTION

Crowds of people can solve some problems faster than individuals or small groups. A crowd can also rapidly generate data about circumstances affecting the crowd itself. This crowdsourced data can be leveraged to benefit the crowd by providing information or solutions faster than traditional means. However, the crowdsourced data can hardly be used directly to yield usable information. Intelligently analyzing and processing crowdsourced information can help prepare data to maximize the usable information, thus returning the benefit to the crowd. This article highlights challenges and investigates opportunities associated with mining crowdsourced data to yield useful information, as well as details how crowdsourced information and technologies can be used for response-coordination when needed, and finally suggests related areas for future research [6]. Text classification is classifying the text into fixed number of predefined categories. There is set of texts in each category which is already trained in the program. Whatever the crowdsourced data we are getting is in the form of text and it will be categorized into one of the category. What we are going to propose is the crowdsourced data will be in larger size and the calculations should be done very fast [2]. For that we are going to use multiple processes for parallel computing and for each processor we use a nested baye's classifier. For each category in text classification we may have sub categories. For that we use a nested baye's classifier.

RELATED WORK

Text classification can be performed within crowdsourced data. For instance, users can categorize documents or can assign labels, also known as classes (i.e., tags), to documents manually [5].

Crowdsourcing is often used to obtain solutions to a problem that are cheaper and superior in quality and

quantity to those that are obtained from traditional professionals in the same industry.

Some websites such as Wikipedia, encyclopaedia and world map should not be developed by individual, they should developed by large number of users individually.

Facebook is another popular application that can be used for crowdsourcing data like business and market analysis urban planning, and product repository generation.

Facebook provides many applications such as designing surveys, opening forums for discussion, dropping a note to bring awareness to a topic, and creating interest groups. Facebook is a mechanism for building brands, calling people to action, or even introducing ideas.

A web crawler(also known as a web spider or web robot) is a program or automated script which browses the World Wide Web in a methodical, automated manner. To visit files or websites in order to index them for searching.

Many legitimate sites, in particular search engines, use spidering as a means of providing up-to-date data.

Parallel computing: crowdsourced data is divided into multiple processes for the purpose of doing the calculations faster. Each process is assigned with nested baye's classifier. This is because to do the calculations faster in nested baye's classifier. How many processes required will be based upon how much crowdsourced data we are getting through the web crawler for classification [1].

Baye's classifier: It is a simple probabilistic approach to categorize the given data into one of the predefined categories. This is based on baye's theorem. This is comes under supervised classification problem. This is because of the set of texts which is trained in the baye's classifier.

Predefined categories and Set of Texts:

Input: read, take, accept, user, keyboard, input

Output: write, display, print, show, monitor

Loop: repeat, iteration, continue, till, goto, as long as

Condition: if, condition

Expression

Input, Output, Loop, Condition, Expression are all predefined categories in which we have set texts as shown above. Now the text which is obtained from web crawler will be classified into one of the category using nested baye's classifier and eventually the algorithm will be converted into the desired program.

CONCLUSION

Basically the current contribution of this project are proposing how the crowdsourced data which is obtained from multiple sources through the web crawler will be classified into categories and the use of the web crawler to crawl the data from many websites and storing the information in database. After this we came across parallel computing to divide the data into multiple processes for the ease of doing calculations in efficient manner.

Set of texts are trained in the predefined categories and the text which is obtained from database of a web crawler will be classified into any one of the category. This will be help for the people who want to see other people algorithms and other people codes for their problem. The users will see how other people write algorithms and they can share their ideas through this and for all of them they can get the code whatever the algorithm they write.

REFERENCES

- [1] Text: Aki, Parallel Computation, Model and Methods Prentice Hall, 1997.
- [2] Manas Joglekar, Adam Marcus, Aditya Parameswaran, and Vasilis Verroios, "Challenges in Data Crowdsourcing", IEEE Transactions on knowledge and data engineering, Vol.28, NO.4 Hector Garcia-Molina, Member, IEEE,
- [3] D. R. Karger, S. Oh, and D. Shah, "Efficient crowdsourcing for multi-class labeling," in Proc. ACM SIGMETRICS/Int. Conf. Meas. Model. Computer Syst., 2013, pp. 81–92.
- [4] Parallel Computing Systems and Applications J.Hollingsworth Dept. of computer science, University of Maryland, USA
- [5] An empirical study of the naive baye's classifier. I.Rish, TJ Watson research centre.
- [6] Maximizing benefits from crowdsourced data, Geoffrey Barbier - Reza Zafarani - Huji Gao Gabriel Fung - Huan Liu) Published online: 25 June 2012 © Springer Science + Business Media, LLC 2012 2012



Jakkula Rajesh is an undergraduate student at Rajiv Gandhi University of Knowledge Technologies-Basar, India. His passions include developing innovative software. His research interest is in the area of data mining and machine learning.



Pathyam Mahesh is an undergraduate student at Rajiv Gandhi University of Knowledge Technologies-Basar, India. His passions include developing innovative software. His research interest is in the area of data mining and machine learning.

BIOGRAPHIES

Venkat Raman B, is working as teaching faculty in the department of Computer Science and Engineering, Rajiv Gandhi University of Knowledge Technologies-Basar, India. His passions include teaching, seminars and conducting workshops. His research interest is in the area of data mining and machine learning.

https://jarce.com/volume-5-issue-3/

International Journal of Advanced Research in Computer and Communication Engineering
A monthly peer-reviewed online and print journal
ISSN Online: 2231-8911
ISSN Print: 2231-8911
Since 2012

Call for Papers

Vol. 9, Issue 3, March 2020
Paper Submission: 10th March 2020
Author Notifications within 2 days
Publication in progress

Downloads:
Paper Format
Copyright Format
Email paper to jarce.paper@gmail.com

IJARCE Management

Aims and Scope
Call for Papers
Editorial Board
Publication Ethics
Subscription
Librarian
Conference Special issue

Archives

2020
2019
2018
2017
2016
2015
2014
2013

March 2016

VOLUME 5, ISSUE 3, MARCH 2016

Cloud Computing Intelligent Management by Melioristic Algorithm of Intelligent Water Drop
Mojid Abdous, Touraj Banirostam
Abstract | PDF | DOI: 10.17148/IJARCE.2016.5308

Performance Evaluation of Different Multipliers in VLSI using VHDL
M. Aravind Kumar, O. Ranga Rao, M. Dilip, C V Pradeep Kumar Reddy, K.P. Mani
Abstract | PDF | DOI: 10.17148/IJARCE.2016.5309

Dynamic Query Form for Relational Database
Priyanka Gupta, Rakesh Kumar Singh, Rambha Agrahari
Abstract | PDF | DOI: 10.17148/IJARCE.2016.5309

https://jarce.com/volume-5-issue-3/

Abstract | PDF | DOI: 10.17148/IJARCE.2016.53172

Keyword Extraction and Clustering For Document Recommendation in Conversations
Pooja Pandit, Umar Farooq Shahbad, Manpreet Singh, Varsha Gaykawad, F.S. Ghodichor
Abstract | PDF | DOI: 10.17148/IJARCE.2016.53178

A Survey Paper on Data mining Techniques and Challenges in Distributed DICOM
P. Haripriya, R. Parkodi
Abstract | PDF | DOI: 10.17148/IJARCE.2016.53179

Efficient Image Classification Using Sum Product Tree Based Parallel Computing Approach Using Large Feature Set
B Venkat Raman, Vaidya Saikumar and Naresh Ashetti
Abstract | PDF | DOI: 10.17148/IJARCE.2016.53180

Text Classification of CrowdSourced Data Using Parallel Computing Nested Baye's Classifier
Venkat Raman B, Rajesh Jakkula and Mahesh Pathiyam
Abstract | PDF | DOI: 10.17148/IJARCE.2016.53181

Controlling Mouse Events Using Eye Blink
Sanjay Ganjala, William Godad, Neelam Phadnis
Abstract | PDF | DOI: 10.17148/IJARCE.2016.53182

Performance Analysis of Hierarchical Location Management Scheme to Locate Mobile Agents
Macron BellBork, Suresh Kannan
Abstract | PDF | DOI: 10.17148/IJARCE.2016.53183

Efficient Image Classification Using Sum Product Tree Based Parallel Computing Approach Using Large Feature Set

B Venkat Raman¹, Vaidya Saikumar² and Naresh Ashetti³

Lecturer, CSE, RGUKT Basar, Hyderabad, India¹

Student, CSE, RGUKT Basar, Hyderabad, India^{2,3}

Abstract: To create an efficient classification method using a multi structural analogy for images. Classification is a division of data into groups of similar objects. Representing the data by fewer clusters necessarily loses certain minor details, to minimize the minute error, come up with a theme is to increase and create an efficient classification technique. When we have a large number of data to be processed and it needs to be clustered for simplification. We have to use efficient approach to consume less time should be taken into consideration. This paper represents creating such methodology in keeping mind all the pros and cons occurred in clustering. We have come up with an idea, using multi features like image feature extraction, parallel computing and distance finding algorithms which bind with sum product tree will results in achieving an efficient classification.

Keywords : Parallel computing, K nearest neighbor, canny edge detection, sobel edge detection, sum product tree.

I. INTRODUCTION

Generally if we want to divide large number of images/data into required number of clusters we use image processing techniques and cluster but processing time is main factor which needs to be reduced. Image Processing with parallel computing is an alternative way to solve image processing problems that require large times of processing or handling large amounts of information in acceptable time. This make use of less resources and results in efficient output. In parallel computing method different objects of the image will be processed at the same time this multitasking makes CPU to be utilized up to our need.

Classification can be done by the idea of sum product trees, the results for nodes of tree will be obtained from parallel computing techniques where we use different image feature techniques like shape, color, texture and distance finding algorithm(nearest neighbor) and with set of rules and procedure we cluster images. Because of the parallel computing we can save time and/or money, we can solve larger problems in very short time periods.

Algorithm

A case is classified by a majority vote of its neighbors, with the case being assigned to the class most common amongst its K nearest neighbors measured by a distance function. If K = 1, then the case is simply assigned to the class of its nearest neighbor.

Distance functions

Euclidean $\sqrt{\sum_{i=1}^k (x_i - y_i)^2}$

Manhattan $\sum_{i=1}^k |x_i - y_i|$

Minkowski $\left(\sum_{i=1}^k (x_i - y_i)^q \right)^{1/q}$

Hamming Distance

$$D_H = \sum_{i=1}^k |x_i - y_i|$$

$$x = y \Rightarrow D = 0$$

$$x \neq y \Rightarrow D = 1$$

X	Y	Distance
Male	Male	0
Male	Female	1

II. LITERATURE REVIEW

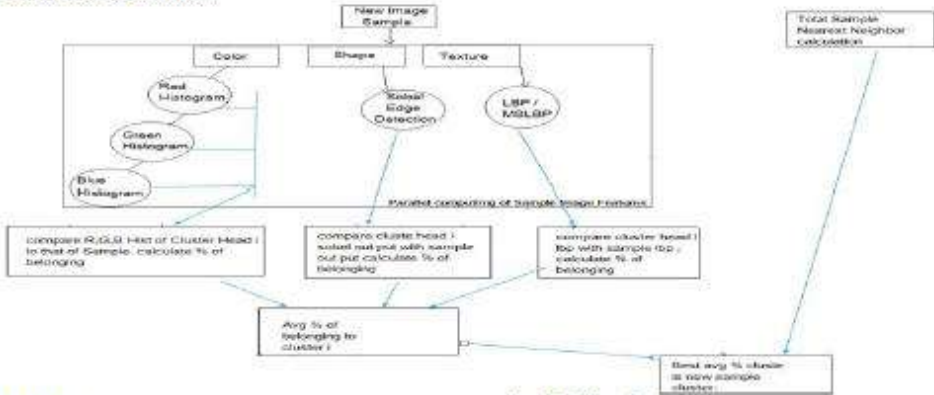
Classification : Classification the groups (or classes) are specified before hand, with each training data instance belonging to a particular class. It is the association between the instances features and the class they belong to that classification algorithms are supposed to learn.

1 .K Nearest Neighbor algorithm

The K-nearest neighbor algorithm stores all available cases and classifies new cases based on a distance functions. KNN has been used in statistical estimation and pattern recognition already in the beginning of 1970's as a non-parametric technique.

III. PROPOSED METHOD

3.1 Architecture of the System



3.2 Methodology

Hardware Requirements

System : Intel® core™ i3-4005U CPU @ 1.70 GHz.
 Hard Disk : 500GB
 Cache Memory : 3 Mb.
 Ram : 4GB

Software Used

Mpj-v0_44 Express software
 Java jdk_1.7.0

3.3 Implementation Procedure

This Classification takes input a large input image set and performs following procedure on it and cluster those images. Image set is randomly taken around 1000 images.

- Initially cluster heads will be defined for each cluster and their properties will be recorder and saved for further usage.
- When a sample image comes from images set to detect into which cluster it belongs,
- Through parallel computing multitasking at a time its image features like color, shape, texture will be acquired.
- Using sum product tree structure defined as in architecture these properties will be compared using image comparison technique to that of each cluster head properties and percentage of matching will be recorded.
- Finally for the cluster which has percentage of belonging is high sample image will go into that cluster.

VI. CONCLUSION

Our proposed method is a simple mechanism for high efficient clustering. It works effectively and is a combination of various existing methods proposed for the process. However, to reduce the complexity in identification and verification we used simple base algorithms in each related field and parallel computing also done in one system with mpj-express software which is specialist in parallel computing tasks.

VII. LIMITATIONS

1. To reduce the complexity in identification and verification we used simple base algorithms in each

- related field and
2. Parallel computing also done in one system with mpj-express software which is specialist in parallel computing tasks.

REFERENCES

- [1] Linda g. Shapiro and George c. stockman, computer visio, Upper saddle River:Prentice-hall,2001
- [2] Trubitskiy k.v.,Anding K.Pote G.A.,Garten D.,Musilimov V.M.(2015)." OUT-OF-FOCUS REGION SEGMENTATION OF 2D SURFACES IMAGES WITH THE USE OF TEXTURE FEATURES"
- [3] Andre Aichert, CAMP MEDICAL SEMINAR WS0708, "Feature extraction techniques", January 9, 2008
- [4] http://www.saedsayad.com/K_Nearest_Neighbors.html

BIOGRAPHIES

Venkat Raman B, is working as teaching faculty in the department of Computer Science and Engineering, Rajiv Gandhi University of Knowledge Technologies-Basar, India. His passions include teaching, seminars and conducting workshops. His research interest is in the area of data mining and machine learning.



Naresh Ashetti is an undergraduate student at Rajiv Gandhi University of Knowledge Technologies-Basar, India. His passions include developing innovative software. His research interest is in the area of data mining and machine learning.



Vaidya Saikumar is an undergraduate student at Rajiv Gandhi University of Knowledge Technologies-Basar, India. His passions include developing innovative software. His research interest is in the area of data mining and machine learning.



INVESTIGATIONS ON COMPACT UWB MONOPOLE ANTENNA

B.Premalatha¹,
Research scholar in ANU
Faculty of ECE, CMRCET.

M.V.S. Prasad²,
Faculty of ECE
RVR & JC college of Engineering, Guntur

M.B.R. Murthy³
Faculty of ECE
RGUKT, Basara

ABSTRACT:

The advances in integrated circuits resulted in drastic reduction in size of electronic gadgets. This necessitated miniature size antennas for use with wireless communication equipments. Many researchers have worked and are working on printed monopole slot antennas to achieve small size and acceptable performance. In this regard several investigations are carried out to ascertain the effect of slot position on antenna performance. In addition to this bevel slots are cut at corners and its effect on antenna performance is studied.

Compact wideband antennas are gaining popularity in view of their features like large bandwidth, low power consumption, low complexity, low cost etc.. Many researches are working to obtain an optimum arrangement for the UWB monopole antenna. In this paper several configurations of wideband antennas are designed, tested and their performance is compared. One arrangement is a compact patch with slot cut at different locations. Another arrangement is the earlier one with two symmetrical bevel cuts on the lower edge of the radiating element. In both schemes a defective ground plane structure (DGS) is used. Further the ground plane dimensions are varied and effect of this on performance is studied. The design and performance evaluation is carried out using HFSS software. The results are presented and discussed.

Keywords: Defective ground plane structure, bevel cuts, returns loss, UWB.

I. INTRODUCTION:

Federal communication commission assigned the frequency band 3.1GHz-10.6 GHz for commercial Applications [1]. Generally monopole antennas used in these applications

give large bandwidth but the drawback with conventional monopoles is that they are not compact as they require large ground plane perpendicular to the radiating element. Research carried out to reduce size of antenna lead to development of UWB printed antennas using partial ground plane. Many researchers are working on UWB monopole antennas with slots in patch and slots even in ground plane. [2-6]. These antennas are gaining attraction because high speed data rate, low power consumption, low complexity, low cost, compact in size, less in weight and large bandwidth.

When a slot is cut on the patch it effects the current distribution. By varying the slot position current distribution on the ground plane varies. The lower limit of the operating frequency depends upon the longest electrical path for the currents generated on the surface of the monopole. Normally the current is concentrated in the bottom as well as at the left and right hand edges of the monopole. So to improve UWB characteristics bevel slots are made on the lower edges of the patch. The ground plane of the antenna is also a part of radiating configuration and the current distribution on radiating element. The gap between ground plane and radiating patch plays a crucial role in obtaining the UWB characteristics. With UWB antennas defective ground structure is used.

In this paper performance of several arrangements of compact UWB antenna with micro strip feed to operate in the frequency band of 3GHz-12GHz is investigated. The arrangements considered are a single slot in patch placed at different positions from feed, slot at different locations along with symmetrical bevel slots. Further investigations are carried out to find the effect of varying ground plane length and varying dimensions of slot on patch performance.

To compare the performance of patch arrangements return loss, VSWR, gains at 5 GHz are considered .The antennas are designed and tested using HFSS software.

The description of the geometry of antennas considered for comparison is given in section II. In section III monopole antenna design details are given. The results obtained through simulation are presented in section IV. Section V deals with discussion of results and conclusions.

II. GEOMETRY OF ANTENNAS:

A rectangular radiating patch with slot is shown in Fig1. The slot position and it's dimensions play a crucial role in achieving wide band .To improve the impedance bandwidth bevel slots are made on lower edges of the radiating patch as shown in Fig 2. To get good radiation characteristics defective ground plane is taken and the gap between the ground plane and patch is optimized [7-11]. By varying the gap between the patch and ground plane return losses, VSWR and radiation characteristics are observed. A 50Ω micro strip feed line is connected to the patch to excite the antenna.

Fig 1 Rectangular radiating patch with slot

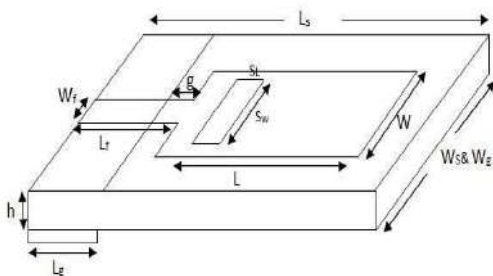
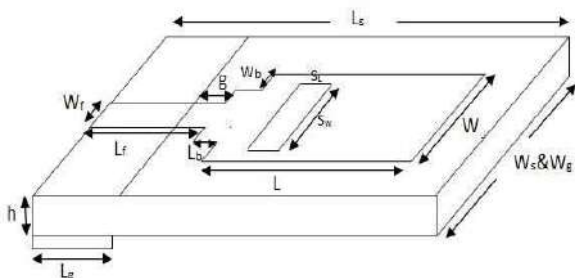


Fig2 Rectangular Radiating patch with slot and bevel slots.



III. MONOPOLE ANTENNA DESIGN:

First a rectangular patch is designed with resonant frequency of 6GHz using FR4 substrate of thickness (h) 1.6mm and dielectric constant (ϵ_r) of 4.4. Patch dimensions are calculated using the design equations [12] given below.

The width of the rectangular patch

$$W = \frac{c}{2f_r} \sqrt{\frac{2}{\epsilon_r + 1}} \quad (1)$$

c = velocity of light in free space, ϵ_r = relative permittivity of substrate.

Length of the patch

$$L = L_{eff} - 2\Delta L \quad (2)$$

L_{eff} is the effective length of patch due to fringing. The effective length L_{eff} of the antenna appears to be more than actual length L and is given by

$$L_{eff} = \frac{c}{2f_r \sqrt{\epsilon_{eff}}} \quad (3)$$

ϵ_{eff} is Effective dielectric constant and is obtained from

$$\epsilon_{eff} = \frac{\epsilon_r + 1}{2} + \frac{\epsilon_r - 1}{2} \left[1 + \frac{12h}{W} \right]^{-0.5} \quad (4)$$

The change in length ΔL that is difference between effective and actual lengths can be estimated from the relation

$$\frac{\Delta L}{h} = 0.412 \frac{(\epsilon_{eff} + 0.3)(\frac{W}{h} + 0.264)}{(\epsilon_{eff} - 0.258)(\frac{W}{h} + 0.8)} \quad (5)$$

The ground plane dimensions length L_g and width W_g are given by

$$L_g \geq 6h + L \quad (6)$$

$$W_g \geq 6h + W \quad (7)$$

Now a monopole antenna can be designed by equating the area of the planar rectangular patch antenna of length L and width W to that of cylindrical wire of radius r and height L.

That is equating

$$2\pi r L = LW \quad (8)$$

Radius of the cylindrical monopole will be

$$r = \frac{w}{2H} \quad (9)$$

The lower resonant frequency of the rectangular monopole antenna is given by [13]

$$f_L = \frac{7.2}{L_f + r + g} \text{ Hz} \quad (10)$$

L_f is the length of 50Ω feed line and g is distance between ground plane and patch.

Using the above expressions the dimensions are calculated and are presented in table I. For UWB monopole defective ground structure is to be used. So instead of taking full ground plane partial ground plane is used and its dimensions also are given in

Table: 1 Dimensions of monopole antenna

Parameter	Dimensions in mm
Height or thickness of the substrate (h)	1.6
Length of the Patch (L)	13.8
Width of the patch (W)	16
Radius of cylindrical monopole r	2.547
Length of the full Ground plane (L_g)	27
Length of the partial Ground plane (variable)	4 to 8.5
Width of the ground plane (W_g)	28
Length of the feed line(L_f)	9.5
Width of the feed line (W_f)	2.8
Gap between ground plane and patch (g)(variable)	1 to 5.5
Width of the slot(S_w)	2
Length of the slot(S_L)	10
Width of Bevel slot(W_b)	1
Length of Bevel slot (L_b)	1

IV. SIMULATION RESULTS:

Using Ansoft HFSS software two configurations (i) and (ii) of monopole patch are designed using above dimensions and their performances are evaluated. The effect of ground plane

dimensions and effect of bevel slots on frequency range and gain are also investigated. The configurations tested are

- (i) Patch Antenna with slot cut at different distances from feed location
- (ii) Configuration(i) with bevel cuts 1mmx1mm on both sides
- (iii) Slot at 12 mm from feed, bevel cuts of 1mmx1mm , ground plane of width 28mm and varying length
- (iv) Slot at 12 mm with varying dimensions of bevel cuts

The results obtained are presented in tables II-V

From the results in table II it is evident that maximum gain is obtained with slot located at 12 mm from feed location for both cases namely with and without bevel cuts. The results in table III indicate that for better performance the ground plane length L_g should be 7 mm and patch to ground spacing g should be 2.5 mm. Using $g=2.5$ mm, $L_g = 9.5$ mm and $r=2.54$ mm in equation 10 the lower resonant frequency is given as 4.96 GHz though initially for design resonant frequency is taken as 6 GHz. Hence gain is recorded for all cases at 5 GHz and presented in the tab

V. CONCLUSIONS:

The effect of slot position and bevel cut dimensions on the monopole patch are investigated and results are presented. From the investigations it can be concluded that for better performance slot of length 10mm, width 2 mm is to be placed at 12 mm from feed location. The partial ground plane can be 7 mm long and 28 mm wide. Bevel cuts on both sides are 1mmx1mm. This arrangement gives a UWB monopole covering 3 to 15 GHz. From the above results it is clear that the radiation pattern is same for the entire frequency band. However gain is constant. The gain reaches a maximum at 7 GHz and thereafter decrease. Further investigations are to be carried to achieve uniform gain for the entire range.

Table: 2 Effect of Ground plane dimensions on resonant frequency, VSWR and Gain

Ground plane length (Lg) mm	patch to ground distance(g) mm	frequency GHz where return loss <10dB	frequency GHz where VSWR<2	Gain at f=5GHz Φ=0, θ=90
4	5.5	1.9 to 3.6	1.8 to 3.7	1.8974
5	4.5	2 to 4.9	1.9 to 6.2	1.9235
6	3.5	2 to 6.6, 10.8to 12.3	2.1 to 6.9, 10.4 to 14.3	2.1814
7	2.5	2.3 to 14.3	2.3 to 14.5	2.2221
8	1.5	2.6 to 15	2.5 to 15	1.9405
8.1	1.4	2.7 to 15	2.6 to 15	1.8453
8.2	1.3	2.9 to 15	2.9 to 15	1.6340
8.3	1.2	2.8 to 15	2.7 to 15	1.85
8.4	1.1	2.8 to 15	2.7 to 15	1.6877
8.5	1.0	2.8 to 15	2.7 to 15	1.8894

Table: 3 Effect of slot position on Performance parameters:

Slot position from feed mm	Frequency GHz with return losses <10dB		Frequency GHz with VSWR is <2		Gain dB at 5 GHz Φ=0, θ=90	
	With bevel cuts	Without bevel cuts	With bevel cuts	Without bevel cuts	With bevel cuts	Without bevel cuts
10	2.6 to 7.2, 9.4 to 15	2.5 to 7.5, 9.4 to 15	2.5 to 7.5, 9.4 to 15	2.6 to 6.5, 9.4 to 11.4	1.82	2.03
11	3 to 15	3 to 15	3 to 15	3.3 to 12.5	1.78	1.61
12	2.8 to 15	2.6 to 15	2.6 to 15	3.4 to 15	1.68	1.88
13	2.8 to 15	2.7 to 15	2.7 to 15	3.2 to 15	1.49	1.80
14	3.1 to 15	2.8 to 15	2.8 to 15	3 to 7.3, 8.8 to 15	1.54	1.76
15	3.4 to 15	3.2 to 15	3.2 to 15	3.5 to 7.5, 8.9 to 15	1.34	1.21
16	3.3 to 15	3.1 to 15	3.1 to 15	3.8 to 6.8, 8.8 to 15	1.35	1.26

Table 4: Effect bevel slot dimensions on Antenna Performance parameters

Bevel cut Size mm (on both sides)	Frequencies GHz where return loss < 10dB	Frequencies GHz where VSWR<2	Gain at 5 GHz Φ=0, θ=90
2	2.9 to 11, 12.7 to 15	2.8 to 11.5, 12.6 to 15	1.72
1.5	2.8 to 11.3, 12.6 to 15	2.7 to 15	1.64
1	2.8 to 15	2.8 to 15	1.83
0.5	3 to 15	3 to 15	1.6275

Table: 5 UWB antenna gain variation with frequency

Freq in GHz	Gain dB Φ=0, and θ=90
3	0.51
4	0.5
5	2.03
6	2.92
7	3.43
8	3.6 (θ= 70)
9	-3
10	-2.6

From the above results it is observed that the radiation pattern is same for the entire frequency band but gain is maximum at 7GHz. The effect of slot position, ground plane dimensions and bevel slot dimensions on antenna parameters are studied and reported.

REFERENCES

- [1].K. George Thomas and M. Sreenivasam “A simple ultra-wide band planar monopole rectangular printed antenna with band dispensation” IEEE Transactions on antennas and propagation, vol. 58, No. 1, January 2010.
- [2].Jamal Nasir, Mohd. H. Jamaluddin, Imdad khan, Muhammad R. Kamarudin, and Muzammil Hussain “Design and Implementation of printed monopole antenna for portable devices” progress in Electromagnetic Research Symposium proceedings, Guangzhou, China, Aug 25-28, 2014.

[3].S.H.Hsuand K.Chang, “Ultra-ThinCPW-fedrectangularslotantenna for UWB applications,” in Proc. IEEE AP.-S Int. Symp., Jul. 2006, pp. 2587–2590.

[4].J.-P.Zhang, Y.S.Xu andW.-D.Wang, “Micro strip-fedsemi-elliptical antenna for ultra-wideband communications,” IEEE Trans. Antennas. Propagation, vol. 56, no. 1, pp. 241–244, Jan. 2008.

[5]. Qi Wu, Ringhong Jin, Junping Geng, and Min Ding “Printed Omni directional UWB Monopole Antenna with Very Compact Size.”IEEE Trans, Antennas propagation, Vol.56, No.3, March2008.

[6.] M. Q.Wu.R.Jin,J. Geng, and J.Lao, “Ultra Wideband Rectangular disk monopole antenna with notched ground,” Electron Lett ., vol. 43 ,no. 11 ,pp. 605-606,May 2007.

[7] C.-Y .Hong, C.-W .Ling,I.-Y. Yam, and S-J Chung, “Design of a planar UWB Antenna with a band notch structure,” IEEE Trans, Antennas propagation, Vol.56, No.55, no.12, Dec 2007.

[8] Y .Gao, B. L.Ooi, and A.P. Popov, “Band notched UWB ring monopole antenna” microwave. opt. tech. letter, Vol.48, No.1, pp.783-785, Jul.2005.

[9] M.N.Moghadasi .H.Rousta, and B.S.Virdee,” Compact UWB planar monopole antenna.” IEEE Antennas Wireless propagation, letter, vol, 7,pp.411-413, 2008.

[10] G Shrikanth Reddy, Anil kamma, Sanjeev.K. Mishra, and Jayanta Mukherjee,” UWB Dual-Band Planar Antenna with Quadruple Band-Notch Characteristics.” IEEE Antennas Wireless propagation, letter, vol, 13, 2014.

[11] D.T.Nguyen, D.H.Lee and H .C .Park,” Compact printed triple band notched UWB antenna with quarter –wavelength slots,” IEEE Antennas Wireless propagation, letter. Vol 11, PP 411-414, 2012.

[12].Constantine A. Balanis “Antenna theory analysis and design” Authorized reprint by Wiley India Pvt.Ltd., Daryaganj, New Delhi 2015.

[13] Daniel valderas,Juan Ignacio sancho,David puente,Cong Ling and Xiaodong chen “ULTRA WIDE BAND ANTENNAS” Design and Applications Imperial College Press.

Authors



B.Premalatha is presently working as a Assoc Professor in the Department of ECE in CMR college of Engineering and Technology. She did her B.Tech in ECE in 2002 and M.Tech in 2009 from JNTUH . She published several papers in National and International journals .She is presently doing Research on Microstrip Antennas in Acharya Nagarjuna university
E-Mail:bpremalatha@cmrcet.org



M.V.S.Prasad is presently working as a Professor in the Department of ECE of R.V.R & J.C. College of Engineering, Guntur Andhra Pradesh. He did his B.E. in Electronics and Communication Engineering in 1989, and M.E in Electronic Instrumentation in 1999 from Andhra University, Visakhapatnam, A.P. He obtained his Ph.D from S.V.University Tirupati in the year 2012. He published several papers in National and International journals. He did his research work on Dielectric rod Antennas. His interesting fields are Antennas, EMC/EMI, Electronic Measurements and Transducers. He is a Fellow of IETE, Life member in ISTE New Delhi and life member in EMC society.

E-Mail:mvs_prasad67@yahoo.co.in



M B R Murthy obtained bachelor’s degree BE Electrical from A U College of Engineering in 1972.He did M S Engg in communication Systems from N I T Rourkela . Obtained Ph D from Karnataka University Dharwad for his research on dielectric studies using microwave techniques. Dr Murthy is in the academic filed for the past 41years. Currently he is working as a senior Professor in ECE department of CMR College of Engineering and Technology, Hyderabad, 501041, India. He has guided two scholars for Ph D and supervised several M Tech and B tech Projects. He has over 100 publications to his credit in National, International Journals and Conferences. His areas of interest are Speech Processing and Communications. He is member of several professional bodies like Senior member IEEE, Life Fellow Institute of Electronics and Telecommunication Engineers India , Life member Institution of Engineers India, Life member Instrument society of India, Life member Indian Society for Technical Education

E-Mail:mbrmurthy@cmrcet.org

RESEARCH ARTICLE

OPEN ACCESS

Image Processing Technique for Drilled Holes Inspection in Large Rectangular Plate

Deepak Sachan¹, A Sainath Chaithanya²

¹Sr. Engineer, BHEL R & D, Hyderabad, Telangana, 500093 India.

²M. Tech, VLSI System Design, Anurag Group of Institutions (autonomous), Hyderabad, Telangana-500088

Corresponding author: Deepak Sachan

ABSTRACT

Baffle plates used in power plants as heat exchangers for the process of condensation are huge in size with large volume of holes meant for inserting and supporting the bundles of condenser tubes are transported to the site, where the tubes assembly is carried out.. Incidentally if a hole is undersized, oversized or not drilled, to rectify the same it is extremely difficult to carry out such operations at site as an oversize hole will lead to tube vibrations leading to physical damages to the condenser tubes. This leads to requirement for inspection of drilled holes in large rectangular plate. At present holes are checked by hand gauges, GO / NOGO Gauges, which is manually carried out and also time consuming. This made a way for optical inspection which offers the desirable characteristics of being non-invasive and non destructive, able to analyze real time objects in a remote sense. The present paper describes an automated method using image processing technique, for measurement of the large number of holes and its parameters for reducing the cycle time of inspection and improve the hole parameter measurement process, in tube sheet or baffle plates.

Keywords Adaptive filters, Baffle plate, Connectivity, Heat Exchangers, Image processing, , Label, NX-UG (CAD tool).

Date of Submission: 05-03-2018

Date of acceptance: 20-03-2018

I. INTRODUCTION

The purpose of baffle plate is to condense exhaust steam from the steam turbine by rejecting the heat of vaporization to the cooling water passing through the condenser tubes; the plate is having with its unique inlet designs to ensure high thermal efficiency where heat transmission takes place.

A sample of Tube sheet or baffle plate is as shown in Figure 1 is having dimensions of 1200mm x 800mm x 25 mm, provided with 415 holes.

Holes are drilled in to the plates using mechanical means such as single or multi-spindle drilling machine for the insertion of bundles of condenser tubes are transported to the site, where the tubes assembly is carried out.

Incidentally if a hole is undersized, oversized or not drilled, to rectify the same it is extremely difficult to carry out such operations at site as an oversize hole will lead to tube vibrations leading to physical

damages to the condenser tubes This lead to drilled hole inspection in baffle plates.

Presently parameters of holes in the Baffle plates sometimes baffle plate are being checked manually, which consumes a lot of time and manpower, hence it is desired to automate the inspection process for large number of holes on plate and this made a way for optical inspection.

A number of research studies being carried out on non-contact type metrological measurement

since it has many advantages over contact type measurements. Image processing [6] is one that aids for non-contact type optical measurements that allow one to enhance image features of interest while attenuating detail irrelevant to a given application and then extracts useful information about the scene from the enhanced image.

The real time capturing of plate needs a special mechanical alignment that takes time for establishment. An alternate source is provided, where a reference sample plate has been designed in NX-Unigraphics (CAD tool). An in built camera tools in NX make us to glance the appearance of plate's top view exactly when it is captured at different elevations practically.

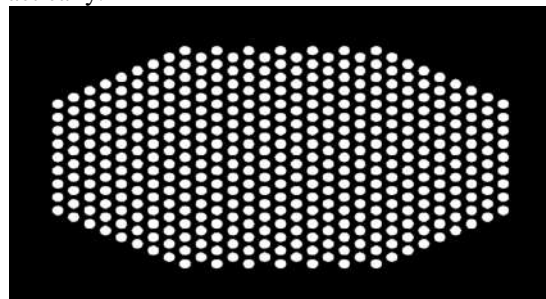


Figure 1: Tube sheet or Baffle plate

Finally Inspection of plate using image processing technique is employed in order to check the source image for different parameters namely hole count,

missing holes, misplaced holes, and the dimension of and to inspect whether holes are drilled at equal intervals. Height between the camera and the plate is adjusted in order to grab entire/section of plate. Parameters of the holes are estimated using image processing algorithm and checked with the reference designed plate in NX; parameter values of holes when the full/section of plate captured at various heights are noted and deviations are observed and plotted.

II. LITERATURE REVIEW AND RESEARCH DEVELOPMENT

In field of image processing applications in metrology, many researchers have done many research works. Some of the distinguished ones, which are relevant and carry basic information for this paper have been highlighted briefly.

An automated visual printed circuit board (PCB) inspection for Defect classification operation is employed in order to identify the source for four types of defects namely, missing hole, pin hole, short-circuit, and open-circuit [1].

Determination of misplaced drills on printed circuit board, the algorithm proposed in this paper uses image processing techniques for automated optical inspection and does not requires the original image of the PCB (original mask) [2].

Bloom diameter are measured using vernier caliper and number of blooms in a bunch is counted manually which may leads to mismatch. The work deals with image processing approach to estimate bloom parameters and total number of blooms in a bunch. To estimate these parameters gradient based circular Hough transformation technique is implemented using MATLAB [3].

Measuring the roundness and roughness of a work piece is essential for the engineering industries which are measured using one of the internationally defined methods of Minimum Zone Circles. This parameter was measured and studied using video measuring machine and image processing technology through Matlab [4].

With the aid of the above references, the current task of ‘Image processing technique for drilled hole inspection in large rectangular plate’ had been made easier and laid a way for developing an algorithm for the inspection of baffle plate using image processing techniques in Matlab.

III. METHODOLOGY

Approach for task

As the real image of the plate are captured by an MP (Mega pixel) camera, which requires specialized mechanical equipment that needs time for collection and establishment. In order to replicate the process an alternate method of is developed where tube sheet is designed in CAD Drawing of UG-NX. By capturing the plate at various positions and heights

holes like area, centroid, perimeter, radius, roundness by camera tool, Inspection of plate images are carried out

NX-Unigraphics:

The input image for processing is taken from NX Unigraphics [8] which is an advanced high end CAD/CAM software package. This is one of the key function in computer aided design engineering drawing, which conveys all critical information like geometry, dimensions before manufacturing a design unit. The capturing view of plate in NX is shown if Figure 2.

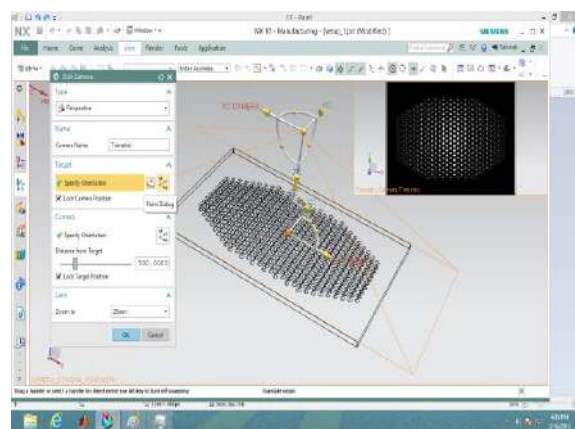


Figure 2: Capturing view of plate by camera in NX

In this study of hole inspection the plate image is inspected by using connectivity and labeling [5], its algorithm is shown in Figure 3.

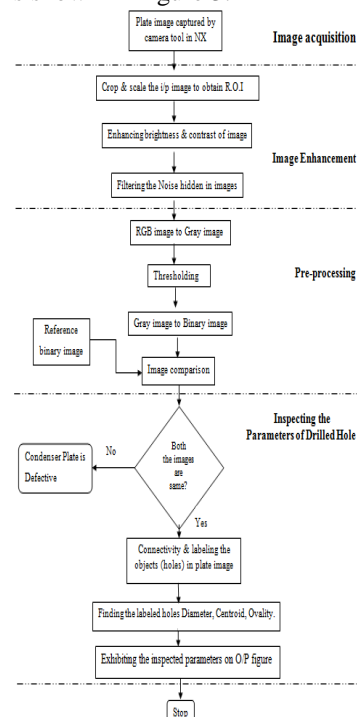


Figure 3: Flow Chart

IV. EMPIRICAL TESTS AND RESULT ANALYSIS

Test 1: Diameter Inspection of holes

The top view of Tube sheet / baffle Plate that has been designed in NX and its diameter values of holes obtained from program are depicted in figure 4 (a, b). appearance of full plate when captured at height of 3000mm and hole diameter values obtained from program are depicted in figures 4(c, d)

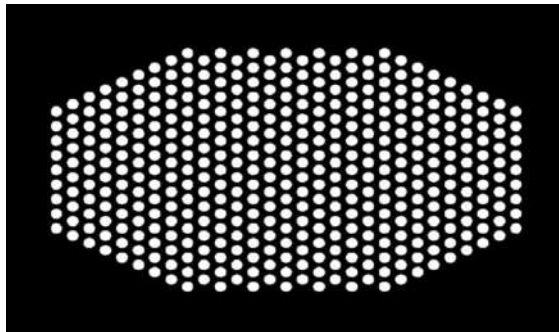


Figure 4 (a): Appearance of baffle plate in NX

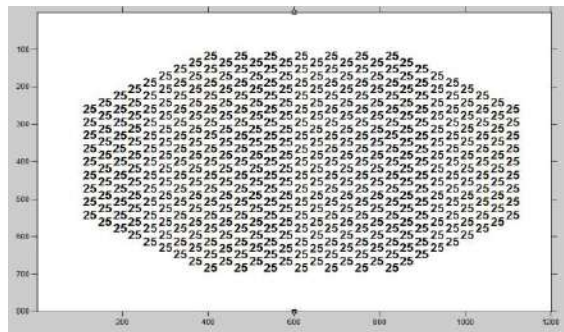


Figure 4 (b): Diameter values of holes obtained from program

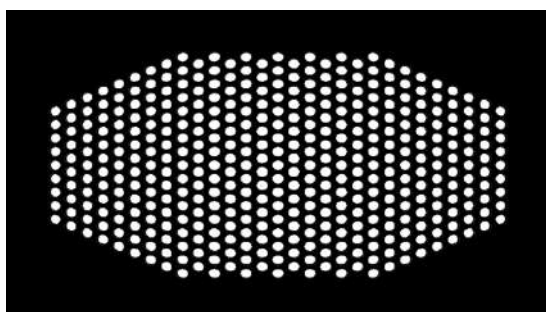


Figure 4(c): Appearance of plate when captured at 3000mm distance

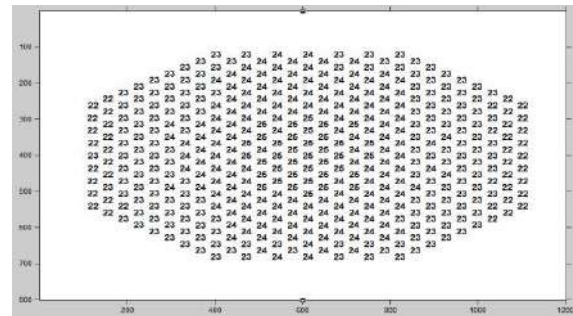


Figure 4 (d): Diameter values of holes obtained from program

As we go on increasing the height of camera tool the inner edges of holes disappear gradually. It is expedient to take camera at 3000mm height to capture plate as it exhibits a minimum diameter of 22pixels (mm) existing at border holes of plate, which is taken as a good consideration from the expected diameter of where the remaining heights like 1000mm shows 16mm of minimum diameter for border holes. We can't exceed the height of camera as the maximum permissible height of camera is 3000mm.

A graph is plotted with hole number to the diameter values obtained from program at various heights along with hole number to its deviation from expected diameter(=25 mm) which are depicted in figures 4 (e, f).

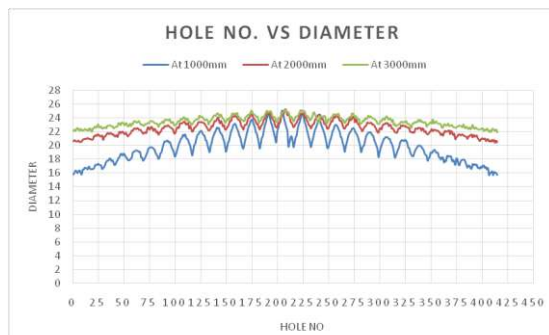


Figure 4 (e): Hole no. vs. obtained diameter from program

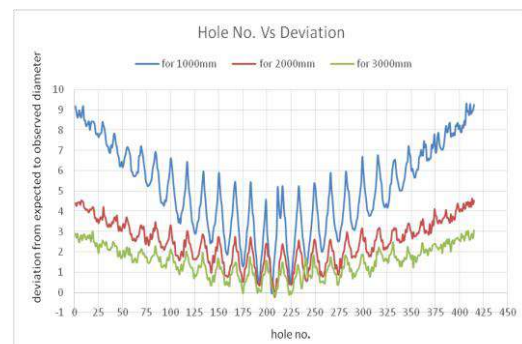


Figure 4 (f): Hole no. vs. observed deviation from program

Test 2: Inspection of distance between vertical holes using Centroid

Difference between the centers coordinates of adjacent row holes infers whether all vertical holes are equally spaced.

The below output figures 5 (a,b) show the centroid values which are arranged in regular order as that of holes in tube sheet or baffle plate.

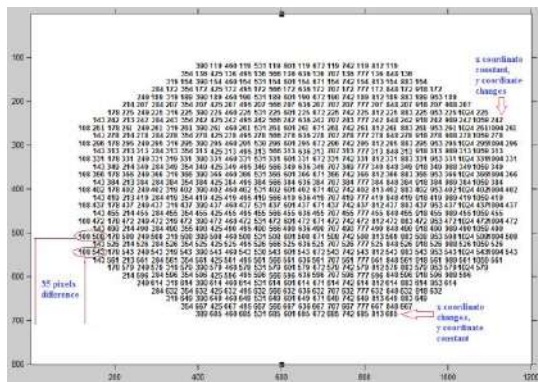


Figure 5(a): Centroid of holes in actual plate obtained by program

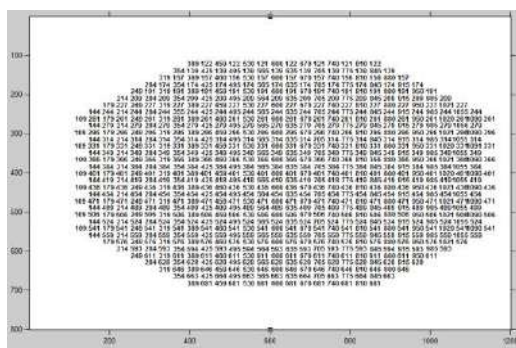


Figure 5 (b): Centroid of holes obtained from program at 3000mm

As the holes are arranged in random, while inspecting if it is detected the hole as the last hole in its column of holes, for which its distance of hole to succeeding hole that comes in next column is ignored which tends to a total of 386 distances for 415 holes.

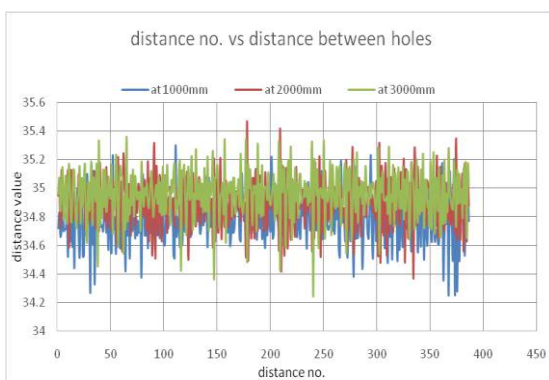


Figure 5 (c): Distance no. vs. hole to hole distance value

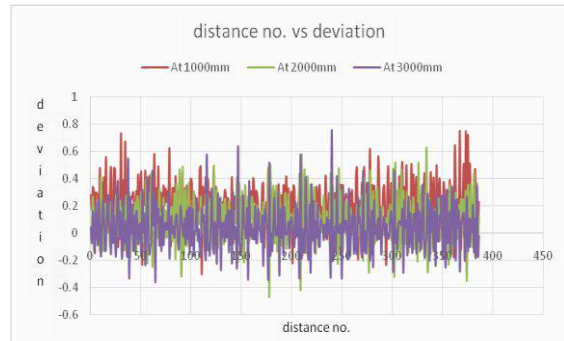


Figure 5 (d): Distance no. vs. Deviation from expected distance

A graph is plotted with distance number to the hole-hole distance values obtained from program at various heights along with distance number to its deviation from expected distance(=35mm) which is depicted in figures 5 (c, d).

Test3: Ovality Inspection of holes in full Plate at different heights

The ovality of circle infers us how round the object is. For ideal case the ovality of perfect circle is 1, in practice it ranges in [0.95 1], the ovality of holes in full plate for ideal case and when captured at 3000mm height is shown in figures 6 (a, b).

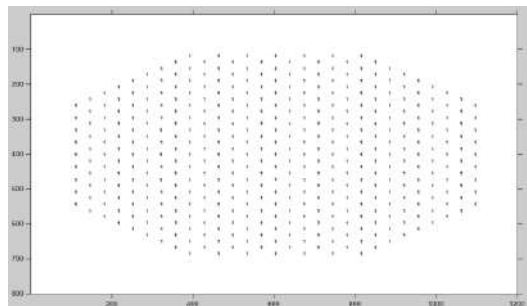


Figure 6 (a): Ovality of holes obtained from program for actual plate

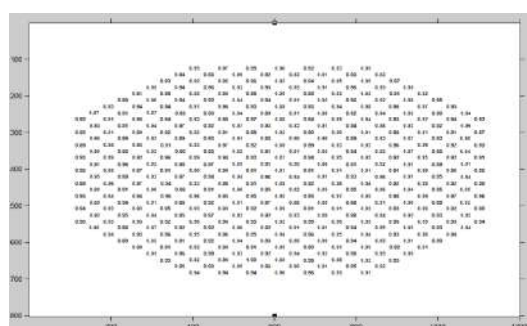


Figure 6 (b): Ovality values of holes obtained from program at 3000mm height

A graph is plotted with hole number to its ovality values obtained from program at various heights along with hole number to its deviation from expected ovality which is depicted in figures 6 (c,d).

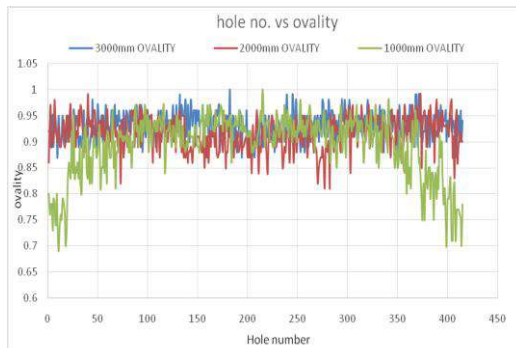


Figure 6 (c): Hole number vs. Obtained ovality

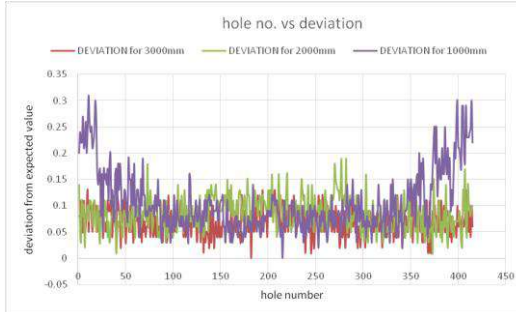


Figure 6 (d): Hole number vs. Deviation from expected ovality

From the Diameter, Centroid for distances between vertical holes, Ovality inspections, the results obtained by capturing the plate at 3000mm are satisfactory and in tolerable deviations when compared to the remaining heights of capturing full plate. We can't increase the camera height beyond 3000mm as 3000mm is maximum permissible height for capturing the full plate.

Inspections of plate as various Sections at 3000mm height

As per the requirement all the holes in plate should exhibit 25 pixels as diameter which is not satisfying with the complete plate (maximum section) by capturing at 3000mm height. The tube sheet / baffle plate on which lines are drawn with specific colors as shown in figure 7 depicts sections of plate

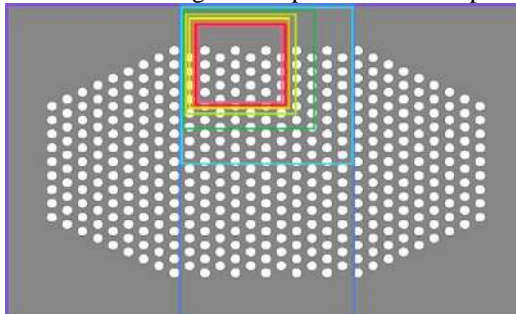


Figure 7: various sections in plate

Table 1: Color identity for various sections with % of holes showing 25mm

Sl no.	color	Dimension of section(mm)	Area section(mm ²)	of % of holes exhibiting 25pixels as diameter
1	Violet	800*1200	960000	5.9
2	Indigo	800*400	320000	6.8
3	Blue	400*400	160000	8.0
4	Green	300*300	90000	23.0
5	Yellow green	250*250	62500	29.0
6	Yellow	225*225	50625	73.0
7	orange	220*220	48400	80.0
8	Red	210*210	44100	100.0

diameter Analyzing the maximum section in to subsections the count of holes having 22 pixels diameter vanishes gradually. By further visualizing in to subsections the count of holes showing 25 pixels as diameter increases and there by 23, 24 pixels hole diameter disappears slowly. The observation of section dimensions (area) to the percentage of holes displaying 25 pixels diameter is depicted in table. By investigations, it is observed that the maximum section dimensions needed for all the holes to exhibit 25 pixels diameter is 210*210 for camera taken at 3000mm height where the lens of camera focuses on center of section. Extraction of 210*210 sections is shown in figure 8.

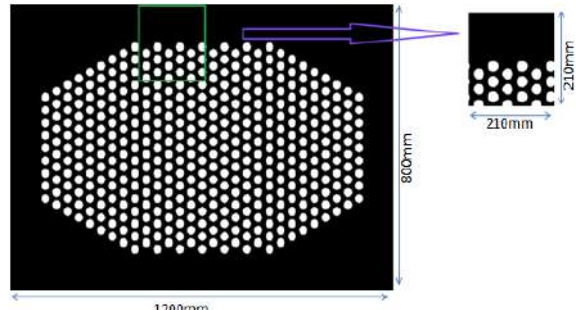


Figure 8: Extracting a 210*210 section from plate

Section appearance and diameter values at 3000mm height are depicted in figure 9(a, b).

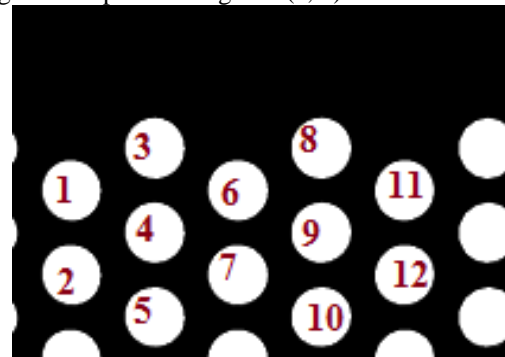


Figure 9 (a): Top view and numbering of section in plate captured at 3000mm height

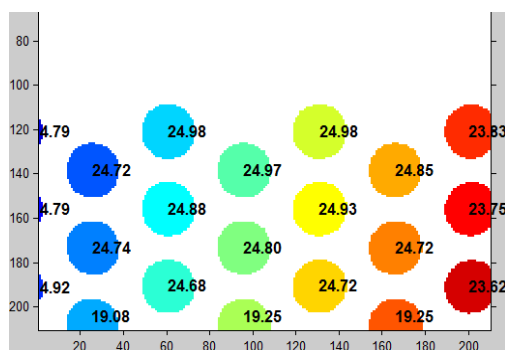


Figure 9 (b): Diameter of holes in a section of plate captured at 3000mm height

A graph is depicted with the Hole number to its deviation from actual diameter ($=25\text{mm}$) which is shown in figure 9(c)

Hence it is observed that 3rd and 8th hole have a diameter of 24.98mm (pixels) from actual value of 25mm (pixels), with deviation of 0.02mm . It requires 24 camera shots for capturing all the sections of plate, which gives full plate analyses.

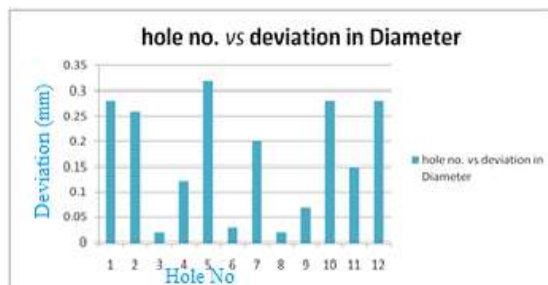


Figure 9 (c): Hole number vs. deviation in diameter in section

V. CONCLUSION

The Proposed method is envisaged to develop and automate a process for drilled hole inspection in large rectangular plate through Image processing technique. The algorithms developed have been applied for detecting holes and inspecting its parameters like area, diameter, centroid, perimeter, ovality when captured at different heights on a tube sheet / baffle plate of size $1200\text{mm} \times 800\text{mm}$, that has been designed using NX-UG (CAD tool). A deviation report has been prepared with expected parameters to the calculated parameters captured at various heights. From the observations, it is noted that when the plate is captured at 3000mm height in NX, holes in a section of $210\text{mm} \times 210\text{mm}$ of the plate are exhibiting maximum deviation of diameter as 0.2mm , which is good consideration. The significance of the end result depicts a considerable reduction in time for inspection of one work piece by automatic programming, elimination of the manual handling, improving the

quality, increasing the productivity, eliminating rework at site.

Further, the developed process and algorithms needs to be applied on real time plate images captured using an MP camera. A lot of filtering process such as adaptive filters or Sobel filters will be required for real time images prior to apply the developed algorithms.

REFERENCES & BIBLIOGRAPHY

- [1] Ismailibrahim1,Syedabdulrahmansyedabubakar2 ,usamohdmokji3, Jameelabdullaahmedmukred4, Zulkiflimdyusof5, Zuwaarie Ibrahim6, "A Printed circuit board Inspection system with defect classification capability" , International Journal of Innovative Management, Information & Production, Volume 3, Number 1, March 2012.
- [2] Tefanoprea 1, Joan lita 2, Ion BogdanCioc 3, Daniel AlexandruViUan 4, "Determination of Misplaced drill holes on a PCB", Electronics, Communications and Computers Department, University of Pitesti Str. Targul din Vale, Nr. 1, Pite,ti, ROMANIA.
- [3] Avadhoot R. Telepatil 1, Shrinivas A.Patil 2, "Parameter Estimation of Metal blooms using Image processing techniques", International Journal Of Innovative Research In Science, Engineering and Technology(ISO 3297: 2007 Certified Organization)Vol. 2, Issue 8, August 2013.
- [4] S.Sivasankar1, R.Jeyapaul2, S.Kolappan3, N.Mohamed Shaahid4, "Procedural Study For roughness, Roundness and waviness Measurement Of EDM Drilled Holes Using Image processing Technology", Computer modeling And New Technologies, 2012, Vol.16, No.1, 49–63.
- [5] Label- <http://in.mathworks.com/help/images/labeling-and-measuring-objects-in-a-binary-image.html/>
- [6] R.C.Gonzalez1, R.E.Woods2 "Digital Image Processing" TMH 3rd edition
- [7] Raman Maini1, Dr. HimanshuAggarwal2, "Study and Comparison of Various Image Edge Detection Techniques", International Journal of Image Processing (IJIP), Volume (3): Issue (1).
- [8] Ming C Leu, Albin Thomas, Krishna Kolan "NX 9.0 for Engineering Design" Department of Mechanical and Aerospace Engineering, Missouri university of science & technology

BIOGRAPHY

Deepak Sachan received the B.Tech. Hons. Degree in ECE from Madam Mohan Malviya Technical University, Gorakhpur in 2009. He has 7 years of experience in automation area. Since 2010, he is working in Research and Development division of Bharat Heavy Electricals Limited, a Maharatna PSU of India. He is working in Technology and Development Lab of BHEL R&D and his main areas of research are Robotic applications, manufacturing automation, image processing, inspection technologies, software development and various new technologies like 3D



printing, RFID, GPS based vehicle tracking system etc.

A Sainath Chaithanya completed B.Tech in ECE from Geethanjali College of engineering & technology, R. R. Dist., Telangana,. Completed M.Tech in VLSI System design from Anurag group of institutions (formerly CVSR college of engineering) an autonomous institution of JNTU Hyderabad, Telangana,. Currently working as Asst. Prof in Dept of ECE in RGUKT, Basar. His interesting fields include VLSI- physical and logical designs, embedded systems, digital system design, Image processing.



Deepak Sachan " Image Processing Technique for Drilled Holes Inspection in Large Rectangular Plate " International Journal of Engineering Research and Applications (IJERA) , vol. 8, no. 03, 2018, pp. 21-27

Metadata of the chapter that will be visualized in SpringerLink

Book Title	Proceedings of 2nd International Conference on Computer Vision & Image Processing	
Series Title		
Chapter Title	A Novel Method for Logo Detection Based on Curvelet Transform Using GLCM Features	
Copyright Year	2018	
Copyright HolderName	Springer Nature Singapore Pte Ltd.	
Corresponding Author	Family Name Particle Given Name Prefix Suffix Division Organization Address Email	Naganjaneyulu 
Author	Family Name Particle Given Name Prefix Suffix Division Organization Address Email	Krishna 
Author	Family Name Particle Given Name Prefix Suffix Division Organization Address Email	A. V. 
Abstract	Automatic logo detection is a key tool for document retrieval, document recognition, document classification, and authentication. It helps in office automation as it enables the effective identification of source of a document. In this paper, a novel approach for logo detection using curvelet transform is proposed. The curvelet transform is employed for logo detection because of its ability to represent curved singularities efficiently when compared to wavelet and ridgelet transforms. The proposed algorithm consists of five steps, namely segmentation, noncandidate elimination, computation of curvelet coefficients, gray level co-occurrence matrix (GLCM) features extraction, followed by classification using a pretrained support vector machine classifier. The proposed algorithm is tested on a standard dataset, and the performance is compared with the state-of-the-art methods. The results show good improvement in the accuracy when compared with the competitors.	

Keywords
(separated by ',')

Logo detection - Curvelet transform - GLCM features

A Novel Method for Logo Detection Based on Curvelet Transform Using GLCM Features

G. V. S. S. K. R. Naganjaneyulu, Ch Sai Krishna and A. V. Narasimhadhan

Abstract Automatic logo detection is a key tool for document retrieval, document recognition, document classification, and authentication. It helps in office automation as it enables the effective identification of source of a document. In this paper, a novel approach for logo detection using curvelet transform is proposed. The curvelet transform is employed for logo detection because of its ability to represent curved singularities efficiently when compared to wavelet and ridgelet transforms. The proposed algorithm consists of five steps, namely segmentation, noncandidate elimination, computation of curvelet coefficients, gray level co-occurrence matrix (GLCM) features extraction, followed by classification using a pretrained support vector machine classifier. The proposed algorithm is tested on a standard dataset, and the performance is compared with the state-of-the-art methods. The results show good improvement in the accuracy when compared with the competitors.

Keywords Logo detection · Curvelet transform · GLCM features

1 Introduction

The detection of logo can be considered as an important clue for document image analysis and retrieval. Logos are special visual objects that are commonly used in business and government documents as a declaration of document source and ownership. Logos are generally used to aid and promote instant public recognition for an organization. The document retrieval is easier using logo recognition than a keyword search. Methods for document retrieval using logo detection are presented in [12, 18, 29, 37]. A method for categorization of documents based on logo detection is described in [26].

G. V. S. S. K. R. Naganjaneyulu (✉) · A. V. Narasimhadhan
National Institute of Technology Karnataka, Surathkal, India
e-mail: snd.786@gmail.com

C. S. Krishna
Rajiv Gandhi University of Knowledge Technologies, Krishna, Nuzvid, India



Many algorithms have been developed by several researchers for logo detection and recognition. A brief literature review is presented in Table 1. These methods are broadly categorized into three types, namely heuristic methods [16, 21, 27, 31, 32], spatial density-based methods [2, 25, 28], and multi-resolution methods [36].

1.1 Heuristic Methods

Seiden et al. [27] used the top-down X-Y cut segmentation algorithm to analyze a binary document to extract 16 features from each connected component, and a rule-based classifier for classification of the logos. Wang et al. [32] extracted all feature rectangles from the entire document to detect the logos. A feature rectangle is a minimum virtual rectangle which fully embraces at least one foreground pixel and their edges have all background pixels. Once all the feature rectangles are extracted from whole document image, classification is performed using a decision tree classifier.

1.2 Spatial Density-Based Methods

Pham [25] and Ahmed [2] proposed logo detection methods that are based on spatial density of foreground pixels within a given window. The fundamental assumption in these methods is that the spatial density related to logo regions is greater than that of non-logo regions. The preprocessing steps are followed by the estimation of spatial density using mountain function [33], and classification is performed using a decision tree classifier.

1.3 Multi-resolution Analysis-Based Methods

Shirdhonkar et al. [28] used discrete wavelet transform (DWT) [24] to calculate spatial density. The document image is divided into different nonoverlapping blocks of fixed size. The DWT coefficients of these blocks of the document image are computed. Using the DWT coefficients, two features namely energy and standard deviation of each window from all the sub-bands are computed to differentiate logo and non-logo blocks in the document image. In [28], author made an assumption that the complete logo is present in a single block. A segmentation step can be used to avoid such an assumption. The DWT coefficients can represent point singularities effectively, but fails to represent curve singularities. Ridgelet transform [6, 10] can represent line singularities; however, it also fails in representing curve singularities. Curvelet transform can represent the curved singularities in a better way when compared to wavelets and ridgelets [7, 22, 23, 30]. The logos generally contain curve singularities, and therefore curvelet transform is a good choice for detection of logos.

Table 1 Literature review of logo detection methods

Papers	Key features of algorithm
Hassanzadeh et al. [16]	Morphological operations, decision tree classifier, and merging separated parts in logo
Shirdhonkar et al. [28]	Discrete wavelet transform, spatial density using two features—mean and variance
Wang [31]	RAG data structure and Bayesian modeling
Li et al. [21]	Axial lines, shape descriptors
Wang et al. [32]	Feature rectangles
Ahmed et al. [2]	Colorimetric uniformity and spatial compactness using mountain function
Zhu et al. [36]	Multi-scale approach
Pham [25]	Mountain function
Seiden et al. [27]	X-Y cut segmentation, rule-based classifier
Doermann et al. [11]	Geometric invariants

On the other hand, in literature, an approach with two features and a decision tree-based classifier for logo detection is typically used. Usage of more number of features and a sophisticated classifier like support vector machine classifier (SVM) [8] can produce a better accuracy. In this work, logo detection is performed by means of segmentation, noncandidate elimination, computation of GLCM features from each sub-band of curvelet coefficients, followed by classification using SVM classifier.

The organization of the paper is as follows. In Sect. 2- theory related to the methods employed is presented. In Sect. 3, a brief description of the different blocks is provided. In Sect. 4, the performance analysis of the proposed method and comparison with the state of the art are analyzed, followed by conclusion in Sect. 5.

AQ4

2 Theory

2.1 Fast Discrete Curvelet Transform

Curvelet transform [5] is a nonadaptive approach of representing images at multiple scales and multiple angles. It is a higher dimensional generalization of the wavelet transform and overcomes the limitation of wavelets in terms of representing curved singularities.

In the proposed method, fast discrete curvelet transform (FDCT) [4] is employed. The FDCT of an image is defined as,

AQ5

$$c(j, \mathbf{k}, l) = \sum_{n_1, n_2 \in P_j} \hat{f}[n_1, n_2 - n_1 \tan \theta_l] \tilde{U}_j[n_1, n_2] e^{i2\pi(\frac{k_1 n_1}{L_{1,j}} + \frac{k_2 n_2}{L_{2,j}})}. \quad (1)$$



75 where $c(j, \mathbf{k}, l)$ is representing discrete curvelet coefficient at scale 2^j , location
 76 $\mathbf{k} = [k_1 \ k_2]$, angle θ_l and U_j (with length $L_{1,j}$ and width $L_{2,j}$)
 77 Cartesian (rectangular) generalization of the polar (circular) window that isolates the digital fre-
 78 quencies $[n_1, n_2]$ at the wedges, $\theta_l = 2\pi 2^{\lfloor \frac{j}{2} \rfloor} l$, $l = 0, 1, 2, \dots$ and $P_j = \{(n_1, n_2) :
 79 n_{1,0} \leq n_1 \leq n_{1,0} + L_{1,j}, n_{2,0} \leq n_2 \leq n_{2,0} + L_{2,j}\}$. The curvelet transform is used in
 80 texture analysis in [3].

81 2.2 GLCM Features

82 The GLCM is a tool to measure texture as it represents the distribution of the co-
 83 occurring values in an image. The texture features generated and used are Haralick
 84 features [15]. GLCM is a matrix in which the number of rows and columns
 85 is equal to the number of gray levels G in the image. The GLCM matrix element
 86 $P(i, j | \Delta x, \Delta y)$ is the relative frequency with which two pixels, separated by a pixel
 87 distance $(\Delta x, \Delta y)$, occur within a given neighborhood. Given an image I of size
 88 $N \times N$, the element of in i th, j th column of normalized GLCM matrix P can be
 89 defined as,

$$90 P(i, j) = \sum_{x=1}^N \sum_{y=1}^N \delta(I(x, y) - i) \delta(I(x + \Delta x, y + \Delta y) - j) \quad (2)$$

91 where $\delta(\cdot)$ is impulse function. Let us assume that μ is the mean value of P , and $\mu_x,
 92 \mu_y, \sigma_x, \sigma_y$ are the means and standard deviations of the marginal densities P_x, P_y .
 93 The marginal densities P_x and P_y are related to $P(i, j)$ as follows.

$$94 P_x(i) = \sum_{j=1}^G P(i, j), P_y(j) = \sum_{i=1}^G P(i, j) \quad (3)$$

95 The expressions for $P_{x+y}(k)$ and $P_{x-y}(k)$ are given below.

$$96 P_{x+y}(k) = \sum_{i=1}^G \sum_{j=1}^G P(i, j)_{i+j=k}; k = 2, 3, \dots, 2N \quad (4)$$

$$97 P_{x-y}(k) = \sum_{i=1}^G \sum_{j=1}^G P(i, j)_{|i-j|=k}; k = 0, 1, \dots, N-1 \quad (5)$$

99 The 12 GLCM features used in this work are defined in Table 2. Angular second
 100 moment gives the homogeneity in the image. Contrast provides an insight into the
 101 local gray level variation in image, while inverse difference moment gives the sim-
 102 ilarity among nonzero entries in the image. The correlation represents gray value

Table 2 Definition of 12 features extracted from GLCM matrix

Angular second moment	$\sum_{i=0}^{G-1} \sum_{j=0}^{G-1} \{P(i, j)\}^2$
Contrast	$\sum_{n=0}^{G-1} n^2 (\sum_{i=1}^G \sum_{j=1}^G i-j =n P(i, j))$
Correlation	$\sum_{i=0}^{G-1} \sum_{j=0}^{G-1} \frac{(i \times j) \times P(i, j) - (\mu_x \times \mu_y)}{\sigma_x \times \sigma_y}$
Variance	$\sum_{i=0}^{G-1} \sum_{j=0}^{G-1} (i - \mu)^2 P(i, j)$
Inverse difference moment	$\sum_{i=0}^{G-1} \sum_{j=0}^{G-1} \frac{1}{1+(i-j)^2} P(i, j)$
Entropy	$-\sum_{i=0}^{G-1} \sum_{j=0}^{G-1} P(i, j) \times \log(P(i, j))$
Average	$\sum_G^{2G-2} i P_{x+y}(i)$
Sum entropy	$-\sum_{i=0}^{2G-2} P_{x+y}(i) \log(P_{x+y}(i))$
Difference entropy	$-\sum_{i=0}^{G-1} P_{x-y}(i) \log(P_{x-y}(i))$
Inertia	$\sum_{i=0}^{G-1} \sum_{j=0}^{G-1} (i - j)^2 \times P(i, j)$
Shade	$\sum_{i=0}^{G-1} \sum_{j=0}^{G-1} (i + j - \mu_x - \mu_y)^3 \times P(i, j)$
Prominance	$\sum_{i=0}^{G-1} \sum_{j=0}^{G-1} (i + j - \mu_x - \mu_y)^4 \times P(i, j)$

linear dependencies in the image. Entropies give the statistical disorderliness in the image. The average and variance represent the central tendency and the spread in GLCM matrix (not of the image). Inertia, cluster prominence, and shade are higher order statistic related to texture. The GLCM features are used in various applications involving texture classification in [17, 35]. GLCM features are also used along with multi-scale transforms in [13, 34].

3 Description of the Algorithm

The block diagram of the proposed method is shown in Fig. 1. The proposed algorithm initially performs segmentation, using morphological operations [14] and connected component analysis (CCA) [9]. The improbable logo candidates are removed based on heuristic features in noncandidate elimination phase. Curvelet coefficients of the remaining logo candidates are obtained using FDCT. Subsequently, 12 features are computed from GLCM matrix obtained from each wedge of curvelet coefficients that are extracted in eight different directions in order to obtain the texture clues in all the directions. A pretrained SVM classifier is used for removal of false logo blocks using the GLCM features. The detailed explanation of each stage is discussed in the following subsections.

**Fig. 1** Block diagram of the proposed method

120 3.1 Segmentation

121 Segmentation is the foremost step in logo detection. The inclusion of segmentation
122 may increase the computational complexity; nevertheless, it gives an advantage of
123 avoiding the assumption that the logo has to be in a single block under consideration,
124 as mentioned in [28]. The proposed scheme employs a segmentation algorithm which
125 is based on connected components analysis. In a document image, a segment is a
126 portion which has all connected components near to each other. Hence, connecting
127 the nearest connected components for clubbing them together to make a segment is
128 achieved by applying morphological operations. A morphological dilation operation
129 with a rectangular structuring element of size 15×90 is performed on the com-
130 plement of the input binary image. This dilation operation is followed by a closing
131 operation with the same structuring element in order to connect the similar patterns
132 in the image. CCA is performed on the resulting image from the morphological
133 operations to find the coordinates of all possible bounding boxes. A typical output
134 of segmentation is shown in Fig. 2.

135 3.2 Noncandidate Elimination

136 The purpose of this step is to remove obvious non-logo candidates in order to reduce
137 the load on classifier and computational complexity. Out of all the blocks obtained
138 from CCA, the obvious false positives are removed using two heuristic clues, namely
139 aspect ratio and foreground pixel density. The connected components with aspect
140 ratio less than 3 and foreground pixel density greater than 70% are considered as logo
141 candidates. These thresholds are obtained by computing the values of aspect ratio and
142 spatial density of 100 logo objects. All probable logo candidates from segmentation
143 step are first filtered with the aspect ratio criteria, and those do not satisfy the criteria
144 are identified as non-logo candidates. The remaining probable logo candidates are
145 further refined using the foreground pixel density criteria. Using the aspect ratio, clue
146 large paragraphs containing text are removed, and using foreground density, criteria
147 typically headings are eliminated as non-logo objects. The remaining possible logo
148 candidates after the removal of non-logo candidates by enforcing the aforementioned
149 constraints are considered for further processing.

150 3.3 FDCT

151 For all the possible logo candidates, FDCT is calculated with number of scales equal
152 to 4. The number of scales is chosen as 4 by trial and error procedure. The computation
153 of FDCT is performed using the non-equispaced FFT method proposed in [4]. Total
154 number of wedges resulting from the computation of FDCT in this work is 130.

Fig. 2 Example image and its segmented blocks

HARVARD MEDICAL SCHOOL

BEW-IN-PRINT

Rafi S. Geha, M.D.
Prince Turki bin Abdul Aziz Al-Saud
Professor of Pediatrics
Harvard Medical School
Chair, Division of Immunology
Children's Hospital



Children's Hospital
300 Longwood Avenue
Boston, Massachusetts 02115-5342
Telephone: (617) 734-7602
Fax: (617) 735-8295

April 27, 1993

James F. Glenn, M.D.
Chairman of the Board
Chief Executive Officer
The Council for Tobacco Research- U.S.A., Inc.
900 Third Avenue
New York, NY 10022

Dear Dr. Glenn:

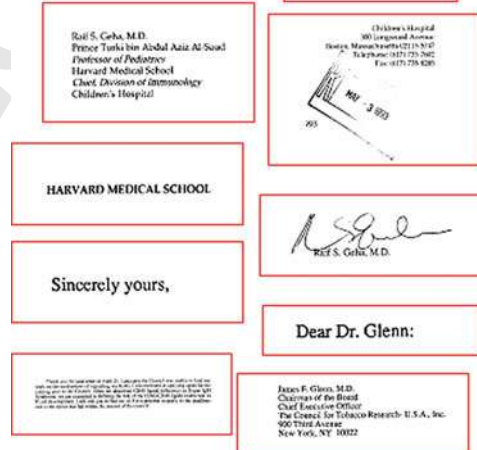
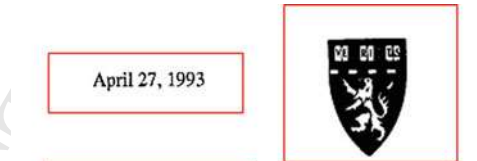
Thank you for your letter of April 21. I am sorry the Council was unable to find our work on the mechanisms of signaling via Fc γ R. I am interested in applying again for the coming year to the Council. Since we described CD40 ligand deficiency in Hyper IgM Syndrome, we are interested in defining the role of the CD40-CD40 ligand interaction in B cell development. I will call you to find out a) if it is possible to apply, b) the deadlines and c) the topics that fall within the interest of the council.

Sincerely yours,

Rafi S. Geha, M.D.

/mz

(a) Input image



(b) Corresponding output blocks of segmentation



155 **3.4 GLCM Features**

156 Texture in logos is an important clue as logos generally contain patterns inside them
 157 along with the text. The GLCM features along with the curvelet coefficients are
 158 used to extract the textural clues in the logos. In the proposed scheme, 12 features
 159 mentioned in Table 2 are extracted from each wedge of FDCT obtained from the
 160 previous step. A total  30 wedges, 8 directions, and 12 features results in 12, 480
 161 features per each block are computed as a part of feature extraction and used for
 162 training a SVM classifier.

163 **3.5 SVM Classifier**

164 A pretrained SVM classifier [8] is used to separate logo candidates from all the
 165 possible logo candidates. SVM classifier is a supervised binary classifier based on
 166 linear discriminants. It considers the extreme data samples near the boundary called
 167 support vectors and maximizes the margin between the classes. In nonlinear boundary
 168 case where it is not a linearly separable problem, SVM treats the nonlinear function as
 169 a linear function by projecting the data into a higher dimensional case. SVM provides
 170 an optimal decision for binary classification problem and is chosen for the binary
 171 classification problem of logo objects. In this work, 20 logos and 200 non-logos are
 172 used for training the SVM classifier with linear kernel which outputs the true logo
 173 objects.

174 **4 Experiments and Results**

175 The proposed method is tested on Tobacco-800 dataset¹ [1, 19, 20] which is com-
 176 posed of 1151 binary images. Tobacco 800 is a public dataset which is a part of IIT
 177 CDIP dataset that contains about 42 million document images collected from UCSF.
 178 This dataset is widely used by many researchers [2, 16, 25, 28, 36] for testing the
 179 logo detection methods. A total of 20 logo candidates and 200 non-logo candidates
 180  are used for training and the remaining for testing. Performance of the proposed work
 181 is evaluated using below performance metrics.

182
$$Accuracy = \frac{TP}{TP + TN} \quad (6)$$

183
$$Precision = \frac{TP}{TP + FP} \quad (7)$$

¹The database is available at <http://www.umiacs.umd.edu/~zhugy/tobacco800.html>.

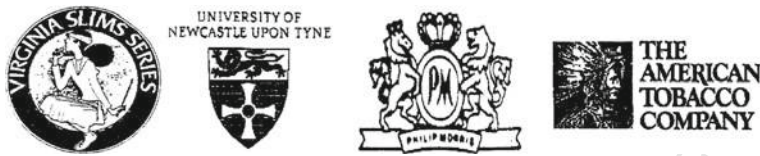


Fig. 3 Examples of logos detected (true positives)

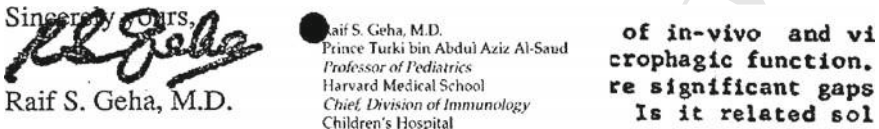


Fig. 4 Examples of non-logos detected as logos (false positives)

Table 3 Results of algorithm

Category	Logos	Non-logos
Training	20	200
Correctly classified	66	1747
Miss classified	6	29
Total	92	1976

184 where

185 TP: True positives (Total number of correctly detected logos)

186 TN: True negatives (Number of non-detected logos)

187 FP: False positives (Not a logo but algorithm detected it as logo)

188 FN: False negatives (Not a logo and the algorithm detected as non-logo).

189 Some of the correctly detected logos are shown in Fig. 3, and false positives are
190 shown in Fig. 4.

191 The proposed algorithm gives an accuracy of 91.47% and precision of 98.1%. The
192 results obtained using the proposed method are presented in Table 3. From Fig. 3, it
193 can be seen that if there is a text block associated with the logo, the proposed method
194 is able to obtain the logo completely along with the text part, which is an advantage.
195 Figure 4 shows typical false positives, and most of the times they are cluttered text
196 regions which almost look like a logo. The accuracy obtained using the proposed
197 method is compared with the state-of-the-art algorithms and is given in Fig. 5. It can
198 be observed that the proposed algorithm outperforms the other methods in terms of
199 accuracy of detection of logos. The significant improvement in the accuracy can be
200 attributed to the ability of curvelet transform in representing the curve discontinuities.
201 The inclusion of segmentation in proposed method removes the assumption that
202 entire logo needs to be in a single block which is fed to the classifier. However, the
203 computational complexity increases because of inclusion of segmentation involving
204 morphological operations.

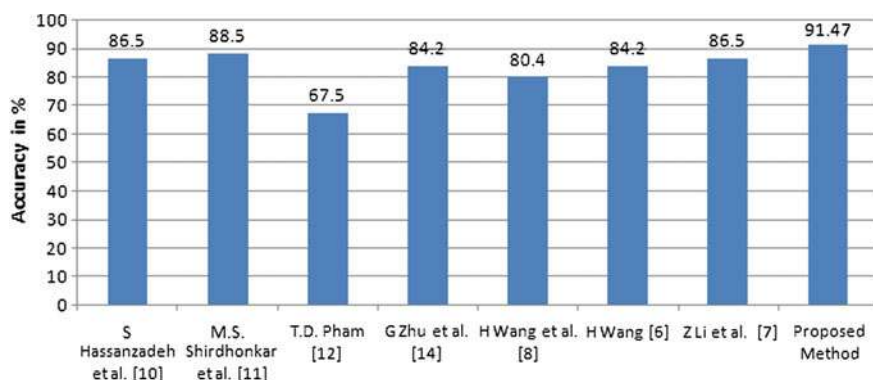


Fig. 5 Comparison of accuracies of different algorithms for logo detection

205 5 Conclusion

206 In this work, a novel approach for logo detection using curvelet transform has been
 207 proposed. The proposed algorithm gives an accuracy of 91.47% with a precision of
 208 98.1%. It has been observed that the accuracy of the proposed algorithm is better than
 209 the other competitors with a competitive precision. The inclusion of segmentation
 210 automated the process of selection of the probable logo candidates. Consequently,
 211 the proposed method has removed the assumption that the logo must be in a single
 212 block that is sent to the classifier which is a drawback in other methods. A better
 213 precision has been obtained because of the noncandidate elimination. The algorithm
 214 is able to include the text part near to the logo, which is an advantage.

215 References

- 216 1. Agam, G., Argamon, S., Frieder, O., Grossman, D., Lewis, D.: The Complex Document Image
 217 Processing (CDIP) Test Collection Project. Illinois Institute of Technology (2006), <http://ir.iit.edu/projects/CDIP.html>
- 218 2. Ahmed, Z., Fella, H.: Logos extraction on picture documents using shape and color density. In:
 219 ISIE IEEE International Symposium on Industrial Electronics, pp. 2492–2496. IEEE (2008)
- 220 3. Arivazhagan, S., Ganesan, L., Kumar, S.T.: Texture classification using curvelet statistical and
 221 co-occurrence features. In: 18th International Conference on Pattern Recognition, ICPR, vol. 2,
 222 pp. 938–941. IEEE (2006)
- 223 4. Candes, E., Demanet, L., Donoho, D., Ying, L.: Fast discrete curvelet transforms. Multiscale
 224 Modeling & Simulation 5(3), 861–899 (2006)
- 225 5. Candes, E.J., Donoho, D.L.: Curvelets: A surprisingly effective nonadaptive representation for
 226 objects with edges. FPO AE 09499-0039 (1999)
- 227 6. Candès, E.J., Donoho, D.L.: Ridgelets: A key to higher-dimensional intermittency? Philosophical
 228 Transactions of the Royal Society of London A: Mathematical, Physical and Engineering Sciences
 229 357(1760), 2495–2509 (1999)

- 231 7. Candes, E.J., Donoho, D.L.: Curvelets: A surprisingly effective nonadaptive representation for
232 objects with edges. Tech. rep., DTIC Document (2000)
- 233 8. Cortes, C., Vapnik, V.: Support-vector networks. Machine learning 20(3), 273–297 (1995)
- 234 9. Dillencourt, M.B., Samet, H., Tamminen, M.: A general approach to connected-component
235 labeling for arbitrary image representations. Journal of the ACM (JACM) 39(2), 253–280
236 (1992)
- 237 10. Do, M.N., Vetterli, M.: The finite ridgelet transform for image representation. IEEE Transac-
238 tions on Image Processing 12(1), 16–28 (2003)
- 239 11. Doermann, D.S., Rivlin, E., Weiss, I.: Logo recognition using geometric invariants. In: Pro-
240 ceedings of the Second International Conference on Document Analysis and Recognition, pp.
241 894–897. IEEE (1993)
- 242 12. Folkers, A., Samet, H.: Content-based image retrieval using fourier descriptors on a logo
243 database. In: Proceedings, 16th International Conference on Pattern Recognition, vol. 3, pp.
244 521–524 (2002)
- 245 13. Francis, S.V., Sasikala, M., Saranya, S.: Detection of breast abnormality from thermograms
246 using curvelet transform based feature extraction. Journal of medical systems 38(4), 1–9 (2014)
- 247 14. Gonzalez, R.C., et al.: Re woods, digital image processing. Addison–Wesely Publishing Com-
248 pany (1992)
- 249 15. Haralick, R.M.: Statistical and structural approaches to texture. Proceedings of the IEEE 67(5),
250 786–804 (1979)
- 251 16. Hassanzadeh, S., Pourghassem, H.: Fast logo detection based on morphological features in
252 document images. In: IEEE 7th International Colloquium on Signal Processing and its Appli-
253 cations (CSPA), pp. 283–286. IEEE (2011)
- 254 17. Jafarpour, S., Sedghi, Z., Amirani, M.C.: A robust brain mri classification with glcm features.
255 International Journal of Computer Applications 37(12), 1–5 (2012)
- 256 18. Jain, R., Doermann, D.: Logo retrieval in document images. In: Document Analysis Systems
257 (2012)
- 258 19. Legacy: The Legacy Tobacco Document Library (LTDL). University of California, San Fran-
259 cisco (2007), <http://legacy.library.ucsf.edu/>
- 260 20. Lewis, D., Agam, G., Argamon, S., Frieder, O., Grossman, D., Heard, J.: Building a test
261 collection for complex document information processing. In: Proc. 29th Annual Int. ACM
262 SIGIR Conference, pp. 665–666 (2006)
- 263 21. Li, Z., Schulte-Austum, M., Neschen, M.: Fast logo detection and recognition in document
264 images. In: 20th International Conference on Pattern Recognition (ICPR), pp. 2716–2719.
265 IEEE (2010)
- 266 22. Ma, J., Plonka, G.: The curvelet transform. Signal Processing Magazine, IEEE 27(2), 118–133
267 (2010)
- 268 23. Ma, J., Plonka, G.: A review of curvelets and recent applications. IEEE Signal Processing
269 Magazine 27(2), 118–133 (2010)
- 270 24. Mallat, S., Zhong, S.: Characterization of signals from multiscale edges. IEEE Transactions
271 on Pattern Analysis & Machine Intelligence (7), 710–732 (1992)
- 272 25. Pham, T.D.: Unconstrained logo detection in document images. Pattern recognition 36(12),
273 3023–3025 (2003)
- 274 26. Rusinol, M., Lladós, J.: Logo spotting by a bag-of-words approach for document categorization.
275 In: 10th International Conference on Document Analysis and Recognition, ICDAR, pp. 111–
276 115. IEEE (2009)
- 277 27. Seiden, S., Dillencourt, M., Irani, S., Borrey, R., Murphy, T.: Logo detection in document
278 images. In: Proceedings of the International Conference on Imaging Science, Systems, and
279 Technology, pp. 446–449 (1997)
- 280 28. Shirdhonkar, M., Kokare, M.: Automatic logo detection in document images. In: IEEE Interna-
281 tional Conference on Computational Intelligence and Computing Research (ICCIC), pp. 1–3.
282 IEEE (2010)
- 283 29. Shirdhonkar, M., Kokare, M.B.: Automatic logo based document image retrieval. International
284 Journal of Knowledge-based and Intelligent Engineering Systems 19(1), 27–33 (2015)

- 285 30. Starck, J.L., Candes, E., Donoho, D.: The curvelet transform for image denoising. *IEEE Transactions on Image Processing*, 11(6), 670–684 (Jun 2002)
- 286 31. Wang, H.: Document logo detection and recognition using bayesian model. In: 20th International Conference on Pattern Recognition (ICPR), pp. 1961–1964. IEEE (2010)
- 287 32. Wang, H., Chen, Y.: Logo detection in document images based on boundary extension of feature rectangles. In: 10th International Conference on, Document Analysis and Recognition, ICDAR, pp. 1335–1339. IEEE (2009)
- 288 33. Yager, R.R., Filev, D.P.: Approximate clustering via the mountain method. *IEEE Transactions on Systems, Man and Cybernetics* 24(8), 1279–1284 (1994)
- 289 34. Youssef, S.M.: Ictedct-cbir: Integrating curvelet transform with enhanced dominant colors extraction and texture analysis for efficient content-based image retrieval. *Computers & Electrical Engineering* 38(5), 1358–1376 (2012)
- 290 35. Zhang, J., Tong, L., Wang, L., Li, N.: Texture analysis of multiple sclerosis: a comparative study. *Magnetic resonance imaging* 26(8), 1160–1166 (2008)
- 291 36. Zhu, G., Doermann, D.: Automatic document logo detection. In: Ninth International Conference on Document Analysis and Recognition, ICDAR, vol. 2, pp. 864–868. IEEE (2007)
- 292 37. Zhu, G., Doermann, D.: Logo matching for document image retrieval. In: 10th International Conference on Document Analysis and Recognition, ICDAR, pp. 606–610. IEEE (2009)

Author Queries

Chapter 1

Query Refs.	Details Required	Author's response
AQ1	Please confirm if the corresponding author is correctly identified. Amend if necessary.	
AQ2	Please check and confirm if the author names and initials are correct.	
AQ3	Please confirm if the inserted city name in "Affiliation 2" is correct. Amend if necessary.	
AQ4	Kindly note that the references "Liet et al." has been changed to "Li et al." so that the citation matches the list.	
AQ5	The sentence "The FDCT of an image..." is missing a closing parenthesis. Please check.	
AQ6	Please check and approve the edit in the sentence "The marginal densities...".	
AQ7	Please check and approve the edit made in the sentence "A total of...a SVM classifier".	
AQ8	Please check and approve the edit made in the sentence "A total of...remaining for testing".	

MARKED PROOF

Please correct and return this set

Please use the proof correction marks shown below for all alterations and corrections. If you wish to return your proof by fax you should ensure that all amendments are written clearly in dark ink and are made well within the page margins.

Instruction to printer	Textual mark	Marginal mark
Leave unchanged	... under matter to remain	①
Insert in text the matter indicated in the margin	↗	New matter followed by ↗ or ↗②
Delete	/ through single character, rule or underline — through all characters to be deleted	↙ or ↙②
Substitute character or substitute part of one or more word(s)	/ through letter or — through characters	new character / or new characters /
Change to italics	— under matter to be changed	←
Change to capitals	== under matter to be changed	≡
Change to small capitals	= under matter to be changed	=
Change to bold type	~ under matter to be changed	~
Change to bold italic	~~ under matter to be changed	~~
Change to lower case	Encircle matter to be changed	≡
Change italic to upright type	(As above)	+
Change bold to non-bold type	(As above)	+
Insert 'superior' character	/ through character or ↗ where required	Y or X under character e.g. ȝ or ȝ
Insert 'inferior' character	(As above)	↗ over character e.g. ↗
Insert full stop	(As above)	○
Insert comma	(As above)	,
Insert single quotation marks	(As above)	Y or X and/or ȝ or ȝ
Insert double quotation marks	(As above)	Y or X and/or ȝ or ȝ
Insert hyphen	(As above)	H
Start new paragraph	↙	↙
No new paragraph	↘	↘
Transpose	↛	↛
Close up	linking () characters	()
Insert or substitute space between characters or words	/ through character or ↗ where required	Y
Reduce space between characters or words	between characters or words affected	T

A Multi Clue Heuristic Based Algorithm For Table Detection

G V S S K R Naganjaneyulu
Department of Electronics and
Communication Engineering
National Institute of Technology,
Surathkal, Karnataka, India
Email: snd.786@gmail.com

N Veerendra Sathwik
Department of Electronics and
Communication Engineering
Rajiv Gandhi University of
Knowledge Technologies
Nuzvid, India
Email: veerendrasathwik@gmail.com

A.V. Narasimhadhan
Department of Electronics and
Communication Engineering
National Institute of Technology,
Surathkal, Karnataka, India
Email: dhan257@gmail.com

Abstract—Research in the field of document analysis and document recognition experienced reverent growth in the past decade as automation of the office document became essential for daily life. Text in documents can take different forms like hand written text, printed text, headings signatures, tables and graphics. Extraction of tables plays a crucial role in layout analysis, and retaining the important information present in tables. In this work, a multi clue heuristic based table detection algorithm using hough lines and corner harris corner is proposed. Hough lines and harris corner points are extracted from the document in two parallel process. The clues extracted from both the process are matched using nearest neighbor framework to yield tables from the documents. The proposed algorithm is a simple paradigm for extraction of tables that are formed by lines. The performance of the proposed algorithm is tested on different types of documents that contain tables to observe an accuracy of 89.7 %.

I. INTRODUCTION

A document image is group of blocks that contains different types of data like general printed text, handwritten text, tabular form text, and mathematical text. In this modern era developing nations like India are giving high importance for digitization of office documents. Specifically, government documents, bank vouchers, and registration documents related to properties indulge important information in the form of text in tables. Hence, automatic table detection plays a pivotal role in office document analysis. Table forms are defined as structured component of documents for the efficient representation of statistical and relational information. Based on the layout of the tables of interest, the methods for table detection in the document images can be categorized into two types, namely methods for the detection of tables that possess layouts with lines and methods for the detection of tables that possess layout without lines. Few works related to table detection methods are found in literature. Watanabe et al. [1], proposed a graph based method which fails for tables with corner imperfections. Naves et al. [2], considered artifacts in tables and presented a method based on morphological operations. S.Mandal et al, [3], observed the gap between columns is significantly greater than the gaps between words in text lines and suggested a significant column gap method. Drawback of the significant column gap method is that the normal text

words that have long gap cause false alarms. Shimotsuji et al [4], Liang et al [5], and Couasnon [6] proposed methods using previous knowledge such as noise and imperfections. Hu J. et al [7], introduced table analyzer with information of distances among lines in the table for the detection of tables. Zheng et al. [8], defined frame line detection based on direction single connected chain (DSCC) method to detect lines and subsequently with the detection of lines, tables are detected to be extracted from the document image. Most of these methods fail if the input document have skew artifact and need skew correction as a preprocessing step. The objective of the current work is to extract the tabular structures with lines from document images in order to enable the layout analysis and retrieval of text with out skew correction. Proposed method is based on Hough lines and Harris corner clues which are rotational invariant. The paper is organized as follows, section II presents a brief description of the key concepts employed for the algorithm. The next section describes the proposed algorithm. Section IV provides analysis of results followed by conclusion and future work in section V.

II. THEORY

A. Hough Transform

Hough Transform [9] is used to detect particular shapes in an image. The classical Hough Transform is concerned with the identification of lines in the image which is later extended to detection of shapes like circles, ellipses, and parabolas. Hough transform maps a line in cartesian space to a single point in radial parameter space. A point in cartesian space is projected as a line in parameter space. Thus a line in the image space has several lines in the parameter space intersecting at point as shown in Fig. 1.

B. Harris corner detection

Harris corner detection algorithm [11] is used to detect the corners in an image. A corner can be defined as the intersection of two edges. A corner can be detected using eigen Harris matrix [11]. If the eigen values of Harris matrix are large and positive then it can be detected as a corner. The result of Harris

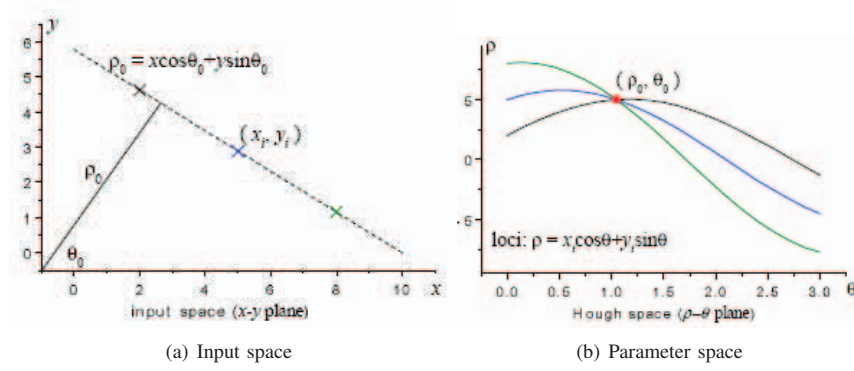


Fig. 1. Illustration of hough Transform [10]

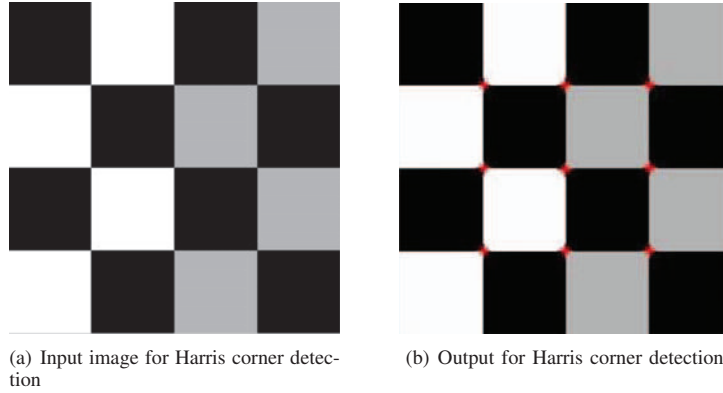


Fig. 2. Harris corner detection on checker board image

corner detection when applied to a checker board is shown in Fig.2.

III. DESCRIPTION OF ALGORITHM

The flow chart of the proposed algorithm is shown in Fig. 3. The proposed heuristic method performs matching of end points of hough lines and the Harris corners, to extract the four corners of the tables. The input to the algorithm is a document image from which the tables need to be extracted. The initial stage of the algorithm is the enhancement of image in order to eliminate noise while preserving the edges. A filter in weighted sobolev space with the parameter $\alpha = 0.3$ [12], [13] is used for image enhancement to enable detection of tables for low resolution images. This preprocessing step improves the accuracy of the algorithm for low resolution document images as the line breakages will reduce. The computation of the Hough and Harris corner clues are computed in parallel processes. To detect the Hough lines edge detection is performed as a preprocessing which is achieved using Canny edge detector [14]. Subsequently detection of hough lines is performed. In a parallel process, binarization is applied on the input image employing Otsu method [15]. The binary image is used for computation of corner clues using Harris interesting points. Detected Hough lines and Harris corner

clues are matched using a heuristic method in order to identify corners of the tables. In order to match the endpoints of the hough lines and corner points, a nearest neighbour frame work is used. Initially an endpoint of a hough line is considered and its nearest end point in corner points is identified using the Euclidean distance measure between two points. After the identification of two nearest end points, a combined nearest corner to the two endpoints is identified using the same distance measure along with an adaptive threshold. Then, the two nearest endpoints of hough lines and combined nearest corner to the two endpoints are identified and matching of identified points is performed to compute the corners of the tables. The same process is executed for all the remaining endpoints for extraction of tables.

IV. EXPERIMENTAL RESULTS

The proposed algorithm is tested on a self developed dataset of 50 images containing 78 tables out of which 70 tables are detected correctly with an accuracy of 89.74 % (on MATLAB platform). A table is considered as correctly detected when the ratio of overlapping area of the detected table with the table in original document to the area of table in the original document is in between 0.9 – 1.1. The accuracy is calculated as the ratio of number of tables detected to total number of tables present.

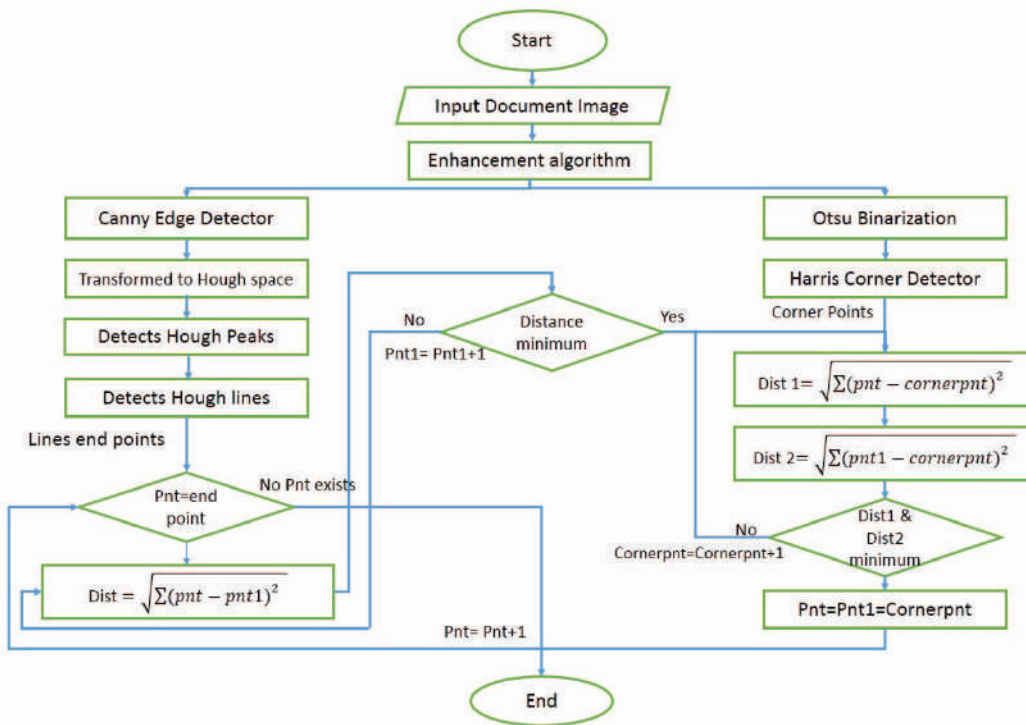


Fig. 3. Flowchart of the proposed algorithm

The typical output of the proposed algorithm is shown in Fig.4 along with input image. Proposed algorithm works efficient for tables with the general rectangular box layout. Proposed algorithm is a rotational invariant method which is the keen advantage of this method. As Hough transform, and Harris corner detection algorithm are rotational invariant methods which the ability of the proposed algorithm to detect tables in documents with skew artefact. The proposed algorithm fails for the tables with spaces as delimitation (with out lines) and irregular table format. Fig.5 is an example of the undetected table due to its structural layout. The computational cost of the proposed method is high as hough transform is computationally expensive. The proposed method allows parallel processing of the image for hough and Harris clues.

V. CONCLUSION AND FUTURE WORK

In this work a multi clue heuristic method for table detection by employing matching between end points of Hough lines and Harris corner clues has been proposed. This method computes Hough transforms and Harris corner clues in two parallel process followed by matching end points of hough lines and Harris corner points. In case of a mismatch, a point near to both the interesting points has been determined using nearest neighbour framework and an adaptive threshold. From the simulation results, it has been shown that the algorithm gives an accuracy of 89.74 % on self developed database of 50 images with 78 tables. The method has an advantage of skew invariance since both the clues that has been used in this

algorithm posses the rotational invariance. It has been observed that the method fails in case of tabular structures with spaces as delimitation and without lines. Extension of this work for detection of tables with spaces as delimitations by using the idea that text lines have a high probability of corners.

REFERENCES

- [1] T. Watanabe, Q. Luo, and N. Sugie, "Toward a practical document understanding of table-form documents: its framework and knowledge representation," in *Document Analysis and Recognition, 1993., Proceedings of the Second International Conference on*, pp. 510–515, Oct 1993.
- [2] L. A. P. Neves, J. M. de Carvalho, and J. F. "Table-form extraction with artefact removal," vol. 14, pp. 252–265, feb 2008.
- [3] S. Mandal, S. Chowdhury, A. Das, and B. Chanda, "A simple and effective table detection system from document images," *International Journal of Document Analysis and Recognition (IJDAR)*, vol. 8, no. 2-3, pp. 172–182.
- [4] S. Shimotsuji and M. Asano, "Form identification based on cell structure," in *Pattern Recognition, 1996., Proceedings of the 13th International Conference on*, vol. 3, pp. 793–797 vol.3, Aug 1996.
- [5] J. Liang, J. Ha, R. Haralick, and I. Phillips, "Document layout structure extraction using bounding boxes of different entities," in *Applications of Computer Vision, 1996. WACV '96., Proceedings 3rd IEEE Workshop on*, pp. 278–283, Dec 1996.
- [6] B. Couasnon, "Dmos: a generic document recognition method, application to an automatic generator of musical scores, mathematical formulae and table structures recognition systems," in *Document Analysis and Recognition, 2001. Proceedings. Sixth International Conference on*, pp. 215–220, 2001.
- [7] J. Hu, R. Kashi, D. Lopresti, and G. Wilfong, "Evaluating the performance of table processing algorithms," *International Journal on Document Analysis and Recognition*, vol. 4, no. 3, pp. 140–153, 2002.

 BANK COPY State Bank of India BRANCH(CODE NO. 20191668)														
Indian Space Research Organisation (ISRO) ICRB Recruitment Application Fee Payment														
Name of the Candidate : souvik maitkar Present Address : 65, Bawali mazar E.V.Palya, Saurashtra Paly Ramt, Kolad - 70061 Kolad - 70061 Advt. Details : 01/2014 - 06/01 [Scientist/Engineer- SC(Electronics)] Category / Sex / Ph / Ex : GN / M / No / No														
<table border="1" style="width: 100%;"> <thead> <tr> <th>Head</th> <th>Amount</th> <th>Credit to</th> </tr> </thead> <tbody> <tr> <td>Application Fees</td> <td>₹ 100</td> <td>32034064593</td> </tr> <tr> <td>Bank's Charges</td> <td>₹ 30</td> <td></td> </tr> <tr> <td>Total</td> <td>₹ 130</td> <td></td> </tr> </tbody> </table>			Head	Amount	Credit to	Application Fees	₹ 100	32034064593	Bank's Charges	₹ 30		Total	₹ 130	
Head	Amount	Credit to												
Application Fees	₹ 100	32034064593												
Bank's Charges	₹ 30													
Total	₹ 130													
Amount in words : Rupees One Hundred and Thirty Only														
Signature of the Candidate/Remitter For Receiving Branch use only														
<table border="1" style="width: 100%;"> <thead> <tr> <th>Registration Number</th> <th>Journal Number (to be filled by bank)</th> </tr> </thead> <tbody> <tr> <td>20191668</td> <td></td> </tr> </tbody> </table>			Registration Number	Journal Number (to be filled by bank)	20191668									
Registration Number	Journal Number (to be filled by bank)													
20191668														
1. Please write the Journal Number in all the challans. 2. Please enter the Registration No. and Name of the Candidate in the menu while posting.														
SEAL:	Authorised Signatory													
DATE:	Note : This part is to be retained by SBI.													

(a) Input image

Head	Amount	Credit to
Application Fees	₹ 100	32034064593
Bank's Charges	₹ 30	
Total	₹ 130	

(c) Extracted table 1

 BANK COPY State Bank of India BRANCH(CODE NO. 20191668)														
Indian Space Research Organisation (ISRO) ICRB Recruitment Application Fee Payment														
Name of the Candidate : souvik maitkar Present Address : 65, Bawali mazar E.V.Palya, Saurashtra Paly Ramt, Kolad - 70061 Kolad - 70061 Advt. Details : 01/2014 - 06/01 [Scientist/Engineer- SC(Electronics)] Category / Sex / Ph / Ex : GN / M / No / No														
<table border="1" style="width: 100%;"> <thead> <tr> <th>Head</th> <th>Amount</th> <th>Credit to</th> </tr> </thead> <tbody> <tr> <td>Application Fees</td> <td>₹ 100</td> <td>32034064593</td> </tr> <tr> <td>Bank's Charges</td> <td>₹ 30</td> <td></td> </tr> <tr> <td>Total</td> <td>₹ 130</td> <td></td> </tr> </tbody> </table>			Head	Amount	Credit to	Application Fees	₹ 100	32034064593	Bank's Charges	₹ 30		Total	₹ 130	
Head	Amount	Credit to												
Application Fees	₹ 100	32034064593												
Bank's Charges	₹ 30													
Total	₹ 130													
Amount in words : Rupees One Hundred and Thirty Only														
Signature of the Candidate/Remitter For Receiving Branch use only														
<table border="1" style="width: 100%;"> <thead> <tr> <th>Registration Number</th> <th>Journal Number (to be filled by bank)</th> </tr> </thead> <tbody> <tr> <td>20191668</td> <td></td> </tr> </tbody> </table>			Registration Number	Journal Number (to be filled by bank)	20191668									
Registration Number	Journal Number (to be filled by bank)													
20191668														
1. Please write the Journal Number in all the challans. 2. Please enter the Registration No. and Name of the Candidate in the menu while posting.														
SEAL:	Authorised Signatory													
DATE:	Note : This part is to be retained by SBI.													

(b) Hough lines, corner clues, and matched points

Registration Number	Journal Number (to be filled by bank)
20191668	

(d) Extracted table 2

Fig. 4. Typical input and output images

OSC 2 TIMETABLE TEMPLATE 2010-2011						
OSC 2						
Time	SUNDAY	MONDAY	TUESDAY	WEDNESDAY	THURSDAY	
MALES	FEmales	MALES	FEmales	MALES	FEmales	MALES
8:00						
8:45						
9:45						
10:15						
10:35						
11:00						
11:15	Loc-1 Approach to the Clinical Presentation of the Patient	Loc-2	Loc-3	Loc-4	Loc-5	Loc-6
12:00						
12:15						
13:00						
13:45						
14:00						
14:45	PBL TUTORIAL DAY 1	CLINICAL SKILLS MODULE 14:05 - 17:00	Self-Directed Learning	CLINICAL SKILLS MODULE 14:05 - 17:00	Self-Directed Learning	PBL WRAP-UP 11:30 - 12:00
15:00						
15:45						
16:00						
16:45	Self-Directed Learning					

Last updated: 24/09/10

Fig. 5. Undetected table using the proposed algorithm

- [8] Y. Zheng, C. Liu, X. Ding, and S. Pan, "Form frame line detection with directional single-connected chain," in *Document Analysis and Recognition, 2001. Proceedings. Sixth International Conference on*,

- pp. 699–703, 2001.
- [9] D. Duan, M. Xie, Q. Mo, Z. Han, and Y. Wan, "An improved hough transform for line detection," in *Computer Application and System Modeling (ICCASTM), 2010 International Conference on*, vol. 2, pp. V2–354–V2–357, Oct 2010.
- [10] X. Lin and K. Otobe, "Hough transform algorithm for real-time pattern recognition using an artificial retina camera," *Opt. Express*, vol. 8, pp. 503–508, Apr 2001.
- [11] Z. Ye, Y. Pei, and J. Shi, "An improved algorithm for harris corner detection," in *Image and Signal Processing, 2009. CISP '09. 2nd International Congress on*, pp. 1–4, Oct 2009.
- [12] G. V. S. S. K. R. Naganjaneyulu, A. Narasimhadhan, and K. Venkatesh, "Performance evaluation of ocr on poor resolution text document images using different pre processing steps," in *TENCON 2014 - 2014 IEEE Region 10 Conference*, pp. 1–4, Oct 2014.
- [13] S. Buzykanov, "Enhancement of poor resolution text images in the weighted sobolev space," in *Systems, Signals and Image Processing (IWSSIP), 2012 19th International Conference on*, pp. 536–539, April 2012.
- [14] W. Xiao and X. Hui, "An improved canny edge detection algorithm based on predisposal method for image corrupted by gaussian noise," in *World Automation Congress (WAC), 2010*, pp. 113–116, Sept 2010.
- [15] N. Level Otsu, "A threshold selection method from gray-level histogram," *IEEE Transactions on Systems, Man and Cybernetics*, vol. 9, no. 1, pp. 62–66, 1979.

R peak delineation in ECG signal based on Polynomial Chirplet Transform using Adaptive Threshold

G V S S K R Naganjaneyulu
 Department of Electronics and
 Communication Engineering
 National Institute of Technology,
 Surathkal, Karnataka, India
 Email: snd.786@gmail.com

Basheeruddin Shah Shaik
 Department of Electrical Engineering
 School of Engineering
 Shiv Nadar University
 Dadri, India
 Email: bs600@snu.edu.in

A.V. Narasimhadhan
 Department of Electronics and
 Communication Engineering
 National Institute of Technology,
 Surathkal, Karnataka, India
 Email: dhan257@gmail.com

Abstract—R peak delineation is fundamental step in any application implicating electrocardiogram (ECG) signal. ECG is non stationary and non linear. Hence, linear transforms like short time fourier transform, wavelet transform and chirplet transform may be inadequate to represent ECG signal and consequently for R peak delineation. Polynomial chirplet transform (PCT) models the frequency into a higher order polynomial to enhance the representation of non stationary signals whose frequency vary non linearly with time. In this paper, PCT based R peak delineation method using adaptive threshold is proposed. The performance of the proposed algorithm is evaluated on ECG ID data base taken from physionet data bank. This work also presents a comparative study of QRS detection methods employing the uni scale family of time frequency analysis methods, short time fourier transform, chirplet transform, stockwell transform , wigner ville distribution, and pseudo wigner ville distribution out of which stockwell transform, pseudo wigner ville distribution along with adaptive threshold are applied to QRS detection for the first time. The results show that the proposed method outperforms the competitors in terms of sensitivity, specificity and detection error rate.

I. INTRODUCTION

Analyzing Electrocardiogram (ECG) via R peak delineation is an important clue for diagnosis to prevent imminent failure of heart [1]–[4], and in other applications [5]–[7]. Many researchers proposed several methods for R peak detection in ECG signal which includes conventional filter theory based methods, transform based methods, and heuristic methods. Few typical algorithms along with the key features of the algorithms are enlisted in Table I. ECG is a non stationary signal with high complex time frequency content. Analyzing ECG signal for QRS detection using fast fourier transform (FFT) is inadequate since FFT doesn't provide time information. In this stand point, time frequency analysis (TFA) methods are very handy. Our previous works, [24], [25] deals with algorithms for QRS delineation based on short time fourier transform, and chirplet transform(CT) using adaptive threshold respectively. The linear transforms congressional to the family of STFT, wavelet, CT may not be commensurate for QRS detection in ECG signal as it contains non linearly varying

TABLE I
 LITERATURE REVIEW ON QRS DELINEATION METHODS

Authors	Key features of Algorithm
M. Okada [8]	Five step digital filter
J. Pan and W. J. Tompkins [9]	Filters, adaptive threshold
V. Afonso et al. [10]	Multi rate signal processing, sub band decomposition
Q. Xue et al. [11]	Neural network modelling and adaptive matching filter
S. Kadamb et al. [12]	Wavelets, Peak matching in different scales
DS Benitez et al. [13]	Hilbert transform, thresholding
Kohler et al. [14]	Count of zero crossings, computationally efficient
J. Martinez et al. [15]	Quadratic spline wavelet, P,QRS, T wave delineation
F. de Oliveira et al. [16]	Hilbert transform of wavelet, peak detector
Mayer C et al. [17]	Combination of wavelet, Pan Tomppmkins methods in a data driven way
Tabakov S [18]	Comb filter to reject powerline interference
N. Uchaipichat and S. Inban [19]	STFT, local maxima finding
Chouakri S.A. et al. [20]	Wavelet packets, and histogram approach
Z. Zidelman et al. [21]	S Transform, shanon energy
Ramakrishnan A.G. et al. [22]	Integrated linear prediction residual (ILPR), dynamic poison index
P. Phukpattaranon [23]	Quadratic filter and single threshold
Shaik B.S. et al. [24]	STFT and adaptive threshold
Shaik B.S. et al. [25]	Chirplet transform, adaptive threshold

low frequency content. Quadratic transforms like wigner ville distribution(WVD), PCT are more appropriate. The shortage of WVD in QRS detection is explained in [26]. WVD suffers from cross term interference which makes it incompatible for R peak delineation. WVD is also permeable to noise in case the signal is contaminated by noise, since it derives the basis from the signal itself. To make WVD commodious for R peak detection, the kernel is multiplied with a smoothing function like gaussian to produce pseudo wigner ville distribution (pseudo WVD). However, stockwell transform (ST) provides a frequency dependent resolution. For low frequency signals ST gives a high frequency resolution, poor time resolution,

and for high frequencies, it gives bad frequency resolution, good time resolution. PCT on the other hand, models the frequency with a higher order polynomial which gives it the ability to represent any non stationary signal whose frequency is varying non linearly with time. This ability of PCT makes it suitable for representing the ECG in a more compatible way. In this work, a method for R peak delineation using polynomial chirplet transform using adaptive threshold is proposed. R peak detection is also accomplished with STFT, CT transform, ST, WVD, and pseudo WVD. The performance of PCT is compared with the aforementioned methods.

The paper is organized as follows. In section II, a brief outline of time frequency analysis methods is presented. Section III describes the proposed algorithm while section IV gives a glimpse in to results followed by conclusion and future work in section V.

II. THEORY

A. Polynomial chirplet transform

The CT fails to generate time frequency distributions (TFD) with good energy concentration if the frequency of the signal is a nonlinear function of time. PCT has the ability to generate a better TFD than CT for signals with frequency that is an arbitrary function of time. PCT of a signal $s(t)$ is defined in [27] as follows.

$$PCT_s(t, \omega, \alpha_1, \dots, \alpha_n; \sigma) = \int_{-\infty}^{\infty} z(\tau) \Phi_{\alpha_1, \dots, \alpha_n}^R(\tau) \times \Phi_{\alpha_1, \dots, \alpha_n}^M(\tau, t) \omega(\sigma)(\tau - t) e^{-j\omega\tau} d\tau \quad (1)$$

where,

$$\begin{aligned} \Phi_{\alpha_1, \dots, \alpha_n}^R(t) &= \exp(-j \sum_{k=2}^{n+1} \frac{1}{k} \alpha_{k-1} t^k) \\ \Phi_{\alpha_1, \dots, \alpha_n}^M(t, t_0) &= \exp(j \sum_{k=2}^{n+1} \alpha_{k-1} t_0^{k-1} t) \end{aligned}$$

are the non linear frequency rotating operator and frequency shifting operator respectively and $z(t)$ is analytical signal of $s(t)$ given by

$z(t) = s(t) + jH(s(t))$, where $H(\cdot)$ represents hilbert transform. $\alpha_1, \dots, \alpha_n$ are the polynomial kernel characteristic parameters corresponds to slope of instantaneous frequency function. Different uniscale TFA transforms are listed in Table II. (In Table II Assume, $\omega_\sigma(t) = \frac{1}{\sqrt{2\pi}\sigma} e^{-\frac{1}{2}(\frac{t}{\sigma})^2}$).

TABLE II
DEFINITIONS OF DIFFERENT TFA METHODS

Method	Formulae
STFFT [28]	$\int_{-\infty}^{\infty} z(\tau) \omega(\sigma)(\tau - t) e^{-j\omega\tau} d\tau$
CT [29]	$\int_{-\infty}^{\infty} z(\tau) \omega_\sigma(\tau - t) e^{j\frac{\alpha}{2}(\tau-t)^2} e^{-j\omega\tau} d\tau$
ST [30]	$\int_{-\infty}^{\infty} z(\tau) \frac{ \omega }{2\pi\sqrt{2\pi}} e^{-\frac{(t-\tau)^2\omega^2}{8\pi^2}} e^{-j\omega\tau} d\tau$
WVD [31]	$\int_{-\infty}^{\infty} z(\frac{t+\tau}{2}) z^*(\frac{t-\tau}{2}) e^{-j\omega\tau} d\tau$
PWVD [32], [33]	$\int_{-\infty}^{\infty} z(\frac{t+\tau}{2}) z^*(\frac{t-\tau}{2}) \omega(\sigma)(\tau - t) e^{-j\omega t} d\tau$
PCT [27]	$\int_{-\infty}^{\infty} z(\tau) e^{(-j \sum_{k=2}^{n+1} \frac{1}{k} \alpha_{k-1} \tau^k)} e^{(j \sum_{k=2}^{n+1} \alpha_{k-1} t^{k-1})} e^{-j\omega\tau} d\tau$

III. DESCRIPTION OF THE PROPOSED ALGORITHM

The block diagram of the proposed algorithm is shown in Fig. 1. The proposed algorithm consists of five steps namely data acquisition, pre processing, computation of polynomial chirplet coefficients, employing the adaptive threshold followed by decision making to output the R peak locations. Data acquisition is not performed in this algorithm, instead recorded ECG recordings from ECG ID data base from physionet databank [34] are used. As a part of pre processing, a low pass butterworth filter with cutoff frequency $40Hz$, passband ripple of $3dB$ and a stop band attenuation of $60dB$ is used to remove the high frequency power line interference. A typical raw ECG signal along with the filtered output is shown in Fig. 2. The polynomial coefficients are computed as in [27]. The time frequency distribution (TFD) of the signal is computed using PCT in the next step. The TFD is computed by considering an atom of size 75 samples and moving in steps of 10 time lags. An adaptive threshold used in [24] is employed for obtaining the peaks in the third and fourth frequency components in the TFD followed. The adaptive thresholding algorithm is a dual threshold method in which one of the threshold is 0.9 of the other threshold. These thresholds are decided using a training step as in [9]. The higher threshold is used for QRS complexes initially. If no QRS complex is found in a stipulated time interval corresponds to 166% of the current RR interval, then lower threshold is used for detection of QRS complex. The adaptive thresholding is followed by a decision making step, in which number of peaks, and peak locations in two successive frequency components of TFD are compared. If the count and locations (approximately) matches in the two, these peaks are considered to be true QRS locations. Otherwise, the process of comparison is repeated in between the next two lower successive frequency components. If no match is found between the two successive components, then the peaks locations in the highest frequency component are considered as true QRS locations.

IV. RESULTS AND DISCUSSIONS

The proposed algorithm is tested on ECG ID database. ECG ID database contains 299 recordings of $10s$ duration pertaining to 90 different persons which are sampled at $500Hz$. Different variations of this algorithm, i.e the same algorithm with PCT replaced by STFT, CT, ST, WVD, and pseudo WVD transforms are tested on the aforementioned data set. The TFDs of an ECG signal computed using different TFA methods are shown in Fig. 3. From Fig. 3, it can be observed that TFD computed using PCT has better frequency resolution and time resolution compared to TFDs produced by STFT and CT which is the reason for better performance of PCT. It can be deduced that the TFD generated by WVD is not good enough to represent the signal, and TFD generated by pseudo WVD is better than that of TFD computed using WVD in terms of frequency resolution. TFD generated by ST lacks clarity in time resolution when compared to TFDs generated by other TFA methods. The following performance metrics are used for

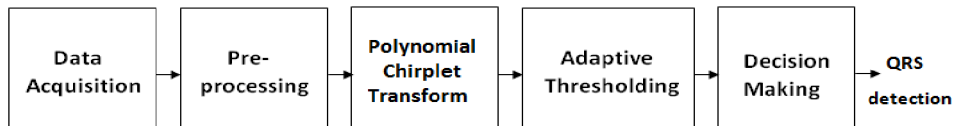


Fig. 1. Block diagram of the proposed algorithm

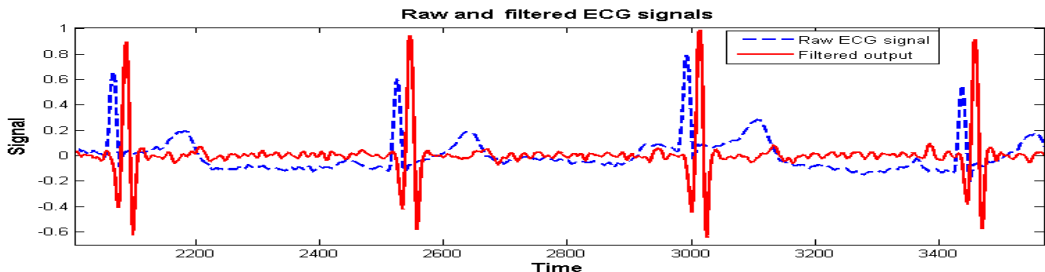


Fig. 2. Raw ECG signal and the filtered signal

TABLE III
COMPARISON OF QRS DETECTION TECHNIQUES USING DIFFERENT TIME FREQUENCY ANALYSIS METHODS

TFA Method	Sens	Spec	DER
STFT	99.19	99.49	1.32
CT	99.46	99.69	0.85
S Transform	99.52	99.56	0.914
WVD	75.10	45.45	115.04
PWVD	98.24	99.28	2.47
PCT	99.49	99.73	0.78

quantifying the results.

$$\text{Sensitivity (Sens in \%)} = \frac{TP}{TP + FN} \times 100 \quad (2)$$

$$\text{Specificity (Spec in \%)} = \frac{TP}{TP + FP} \times 100 \quad (3)$$

$$\begin{aligned} \text{Detection error rate (DER)} &= \\ &\frac{FP + FN}{\text{Total number of QRS complex}} \end{aligned} \quad (4)$$

where TP is number of true positive (correctly detected beats), FP is number of false positives (false alarms i.e non R peak detected as R peak), and FN represents false negatives (R peak not detected by the algorithm). The sensitivity, specificity and DER for various methods are computed as per equations 2, 3, 4 and tabulated in Table III. The values given in Table III are shown in pictorial form in Fig. 4. For the sake of convenience results corresponding to WVD are not shown in Fig. 4. From Table III, it is ascertained that the performance of WVD in detection of R peak is poor which supports [26]. The pseudo WVD applied in this work for R peak detection achieved a very good sensitivity, specificity and DER than WVD. It can be also be discovered that PCT is outrunning the other methods in terms of specificity and DER and sensitivity is very much near to that of ST. It is not surprising that ST is handy in

R peak detection because of it's ability to produce frequency dependent resolution.

V. CONCLUSION AND FUTURE WORK

A method for R peak delineation based on PCT using adaptive threshold has been proposed in this work. It has been shown that because of the ability of PCT to represent a non stationary signal with frequency varying non linearly with respect to time, PCT is a better choice for R peak delineation in ECG signal. The performance of different variants of the proposed algorithm with PCT replaced by STFT, CT, ST, WVD, and pseudo WVD has been evaluated on ECG ID database along with the proposed algorithm. In terms of sensitivity ST performed well with 99.52 % which is closely followed by the proposed algorithm with sensitivity of 99.49. However in terms of specificity and DER the proposed algorithm outperformed the other competitors with specificity of 99.73 and DER of 0.78. It has been also shown that by multiplying the WVD kernel with smoothing function like gaussian WVD can be made suitable for R peak detection. The results obtained using pseudo WVD are superior to that of WVD and comparable with the other TFA methods with sensitivity of 98.24, specificity of 99.28 and DER of 2.47. Application of different multi resolution techniques for QRS delineation and comparative study of multi resolution techniques for QRS detection is author's current objective.

REFERENCES

- [1] H. G. Hosseini, D. Luo, and K. Reynolds, "The comparison of different feed forward neural network architectures for ECG signal diagnosis," *Medical Engineering & Physics*, vol. 28, no. 4, pp. 372–378, 2006.
- [2] P. de Chazal, M. O'Dwyer, and R. Reilly, "Automatic classification of heartbeats using ECG morphology and heartbeat interval features," *IEEE Transactions on Biomedical Engineering*, vol. 51, pp. 1196–1206, July 2004.
- [3] S. C. Saxena, V. Kumar, and S. T. Hamde, "Feature extraction from ECG signals using wavelet transforms for disease diagnostics," *International Journal of Systems Science*, vol. 33, no. 13, pp. 1073–1085, 2002.

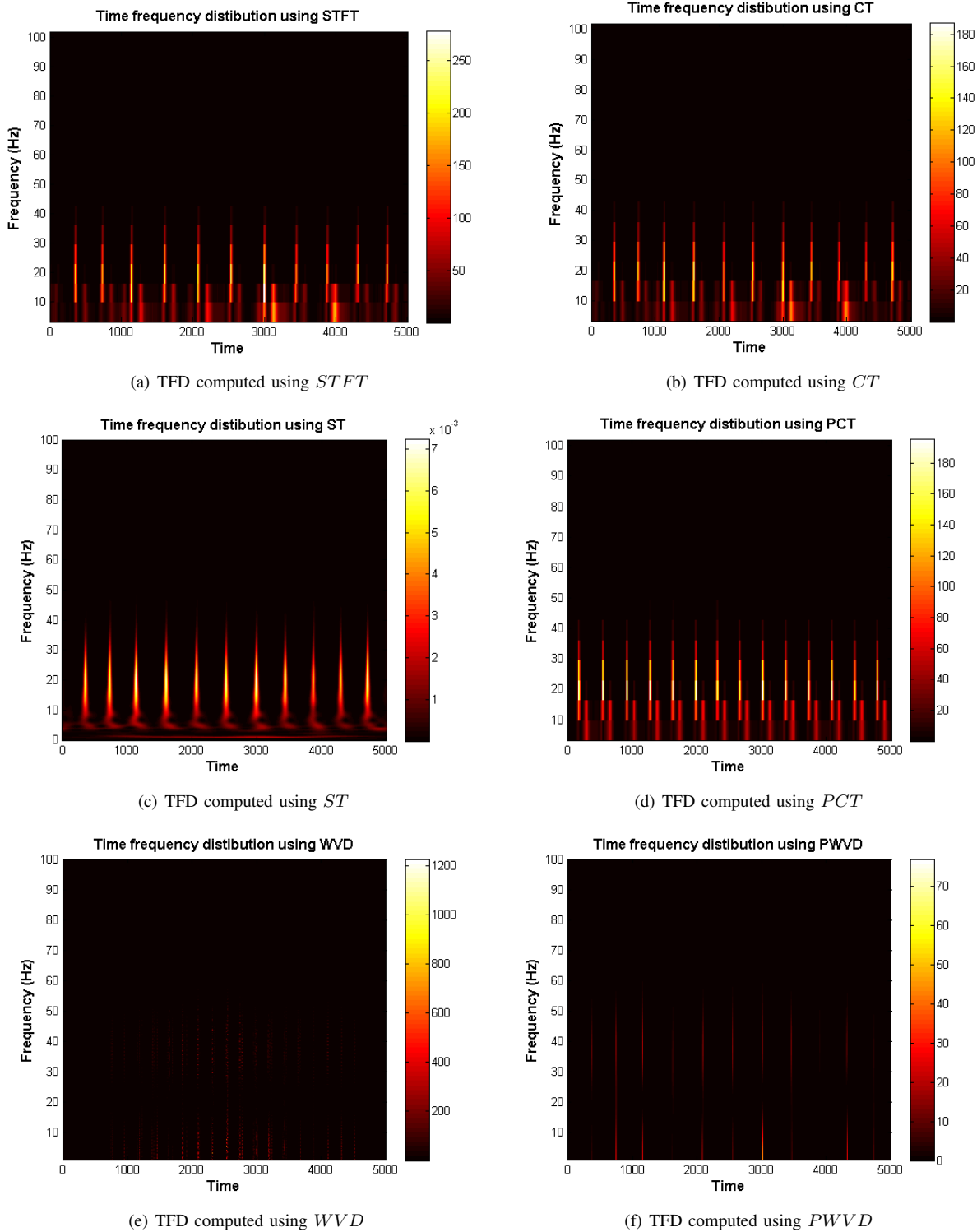
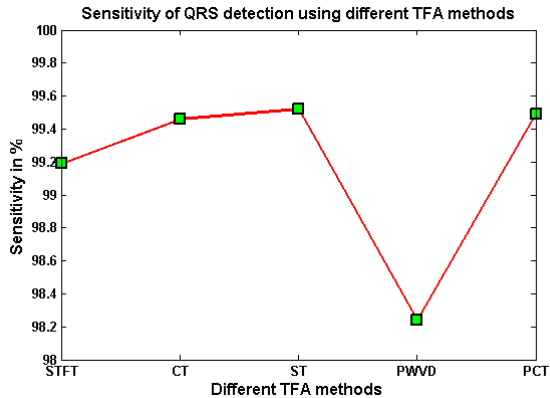


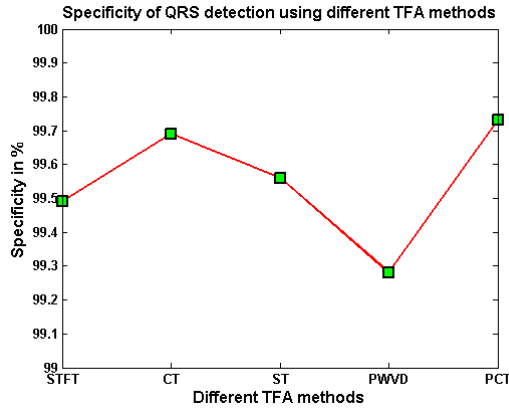
Fig. 3. TFD computed using different TFA methods

- [4] D. Hayn, B. Jammerbund, and G. Schreier, "QRS detection based ECG quality assessment," *Physiological measurement*, vol. 33, no. 9, p. 1449, 2012.
- [5] Y. Singh and P. Gupta, "ECG to individual identification," in *2nd IEEE International Conference on Biometrics: Theory, Applications and Systems, BTAS*., pp. 1–8, Sept 2008.
- [6] A. Lourenço, H. Silva, and A. Fred, "Unveiling the biometric potential

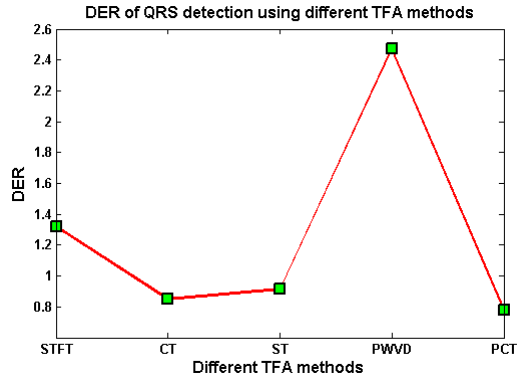
- of finger-based ECG signals," *Intell. Neuroscience*, vol. 2011, pp. 5:1–5:8, Jan. 2011.
- [7] T.-W. Shen, W. Tompkins, and Y. Hu, "One-lead ECG for identity verification," in *Proceedings of the Second Joint EMBS/BMES Conference, Houston*, vol. 1, pp. 62–63, IEEE, 2002.
- [8] M. Okada, "A digital filter for the QRS complex detection," *IEEE Transactions on Biomedical Engineering*, vol. BME-26, pp. 700–703,



(a) Sensitivity of QRS detection using different TFA methods



(b) Specificity of QRS detection using different TFA methods



(c) DER of QRS detection using different TFA methods

Fig. 4. Performance of QRS detection algorithms using different TFA methods

Dec 1979.

- [9] J. Pan and W. J. Tompkins, "A real-time QRS detection algorithm," *IEEE Transactions on Biomedical Engineering*, vol. BME-32, pp. 230–236, March 1985.
- [10] V. Afonso, O. Wieben, W. J. Tompkins, T. Nguyen, and S. Luo, "Filter bank-based ECG beat classification," in *Proceedings of the 19th Annual International Conference of the IEEE Engineering in Medicine and Biology Society*, 1997., vol. 1, pp. 97–100 vol.1, Oct 1997.
- [11] Q. Xue, Y. Hu, and W. J. Tompkins, "Neural-network-based adaptive matched filtering for QRS detection," *IEEE Transactions on Biomedical Engineering*, vol. 39, pp. 317–329, April 1992.
- [12] S. Kadambe, R. Murray, and G. F. Boudreux-Bartels, "Wavelet transform-based QRS complex detector," *Biomedical Engineering, IEEE Transactions on*, vol. 46, no. 7, pp. 838–848, 1999.

- [13] D. Benitez, P. Gaydecki, A. Zaidi, and A. Fitzpatrick, "A new QRS detection algorithm based on the hilbert transform," in *Computers in Cardiology*, pp. 379–382, 2000.
- [14] B. Kohler, C. Hennig, and R. Orglmeister, "QRS detection using zero crossing counts," *Applied genomics and proteomics*, vol. 2, no. 2, pp. 138–145, 2003.
- [15] J. Martinez, R. Almeida, S. Olmos, A. Rocha, and P. Laguna, "A wavelet-based ECG delineator: evaluation on standard databases," *IEEE Transactions on Biomedical Engineering*, vol. 51, pp. 570–581, April 2004.
- [16] F. de Oliveira and P. Cortez, "A QRS detection based on hilbert transform and wavelet bases," in *IEEE Workshop on Machine Learning for Signal Processing*, pp. 481–489, Sept 2004.
- [17] C. Meyer, J. Gavela, and M. Harris, "Combining algorithms in automatic detection of QRS complexes in ECG signals," *IEEE Transactions on Information Technology in Biomedicine*, vol. 10, pp. 468–475, July 2006.
- [18] S. Tabakov, I. Iliev, and V. Krasteva, "Online digital filter and QRS detector applicable in low resource ECG monitoring systems," *Ann Biomed Eng*, vol. 36, pp. 1805–1815, Nov 2008.
- [19] N. Uchaipichat and S. Inban, "Development of QRS detection using short-time fourier transform based technique," *IJCA, Special Issue on CASCT*, no. 1, pp. 7–10, 2010.
- [20] S. Chouakri, F. Berekhi-Reguig, and A. Taleb-Ahmed, "QRS complex detection based on multi wavelet packet decomposition," *Applied Mathematics and Computation*, vol. 217, no. 23, pp. 9508–9525, 2011.
- [21] Z. Zidemal, A. Amirou, D. Ould-Abdeslam, A. Moukadem, and A. Dieterlen, "QRS detection using s-transform and shannon energy," *Computer Methods and Programs in Biomedicine*, vol. 116, no. 1, pp. 1 – 9, 2014.
- [22] A. Ramakrishnan, A. Prathosh, and T. Ananthapadmanabha, "Threshold-independent QRS detection using the dynamic plosion index," *Signal Processing Letters, IEEE*, vol. 21, pp. 554–558, May 2014.
- [23] P. Phukpattaranont, "QRS detection algorithm based on the quadratic filter," *Expert Systems with Applications*, vol. 42, no. 11, pp. 4867 – 4877, 2015.
- [24] B. S. Shaik, G. V. S. S. K. R. Naganjaneyulu, T. Chandrasheker, and A. Narasimhadhan, "A method for QRS delineation based on stft using adaptive threshold," *Procedia Computer Science*, vol. 54, pp. 646–653, 2015.
- [25] B. S. Shaik, G. V. S. S. K. R. Naganjaneyulu, and A. V. Narasimhadhan, "A novel approach for QRS delineation in ECG signal based on chirplet transform," in *International Conference on Electronics, Computing and Communication Technologies (CONECCT) 2015*, pp. 1–5, July 2015.
- [26] A. Mousa and R. Saleem, "The shortage of wvd in analyzing abnormal ECG signal," in *IEEE Symposium on Industrial Electronics Applications (ISIEA)*, pp. 651–654, Oct 2010.
- [27] Z. Peng, G. Meng, F. Chu, Z. Lang, W. Zhang, and Y. Yang, "Polynomial chirplet transform with application to instantaneous frequency estimation," *IEEE Transactions on Instrumentation and Measurement*, vol. 60, no. 9, pp. 3222–3229, 2011.
- [28] P. D. Welch, "The use of fast fourier transform for the estimation of power spectra: A method based on time averaging over short, modified periodograms," *IEEE Transactions on audio and electroacoustics*, vol. 15, no. 2, pp. 70–73, 1967.
- [29] S. Mann and S. Haykin, "The chirplet transform: A generalization of gabors logon transform," in *Vision Interface*, vol. 91, pp. 205–212, 1991.
- [30] R. G. Stockwell, L. Mansinha, and R. Lowe, "Localization of the complex spectrum: the s transform," *IEEE Transactions on Signal Processing*, vol. 44, no. 4, pp. 998–1001, 1996.
- [31] T. Claesen and W. Mecklenbrauker, "The wigner distribution—a tool for time frequency analysis, 1-3," *Philips J. Res*, vol. 35, no. 3, p. 217.
- [32] L. Cohen, *Time-frequency Analysis*. Electrical engineering signal processing, Prentice Hall PTR, 1995.
- [33] P. Flandrin and B. Escudie, "An interpretation of the pseudo-wigner-ville distribution," *Signal Processing*, vol. 6, no. 1, pp. 27–36, 1984.
- [34] G. Moody, R. Mark, and A. Goldberger, "PhysioNet: A web-based resource for the study of physiologic signals," *IEEE Engineering in Medicine and Biology Magazine*, vol. 20, pp. 70–75, May 2001.

A Novel Method for Pitch Detection via Instantaneous Frequency Estimation using Polynomial Chirplet transform

G V S S K R Naganjaneyulu
Department of Electronics and
Communication Engineering
National Institute of Technology,
Surathkal, Karnataka, India
Email: snd.786@gmail.com

M Venkata Ramana
Department of Electronics and
Communication Engineering
Rajiv Gandhi University of
Knowledge Technologies
Nuzvid, India
Email:mvramanaece@gmail.com

A.V. Narasimhadhan
Department of Electronics and
Communication Engineering
National Institute of Technology,
Surathkal, Karnataka, India
Email: dhan257@gmail.com

Abstract—Speech processing and synthesis have been the interests of many researchers for the past few decades. One of the primary task in speech processing is the estimation of fundamental frequency of speech (also known as pitch). Speech is a non stationary signal whose frequency varies arbitrarily with time. Linear time frequency analysis tools such as short time fourier transform may not be convenient for estimation of pitch of speech. Polynomial chirplet transform models the frequency of speech signal by a higher order polynomial of time, which makes it suitable for analysis of speech to extract pitch. In this work, a novel algorithm is proposed for pitch detection in speech by estimating instantaneous frequency (IF) using polynomial chirplet transform. The proposed algorithm is applied on a part of TIMIT speech database to find the pitch of speech of different male and female persons.

I. INTRODUCTION

Pitch is defined as the fundamental frequency of speech signal i.e., the frequency at which the vocal cord vibrates periodically during voiced parts of speech. The value of pitch varies with gender and age of human beings. For males, pitch is in the range 50 – 150 Hz, for females, pitch is in between 180 – 300 Hz and for children pitch varies in the range of 350–500 Hz. Estimation of pitch of speech signal is a critical step in many speech processing applications [1]–[3]. Pitch estimation is achieved in past utilizing different approaches like time domain methods [4]–[8], cepstral methods [9], [10], time frequency analysis methods [11]. Comparative studies on different pitch detection methods are presented in [12]–[15]. Except [11], other methods assumes local stationary of the speech signal which is a limitation. In [11], this assumption is removed by employing time frequency analysis method to represent speech signal using time frequency distribution and combined with dyadic wavelet transform for converting speech into a mono component signal by removing harmonics to compute pitch via estimation of instantaneous frequency (IF). However, time frequency (scale) distributions obtained using linear transforms such as short time fourier transform (STFT), wavelet transform (WT) may fail to represent speech signal

in an adequate manner. Quadratic transform like wigner ville distribution (WVD) can perform better. However, WVD has the disadvantage of cross term. Polynomial chirplet transform (PCT) provides a higher order generalization by representing frequency as a higher order polynomial function of time. PCT also has an ability to represent multi component signal which makes it attractive to represent speech signal which is a multi component non stationary signal whose frequency varies arbitrarily with time. In this work, a similar approach to [11], is considered to estimate pitch from speech signal via instantaneous frequency estimation using polynomial chirplet transform. The estimation of instantaneous frequency is based on [16].

II. THEORY

A. Analytical signal

Discarding negative frequencies is critical in IF estimation. This can be achieved by computing the analytical signal of the signal. The analytic signal of a real signal is a complex signal which contains only the non negative frequency component of the original signal. The analytical signal $z(t)$ of a real signal $s(t)$ is computed using equation 1.

$$z(t) = s(t) + j\hat{s}(t) \quad (1)$$

where, $\hat{s}(t)$ is the Hilbert transform of the signal.

B. PCT

PCT has the ability to produce time frequency distribution (TFD) with good energy concentration for non stationary signals with arbitrary frequency where the linear transforms like STFT, WT and chirplet transform (CT) fail.

The PCT [16] of the signal $z(t)$ is defined as

$$\begin{aligned} PCT_s(t_0, \omega, \alpha_1, \dots, \alpha_n; \sigma) = & \int_{-\infty}^{\infty} z(t) \Phi_{\alpha_1, \dots, \alpha_n}^R(t) \times \\ & \Phi_{\alpha_1, \dots, \alpha_n}^M(t, t_0) \omega_{(\sigma)}(t - t_0) e^{-j\omega t} dt \end{aligned} \quad (2)$$

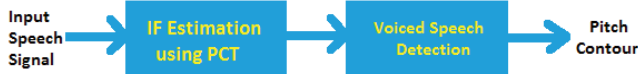


Fig. 1. Block diagram of the proposed algorithm

where

$$\Phi_{\alpha_1, \dots, \alpha_n}^R(t) = \exp(-j \sum_{k=2}^{n+1} \frac{1}{k} \alpha_{k-1} t^k)$$

$$\Phi_{\alpha_1, \dots, \alpha_n}^M(t, t_0) = \exp(j \sum_{k=2}^{n+1} \alpha_{k-1} t_0^{k-1} t)$$

are the frequency rotating operator and frequency shifting operator respectively. $\alpha_1, \alpha_2, \dots, \alpha_n$ are the coefficient of powers of time in polynomial kernel.

III. DESCRIPTION OF ALGORITHM

The block diagram of the proposed algorithm is shown in Fig. 1. The proposed algorithm for pitch extraction consists of two fundamental steps namely IF estimation and voiced speech detection. The IF of the signal is estimated using PCT which includes both voiced and non voiced parts of speech. Voiced speech detection is used to remove the unvoiced parts of speech so as to yield the true pitch contour of the speech signal. The pitch of the speech signal is calculated by averaging the IF values over all time values pertaining to voiced speech regions.

A. IF Estimation

The IF estimation method used in this work is adopted from [16]. In IF estimation based on PCT, all polynomial kernel characteristic parameters ($\alpha_1, \dots, \alpha_n$) are initialized to zero to compute TFD (which is equivalent to computing TFD using STFT) and estimate IF using peak detection from TFD. Subsequently, the estimated IF trajectory is approximated to a polynomial function of time by calculating coefficients of polynomial employing least squares framework. Using the estimated polynomial kernel, TFD is recomputed by utilizing PCT. This process is repeated till the average change in instantaneous frequencies in successive iterations ξ , computed using simpson's rule (used for evaluating the area under curve for computation of average value) goes below a certain threshold δ . The flow chart of IF estimation method using PCT is shown in Fig. 2.

B. Voiced speech detection

The output of IF estimation block consists frequencies of both voiced and unvoiced parts of speech signal. However, pitch represents the fundamental frequency of the voiced parts of speech signal as pitch is the frequency at which vocal cord vibrates. Vocal cord vibrates periodically for voiced part of speech signal, and randomly for unvoiced parts. Hence segmenting speech into voiced and unvoiced parts is crucial for avoiding false pitch prediction. The following criteria (similar to [11]), is used to recognize and eliminate the unvoiced parts of speech.

- Frequencies higher than 300Hz.
- Frequencies lower than 50Hz.

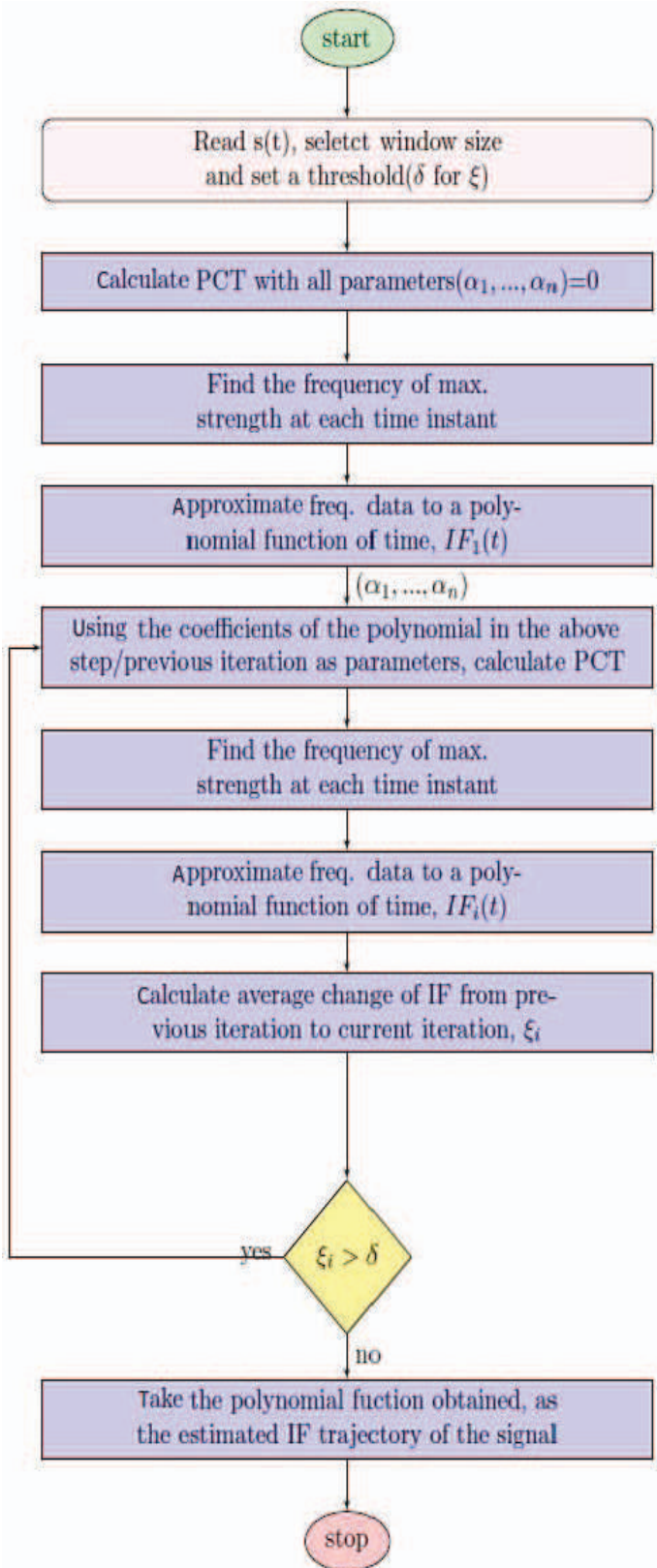
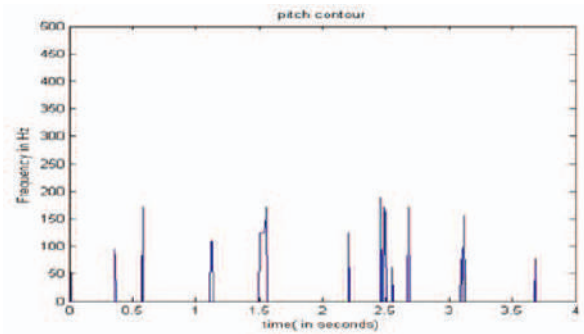
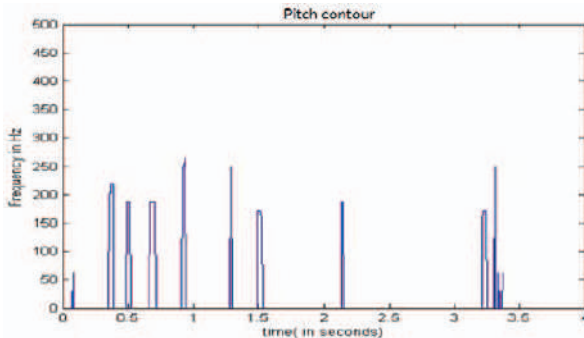


Fig. 2. Flowchart of IF estimation



(a) Pitch contour of a speech uttered by male person



(b) Pitch contour of a speech uttered by female person

Fig. 3. Pitch contours of speech

IV. RESULTS AND DISCUSSIONS

In this paper, TIMIT speech sample corpus [17] from MIT is used for the analysis. Database contains total 160 recordings, obtained from 16 persons 8 male voices and 8 female voices and each record contains 3-4 seconds recorded speech sampled at 16 kHz. Out of 160 records, 16 records are used in this work for analysis. In this work, all the simulations are performed on MATLAB platform. For each signal, IF is estimated using a seventh order polynomial (the order is decided by trial and error), as described in section III, with window length equal to 1024 samples, in step intervals of 100 samples, and δ set to 0.001. The value of δ is same for both female and male speeches. Voiced parts of speech are detected for estimation of IF. The speech used in this work consists of a sentence, "she had your dark suit and greasy wash water all year". The pitch contours of both the male and female signal are computed and shown in Fig. 3. The TFD of a speech signal computed using PCT is presented in Fig. 4. The pitch of speech uttered by 8 male and 8 female persons are calculated and tabulated in Table I which is also represented in pictorial form in Fig. 5. From Fig. 5, it can be observed that the average pitch of female voices are in between 186.06 – 238.06 Hz while the average pitch of male voices are in the range of 117.78 – 154.21 Hz. These values are in the same range of the general ranges of pitch values of male and female voices (50 – 150 Hz, 180 – 300 Hz respectively). This

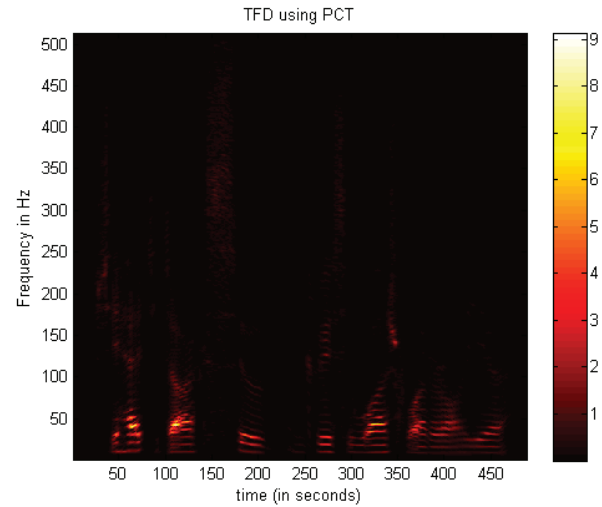


Fig. 4. TFD of a speech computed using PCT

Comparison of pitch values of speech of male, female persons

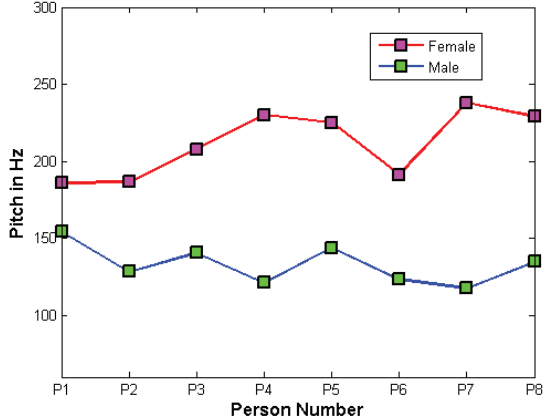


Fig. 5. Pitch of speech uttered by male and female

indeed verifies the results obtained. This method also relaxes the assumption that speech is locally stationary.

V. CONCLUSION AND FUTURE WORK

In this work, a novel approach for pitch detection by estimating instantaneous frequency using polynomial chirplet transform has been proposed. The IF of speech has been modeled as a high order polynomial function of time to compute the TFD of speech signal. The proposed method has been applied on speech signals of 8 male and 8 female persons saying "she had your dark suit and greasy wash water all year" selected from TIMIT database for computation of pitch. The values obtained for female voices are in the range of 186.06 – 238.06 Hz and for male voices have the pitch values varying in the range of 117.78 – 154.21 Hz, which are in concurrence with the general range of pitch values of

Gender	P1	P2	P3	P4	P5	P6	P7	P8
Male	154.21	128.28	140.62	121.09	143.97	123.48	117.78	134.76
Female	186.06	186.69	207.78	230.04	225.03	191.23	238.06	229.07

TABLE I
COMPARISON OF PITCH OF MALE AND FEMALE

female voices ($180 - 300\text{ Hz}$), and male voices ($50 - 150\text{ Hz}$). This indeed verifies the results. Performance evaluation of different time frequency analysis methods such as short time fourier transform, wavelet, chirplet transform, polynomial chirplet transform for pitch detection in speech on different standard speech corpora is author's current objective.

ACKNOWLEDGMENT

The authors would like to thank Mr. B. Sreenivasulu M.Tech., Department of Electronics and Communication Engineering, NITK for his support in this work.

REFERENCES

- [1] B. D. Barkana and J. Zhou, "A new pitch-range based feature set for a speakers age and gender classification," *Applied Acoustics*, vol. 98, pp. 52 – 61, 2015.
- [2] C. Adnene, B. Lamia, and M. Mounir, "Analysis of pathological voices by speech processing," in *Proceedings of Seventh International Symposium on Signal Processing and Its Applications*, vol. 1, pp. 365–367 vol.1, July 2003.
- [3] J. Marks, "Real time speech classification and pitch detection," in *Southern African Conference on Communications and Signal Processing, Proceedings. COMSIG*, pp. 1–6, Jun 1988.
- [4] L. Rabiner, M. Cheng, A. Rosenberg, and C. McGonegal, "A comparative performance study of several pitch detection algorithms," *IEEE Transactions on Acoustics, Speech and Signal Processing*, vol. 24, pp. 399–418, Oct 1976.
- [5] D. Talkin, "A robust algorithm for pitch tracking (rapt)," 1995.
- [6] M. Ross, H. Shaffer, A. Cohen, R. Freudberg, and H. Manley, "Average magnitude difference function pitch extractor," *IEEE Transactions on Acoustics, Speech and Signal Processing*, vol. 22, no. 5, pp. 353–362, 1974.
- [7] H. Zhao and W. Gan, "A new pitch estimation method based on amdf," *Journal of Multimedia*, vol. 8, no. 5, 2013.
- [8] P. Ghahremani, B. BabaAli, D. Povey, K. Riedhammer, J. Trmal, and S. Khudanpur, "A pitch extraction algorithm tuned for automatic speech recognition," in *IEEE International Conference on Acoustics, Speech and Signal Processing (ICASSP)*, pp. 2494–2498, IEEE, 2014.
- [9] A. M. Noll, "Cepstrum pitch determination," *The journal of the acoustical society of America*, vol. 41, no. 2, pp. 293–309, 1967.
- [10] L. Gu and K. Rose, "Perceptual harmonic cepstral coefficients for speech recognition in noisy environment," in *IEEE International Conference on Acoustics, Speech, and Signal Processing, Proceedings ICASSP*, vol. 1, pp. 125–128, IEEE, 2001.
- [11] H. Yang, L. Qui, and S.-N. Koh, "Application of instantaneous frequency estimation for fundamental frequency detection," in *Proceedings of the IEEE-SP International Symposium on Time-Frequency and Time-Scale Analysis*, pp. 616–619, IEEE, 1994.
- [12] L. Rabiner, M. J. Cheng, A. E. Rosenberg, C. McGonegal, et al., "A comparative performance study of several pitch detection algorithms," *IEEE Transactions on Acoustics, Speech and Signal Processing*, vol. 24, no. 5, pp. 399–418, 1976.
- [13] K. Oh, C. Un, et al., "A performance comparison of pitch extraction algorithms for noisy speech," in *IEEE International Conference on ICASSP Acoustics, Speech, and Signal Processing*, vol. 9, pp. 85–88, IEEE, 1984.
- [14] O. Babacan, T. Drugman, N. d'Alessandro, N. Henrich, and T. Dutoit, "A comparative study of pitch extraction algorithms on a large variety of singing sounds," in *IEEE International Conference on Acoustics, Speech and Signal Processing (ICASSP)*, pp. 7815–7819, IEEE, 2013.
- [15] D. Gerhard, *Pitch extraction and fundamental frequency: History and current techniques*. Regina: Department of Computer Science, University of Regina, 2003.
- [16] Z. Peng, G. Meng, F. Chu, Z. Lang, W. Zhang, and Y. Yang, "Polynomial chirplet transform with application to instantaneous frequency estimation," *IEEE Transactions on Instrumentation and Measurement*, vol. 60, no. 9, pp. 3222–3229, 2011.
- [17] W. E. Fisher, G. R. Doddington, and K. M. Goudle-marshall, "The darpa speech recognition research database: specifications and status," 1986.

Reconstruction of Edges from Fan-Beam Projections

A V Narasimhadhan

Electronics and Communication Engineering
National Institute of Technology
Karnataka, Surathkal, India.
Email: dhan257@gmail.com

Aman Sharma

Electronics and Electrical Engineering
National Institute of Technology
Goa, India.

Shashidhar G. Koolagudi

Computer Science and Engineering
National Institute of Technology
Karnataka, Surathkal, India.

G V S S K R Naganjaneyulu

Electronics and Communication Engineering
National Institute of Technology
Karnataka

Sure Avinash

Electronics and Communication Engineering
National Institute of Technology
Karnataka

Vinay Peddireddy

Electronics and Communication Engineering
National Institute of Technology
Karnataka

N Bal Kishan

Electronics and Communication Engineering
National Institute of Technology
Karnataka.

Jeny Rajan

Computer Science and Engineering
National Institute of Technology
Karnataka.

Abstract—The goal of computerised tomography is to reconstruct cross sectional image of the object under consideration from its projections whereas edge detection is an image analysis problem of utmost importance in medical imaging to outline the boundaries of tumours, bones etc. In this paper, a technique to reconstruct the edges directly from fan-beam projections, using the Marr-Hildreth operator, is presented. To obtain the edge map of object under consideration, the divergent beam transform of Marr-Hildreth operator is convolved with ramp filter to yield an edge reconstruction filter which is finally convolved with the acquired fan-beam projections and back-projected, resulting in a convolution back-projection, to reconstruct the edges. The paper also discusses about the utilisation of state-of-the-art Noo's algorithm to reconstruct the edges directly from equi-angular fan beam projections. Finally, the proposed technique is simulated to make relevant conclusions and inferences.

I. INTRODUCTION

The ultimate goal of large number of image processing applications and computer vision is to extract the important features from an image and pass it over to a machine which is apt in analysing and interpreting the data contained in it. Several applications can be found in [1]. In the domain of medical image analysis, edge detection is used in the detection of boundaries of tumors and internal organs, to study their size and shape. Since specific information is needed in the aforementioned applications, reconstructing a high resolution image is not of utmost importance. Also, in case of positron emission tomography, object contours need to be determined in the reconstruction of cross-sections [2], [3].

The conventional Edge detection procedures given in [4], [5] follow a two step methodology: first, to reconstruct the entire cross sectional image of the object being imaged and secondly, filtering the obtained image with an edge detection filter to detect the edges. There are problems associated with this execution strategy: 1. Post image processing is a challenge,

which is evident from [6], as even when the noise in the acquired projections is white, the noise in the reconstructed image is non-white. 2. A good number of projections are to be acquired for reconstructing a fair quality image. 3. The computational burden is high as compared to directly reconstructing the edges from projections [7].

To avoid the aforementioned problems, it is advantageous to reconstruct the edges directly from the acquired sequential projections. *N. Srinivasa et. al.* [7] addressed this issue by introducing a technique to reconstruct the edges directly from acquired sequential parallel beam projections, using the Marr-Hildreth operator. The main reason for the theoretical validity of technique described in [7] is the fact that the Radon transform of the 2-D convolution of two functions is equal to the 2-D convolution of Radon transform of individual functions [8].

In this paper, the idea mentioned above is utilized to reconstruct the edges of cross section directly from equi-angular fan-beam projections by using the following reconstruction strategies: 1. Classical Fan beam FBP reconstruction algorithm [9] and 2. State of art Fan beam reconstruction algorithm given by *Noo et. al.* [10]. The paper aims to facilitate good image to the machine, consequently leading to minimizing the errors associated with boundary identification, shape and size estimation of tumors, internal organs etc.

The paper is organized as follows; first, mathematical reasoning of 'why the proposed technique is possible?' will be formulated followed by a brief description of classical fan-beam FBP algorithm and the state of art algorithm described in [10]. In the following section, mathematics of proposed technique are presented followed by its incorporation procedure in the aforementioned algorithms. Next, the validity of proposed technique is tested by means of computer simulations and finally advantages of reconstructing edges directly from

fan beam projections, as compared to the conventional two step procedure, are enlisted.

II. DETECTING EDGES DIRECTLY FROM DIVERGENT BEAM PROJECTIONS

Let $f(\mathbf{x})$ be the image of the cross-section obtained from FBP reconstruction algorithm where $\mathbf{x} = [x \ y]^T$ and $h(\mathbf{x})$ be an arbitrary linear edge detection filter. The straightforward approach to detect the edges would involve filtering the given image with the edge detection filter to yield the image depicting only edges

$$g(\mathbf{x}) = f(\mathbf{x}) * h(\mathbf{x}), \quad (1)$$

where $*$ is convolution operator. The goal is to reconstruct edges directly from fan-beam projections and therefore $f(\mathbf{x})$ is unknown, however its divergent beam transform $-D(\lambda, \gamma)$ is known, where λ is the angle subtended by the line joining X-ray source to the origin with respect to horizontal axis and γ is the angle between a ray with in a fan and central fan-beam ray passing through the origin. The transformation is given by:

$$\mathcal{T}[f(\mathbf{x})] = D(\lambda, \gamma), \quad (2)$$

where \mathcal{T} denotes the divergent beam transformation operator and

$$D(\lambda, \gamma) = \int_0^\infty f(\mathbf{a}(\lambda) + t\boldsymbol{\alpha}) dt. \quad (3)$$

Here, $\mathbf{a}(\lambda) = R_0 [\cos \lambda \ \sin \lambda]^T$ and $\boldsymbol{\alpha} = \cos \gamma \mathbf{e}_u(\lambda) + \sin \gamma \mathbf{e}_v(\lambda)$. R_0 is the radius of circular scan trajectory and $\mathbf{e}_u, \mathbf{e}_v$ are orthogonal unit vectors defined as $\mathbf{e}_u(\lambda) = [-\sin \lambda \ -\cos \lambda]^T$ and $\mathbf{e}_v(\lambda) = [-\sin \lambda \ \cos \lambda]^T$.

Let J be a variable defined as:

$$J(\lambda, \gamma) = \mathcal{T}[f(\mathbf{x})] * \mathcal{T}[h(\mathbf{x})]. \quad (4)$$

It can be mathematically shown that,

$$J(\lambda, \gamma) = \mathcal{T}[f(\mathbf{x}) * h(\mathbf{x})] \quad (5)$$

also,

$$g(\mathbf{x}) = \mathcal{T}^{-1}[J(\lambda, \gamma)], \quad (6)$$

therefore, equation (6) proves the fact that edge reconstruction is indeed possible directly from acquired divergent beam projections by inverting the divergent beam transform of $J(\lambda, \gamma)$. The algorithms discussed in [10], [9] are used to invert the divergent beam transform. Additionally, J can be obtained practically from (4).

III. EDGE DETECTION FILTER

Marr-Hildreth operator is used as the edge detection filter to reconstruct edges directly from fan-beam projections. However, any linear and circularly symmetric (isotropic function) edge detection filter may be employed to accomplish the desired objective. Let $\mathcal{M}(\mathbf{x})$ denote the Marr-Hildreth operator, which is defined below:

$$\mathcal{M}(\mathbf{x}) = \nabla^2 \mathcal{G}(\mathbf{x}) \quad (7)$$

and $\mathcal{G}(\mathbf{x})$ represent a 2-D Gaussian function with standard deviation σ , given by:

$$\mathcal{G}(\mathbf{x}) = \frac{1}{2\pi\sigma^2} e^{-\left(\frac{\|\mathbf{x}\|^2}{2\sigma^2}\right)}. \quad (8)$$

Equation (7) further evaluates to

$$\mathcal{M}(\mathbf{x}) = -\frac{1}{\pi\sigma^4} \left(1 - \frac{\|\mathbf{x}\|^2}{2\sigma^2}\right) e^{-\left(\frac{\|\mathbf{x}\|^2}{2\sigma^2}\right)}, \quad (9)$$

To compute J , divergent beam transform of Marr-Hildreth operator needs to be convolved with acquired fan beam projections as per equation (4), yielding,

$$J(\lambda, \gamma) = \mathcal{T}[f(\mathbf{x})] * \mathcal{T}[\mathcal{M}(\mathbf{x})]. \quad (10)$$

With reference to [7], Radon transform of Marr-Hildreth operator is given by

$$\mathcal{R}[\mathcal{M}(\mathbf{x})] = \frac{1}{\sqrt{2\pi}\sigma^5} (s^2 - \sigma^2) e^{-\frac{s^2}{2\sigma^2}}, \quad (11)$$

where Radon transform is defined as:

$$P(\mathbf{n}, s) = \mathcal{R}[f(\mathbf{x})], \quad (12)$$

\mathcal{R} is the Radon transformation operator. Let \mathbf{n} describe the direction of normal to the Parallel beam rays and s is the distance of an individual ray from the origin along \mathbf{n} , concretely

$$P(\mathbf{n}, s) = \int_{R^2} f(\mathbf{x}) \delta(\mathbf{x} \cdot \mathbf{n} - s) d\mathbf{x}. \quad (13)$$

By using the rebinning relation between a parallel beam and fan beam ray [9], one can directly write $s = R_0 \sin \gamma$ and substitute it in (11) to obtain the divergent beam transform of Marr-Hildreth operator

$$\mathcal{R}[\mathcal{M}(\mathbf{x})] = \frac{1}{\sqrt{2\pi}\sigma^5} ((R_0 \sin \gamma)^2 - \sigma^2) e^{-\frac{(R_0 \sin \gamma)^2}{2\sigma^2}}. \quad (14)$$

By substituting the above value obtained for $\mathcal{R}[\mathcal{M}(\mathbf{x})]$ in equation (10), $J(\lambda, \gamma)$ can be computed and the algorithms described in [10], [9] can successfully reconstruct the edges directly from acquired fan-beam projections.

IV. IMAGE RECONSTRUCTION ALGORITHMS FROM FAN-BEAM PROJECTIONS

In this section, two image reconstruction algorithms, which serve as the recipient of our proposed technique to reconstruct edges from divergent beam projections, are briefed.

A. Classical fan-beam FBP reconstruction algorithm:

With reference to [9], image reconstruction formula from equi-angular fan-beam projections is given by:

$$f(\mathbf{x}) = \int_0^{2\pi} \frac{1}{L^2} d\lambda \int_{-\gamma_{max}}^{\gamma_{max}} D(\lambda, \gamma) p(\gamma' - \gamma) R_0 \cos \gamma d\gamma \quad (15)$$

where,

$$L = \sqrt{[R_0 + \mathbf{x} \cdot \mathbf{e}_u(\lambda)]^2 + [\mathbf{x} \cdot \mathbf{e}_v(\lambda)]^2}$$

$$\gamma' = \tan^{-1} \left(\frac{\mathbf{x} \cdot \mathbf{e}_v(\lambda)}{R_0 + \mathbf{x} \cdot \mathbf{e}_u(\lambda)} \right)$$

$$p(\gamma) = \frac{1}{2} \left(\frac{\gamma}{\sin \gamma} \right)^2 h_F(\gamma)$$

and $h_F(\gamma)$ is the impulse response of a ramp filter, given by:

$$h_F(\gamma) = \int_{-\infty}^{\infty} |\omega| e^{j2\pi\omega\gamma} d\omega. \quad (16)$$

The time invariant filter is practically implemented due to its simplicity as compared to time variant filter [11]; the latter should be implemented as suggested by the theoretical work demonstrated in [12]. The implementation of the time invariant filter results in the quality of image being affected at regions where the object is close to the source.

B. State of art fan-beam FBP reconstruction algorithm proposed by Noo. et. al.:

With reference to [10], image reconstruction formula from equi-angular divergent beam projections is given by:

$$f(\mathbf{x}) = \frac{1}{2\pi} \int_0^{2\pi} \frac{1}{\|\mathbf{x} - \mathbf{a}(\lambda)\|} D_F^m(\lambda, \gamma') d\lambda \quad (17)$$

where,

$$D_F^m(\lambda, \gamma') = \int_{-\gamma_{max}}^{\gamma_{max}} h_H(\sin(\gamma' - \gamma)) \left(\frac{\partial}{\partial \lambda} + \frac{\partial}{\partial \gamma} \right) D(\lambda, \gamma) d\gamma$$

and $h_H(\gamma')$ is the impulse response of a Hilbert filter given by

$$h_H(\gamma') = -\frac{1}{2\pi} \int_{-\infty}^{\infty} j \operatorname{sgn}(\omega) e^{j2\pi\omega\gamma'} d\omega, \quad (18)$$

with $j = \sqrt{-1}$ and $\operatorname{sgn}(\omega)$ denoting the Signum function. Since the above reconstruction formula is basically derived from the rebining formula [13], it avoids the presence of variable cut off frequency limits and hence the notion of time variant filter is out of the scenario. This paper is all about edge detection by means of retaining the higher frequencies. The filtering part of (17) says that first derivative of projections is implemented followed by Hilbert filtering, resulting a relatively smooth image being obtained as compared to the image obtained by using conventional FBP algorithm [14].

V. INCORPORATION OF EDGE DETECTION METHOD IN THE FAN BEAM FBP RECONSTRUCTION ALGORITHM

So far all the tools required to develop the proposed technique have been introduced. This section is devoted to putting all the presented tools together to derive the edge reconstruction formula from equi-angular fan-beam projections. The image reconstruction formula depicted in equation (15) involves back-projection of ramp-filtered fan-beam projections. By imbibing our proposed technique into this reconstruction formula, the following edge reconstruction formula is obtained

$$g(\mathbf{x}) = \int_0^{2\pi} \frac{1}{L^2} d\lambda \int_{-\gamma_{max}}^{\gamma_{max}} J(\lambda, \gamma) p(\gamma' - \gamma) R_0 \cos \gamma d\gamma. \quad (19)$$

In words, the projections are first filtered through the Marr-Hildreth edge detection filter and then undergo the conventional FBP reconstruction algorithm. This formula is referred to as modified conventional FBP formula.

To convert the image reconstruction formula depicted in equation (17) to an edge reconstruction formula, the proposed technique is incorporated into the algorithm to yield

$$g(\mathbf{x}) = \frac{1}{2\pi} \int_0^{2\pi} \frac{1}{\|\mathbf{x} - \mathbf{a}(\lambda)\|} J_F^m(\lambda, \gamma') d\lambda, \quad (20)$$

where $J_F^m(\lambda, \gamma')$ is given by

$$J_F^m(\lambda, \gamma') = \int_{-\gamma_{max}}^{\gamma_{max}} h_H(\sin(\gamma' - \gamma)) \left(\frac{\partial}{\partial \lambda} + \frac{\partial}{\partial \gamma} \right) J(\lambda, \gamma) d\gamma.$$

In words, the fan-beam projections are first filtered through the Marr-Hildreth window and subsequently undergo the Noo's algorithm. This formula is referred to as modified Noo's FBP formula for further reference.

Please note that Due to the validity of (21), the methodology described in the abstract is implicitly incorporated in the proposed technique:

$$D(\lambda, \gamma) * (h_F(\gamma) * \mathcal{T}[\mathcal{M}(\mathbf{x})])|_{\gamma=\gamma'} = (D(\lambda, \gamma) * \mathcal{T}[\mathcal{M}(\mathbf{x})]) * h_F(\gamma)|_{\gamma=\gamma'}. \quad (21)$$

The edge reconstruction formula, in a nutshell, is the inverse divergent beam transform of Marr-Hildreth (or any other linear circularly symmetric edge detection operator) filtered fan-beam projections. The aforementioned algorithm theoretically invert the windowed divergent beam projection data to reconstruct the edges. The following section gives validation of the theoretical formulations by means of computer simulations.

VI. SIMULATION RESULTS

Equi-angular fan-beam projections of a low contrast Shepp Logan phantom is generated, followed by reconstruction of edges directly from acquired projections by employing the proposed technique. In the simulation, firstly, the edges from acquired fan-beam projections are reconstructed for a scan radius which is twice the radius of field of view (FOV) of the phantom for different values of standard deviation σ using both the discussed reconstruction algorithms. This procedure helps to select the best value of σ . For the chosen best σ , edges are reconstructed from fan-beam projections for a couple of values of scan radius comparable to the radius of FOV.

Following the qualitative simulation results, data pertaining to computational cost are presented to ascertain the readers about the advantage of proposed algorithm over conventional edge detection algorithms.

A. Scan parameters:

The above mentioned procedure is simulated for the scanning parameters mentioned in Table I. The edge map will be reconstructed on a 2-D plane with 360 X 360 pixels for a total of 512 detectors with angular spacing of 0.002° . The radius of FOV is taken as 1 and the scanning radius is set to twice the value of radius of FOV, i.e. 2. Later this value is set to 1.2 and 1.1 to compare the performance of the illustrated reconstruction algorithms at scanning radius comparable to the radius of FOV at the best σ .

TABLE I: Fan-beam imaging parameters used in simulations

Imaging Parameter	Value
Number of pixels ($N_{pic} \times N_{pic}$)	360 ²
Object radius (FOV) (r)	1.0
Scanning radius (R_0)	2, 1.2, 1.1
Source to detector distance	4, 2.4, 2.2
Number of source positions	512
Detector element angular width ($\Delta\gamma$)	0.002°
Number of Detectors (N)	512

TABLE II: Computational Burden

Methodology	Time (seconds)
Conventional fan beam FBP followed by edge detection	11.4
Proposed conventional fan-beam FBP edge detection	10.1
Conventional Noo's algorithm followed by edge detection	13.1
Proposed variant of Noo's algorithm for edge detection	11.5

B. Observations:

On simulating the proposed technique for conventional fan-beam FBP algorithm and Noo's algorithm, the results obtained are shown in Fig. 1, 2, 3. The original Shepp Logan phantom is depicted in Fig. 1(a), which undergoes a divergent beam transformation upon illuminated by a fan of equi-angular rays for a scanning radius of 2 and series of values of $\sigma = 0.1, 0.01, 0.005, 0.001$. The edges reconstructed are shown in figure 1(b),(c),(d),(e) and 2(a),(b),(c),(d). From visual inspection, the value of $\sigma = 0.005$ results in reconstructing sharpest edges as compared to other values for both the reconstruction algorithms –1(d) and 2(c). Therefore $\sigma = 0.005$ is chosen to evaluate the performance of our proposed technique, incorporated in both the reconstruction algorithms, for scanning radii comparable to the radius of FOV.

Two values of scanning radius i.e. 1.2 and 1.1 are chosen to simulate the proposed technique for both the reconstruction algorithms. The results of edge detection for modified conventional fan-beam FBP reconstruction algorithm is depicted in Fig. 3(a),(b) and for modified Noo's algorithm, it is depicted in Fig. 3(c),(d).

C. Juxtaposition of Computational Cost:

To obtain the computational burden on a processor, executing the conventional and proposed edge detecting algorithms, Compute Unified Device Architecture (CUDA) has been utilised. The machine used have the following hardware specifications:

CPU - Intel i7-2640M @ 2.80GHz

GPU - NVIDIA GeForce GT 525M

It has been observed that conventional fan beam FBP reconstruction algorithm followed by edge detection filtering took 11.4 seconds whereas detecting edges, post state of art Noo's algorithm took 13.1 seconds. The methodology proposed in the paper, on both of the aforementioned strategies, successfully reduced the computational time to 10.1 and 11.5 seconds respectively. The results are tabulated and summarised in Table

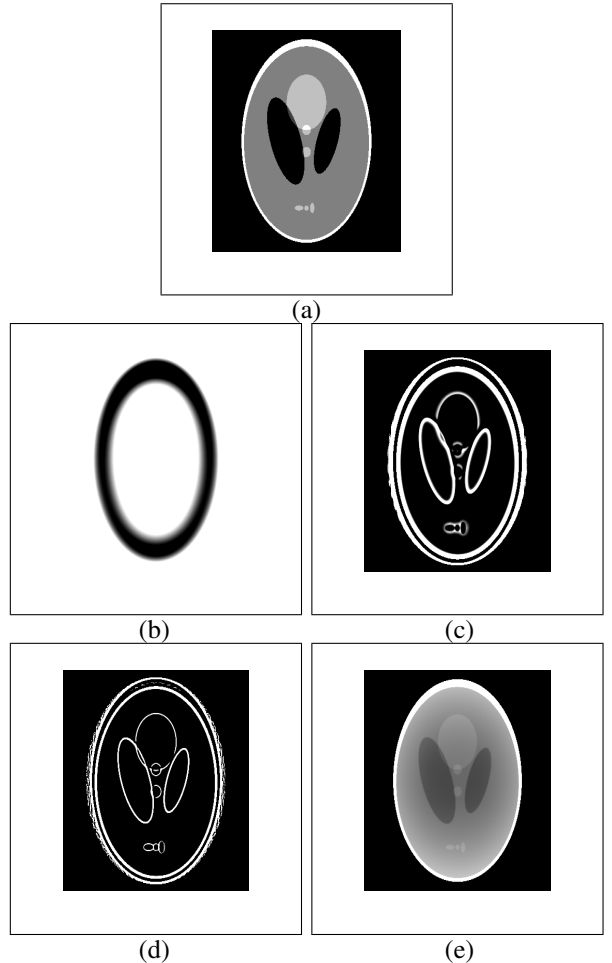


Fig. 1: Reconstruction edges of Low contrast Shepp-Logan phantom from fan-beam projections using modified conventional fan-beam algorithm (a) Original Phantom. (b) with $R = 2$ and $\sigma = 0.1$. (c) with $R = 2$ and $\sigma = 0.01$. (d) with $R = 2$ and $\sigma = 0.005$ and (e) with $R = 2$ and $\sigma = 0.001$.

II. The computational efficiency can be achieved relatively high, if the proposed method is extended to 3D reconstruction.

D. Inference/Discussion:

It is very evident from the observed results that the proposed technique successfully reconstructs the edges of a low contrast phantom from its acquired sequential fan-beam projections. The proposed conventional fan-beam FBP edge detection algorithm reduced the computational burden by 11.4% over conventional methodology whereas modified Noo's algorithm for edge detection reduced the computation burden by 12.2%.

Secondly, as the scanning radius becomes small, artefacts can be witnessed along the boundary of the semi-major axis of the biggest ellipse (of the phantom) as shown in figure 3(a),(b),(c),(d). These artefacts, abrupt changes in intensity, are predominant in the images reconstructed by employing the proposed modified conventional fan-beam FBP algorithm, see Fig. 3(a),(b) as compared to the images reconstructed from modified Noo's algorithm as shown in Fig. 3(c),(d) due to

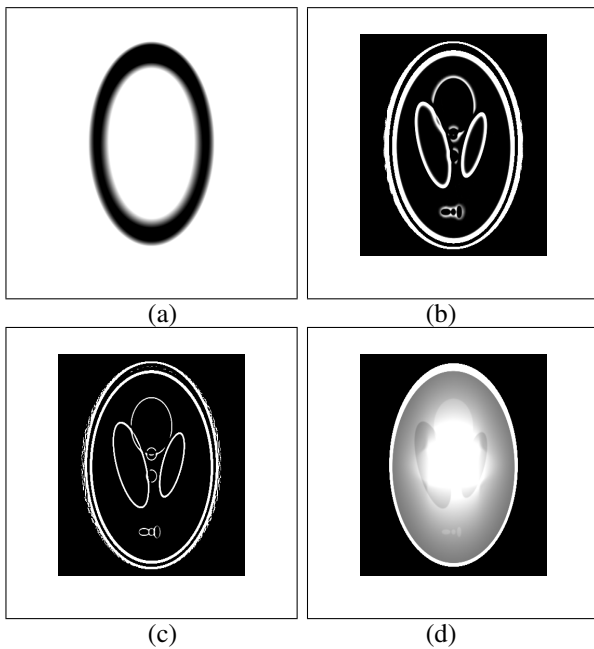


Fig. 2: Reconstruction of edges of Low contrast Shepp-Logan phantom from fan-beam projections using modified Noo's fan-beam algorithm for edge detection (a) with $R = 2$ and $\sigma = 0.1$. (b) with $R = 2$ and $\sigma = 0.01$. (c) with $R = 2$ and $\sigma = 0.005$ (d) with $R = 2$ and $\sigma = 0.001$.

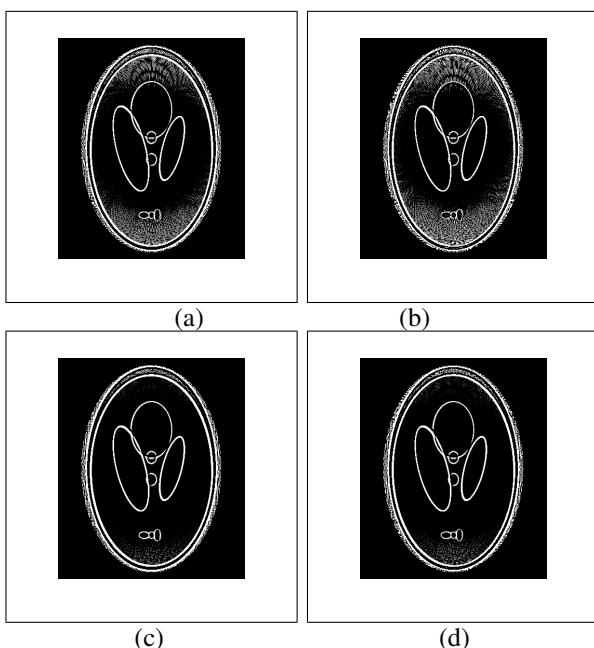


Fig. 3: Reconstruction of edges of Low contrast Shepp-Logan phantom from fan-beam projections using (a) modified conventional FBP algorithm with $R = 1.2$ and $\sigma = 0.005$ and (b) with $R = 1.1$ and $\sigma = 0.005$. (c) modified Noo's fan-beam algorithm with $R = 1.2$ and $\sigma = 0.005$ and (d) with $R = 1.1$ and $\sigma = 0.005$

the Hilbert filtering of differentiated acquired projections in the latter algorithm and time invariant filter implemented in the former algorithm. The reason for the artefacts to occur primarily only along the vertical axis is due to the very small distance of the vertical tip of the phantom from the X-ray source as compared to a relatively large distance along the horizontal.

VII. CONCLUSION

Presented paper theoretically formulated the mechanics of detecting edges from fan-beam projections and indeed corroborated the purported claim by means of articulated modified fan beam FBP edge detection algorithm and modified Noo's edge detection methodology (utilising the Marr-Hildreth operator). The methodology developed in the paper has also been found to be effective in reducing the computational burden on the processor by 11.4% and 12.2% respectively for fan-beam FBP and Noo's algorithm, as in the conventional two-step method for detecting edges, reconstructed image has to undergo 2-D filtering to yield the edges whereas in the proposed technique, 1-D filtering is required (in the projection domain). Moreover, the proposed technique is advantageous in terms of preventing one in getting into post image processing challenges. The developed theory in this paper can be extended to the recent fan- and cone-beam algorithms [15], [16].

REFERENCES

- [1] Anil K. Jain, 1989, Fundamentals of Digital Image Processing, *Prentice-Hall, Inc.*
- [2] Bergstrom M, Litton J, Eriksson L, Bohm C, and Blomqvist G, 1982, Determination of object contour from projections for attenuation correction in cranial positron emission tomography, *J. Comput. Assist. Tomogr.*, **6**, 356-372.
- [3] Knoll G F, 1983, Single photon emission computed tomography, *Proc. IEEE*, **71**, 320-328.
- [4] Belanger M G, Yasnoch W A, Penn R D, and Bacus J W, 1979, Automated scene analysis of CT scans, *Computerized Tomography*, **3**, 201-211.
- [5] Selfridge P G, Prewitt J M S, 1981, Organ detection in abdominal computerized tomography scans: Applications to the kidney, *Comput. Graphics Image Processing*, **15**, 265-278.
- [6] Riedere S T, Pelec N J, and Chesler D A, 1978, The noise power spectrum in computed X-ray tomography, *Phys. Med. Biol.*, **6**, 441-451.
- [7] Srinivasa N, Ramakrishnan K R, K. Rajgopal, 1992, Detection of Edges from Projections, *IEEE Trans. Medical Imaging*, **11(1)**, 76-80.
- [8] Deans S R, 1983, The Radon transform and some of its Applications, *New York: Wiley*.
- [9] Kak A C, Slaney M, 1987, Principles of Computerized Tomography, *IEEE Press, New York*.
- [10] Noo F., Defrise M., Kudo H., 2002, Image reconstruction from fan beam projections on less than a short-scan, *Phys. Med. Biol.*, **47**, 2525-2546.
- [11] Zeng G L, 2004, Nonuniform noise propagation by using the ramp filter in fan-beam computed tomography, *IEEE Trans. Med. Imag.*, **23(6)**, 690-695.
- [12] Pan X and Yu L, 2003, Image reconstruction with shift-variant filtration and its implication for noise and resolution properties in fan-beam computed tomography *Med. Phys.* **30** 590-600.
- [13] Hamaker C, Smith K T, Solmon D C, and Wagner S L, 1980, The divergent beam x-ray transform, *Rocky Mountain J. Math.*, **10**, 253-283.
- [14] Zamyatin A A, Taguchi K and Silver M D, 2006, Practical hybrid convolution algorithm for helical CT reconstruction, *IEEE Trans. Nucl. Sci.*, **53(1)**, 167-174.
- [15] Dennerlein F, Noo F, Hornegger J and Lauritsch G, 2007, Fan-beam filtered-backprojection reconstruction without backprojection weight, *Phys. Med. Biol.*, **52**, 3227-3240.

- [16] Narasimhadhan A V and Rajgopal K, 2012, FDK-Type algorithms with no backprojection weight for circular and helical cone-beam CT, *International Journal of Biomedical Imaging*, **2012**.
- [17] Narasimhadhan A V, Aman Sharma and Dipen Mistry, 2013 Image Reconstruction from Fan-Beam Projections without Back-Projection Weight in a 2-D Dynamic CT: Compensation of Time-Dependent Rotational, Uniform Scaling and Translational Deformations, *Open Journal of Medical Imaging*, **3**.

DESIGN AND INTERFACING OF I2C MASTER WITH REGISTER AND LCD SLAVES

A.Sainath Chaithanya¹

¹Asst. Prof,

Department of ECE,
RGUKT Basar,
Telangana, India.
chaithanya.aravalli@gmail.com

D.Sindhuja²

²B'tech Student,
Department of ECE,
RGUKT Basar,
Telangana, India.
sindhudarra55@gmail.com

D.Bhavana³

³B'tech Student,
Department of ECE,
RGUKT Basar,
Telangana, India.
dablikarbhavana96@gmail.com

P. Vennela⁴

⁴B'tech Student,
Department of ECE,
RGUKT Basar,
Telangana, India.
vennela1599@gmail.com

Abstract-- One of the foremost well-liked Serial communication standards I2C a bus protocol developed by Philips Semiconductors for exchange of transactions among the peripherals residing on constant circuit card. It supports communication between multiple masters with multiple slaves by employing a two-wire duplex serial bus, one for data and further for clock, emphasizing simple and economical technique of information exchange. This work involves I2C controller interfacing with two slaves, one is register memory makes data to write or scan from, followed with implementation of single master I2C on Spartan 3E FPGA such that LCD acting as slave2 for effective read/write operations. The entire module developed in Verilog, simulated in ISim 10.0b and synthesized by XST of Xilinx ISE14.4 tool.

Keywords— I2C Bus, SDA, SCL, Verilog, FPGA, Xilinx14.4 tool.

I. INTRODUCTION

Serial bus communication protocols [8] SPI, UART, USB, IEE1394 uses multiplexing of information and forwarding of messages to service multiple devices are just straight line data transfer bus protocols. To beat this drawback, I2C bus developed by Philips Company could be a single two-way serial bus that supports multiple masters and slaves for communication between them within a circuit board. Samples of uncomplicated I2C [3] compatible devices found in embedded systems embrace EEPROMs, thermal sensors, and real time clocks as shown in figure1.

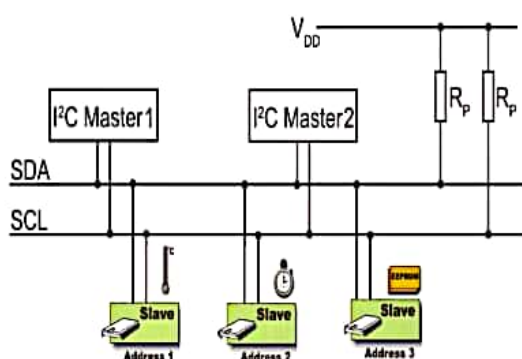


Fig 1: I2C Multi master and slave

Serial information communication protocols like RS-232, RS-422, RS-485, SPI interfacing high speed and low speed peripherals requires more pin connection and size in the IC realization, for past few decades the physical size of IC has slashed that created a thirst of requiring less quantity of pin association for serial data transfer hence I2C evolved that not solely simplifies the system level interconnect design however conjointly improves system performance since the transmission of digital data information is a lot of less prone to interference from environmental noise sources.

This article enlightens I2C bus protocol and its electrical characteristics, working methodology, technique of interface through simple register memory following with the hardware implementation [11] of I2C master bus controller on Spartan 3E FPGA where I2C interfaces with LCD slaves.

II. I2C PROTOCOL

The I2C Controller is a bi-directional serial bus for infrequent short distance communication between devices employs two wires----

SDA: Transmission of any information takes places through this line.

SCL: A clock line that is liable for monitoring and synchronizing the communication.

A master device that initiates a data transfer on the bus also generates the clock signals to permit data transfer as delineate in figure 2. Any device it addresses is taken into account as a slave is recognized by a novel address whether or not it's a microcontroller, LCD driver, memory or keyboard interface which may operate as either a transmitter or receiver, reckoning on the requirement.

Electrical Characteristics

I2C associates open-drain/open-collector [1] with an input buffer on the data line, which permits a same line to be used for an information flow.

Switched Inductor Quazi Switched boost Converter for the Nano-Grid Applications

Mohammad Meraj,
Dept. of Electrical Engg.,
Qatar University, Al-Dafna,
Doha, Qatar
meraj@qu.edu.qa,

Md Arif Ali
Dept. of Electrical Engg.,
RGUKT Basar,
Nizamabad, India
arifmd4073@gmail.com

Syed Rahman, Sagar Mahajan Bhaskar, Atif Iqbal,
Mohammad Abdulla E Al Hitmi
Dept. of Electrical Engg.,
Qatar University, Al-Dafna,
Doha, Qatar
syed.rahman@qu.edu.qa, sagar25.mahajan@gmail.com,
atif.iqbal@qu.edu.qa, m.a.alhitmi@qu.edu.qa

Abstract — Each commercial and residential buildings energy management system can be efficiently/ economically realized by integration of the solar photovoltaics (acting as the renewable power generator), battery energy storage system (ESS) along with the power electronic converters. The switched boost converters are the attractive solutions for the nano-grid applications where with a single stage operation, voltage boost, storage in battery and simultaneously inversion to the required AC voltage levels can be achieved. Here, a novel switched inductor Quasi switched boost converter is proposed. The proposed converter can operate in different modes such as multiple inputs and multiple outputs for the battery storage, PV and the load. The proposed converter reduces the shoot through requirement and improves the modulation index by increasing the gain of the DC-DC stage. The benefits of the proposed converter are: 1) high gain during PV to BESS mode, 2) high modulation index for the DC-AC stage, 3) continuous input current, 4) reduced shoot-through time which reduces the current ripple, 5) high efficiency and 6) increased reliability. The different operating modes to achieve these benefits are also presented in this paper. The detailed mathematical modelling of the proposed converter is carried out. MATLAB/SIMULINK simulation results which validates the benefits with proposed converter are given. Experimental results are obtained by developing a 120W prototype in the laboratory.

Keywords—DC – AC converter, DC – DC converter, Pulse width modulation (PWM), Photovoltaic (PV), Shoot-through (ST) duty cycle, Micro-grid, Nano-grid.

I. INTRODUCTION

Distributed Generation (DG) is a replacement for centralized conventional power plants which is based on Renewable Energy Resources (RES). To decrease the degrading effects of fossil fuels, DGs are being integrated to conventional power system to meet the energy requirement in islanded as well as grid connected modes. DGs make exclusive use of solar PV and wind to exhibit least environmental effect. By making this practice more popular, carbon dioxide emission can be effectively decreased in residential and commercial building. Along with the use of DGs, reliability of RES can be improved by adding Battery Energy Storage (BES) to RES. With this integration, we can expect drastic changes in power system structure of both residential and commercial spaces. One such distributed energy management system is Nano-grid (NG). It includes generation source (PV/wind), BES and in-house power distribution system

as well as home appliances (acting as load). In other words, NG can be defined as the downscaled version of the Micro-Grid (MG), ranging from watts to several kW and usually operate along with the common power line [6]. Furthermore, NG can operate in integration with the utility grid or in the islanded mode. It can be used to feed either AC or DC load [7]. Fig. 1, represents multiple NGs (cumulatively connected to forms a MG), AC-NG power conversion stages and interconnecting gateway. Here the gateway links the utility grid to the MG. It is required to make the utility grid connected NG to effectively operate in an off-grid mode optionally as it can handle the power failures in the national utility grid, in addition to that, it can function even without the national grid [8]. Finally, NG is small and closely packed power electronic converter-based grid system. It controls the power between PV, home /commercial appliances and BES with variety of usage patterns by taking into consideration factors like cost, CO₂ release and energy availability [9].

Conventional methods provided low output voltage as voltage of PV panels is also low and was changing in nature because of change in solar irradiance, temperature and dust accumulation on PV panels. To obtain higher values of AC peak to peak voltages, additional DC-DC converters are necessary to obtain MPPT operation and also to boost up the applied input voltage. To encounter this issue, two-stage power conversion was introduced, but it has shortcomings like delay losses and shoot-through (ST). Z Source Inverter (ZSI) was developed to

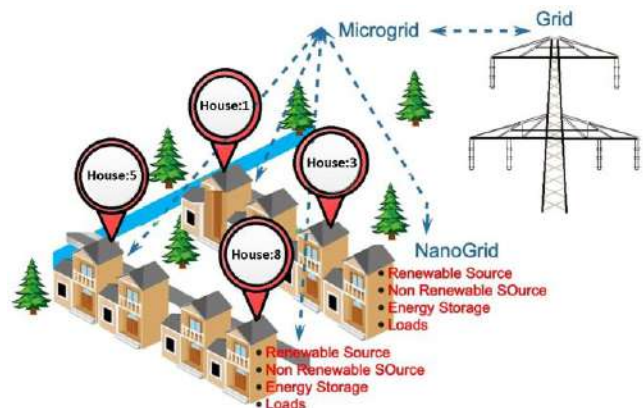


Fig. 1. Structure of National Grid, Micro-grid & Nano-grid

deal with shoot-through (ST) issue and achieve single stage

power conversion. In order to decrease the size of capacitors and achieve continuous input current, Quasi Z-Source Inverters (qZSI) are introduced. PWM modelling, methods and controlling techniques of ZSI/qZSI for specific applications are explained in detail [14-19]. Converter efficiency decreases in ZSI/qZSI because of usage of bulky and costly two inductors and two capacitors. Size, weight, conversion efficiency and cost are important factors of micro inverter application which make the adoption of ZSI/qZSI for PV power generation difficult. For low power applications, Switch Boost Inverter (SBI) was suggested in [20]. The working principle of ZSI/qZSI is similar to SBI. Fewer components like only one capacitor and one inductor are used with additional MOSFET and a diode. The PWM control technique with its circuit analysis is depicted in [21]. SBI is utilized for providing AC and DC load of NG as suggested in [22], adding one more bidirectional converter for the BES. However, discontinuous PV current is the major shortcoming. To enhance the continuous input current and boost factor, current fed SBI [23] is developed. BES stores the additional PV power available when it is connected across capacitor and the same is suggested in energy stored qZSI [24]. Discharging of energy stored is possible at the time of direct operation from BES.

In this article, for NG application battery energy stored quasi-SBC (BES q-SBC) is suggested. Here we can feed BES, AC and DC loads simultaneously. As per the control given, it can be charged from AC-grid. In this article efforts have been made to suggest a modulation technique which has high modulation index to obtain same AC-voltage gain. The PWM presented here decreases the voltage stress across capacitors, diodes, MOSFETs and other components. Complete component design is presented and is compared with traditional PWM method of SBI. Simulation and synthesis results verifying the suggested circuits and related PWM are also explained. The remaining paper is arranged as follows: section II explains the suggested qSBC for NG application as power converter. Section III explains mathematical analysis and complete PWM switching models. Comparison with available techniques and component design are presented in section IV. Complete simulation and synthesis reports are shown in section V, conclusion is made in section VI.

II. PROPOSED SWITCHED INDUCTOR QUASI SWITCEHD BOOST CONVERTER FOR THE NANO-GRID ARCHITECTURE

Fig. 2(a) depicts the traditional NG structure. It contains several power electronic converter stages like high gain DC-DC converter for DC-bus formation, DC-AC converter for AC load along with utilization of grid interlink and bidirectional DC-DC converter for the BES. Fig 2(b) represents single stage SBI for DC bus formation, load interface and concurrent AC grid. It contains different converter for BES system. The proposed NG architecture is depicted in Fig. 2(c). It consists of single stage high voltage DC-bus directly including the BES and AC bus for grid and load. The suggested system has less number of components in comparison to traditional structure. Fig 3 shows power converter called qSBC which has two switches (S_5 and S_6) one inductor, one diode and DC-bus capacitor interlinked between inverter bridge and PV source (V_{pv}). PWM control logic controls the voltage boost and BES. Complete PWM performance was explained in section III. The proposed NG-

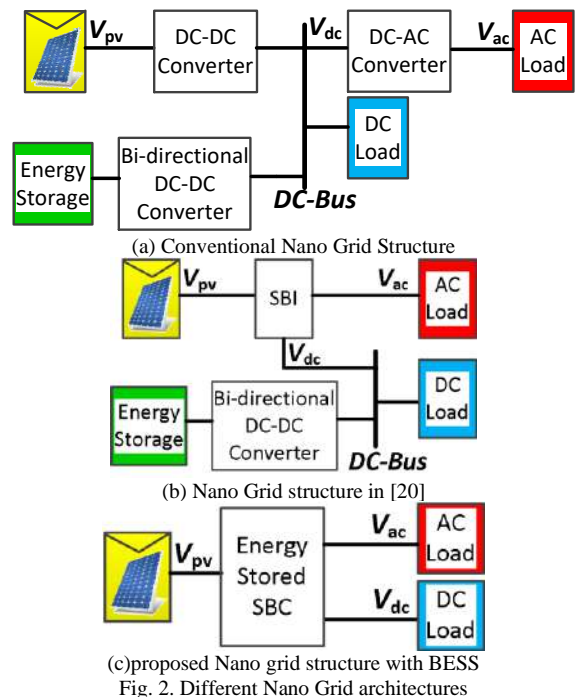


Fig. 2. Different Nano Grid architectures

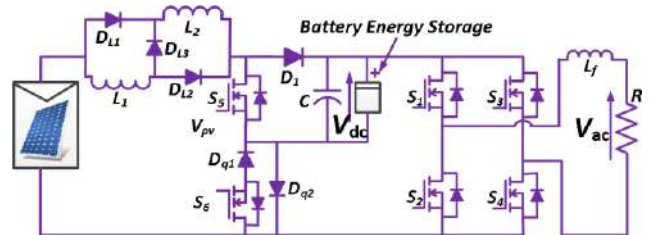


Fig. 3. Proposed Switched inductor qSBC

structure has the following advantages: 1) Maintaining peak shaving and load levelling the power that can be supplied to grid and can be stored with the help of BES System. 2) qSBC can supply AC & DC concurrently and is a single stage power converter. In addition, it can store power in BES and can supply AC directly even when there is no PV power thereby reducing overall cost and size of the system. 3) In comparison to the conventional VSI, qSBC shows better electromagnetic interference (EMI) since there are no delays in PWM signals and dead short circuits qSBC systems are compact, reliable and less protection is needed.

III. DEVELOPED PWM SCHEME FOR THE SL-QSBC

A. PWM scheme for PV supplying BESS and AC load

Fig. 4 depicts the explanation of PWM control of qSBC converter for NG BES. Switching frequency (triangular carrier) with unit amplitude is compared with constant (ST reference-Green) in order to produce shoot through pulses (waveform) for S_5 and inverter leg. Identically, comparison is made between sawtooth (amplitude = two) and modulation signal. To produce switching pulse, OR (logic) is applied between these two pulses to achieve final switching pulse for S_5 . To decrease switching losses of MOSFET switch, S_6 is kept in OFF condition for complete operating mode. Upper triangular carrier produces switching pulses for S_1 and S_2 during positive half cycle. On the

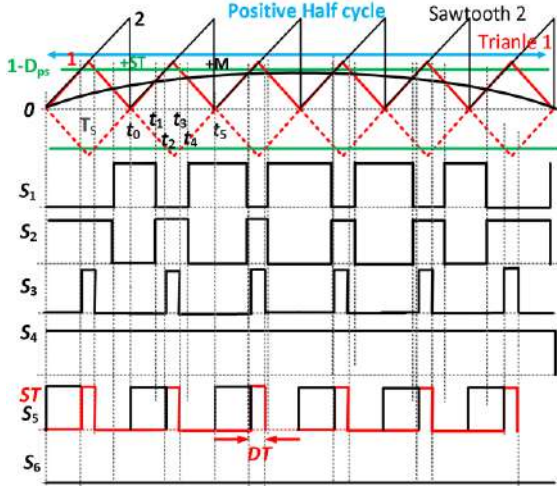


Fig. 4. Proposed PWM for PV to BESS and the AC load

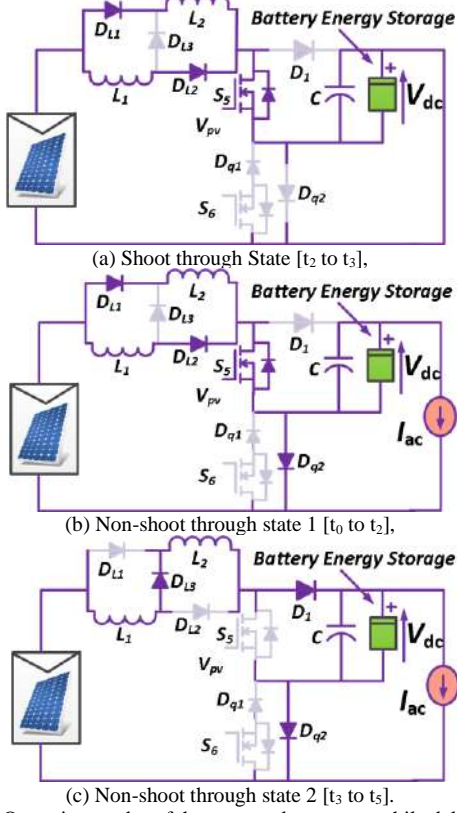


Fig. 5. Operating modes of the proposed converter while delivering power from the PV to the BESS and the AC load

other hand, lower triangle puts S_3 and S_4 ON. In a similar way in negative half cycle, the lower triangle will produce switching pulse for S_3 and S_4 . Whereas the upper triangle turns S_1 OFF and S_2 ON. For achieving the shoot through state, only S_3 is ORed (logic) with ST pulse during positive half cycle and the switches S_1, S_2, S_4 are kept same. This will decrease the switching loss of H-Bridge (HB). Only S_2 is ORed (logic) with ST pulse and S_1, S_2 and S_4 are kept as it is for the generation of shoot through state in negative half cycle resulting in reduction of switching loss of HB. ON time in the suggested PWM control is greater than traditional SBI and SBC. Simultaneously S_1-S_4 are changed for decreasing the switching losses of S_1-S_4 in comparison with

traditional qZSI logic regular comparison with triangle is mentioned as shoot through duty cycle when compared with sawtooth $(1-D)/2$ will be mentioned represents the proposed PWM control of the qSBC converter for the NG BES system. A constant (ST reference-Green) is compared with the switching frequency (triangle 1) having unity amplitude, to generate shoot through pulse for the inverter leg and the S_5 . Similarly, it compares the modulation signal with sawtooth 2 (having amplitude equal to two), to generate the switching pulse which are then ORed (logic) with the ST pulse to finally achieve the switching pulse for S_5 . Switch S_6 is kept OFF for the entire operating mode to reduce the switching losses of the MOSFET. During the positive half cycle operation, the upper triangular carrier generates the switching pulses for S_1 and S_2 , whereas the lower triangle keeps S_3 off and S_4 ON. Similarly, for the negative half cycle, the lower triangle will generate the switching pulses for the S_3 and S_4 , while the upper triangle keeps S_1 OFF and S_2 ON. For generation of the shoot through state, for the HB in positive half cycle, only S_3 is ORed (Logic gate) with the ST pulse and remaining S_1, S_2 and S_4 are kept as it is. This will reduce the switching loss of the HB. For generation of the shoot through state for the HB in negative half cycle, only S_2 is ORed (Logic gate) with the ST pulse and remaining S_1, S_3 and S_4 are kept as it is. This will reduce the switching loss of the HB. ON time in the proposed PWM control is more than the conventional SBC and SBI. At the same time, S_1-S_4 are changed for reducing the switching losses of the S_1-S_4 when compared to conventional qZSI logic. Constant comparing with the triangle is considered as the shoot through duty cycle D while for comparison with sawtooth, $(1-D)/2$ will be considered.

B. Operating Modes of Proposed PWM control

In presented PWM control scheme of SBC three operating modes are available. All modes with simple figures are depicted in Fig 5. Duration t_2 to t_3 is shoot through state obtained by applying the ON pulses to one of the inverter legs, HB can be short-circuited. At the same time S_5 is turned ON. The time interval is DT_s , where T_s is switching time of AC output in this mode.

$$L_1 \frac{di_{L1}}{dt} = L_2 \frac{di_{L2}}{dt} = V_{pv} + V_C; C \frac{dv_C}{dt} = -I_{in} \quad (1)$$

Duration t_0 to t_2 is non-shoot through state-1. When we turn ON S_5 , inductor will charge from the excitation (input) PV voltage since the diode is in forward biased condition. AC load will receive power from BESS or capacitor. During HB operation, active state is followed by zero state. This will continue for $(1-D)/2$ period . In this mode,

$$L_1 \frac{di_{L1}}{dt} = L_2 \frac{di_{L2}}{dt} = V_{pv}; C \frac{dv_C}{dt} = -I_{ac} \quad (2)$$

Non-shoot through state 2 is considered from $[t_3$ to $t_5]$. Active and zero state occur when HB switch S_5 is turned OFF. As the current flows continuously in inductor. Its energy is delivered to capacitor output voltage. The time duration is $(1-D)/2$ to obtain symmetry of the carriers. During this mode,

$$L_1 \frac{di_{L1}}{dt} + L_2 \frac{di_{L2}}{dt} = V_{pv} - V_C; C \frac{dv_C}{dt} = I_{L1} - I_{ac} \quad (3)$$

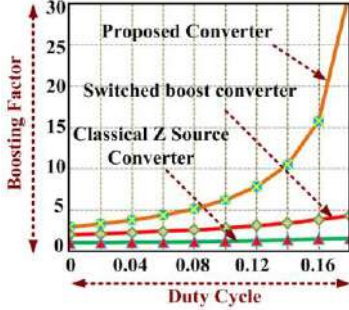


Fig. 6. Gain comparison with shoot through state (STS) duty

The following equation is obtained by the application of volt-second balance principle (to inductor) and charge balance (for capacitor).

$$V_C = \frac{3+D}{1-5D} V_{pv}; I_{ac} = \frac{1-3D}{2(1-D)} I_{in} \quad (4)$$

The DC-link voltage for the HB and the peak voltage across the capacitor are equal at the time of non-shoot through states, the DC-link is obtained as follows,

$$V_C = \frac{3+D}{1-5D} V_{pv}; I_{ac} = \frac{1-3D}{2(1-D)} I_{in} \quad (5)$$

The boost factor for the suggested qSBC converter of the PV panel to the capacitor (BES) and AC load is given as:

$$B = \frac{V_C}{V_{pv}} = \frac{3+D}{1-5D} \quad (6)$$

Comparison between boost factors of suggested qSBC and the traditional SBI and SBC are shown in Fig 6. With the suggested PWM control, improved gain can be achieved with same shoot through cycle and additional non-shoot through state is included in PWM strategy. The voltage stress improves drastically across the HB switches. The presented method can be extended to DC-link type [22] for qSBI topologies, which improves the gain. Impedance source inverters (ISI) are used to obtain high quality response and maximize duty cycle of the STS is 1-M. The suggested method derives voltage gain as follows:

$$G_{c.qzs} = \frac{M}{2M-1}; G_{c.qsbc} = \frac{2M}{3M-1}, G_{p.qsbc} = \frac{M(4-M)}{5M-4} \quad (7)$$

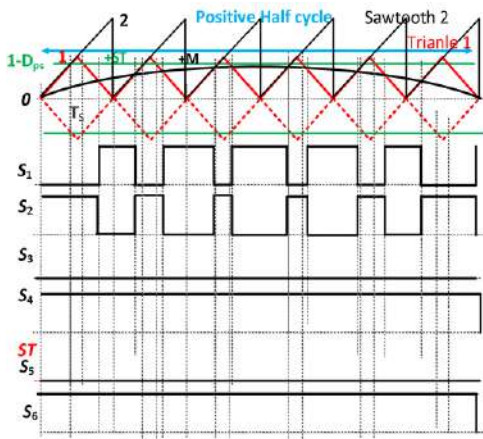


Fig. 7. Proposed PWM for the BES to AC load

With the suggested control technique, for the same modulation index, gain can be improved.

C. PWM control during BES feeding AC load

As the switch S5 is turned OFF, the connection between the converter and inductor, input PV is unavailable. During this operation, the Switch S6 is turned ON. AC load can be powered directly by BES. The proposed PWM control is shown in Fig. 7. BES delay must be included in order to avoid dead short circuit in HB switches.

D. Component design

The expression for capacitor voltage ripple and high frequency peak to peak inductor current under the non-shoot through state 2 for the PWM are given by:

$$\Delta I_L = \frac{(1-D)(V_{dc} - V_C)}{2L}; \Delta V_C = \frac{(1-D)(I_L - I_{ac})T}{2C} \quad (8)$$

The inductor current high frequency and peak to peak capacitor voltage are expressed as:

$$\Delta I_L = \frac{(1-D)(1+3D)*T*V_{dc}}{L*(1-5D)}; \Delta V_C = \frac{(1+D)*I_{in}*T}{4C} \quad (9)$$

When compared to traditional SBC and SBI, the high frequency inductor and capacitor component values are large. Double frequency analysis for the developed PWM technique is applicable for qSBC. The inductor and the capacitor currents of low frequency ripple are expressed as:

$$\hat{i}_L = \frac{(1-5D)*M*I_m}{16LC\omega^2 - (1-5D)^2}; \hat{v}_C = \frac{4\omega L M I_m}{16LC\omega^2 - (1-5D)^2} \quad (10)$$

When compared to traditional SBI and SBC, the low frequency inductor and capacitor component values are very small. So the eventual obtained values of inductor and capacitor are expressed as:

$$L > \frac{(1-D)(1+3D)*T*V_{pv}^2}{r_L \% (1-5D)P_o}; C > \frac{(1-D)(1-5D)*T*P_o}{4r_C \% (3+D)V_{pv}^2} \quad (11)$$

IV. SIMULATION AND EXPERIMENTAL VERIFICATION

To explain the sustainability of nano-grid implementations, solar powered qSBC interlinked to ac powered RL load and dc

Table. II Component specifications for Proposed qSBC

Component name	MATLAB R18a Simulink	Experimental qSBC
Inductors L_1, L_2	Series RLC branch type	Ferrite core, 1.6 mH, 15A
Capacitor C	Series RLC branch type	Electrolytic capacitor, 2000 uF, 400 V
Diode $D_{L1}, D_{L2}, D_{q1}, D_{q2}, D_I$	Simscape, power electronic library	STTH30R04, 400V, 15A
SIC-MOSFET S_1-S_6	Simscape, power electronic library	FDP19N40, 1200V, 40 A
Frequency	50KHz	50KHz
RL-load	640W	120W
Modulation Index	0.9	0.9
Control Board	Computer PC	Virtex-5 FPGA

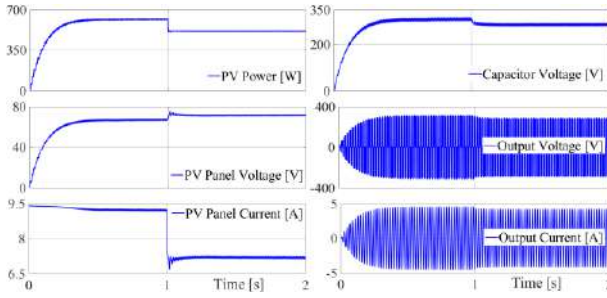


Fig. 8. Steady state simulation results of the proposed converter powered with PV array. Solar insolation is changed from 1 to 0.8kW/m^2 at $t = 1\text{s}$.

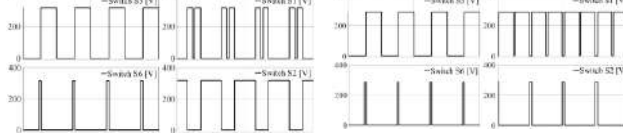
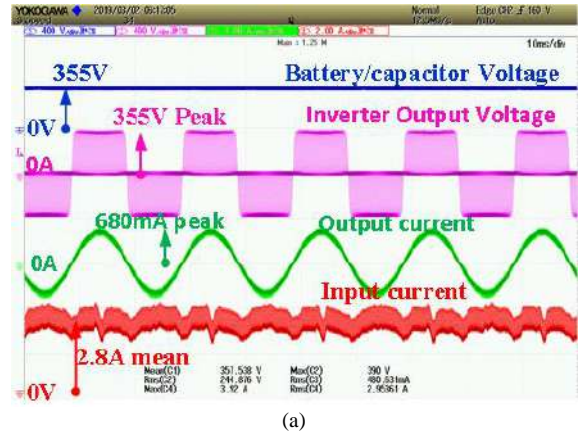


Fig. 9. Component voltage stress in simulation: V_L – voltage across the inductor ($V_{\text{pv}}+V_{\text{dc}}=410\text{V}$ peak), S_5 voltage (350V peak), D voltage (350V peak), S_6 voltage (350V peak).

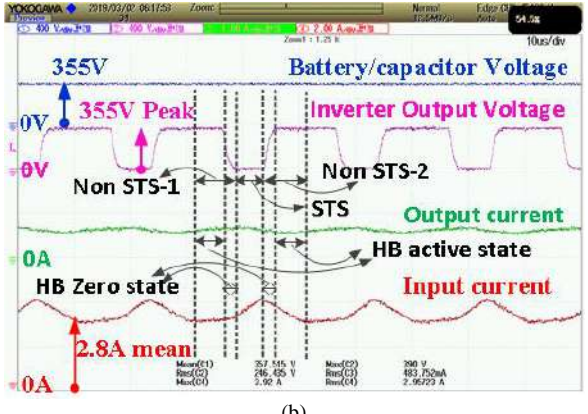
resistive load are drafted in MATLAB. Tools and components utilized for hardware presentation and simulation are represented in Table-I. PV Ratings are 320W, 36V at MPPT at 1kW/m^2 and 25°C . To get the input of qSBC of 72V, two panels are interlinked in series connection. Applied excitation voltage is enhanced to 310V at 1kW/m^2 (with $D = 0.07$) and 295V at 0.8kW/m^2 operation of MPPT. At the time of operation, dc voltage bus capacitor consumes power and across it dc resistive load is connected. In comparison with qSBC supplying ac RL load the shoot through duty varies.

Different solar irradiations (1kW/m^2 , 640W and 0.8kW/m^2 , 515W) and their steady state responses of qSBI are depicted in Fig. 8. MPPT algorithm is used to give shoot through duty ratio for boost voltage which is forced by PV panel response beside capacitor voltage (which is dc bus voltage), PV panel output voltage and output current are also depicted. At $t = 1\text{s}$, solar insolation is varied from 1kW/m^2 to 0.8kW/m^2 (temperature is maintained at 25°C). Shoot through duty ratio varies (from $D = 0.07$ to $D = 0.05$) to follow MPPT point at new value of solar insolation. MPPT point is tracked without any transient overshoot are depicted in Fig. 9. Decline in solar insolation is obtained as there is decline in output voltage and current. the decline which is obtained in output voltage and current due to partial shading because of this power flowing to resistive load varies. Voltage stress levels at different switches of two different steady states are depicted in Fig. 9(a) and Fig. 9(b). Here, maximum voltage stress with respect to the switches remains same. Switch S_6 also receives same amount of voltage stress. Switch S_6 works for DC fault blocking protection to provide power to ac load at night time when PV cannot produce power. Thus, by using switch S_6 with developed PWM improves the suitability and reliability of converter for nano-grid implementations.

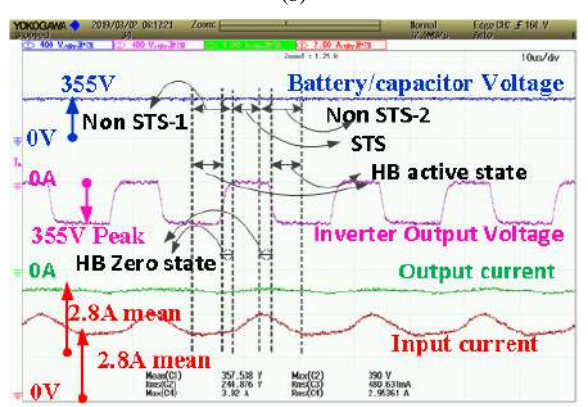
For practical verification, prototype of 120W is developed in the laboratory. DC resistive load is interlinked across dc bus voltage and ac load ($R = 100\Omega$, 33mH) is connected at output of inverter. Vertex-5 FPGA is used at 100nS for producing carrier signal at 50kHz. Input voltage of 75V is given by dc voltage source to boost it up to 330V as depicted in Fig. 10 thereby



(a)



(b)



(c)

Fig. 10. Experimental results of the proposed qSBC, (a) BES voltage (V_{dc}) 355V , three level AC output voltage 240V rms (V_{ac}), AC load current 0.5A rms and the continuous input current 2.3 A mean, (b) Zoomed positive cycle of the NSTS-1 & 2, STS, active state and zero states of the HB, (c) Zoomed negative cycle of the NSTS-1 & 2, STS, active state and zero states of the HB.

achieving 4.4 times of boosting. The dc current through DC resistive load is 0.5A and current through AC load RL is 0.58A . Amplified waveforms depict the operation qSBC in all the three modes of operation as shown in Fig. 10(b) and Fig. 10(c).

Fig. 10(c) depicts amplified version of five switching cycles of basic positive half cycle. Here all the modes of operation of developed PWM algorithm described as NSTS-1(inductor is charging with V_{pv}), NSTS-2 (inductor is discharging with $V_{\text{pv}}-V_{\text{dc}}$), STS (inductor is charging with $V_{\text{pv}}+V_{\text{dc}}$), active and Zero states of the HB. Inductor and capacitor both operate

concurrently for both positive half cycle and negative half cycle and maximum voltage across them is 330V. It is depicted that STS are added into zero states for HB. Modulation index of M=0.75, maximum gain of G=7.54 are obtained at D=0.245. The expression M=1-D is used to obtain nominal harmonic performance of the output voltage. At 120W, output peak efficiency of 87.9% is achieved.

V. CONCLUSION

In this paper, a novel BES embedded qSBC converter for operation in single-phase grid connected or islanded mode was presented. Two novel PWM control techniques are described for operation in all the operating modes consisting of power exchange between PV, AC utility grid, BES and DC – AC load for the NG implementations. In comparison to traditional SBI, SBC and qZSI, the developed PWM techniques have higher modulation index and achieves the desired output voltage with low shoot – through duty cycle ($D = 0.05$ to 0.07). Minimizing of shoot – through duty cycle is essential as it reduces the stress on passive as well as semiconductor components. Simulation results validates the advantages associated with this converter and PWM control for renewable energy application. In addition to this, condition of partial shading is also emulated by varying the solar irradiation from 1 to 0.8 kW/m^2 during operation. Even during this perturbation, the system performance is satisfactory. Hardware results pertaining to circuit performance are also presented.

ACKNOWLEDGMENT

This publication was made possible by QUCG grant # [CENG-19/20-5] from the Qatar National Research Fund (a member of Qatar Foundation). The statements made herein are solely the responsibility of the authors.

REFERENCES

- [1] J. M. Guerrero, F. Blaabjerg, T. Zhelev, K. Hemmes, E. Monmasson, S. Jemei, M. P. Comech, R. Granadina, and J. Frau, "Distributed generation: toward a new energy paradigm," *IEEE Ind. Electron. Mag.*, vol. 4, no. 1, pp. 52–64, Mar. 2010.
- [2] S. Bacha, D. Picault, B. Burger, I. Etcheverria-Otadui and J. Martins, "Photovoltaics in Microgrids: An Overview of Grid Integration and Energy Management Aspects," in *IEEE Industrial Electronics Magazine*, vol. 9, no. 1, pp. 33-46, March 2015.
- [3] M. H. Nehrir, W. K. Strunz, H. Aki, R. Ramakumar, J. Bing, Z. Miao, and Z. Salameh, "A review of hybrid renewable/alternative energy systems for electric power generation: configurations, control, and applications," *IEEE Trans. Sustain. Energy*, vol. 2, no. 4, pp. 392-403, Oct. 2011.
- [4] A. Iqbal, M. S. B. Ranjana, M. Meraj, S. Padmanaban and R. Syed, "Closed-Loop Control and Boundary for CCM and DCM of Non-Isolated Inverting Nx Multilevel Boost Converter for High Voltage Step-Up Applications," in *IEEE Transactions on Industrial Electronics*.
- [5] H. Abu-Rub, M. Malinowski, and K. Al-Haddad, "Power electronics for renewable energy systems," in *Trans. and Ind. Appl.*, Hoboken, NJ, USA: Wiley, Jul. 2014.
- [6] S. Javaid, T. Kato and T. Matsuyama, "Power Flow Coloring System Over a Nanogrid With Fluctuating Power Sources and Loads," in *IEEE Trans. Ind. Inf.*, vol. 13, no. 6, pp. 3174-3184, Dec. 2017.
- [7] G. Manavalan, H. M. Tania, J. K. Patra, M. G. Poongothai and S. Prema, "A closed loop system to stabilize a 24V solar DC Nano grid," *2017 International Conference on Smart grids, Power and Advanced Control Engineering (ICSPACE)*, Bangalore, 2017, pp. 177-182.
- [8] P. K. Maroti, S. Padmanaban, J. B. Holm-Nielsen, M. Sagar Bhaskar, M. Meraj and A. Iqbal, "A New Structure of High Voltage Gain SEPIC Converter for Renewable Energy Applications," in *IEEE Access*, vol. 7, pp. 89857-89868, 2019.
- [9] A. Riccobono *et al.*, "Next generation automation architecture for DC smart homes," *2016 IEEE International Energy Conference (ENERGYCON)*, Leuven, 2016, pp. 1-6.
- [10] R. Adda, S. Mishra, and A. Joshi, "A PWM control strategy for switched boost inverter," in Proc. 3rd IEEE Energy Convers. Congr. Expo., Phoenix, AZ, 2011, pp. 4208-4211.
- [11] M. Meraj, S. Rahman, A. Iqbal and L. Ben-Brahim, "Common Mode Voltage Reduction in a Single-Phase Quasi Z-Source Inverter for Transformerless Grid-Connected Solar PV Applications," in *IEEE Journal of Emerging and Selected Topics in Power Electronics*, vol. 7, no. 2, pp. 1352-1363, June 2019.
- [12] K. Hada, A. Kumar Sharma, J. Gupta and P. S. Tomar, "Comparative analysis of isolated and non-isolated quasi impedance source converters," *2017 International Conference On Smart Technologies For Smart Nation (SmartTechCon)*, Bangalore, 2017, pp. 460-464.
- [13] J. Anderson and F. Peng, "A class of quasi-Z-source inverters," in Proc. Annu. Meet. IEEE Ind. Appl. Soc., 2008, pp. 1-7.
- [14] J. Khajesalehi, K. Sheshyekani, M. Hamzeh and E. Afjei, "Maximum constant boost approach for controlling quasi-Z-source-based interlinking converters in hybrid AC-DC microgrids," in *IET Generation, Transmission & Distribution*, vol. 10, no. 4, pp. 938-948, 10 3 2016.
- [15] N. Sabeur, S. Mekhilef and A. Masaoud, "Extended maximum boost control scheme based on single-phase modulator for three-phase Z-source inverter," in *IET Power Electronics*, vol. 9, no. 4, pp. 669-679, 30 3 2016.
- [16] S. Rahman, M. Meraj, A. Iqbal, L. Ben-Brahim, R. Alammari and H. Abu-Rub, "Failure mode analysis for single-phase Multi-level qZSI interfacing PV system to utility grid," *2017 11th IEEE International Conference on Compatibility, Power Electronics and Power Engineering (CPE-POWERENG)*, Cadiz, 2017, pp. 504-509.
- [17] Y. Liu, B. Ge, H. Abu-Rub and D. Sun, "Comprehensive Modeling of Single-Phase Quasi-Z-Source Photovoltaic Inverter to Investigate Low-Frequency Voltage and Current Ripple," in *IEEE Trans. Ind. Electron.*, vol. 62, no. 7, pp. 4194-4202, July 2015.
- [18] B. Ge, Y. Liu, H. Abu-Rub, and F. Z. Peng, "State-of-charge balancing control for a battery-energy-stored quasi-Z-source cascaded-multi level inverter-based photovoltaic power system," *IEEE Trans. Ind. Electron.*, vol. 65, no. 3, pp. 2268-2279, Mar. 2018.
- [19] A. A. Abdullaah, A. Iqbal, M. Meraj, L. Ben-Brahim, R. Alammari and H. Abu-Rub, "Discontinuous space vector pulse width modulation techniques for a five-phase quasi Z-source inverter," *IECON 2015 - 41st Annual Conference of the IEEE Industrial Electronics Society*, Yokohama, 2015, pp. 004205-004210.
- [20] A. Ravindranath, S. Mishra, and A. Joshi, "Analysis and PWM control of switched boost inverter," *IEEE Trans. Ind. Electron.*, vol. 60, no. 12, pp. 5593-5602, Dec. 2013.
- [21] M. H. B. Nozadian, F. Ebrahimzadeh, E. Babaei and E. S. Asl, "Current-fed switched Z-source inverters," *2017 14th International Conference on Electrical Engineering/Electronics, Computer, Telecommunications and Information Technology (ECTI-CON)*, Phuket, 2017, pp. 769-772.
- [22] M. Nguyen, Y. Lim and S. Park, "A Comparison Between Single-Phase Quasi-\$Z\$-Source and Quasi-Switched Boost Inverters," in *IEEE Trans. on Ind. Electron.*, vol. 62, no. 10, pp. 6336-6344, Oct. 2015.
- [23] M. Meraj, A. Iqbal, N. Al-emadi, S. Rahman and M. S. Bhaskar, "Novel PWM Technique for Quasi Switched Boost Converter for the Nano-grid Applications," *2019 IEEE 28th International Symposium on Industrial Electronics (ISIE)*, Vancouver, BC, Canada, 2019, pp. 2659-2664.
- [24] A. Ho, T. Chun and H. Kim, "Extended Boost Active-Switched-Capacitor/Switched-Inductor Quasi-Z-Source Inverters," in *IEEE Trans. Power Electron.*, vol. 30, no. 10, pp. 5681-5690, Oct. 2015.
- [25] B. Xu and X. Ran, "Sliding Mode Control for Three-Phase Quasi-Z-Source Inverter," in *IEEE Access*, vol. 6, pp. 60318-60328, 2018.

Quasi Z Source Inverter Fed V/f Controlled Five Phase Induction Motor Drive Powered

Syed Rahman

Dept. of Electrical Engg., Qatar University, Al-Dafna, Qatar
syed.rahman@qu.edu.qa

Mohammad Meraj

Dept. of Electrical Engg., Qatar University, Al-Dafna, Qatar
meraj@qu.edu.qa

Khaliquar Rahman

Dept. of Electrical Engg., Aligarh Muslim University, India
er.khaliqurrahman@gmail.com

Md Arif Ali

Dept. of Electrical Eng., RGUKT Basar, Nizamabad, India
arifmd4703@gmail.com

Atif Iqbal

Dept. of Electrical Engg., Qatar University, Al-Dafna, Qatar
atif.iqbal@qu.edu.qa

Abstract – Impedance Source Inverters are extremely popular these days. They offer simultaneous boosting of input voltage applied as well as inversion operation. The converter achieves this by means of a specially designed impedance network along with H - Bridge. Unlike conventional H – Bridge (HB) inverters, impedance source inverters can boost the supply voltage thereby achieving boost operation. Utilizing this feature, voltage transient due to grid side disturbance, improved control and enhanced fault tolerance capability can be achieved. There are two types of impedance source-based inverters namely Z Source Inverters (ZSI) and quasi Z Source Inverters (qZSI). In this paper, five phase qZSI fed five phase induction motor drive is discussed. V/f control is implemented to induction motor in synchronism with closed loop voltage control of quasi network output voltage. Constraints in the integrated performance are discussed and taken into consideration for development of control algorithm. Simulation results are presented for the system when subjected to different load transients thereby validating the integrated control.

Keywords: Five phase Induction motor drive, V/f control, quasi Z Source Inverter, Shoot through duty cycle.

I. INTRODUCTION

Modern drive systems usually consist of electric motor controlled by means of power converter. Analog or digital control is embedded with the system to achieve desired response. In addition to this, signal conditioning circuits are added to the system to achieve closed loop control. Three phase systems are preferred when compared to single phase because of higher efficiency, lower rating of individual components, easier control, balanced operation, fault tolerant capability etc. As a result, three phase systems are commercially available and most suitable for industrial applications. However, in applications where a machine is not readily available, multiphase machines are preferred because of the following advantages: possibility of splitting the required per-phase power rating, significant improvement in

fault tolerance capability of the drive, sinusoidal input current, reduced torque pulsation and better noise characteristics. However, it also suffers from drawbacks of customized machine design and readily available three phase grid supply [1-3].

Five phase induction motor drive fed from voltage inverter is introduced way back in 1969. For the next two decades, there has been limited research in this area. But from early 2000s, development of application specific electric drives where the three-phase grid is not readily available (ship propulsions, aircrafts), led to accelerated growth and research in this area. PWM techniques have been developed and tested for desired operation of inverter fed multiphase machine drives [4-5]. Modelling of five phase induction motor is reported in literature by using the dynamic equations based on the circuit operation [6]. Advanced optimization techniques have also been reported to improve drive performance and fault tolerance capability [7]. Common mode voltage reduction techniques are also discussed in the literature [8].

Conventionally, two level inverters fed from a fixed voltage source are used to power the five phase machine drives. Control of these drives is achieved by varying the modulating signal, which is used for switching pulse generation by simple comparison with triangular carrier signal. However, with the new breed of impedance converters it is possible to control the input voltage to the inverter by means of impedance network. This feature in renewable energy applications eliminates the need for additional dc-dc converter [9-10].

qZSI consists of two inductors, two capacitors and one diode followed by the conventional H Bridge. In conventional inverters, shorting of leg is avoided by introducing delay time in between incoming and outgoing switches. However, in impedance source-based inverters, this feature is utilized to boost the input voltage. By varying this period, it is possible to control the voltage boost. Different techniques of switching

have been reported in literature to achieve the desired performance along with voltage boost [11-12]. Energy Efficient qZSI, component optimization and application of advanced control techniques are also discussed in the literature [13-15]. For renewable energy applications, grid connected qZSI are also developed. Their integration with different conventionally existing techniques is also discussed to suggest improvement of response and cost optimization [16]. Multilevel qZSI is also reported in the literature which improves the harmonic performance of the inverter along with reduced rating per switch as well increases the fault tolerance capability [17-18].

In this paper, five phase induction motor is fed from five phase qZSI. The system description is discussed in Section II. V/f control of induction motor is achieved by controlling its speed during starting and transients. Control algorithm is discussed in detail in Section III. Simulation results which validates the control are discussed in Section IV. Finally, summarized conclusions are presented in Section V.

II. SYSTEM DESCRIPTION

The system consists of five phase quasi Z Source Inverter (qZSI) powering five phase Induction motor as shown in Fig. 1. DC voltage source is applied at the input of the qZSI.

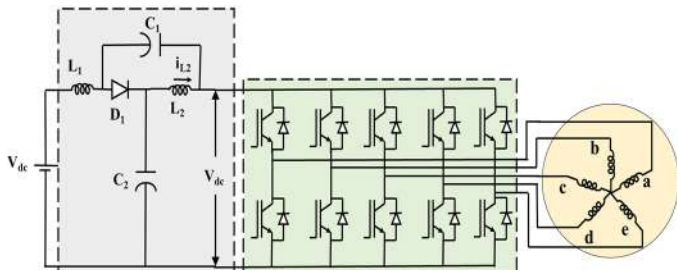


Fig. 1 – Five Phase Induction Motor powered with qZSI

a) Five Phase Quasi Z Source Inverter

Quasi network consists of two capacitors, two inductors and one diode. Boosting of the applied input voltage is possible with this inverter. This boosting of applied input voltage is achieved by simultaneous shorting of all the inverter legs for a short period of time. This duration is called as Shoot through duty cycle (D) of the quasi Z Source Inverter. Operation of the qZSI can be divided into two modes namely powering mode and shoot through mode shown in Fig. 2(a) and Fig. 2(b) respectively.

i) Shoot through Mode

During this mode, all the inverter legs are shorted by simultaneous application of switching pulse to both the switches of the same leg. The Inductors are charged during this mode and the output voltage of the quasi network is zero.

During this mode, the input voltage and voltage across the inductors are opposite in nature. Due to this, the voltage across the diode is negative and hence it is reverse biased. The current during the shoot through mode is shared between the five legs of the inverter.

Applying KVL to the circuit we get:

$$V_{diode} = V_{in} - V_{c2} - V_{L1} \quad (1)$$

Applying KCL to the circuit:

$$I_{L1} = I_{c1} \text{ and } I_{L2} = I_{c2} \quad (2)$$

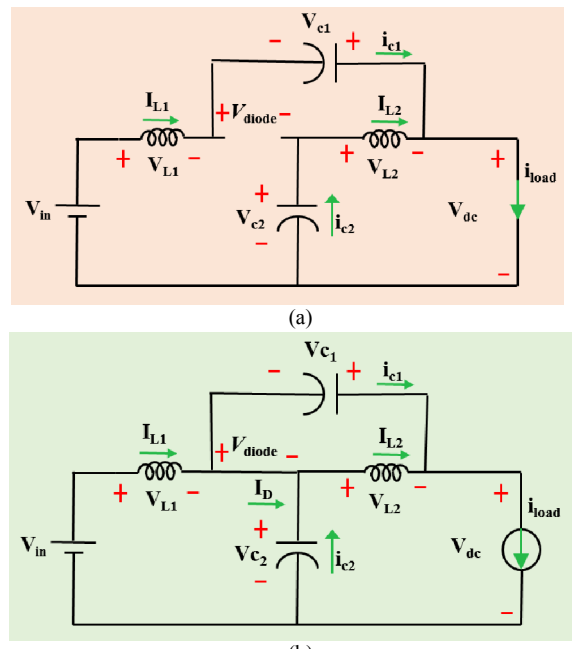


Fig. 2 Equivalent circuit during (a) Shoot through Mode
(b) Powering Mode

ii) Powering Mode

This mode is like the operation of conventional inverter. During this mode, the current flowing through the inductors decreases and hence the diode gets forward biased due to change in polarity of $L \frac{di}{dt}$. The energy stored in the inductors will charge the capacitors and the output voltage of the quasi network will be higher than the input voltage.

Applying KVL to the circuit:

$$0 = V_{in} - V_{c1} - V_{L1} \quad (3)$$

Applying KCL to the circuit:

$$I_{L1} + I_{c2} = I_{L2} + I_{c1} \quad (4)$$

Ratio of shoot through mode to the period of switching cycle is defined as shoot through duty cycle (D). Simplifying the above equations, the relations of the circuit can be given by:

$$V_{c2} = \frac{1-D}{1-2D} V_{in}; V_{c1} = \frac{D}{1-2D} V_{in}; V_{dc} = \frac{V_{in}}{1-2D} \quad (5)$$

where, shoot through duty cycle $D = \frac{T_0}{T_s}$

T_0 = Shoot through duration and T_s = Switching Cycle duration.

b) Five Phase Induction Motor

Five legs of qZSI feeds the five phase Induction motor. Phase Shift in the applied input voltage and spatial displacement of the five-winding construction ensures the operation of five phase Induction motor. Mechanical load is connected to the shaft of the motor. Speed sensor senses the speed of the motor and it is given as input to the control loop.

III. CONTROL ALGORITHM

The control structure is shown in Fig. 3. Control structure consists of V/f control of induction motor and dc link voltage control of qZSI. These two sections are described below in detail:

i) V/f Control of Five Phase Induction Motor

Speed reference of the motor (designated by ω_m^*) is compared with the sensed mechanical speed of the motor. The error is passed through to the controller to give slip speed (ω_{sl}^*). The mechanical speed is converted to electrical speed by multiplying with no. of pole pairs. This electrical speed is added to the slip speed to give synchronous speed. The ratio of rated voltage to the rated frequency (ω_s) gives the rated flux. Synchronous speed is multiplied with rated flux to give the required voltage V_{ref} . Using V_{ref} and w_s , five 72° degree displaced modulating signals are generated. This voltage signal is divided with output of quasi network to give normalized modulating signal. To ensure steady state operation, relation of $m = 1 - D$ between the peak of modulation signal (m) and maximum shoot through duty cycle (D) should be maintained. The normalized modulating signal is saturated to m (or) $1 - D$. Conventional Sine PWM is used for generation of switching pulses by comparing the modulating signal with carrier signal. In addition to this, Carrier signal is compared with $(1 - D)$ and $-(1 - D)$ to give boosting pulses. OR operated is performed between boosting pulses and pulses generated by conventional comparison.

These pulses are given to five leg qZSI to achieve desired V_{dc} and output voltage at the legs of the inverter.

ii) DC Link Voltage Controller

Capacitor voltage V_{c2} is sensed into the control system. Output voltage of the quasi network (V_{dc}) is estimated by using the steady state equations using V_{c2} and shoot through duty cycle (D). V_{dc} is compared with dc bus reference voltage and the error is fed to the PI controller to give reference inductor current value i_{L2}^* . This is fed to the PI control loop to give shoot through duty cycle (D).

IV. SIMULATION RESULTS FOR V/F CONTROL

By implementation of V/f control to qZSI powered five phase induction motor drive, the following points should be ensured:

- Starting of Induction motor must not be subjected to huge torque transients
- V/f control must be ensured during all transients
- Motor must be subjected to load-side transients to ensure stability of drive
- Control of output voltage of quasi network must be ensured
- Boosting of input voltage to the required level must be achieved to utilize the advantage of using qZSI
- Steady state relation of $m = 1 - D$ must be ensured during operation

Table -1 gives the parameters of the five-phase induction motor and Table -2 gives the parameters of qZSI.

Table -1: Specifications of Five Phase Induction Motor

Parameter	Specification
Power (P)	3 kW
Supply Voltage (V_s)	230 V
Rated Speed (N_r)	970 RPM
Stator Resistance (R_s)	25.3 Ohm
Rotor Resistance (R_r)	15.5 Ohm
Stator Inductance (L_s)	103.1 mH
Rotor Inductance (L_r)	92.2 mH
Moment of Inertia (J_m)	0.021 Kg.m ²

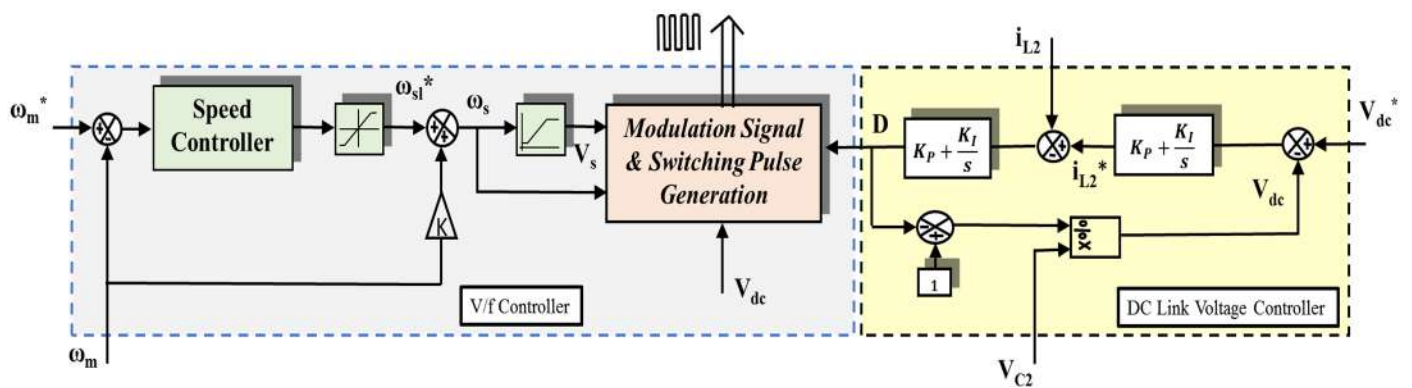


Fig. 3 Control Algorithm for V/f Control of Five Phase Induction Motor Drive fed with voltage controlled qZSI

Table -2: Specification of quasi Z Source Inverter

Parameter	Specification
Switching Frequency (f_s)	10 kHz
Quasi Inductor ($L_1 = L_2$)	1.2 mH
Quasi Capacitor ($C_1 = C_2$)	2 mF
Modulation Index (m)	0.8
Maximum Shoot through duty cycle (D_{max})	0.2

The modelled system is tested by applying the speed reference and its response is observed. The disturbance is also applied from the output side by application of load torques in a stepped manner.

The sequence of the speed references and load torque application is as given below:

- At $t = 0$ sec, the speed reference is set to 154 rad/sec.
- At $t = 2$ sec, load torque of -2 Nm is applied.
- At $t = 4$ sec, the speed reference is changed to 235 rad/sec.
- At $t = 6$ sec, the load torque changes from -2 Nm to 2 Nm.

Fig. 4 shows the speed and torque response of the system for given speed references and load torque demands.

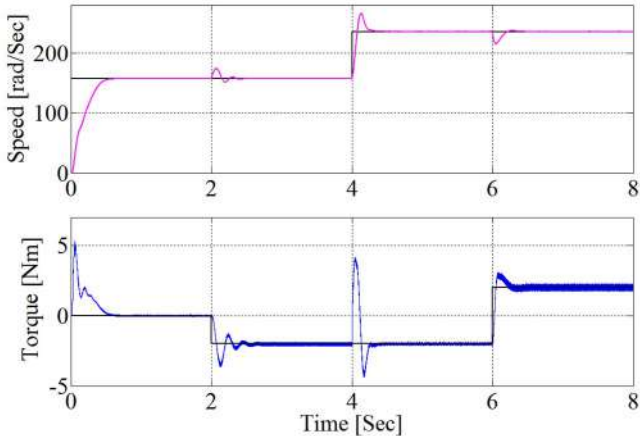


Fig. 4 Speed and torque response of the controlled system

At starting, the machine steadily rises to approach the required steady state speed. Once the motor reaches its steady state speed, the torque developed by the motor is reduced as there is no more requirement of acceleration of the motor. The modulating signal shown in Fig. 5 varies accordingly to keep the ratio Volt/Hertz constant. It can also be observed that the frequency of the modulating signal is low at the starting with corresponding magnitude keeping V/f constant as shown in Fig. 5(b).

The peak of the modulation signal should never exceed m (or) $1-D_{max}$. In the control algorithm D_{max} is ensured to be 0.2, which means the peak of modulation signal should not be above 0.8 which can be observed in Fig. 5.

At $t = 2$ sec, the load torque demand is changed to -2 Nm. For a drive operating in stable region, there should be a decrease in speed when positive load torque is applied to the system and the speed should increase when load is reduced. This behavior can be clearly observed in the response shown. After the speed increases momentarily, the control algorithm comes into action to restore the speed back to the reference value.

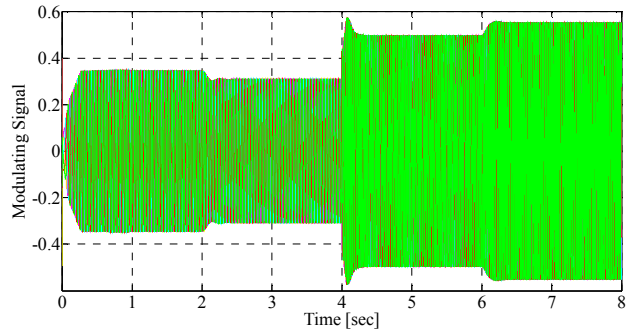


Fig. 5(a) Modulating Signal of the five phases ensuring V/f control is achieved during all operating modes

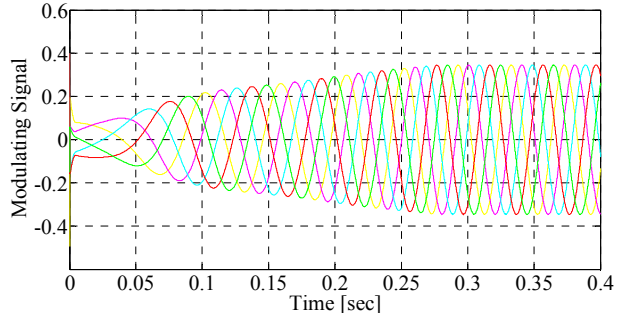


Fig. 5(b) During starting, frequency and magnitude of the modulating signal increases steadily

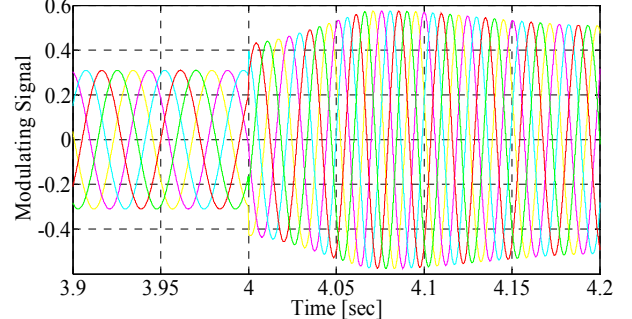


Fig. 5(c) When the speed reference is increased, frequency and magnitude of modulating signal increases steadily

Fig. 5 Variation of modulation signal magnitude and frequency during Volt/Hertz control.

At $t = 4$ sec, the speed reference is increased to 235 rad/sec from 154 rad/sec. To ensure fastest possible acceleration of the motor to the required speed, maximum torque should be applied. Once the speed exceeds the required speed, the torque becomes negative and the speed settles to

the new reference value. Fig. 4 shows that control can meet the load torque demand without any decrease in the steady state speed of the motor drive. Fig. 5(b) shows that during speed transient, the modulating signal increases its magnitude and frequency steadily to ensure minimization of transients. At $t = 6$ sec, the load torque demand increases to 2 Nm. For stable region operation, the speed should decrease when there is a sudden change in load torque. The speed decreases momentarily and then control algorithm brings it back to the desired speed. Proper tuning of controllers ensures that transients are minimized, and fast settling of the drive response is achieved.

Output current of phase A of five phase induction motor is shown in Fig. 7(a). As already discussed, torque reference is changed at $t = 2$ sec. It can be observed as increase in the phase current magnitude. It is shown in Fig. 7(b). When speed reference is changed, the torque first increases then decreases which is reflected in the current waveform shown in Fig. 7(c). Fig. 7(a) shows the boosting of the input voltage in qZSI. The input voltage is 300 V and dc bus input voltage for the inverter must be 350 Volts. Output of the quasi network forms the dc bus voltage of the five-phase inverter. Utilizing the shoot through mode of the inverter, boosting of input voltage is achieved. It should also be ensured that the dc bus voltage is maintained constant throughout the operation of the drive.

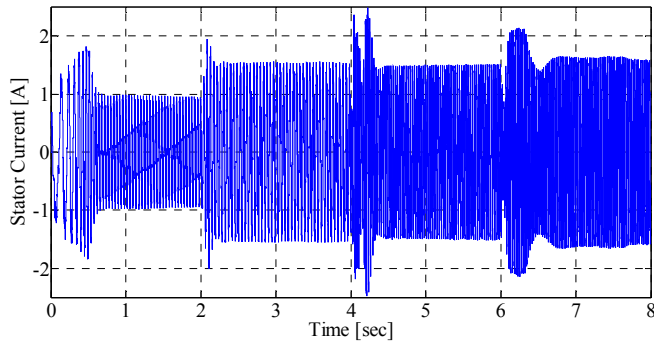


Fig. 6 Phase current of five phase induction motor

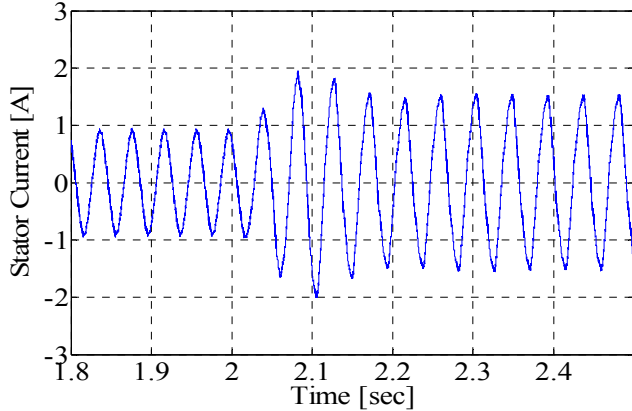


Fig. 6(b) Stator current during load torque change from 0 to -2 Nm

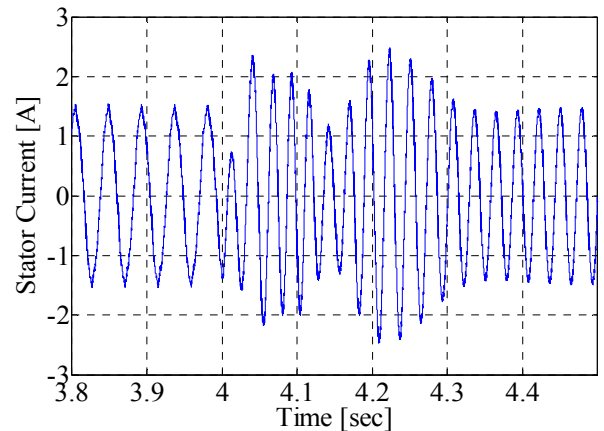


Fig. 6(c) When the speed reference is increased, frequency and magnitude of modulating signal increases steadily

As it can be observed in Fig. 7(a), the dc bus voltage remains constant during speed and load torque transients. Fig. 7(b) shows the inverter output phase voltage measured by connecting high impedance in star at the input of the motor terminal. The voltage measured between one point of high impedance and its star point will give the phase voltage of the motor.

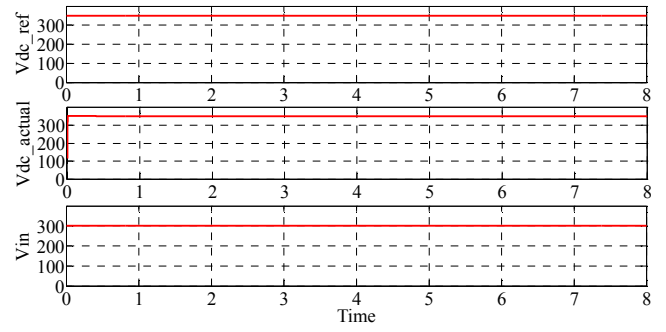


Fig. 7(a) DC bus voltage tracking

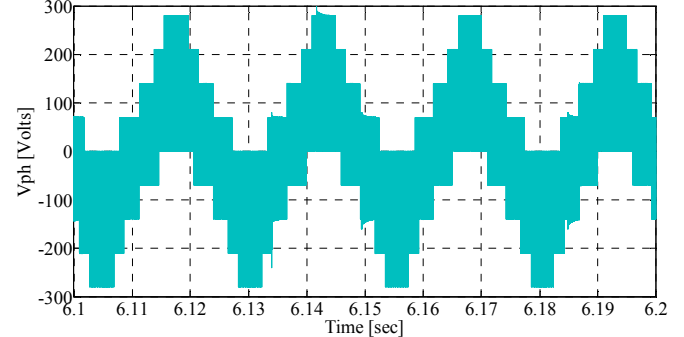


Fig. 7(b) Inverter output phase voltage

V. CONCLUSION

Five phase induction motor powered with five phase quasi Z Source Inverter is presented in this paper. Closed loop voltage control of qZSI is achieved by cascaded PI controllers. Boosting of input voltage is achieved by

implementation of shoot through mode of qZSI. Voltage control of the motor is achieved by controlling the output voltage of quasi network and modulation index of the modulating signal. For implementation of V/f control of Five Phase Induction motor, mechanical speed is sensed and fed as input to the control algorithm. The system is tuned for voltage control of quasi network and tracking of mechanical speed of the motor when subjected to load perturbations. Performance optimization is ensured by considering the constraints of circuit relations during control algorithm implementation.

ACKNOWLEDGEMENT

This publication was made possible by NPPR-EP grant # [X-033-2-007] from the Qatar National Research Fund (a member of Qatar Foundation). The statements made herein are solely the responsibility of the authors

REFERENCES

- [1] M. Jones; E. Levi; "A literature survey of state-of-the- art in multiphase ac drives," Proc. 37Th Int. Universities Power Eng. ConJ UPEC, Stafford, UK, 2002, pp. 505-510.
- [2] E. Levi, R. Bojoi, F. Profumo, H. A. Toliyat and S. Williamson, "Multiphase induction motor drives - a technology status review," in IET Electric Power Applications, vol. 1, no. 4, pp. 489-516, July 2007.
- [3] L. Parsa, "On advantages of multi-phase machines." 31st Annual Conference of IEEE Industrial Electronics Society, 2005. IECON 2005., 2005, pp. 6 pp. DOI: 10.1109/IECON.2005.1569139
- [4] J. Prieto, M. Jones, F. Barrero, E. Levi and S. Toral, "Comparative Analysis of Discontinuous and Continuous PWM Techniques in VSI-Fed Five-Phase Induction Motor," in IEEE Transactions on Industrial Electronics, vol. 58, no. 12, pp. 5324-5335, Dec. 2011.
- [5] Rahman, K., Iqbal, A., Abdullah, A. A., Abu-Rub, H., Al-Ammari R., (2014), "Space vector PWM technique for a three-phase to seven-phase matrix converter", *IEEE APEC*, 16-20 March, Texas, USA, pp. 595-601.
- [6] A. Iqbal, S. M. Ahmed, M. A. Khan, M. R. Khan and H. Abu-Rub, "Modeling, simulation and implementation of a five-phase induction motor drive system," 2010 Joint International Conference on Power Electronics, Drives and Energy Systems & 2010 Power India, New Delhi, 2010, pp. 1-6. DOI: 10.1109/PEDES.2010.5712373
- [7] H. Guzman, M. J. Duran, F. Barrero, B. Bogado and S. Toral, "Speed Control of Five-Phase Induction Motors With Integrated Open-Phase Fault Operation Using Model-Based Predictive Current Control Techniques," in IEEE Transactions on Industrial Electronics, vol. 61, no. 9, pp. 4474-4484, Sept. 2014.
- [8] Rahman, K., Iqbal, Atif, Al-Emadi, Nasser, Ben-Brahim, Lazhar. (2017), 'Common mode voltage reduction in a three-to-five phase matrix converter fed induction motor drive', IET Power Electronics, 10, (7), p. 817-825.
- [9] D. Vinnikov and I. Roasto, "Quasi-Z-Source-Based Isolated DC/DC Converters for Distributed Power Generation," in IEEE Transactions on Industrial Electronics, vol. 58, no. 1, Jan. 2011, pp. 192-201.
- [10] Y. Liu, H. Abu-Rub, B. Ge, F. Blaabjerg, O. Ellabban, and P. C. Loh: Impedance Source Power Electronic Converters, John Wiley & Sons Ltd., ISBN-13: 978-1119037071.
- [11] Y. Liu, B. Ge, H. Abu-Rub and F. Z. Peng, "Phase-shifted pulse-width-amplitude modulation for quasi-Z-source cascade multilevel inverter-based photovoltaic power system," in IET Power Electronics, vol. 7, no. 6, pp. 1444-1456, June 2014.
- [12] I. Roasto, D. Vinnikov, J. Zakis and O. Husev, "New Shoot-Through Control Methods for qZSI-Based DC/DC Converters," in IEEE Transactions on Industrial Informatics, vol. 9, no. 2, pp. 640-647, May 2013.
- [13] M. Meraj, S. Rahman, A. Iqbal, L. Ben-Brahim, R. Alammari, H. Abu-Rub, "A Hybrid Active Power and Reactive Power Control with Quasi Z-Source Inverter in Single Phase Grid Connected PV systems", IECON 2016 – 42nd Annual Conference of the IEEE Industrial Electronics Society, Florence, 2016.
- [14] M. Meraj, S. Rahman, A. Iqbal and L. Ben-Brahim, "Common Mode Voltage Reduction in a Single-Phase Quasi Z-Source Inverter for Transformerless Grid-Connected Solar PV Applications," in IEEE Journal of Emerging and Selected Topics in Power Electronics, vol. 7, no. 2, pp. 1352-1363, June 2019.
- [15] S. Rahman, M. Meraj, A. Iqbal and L. Ben-Brahim, "Novel voltage balancing algorithm for single-phase cascaded multilevel inverter for post-module failure operation in solar photovoltaic applications," in IET Renewable Power Generation, vol. 13, no. 3, pp. 427-437, 25 2 2019.
- [16] S. Rahman, M. Meraj, A. Iqbal, L. Ben-Brahim and R. Alammari, "Thyristor based SVC and multilevel qZSI for Active and Reactive power management in solar PV system," 2017 11th IEEE International Conference on Compatibility, Power Electronics and Power Engineering (CPE-POWERENG), Cadiz, 2017, pp. 528-533.
- [17] M. Trabelsi, H. Abu-Rub and B. Ge, "1-MW quasi-Z-source based multilevel PV energy conversion system," 2016 IEEE International Conference on Industrial Technology (ICIT), Taipei, 2016, pp. 224-229.
- [18] V. F. Pires, D. Foito and A. Cordeiro, "Three-phase qZ-source inverter with fault tolerant capability," in *IET Power Electronics*, vol. 10, no. 14, pp. 1852-1858, 17 11 2017.

Solar Powered Water Pumping Using BLDC Motor Drive with Boost-Buck converter for Telangana State

K. Ajith

Assistant Professor, EEE Dept.,
Kakatiya Institute of Technology &
Science, Warangal
mr.a.k@ieee.org

N. Rakesh

Assistant Professor, EE Dept.
Rajiv Gandhi University of Knowledge
Technologies (RGUKT), Basar
namanirakesh@gmail.com

M. Srinivas

Assistant Professor, EEE Dept.,
Kakatiya Institute of Technology &
Science, Warangal
srinivas.mavurapu@gmail.com

K. Aravind

Trainee Development Engineer,
OPTOMECH Engineers Pvt. Ltd.
Kukatpally, Hyderabad
kotaaravind1993@gmail.com

Abstract— DC to DC converters are used to improve the power from Solar PV array and then it is fed to the motor through Voltage Source Inverter (VSI) in order to optimize the power output from the solar PV array. There are many configurations in the DC to DC converters. Boost converter is commonly used for various solar applications. High voltage output of the boost converter is not considered for smooth starting of BLDC motor. Buck converters decrease the output voltage and hence it is not considered for this application. Cuk converters have poor switch utilization and high stress on power devices. A Boost-Buck converter is proposed in this paper for its performance and features of both Boost and Buck operation. PV array fed to BLDC motor through a Boost-Buck (BB) converter and a VSI. PV array is simulated using real time solar radiation data from National Renewable Energy Laboratory (NREL) for Telangana State. The simulation is carried out through MatLAB/Simulink environment and simulation results shows that the operation of the boost buck converter was smooth. During dynamic simulation, the sudden change in the solar radiation and the variation in solar power are smoothly stepped up by the boost converter.

Index Terms— Solar radiation in Telangana, Solar PV Array, BLDC Motor, Boost-Buck Converter

I. INTRODUCTION

In order to effectively obtain the solar power from the solar radiation, it is important to constantly track the solar radiation. As the solar output depends on the irradiance and temperature of the radiation that is being received by the earth surface, constant monitoring of solar radiation is required. Generally, it is difficult to constantly track the solar radiation parameters for a normal person. But there are some organizations that provide estimated or approximate values of solar radiation for a particular region. But National Renewable Energy Laboratory (NREL) [1] of United States of America has provided accurate data of solar radiation of both USA and India under the program Renewable Resource Data Center (RRDC). This data includes temperature, different irradiance values, and pressure and azimuth angle of the solar radiation of hourly solar radiation. Based on this data appropriate data for the year 2014 is collected of the Telangana, India region is collected and utilized. The collected data is presented below in the table 1.1. Since 1960 many algorithms have been proposed for extracting Maximum Power from Solar PV array, these algorithms are called as Maximum Power Point Tracking (MPPT) algorithms. MPPT algorithms mainly classified as direct and indirect methods.

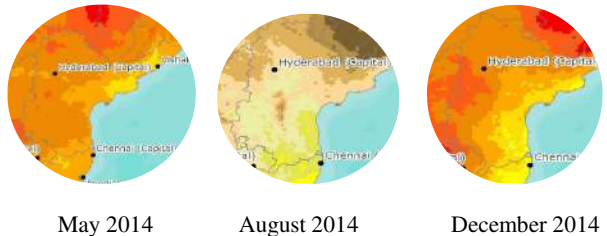


Fig 1 Average solar radiation of Telangana State May, August, December months in 2014 (Source: NREL) [1]

Table 1 Monthly minimum and maximum irradiances and temperatures of Telangana State in the year 2014 (Source: NREL) [1]

Month	Maximum and Minimum solar radiation and temperature				Season
	Average Irradiance		Average Temperature		
	Min	Max	Min	Max	
Jan	78.5	694	20.69	28.11	Rabi
Feb	107.25	862.5	20.58	31.9725	
Mar	178	914.25	26.9275	38.825	
Apr	201.75	961	31.85329	44.01603	
May	269.75	950.25	32.33742	40.6777	Summer
Jun	230.25	896.25	29.73949	36.36104	
July	173.5	764.75	26.84087	30.48676	
Aug	198.75	812.75	26.1244	29.96178	
Sep	140.5	712.25	25.23419	29.61552	Kharif
Oct	177	867.25	24.0265	30.06392	
Nov	144.5	733	20.22501	27.97588	
Dec	107.25	752.25	17.91771	27.19034	

Most popular methods for maximum power extraction from Solar PV arrays are Perturb and Observe (P&O) algorithm, Fixed step MPPT, Variable step MPPT, Incremental conductance (IC) and Fuzzy logic based MPPT etc., In this paper IC algorithm is used for tracking maximum power from Solar PV array since it optimizes the energy recovered especially when solar irradiation is low [4, 6, 7, 8, 11].

Conventional way to lift the water from very deep wells or bores for irrigation is by using 3-phase induction motor based centrifugal pumps. With solar power as input researchers proposed use of induction motor, DC motor, PMSM motor and BLDC motor fed centrifugal pump. BLDC motor is best suited for Solar PV array fed water pump among all other motors because of its higher efficiency and reliability than an induction motor, low Electro Magnetic Interference and noise which do not require any maintenance. [5, 12]

Since output voltage from the solar panel is constant as the temperature and irradiance are continuously varying parameters throughout a day, DC to DC converter is required to maintain the common DC bus voltage before Voltage Source Inverter. Many DC to DC converters have been used by researchers for water pumping applications like Boost converter, Buck converter, SEPIC converter, Cuk converter and Boost-Buck converter [2,10,13,14]. In this paper Boost-Buck converter is used for maintaining constant DC bus voltage.

II. POWER CONVERTERS

The output from the solar panel depends on the solar radiation the surface is receiving. As the radiation changes its temperature and irradiance the output parameters like voltage, current and power also vary. This rapidly varying output can be modified into input suitable to the load by using different power converters like boost, buck, buck-boost etc. These converter blocks modify the output power from the solar generator into fixed power and feeds to the load.

1) Boost-Buck Converter

This paper is implemented with Boost-Buck (BB) Converter. Boost-Buck converter is obtained by connecting a boost converter immediately after the DC source followed by a Buck Converter followed by load. The major advantage of this connection is it provides the advantages of both boost and buck converter simultaneously. All the four possible combinations of switching states of the two switches of boost-buck converter are considered for elaboration of the operation and working principle. According to the position of switches, the operation of the converter is categorized in two modes; (i) synchronized control mode and (ii) combined control mode.

(i) When the position of both the switches is same i.e. both the switches are either on or off, the converter operates in the synchronized control mode.

(ii) When the position of both the switches is different i.e. one is on and other is off, the converter operates in combined control mode.

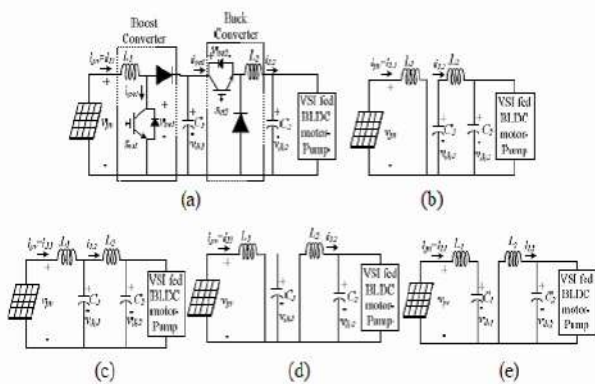


Fig 2 Boost-Buck converter fed BLDC motor pump

When the boost converter operates in continuous conduction mode, V_{dc1} is expressed as,

$$V_{dc1} = \frac{1}{1-D_1} V_{pv} \quad (1)$$

Similarly, when the buck converter operates in continuous conduction mode, V_{dc1} is expressed as,

$$V_{dc1} = \frac{1}{D_2} V_{dc2} \quad (2)$$

Where V_{dc1} and V_{dc2} are average values of output voltages of boost-buck converter. By solving the above equations we get a relation between output and input voltages of this converter as,

$$\frac{v_{DC2}}{v_{pv}} = \frac{D_2}{1-D_1} \quad (3)$$

It is clear from (3) that the Boost Buck converter operates as a non inverting buck-boost converter with independent control of both the boost and buck converters.

Boost-Buck converter is designed for standard solar radiation parameters of $1000W/m^2$ and $25 C$. The voltage at the input of the buck converter which is the output voltage of the boost converter is maintained at $V_{dc1} = 225 V$. On the other hand, V_{mpp} is the input voltage of boost converter which appears as, $v_{pv} = V_{mpp} = 170 V$. Using (1), D_1 is estimated as,

$$D_1 = \frac{V_{dc1}-V_{pv}}{V_{dc1}} = \frac{225-170}{225} = 0.24 \quad (4)$$

Switching frequencies $f_{sw1} = f_{sw2} = 20 \text{ kHz}$ are selected to minimize the amount of ripples in $iL1$, $iL2$ and $vdc1$ even with the lower values of the converter elements. The current of the PV array at MPPT, I_{mpp} flows through L_1 resulting in an average current, $IL1 = ipv = I_{mpp} = 30 A$. Limiting the current ripple, $IL1$ in $iL1$ at 8%, $L1$ is estimated as

$$L_1 = \frac{v_{pv} D_1}{f_{sw1} \Delta IL1} = \frac{170 * 0.24}{20000 * 30 * 0.005} = 1mH \quad (5)$$

Neglecting the converter power loss, average current at the output of boost converter, $Idc1 = P_{mpp}/V_{dc1} = 5100/225 = 22.67A$. Limiting the voltage ripple in $vdc1$ at 6%, $C1$ is estimated as

$$C1 = \frac{Idc1 * d_1}{f_{sw1} * \Delta v_{dc1}} = \frac{22.67 * 0.24}{20000 * 225 * 0.006} = 20\mu F \quad (6)$$

The average value of the output voltage of the buck converter which is the DC voltage rating of the BLDC motor is as, $V_{dc2} = 200 V$. Using (3.2), $D2$ is estimated as,

$$D2 = \frac{V_{dc2}}{V_{dc1}} = \frac{200}{225} = 0.89 \quad (7)$$

Neglecting, converter power losses, average current flowing through $L2$ is as, $IL2 = P_{mpp}/V_{dc2} = 5100/200 = 25.5 A$. Limiting the current ripple, $IL2$ in $iL2$ at 5%, $L2$ is estimated as,

$$L2 = \frac{V_{dc2} * (1-D1) * D2}{f_{sw2} * \Delta IL2} = 1mH \quad (8)$$

The lowest and highest frequencies of VSI output voltage are used to estimate the value of DC link capacitor, $C2$.

The maximum value of output frequency ω_h is calculated using rated speed of the motor

$$\begin{aligned} \omega_h &= 2 * \pi * f = 2 * \pi * (N_{rated} * P) / 120 \\ &= 2 * \pi * (2000 * 6) / 120 = 628.3 \text{ rad/sec} \end{aligned}$$

The lowest value ω_l is calculated using minimum speed of a motor required to pump the water

$$\begin{aligned} \omega_l &= 2 * \pi * f = 2 * \pi * (N * P) / 120 \\ &= 2 * \pi * (1100 * 6) / 120 = 345.6 \text{ rad/sec} \end{aligned} \quad (9)$$

Where $f \rightarrow$ frequency in Hz

N_{rated} \rightarrow rated speed of the motor

$P \rightarrow$ numbers of poles

Neglecting a very low current flowing through C_2 , an average current flowing through the DC link of VSI, I_{dc2} is equal to I_{L2} i.e. $I_{dc2} = I_{L2} = 25.5$ A.

The voltage ripple is limited to 10% as the 6th harmonic component of the motor voltage will appear on the DC link of VSI, C_2 is calculated corresponding to ω_h and ω_l as,

$$C_2 (\text{corresponding to } \omega_h) = \frac{I_{dc2}}{6 * \omega_h * \Delta V_{dc2}} = \frac{25.5}{6 * 628.3 * 200 * 0.1} = 338 \mu F \quad (10)$$

$$C_2 (\text{corresponding to } \omega_l) = \frac{I_{dc2}}{6 * \omega_l * \Delta V_{dc2}} = \frac{25.5}{6 * 345.6 * 200 * 0.1} = 615 \mu F \quad (11)$$

In order to ensure the satisfactory performance of the BLDC motor pump system, the value of $C_2 = 615 \mu F$ or $620 \mu F$ (approx.) is selected out of the two estimated values. The proposed BB converter is designed as per these estimated values of the components.

III. BRUSH LESS DC MOTOR (BLDC) DRIVE

Brushless DC motors were introduced to overcome the drawbacks of DC motors and Induction motors used for water pumping applications when fed with solar PV arrays. The overall efficiency of the system using BLDC and helical motor pumps varies from 30% to 50%. Fig 3 represents the switching of devices and the corresponding phases back emf waveform of BLDC motor.

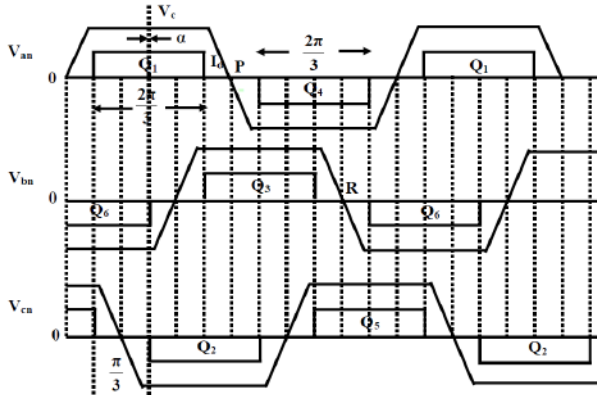


Fig 3 Back EMF waveform and corresponding operating switches

i) Control of BLDC Motor

BLDC motor is often connected with a Voltage Source Inverter to have a control on the motor's speed and torque. By controlling the switching sequence of the inverter, the motor's speed and torque can be controlled. This arrangement is possible mainly due to the absence of brushes. This arrangement also provides a variety of control strategies that efficiently control the motor without any hassle. This is the most significant feature of the BLDC motor which is helping various applications to choose BLDC motor. Various control strategies are in use in current technological world. Out of them the most prominent ones are sensor control and sensor less control. This is also called as electronic commutation. This project employs this electronic commutation as the control strategy of BLDC motor.

ii) Hall Sensors:

Hall sensors are devices that generally detect the position of the rotor and its rotatory motion through a principle called Hall Effect. Table 2 is presented below to determine the hall sensor outputs and the energizing of corresponding phases for the operation required.

Table 2 Output signals of hall sensors and switching sequence for different operation of BLDC motor

Rotor Position Sensor Signals			Forward Operation			Reverse Operation						
S1	S2	S3	Output Control Signals			Motor Windings						
			A	B	C	A	B	C				
0	0	0	1	5	+	-	OFF	2	4	-	+	OFF
1	0	0	3	5	OFF	-	+	2	6	OFF	+	-
1	1	0	3	4	-	OFF	+	1	6	+	OFF	-
1	1	1	2	4	-	+	OFF	1	5	+	-	OFF
0	1	1	2	6	OFF	+	-	3	5	OFF	-	+
0	0	1	1	6	+	OFF	-	3	4	-	OFF	+

PMSM Motor in Matlab/Simulink Library is used as a BLDC motor. As BLDC motor can be represented using PMSM motor by implementing a trapezoidal back EMF waveform.

This is backed by the properties of BLDC motor that are similar to PMSM Motor, as discussed. The motor parameters are mentioned in Table 3.

Table 3 BLDC motor parameters

Stator Resistance	$R_S = 0.23$ Ohms
Stator Inductance	$L_S = 1.3$ mH
Voltage Constant	$K_e = 78$ V _{L-L} /krpm
Rated Speed	$N_{Rated} = 2000$ rpm
Number of Poles	P= 6
Torque	1.2 Nm

IV. SIMULATION RESULTS

Proposed circuit is simulated using Matlab/Simulink environment version r2009a. 250V, 2.5kW Solar PV array is designed specifically based on the mathematical model of the panel. Inputs to the Solar PV array are given using repeating sequence using the collected solar radiation data from NREL's RRDC program. The Incremental Conductance MPPT can be realized by using various methods like the state flow method, block diagram using the mathematical modeling. But the MPPT is implemented by writing a code in the Matlab function block available in the Simulink library. The MPPT technique produced triggering pulses which are given to boost converter that boost up the output voltage of Solar PV array. This voltage is stabilized by using Buck converter connected. Triggering pulses for the buck converter are produced using input voltage comparator technique. This technique compares the input voltage to the buck converter with the predefined reference value to produce an error that is then compared with a high frequency carrier wave generated by comparing the error with 1, which is the highest value of triggering pulse. The output voltage of buck converter is given to VSI fed BLDC drive. The inverter switches are controlled by using the electronic commutation principle of the BLDC motor using inbuilt hall sensors. The hall signals are decoded using a logic circuit to generate triggering pulses to the

switches of VSI. These hall sensors control the operation of the BLDC motor through controlling the switching sequence of the VSI.

The performance of the model is simulated in Steady state and Dynamic mode. The dynamic mode includes the variation in the solar irradiance and temperature values for the data shown in Table1 for different seasons. Solar panel is modeled for different input irradiance and temperature values.

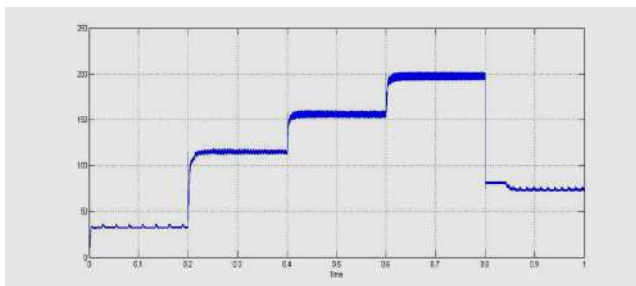


Fig 4 Solar PV Array output voltage during dynamic performance

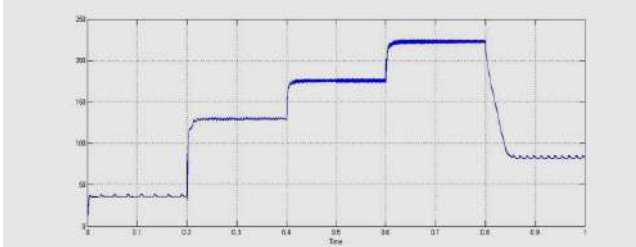


Fig 5 Boost converter output during dynamic performance

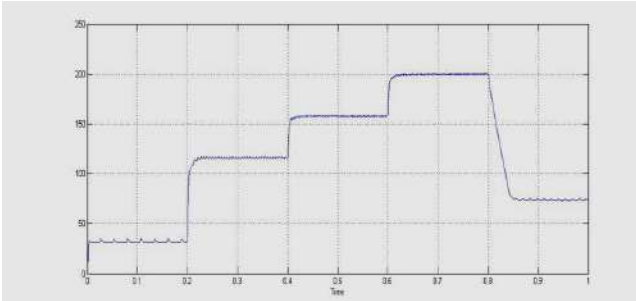


Fig 6 Buck converter output voltage during dynamic performance

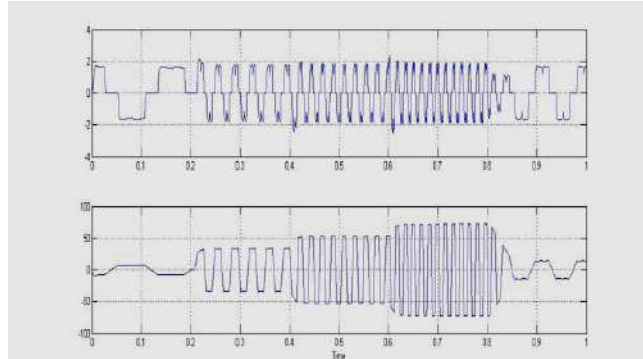


Fig 7 Stator Back emf and phase current of BLDC motor during dynamic performance

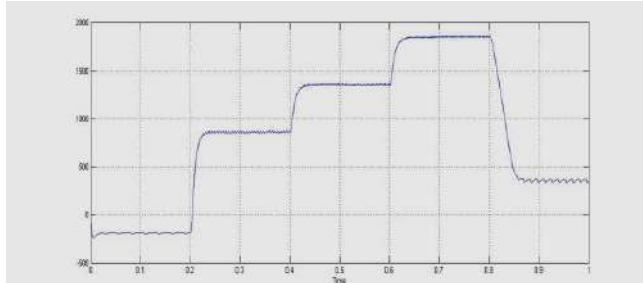


Fig 8 BLDC motor speed during dynamic performance

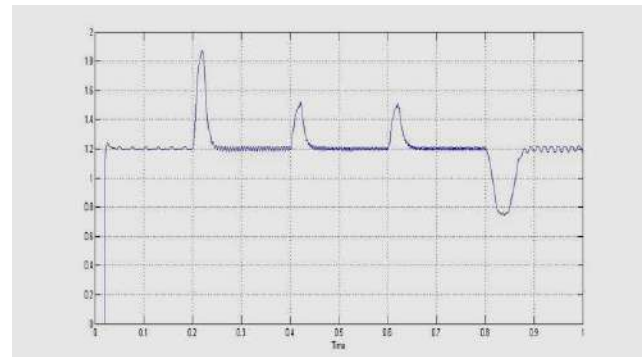


Fig 9 BLDC motor torque during dynamic performance

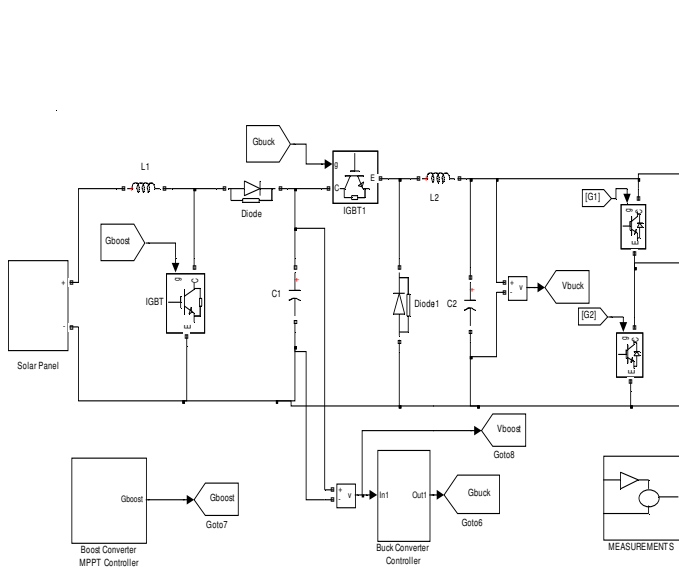
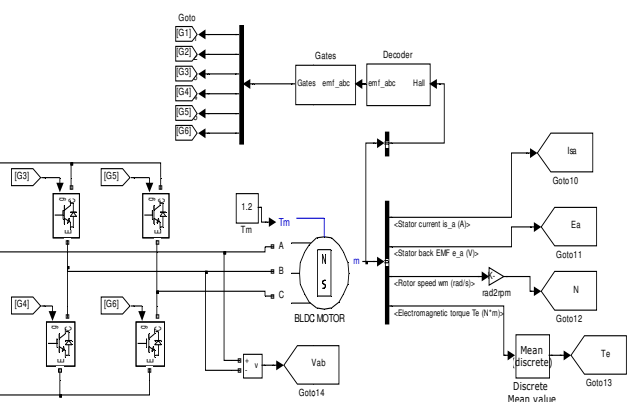
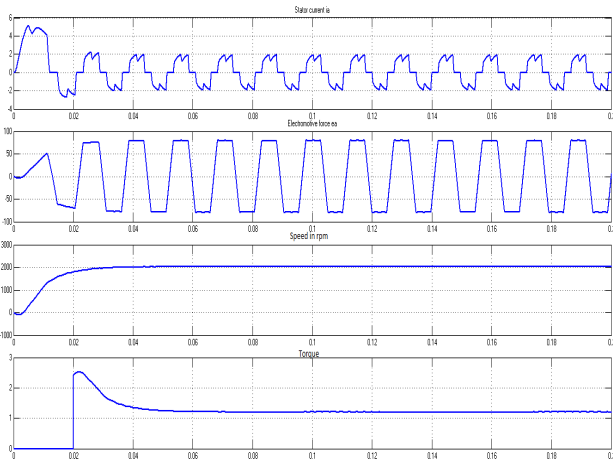
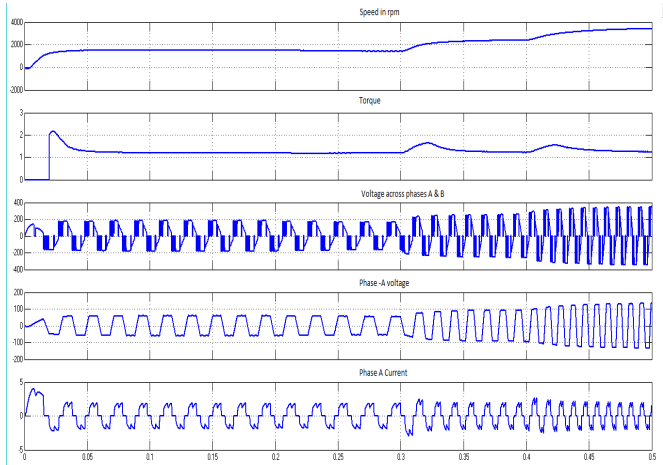


Fig 10 Simulation Model of Solar PV Boost Buck Converter Fed BLDC Motor





**Fig 11 Steady state performance of BLDC motor
(1000 W/m² Irradiance & 25 deg Temperature)**



**Fig 12 Dynamic performance of BLDC motor during Rabi Season
(November - March)**

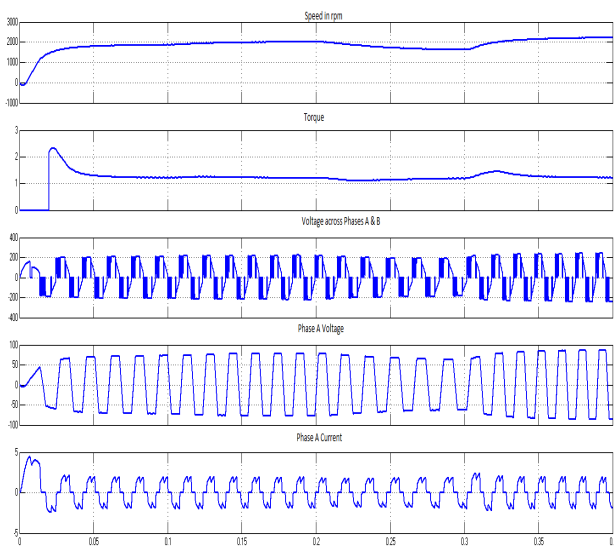


**Fig 13 Dynamic Performance of BLDC motor during Kharif Season
(July - October)**

V. CONCLUSION

It is evident from the results that operation of the boost buck converter was smooth. The output of boost converter is produced as per modeling and design of the boost converter. During dynamic simulation, with the data collected from NREL for the state of Telangana, the sudden change in the solar radiation and the variation in solar power are smoothly stepped up by the boost converter. Buck converter is employed to stabilize the output of boost converter. The performance of buck converter during steady state and dynamic simulation was satisfactory. The buck converter's output is fed to BLDC motor drive. The motor drive operates smoothly in the steady state simulation. During the dynamic simulation a few transient states are observed that is caused by the sudden change in the input parameters. The motor operation is observed to be smooth by observing the output waveforms in both the stages. Hardware model of Boost Buck converter fed BLDC drive can be analyzed for the future scope of irrigation in Telangana State.

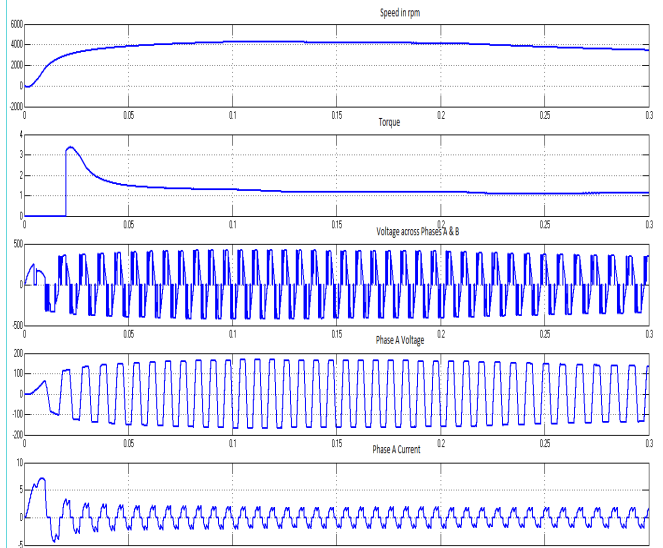


Fig 14 Dynamic Performance of BLDC motor during Summer Season (April - June)

REFERENCES

- [1] "Solar Irradiance and temperature data for the year 2014", National Renewable Energy Laboratory (NREL)
- [2] USA R. Kumar, B. Singh, A. Chandra and K. Al-Haddad, "Solar PV array fed water pumping using BLDC motor drive with boost-buck converter," 2015 IEEE Energy Conversion Congress and Exposition (ECCE), Montreal, QC, 2015, pp. 5741-5748.
- [3] C. Gopal, M. Mohanraj, P. Chandramohan and P. Chandrasekaran, "Renewable Energy Source Water Pumping Systems-A Literature Review", Renewable and Sustainable Energy Reviews, vol. 25, pp. 351-370, September 2013.
- [4] Mehmet Akbaba, "Matching Induction Motors to PVG for Maximum Power Transfer", Desalination, vol. 209, no. 1–3, pp. 31-38, 2007.
- [5] N. Chandra sekaran, G. Ganesh prabu and K. Thyagarajah, "Comparative Study of Photovoltaic Pumping System Using a DC Motor and PMDC Motor", International Conference on Advances in Engineering Science and Management (ICAESM), pp. 129-132.

- [6] Zhou Xuesong, Song Daichun, Ma Youjie and Cheng Deshu, "The Simulation and Design for MPPT of PV System Based on Incremental Conductance Method", WASE International Conference on Information Engineering (ICIE), vol. 2, pp. 314-317.
- [7] Issam Houssamo, Fabrice Locment and Manuela Sechilariu, "Experimental Analysis of Impact of MPPT Methods on Energy Efficiency for Photovoltaic Power Systems", International Journal of Electrical Power & Energy Systems, vol. 46, pp. 98-107, March 2013.
- [8] T. K. Soon and S. Mekhilef, "Modified Incremental Conductance MPPT Algorithm to Mitigate Inaccurate Responses Under Fast-Changing Solar Irradiation Level", Solar Energy, vol. 101, pp. 333-342, 2014.
- [9] Mohan Ned, Tore M. Undeland and William P. Robbins, Power Electronics: Converters Applications and Design, 2009, Jhon Wiley & sons Inc.
- [10] B.Singh and V.Bist, "Improved Power Quality Bridgeless Cuk Converter Fed Brushless DC Motor Drive for Air Conditioning System", IET Power Electronics, vol. 6, no. 5, pp. 902-913, May 2013.
- [11] Stefan Moring, Anton Pols, 27-June-2012, "Maximum Power Point Tracking: Algorithm and Software Development" (Bachelor Thesis), Delft University of Technology.
- [12] Ward Brown, 2002, Brushless DC Motor Control Made Easy, Microchip
- [13] Rajan Kumar, Bhim Singh, "Solar PV Array Fed Water Pumping System Using SEPIC Converter Based BLDC Motor Drive", Eighteenth National Power Systems Conference (NPSC), 2014
- [14] Bhim Singh , Rajan Kumar, "Solar PV Array Fed Brushless DC Motor Driven Water Pump", IEEE 6th International Conference on Power Systems (ICPS), 2016

Modelling and Simulation of the Wind Energy Electric Conversion System to Extract The Maximum Power From the Wind Using MATLAB

N. Rakesh¹, A.Nitya² and Gautham Ram²

¹Department of EEE, Kakatiya Institute of Technology & Science (KITS), Warangal, Andhra Pradesh, India.

²Department of EEE, National Institute of Technology (NIT), Tiruchirappalli, Tamil Nadu, India.

Email: nr@eee.kitsw.ac.in

Abstract— This paper describes the development of a simple maximum power extracting (MPE) scheme for Wind Electric Energy Conversion System (WECS) comprising of an induction generator, capacitor banks, a diode bridge rectifier, dc link inductor and a line commutated inverter feeding the grid. Steady state analysis of Self Excited Induction Generator (SEIG) is done with the MATLAB programming. The operational speed range of SEIG is decided by proper choice of excitation capacitor banks. MPE is achieved over this speed range by the adjustment of the inverter firing angle that loads the system appropriately to extract maximum power for any given value of input rotor speed. A unique one-to-one relation between per unit rotor speed input and the predetermined inverter firing angle corresponding to MPE has been developed in the form of look-up table. The entire system has been simulated and modelled using the power system block set in MATLAB to obtain the results. The experimental and simulated waveforms validate the system performance.

Keywords— SEIG, Renewable power generation, Line-commutated inverter, MPPT, steady state analysis, Power generation systems.

I. INTRODUCTION

The rate at which conventional non renewable sources of energy are facing depletion poses a severe element of doubt on the ability of utilities to satisfy the growing power demand. Naturally a search for alternatives is prevalent especially in developing countries wherein the rate of increase in demand is bound to overtake the rate of increase in installed capacity, which attempts to meet the demand. The potential of non-conventional, renewable sources of energy in meeting future claims of power has been under detailed investigation over the past two decades [1]. In fact, the possible contribution of wind energy in minimizing the rate of depletion of fossil fuels is at present of great interest as it has been estimated that there is about 106 MW potentially recoverable from the wind on a global basis and that amounts to nearly 10 times the hydropower capacity [2-3]. Hence wind power conversion schemes are regarded as power saving solutions and considerable research has yielded many models for the same. Fig.1 shows the layout of such a WECS. The prime mover employed is generally a wind turbine. The variable speed generator in use is generally a SEIG on account of its simplicity, ruggedness, ease of implementation and low cost [4-6]. On account of the erratic nature of wind speed, the generator acts as a source of variable voltage and frequency. Directly interfacing this generator to the grid gives rise to the

following problems like the inability of the generator to extract and feed power to the grid at speeds below the synchronous speed and the added tendency to act as a motor, drawing power from the system and posing a supplementary burden on the same and Voltage fluctuations, flickering and generation of sub harmonics or harmonics associated with the pulsating torque characteristic of the wind turbine driving the induction generator [7]. Moreover, the inability to extract the maximum power over a large speed ranges thereby favouring incomplete utilization of the wind energy. This justifies the requirement of the above scheme that involves a SEIG feeding the grid via power electronic interface. Provided the critical value of magnetizing reactance is not exceeded the machine will function as a generator for any value of input rotor speed. Also the employment of such a system will increase the operating speed range, reduce voltage and torque pulsations and allow the implementation of flexible MPE. The configuration of the interface employed is generally a rectifier-inverter system connected through an asynchronous DC link.

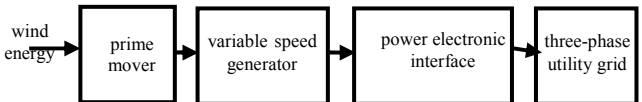


Fig.1. Generalized block diagram of wind energy conversion scheme

II. MACHINE MODELLING WITH CONCEPTION OF THE POWER SOURCE

This system deals with the design and development of a practical system for achieving MPE from the wind over a fairly large range of wind speeds. It comprises wind driven SEIG, diode bridge rectifier, dc link, three phase line commutated inverter and grid as shown in Fig.2. The system is simulated by connecting the different type of entities. Each entity requires to be configured in terms of its design and function to match the goal of the MPE. The wind driven self excited induction generator had modelled with the simple mathematical relations to get the variable voltage and the variable frequency. Hence by employing the system model, it has been realized the source of power as a simple mathematical input-output relation. Each solution of this relation will correspond to a unique condition of steady state MPE. In other words, the user will view the source of power as a black box that will receive the input, perform a manipulation as governed by the relation inscribed and

produce an output that is fed to the system. The input fed to the source is per unit rotor speed and the output is the per phase stator voltage that is fed to the system. Two minor issues need to be reasoned out here with regard to the choice of the input and output. The range of rotor speed under analysis corresponds to a unique range of wind speed [1,4] as a straightforward one-to-one relation. This is because for each value of wind speed, MPE takes place only at a particular value of rotor speed. Furthermore while validating the system model by experimentation DC shunt motor will be employed to feed in a fixed speed to the induction generator and the rotational speed of the shaft is the data to be recorded as input for verification. Hence despite terming the source as a wind-driven SEIG we are completely justified in using the rotor speed and not the wind speed as input for the system.

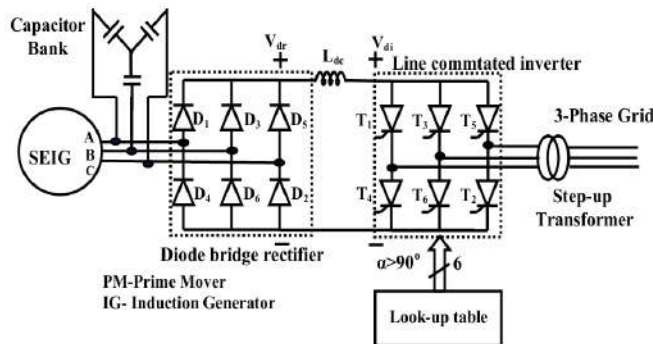


Fig.2. Overall schematic diagram of the proposed wind energy conversion system

The choice of per phase stator voltage as the output variable of the black box is justified thus. The load on the SEIG cannot be obtained in a simple manner and involves multiple stage reflections beginning from the grid. However the stator voltage is a controllable parameter. Hence a predetermination is done in coding, wherein the stator voltage corresponding to each steady state condition of MPE is recorded in terms of its rms magnitude V_s and per unit frequency a by subjecting the machine to a fairly expansive range of loading. Having decided the input and output, the mathematical relation is derived by studying the variation of the output with respect to the input, fitting the relation into a suitable curve. The steady state model of the SEIG is realized as a linear time invariant circuit, i.e. as a purely passive circuit with fixed values of parameters. The load on the SEIG is also assumed to be linear and purely resistive. The assumption of a purely resistive load is justified in the following manner. The entities following the SEIG are the diode bridge rectifier and the DC Link. If a continuous current requirement is imposed on the DC link then unity power factor will be maintained at the input of the Diode Bridge Rectifier, which corresponds to resistive loading of the induction generator [8-9]. So apart from the sheer convenience offered by the choice of resistive loading the constraints on the system in addition are in its favour. Having justified the linearity of the source and load, it follows that a variation in the applied load from 0 to infinity will result in a bell shaped curve for the power extracted from the system with a well-defined maximum at a given value of load, the input remaining constant in the course of the

variation [10]. This is termed as the machine loading characteristic. It has also been established that the relationship between maximum power extracted from the wind and wind speed is a cubic polynomial [6, 8]. For the sake of simplicity we neglect the lower exponentials and assume a pure cubic relationship between the maximum power extracted from the wind and wind speed. The presence of a unique rotor speed corresponding to each wind speed at the maximum power point provides sufficient room to believe that a similar cubic relation holds between the maximum power extracted and the rotor speed as shown below:

$$P_{b\max} \propto b^3 \quad (1)$$

Assuming that the machine has been designed wisely such that the maximum power extracted at rated speed ($b = 1$ p.u.) equals the rated power of the machine, then the maximum power extracted at any fraction of the rated speed will follow the simple proportionate relationship shown below:

$$P_{b\max} = b^3 \times P_{\text{rated}} \quad (2)$$

The variation of power for different per unit speeds based on equation (2) over the operational speed range and its operation is described in [11, 12]. So, To ascertain the existence of such an operating point over a practically feasible range of rotor speed by loading it appropriately for each value of input rotor speed and produce a database of such operating points. To achieve a series of maximum power operating points over a fairly large range of rotor speed scaling downwards from the maximum value, which is the rated value. For the first stage of analysis, the performance is predetermined over a wide speed range and a wide load resistance range with a fixed value of excitation capacitance. This is done to first ascertain the presence of an operating point over the given range. A star connected capacitance of 60 μF per phase is employed for excitation as was done in the predetermination and experimental verification routine. The range of per unit speed variation is initially fixed at (1:0.1:0.1). The maximum value of load resistance available is 165 ohms per phase. Hence for each value of per unit speed the load resistance variation is initially taken as (5:5:165). The range and step size of loading are then restricted and reduced respectively to elaborate on results close to the intersection of power curve with the maximum power point. The result was that operating points were found to exist over a per unit speed range of (1:0.94) for 60 μF excitation capacitance following which the machine loading characteristic (MLC) failed to intersect the maximum power extraction (MPE) characteristic of wind. This can be attributed to the demagnetization of E with decrease in b till a point where the magnetizing reactance surpasses its critical value. However research has proved that an increase in the value of excitation capacitance per phase increases the allowable speed range of an induction machine for a given range of loading [13]. A two-stage successive connection of 20 μF each in parallel to the existing 60 μF connection was applied and the above analysis was repeated. This resulted in an extension in per unit speed range of (0.93:0.77) for the first stage and (0.76:0.66) for the second stage, with operating points available over the entire speed

range. Hence three subsidiary ranges of per unit speed are obtained to form a cumulative range of (1:0.66). The range of rotor speeds at which an operating point was obtained found to be limited. Because the machine fails to excite as the critical value of magnetizing reactance was exceeded at these operating points and even if the machine excites, it is unable to extract the maximum power entirely (i.e. power is less than that of ideal cube law power).

For each subsidiary speed range or excitation capacitance there are two MATLAB code files. The first MATLAB code file contains the mathematical model of the SEIG along with the definition and declaration of the function to be minimized. The second MATLAB code file varies the per unit speed over the subsidiary speed range and the load resistance over a condensed range in steps of 0.5 and obtains the power supplied by the machine and the stator voltage magnitude and per unit frequency for each calculation. A plot of power supplied by the machine versus load resistance is also obtained. The operating point was defined as the intersection of the Machine Loading Characteristics (MLC) with the Maximum Power Extraction (MPE) characteristic. Naturally for a null error margin there will be two points of intersection as shown in Fig.3 except for the case of a single operating point being present at the maxima of the MLC. So for each run of calculation a minimum of two operating points will be get. One corresponds to the upward slope of the MLC and the other corresponds to the downward slope.

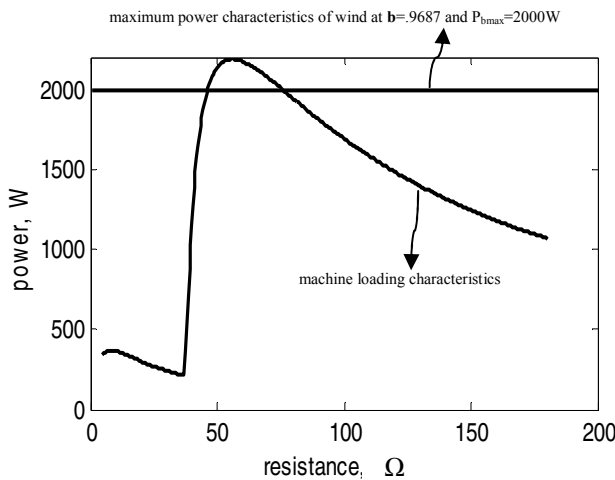


Fig. 3. Intersection of MLC and MPE characteristics

Table.1 Results of convergence at downward slope for error margin = 10W

expected maximum power = 2000 W		
load resistance(R),Ω	three phase load power(P), W	source line voltage(V _s), V
46.00	1980.8	301.68
46.50	2009.6	305.68
47.00	2035.0	309.25

A choice must be made between these two if we are to get a unique relation for our source model. It is found that at the downward slope intersection an increase in load or a decrease

in load resistance leads to an increase in power extracted from the machine which is an indication of operating point stability, not offered by the upward slope intersection. Hence for each value of per unit speed the downward slope intersection is chosen as the operating point. Table.1 and Fig.3 Shows the important results of the analysis described so far for a particular value of per unit speed ($b = 0.9687$). However an error margin of 0.45% is provided as the variation of speed and load are discrete. It is possible that more than one point might lie within this error range and hence many points may be recorded and under such circumstances the relevant details corresponding to maximum power extraction are averaged. Once the operating points are chosen the corresponding values of per phase voltage magnitude and per unit frequency are stored against per unit speed as an array. The results of this simulation routine are shown in fig.4 and yield a unique set of operating points. The fig.4 shows the discrete values over the entire speed range. The values of b and the corresponding unique values of V_s and a are hence fit into a suitable curve for each subsidiary speed range and the governing equations of their relation for each range is shown in Fig.4(a) and Fig.4(b) with the corresponding equations.

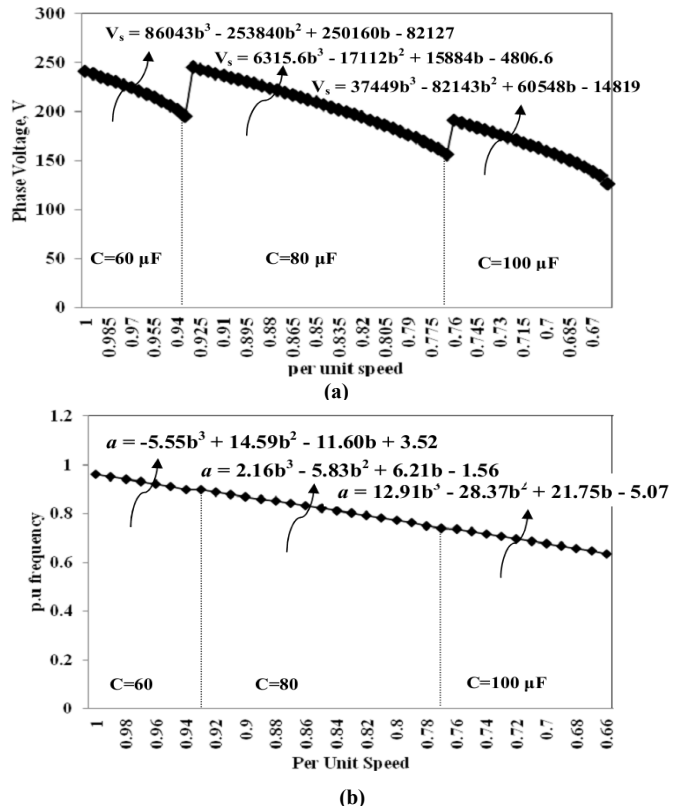


Fig.4. curve fit equations and waveforms

- (a) curve fit of V_s versus b
- (b) curve fit of a versus b

A

III. SYSTEM MODELLING

The system is essentially a wind-driven SEIG synchronized to the grid by means of a power electronic interface. The induction generator is modelled as a three-phase

source with a controllable value of per phase voltage, V_s and per unit frequency, a . The grid is modelled as a fixed voltage-fixed frequency source. The interface comprises of a diode bridge rectifier feeding a three-phase fully controlled converter by means of a DC transmission link. An uncontrolled diode-bridge rectifier is employed at the generator end, which implies an additional reactive power burden on the capacitor bank is effectively avoided (input displacement factor is zero and draws no reactive power) [8]. The remaining part of the system as viewed from the output terminals of the diode bridge rectifier is an RLE load.

The three-phase inverter is designed using SCRs and the connection of its AC terminals to the grid assures line commutation, avoiding the additional expense over complex forced commutation circuitry. The converter operation as an inverter is demanded here as real power needs to be fed to the grid. Hence the firing angle range is chosen to lie between 90 degrees and 180 degrees with respect to the natural zero of the three phase system. Also the positive terminal of the diode bridge output is connected to the negative terminal of the inverter input and vice versa via the DC link. This facilitates flow of real power from the DC side at the inverter input to the grid [8]. The variation of the inverter firing angle reflects as a variation in load at the terminals of the induction machine. For a given value of input rotor speed, the value of firing angle must be chosen such that the machine is loaded appropriately to extract maximum power at that speed. Although the real power flow is the major concern of analysis. Consider the system comprising of the induction machine and the diode bridge rectifier. The load on the machine is mapped either as a purely resistive load or a fairly inductive load depending on whether continuous or discontinuous conduction is maintained at the DC link respectively [9]. Hence on account of the converter configuration used and the nature of load connected there is no possibility of the grid to extend any contribution towards the reactive power requirement of the induction machine. Then for the system [8] comprising of the line commutated inverter provides the entire range of firing angle variation, the inductive load of the dc link forces reactive power to be drawn from the grid. The dc link is modelled as a series reactor as mentioned earlier. The design of the dc link was carried out by conducting a series of simulations by employing different values of link parameters at each stage. The final choice of the design was reached based on which model guaranteed an operating point with permissible values of voltage and current over the entire range of per unit speed.

IV. PREDETERMINATION OF THE INVERTER FIRING ANGLE

The system model is configured by obtaining a simple input-output relation between per unit speed and inverter firing angle. The system parameter thus chosen for control is the inverter firing angle. This is because the variation of the inverter firing angle is mapped as an equivalent load variation at the terminals of the induction machine. Hence for each value of per unit speed input the required loading of the induction machine to achieve MPE by suitably fixing the firing angle. For each value of per unit speed, the per phase stator voltage

magnitude and frequency are set to correspond to conditions of MPE. For each value of b , the value of the firing angle at which the power generated at the source end is within a 1.0% tolerance margin of the maximum extractable power from the wind at that speed is recorded. The inverter firing angle that would appropriately load the source to extract maximum power was predetermined over the operational speed range. The unique one-one relation between per unit speed b and inverter firing angle α is drafted as a lookup table. The tabulated values of b and α correspond to discrete points over the speed range are displayed in table.2. Derivation of a mathematical relation between b and α followed by a curve fit is avoided on account of the small variation in α for a step change in b . Hence the relation is coded as a look-up table.

Table.2.look-upable

$C=60\mu F$	b (p.u)	1	0.99	0.98	0.97	0.96	0.95	0.94	-	-	-
	α (deg)	171	164.3	160	156.2	152.6	148.7	144.5	-	-	-
$C=80\mu F$	b (p.u)	0.93	0.92	0.91	0.9	0.89	0.88	0.87	0.86	0.85	0.84
	α (deg)	177.1	176.5	168.5	164.2	160.7	157.8	155.1	152.6	150.2	147.8
	b (p.u)	0.83	0.82	0.81	0.8	0.79	0.78	0.77	-	-	-
	α (deg)	145.5	143.3	140.9	138.7	136.2	132.8	129.3	-	-	-
$C=100\mu F$	b (p.u)	0.76	0.75	0.74	0.73	0.72	0.71	0.7	0.69	0.68	.67
	α (deg)	142.7	140.5	138.6	136.8	135.1	133.3	131.4	129.3	127	124.4

V. HARDWARE AND SIMULATION RESULTS

A particular value of the rotor speed was chosen from each of the speed ranges and the values of system variables at each stage were recorded at the source, dc link and the grid. These values are tabulated in Table.3.

Table.3 System variables at specific operating points

	$b = 0.95$	$b = 0.8$	$b = 0.7$
V_s	210.4	182.6	160.4
I_s	3.21	2.12	1.75
I_{s1}	3.01	1.96	1.57
$O_{il}(+ : lead)$	+0.25	-1.93	-0.71
P_s	1896	1107	753
V_{dr}	490.4	423.5	373
I_{de}	-3.87	-2.57	-2.05
V_{di}	463.1	407.2	358.5
I_g	3.14	2.12	1.75
I_{g1}	2.98	1.96	1.56
O_{ol}	31.86	41.82	49.54
P_g	1764	1014	702

The experimentation and simulation waveforms are observed with per unit speed $b=0.9687$ and the same are displayed in Fig.5.

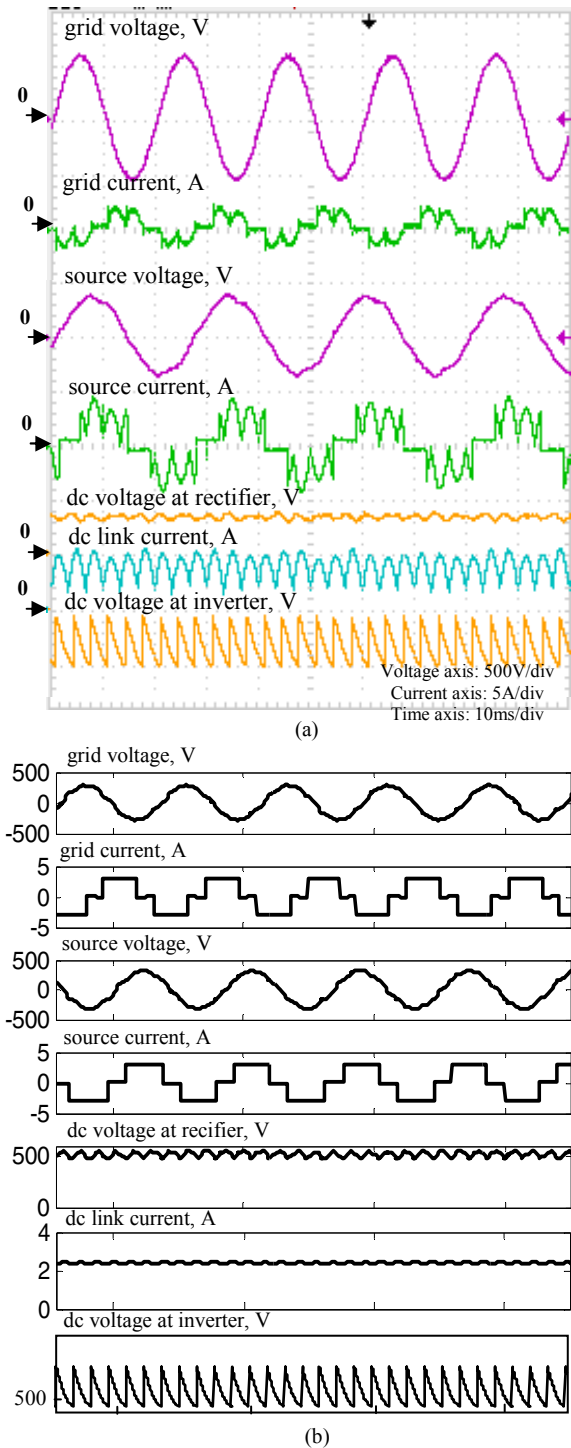


Fig: 5. Proposed system waveforms at different stages
 (a) Experimental waveforms
 (b) Simulated waveforms

VI. CONCLUSION

A new maximum power extraction scheme for wind energy electric conversion scheme had been developed by employing

induction machine and associated power electronic controllers. The maximum power extraction from the wind over a fairly large range of wind speed by variation of the line-commutated inverter firing angle had been achieved. The SEIG was coded successfully in software as a steady state mathematical model. It was then subject to various stages of analysis resulting in a black box model. The source conceived as a black box model was employed to feed power to the system and the inverter firing angle was varied for each value of input speed to obtain the precise level of loading corresponding to the operating point of maximum power extraction. The corresponding simulated and experimental waveforms had been brought out.

NOMENCLATURE

<i>a</i>	: per unit (p.u.) frequency = f_g / f_r
<i>b</i>	: p.u. speed = N/N_s
<i>C</i>	: excitation capacitance per phase μF
<i>E</i>	: air-gap voltage per phase V
I_{dc}	: dc link current A
I_g, I_{g1}	: rms value of grid current, fundamental value of grid current, respectively A
I_s, I_{s1}	: stator line current, fundamental stator line current, respectively A
L_{dc}	: dc link inductance mH
P_{bmax}	: maximum power extracted from the wind at a given value of <i>b</i> W
P_{rated}	: maximum power extracted at rated speed W
P_g, P_s	: grid power, power output of the generator, respectively W
<i>R</i>	: load resistance Ω
V_{di}	: average dc input voltage of LCI terminals V
V_{dr}	: average dc output voltage of the diode bridge rectifier V
V_s	: line voltage at the generator terminals V
V_g	: phase voltage at the grid V
α	: firing angle Degree
ϕ_{il}	: input fundamental power factor angle Degree
ϕ_{ol}	: output fundamental power factor angle Degree

REFERENCES

- [1] Ion. Boldea, "The Electric Generators Handbook: Variable Speed Generators," Taylor and Francis Publications, 2006.
- [2] T. S. Jayadev, "Windmills stage comeback," IEEE Spectrum, pp.45-49, 1976.
- [3] G. L. Johnson, "Economic design of wind electric systems," IEEE Trans., PAS 97, pp. 554-562, 1978.
- [4] B. Watson, J. Arrillaga, and T. Densem, "Controllable dc power supply from wind-driven self-excited induction machines," Proc. IEE, Vol.126, No:12, pp. 1245-1248, 1979.
- [5] N. Mohan, and A. Riaz, "Wind driven capacitor excited induction generators for residential electric heating," IEEE PES Winter Meeting, New York, 1978.
- [6] D. B. Watson, and J. Arrillaga, "Static power conversion from self excited induction generators," IEE Proc., Vol. 125, No:8, pp. 743-746, 1978.
- [7] R. M. Hilloowala, A. M. Sharaf, and M. Lodge, "Wind energy conversion schemes and electric power supply quality," European Wind Energy Conference, Madrid, 1990.
- [8] R. M. Hilloowala and A. M. Sharaf, "A Utility Interactive Wind Energy Conversion Scheme with an Asynchronous DC link using

- Supplementary Control Loop," IEEE Transactions on Energy Conversion, vol. 9, No:3, pp. 558 -563, 1994.
- [9] N. Kumaresan, N. Ammasaigounden, and M. Subbiah, "Certain control strategies for three-phase semi-converters for the operation of selfexcited induction generators," Proc. IEEE ICIT 2002, Vol. 2, pp. 986-991, December 2002.
- [10] Hou-Tsan Lee, Li-Chen Fu, and Hsin-Sain Huang, "Sensorless speed tracking of induction motor with unknown torque based on maximum power transfer," IEEE Transactions on Industrial Electronics, Vol.49, No:4, pp.911-924, 2002.
- [11] R. Karthigaivel, N. Kumaresan, and M. Subbiah, "Analysis and control of self-excited induction generator-converter systems for battery charging applications," IET Electr. Power Appl., Vol. 5, pp.247-257, 2011.
- [12] S. Senthil kumar, N. Kumaresan, N. Ammasai gonden, and N. Rakesh, "Analysis and control of wind-driven self-excited induction generators connected to the grid through power converters," Frontiers in Energy with Springer Publications, Front. Energy, Vol. 6, No. 4, pp. 403-412, 2012.
- [13] S. M. Alghuwainem, "Control of a Wind-Driven Self-Excited Induction Generator Supplying an Induction Motor Load for Maximum Utilization," Canadian Conference on Electrical and Computer Engineering, Vol.1, pp.531-534, 2000.

A New Technique to Enhance Output Power from Solar PV Array under Different Partial Shaded Conditions

Namani Rakesh¹, Venkata Madhavaram.T², K. Ajith³, G. Rajendra Naik⁴ and P. Nagarjun Reddy⁵

Department of Electrical and Electronics Engineering

Kakatiya Institute of Technology and Science, Warangal, Telangana, India

namanirakesh@gmail.com¹, madhavaram92@gmail.com², ajitkatanguri@gmail.com³, rajendra.ksg@gmail.com⁴, nagarjunreddyp@gmail.com⁵

Abstract – The performance of the Solar PV array is dependent on solar irradiation, temperature, power mismatch and shading. Solar PV arrays are losing its efficiency by the effect of shading. Solar PV array applications around the globe are reported with the problems of shading. Passing clouds, shade of a big tree, the neighbours building completely reduce the output power yield even though the size of Solar Power Plant is large. So, in order to solve this issue, a New Technique (Magic Square) is proposed in this paper to increase the generated power by configuring the modules of a shaded photovoltaic array. In this approach, the physical location of the modules in Total Cross Tied (TCT) connected in the solar PV array is arranged based on Magic Square arrangement pattern. The arrangement is done in such a way that, only the physical locations of the modules are changed and the electrical connections remained unaltered. In this work, the Global Peaks are achieved by plotting PV characteristics. For different types of shading patterns, the performance is calculated. The theoretical calculations are compared with MATLAB simulations to validate the results.

Keywords - Photovoltaic cells, partial shading patterns, Magic Square, Global peaks and TCT

I. INTRODUCTION

Higher energy prices, environmental problems such as pollution and depleted non-renewable energy resources have urged the demand to the affordable, inexhaustible and clean renewable sources of energy. Of these renewable energy sources, such as solar energy, wind energy, tidal energy, etc., solar energy has grabbed much more advantages as it can be used as a compliment to other energy sources. For example, solar photovoltaic energy supplies electricity on sunny days (in general with low wind) while on cold and windy days, which are frequently cloudy, the wind generators are in position to supply more electric energy [1], [2].

Solar energy can be generated anywhere around the globe provided that there is some solar irradiation. It is import – independent, enhances sustainability, reduces pollution and is mainly, above all, maintenance free [3]. The photovoltaic cell or solar cell, which is an electric device that converts the light energy into electricity, is much affordable. Solar radiation can be trapped by the means of the Photovoltaic cells (panels) and the obtained DC power can be used for low DC voltage applications or can be converted into AC. There are wide ranges of applications of generating power from solar PV array varying from few kW to numerous MW [4], [5].

In order to meet the load requirements, the solar PV cells are connected in series and parallel. But, when an array or two is subjected for shading, we observe a decrease in the output power of solar PV array [6].

Passing clouds, shade of a big tree, poles, and the neighbours building affects the output of solar PV energy as these are also roots for partial shading [7]. Because of this partial shading, there is reducing in the output yield. This power loss obtained due to shading depends upon the shading pattern and location of shaded modules. So, in this proposed arrangement, we change the physical location of the modules and the electrical connection remains unaltered. The multiple peaks in the solar PV characteristics arises which affect MPPT algorithms and the Global Peak (GP) is settled at Local Peak (LP) [8], [9]. To track the GP for shading conditions, various MPPT algorithms are proposed in [10].

This paper deals with a new technique to configure the physical location of modules in a Total Cross Tied (TCT), connected Solar PV array to boost up the output power under shaded conditions. When the physical locations are changed from TCT to Sudoku pattern, the power increase is 6% [11]. However, the main disadvantage that the Sudoku possesses is that it can be performed only on a 9 X 9 array. So the generalized partial dispersion technique is proposed in [12], where the power enhancement takes place which is given in [12]. In this proposed system, in order to overcome the disadvantage of Sudoku, the physical location of the TCT configured modules are changed by a new technique called as Magic Square.

The physical locations of modules of solar PV array are changed and the electrical connections are unaltered. This arrangement distributes the shading effect over the entire array and hence it reduces the affect of shaded modules in the row [11], [13]. In this work, we compare the output powers of TCT and Magic Square arrangement.

But some studies [14] also proved that electrical reconfiguration technique also distributed the effect of shading. When this Electrical reconfiguration technique is put into practice virtually, it involves various current and voltage sensors, it is mandatory to adjust the electrical connections which require switches for operation. So in this Magic Square Technique, there is no need of any switches or sensors. The reconfiguration technique in large solar PV systems consists of variety of switches and sensors. The increase in array size increases the number of Switches used and a huge complex control circuit is obtained.

The paper is as follows: Section II deals with proposed technique design configuration. The results are explained in Section III and Section IV gives the conclusion of the proposed work.

II. Proposed Technique Design Configuration

a. Photo Voltaic Panel Model

Solar energy is the renewable energy which is mostly abundant in the nature. The energy radiated by the sun can be trapped by the means of the Photovoltaic cells. These cells are connected to form a Solar PV panel. The specifications of solar panel at standard test conditions are given in Table-1.

Table - 1: PV Specifications at 1000W/m^2 and 25°C

Output Power	80 W
Open Circuit Voltage	21.6 V
Short Circuit Current	4.7 A
Nominal Voltage	18 V
Nominal Current	4.4 A

b. TCT structure of a Solar PV array

A 4×4 panel is considered, Column – 1 consists of modules labelling from 01 – 04; column – 2 consists of modules from 05 – 08 and so on as in fig. 1.

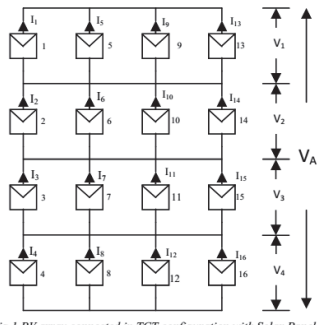


Fig.1 PV array connected in TCT configuration with Solar Panels

For different types of shading patterns, The PV characteristics are obtained for both TCT and Magic Square and the results are presented in Section III.

c. Magic Square Configured structure of a Solar PV array

A magic square is an arrangement of the numbers from 1 to n^2 in an ' $n \times n$ ' matrix, with each number occurring exactly once, and such that the sum of the entries of any row, any column, or any main diagonal, is the same.

The following technique is applied for 4×4 square matrix. Consider TCT arrangement of panels as shown in fig. 1. All the diagonal numbering panels of magic square configuration are connected same as in TCT configuration, leaving all the remaining as shown in Fig. 2(ii). In the proposed 4×4 configuration, there exists 16 panels and starting from the last, i.e., 16th number panel, in the descending order, all the unused numbering panels are arranged in column – wise to fill all the remaining left out as in Fig. 2(ii).

1			13
6	10		
7	11		
4		16	

1	12	8	13
15	6	10	3
14	7	11	2
4	9	5	16

Fig. 2 (i) Diagonal elements of TCT configuration (ii) Magic Square pattern

In this arrangement, the physical locations of modules are changed, without affecting the electrical connections. The panels in the row of TCT configuration are moved to different rows in Magic Square Technique. The Proposed Magic Square

technique is shown in Fig. 3(i) and its arrangement with solar panels are represented in Fig. 3(ii). For few solar panels the physical movement is shown with the extending lines as in Fig. 3(ii) and the remaining connections are understood with Fig. 3(i). In this technique, the incoming current at a particular node is increased and reduces the bypassing of panels. Therefore the generated power is increased for the identical shading pattern. This allows reducing the shading effect on a single row by distributing the shade over the entire array.

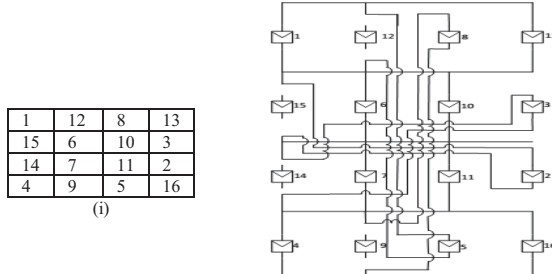


Fig.3 (i) Chosen Magic Square pattern (ii) Magic Square Arrangement with solar panels

III. SIMULATION RESULTS

In order to evaluate performance of the proposed system, a 4×4 solar PV array, shown in fig. 3, is subjected to four types of different shading patterns.

Case 1: Short Wide (SW)

In this case we consider 4 different irradiation levels to calculate the performance of the system. The group one receives the irradiation of 900W/m^2 ; group two receives 600W/m^2 ; group three and group four receives 400W/m^2 and 200W/m^2 respectively.

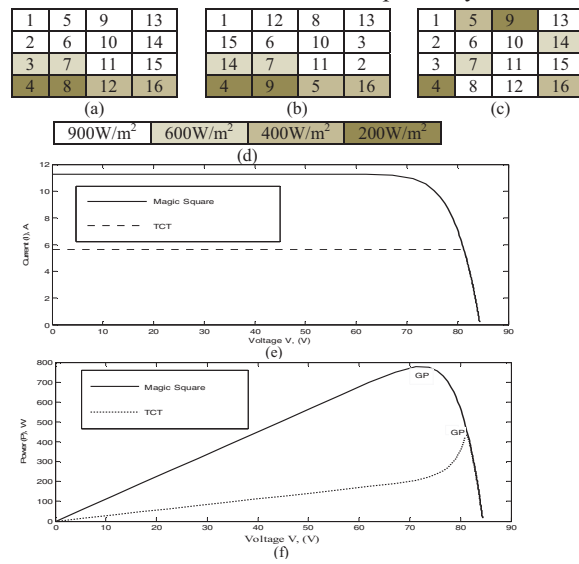


Fig. 4 Shading pattern for 4×4 arrangements for case 1. (a) TCT Arrangement (b) Magic Square arrangement (c) Shade dispersion with Magic Square technique (d) irradiation levels (e) I-V characteristics for case 1 (f) P-V characteristics for case 1

In the TCT configuration, all the panels in row – 1 and row – 2 receive an irradiation level of 900W/m^2 . Current equation for row – 1 is expressed as:

$$I_{R1} = k_1 I_1 + k_2 I_2 + k_3 I_3 + k_4 I_4 \quad (4)$$

Where, $k_1 = G_1/G_0 = 0.9$ where G_1 is the solar irradiance of the module 1 and I_1 is the current generated by the module 1. Assuming the current generated by single panel as I_m at $G=1000\text{ W/m}^2$.

$$I_{R1} = I_{R2} = 4 \times 0.9I_m \quad (5)$$

In row 3, two panels receive an irradiation of 900 W/m^2 and the remaining two receives 600 W/m^2 . The current generated in the other rows is given as

$$I_{R3} = 2 \times 0.6I_m + 2 \times 0.9I_m = 3I_m \quad (6)$$

$$I_{R4} = 2 \times 0.4I_m + 2 \times 0.2I_m = 1.2I_m \quad (7)$$

As the currents in four rows are different to each other, there will be multiple peaks in PV characteristics. The power when no array is bypassed

$$P_a = 9V_m I_m \quad (8)$$

For magic square arrangement, rearranged for shade dispersion, the current in each row is calculated as,

$$I_{R1} = I_{R4} = 2 \times 0.9I_m + 0.6I_m + 0.2I_m = 2.6I_m$$

$$I_{R2} = I_{R3} = 3 \times 0.9I_m + 0.6I_m = 3.3I_m \quad (9)$$

The calculated voltage and power are noted down in Table – 2. The results are verified with the MATLAB/Simulink and these are compared with theoretical results. From practical values it is clear that maximum power generated is 435W for TCT and that of Magic Square is 780W . The power is increased by 44.23% from TCT to Magic Square.

This increase in power is because of changing of the physical locations of the array which distributes the shading effect from a row to the entire array.

Table – 2: Location of GP in TCT and Magic Square

TCT Arrangement			MAGIC SQUARE		
Row current in the order in which panels are bypassed	V_a	P_a	Row current in the order in which panels are bypassed	V_a	P_a
I_{R4}	$1.2I_m$	$4V_m$	I_{R4}	$2.6I_m$	$4.8V_m I_m$
I_{R3}	$3I_m$	$3V_m$	I_{R1}	$2.6I_m$	$6.6V_m I_m$
I_{R2}	$3.6I_m$	$2V_m$	I_{R3}	$3.3I_m$	$2V_m$
I_{R1}	$3.6I_m$	-	I_{R2}	$3.3I_m$	-

Case 2: Long Wide (LW)

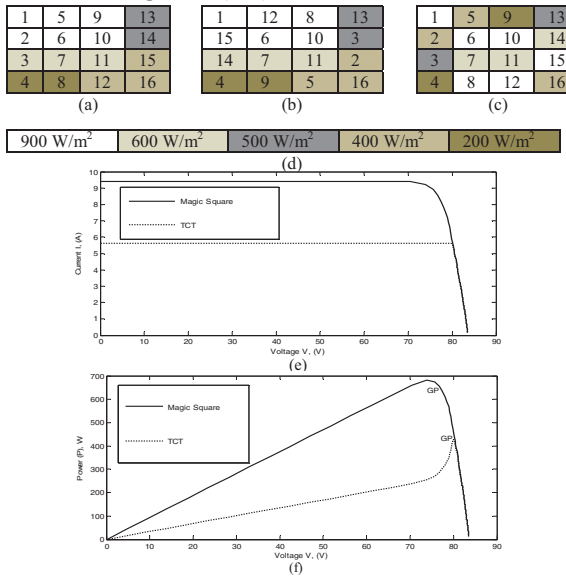


Fig. 5 Shading pattern for 4×4 arrangements for case 2. (a) TCT Arrangement (b) Magic Square arrangement (c) Shade dispersion with Magic Square technique (d) Irradiation levels (e) I-V characteristics for case 2 (f) P-V characteristics for case 2

A Solar PV array with five distinct groups of 900 W/m^2 , 600 W/m^2 , 500 W/m^2 , 400 W/m^2 and 200 W/m^2 is taken in this case of shading pattern which is shown in fig. 5.

The current in each row is calculated as

$$I_{R1} = I_{R2} = 3 \times 0.9I_m + 1 \times 0.5I_m = 3.2I_m$$

$$I_{R3} = 3 \times 0.6I_m + 1 \times 0.4I_m = 2.2I_m$$

$$I_{R4} = 2 \times 0.4I_m + 2 \times 0.2I_m = 1.2I_m \quad (10)$$

The shade dispersion is done by Magic Square method the current in each row is determined by

$$I_{R1} = 1 \times 0.9I_m + 0.5I_m + 0.4I_m + 0.2I_m = 2I_m$$

$$I_{R2} = 2 \times 0.9I_m + 0.4I_m + 0.6I_m = 2.8I_m$$

$$I_{R3} = 1 \times 0.9I_m + 2 \times 0.6I_m + 0.4I_m = 2.6I_m$$

$$I_{R4} = 2 \times 0.9I_m + 0.4I_m + 0.2I_m = 2.4I_m \quad (11)$$

The maximum power obtained in TCT and Magic Square is 429W and 682W respectively. There is a hike of 37.1% from TCT to Magic Square due to the dispersion of shaded modules.

Table – 3: Location of GP in TCT and Magic Square

TCT Arrangement			MAGIC SQUARE		
Row current in the order in which panels are bypassed	V_a	P_a	Row current in the order in which panels are bypassed	V_a	P_a
I_{R4}	$1.2I_m$	$4V_m$	I_{R4}	$2I_m$	$4V_m$
I_{R3}	$2.2I_m$	$3V_m$	I_{R4}	$2.4I_m$	$3V_m$
I_{R2}	$3.2I_m$	$2V_m$	I_{R3}	$2.6I_m$	$2V_m$
I_{R1}	$3.2I_m$	-	I_{R2}	$2.8I_m$	V_m

Case 3: Short and Narrow (SW)

In this case the array is subjected to three irradiations, viz. 900 W/m^2 , 600 W/m^2 and 400 W/m^2 and is shown in fig. 6. The location of GP in both TCT and Magic Square is tabulated in Table – 4.

The maximum power obtained in TCT and Magic Square is 943W and 1016W respectively. The power hike of 7.18% is obtained from TCT to Magic Square due to dispersion of shaded modules.

1	5	9	13
2	6	10	14
3	7	11	15
4	8	12	16

(a)

1	12	8	13
15	6	10	14
14	7	11	2
4	9	5	16

(b)

1	5	9	13
2	6	10	14
15	6	10	3
14	7	11	2

(c)

900 W/m^2 600 W/m^2 400 W/m^2

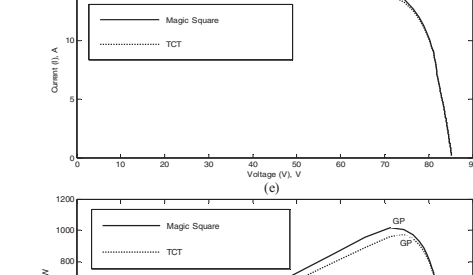


Fig. 6 Shading pattern for 4×4 arrangements for case 2. (a) TCT Arrangement (b) Magic Square arrangement (c) Shade dispersion with Magic Square technique (d) Irradiation levels (e) I-V characteristics for case 3 (f) P-V characteristics for case 3

Table – 4: Location of GP in TCT & Magic Square

TCT Arrangement			Magic Square		
Row current in the order in which panels are bypassed	V_a	P_a	Row current in the order in which panels are bypassed	V_a	P_a
I_{R3}	$2.8I_m$	$4V_m$	I_{R4}	$3.1I_m$	$4V_m$
I_{R4}	$3I_m$	$3V_m$	I_{R1}	$3.3I_m$	$3V_m$
I_{R1}	$3.6I_m$	$2V_m$	I_{R3}	$3.3I_m$	-
I_{R2}	$3.2I_m$	-	I_{R4}	$3.3I_m$	-

Case 4: Long and Narrow (LN)

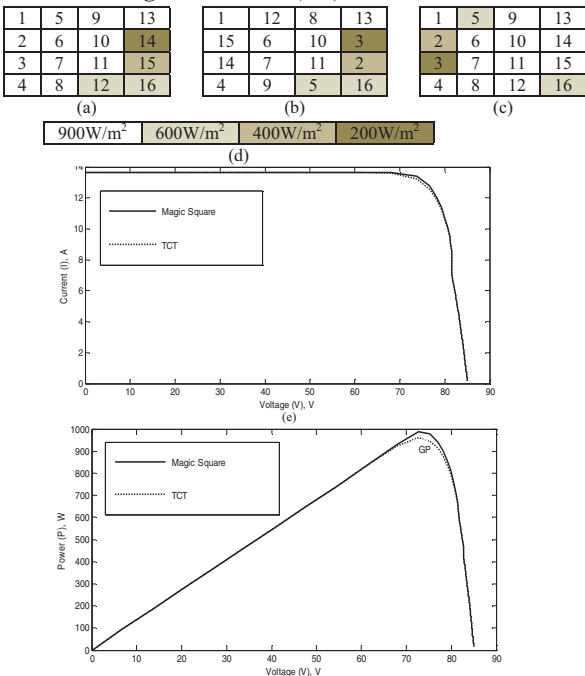


Fig. 7 Shading pattern for 4×4 arrangements for case 4. (a) TCT Arrangement (b) Magic Square arrangement (c) Shade dispersion with Magic Square technique (d) irradiation levels (e) I-V characteristics for case 4 (f) P-V characteristics for case 4

In this case, the array is subjected to 900W/m^2 , 600W/m^2 , 400W/m^2 and 200W/m^2 as shown in fig. 7.

Table – 5: Location of GP in TCT & Magic Square

TCT Arrangement			Magic Square		
Row current in the order in which panels are bypassed	V_a	P_a	Row current in the order in which panels are bypassed	V_a	P_a
I_{R3} $2.9I_m$	$4V_m$	$11.6V_mI_m$	I_{R3} $2.9I_m$	$4V_m$	$11.6V_mI_m$
I_{R4} $3I_m$	$3V_m$	$9V_mI_m$	I_{R2} $3.1I_m$	$3V_m$	$9.3V_mI_m$
I_{R2} $3.1I_m$	$2V_m$	$6.2V_mI_m$	I_{R1} $3.3I_m$	V_m	$3.3V_mI_m$
I_{R1} $3.6I_m$	V_m	$3.6V_mI_m$	I_{R4} $3.3I_m$	-	-

In this case the theoretical values of both TCT and Magic Square Configuration are same. When practically implemented the power generated by Magic Square is 2.831% more than TCT

From Table – 6 and Table – 7, the power generated by the Magic Square configuration is higher than TCT arrangement in all the four cases.

Table – 6: Theoretical summary of power generated in TCT and Magic Square configurations

Case	Maximum Power (W)		Power Enhancement (%)
	TCT Structure	Magic Square Configuration	
1(SW)	713	824	13.471
2(LW)	522	633	17.536
3(SN)	888	982	9.572
4(LN)	918	918	0

Table – 7: Practical summary of power generated in TCT and Magic Square configurations

Case	Maximum Power (W)		Power Enhancement (%)
	TCT Structure	Magic Square Configuration	
1(SW)	435	780	44.23
2(LW)	429	682	37.096
3(SN)	943	1016	7.185
4(LN)	961	989	2.831

IV. CONCLUSIONS

This paper proposed a 4×4 magic square configuration, to enhance the output power under partial shading conditions. In this configuration, the

physical locations of the modules are changed without changing the electrical connections such that the shading effect on a row is distributed over the entire array. The performance of the system is studied through analysis and simulations for various types of shading patterns and it is observed that, the magic square arrangement yields better results than TCT under partial shaded conditions.

REFERENCES

- [1] M.Liserre, T.Sauter and J.Y.Hung "Future energy systems: Integrating renewable energy sources into the smart power grid through industrial electronics", *IEEE Ind. Electron. Mag.*, vol. 4, no. 1, pp.18 -37, 2010.
- [2] Nabeel A.Al-Rawi, Maan M.Al-Kaisi and Dhaia J.Asfer "Reliability of photovoltaic modules II. Interconnection and bypass diodes effects", *Solar Energy Mater. Solar Cells*, vol. 31, no. 4, pp.469 – 480, 1994.
- [3] B. E. A. Saleh and M. C. Teich, "Fundamentals of Photonics", New York: Wiley, 1991.
- [4] G. Petronea and C. A. Ramos Pajab, "Modelling of photovoltaic fields in mismatched conditions for energy yield evaluations," *Elect. Power Syst. Res.*, vol. 81, no. 4, pp. 1003–1013, Apr. 2011.
- [5] W. Xiao, N. Ozog, and W. G. Dunford, "Topology study of photovoltaic interface for maximum power point tracking," *IEEE Trans. Ind. Electron.*, vol. 54, no. 3, pp. 1696–1704, Jun. 2007.
- [6] Y. J. Wang and P. C. Hsu, "Analytical modelling of partial shading and different orientation of photovoltaic modules," *IET Renew. Power Gener.*, vol. 4, no. 3, pp. 272–282, May 2010.
- [7] L.Gao, R.A.Dougal, S.Liu, and A. P. Iotova, "Parallel-connected solar PV system to address partial and rapidly fluctuating shadow conditions," *IEEE Trans. Ind. Electron.*, vol.56, no.5, pp. 1548–1556, 2009.
- [8] X. Weidong, N. Ozog, and W.G. Dunford, "Topology Study of Photovoltaic Interface for Maximum Power Point Tracking," *IEEE Transactions on Industrial Electronics*, vol. 54, no 3, pp. 1696-1704, Jun. 2007.
- [9] H. P. Desai and H. K. Patel "Maximum power point algorithm in PV generation: An overview", *7th Int. Conf. Power Electron. Drive Syst.*, pp. 624 - 630, 2007.
- [10] T. L. Nguyen and K. S. Low, "A global maximum power point tracking scheme employing direct search algorithm for photovoltaic systems," *IEEE Trans. Ind. Electron.*, vol.57, no.10, pp. 3456–3467, Oct.2010.
- [11] B.I Rani, G.S. Ilango, And C. Nagamani "Enhanced Power Generation from PV Array under Partial Shading Conditions by Shade Dispersion Using Su Do Ku Configuration" *IEEE Trans. Sustain Energy*, Vol.4, no.3, pp. 594 – 601, 2013.
- [12] P. Srinivasa Rao, G. Saravana Ilango, and Chilakapati Nagamani, "Maximum Power from PV Arrays Using a Fixed Configuration under Different Shading Conditions" *IEEE journal PV*, vol.4, no. 2, 2014.
- [13] Mohammad A S Masoum, Hooman Dehboneyi, and Ewald F Fuchs, "Theoretical and experimental analysis of Photovoltaic systems with voltage and current based maximum power point tracking", *IEEE Trans. Energy conversion*, vol.17, no. 4, 2002.
- [14] G. Velasco Quesada, F. Guinjoan Gispert, R. Pique Lopez, M. Roman Lumbieras, and A. Conesa Roca, "Electrical PV array reconfiguration strategy for energy extraction improvement in grid connected systems," *IEEE Trans. Ind. Electron.*, vol. 56, no. 11, pp. 4319–4331, Nov. 2009.

Major methods of steady-state analysis of three-phase SEIGs – A summary

Namani Rakesh¹, N. Kumaresan¹, S. Senthil Kumar¹ and M. Subbiah²

¹NIT, Tiruchirappalli, Tamil Nadu, India and ²REC, Chennai, Tamil Nadu, India

E-mail : 307110009@nitt.edu, nkumar@nitt.edu, skumar@nitt.edu, eesubbiah@yahoo.co.in

Abstract- Through an elaborate survey of the papers published so far, a summary of three major methods of performance analysis of Self-Excited Induction Generators (SEIGs) has been presented. Among the various methods, the optimization approach has been shown to be the best in handling the variation in the generator and load parameters. The comparative study presented herein would be useful for any researcher as a starting platform, for further investigations in this field of wind energy electric conversion systems.

Notations:

- a : per unit (p.u.) frequency
- b : p.u. speed
- C : excitation capacitance per phase, μF
- E : air-gap voltage per phase, V
- f_g : generated frequency, Hz
- f_r : rated frequency, Hz
- I_p : phase current of the three-phase load on the generator, A
- P_e : power output of the generator, W
- R, X : per phase load resistance and reactance at the generator terminals, respectively, Ω
- R_m : core loss resistance per phase, Ω
- R_1, X_1 : per phase stator resistance and leakage reactance, respectively, Ω
- R_2, X_2 : per phase rotor resistance and leakage reactance (both referred to stator), respectively, Ω
- X_m : magnetizing reactance per phase, Ω
- X_{mc} : critical magnetizing reactance per phase, Ω
- X_C : capacitive reactance per phase of the excitation capacitance, Ω

I. INTRODUCTION

Among the various renewable energy sources, wind energy electric conversion systems have proved to be very promising in producing significant amount of electrical power for supplementing the conventional sources. The installation of these systems in locations where adequate wind potential is available and their operation and maintenance have also been found to be quite economical. The wind energy systems are broadly classified into two categories, namely (i) grid connected systems, where larger wind power generators with ratings in the order few MW are directly connected to the local power grid and (ii) stand-alone systems for isolated power supplies of up to about 100 kW. For the grid connected systems, invariably, from the beginning, squirrel-cage induction motors have been mainly used. But in recent times, slip-ring induction motors are employed which offer an additional control flexibility through the rotor terminals [1-2].

For the stand-alone systems, several options are available, such as capacitor-excited induction generators, permanent magnet alternators and conventional synchronous generators. However, of these various types of generators, capacitor excited induction generators have been found to be very suitable for wind energy electric conversion systems, owing to their rugged rotor construction, absence of slip-rings, brushes and a separate dc source for excitation and ease of maintenance. In the case of grid connected generators, the terminal voltage and frequency are known, being same as that of the grid. Hence their analysis is simple and straightforward using the conventional equivalent circuit of the induction machines as shown in Fig. 1 [3-4].

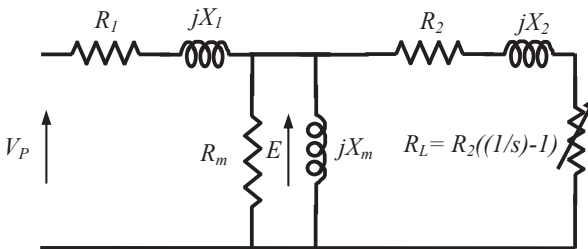


Fig. 1. Conventional Equivalent circuit of Three-phase Induction Machine.

In the Self Excited Induction Generators used for supplying isolated loads, both terminal voltage and frequency are not known constant values, since these quantities vary with the values of the prime-mover speed, excitation capacitor and load parameters. Further, owing to saturation, the magnetizing reactance of the machine varies with the operating point. A large number of papers have appeared on the analysis and predetermination of performance of these stand-alone generators [5-25]. Any researcher commencing the work on developing newer type of power electronic controllers for these generators, require a thorough knowledge of these aspects. Further, the value of the exciting capacitor has to be chosen to obtain a terminal voltage based

on the load requirement. To enable such researchers, the major methods of analysis have been summarized in this paper, which would provide a good platform for starting the further investigations on the overall design of system for isolated power supply.

A survey of literature published since 1983 shows that, invariably the various authors had started the analysis from the formulation of an equation for either the loop impedance or the nodal admittance of the equivalent circuit of the generator [5-17]. Again, as the p.u. frequency (a) varies with p.u. speed (b) of the rotor; two types of procedures have been developed; viz. one in which, b is taken as known and the corresponding a is calculated and the other in which a is assumed and b is calculated for any operating point. Both these methods are briefly described in the succeeding sections.

II. STEADY-STATE ANALYSIS

The conventional equivalent circuit of the induction machine shown in Fig. 1 has to be suitably modified for the analysis of SEIGs to take into account the variable frequency operation of the generator with rotor speed. In such modifications the following assumptions are made [15]:

- (i) Only the magnetizing reactance is considered to vary with the level of saturation, all other parameters being constant
- (ii) The magneto motive force (MMF) space harmonics and time harmonics in the induced voltage and current waveforms are ignored
- (iii) Core loss components are ignored

Hence the modified equivalent circuit for the steady-state analysis of SEIGs is shown in Fig. 2. In this Fig., a = p.u. frequency = f_g/f_r and b = p.u. speed = N/N_s .

Then the operating slip of the machine is $s = (a - b)/a$. Where N = actual rotor speed, r/min., N_s = synchronous speed corresponding to the rated frequency, r/min., f_g = generated frequency, Hz and f_r = rated frequency, Hz.

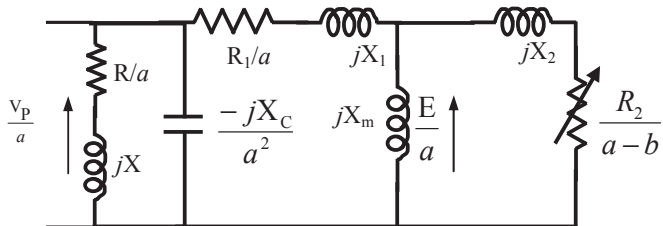


Fig. 2. Equivalent circuit of SEIG with load.
All reactances correspond to rated frequency.

III. CALCULATION OF p.u. FREQUENCY FOR A GIVEN p.u. SPEED

A. Nodal admittance method

For the circuit shown in Fig. 2, the nodal equation can be written as

$$EY=0 \quad (1)$$

Since under steady state excitation $E \neq 0$, it follows from equation (1), that $Y = 0$ i.e.,

$$Y = \frac{1}{\left[\frac{R}{a} + jX \right] \| e^{j\theta} \left[\frac{-jX_C}{a^2} \right] + \left\{ \frac{R_1}{a} + jX_1 \right\}} + \frac{1}{jX_m} + \frac{1}{\left[\frac{R_2}{a-b} + jX_2 \right]} \quad (2)$$

B. Loop impedance method

Similarly, for the circuit shown in Fig. 2 the loop equation can be written as

$$IZ = 0 \quad (3)$$

Since under steady state excitation $I \neq 0$, it follows from equation (3), that $Z = 0$ i.e.,

$$\left\{ \left[\frac{R}{a} + jX \right] \| e^{j\theta} \left[\frac{-jX_C}{a^2} \right] \right\} + \left\{ \frac{R_1}{a} + jX_1 \right\} + \left\{ jX_m \| e^{j\theta} \left[\frac{R_2}{a-b} + jX_2 \right] \right\} = 0 \quad (4)$$

Then, the real and reactive parts of equation (2), or equation (4), are separately equated to zero and then going through a long derivation, a polynomial in p.u. frequency is obtained when p.u. speed is taken as the input parameter. For example, such a polynomial for an impedance load on the generator would come out to be [5-7].

$$P_7 a^7 + P_6 a^6 + P_5 a^5 + P_4 a^4 + P_3 a^3 + P_2 a^2 + P_1 a + P_0 = 0 \quad (5)$$

where the coefficients P_0 to P_7 are functions of the generator and load parameters and p.u. speed.

The solution for such polynomials given in equation (5), requires the adoption of some numerical method. After evaluating the p.u. frequency and then the magnetizing reactance (for any p.u. speed, load and excitation capacitance), the induced emf is determined from the magnetization characteristic. Then, the load phase voltage (V_p), load current (I_p) and power output (P_e) can be computed from the expressions derived from the equivalent circuit shown in Fig. 2 and they are summarized in Appendix. The procedure for obtaining the magnetisation characteristic of the generator is given in [15-16]. The steps involved in the predetermination of performance of SEIGs using this nodal or loop method is given in the flowchart of Fig. 3.

IV. CALCULATION OF p.u. SPEED FOR A GIVEN p.u. FREQUENCY

It is to be mentioned that, in addition to the lengthy derivation, adoption of some numerical method is needed for solving the equation (5), to obtain the p.u. frequency and then the magnetizing reactance for the given p.u. speed. To overcome this, Ammasaigouden et al and Kumaresan et al have followed two different approaches by taking p.u. frequency as the known variable, which lead to quadratic

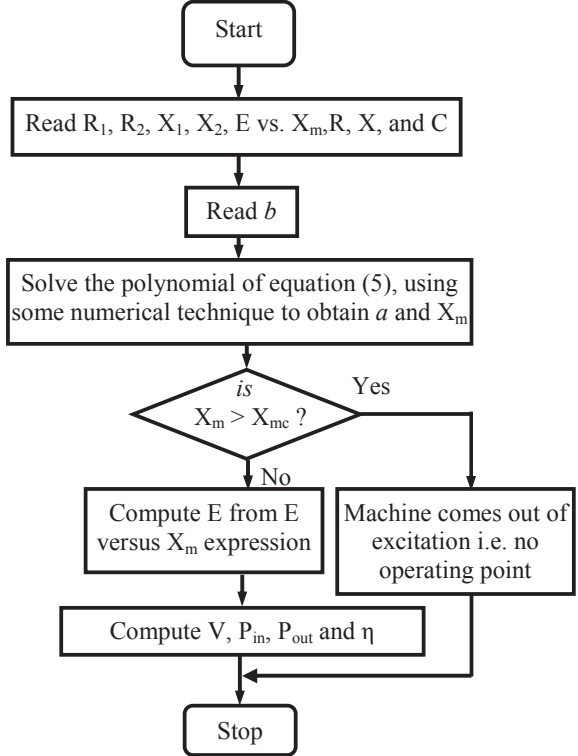


Fig. 3. Flow chart for the Performance predetermination of SEIGs

equations only to be solved and these procedures are briefly explained for the sake of continuity [15, 17].

A. Nodal admittance method

Equating the net real part of equation (2) to zero, the following quadratic equation is obtained with p.u. speed, b as the variable:

$$C_2 b^2 + C_1 b + C_0 = 0 \quad (6)$$

Solving equation (6), the value of b can be obtained for an assumed a . Knowing the values of a and b thus determined, X_m can be determined upon equating net reactive part of equation(2) to zero. The expression for X_m is given in appendix.

B. Loop Impedance Method

Kumaresan et al [17] have adopted the loop impedance expression, and obtained the following quadratic equation with the magnetizing reactance, X_m of the generator as the variable, by equating the real and reactive parts of equation (4) separately to zero:

$$C_5 X_m^2 + C_4 X_m + C_3 = 0 \quad (7)$$

Solving equation (7), the value of X_m can be obtained for an assumed a . Knowing the values of a and X_m thus arrived at, the p.u. speed b can be determined using

$$\begin{aligned} b &= a + (M_2 / M_1) \\ &= a + (N_2 / N_1) \end{aligned} \quad (8)$$

In equations (6), (7) and (8) $C_0, C_1, C_2, C_3, C_4, C_5, M_1, M_2, N_1$ and N_2 are all functions of machine parameters, load parameters, excitation capacitance and p.u. frequency.

V. OPTIMIZATION METHODS

In general, the p.u. rotor speed is the known independent variable in the operation of the wind driven generator. However, the quadratic equations {(6) or (7)} mentioned in section-IV could be solved only for an assumed p.u. frequency and then the corresponding p.u. speed and the performance quantities are calculated. Moreover, it should be noted that the formulation of quadratic equation is possible, only if core loss component of the machine is neglected.

So, subsequently, a much simpler methods have been proposed by a few authors for the analysis of SEIGs by making use of optimization techniques [16, 18-22]. The core loss component R_m/a , can also be considered in parallel to X_m in the equivalent circuit. In such methods, loop impedance / nodal admittance equation written for the equivalent circuit is taken and solved straightforwardly without any further manipulation and minimized using Genetic Algorithm technique to arrive at the values of p.u. frequency, magnetizing reactance and core loss resistance of the generator, for a given p.u. rotor speed, machine parameters and load parameters. As an example, considering also the core loss component R_m/a , in parallel to X_m in the equivalent circuit, the objective function whose value is to be minimized is [16, 22]

$$f(a, X_m, R_m) = \text{abs}(Z) + WF \times \text{abs}(R_m - R_m') \quad (9)$$

where WF is a suitable weighting factor and.

$$Z = \left\{ \left[\frac{R}{a} + jX \right] \parallel \left[\frac{-jX_C}{a^2} \right] \right\} + \left\{ \frac{R_1}{a} + jX_1 \right\} + \left\{ jX_m \parallel \frac{R_m}{a} \parallel \left[\frac{R_2}{a-b} + jX_2 \right] \right\}$$

It has also been shown earlier that the result obtained using GA technique will be unique i.e., for a given generator, load, excitation capacitance and speed, there will be only one operating point for a and X_m , when $|Z| = 0$ [16]. Further, for starting the minimization process of the objective function, an estimate for the ranges of the unknown variables is needed. Such an estimation of the ranges for the unknown variables a , X_m , and R_m are described in [16, 21-22] and for the sake of continuity they are given here:

- (i). In SEIGs, the generated frequency, a and hence the synchronous speed of the rotating magnetic field also vary with variation in b . So, the negative slip $\{(a-b)/a\}$ remains small, and hence, the range for a can be specified as 0.9 to 0.999 times the value of b .
- (ii). The SEIGs operate only in the saturated region of the magnetization characteristics, where X_m starts from a small value at the higher rotor speed and goes on increasing as the speed reduces and comes out of excitation at drop out speed, the corresponding X_m being denoted as critical magnetizing reactance (X_{mc}). So the

- range for X_m can be chosen from about 40 % to 100 % of X_{mc} .
- (iii). For well designed SEIGs, the core loss may vary from about 3 to 10 % from full-load to no-load conditions. Using these values and rated voltage, the range of R_m can be estimated.

Following are the steps involved for the predetermination of performance of SEIGs employing GA technique:

- Step 1 : Read : R_1, R_2, X_1, X_2, E vs. X_m, R_m vs E, R, X and C
- Step 2 : Assign values for ranges for a, X_m and R_m
- Step 3 : Set values for Population Size (PS), number of Chromosomes (Chr) and Generations (Gen) and Tolerance (ϵ).
- Step 4 : Read b and set Gen = 1.
- Step 5 : Generate initial population
- Step 6 : Identify the variable for the first Chr
- Step 7 : Evaluate the objective $f(a, X_m, R_m)$ given in (9)
- Step 8 : If $f(a, X_m, R_m) \leq \epsilon$ go to step 11.
Else go to next step
- Step 9 : If Chr \leq PS, Take the variables from the next Chr and go to step 7. Else go to next step.
- Step 10 : Generate new set of chromosomes using GA process and go to Step 6
- Step 11 : Print a, X_m and R_m and Compute generator performance and stop

VI. PERFORMANCE OF SHORT-SHUNT AND LONG-SHUNT CONFIGURATIONS

To improve the voltage regulation of SEIGs, the earlier authors have suggested the following two types of capacitor connections in each phase, in addition to the shunt excitation capacitor 'C' [23-25]:

- (i). a capacitor C_L in series with the load.
- (ii). a capacitor C_G in series with the generator.

To distinguish from the conventional generators which are excited only with shunt capacitor, these two configurations are termed as short shunt and long shunt respectively. These compound generators have been analyzed by the earlier authors using the conventional approach, which again involves higher order polynomials in p.u. frequency. The expression for load voltage for short shunt connection is given in Appendix. In general, the performance of short shunt configuration has been found to be better than the long shunt configuration. Calculation of the performance of such compound generator configurations also become straightforward, if the proposed GA method is used, since it requires only the loop impedance equation to be written for the corresponding equivalent circuit.

VII. RESULTS AND DISCUSSIONS

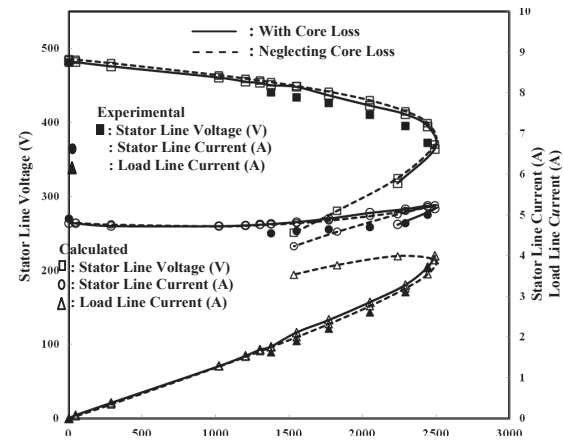
To demonstrate the advantage of the method using optimisation technique for SEIGs, predetermination of performance was carried out using GA for a 3-phase, 4-pole,

400 V, 50 Hz (1 p.u. frequency), 2.2 kW, star-connected squirrel-cage induction machine with a 3-phase star-connected capacitor bank of 55 μ F per phase using GA. The measured parameters of the generator are $R_1 = 3.7 \Omega$, $R_2 = 2.7 \Omega$, $X_1 = X_2 = 3.4 \Omega$. The variation of air-gap voltage, (E/a) with respect to the variation of X_m and also R_m / a obtained experimentally are as follows:

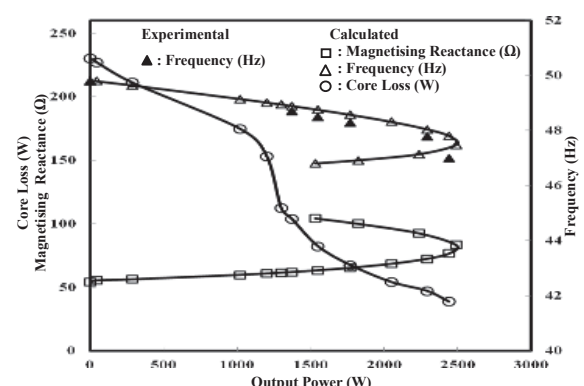
$$E/a = -0.0003 X_m^3 + 0.033 X_m^2 - 1.4545 X_m + 295.53 \quad (10)$$

$$R_m/a = -29.3 \times 10^{-9} (E/a)^6 + 4 \times 10^{-6} (E/a)^5 - 0.001 (E/a)^4 + 0.472 (E/a)^3 - 63.06 (E/a)^2 + 4381 (E/a) - 12268 \quad (11)$$

Fig. 4 shows the predetermined performance characteristics of the machine employing GA technique. Load tests were also conducted on the generator with a terminal capacitance of 55 μ F per phase and the experimental performance characteristics are also shown in Fig. 4 along with the corresponding predicted results. A close agreement is seen between the experimental and predicted values.



(a) Variation of stator voltage and currents against output power



(b) Core loss, Magnetizing Reactance and Frequency against Output Power

Fig. 4. Performance of the SEIG for R load.
 $b = 1$ p.u and $C = 55 \mu\text{F}/\text{phase}$

VIII. CONCLUSIONS

Wind energy electric conversion has proved to be very promising among the various renewable energy systems in producing electrical power. In such conversion systems, SEIGs have been found to be very suitable for stand-alone units for supplying isolated loads and a large number of papers have been published on the steady state performance analysis of these generators since 1980s. This paper has summarised the three major methods for the analysis, after making an elaborate survey of the available literature. It has been shown that the optimisation method is the best, since the readily available Genetic Algorithm tool box in MATLAB software can be straightaway employed, without the need for making any complex derivations or handling higher order polynomials. Moreover, in this method, the effect of variation of excitation capacitor or the load parameters on the performance of the system can be easily studied. Thus the summary presented herein would be very helpful for those who enter into this field of research, for a quick understanding of the methods of analysis so that further developments can be attempted, particularly in the design of the associated power electronic controllers.

REFERENCES

- [1] M. Tazil, V. Kumar, R. C. Bansal, S. Kong, Z. Y. Dong, W. Freitas, and H. D. Mathur, "Three-phase doubly fed induction generators: an overview," *IET Electr. Power Appl.*, Vol. 4, pp.75-89, 2010.
- [2] H. Li, and Z. Chen, "Overview of different wind generator systems and their comparisons," *IET Renew. Power Gener.*, Vol. 2, pp.123-138, 2008.
- [3] M.G. Say, *Alternating current machines*. Edinburgh, UK: The English Language Book Society and Pitman Publishing, 1976.
- [4] Ion Boldea, *The electric generators handbook. Vol.2 Variable speed generators*. CRC Press, Taylor & Francis Group. 2006
- [5] S. S. Murthy, O. P. Malik, and A. K. Tandon, "Analysis of self-excited induction generators," *Proc. Inst. Electr. Eng. C. C*, Vol. 129, pp. 260-265, November 1982.
- [6] Lahcene Ouazene, and George McPherson, "Analysis of the isolated induction generator," *IEEE Trans. Power apparatus and systems*, Vol. PAS-102, pp. 2793-2797, August 1983.
- [7] A. K. Tandon, S. S. Murthy, and J. G. Berg, "Steady-state analysis of capacitor self-excited induction generators," *IEEE Transactions on Power Apparatus and Systems*, Vol. PAS-103, pp. 612-618, April 1984.
- [8] N. H. Malik, and S. E. Haque, "Steady state analysis and performance of an isolated self-excited induction generator," *IEEE Trans. on Energy conversion*, Vol. 1, pp. 134-139, September 1986.
- [9] K. Al Jabri, and A. I. Alolah, "Capacitance requirement for isolated self excited induction generator," *IEE Proc., Pt. B*, Vol. 137, pp. 154-159, May 1990.
- [10] S. Rajakaruna, and R. Bonert, "A technique for the steady state analysis of induction generator with variable speed," *IEEE Trans. on Energy conversion*, Vol. 8, pp. 757-761, December 1993.
- [11] T. F. Chan, "Steady state analysis of self-excited induction generators," *IEEE Trans. on Energy conversion*, Vol. 9, pp. 288-296, June 1994.
- [12] T. F. Chan, "Self-excited induction generators driven by regulated and unregulated turbines," *IEEE Trans. on Energy Conversion*, Vol. 11, pp. 338-343, June 1996.
- [13] L. Wang, and C. H. Lee, "A novel analysis of the performance of an isolated self-excited induction generator," *IEEE Trans. on Energy Conversion*, Vol. 12, pp.109-115, June 1997.
- [14] K. S. Sandhu, and S. K. Jain, "Operational aspects of self-excited induction generator using a new model," *Electric Machines and Power Systems*, Vol. 27, pp.169-180, 1999.
- [15] N. Ammasaigounden, M. Subbiah, and M. R. Krishnamurthy, "Wind-driven self-excited pole-changing induction generators," *IEE Proc. Pt. B*, Vol. 133, pp. 315-321, September 1986.
- [16] R. Karthigaivel, N. Kumaresan, P. Raja, and M. Subbiah, "A novel unified approach for the analysis and design of Wind-driven SEIGs using nested GAs," *Wind Engineering*, vol. 33, pp. 631-647, 2009.
- [17] N. Kumaresan and M. Subbiah, "Analysis and control of wind driven self-excited induction generators with load matching , " *Proc. Of the Eleventh national power system conference NPSC 2000 Vol (I)IISC Bangalore*, pp. 21-26, 2006.
- [18] A. L. Alolah, and M. A. Alkanhal, "Optimization based steady state analysis of three phase self excited induction generator," *IEEE Trans. EC*, Vol.15, pp. 61-65, 2000.
- [19] M. H. Haque, "A novel method of evaluating performance characteristics of a Self excited induction generator," *IEEE Trans. EC*, Vol. 24, pp. 358-365, 2009.
- [20] D. Joshi, K. S. Sandhu, and M. K. Soni, "Performance analysis of three-phase self-excited induction generator using genetic algorithm," *Electr. Power Syst. Res.*, Vol. 34, pp. 461-470, 2006.
- [21] N. Kumaresan, "Analysis and control of three-phase self-excited induction generators supplying single-phase AC and DC loads," *IEE Proc. Electr. Power Appl.*, Vol. 152, pp. 739-747, 2005.
- [22] R. Karthigaivel, N. Kumaresan, and M. Subbiah, "Analysis and control of self-excited induction generator-converter systems for battery charging applications," *IET Electr. Power Appl.*, Vol. 5, pp. 247-257, 2011.
- [23] L. Shridhar, Bhim Singh, C. S. Jha, B. P. Singh, and S. S. Murthy, "Selection of capacitors for the self regulated short shunt self-excited induction generator," *IEEE Trans. on Energy conversion*, Vol. 10, pp.10-17, March 1995.
- [24] Li Wang and Jian-Yi Su, "Effects of long-shunt and short connections on voltage variations of a self-excited induction generator," *IEEE Trans. on Energy conversion*, Vol. 12, pp.368-374, December 1997.
- [25] M. H. Haque, "Comparison of steady state characteristics of shunt, short shunt and long shunt induction generators," *Electr. Power Syst. Res.*, Vol. 79, pp. 1446-1453, 2009.

Appendix

Expressions for the performance quantities of SEIGs are

$$V_p = \left\{ \frac{R_L^2 + X_L^2}{[(R_1/a) + R_L]^2 + (X_1 - X_L)^2} \right\}^{1/2} E \quad (12)$$

$$I_p = V_p/Z_L \quad \text{and} \quad P_e = 3V_p I_p (R/Z_L)$$

$$X_m = \frac{[R_L + (R_1/a)][X_2^2 + \{R_2/(a-b)\}^2]}{[R_2/(a-b)][X_1 - X_L] - X_2[R_L + (R_1/a)]} \quad (13)$$

where

$$R_L = \frac{RX_C^2}{a[a^2R^2 + (a^2X - X_C)^2]},$$

$$X_L = \frac{[-XX_C + R^2 + a^2X^2]X_C}{[a^2R^2 + (a^2X - X_C)^2]} \quad \text{and}$$

$$Z_L = [R^2 + a^2X^2]^{1/2}$$

The expression for the load voltage of short shunt machine is

$$V_p = \left[\frac{R_L^2 + X_L^2}{[(R_1/a) + R_L]^2 + (X_1 - X_L)^2} \right]^{1/2} \times \left[\frac{(R/a)^2 + X^2}{(R/a)^2 + (X - (X_{C_L}/a^2))^2/2} \right]^{1/2} E \quad (14)$$

IMPROVED POWER QUALITY CONTROL STRATEGY FOR DISTRIBUTED GENERATION SYSTEMS

A. Vamshi Kumar^{#1}, K. Ajith^{#2}, P. Nagarjuna Reddy^{#3}, G. Rajender Naik^{#4}, N. Rakesh^{#5}
^{#1}PG Scholar, ^{#2-5}Assistant Professor,

Department of Electrical and Electronics Engg., Kakatiya Institute of Technology & Science, Warangal, Andhra Pradesh, India

^{#1}vamshikumar208@gmail.com, ^{#2}ajitkatanguri@gmail.com, ^{#3}nagarjunreddyp@gmail.com, ^{#4}rajendra.ksg@gmail.com
^{#5}namanirakesh@gmail.com

Abstract—Distribution Generation aims at integrating different power plants to increase the reliability and provide additional power quality benefits. Coming to the grid-connected mode, almost all the commercial single-phase inverters for DG systems inject only active power to the grid, i.e., the reference current is computed from the reference active power p^* that must be generated. This paper deals with a single-phase inverter acquiring power quality features, i.e., active and reactive power generation along with current harmonics compensation. This is achieved by integrating the functions of shunt Active Power Filter (APF) to the control scheme. The control scheme employs a current reference generator with a dedicated repetitive current controller. Two phase conversion of single phase system is used in this paper for the extraction of harmonic components and also for supplying required reactive power by load. The simulation results are presented for the grid connected inverter that generates active power and compensates the reactive power and current harmonics of local loads, thus achieving complete power quality features.

Keywords— *Distributed Generation (DG), Power Quality (PQ), Instantaneous Reactive Power (IRP).*

I. INTRODUCTION

The increasing demand for energy has stimulated the development of alternative power sources such as photovoltaic panels, fuel cells, wind turbines, etc[1]-[3]. The Distributed Generation (DG) concepts emerged as a way to integrate different power plants, increasing the DG owner's reliability, reducing emissions and providing additional power quality benefits [4].

Power electronics is an essential part for the integration of dispersed generation unit to achieve high efficiency and performance in power systems. The power electronic front-end converter is an inverter whose dc link is fed by an ac/dc converter or by a dc/dc converter, according with the DG source type. The commercial front-end inverters are designed to operate either as grid-connected or in island mode. In grid-connected mode, the voltage at the point of common coupling (PCC) is imposed by the grid; thus, the inverter must be current-controlled. When operated in island mode, the inverters are voltage-controlled, generating the output voltage at a specified amplitude and frequency. All the commercial single-phase inverters for DG systems inject only active power

to the grid, i.e., the reference current is computed from the reference active power p^* that must be generated [7].

The integration of APF capability in single-phase inverters needs a particular attention since the control techniques (for example, to find the reference current) were developed for three phase APFs, and consequently, must be adapted for single-phase systems. Different solutions are proposed in the literature to compute the harmonic extraction task for single-phase APFs [8]-[19]. The methods are classified in direct and indirect method [8]. The direct methods include the Fourier transform method, the instantaneous reactive power (IRP) theory [11]-[14] and the synchronous reference frame (SRF) theory [15]-[18]. On the other hand, the indirect methods include the use of enhanced phase-locked loop (EPLL) scheme or a controller such as proportional–integral (PI) to find the reference current.

The IRP and the SRF theories are most widely used in the literature [11]-[18]. These strategies were originally proposed for three-phase systems, but they can be adapted for single-phase systems due to their effectiveness. In three-phase systems, both IRP and SRF techniques operate in a reference system with two orthogonal axes ($\alpha\beta$ for IRP and dq for SRF). In single-phase systems, since only one-phase variable exists, it is necessary to create one “fictitious” or imaginary variable in which all frequencies are phase-shifted by 90 electrical degrees with respect to the original variable. With this procedure, a system with two orthogonal variables is created from a single variable, allowing the application of the IRP and SRF theories.

Hilbert transform method used in [14] reduces the computational burden in calculating fictitious variable but leads to a no causal system which can not be implemented. Introducing phase delays in the fictitious variable i.e., in the inverter current reference through finite-impulse response (FIR) filter will solve the problem [19].

Alternatively, the computation of the reference current can be performed by using a sinusoidal signal integrator (SSI) along with the IRP theory. This approach allows obtaining without any delay the fictitious variables that are needed to apply the IRP theory or other techniques originally applied for three-phase systems [21].

The present paper proposes an enhanced power quality control strategy for single-phase inverters used in DG systems. Fig.1 shows the general scheme of DG unit connected to the grid. The DG unit functions are integrated with shunt APF capabilities. This approach controls the inverter active power flow from the energy source to the grid and also performs the compensation of reactive power and the nonlinear load current harmonics, keeping the grid current almost sinusoidal.

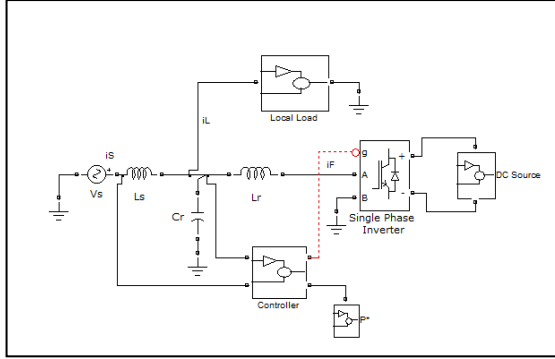


Fig.1. General Scheme of a DG unit connected to the grid.

II. CONTROL SCHEME

A dedicated inverter current control scheme based on a repetitive controller implemented with a FIR filter approach has been employed in the current work. The present method allows halving the number of the FIR filter taps, making the implementation easier from the point of view of the computational effort.

The block diagram of the single-phase inverter control scheme with enhanced power quality features is shown in Fig. 2. The inverter reference current i_F^* is generated by the reference current generator block and the current control is based on a repetitive controller.

The reference current generation scheme is shown in Fig. 3 and can be divided into two parts: the computation of the harmonic current reference i_{ha}^* and the generation of the fundamental reference current i_{1a}^* corresponding to the active and the reactive power to be generated.

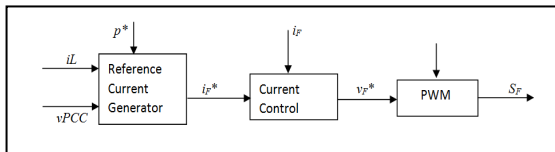


Fig.2. Inverter control scheme

A. Reference Current Generation Scheme:

1) Harmonic Reference Current Generation:

The nonlinear load current i_L and the PCC voltage v_{PCC} are used to calculate the reference current for current harmonics compensation. A filter based on SSIs (hereinafter called SSI filter) extracts the fundamental frequency component $\omega_0 = 2\pi \times 50$ (in radian per second) of the load current in stationary $\alpha\beta$ frame, as shown in Figs. 2 and 3 [20]. The harmonic reference current i_{ha}^* is obtained from the subtraction of the load current from the output of the SSI filter ($i_L - i_{L1a}$).

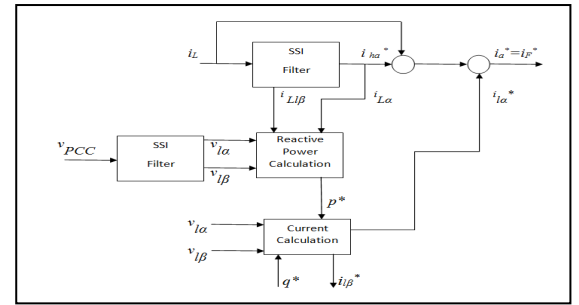


Fig.3 Reference current generation scheme

2) Fundamental Reference Current Generation:

In steady-state operation, the SSI filter shown in Fig.3 has two sinusoidal states x_1 and x_2 having the same amplitude and being phase-shifted by 90 electrical degrees [20][21]. So, it is possible to obtain two outputs from a SSI filter, i_{L1a} and $i_{L1\beta}$ (which is always 90° shifted respect to i_{L1a}). This can be seen by analysing the two transfer functions of the SSI filter.

$$H_1(s) = \frac{I_{L1a}(s)}{I_L(s)} = \frac{2k_A * s}{s^2 + 2k_A * s + \omega_0^2} = \frac{V_{1a}(s)}{V_{PCC}(s)} \dots\dots\dots(1)$$

$$H_2(s) = \frac{I_{L1\beta}(s)}{I_L(s)} = \frac{2k_A * \omega_0}{s^2 + 2k_A * s + \omega_0^2} = \frac{V_{1\beta}(s)}{V_{PCC}(s)} \dots\dots\dots(2)$$

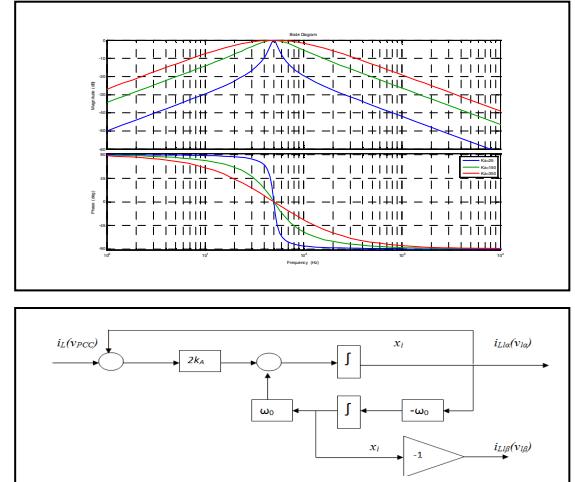


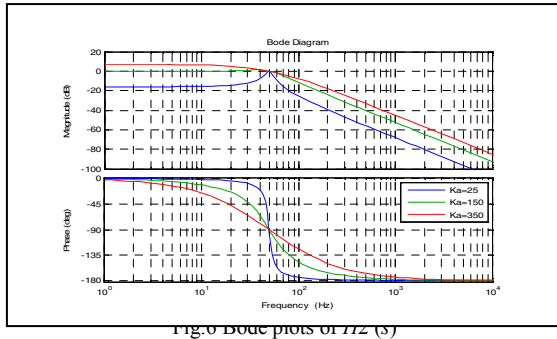
Fig.4 SSI filter applied for the load current (input is i_L and the outputs are i_{L1a} and $i_{L1\beta}$) and for the PCC voltage (input is v_{PCC} and outputs are v_{L1a} and $v_{L1\beta}$)

Fig.5 Bode plots of $H1(s)$

In steady-state operation, the relationship between the phases of the transfer functions (1) and (2) in the frequency domain is

$$\angle H_1(j\omega) = \angle H_2(j\omega) + \frac{\pi}{2} \dots\dots\dots(3)$$

The Bode diagrams of equations 1 and 2 that are shown in Figs. 5 and 6 for different values of k_A confirm (3). It is also possible to see that when k_A becomes smaller, the filter becomes more selective. However, when this happens, the phase delay becomes higher around the fundamental frequency ω_0 .



This property is useful for obtain

This property is useful for obtaining the orthogonal fundamental components needed to perform the reactive power compensation of the local load. The signal $i_{L1\beta}$ is generated by the SSI only to calculate the fundamental reactive power reference q^* , using the definition of reactive power from IRP theory as follows:

To obtain v_{1a} and $v_{1\beta}$, another SSI filter is used in the PCC voltage v_{PCC} by generating v_{1a} and a signal ($v_{1\beta}$) with the same amplitude and phase-shifted by 90 electrical degrees from v_{1a} , as shown in Fig. 4. The use of an SSI filter in the PCC voltage makes the reference current generator insensitive to grid voltage distortions. The fundamental components of the inverter reference current i_{1a}^* and $i_{1\beta}^*$ are calculated by imposing the reference power p equal to the amount of active power to be injected into the grid, as follows:

Since the system is single phase, the current $i_{1\beta}^*$ is neglected and i_{1a}^* is added to the harmonic reference current i_{ha} to obtain the inverter reference current. The SSI filter used to extract the fundamental component of the nonlinear load current is very flexible, and the gain k_A (see Fig. 4) can be adjusted to improve the selectivity of the reference generator or to improve its transient response. It is important to emphasize the difference between the solution used in this paper to create the fictitious variable and another existing method [14]. In the proposed technique, the orthogonal fundamental component signals, used for current reference generation and obtained from the SSI filter, are sinusoidal and phase shifted by 90° . In the existing method, the obtained fictitious variable is a signal with a high harmonic content generated by phase shifting all frequencies of the load current by 90° . In this case, some phase delay is introduced in the fictitious variable and implicitly in the inverter current reference [19].

B. Current Control Scheme

For inverters that generate active power and also compensate the reactive power, the reference current is sinusoidal at fundamental frequency, so the use of conventional PI controllers would probably suffice if their bandwidth is high enough. If the inverter must also compensate the current harmonics, the reference current will

become non sinusoidal. In this case, achieving zero -steady-state error is not possible with PI controllers.

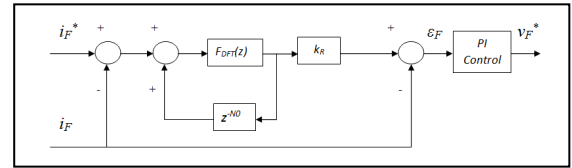


Fig.7 Current control scheme

The current control scheme adopted is shown in Fig. 7 and is based on a repetitive controller along a conventional PI regulator in order to achieve zero steady-state error when the reference current has a high harmonic content. In this scheme, the key issue is the implementation of the repetitive control scheme. The repetitive controller is nothing else than an FIR filter of N taps. The filter can be designed by using the discrete Fourier transform (DFT) to achieve unity gain for every single harmonic to be compensated.

III. SIMULATION RESULTS

The simulation has been performed with the inverter having only a 2-kW resistive local load. The steady-state operation for the inverter, injecting 2 kW of active power, is shown in Fig.8. In this case, it can be seen that the grid current (i_S) is almost zero because the local load power request is completely supplied by the inverter ($i_S = i_L - i_F$).

The steady-state operation of the inverter, injecting 3 kW of active power, is presented in Fig 9. It can be seen that the grid current is out of phase with respect to the PCC voltage by 180 electrical degrees, which means active power generation.

The simulation has been done with the inverter having a local load consisted of the resistance R_2 and the diode rectifier. The steady-state operation of the inverter, injecting 1 kW of active power and compensating the current harmonics of the local load, is shown in Fig.11 and Fig.12.

TABLE I. SYSTEM PARAMETERS

Parameter	Value
Mains voltage (V_s)	220V
Interface capacitance (C_F)	$7.5\mu F$
Interface inductance (L_F)	$700\mu H$
DC- link capacitance (C_d)	2.2mF
DC- link voltage setpoint (V_{dc})	400V
Switching/Sampling frequency (f_{sw}, f_s)	10KHz
Fundamental frequency (f_1)	50Hz
Linear load resistance (R_2)	25Ω
Linear load inductance (L_2)	30mH
Nonlinear load input inductance (L_1)	$900\mu H$
Nonlinear load output capacitance (C_1)	1mF
Nonlinear load output resistance (R_1)	50Ω

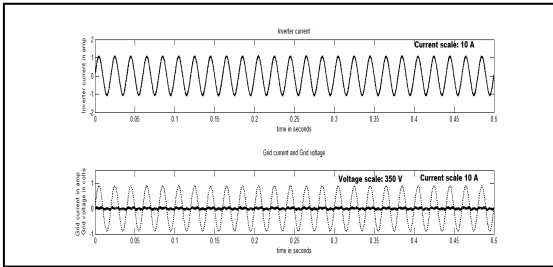


Fig. 8 Steady-state operation of the inverter injecting the active power requested by the resistive load (2kW)

The inverter current waveform in Fig 9 shows that the injected current is almost sinusoidal. The grid current total harmonic distortion (THD) value was about 2%.

The inverter transient response during a step-up of the injected active power reference from 1 to 3 kW is shown in Fig.10, and the results indicate a good transient performance of the inverter control. Before the transient, the inverter-delivered active power (1kW) was less than the power required by the local load (2 kW), so additional power is absorbed from the grid. After the active power reference step-up transient from 1 to 3 kW, the inverter supplies the active power requested by the local load and the remaining power is injected into the grid.

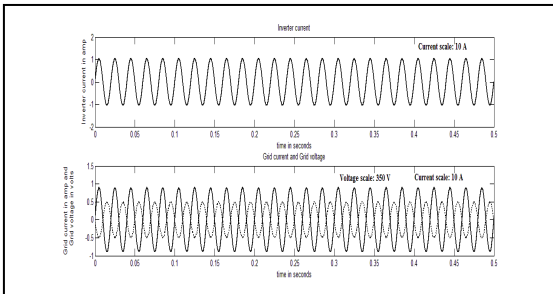


Fig. 9 Steady-state operation for 3 kW active power generation. Only the 2 kW linear load is connected.

The inverter current i_F , the PCC voltage v_{PCC} , and the local load current i_L are shown in Fig.11, while Fig. 12 contains the inverter current i_F , the PCC voltage v_{PCC} , the grid current i_S . It can be seen from Fig.11 and Fig.12 that even if the local load current is highly distorted, the mains current is almost sinusoidal. Also, it can be noted that the grid current is in phase with the PCC voltage, so in this case, the local load still draws active power from the grid. This happens because the inverter-injected active power of 1 kW is smaller than the active power requested by the local load.

The inverter dynamic performance has been evaluated by turning on the load diode rectifier, as shown in Fig.13 and Fig.14. The figures reveal a fast transient response of the inverter with a settling time of about 20 ms.

To clearly emphasize the inverter capability to compensate the local load reactive power, the inverter has been operated only with an RL load obtained as the series connection between the resistance R_2 and the inductance L_2 . The load current lags the load voltage by about 20 electrical degrees, as shown in Fig.15.

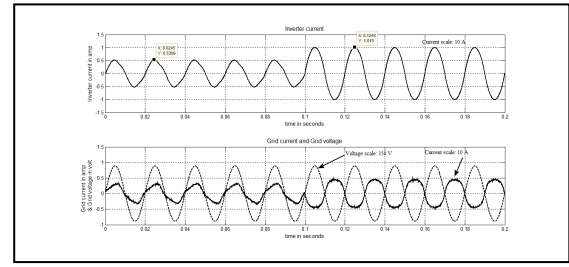


Fig. 10 Inverter transient response during a step-up of the injected active power (1-3 kW). Only the 2 kW linear load is connected

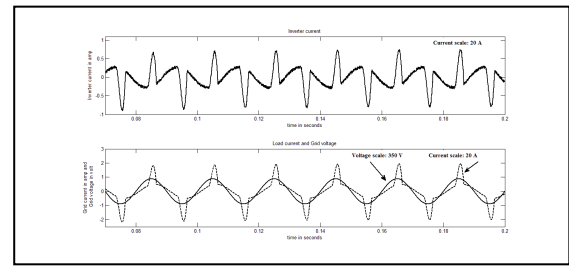


Fig. 11 Steady-state operation of the inverter Injecting 1 kW active power and compensating the current harmonics of the local load

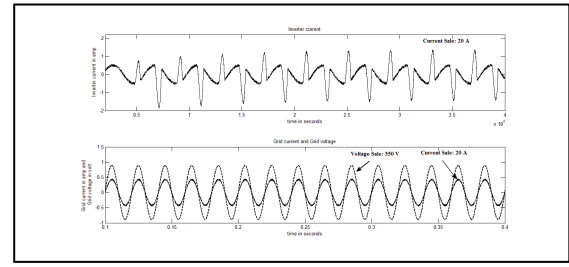


Fig. 12 Steady-state operation of the inverter injecting 1 kW active power and compensating the current harmonics of the local load

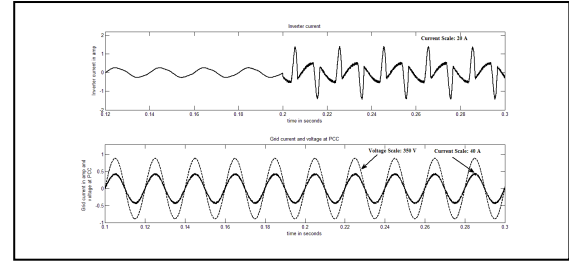


Fig. 13 Inverter transient response during nonlinear load turn-on

The inverter transient operation is obtained for zero active power generation when the reactive power is enabled in a step fashion is shown in Fig.16. It can be noted how the grid current becomes pure active since the inverter completely compensates the local load reactive power. As expected, the inverter current i_F is pure reactive and leads the PCC voltage by 90 electrical degrees (see Fig.16).

The steady-state operation of the inverter, injecting 3 kW of active power and compensating the entire load reactive

power, is shown in Fig.17. The grid current is out of phase with respect to the PCC voltage by 180 electrical degrees, which means active power generation since the inverter generates more active power than the active power required by the load.

Finally, the transient response for step reactive power compensation when the generated active power was 3 kW is illustrated in Fig.18, showing a time response of less than one grid period.

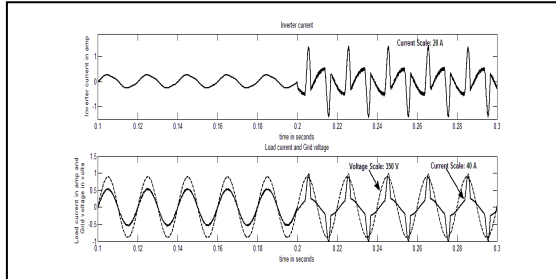


Fig. 14 Inverter transient response for nonlinear load turn-on

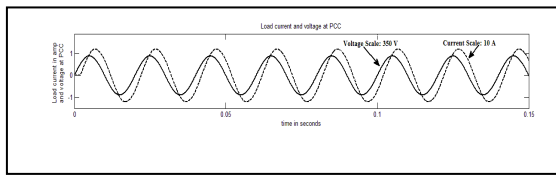


Fig. 15 Steady-state linear resistive-inductive load operation

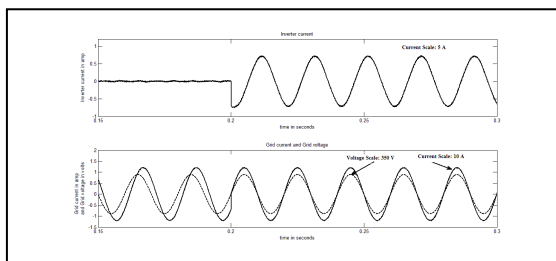


Fig. 16 Inverter transient response when only the reactive power compensation is enabled and the load is resistive-inductive

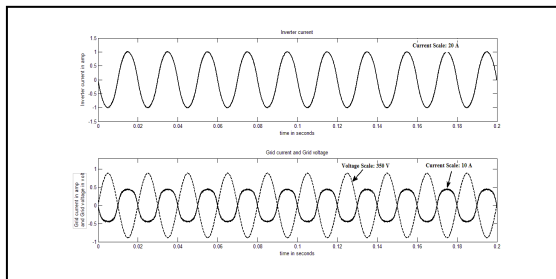


Fig. 17 Steady-state operation for 3 kW active power generation with reactive power compensation

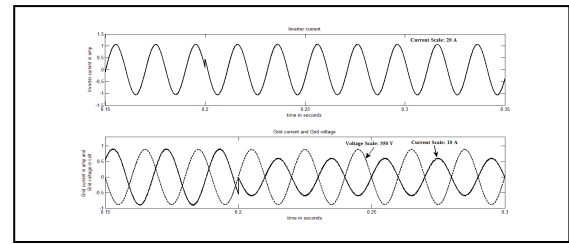


Fig. 18 Inverter transient response for step reactive power compensation when the injected active power is 3 kW

IV. CONCLUSIONS

This paper deals with a single-phase inverter for DG systems, acquiring power quality features as harmonic and reactive power compensation for grid-connected operation. The proposed control scheme employing a current reference generator based on SSI and IRP theory, together with a dedicated repetitive current controller, has resulted in a better transient performance of the inverter control. Also the inverter employed delivers active and reactive power to the load with a better power quality with low THD.

REFERENCES

- [1] M. G. Villalva, et al, "Comprehensive approach to modelling and simulation of photovoltaic arrays," IEEE Trans. Power Electron., vol. 24, no. 5, pp. 1198–1208, May 2009.
- [2] B. Yang, W. Li, Y. Zhao, and X. He, "Design and analysis of a grid connected photovoltaic power system," IEEE Trans. Power Electron., vol. 25, no. 4, pp. 992–1000, Apr. 2010.
- [3] Z. Chen, et al, "A review of the state of the art of power electronics for wind turbines," IEEE Trans. Power Electron., vol. 24, no. 8, pp. 1859–1875, Aug. 2009.
- [4] T. E. McDermott and R. C. Dugan, "Distributed generation impact on reliability and power quality indices," in Proc. IEEE Rural Electr. Power Conf., 2002, pp. D3–D3_7.
- [5] F. Blaabjerg, R. Teodorescu, M. Liserre, and A. V. Timbus, "Overview of control and grid synchronization for distributed power generation systems," IEEE Trans. Ind. Electron., vol. 53, no. 5, pp. 1398–1409, Oct. 2006.
- [6] F. Blaabjerg, et al, "Power electronics as efficient interface in dispersed power generation systems," IEEE Trans. Power Electron., vol. 19, no. 5, pp. 1184–1194, Sep. 2004.
- [7] P. Rodriguez, A. V. Timbus, R. Teodorescu, M. Liserre, and F. Blaabjerg, "Flexible active power control of distributed power generation systems during grid faults," IEEE Trans. Ind. Electron., vol. 54, no. 5, pp. 2583–2592, Oct. 2007.
- [8] M. K. Ghartemani, et al, "A signal processing system for extraction of harmonics and reactive current of single phase systems," IEEE Trans. Power Electron., vol. 19, no. 3, pp. 979–986, Jul. 2004.
- [9] L. P. Kunjumuhammed and M. K. Mishra, "Comparison of single phase shunt active power filter algorithms," in Proc. IEEE Power India Conf., 2006, pp. 8–15.
- [10] L. P. Kunjumuhammed and M. K. Mishra, "A control algorithm for single-phase active power filter under non-stiff voltage source," IEEE Trans. Power Electron., vol. 21, no. 3, pp. 822–825, May 2006.
- [11] M. T. Haque and T. Ise, "Implementation of single-phase pq Theory," in Proc. IEEE PCC Conf. Rec., 2002, pp. 761–765.
- [12] M. Saitou, N. Matsui, and T. Shimizu, "A control strategy of single-phase active filter using a novel d-q transformation," in Proc. IEEE IAS Conf. Rec., 2003, pp. 1222–1227.
- [13] M. Saitou and T. Shimizu, "Generalized theory of instantaneous active and reactive powers in single-phase circuits based on Hilbert transform", in Proc. IEEE PESC Conf. Rec., 2002, pp. 1419–1424
- [14] J. Liu, et al, "A new approach for single-phase harmonic current detecting and its application in a hybrid active power filter," Proc. IEEE IECON Conf. Rec., pp. 849–854, 1999.

- [15] Y. J. Kim, et al, "Single-phase active power filter based on rotating reference frame method," in Proc. IEEE ICEMS Conf. Rec., 2005, pp. 1428–1431.
- [16] M.Gonzalez, et al, "DQ transformation development for single-phase systems to compensate harmonic distortion and reactive power," in Proc. IEEE CIEP Conf. Rec., 2004, pp. 177–182.
- [17] S.M. Silva, et al, "Performance evaluation of PLL algorithms for single-phase grid connected systems," in Proc. IEEE IAS Conf. Rec., 2004, pp. 2259–2263.
- [18] R. I. Bojoi, et al, "Current control strategy for power conditioners using sinusoidal signal integrators in synchronous reference frame," IEEE Trans. Power Electron., vol. 20, no. 6, pp. 1402–1412, Nov. 2005.
- [19] P. Rodriguez, et al, "New positive-sequence voltage detector for grid synchronization of power converters under faulty grid conditions," in Proc. IEEE PESC Conf. Rec., 2006, pp. 1–7.
- [20] P.Mattavelli and F. P.Marafao, "Repetitive-based control for selective harmonic compensation in active power filters," IEEE Trans. Ind. Electron., vol. 51, no. 5, pp. 1018–1011, Oct. 2004.
- [21] L. R. Limongi, et al, "Single-phase inverter with power quality features for distributed generation systems," in Proc. IEEE OPTIM Conf. Rec., 2008, pp. 313–318.



Vamshi Kumar was born in Andhra Pradesh, India. He is pursuing his M.Tech Power Electronics in Kakatiya Institute of Technology & Science, Warangal. His areas of interests are Micro Grids, Distributed Generation and Advanced Converters.



K. Ajith Reddy (M' 2011) was born in Andhra Pradesh, India in 1985. He received M.E. degree in Power systems from GCT – Coimbatore, India in 2009. Presently he is working as an Assistant Professor in the department of Electrical and Electronics Engineering, Kakatiya Institute of Technology & Science, Warangal, A.P., India. His research interests are Communication Technologies, Micro Grids, Distributed Generation, Power System operation, Stability & Analysis.

P. Nagarjuna Reddy P Nagarjuna Reddy was born in Kurnool, India in 1983. He completed his Bachelor degree in Electrical & Electronics Engineering from Jawaharlal Technological University (JNTU) Hyderabad in 2004 and Master's programme in Electrical Engineering at JNTU, Kakinada in 2009. He is presently pursuing his Doctoral degree from Jawaharlal Nehru Technological University, Hyderabad. He is also working as Assistant Professor in the Department of Electrical and Electronics Engineering, Kakatiya Institute of technology & Science, Warangal. His areas of interests are High Voltage Engineering and FACTS.



G. Rajender Naik G Rajender Naik was born in Karimnagar, India in 1984. He completed his Bachelor degree in Electrical & Electronics Engineering from Kakatiya Institute of Technology & Science (KITSW), Warangal in 2005 and Master's programme in Electrical Engineering at NIT, Calicut, Kerala in 2009. He is presently pursuing his Doctoral degree from Kakatiya University, Warangal. He is also working as Assistant Professor in the Department of Electrical and Electronics Engineering, Kakatiya Institute of Technology & Science, Warangal. His areas of interests are Control Systems, Power Electronics and FACTS.



N. Rakesh (M' 2014) Namani Rakesh was born in Warangal on 10th Nov, 1987. He graduated in Electrical and Electronics Engineering from Kakatiya University, Warangal. He completed his M.S (by Research) in Electrical and Electronics Engineering in National Institute of Technology, Tiruchirappalli as a full time Research Scholar in 2012. He worked as a lecturer in Rajiv Gandhi University of Knowledge Technologies, Andhra Pradesh. Presently, He is working as Assistant Professor in Kakatiya Institute of Technology & Science, Warangal, Andhra Pradesh. His Research interests are Power Electronics, Renewable Power Generation Sources and Distributed Generation.

Performance Predetermination of variable speed wind-driven Grid connected SEIGs

Namani Rakesh, N. Kumaresan, S. Senthil Kumar
Department of Electrical and Electronics Engineering
National Institute of Technology,
Tiruchirappalli, Tamil Nadu, India
307110009@nitt.edu, nkumar@nitt.edu, skumar@nitt.edu

Abstract—A Self Excited Induction Generator (SEIG) system has been proposed for supplying power to the grid through a combination of a three-phase semi-converter (SC) and a line commutated inverter. This system is capable of operating at variable speed to enable maximum power, proportional to the cube of the wind speed, to be extracted from the wind. The method of analysing the system has been explained by deriving the relevant expressions for the various performance quantities. The different control schemes to be adopted for the SC to suit the various speed ranges of the generator has been described with an example along with the predetermined performance characteristics of the system, following cube law power curve. The simulated waveforms of voltage and current at the various stages of the proposed system are also presented.

Keywords—*Self-excited induction generator, Renewable power generation, Semi- converter, Line-commutated inverter, MPPT, steady state analysis, Power generation systems.*

I. INTRODUCTION

The design and development of renewable energy sources are very much emphasized now-a-days due to the fast depletion of conventional energy sources and the environmental pollution caused by them. It has been established that, among various renewable sources, wind energy electric conversion systems can produce significant quantum of electrical power output, in locations identified with fairly high wind velocity over most part of the year. Further, in such wind energy systems, squirrel cage induction machines are commonly used as generators due to their low cost, simple and robust construction and almost nil maintenance requirements [1-4]. These generators are operated either for feeding power directly to the grid or for supplying power to isolated loads with capacitor excitation. The Grid-Connected induction generators (GCIGs) run with a very small variation in rotor speed from no load to full load, whereas in the case of the Self-excited induction generators, the rotor speed varies along with the variation in wind speed.

However, due to the aerodynamic characteristics of the wind turbine, if the rotational speed is allowed to vary with varying wind speed, the maximum power (MP) output could be obtained from the generator and this power varies approximately as the cube of the wind speed [5-8]. So, even in the case of generators feeding power to the grid (GCIGs), variable speed operation is possible, if the generator output terminals are connected to the grid through suitable power electronic controllers, instead of feeding directly to the grid.

M.Subbiah
Department of Electrical and Electronics Engineering
Rajalakshmi Engineering College,
Chennai, Tamil Nadu, India
eesubbiah@yahoo.co.in

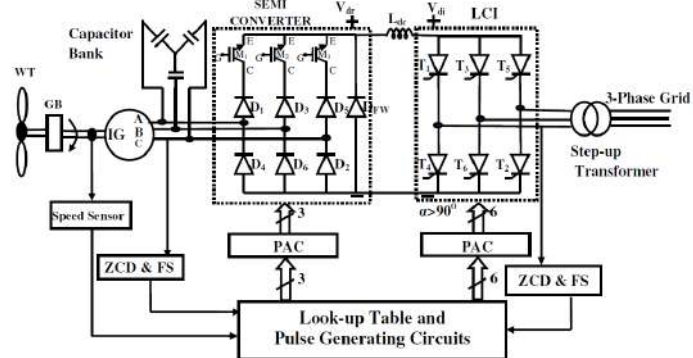
To achieve this, several authors have proposed induction generators with back-to-back PWM converter systems. The attractive features of these systems are (i) low harmonic distortion at the generator and grid terminals and (ii) controllable power factor. However, the drawbacks of these systems are (i) the PWM converters must be oversized in order to supply the reactive power requirement of the generator, (ii) complex control strategy in operating the systems and (iii) issues in synchronising with the grid [9-11].

In this paper, a three-phase semi converter (SC) and a line commutated inverter (LCI) topology have been employed for the SEIG- Grid interactive system. Certain firing angle control schemes other than the conventional phase angle control (PAC), namely, Negative Firing Angle Control (NFAC), Extinction Angle Control (EAC) and Symmetrical Angle Control (SAC) have been adopted for the semi-converter [12,13]. The need for each of these control schemes to accommodate a wide variation in wind speed, has also been brought out with an example. The relevant analytical expressions have been derived for the design of such systems. Starting from the analysis of SEIG, the performance predetermination with grid interaction and the relevant Matlab/Simulink simulation results are presented in the succeeding sections.

II. PROPOSED SEIG-GRID INTERACTIVE SYSTEM

The schematic diagram of the proposed wind energy conversion scheme is shown in Fig.1. Since only one quadrant operation is required in renewable energy conversion systems, i.e., converting renewable energy to dc electrical output, a three-phase semi-converter circuit would be sufficient for such applications. The dc power output is converted back into ac power through an LCI and fed to the grid. The power circuit of the semi-converter employs three IGBTs and six diodes, together with a free-wheeling diode. The three diodes shown in series with the IGBTs are meant for blocking the reverse current flow through the inbuilt diode in the IGBTs, i.e., to provide unidirectional current conduction. The dc power output from the semi-converter is fed to the inverter through a dc link inductance [14,15]. This inductance is used to obtain a steady direct current from the SC. The inverter transfers the power to the utility grid via a step-up transformer of suitable voltage ratio. If the thyristors in the line commutated inverter are numbered as shown in Fig.1, the normal firing sequence is T₁&T₂, T₂&T₃, T₃&T₄, T₄&T₅, T₅&T₆, and T₆&T₁, with the firing

angle α_l being greater than 90° . The look-up table built in the set-up shown in Fig.1 takes three inputs, namely the rotor speed, N of the SEIG and the generator and grid frequencies. Based on these quantities, an appropriate firing scheme and the firing angle α_s for the three-phase semi-converter is calculated. The firing angle, α_l for the inverter is kept fixed such that maximum power at that speed is extracted and fed to the grid. This angle α_l is determined by a trial and error process, in such a way that the generator is not overloaded at any speed and this aspect has been further illustrated for the example system considered in section IV.



WT- Wind Turbine, IG - Induction Generator, PAC - Pulse Amplifier Circuit, ZCD - Zero Crossing Detector, PM- Prime Mover FS- Frequency Sensor, GB- Gear Box

Figure.1 Overall schematic diagram of the proposed wind energy conversion system

For each of the semi-converter control schemes, the expressions for the average dc voltage and the displacement angle for the fundamental component of input current are known [13]. These expressions are given in Table 1 along with the other expressions derived in the next section needed for the analysis of the proposed system.

III. STEADY-STATE ANALYSIS OF SEIG USING GA TECHNIQUE

The analysis of SEIGs can be made under steady state operation using the equivalent circuit shown in Fig.2, where all the parameters are referred to the rated frequency. In this circuit all the parameters are assumed to be known, except the magnetizing reactance, X_m which varies with the wind speed and the core loss in the machine is neglected. Traditionally, the steady state performance of SEIG is carried out, first by writing the loop or nodal equation of the circuit shown in Fig.2. Then, equating the real and reactive parts of the loop impedance or nodal admittance of the circuit to zero, a higher order polynomial is derived in terms of the unknown variables, X_m and the per unit frequency(a). This polynomial is solved by some numerical method for determining these unknown values, for the given values of per unit speed (b), excitation capacitance and machine and load parameters. Such traditional methods involve the derivation of lengthy equations and are also time consuming [16, 17]. So, in this paper, SEIG has been analyzed using Genetic algorithm, an approach recently suggested in [18-20] which has been shown to be simple compared to all other earlier methods. In this analysis, the loop impedance expression is taken as such without any further simplification and its absolute value is taken as the objective function. Thus, the objective function to be minimized using

Genetic Algorithm for obtaining the unknown values a and X_m for the given values of b , excitation capacitance, machine and load parameters is

$$f(a, X_m) = \text{abs}(Z) \quad (1)$$

where

$$Z = \left\{ \left[\frac{R}{a} + jX \right] \parallel \left[\frac{-jX_c}{a^2} \right] \right\} + \left\{ \frac{R_1}{a} + jX_1 \right\} + \left\{ jX_m \parallel \left[\frac{R_2}{a-b} + jX_2 \right] \right\}$$

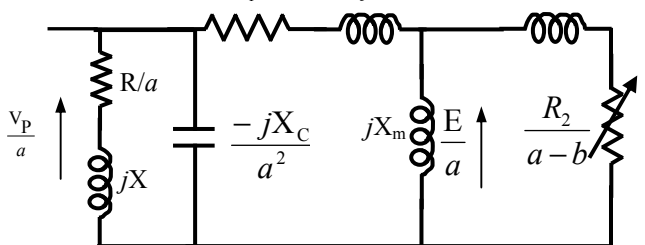


Figure.2 Equivalent circuit of SEIG with load
All reactances correspond to rated frequency

Thus, after arriving at the values of a and X_m for a given b using the methods described in [18], the induced emf can be determined from the magnetization characteristic of the machine. Then, the load phase voltage (V_p), load current (I_{R1}) and power output (P_g) can be computed from the expressions derived from the equivalent circuit shown in Fig.2 and they are summarized in Appendix.

A. Steady-state analysis of the proposed system

The performance analysis of the proposed system consisting of SEIG, power converters and grid can also be carried out using the equivalent circuit shown Fig.2 and employing GA technique. However, for using this method, the power supplied to the grid, P_{gr} should be appropriately reflected at the output terminals of the generator as an equivalent impedance i.e., R and X in the equivalent circuit of Fig.2 should be replaced with equivalent values, R_e and X_e of the proposed system. The values of R_e and X_e depend on the firing angle (α_s) and the control scheme adopted for the SC, firing angle of the LCI (α_l), power supplied to the grid (P_{gr}) and the phase voltage at the output terminals of the LCI (V_{gp}). As an illustration, the derivation of R_e and X_e is explained for the Negative Firing Angle scheme as follows:

The dc link inductor (L_d) is assumed to be lossless and large enough so that the dc current is constant and continuous. Let it be assumed that the generator terminal voltage i.e., per phase voltage at the input terminals of the SC is

$$v_p = \sqrt{2} V_p \sin \alpha \quad (2)$$

The fundamental component of ac input current per phase at SC is

$$i_{R1} = \sqrt{2} I_{R1} \sin(\omega t \pm \phi_l) \quad (3)$$

+ sign for NFAC/EAC and – sign for PAC

Then, the power supplied by the generator at the SC input terminals is

$$P_g = 3 V_p I_{R1} \cos \phi_l \quad (4)$$

where

$\phi_l = (\alpha_S / 2)$ for NFAC scheme. Then

$$I_{R1} = P_{gr} / 3V_p \cos\left(\frac{\alpha_S}{2}\right) \quad (5)$$

where P_{gr} = Power supplied to the grid = P_g (neglecting converter losses)

Thus, the equivalent impedance per phase at the generator terminal is

$$Z_e = \frac{V_p}{I_{R1}} \angle \pm \phi_l = R_e + jX_e \quad (6)$$

- sign indicates NFAC/EAC and + sign indicates PAC.

The average dc voltage at the output of SC for NFAC firing angle control scheme is [13].

$$V_{ds} = \frac{3\sqrt{6}}{2\pi} V_p (1 + \cos \alpha_S) \quad (7)$$

The average dc voltage, the fundamental component of ac current and power factor at the input of LCI are

$$V_{di} = \frac{3\sqrt{6}}{\pi} V_{gp} \cos \alpha_I \quad (8)$$

$$I_{g1} = \frac{\sqrt{6}}{\pi} I_d \quad (9)$$

$$P.F. = \frac{3}{\pi} \cos \alpha_I \quad (10)$$

The three-phase grid power can be evaluated as

$$P_{gr} = 3 V_{gp} I_{g1} (3/\pi) \cos \alpha_I \quad (11)$$

Further, for the lossless dc link inductor $V_{ds} \approx V_{di}$ and using V_{ds} and V_{di} , the per phase voltage at the generator terminals for NFAC scheme is

$$V_p = \frac{2V_{gp} \cos \alpha_I}{1 + \cos \alpha_S} \quad (12)$$

Then by substituting the V_p and I_{R1} in (6), the expressions obtained for the equivalent impedance, resistance and reactance at the generator terminals are

$$Z_e = \left(3/P_{gr}\right) V_p^2 \cos\left(\frac{\alpha_S}{2}\right) \angle -\frac{\alpha_S}{2} \quad (13)$$

$$R_e = \left(\frac{3}{P_{gr}}\right) \frac{(V_{gp} \cos \alpha_I)^2}{\cos^2\left(\frac{\alpha_S}{2}\right)} \quad (14)$$

$$X_e = -6/P_{gr} \frac{(V_{gp} \cos \alpha_I)^2}{(1 + \cos \alpha_S)^2} \sin \alpha_S \quad (15)$$

Similarly the expressions for R_e and X_e for the other control schemes have been derived and all the relevant expressions are listed in Table -1.

IV. PREDETERMINATION OF PERFORMANCE

To illustrate the efficacy of the proposed system consisting of SEIG-SC-LCI and the method of its analysis, an example of a 3-phase, 4-pole, 50 Hz (1p.u. frequency), 1500 rpm (1p.u. speed), 400V, 2.2 kW, star-connected squirrel cage induction motor with a 3-phase, star connected capacitor bank of 55 μ F per phase was considered.

The measured parameters of the generator are $R_1=3.7\Omega$, $R_2=2.7\Omega$, $X_1=X_2=3.4\Omega$.

The (E/a) against X_m characteristic was obtained experimentally at the rated frequency of 50 Hz, following the procedure described in [17,18]. This characteristic expressed as a 3rd order polynomial is

$$E/a = -0.0003 X_m^3 + 0.0330 X_m^2 - 1.4545 X_m + 295.53 \quad (16)$$

TABLE I: PERFORMANCE EQUATIONS FOR DIFFERENT CONTROL SCHEMES OF THE SEMI-CONVERTER

NFAC / PAC	SAC	EAC ($\beta_S \leq 60$)	EAC ($\beta_S > 60$)
$V_{ds} = \frac{3\sqrt{6}}{2\pi} V_p (1 + \cos \alpha_S)$	$V_{ds} = \frac{3\sqrt{6}}{2\pi} V_p (1 + 2\cos(\gamma_S + \pi/3))$	$V_{ds} = \frac{3\sqrt{6}}{2\pi} V_p (0.5 - \cos(\beta_S + \pi/3))$	$V_{ds} = \frac{3\sqrt{6}}{2\pi} V_p (1.5 - \cos \beta_S)$
$V_p = \left(\frac{2V_{gp} \cos \alpha_I}{1 + \cos \alpha_S}\right)$	$V_p = \left(\frac{2V_{gp} \cos \alpha_I}{1 + 2\cos(\gamma_S + \pi/3)}\right)$	$V_p = \left(\frac{2V_{gp} \cos \alpha_I}{0.5 - \cos(\beta_S + \pi/3)}\right)$	$V_p = \left(\frac{2V_{gp} \cos \alpha_I}{1.5 - \cos \beta_S}\right)$
$\phi_l = \frac{+\alpha_s}{2}$ (+: lag)	$\phi_l = 0$	$\phi_l = (\pi/6) - (\beta_S/2)$ (lead)	$\phi_l = \tan^{-1} \left(\frac{\sin \beta_S - \sqrt{3}/2}{3/2 - \cos \beta_S} \right)$ (lead)
$I_{ri} = \frac{P_\sigma}{3V_p \cos\left(\frac{\alpha_s}{2}\right)}$	$I_{ri} = \frac{P_\sigma}{3V_p}$	$I_{ri} = \frac{P_\sigma}{3V_p \cos((\pi/6) - (\beta_S/2))}$	$I_{ri} = \frac{P_\sigma}{3V_p \cos \phi_l}$
$Z_e = \left(3/P_\sigma\right) V_p^2 \cos\left(\frac{\alpha_s}{2}\right) \angle +\frac{\alpha_s}{2}$	$Z_e = \left(3/P_\sigma\right) V_p^2 \angle 0$	$Z_e = K_1 \angle -\phi_l$	$Z_e = K_1 \angle -\phi_l$
$R_e = \left(\frac{3}{P_\sigma}\right) \left(\frac{V_{gp} \cos \alpha_I}{\cos\left(\frac{\alpha_s}{2}\right)}\right)^2$	$R_e = \left(\frac{3}{P_\sigma}\right) \left(\frac{2V_{gp} \cos \alpha_I}{1 + 2\cos(\gamma_S + \pi/3)}\right)^2$	$R_e = \left(\frac{3}{P_\sigma}\right) \left(\frac{2V_{gp} \cos \alpha_I \cos \phi_l}{0.5 - \cos(\beta_S + \pi/3)}\right)^2$	$R_e = \left(\frac{3}{P_\sigma}\right) \left(\frac{2V_{gp} \cos \alpha_I \cos \phi_l}{1.5 - \cos \beta_S}\right)^2$
$X_e = \left(\frac{+6}{P_\sigma}\right) \left(\frac{V_{gp} \cos \alpha_I}{1 + \cos \alpha_s}\right)^2 \sin \alpha_s$	$X_e = 0$	$X_e = \left(\frac{-6}{P_\sigma}\right) \left(\frac{2V_{gp} \cos \alpha_I}{0.5 - \cos(\beta_S + \pi/3)}\right)^2 \sin(2\phi_l)$	$X_e = \left(\frac{-6}{P_\sigma}\right) \left(\frac{2V_{gp} \cos \alpha_I}{1.5 - \cos \beta_S}\right)^2 \sin(2\phi_l)$

$$K_1 = \left(3/P_\sigma\right) V_p^2 \cos((\pi/6) - (\beta_S/2))$$

Since the proposed SEIG-converter system is meant for extracting the maximum possible power from the wind, the performance of the system should be evaluated for the given values of power supplied to the grid and the inverter output voltage. The first step in such an evaluation is to calculate the constant control angle to be set in the LCI so that the requirement of power and voltage are achieved without overloading the generator. Such trial calculations are made for the different firing control schemes that could be adopted in the SC and the results are shown in Table-II.

It can be observed from this Table that starting from the rated speed of 1500 rpm, the SAC scheme could be used till 1428 rpm; then EAC scheme till 1320 rpm and NFAC scheme till 1114 rpm. If the appropriate control scheme is not adopted in the various speed ranges, either there will be a power mismatch or the generator will be overloaded or the rated voltage at the generator terminals would be exceeded. These aspects are also evident from Table-II.

TABLE II: CALCULATION OF FIRING ANGLE α_t FOR THE LCI AS PER CUBE LAW POWER CURVE

	N	V _L	I _s	I _R	P _g	P _{gr}	α_s	α_t
SAC	1500	319.20	4.97	3.97	2200	2200	52.5	117
	1453	323.72	4.63	3.57	2000	2000	51.10	117
	1428	333.28	4.46	3.29	1900	1900	47.80	117
	1402	333.72	4.21	2.98	1800	1800	45.00	117
EAC	1500	431.77	5.24	2.95	2200	2200	49.85	117
	1476	416.37	4.99	2.91	2100	2100	51.76	117
	1453	396.99	4.74	2.91	2000	2000	54.46	117
	1428	365.43	4.48	3.00	1900	1900	59.60	117
	1403	334.30	4.35	3.11	1800	1800	65.82	117
	1376	320.14	4.24	3.07	1700	1700	69.20	117
	1320	303.28	4.01	2.87	1500	1500	74.00	117
	1290	348.39	3.81	1.96	1164	1400	80.00	127
NFAC	1500	461.17	6.57	3.15	2200	2200	59.70	151
	1453	441.78	6.02	2.92	2000	2000	55.78	151
	1402	418.97	5.43	2.69	1800	1800	50.00	151
	1376	404.97	5.10	2.59	1700	1700	45.55	151
	1348	386.54	4.72	2.50	1600	1600	38.10	151
	1320	218.59	4.76	4.06	1500	1500	30.38	121
	1258	218.72	4.21	3.51	1300	1300	31.00	121
	1225	219.82	3.95	3.23	1200	1200	32.48	121
	1190	222.03	3.69	2.94	1100	1100	35.10	121
	1153	227.04	3.45	2.63	1000	1000	40.17	121
	1114	242.24	3.26	2.27	900	900	51.80	121
	1070	246.38	2.81	1.62	621	800	70.00	121

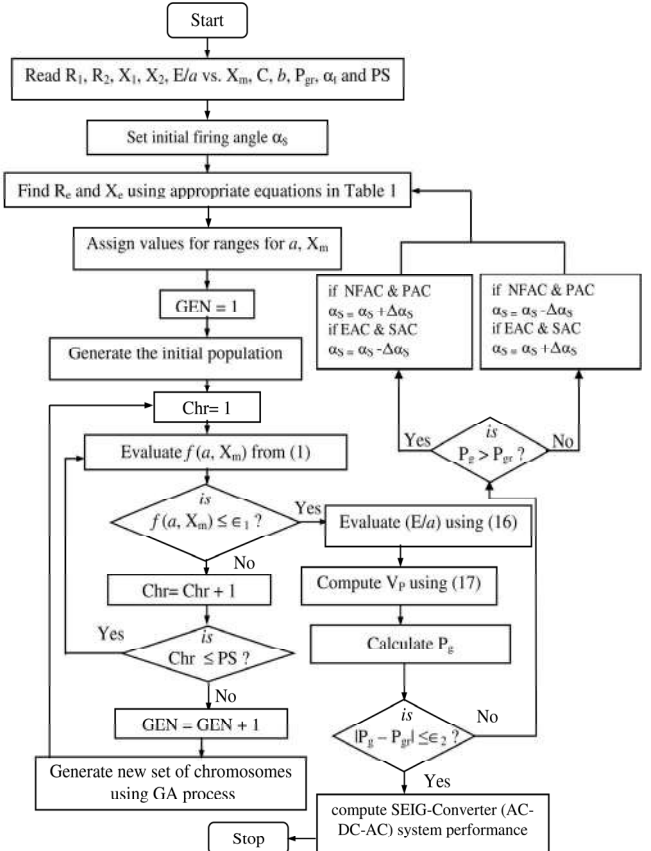
Thus, for the chosen example system, the values of α_t are 117°, 117° and 121° for SAC, EAC and NFAC schemes respectively. The next step is to predetermine the performance as explained in section IIIA. The sequence of steps involved in such a process of predetermination, i.e., calculating α_s for the chosen control scheme, till the required power, P_g is obtained at the output of LCI and then computing the system performance is given in the flowchart of Fig.3.

As a further illustration, the variation of stator line voltage and current and output power, with variation in speed are also graphically shown in Fig.4. This figure explicitly shows the cube law power variation with speed.

V. SYSTEM SIMULATION USING MATLAB /SIMULINK

For assessing the satisfactory working of the system, Simulation studies were also made on the proposed system

using Matlab/Simulink. The sets of simulated waveforms of voltage and current at the input and output of the converter and inverter were obtained on the same SEIG system mentioned in the earlier section and they are shown in Fig.5. The experimentally obtained voltage-current characteristic of the SEIG mentioned in earlier section has been used for representing it in the simulation block of the induction machine.



PS : Population Size, Chr : Chromosomes, GEN:No. of Generations, $\epsilon_1=0.01$ & $\epsilon_2=0.1$
Figure.3 Flow chart for computing the performance of the proposed system using GA

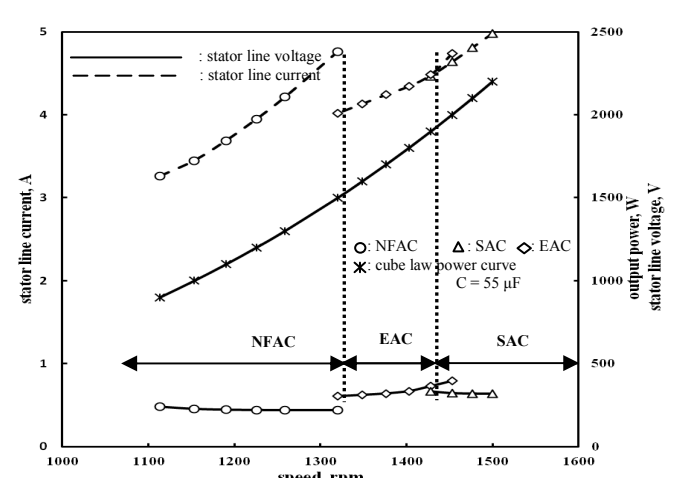
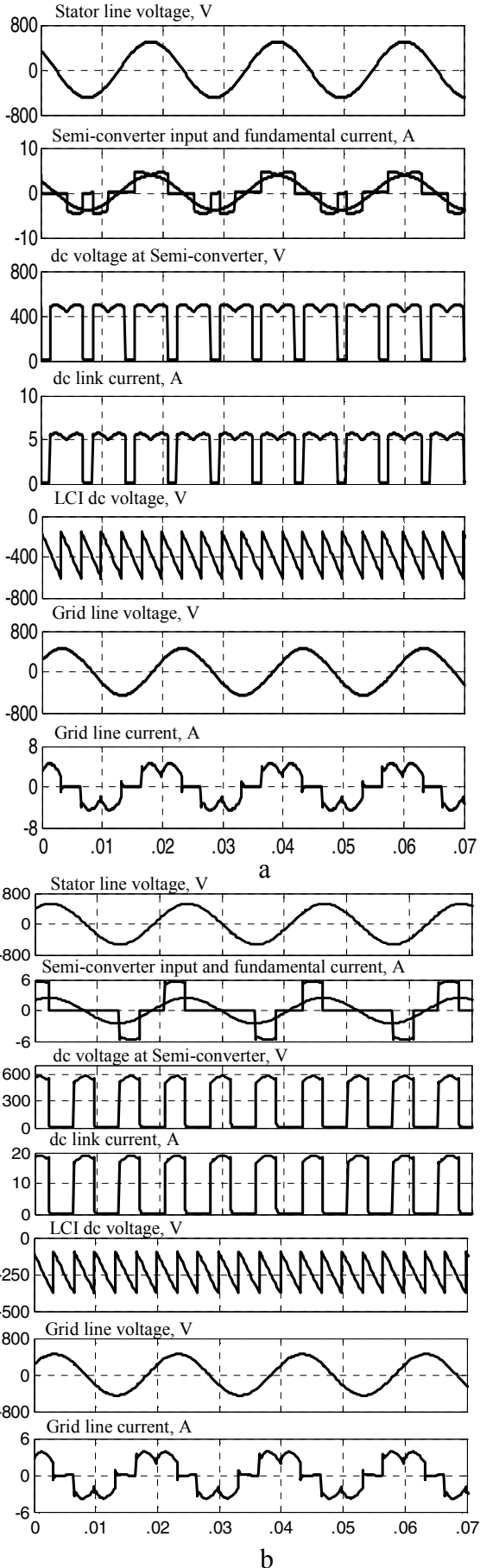
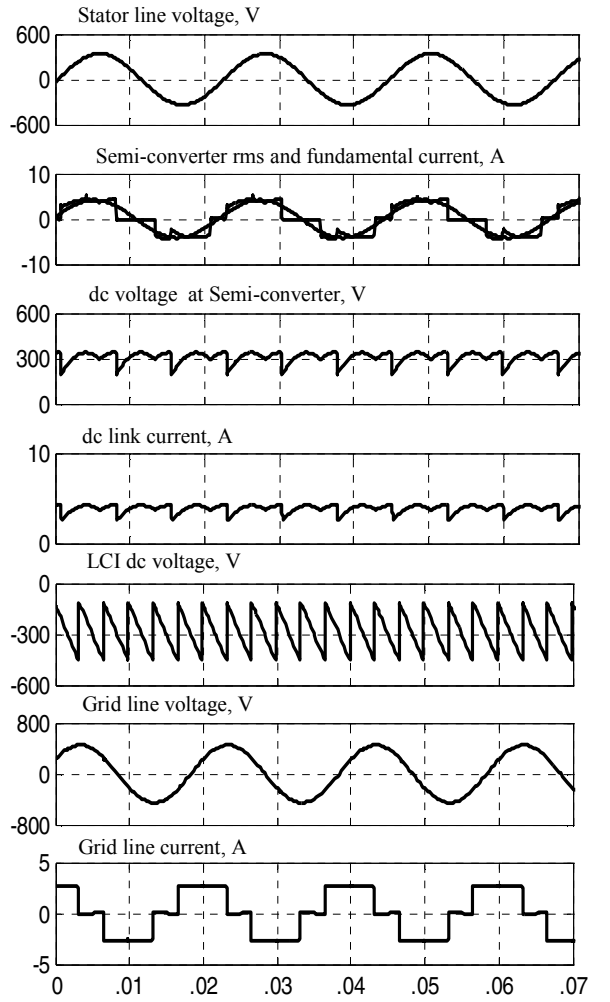


Figure.4 Characteristics of the proposed SEIG-Converter system



a



c

Figure 5 Simulated waveforms of an SEIG-SC-LCI system with $C = 55 \mu\text{F}$ for MPPT

- SAC with $N=1453$ rpm, $\alpha_S = 51^\circ$ and $\alpha_I = 117^\circ$
- EAC with $N=1428$ rpm, $\alpha_S = 59^\circ$ and $\alpha_I = 117^\circ$
- NFAC with $N=1258$ rpm, $\alpha_S = 31^\circ$ and $\alpha_I = 121^\circ$

VI. CONCLUSION

A wind energy electric conversion system, consisting of a self-excited induction generator, a three-phase IGBT semi-converter and a line commutated thyristor inverter, has been developed for supplying power to the grid. This system enables the rotor speed of the generator to vary with variation in wind speed, so that the operating point of the turbine can be close to its optimum power coefficient and maximum power can be extracted and fed to the grid. The necessity for the various control schemes, to be adopted in the converter at the various ranges of rotor speed to achieve this maximum power has been clearly demonstrated with an example. It has also been explained that a suitable firing angle should be set at the inverter, to ensure that the generator works within its rated voltage and current. The method of analysing the performance of the system by representing the grid power at the generator terminals with equivalent impedance has been illustrated. The expressions for such equivalent values have been derived for

the various control schemes and tabulated. The predetermined performance characteristics of the example system show that cube law power curve could be obtained by employing the proposed system. The simulated voltage and current waveforms shown at the various input and output stages of the system further confirm its satisfactory working.

ACKNOWLEDGEMENTS

The authors wish to thank the authorities of the National Institute of Technology, Tiruchirappalli, India for all the facilities provided for carrying out the experimental and simulation work for the preparation of this paper.

REFERENCES

- [1] H. Li, Z. Chen, "Overview of different wind generator systems and their comparisons," IET Renew. Power. Gener., Vol. 2, pp.123-128, 2008.
- [2] G.K. Singh, "Self excited induction generator research—a survey," Electr. Power Systems Res., Vol.69, pp.107–114, 2004.
- [3] R.C. Bansal, T.S. Bhatti, and D.P. Kothari, "Bibliography on the application of induction generators in nonconventional energy systems," IEEE Trans. Energy Convers., Vol.18, pp.433–439, 2003.
- [4] N. Kumaresan, and M.Subbiah, "Innovative reactive power saving in wind-driven grid-connected induction generators using a delta-star stator winding: part II, Estimation of annual Wh and VARh of the delta-star generator and comparison with alternative schemes," International journal in Wind Engineering, Vol.27, pp.195-204, 2003.
- [5] E. Muljadi, and C.P.Butterfield, "Pitch-controlled variable-speed wind turbine generation," IEEE Trans. Ind. Appl., Vol.37, pp.240-246, 2001.
- [6] S.M.R .Kazmi, H.Goto, Hai-Jiao Guo, and O. Ichinokura, "A Novel algorithm for fast and efficient speed-sensorless maximum power point tracking in wind energy conversion systems," IEEE Trans. on Ind. Electron., Vol.58, pp.29-36, 2011.
- [7] S. Srinivasa Rao, and B.K. Murthy, "A new control strategy for tracking peak power in a wind or wave energy system," Renew. Energy, Vol.34, pp.1560–1566, 2009.
- [8] Tomonobu Senju, Yasutaka Ochi, Yasuaki Kikunaga, Motoki Tokudome, Atsushi Yona, Endusa Billy Muhando, Naomitsu Urasaki, and Toshihisa Funabashi, "Sensor-less maximum power point tracking control for wind generation system with squirrel cage induction generator," Renew. Energy., Vol.34, pp.994-999, 2009.
- [9] J. Marques, H. Pinheiro, H.A. Gründling, J.R. Pinheiro, and H.L. Hey, "A survey on variable-speed wind turbine system," Brazilian conference of electronics of power., Vol.1, pp.732-738, 2003.
- [10] F.M. Fayez, E.L.Sousy, M. Oabi, and H. Godah, "Maximum Power Point Tracking Control Scheme for Grid Connected Variable Speed Wind Driven Self-Excited Induction Generator," J. Power Electronics., Vol.6, pp.52-56, 2006.
- [11] C. Zhe, J.M. Guerrero, and F. Blaabjerg, "A Review of the State of the Art of Power Electronics for Wind Turbines," IEEE Trans. on Power. Electron., Vol.24, pp.1859-1875, 2009.
- [12] N. Kumaresan, N. Ammasaigouden, and M. Subbiah, "Certain control strategies for three-phase semi-converters for the operation of self-excited induction generators," Proc. IEEE ICIT 2002, Vol. 2, pp. 986-991, 2002.
- [13] R. Karthigaivel, N. Kumaresan, and M. Subbiah, "Analysis and control of self-excited induction generator-converter systems for battery charging applications," IET Electr. Power Appl., Vol. 5, pp.247-257, 2011.
- [14] R.M. Hilloowala, and A.M. Sharaf, "A utility interactive wind energy conversion scheme with an asynchronous dc link using a supplementary control loop," IEEE Trans. on Energy Convers., Vol.9, pp.558-563, 1994.
- [15] V. Lavanya, N. Ammasaigouden, and Polimera Malleswara Rao, "A Simple Controller using Line Commutated Inverter with Maximum Power Tracking for Wind-Driven Grid-Connected Permanent Magnet Synchronous Generators," IEEE International Conference on Power Electronics, Drives and Energy Systems, pp.01-06, 2006.
- [16] L. Quazene, and G. McPherson, "Analysis of the isolated induction generator," IEEE Trans on Power Apparatus and Systems, Vol. PAS-102, pp. 2793-2798, 1983.
- [17] N. Ammasaigouden, M. Subbiah, and M.R. Krishnamurthy, "Wind-driven self-excited pole-changing induction generators," IEE Proc. B., Vol. 133, pp. 315-321, 1986.
- [18] R. Karthigaivel, N. Kumaresan, P. Raja, and M. Subbiah, "A novel unified approach for the analysis and design of Wind-driven SEIGs using nested GAs," International journal in Wind Engineering, Vol. 33, pp.631- 647, 2009.
- [19] A.L. Alolah, and M.A. Alkanthal, "Optimization based steady state analysis of three-phase self-excited induction generator," IEEE Trans. Energy Convers., Vol.15, pp.61-65, 2000.
- [20] Namani Rakesh, N. Kumaresan, S. Senthil Kumar and M. Subbiah, "Major methods of steady-state analysis of three-phase SEIGs – A summary" Proc. IEEE ICSET 2012, Nepaal, pp. 415-419, 2012.

NOMENCLATURE

a	per unit (p.u.) frequency = f_g / f_r	
b	p.u. speed = N/N_s	
E	air-gap voltage per phase	V
I_{dc}	dc link current	A
I_{R1}	fundamental value of semi-converter input current	A
I_s	stator line current	A
P_{gr}	three-phase grid power	W
P_g	output power of the generator	W
R_e, X_e	equivalent resistance and reactance at the generator terminals corresponding to the value of grid power	Ω
R_1, X_1	per phase stator resistance and leakage reactance respectively	Ω
R_2, X_2	per phase rotor resistance and leakage reactance respectively	Ω
V_{di}	average dc input voltage of LCI terminals	V
V_{ds}	average dc output voltage of the semi-converter	V
V_{gp}, V_{gL}	phase and line voltages, respectively, at the grid terminals	V
V_p, V_L	phase and line voltage, respectively, at the generator terminals	V
X_C	capacitive reactance per phase of the excitation	Ω
X_m	capacitance	Ω
	per phase magnetizing reactance	Ω

APPENDIX

Expressions for the performance quantities of SEIGs are

$$V_p = \left\{ \frac{R_L^2 + X_L^2}{\{(R_1/a) + R_L\}^2 + (X_1 - X_L)^2} \right\}^{1/2} E \quad (17)$$

$$I_{R1} = V_p/Z_e \quad \text{and} \quad P_g = 3V_p I_{R1} (R_e/Z_e) \quad (18)$$

$$\text{where } R_L = \frac{R_e X_c^2}{a [a^2 R_e^2 + (a^2 X_e - X_c)^2]}, \quad X_L = \frac{[-X_e X_c + R_e^2 + a^2 X_e^2] X_c}{[a^2 R_e^2 + (a^2 X_e - X_c)^2]} \quad \text{and} \\ Z_e = [R_e^2 + a^2 X_e^2]^{1/2} \quad (19)$$

Maximizing the Power Output of Partially Shaded Solar PV Array using Novel Interconnection Method

Namani Rakesh^{1*}, and Udagula Malavya²

Department of Electrical Engineering

¹Rajiv Gandhi University of Knowledge Technologies, Basar, Telangana, India

²Kamala Institute of Technology and Science, Singapur, Telangana, India

*e-mail: namanirakesh@rgukt.ac.in

Abstract – Solar Photo Voltaic Array performance severely effect by the partial shading and fast changing irradiance conditions. The performance depends on shading patterns and position of the solar panels in solar PV array. This paper proposes a novel interconnection method (Magic Square method), which disburse the shade to maximize the power output of partially shaded solar PV Array. The proposed system is tested under different partial shaded conditions for change in irradiation. As the solar panels receive continuous change in irradiation, the P-V characteristics of solar array experience multiple peaks or local peaks. The multiple peaks with conventional Total Cross Tied (TCT) connection are avoided with a novel interconnection method. A novel interconnection method (Magic Square method) gives enhanced output power than the conventional TCT connection. The proposed interconnection method is tested with two groups of irradiations for every chosen shading pattern. The performance of the proposed method for 3x3 solar PV Array is tested using theoretical calculations, MATLAB simulations and experimental results on laboratory built hardware setup. The successful working of magic square method on laboratory setup assures for large number of panels in solar PV array and its usefulness of the system.

Keywords - maximum power, interconnection method, shading dispersion, partial shading, TCT and Magic Square

I. INTRODUCTION

The non-renewable fossil fuels are the foremost resources used to generate electricity and heat energy worldwide. The need to move towards Renewable Energy solutions is highlighted because of increase in greenhouse gas emissions resulting from the use of fossil fuels [1]. Renewable energy generated at any place (even on roof top) rather than national can be considered as one of the key Solution of the global energy challenges and to establish a secure energy supply system. The increasing in energy requirement and an optimistic concern about environmental problems has ignited gigantic attention in the consumption of renewable energy [2]. One most important source of RE is the sun. Solar energy is currently considered to be an important energy since this energy source is free of cost, abundantly available everywhere on the earth, sustainable and environmental friendly, and is one of the major energy source of the future. Solar energy can be trapped by the Photo Voltaic (PV) panels [3]. Solar

PV panel is a power source having non linear internal resistance. Several Reconfiguration techniques are available which can be used in very wide range of applications [4]. The output power yield of the panel varies with temperature and insolation. In order to operate the panel in economic conditions, the maximum power point should be followed [5, 6].

The limitations of the solar energy are the high cost of the PV module and its shading effects. The initial cost is basically on the higher side, and running cost is comparatively low. The effect of partial shading is the mismatching effects of the PV output due to partial shading of the modules, which may result in sudden change in the parameters of the Solar PV array [7-9]. Weather changes obstruction of buildings, trees, poles etc., affects the output power of solar PV Array as these are also the cause for partial shading. The reduce in this output power yield is because of this partial shading effect [10-12]. The multiple peaks in the solar PV characteristics arise and the Global Peak (GP) is settled at Local Peak (LP) [13].

When the Solar PV Arrays are partially shaded, the Mismatch conditions arise. When any panel (cell) of the Solar PV array is partially shaded, the output will be reduced and the variation in magnitude of the parameter will also depend on electrical configuration of that array. So, by lowering the light intensity the output of shaded cell or module will be lowered. As this Shaded cell (Panel) is electrically connected to another unshaded panels or cells, the performance of the unshaded cell (panels) is also lessened; this is called a mismatch condition. One completely shaded cell can reduce a solar module's output by 40% to 95%. For PV systems, it is impossible to avoid all shading without severely restricting the size of the array and hence losing output at all times. In these systems, partial shading losses are estimated to contribute between 5% to 25% annual power losses [14 – 16].

This paper presents a new interconnection method to increase the output power from partially shaded solar PV Array. The paper is as follows: Section II deals with System Configuration, different types of topologies of the solar PV arrays and types of shading patters. The Simulation and Hardware results are

discussed in Section III, followed by conclusions and references.

II. SYSTEM CONFIGURATION

a. Photo Voltaic Model

The solar cell can be seen as a current generator which generates the current I_m . The current in the diode I_D flows in opposite direction and is caused by a potential between the + and - terminals. In addition two resistances; one in series (R_s) and one in parallel (R_{sh}), represented in the equivalent circuit diagram as shown in fig. 1. The series resistance is caused by the fact that a solar cell is not a perfect conductor. The parallel resistance is caused by leakage of current from one terminal to the other due to poor insulation. For an ideal solar cell, $R_s = 0$ and $R_{sh} = \infty$.

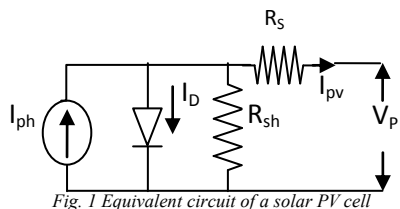


Fig. 1 Equivalent circuit of a solar PV cell

The equation describes the model, where the output current and the voltage of a PV module at an irradiance 'G' can be given as

$$I_m = I_{ph} - I_0 \left[\exp \left(\frac{V_p + R_s I_m}{A} \right) - 1 \right] - \left[\frac{V_p + R_s I_m}{R_{sh}} \right] \quad (1)$$

$$A = \frac{n k T}{q} \quad (2)$$

The photovoltaic current is obtained as

$$I_{ph} = I_{sco} \left(\frac{G}{G_0} \right) (1 + \alpha_1 (T - T_0)) \frac{R_s + R_{sh}}{R_{sh}} \quad (3)$$

The specifications of the module at standard test conditions are given in Table – 1.

Table - 1: PV Specifications at 1000W/m^2 and 25°C

PV Power	384 mW
Open Circuit Voltage	3 V
Short Circuit Current	150 mA
Nominal Voltage	2.74 V
Nominal Current	140 mA

Different Types of Topologies:

This paper explains three basic topologies: Series – Parallel (SP), Bridge –Link (BL), Total Cross Tied connection (TCT) as shown in fig. 2 [9].

Series – Parallel (SP): In this connection, the solar panels are connected in series with one other and the series connected panels are connected in parallel to obtain the series – parallel configuration.

Bridge – Linkage (BL): This configuration is inspired by the wheat-stone bridge connection, The BL interconnection scheme is derived from the connections in a bridge rectifier.

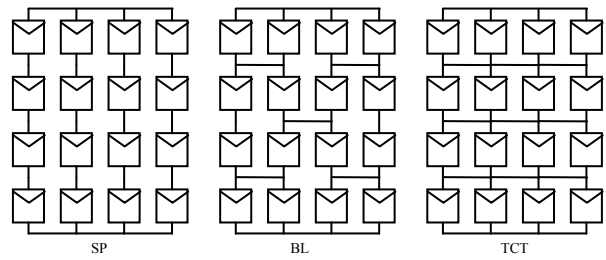


Fig. 2 Different topologies to connect Solar PV array

TCT Configuration: A TCT configuration is obtained by connecting ' $n \times n$ ' branches, in series and parallel with one another. Now cross ties are connected across the branches after each row of panels. All the panels in a column are connected in series and each panel in a row has connected in parallel. The bypass diodes are also connected across each solar panel to allow the current to be bypassed, when solar panel is shaded. This solar PV array consists of n rows and n columns totally of n^2 modules in an ascending order of numbers in column wise.

b. Different types of shading Patterns

Based on the number of shaded columns [Width (wide or narrow)] and shaded modules per column [Length (short or long)], to verify the proposed technique, four different Shading conditions for solar PV arrays [8, 11,12] are employed, Short Wide (SW), Long Wide (LW), Short Narrow (SN) and Long Narrow (LN). For each shading condition, The PV characteristics are obtained for both TCT and Magic Square, The results are presented in Section III.

c. Magic Square Configured structure of a Solar PV array

A magic square is an arrangement of the numbers from 1 to n^2 in an $n \times n$ matrix, with each number occurring exactly once, and such that the sum of the entries of any row, any column, or any main diagonal is the same.

The following technique is observed for any $(2n+1)$ square matrix, where ' $n \geq 1$ '. Starting with '1' in the exact middle block of the first column, the succeeding number is filled in the block which is down left to the present block and the technique continues till a contradictory occurs where the next block is being already filled. In this case, the succeeding number is filled in the immediate right block. The important thing to remember in this technique is to imagine the matrix has "wrap-around", i.e., if you move off one edge of the magic square, you re-enter on the other side.

In this arrangement, the physical locations of panels are changed, without affecting the electrical connections. As the electrical connection is unaltered, the current and voltage equations also remain the same as in TCT connection. The panels in the row in TCT configuration are now in different rows in Magic Square Technique. This allows reducing the shading effect on a single row by distributing the shade over the entire array. Thus, using this technique in the partial shaded conditions, the incoming current

at a particular node is increased and reduces the bypassing of panels. Therefore the generated power is increased for the identical shading pattern.

To generalize, the magic square technique is compared with TCT for 3X3 panels. For this study consider a 3X3 solar PV array which is connected in TCT arrangement as shown in fig. 3(i). This solar PV Array consists of 3 rows and 3 columns totally of 9 panels. Each panel is labelled from 1 to 9 in an increasing order of their numbers in column wise. For example, Column – 1 consists of panels labelling from 01–03; column – 2 consists of panels labelling from 04–06; and column – 3 consists of panels labelling from 07–09. The magic square connection Fig. 3(a) is as shown in Fig. 3(b).

1	4	7
2	5	8
3	6	9

8	3	4
1	5	9
6	7	2

Fig. 3. Solar panels connections in Solar PV array
(a) TCT Connection (b) Magic Square Connection

In this arrangement, the physical locations of panels are changed, without affecting the electrical connections. As the electrical connections are unaltered, the current and voltage equations also remain the same as in TCT connection. The panels in the row in TCT configuration are now in different rows in Magic Square Technique. The bypass diodes are connected across each solar panel in Magic Square technique also. When the solar panel is shaded, these diodes allow the current to be bypassed through them. This TCT technique taken is as shown in Fig. 4(a) and its Magic Square arrangement is as shown in 4(b).

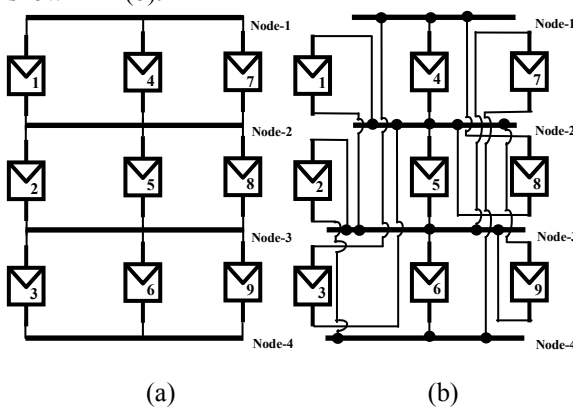


Fig. 4. Solar panels connections in Solar PV array
(a) TCT connection
(b) Magic square connection

The Magic Square arrangement is reducing the shading effect on a single row by distributing the shade over the entire array. Thus, using this technique

in the partial shaded conditions, the incoming current at a particular node is increased and reduces the bypassing of panels. Therefore the generated power is increased for the identical shading pattern.

III. HARDWARE AND SIMULATION RESULTS

The proposed method has been simulated using MATLAB/Simulink and later a 384 mW hardware setup is built in the laboratory. The hardware setup is experimentally tested to verify the analysis and simulations. Theoretical calculations of current, voltage and power for TCT and Magic Square and its simulations are performed on 3x3 solar PV Array for all shading patterns. The regulated power supplies are used to adjust the irradiation levels based on the short circuit currents of solar panels. By choosing suitable irradiation levels for all cases voltages, currents and powers are noted for change in load resistance. For different shading pattern to calculate the location of GP, first calculate the current which is generated in each row of the solar PV array.

Current equations for row-1, row-2 and row-3 are expressed as:

$$I_{R1} = k_1 I_1 + k_2 I_2 + k_3 I_3$$

$$I_{R2} = k_4 I_4 + k_5 I_5 + k_6 I_6$$

$$I_{R3} = k_7 I_7 + k_8 I_8 + k_9 I_9$$

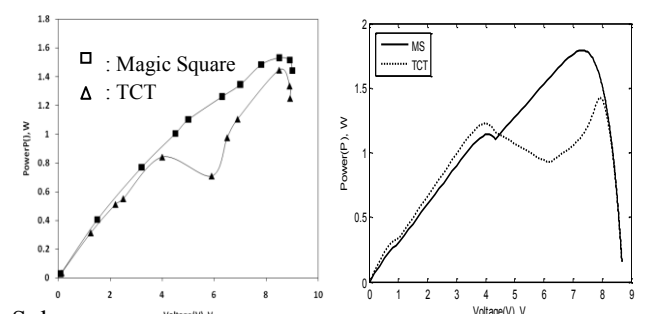
Where $k_y = G_y / G_o$, where ' G_y ' is the solar irradiance of the panel-y and ' I_y ' is the current generated by the Panel-y (where $y=1,2,3,\dots,9$).

The power produced by the solar array is given by

$$P_a = 3 \times 0.9 I_m V_a = 3 \times 0.9 I_m (3V_m);$$

$P_a = 8.1 V_m I_m$; If no panel is bypassed [16].

Case-1 (Short Narrow)



Solar array with three distinct groups of panels are taken in this case of shading pattern as shown in Fig. 5. The group one receives an irradiation 900 W/m^2 and the remaining groups receive 600 W/m^2 and 200 W/m^2 respectively.

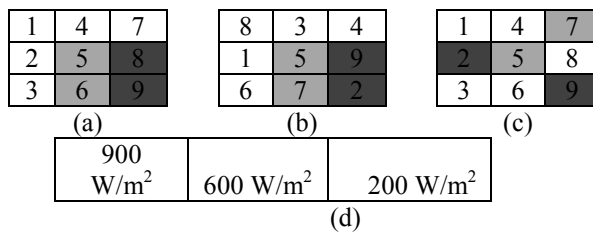


Fig.5. Shading pattern for 3X3 arrangements for case-1.

- (a) TCT Arrangement
- (b) Magic Square arrangement
- (c) Shade dispersion with Magic Square technique
- (d) irradiation levels

The current calculations for each row in solar PV array for TCT and Magic Square are given in table-2. The calculations for voltage and powers are noted down in table-3.

Current Equations	TCT		MAGIC SQUARE	
	I _{R1} = 3 X 0.9I _m = 2.7 I _m	I _{R1} = 2 X 0.9I _m + 1X0.6I _m = 2.4 I _m	I _{R2} = 1 X 0.9I _m + 1X0.6I _m +1X0.2I _m = 1.7 I _m	I _{R2} = 1 X 0.2I _m + 1X0.6I _m +1X0.9I _m = 1.7 I _m
Row-1	I _{R3} = 1 X 0.9I _m + 1X0.6I _m +1X0.2I _m = 1.7 I _m	I _{R3} = 2 X 0.9I _m + 1X0.2I _m = 2.0 I _m		
Row-2				
Row-3				

Table-2: Current equations for different rows

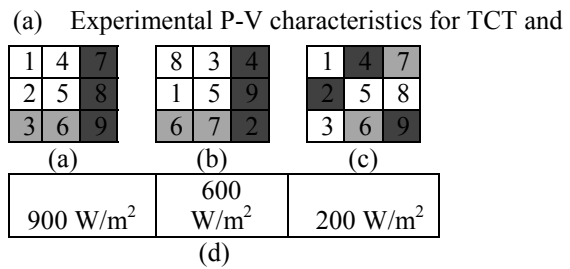
Table-3: Location of GP in TCT and Magic Square

TCT Arrangement			MAGIC SQUARE		
Row current in the order in which panels are bypassed	Volta	Pow	Row current in the order in which panels are bypassed	Volta	Pow
	ge	er		ge	er
I _{R3}	1.7I _m	3V _m	5.1 V _m I _m	I _{R2}	1.7 I _m
I _{R2}	1.7I _m	2V _m	3.4 V _m I _m	I _{R3}	2.0 I _m
I _{R1}	2.7I _m	1V _m	2.7 V _m I _m	I _{R1}	2.4 I _m

The experimental and simulated P-V characteristics are shown in Fig. 6(a) and Fig. 6(b) respectively for

TCT and Magic Square. The corresponding maximum powers obtained in TCT are 1.445W, 1.425W and to that of Magic Square are 1.53W, 1.793W. After the physical locations of the modules are changed, the power generated in the array is increased by 5.88% and 25.82% from TCT to Magic Square.

Fig.6. Power versus Voltage characteristics for Case-1



(a) Experimental P-V characteristics for TCT and MS

Case-2 (Long Wide)

Solar array with three distinct groups of panels are taken in this case of shading pattern as shown in Fig. 7. The group one receives an irradiation 900W/m² and the remaining groups receive 600W/m² and 200W/m² respectively.

Fig.7. Shading pattern for 3X3 arrangements for case-2.

- (a) TCT Arrangement
- (b) Magic Square arrangement
- (c) Shade dispersion with Magic Square technique
- (d) irradiation levels

The current calculations for each row in solar PV array for TCT and Magic Square are given in table-4.

Table-4: Current equations for different rows

Current Equations	TCT	MAGIC SQUARE
Row-1	I _{R1} = 2 X 0.9I _m + 1X0.2I _m = 2.0 I _m	I _{R1} =1X0.9I _m +1X0.2I _m +1X0.6I _m =1.7I _m
Row-2	I _{R2} = 2 X 0.9I _m + 1X0.2I _m = 2.0 I _m	I _{R2} = 2 X 0.9I _m + 1X0.2I _m = 2.0 I _m
Row-3	I _{R3} = 2 X 0.6I _m + 1X0.2I _m = 1.4 I _m	I _{R3} =1X0.9I _m +1X0.6I _m +1X0.2I _m =1.7 I _m

The calculations for voltage and powers are noted down in table-5

Table-5: Location of GP in TCT and Magic Square

TCT Arrangement			MAGIC SQUARE		
Row current in the order in which panels are bypassed	Volta ge	Power	Row current in the order in which panels are bypassed	Volta ge	Power
	V _a	P _a		V _a	P _a
I _R ₃	1.4 I _m	3V _m	4.2 V _m I _m	I _{R3}	1.7 I _m
I _R ₂	2.0 I _m	2V _m	4.0 V _m I _m	I _{R1}	1.7 I _m
I _R ₁	2.0 I _m	1V _m	2.0 V _m I _m	I _{R2}	2.0 I _m

The experimental and simulated P-V characteristics are shown in Fig. 8(a) and Fig. 8(b) respectively for TCT and Magic Square. The corresponding maximum powers obtained in TCT are 1.52W, 1.487W and to that of Magic Square are 1.638W, 1.672W. After the physical locations of the modules are changed, the power generated in the array is increased by 7.76% and 12.44% from TCT to Magic Square.

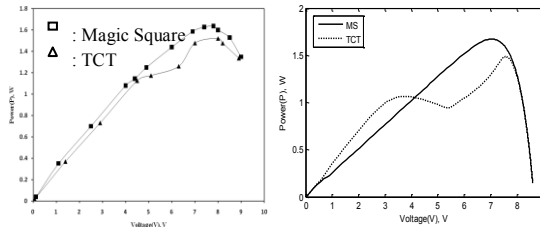


Fig.8. Power versus Voltage characteristics for Case-2

- (a) Experimental P-V characteristics for TCT and MS
- (b) Simulated P-V characteristics for TCT and MS

Case-3 (Short Wide)

Solar array with three distinct groups of panels are taken in this case of shading pattern as shown in Fig. 9. The group one receives an irradiation 900W/m² and the remaining groups receive 600W/m² and 200W/m² respectively.

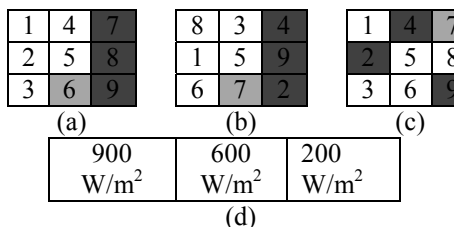


Fig.

9. Shading pattern for 3x3 arrangements for case-3.

- (a) TCT Arrangement (b) Magic Square arrangement

(c) Shade dispersion with Magic Square technique

(d) irradiation levels

The calculations for voltage and powers are noted down in table-6.

Table-6: Location of GP in TCT and Magic Square

TCT Arrangement			MAGIC SQUARE		
Row current in the order in which panels are bypassed	Volta ge	Power	Row current in the order in which panels are bypassed	Volta ge	Power
	V _a	P _a		V _a	P _a
I _R ₃	1.7I _m	3V _m	5.1 V _m I _m	I _R ₁	1.7I _m
I _R ₂	2.0I _m	2V _m	4.0 V _m I _m	I _R ₂	2.0I _m
I _R ₁	2.0I _m	-	I _R ₃	2.0I _m	-

The experimental and simulated P-V characteristics are shown in Fig. 10(a) and Fig. 10(b) respectively for TCT and Magic Square. The corresponding maximum powers obtained in TCT are 1.184W, 1.43W and to that of Magic Square are 1.596W, 1.793W. After the physical locations of the modules are changed, the power generated in the array is increased by 34.8% and 25.38% from TCT to Magic Square.

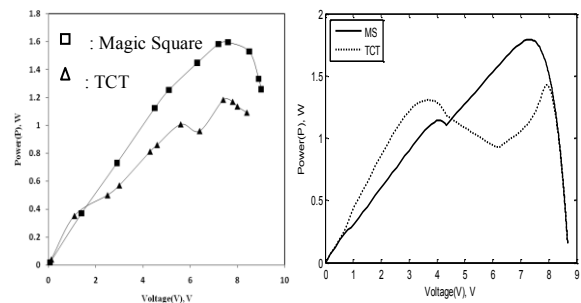


Fig.10. Power versus Voltage characteristics for Case-3

- (a) Experimental P-V characteristics for TCT and MS
- (b) Simulated P-V characteristics for TCT and MS

Case-4 (Long-Narrow)

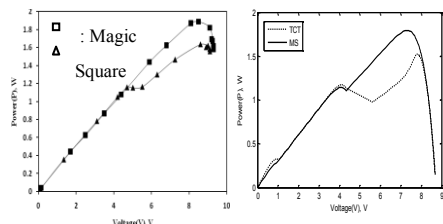
Solar array with three distinct groups of panels are taken in this case of shading pattern as shown in Fig. 11. The group one receives an irradiation 900W/m² and the remaining groups receive 600W/m² and 200W/m² respectively.

Fig.11. Shading pattern for 3X3 arrangements for case-4. (a) TCT Arrangement (b) Magic Square arrangement
(c) Shade dispersion with Magic Square technique
(d) irradiation levels

The experimental and simulated P-V characteristics are shown in Fig. 12(a) and Fig. 12(b) respectively

Case	Maximum Power (W) (900W/m ² , 600W/m ² and 200W/m ²)		Power Enhancement (%)
	TCT Configura- tion	Magic Square Configura- tion	
1(SN)	1.445	1.53	5.88
2(LW)	1.52	1.638	7.76
3(SW)	1.184	1.596	34.8
4(LN)	1.634	1.887	15.48

for TCT and Magic Square. The corresponding maximum powers obtained in TCT are 1.634W, 1.522W and to that of Magic Square are 1.887W, 1.793W. After the physical locations of the modules are changed, the power generated in the array is increased by 15.48% and 17.81% from TCT to Magic Square.

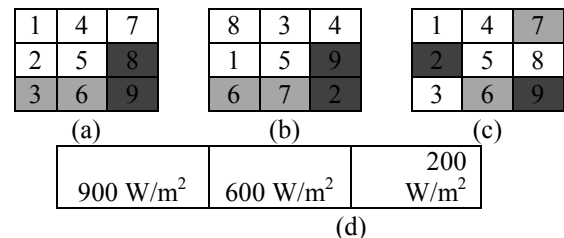


Case	Maximum Power (W) (900W/m ² , 600W/m ² and 200W/m ²)		Power Enhancement (%)
	TCT Configura- tion	Magic Square Configura- tion	
1(SN)	1.425	1.793	25.82
2(LW)	1.487	1.672	12.44
3(SW)	1.43	1.793	25.38
4(LN)	1.522	1.793	17.81

Fig. 12. Power versus Voltage characteristics for Case-4

- (a) Experimental P-V characteristics for TCT and MS
- (b) Simulated P-V characteristics for TCT and MS

It is clearly observed from Table-7 and Table-8, In all the four cases the power generated by the Magic



Square configuration is higher when it is compared with TCT arrangement.

Table-7: Simulated summary of power generated in TCT and Magic Square configurations

Table-8: Experimental summary of power generated in TCT and Magic Square configurations

CONCLUSIONS

This paper presents a novel interconnection method to maximize the power output of partially shaded solar PV array. The detailed explanation for changing panel locations without changing electrical connections is illustrated with tables and figures. Simulation and experimental results clearly confirm and demonstrate that the magic square connection gives better power output than TCT configuration. The magic square method successfully eliminated the local peaks presented in TCT configuration, which makes ease for the maximum power point tracking. The proposed method is easy to implement and eliminates the use of current sensors. The proposed method is simple and scalable for higher power applications. These merits make the proposed method to implement in high power solar PV arrays.

REFERENCES

- [1] El Badawe M, Iqbal T, Mann G K, "Optimization and a comparison between renewable and non-renewable energy systems for a telecommunication site", 25th IEEE Canadian Conference on Electrical & Computer Engineering (CCECE), pp.1 – 5, 2012.
- [2] De Soto, W., "Improvement and Validation of a Model for Photovoltaic Array Performance", Solar Energy, pp.78-88, 2006.
- [3] D. King, J. Dudley, and W. Boyson, "PVSIM: a simulation program for photovoltaic cells, modules, and arrays", 25th Photovoltaic Specialists Conf., 1295-1297, 1996.
- [4] Kumar.P, Biswas.S and Kumari.S; "Building integrated photovoltaic generation system", 1st International Conference on Non Conventional Energy (ICONCE); pp.80 – 83, 2014.
- [5] Nabeel A.Al-Rawi, Maan M.Al-Kaisi and Dhaia J.Asfer, "Reliability of photovoltaic modules II. Interconnection and bypass diodes effects", Solar Energy Mater. Solar Cells, vol. 31, no. 4, pp.469 -480, 1994.
- [6] Patnaik, B. ; Sharma, P. ; Trimurthulu, E. ; Duttagupta, S.P. ;Agarwal, V., "Reconfiguration strategy for optimization of solar photovoltaic array under non-uniform illumination conditions", 37th IEEE Photovoltaic Specialists Conference (PVSC), pp. 1859 – 1864, 2011
- [7] Young-Hyok Ji ; Jun-Gu Kim ; Sang-Hoon Park ; Jae-Hyung Kim ;Chung-Yuen Won "C – language based PV array simulation technique considering effects of partial shading", IEEE International Conference on Industrial Technology, ICIT 2009, pp. 1-6, 2009.
- [8] B.J Rani, G.S. Ilango, And C. Nagamani "Enhanced Power Generation from PV Array under Partial Shading Conditions by Shade Dispersion Using Su Do Ku Configuration", IEEE Trans. Sustain Energy, Vol.4, no.3, 594 – 601, 2013

- [9] P. Srinivasa Rao, , G. Saravana Ilango, , and Chilakapati Nagamani, "Maximum Power from PV Arrays Using a Fixed Configuration Under Different Shading Conditions", IEEE journal PV, vol. 4, no. 2, 2014
- [10] L. F. L. Villa, D. Picault, B. Raison, S. Bacha, and A. Labonne, "Maximizing the power output of partially shaded photovoltaic plants through optimization of the interconnections among its modules", IEEE Photovol., vol. 2, no. 2, pp. 154–163, Apr. 2012.
- [11] Namani. Rakesh, T.V. MadhavaRam, K. Ajith, G. RajendraNaik,P.NagarjunReddy., "A new technique to enhance output power from solar PV array under different partial shaded conditions", IEEE Conference on Electron Devices and Solid State Circuits(EDSSC), pp. 345 - 348, 2015
- [12] Namani. Rakesh, T.V. MadhavaRam, "Performance enhancement of partially shaded solar PV array using novel shade dispersion technique", Front. Energy in Springer, Vol. 10, No.2, pp. 227–239, 2016
- [13] Bidram, A., Davoudi, A., Balog, S., "Control and circuit techniques to mitigate partial shading effects in Photovoltaic arrays", IEEE Photovoltaic's, pp. 532 –546, 2012.
- [14] Gazoli, J.R., Ruppert, E., Villalva, M.G., "Modeling and circuit – based simulation of photovoltaic arrays", Braz. J. Power Electron., pp.35–45, 2009.
- [15] Yaw-Juen Wang, Po-Chun Hsu, "An investigation on partial shading of PV modules with different connection configurations of PV cells", Energy 36, pp.3069 – 3078, 2011.
- [16] Srinivasa Rao. P, Saravana Ilango. G, Dinesh. P, Nagamani.C,"Optimal Su-Do-Ku based interconnection scheme for increased power output from PV array under partial shading," Front. Energy in Springer, Vol. 9, No. 2, pp. 199 – 210, 2015

Design, Development and Testing of Solar Iron Box

¹ Md. Mehar Ali, ² Kala Devi Supriya
^{1,2}School of Renewable Energy and Environment
JNTU, Kakinada, India

^{3*} Namani Rakesh, ⁴ Udagula Malavya
Department of Electrical Engineering
³ RGUKT, Basar, Nirmal, Telangana, India
⁴ CITS, Warangal, Telangana, India
* namanirakesh@rgukt.ac.in

Abstract— The under developed smart cities are facing a problem of minimization of domestic charcoal supply for heating in cloth ironing. Cloth ironing run by charcoal have mostly influenced the domestic coal utilization. Use of charcoal for cloth iron work causes environmental pollution. Due to presence of sulphur dioxide content in coal, burning of coal liberates SO₂ which has detrimental effect on our respiratory system. Carbon dioxide, Carbon monoxide and particulates emission from coal based thermal cloth iron work also forms major Environmental pollutants. To address these problems a solar based iron press has been developed and tested through experimentation. Finally, the proposed system has analysed for compatibility check to develop the product in real market. The proposed system has analysed, tested and payback calculations have done for feasibility of product development and also validated through experimental results.

Keywords— *Solar Iron Box, Cloth Ironing, Solar PV energy and Domestic Coal*

1. INTRODUCTION

Now days, Energy is the major resource. The global primary energy demands are met from coal, oil, natural gas, nuclear etc. It is well known that utility of electricity has been drastically increased which led to power crisis problem. In order to overcome this problem additional generation is required. Coal, oil etc are playing a vital role in generation of electricity, in order to cope up with present day demand. Due to this drastic usage of conventional sources, there raising an enormous impact on environment. By burning of these fossil fuels leading to emission of harmful gases like CO₂ into the atmosphere, causing green house effect and exhaust of fuels [1]. As this is the burning issue today, it can be answered with the generation of power through renewable sources. In spite of advantages of the renewable resources such as reliability, free of cost, requires less maintenance etc, the renewable generation mix technology with hydro, wind and solar energy has been integrated in the power system [2].

In spite of all advantages of renewable sources, the solar power generation is most preferable compared to other renewable sources because solar energy is widely available and it is free of cost. Solar energy can be converted into direct current electricity by photo voltaic effect. In view of the solar power generation, the utilization of solar energy has become popular in building solar wall system & stand-alone system [3], [4]. Due to variation in light intensity and temperature

from solar irradiations, there are various techniques has been adopted in order to track the maximum power. To maintain high efficiency, PV system should be operated optimally in all conditions including during partial shading. To obtain the maximum power, PV system is normally equipped with Maximum Power Point (MPP) tracker in their power converter control algorithm. In order to track the Global Peak (GP), many MPP tracking techniques have been proposed [5–7]. Recently artificial intelligence methods which include Fuzzy [8] and Neural Network [9] have been applied to track the MPP. In these methods, vast amount of training data is required for the system to be modeled accurately. The generated power is in the form of low voltage which can be increased by using DC-DC converters for utilization. The high voltage output from the converter is used by the inverter to generate the AC power for driving the induction motor [10].

Today in our modern world we have every new technology like washing machine for clothes, vacuum cleaners for cleaning, refrigerators for cooling and in some cases, even cooking machines also finding their way in our home. But from long time we do not have an Efficient Ironing Machine in our homes. The main reason why we do not have any ironing machine is the large variety of clothes that are used around the world. One of the motives of designing this machine is to ease out the efforts needed in ironing. Also it will lead us one-step closer to smart homes, which is going to be the technology of the future.

2. HISTORY OF IRONING

Chinese are first to introduce the ironing, they used pans packed with hot coals were pressed above stretched. This method of ironing started 1000 years ago. People in North Europe have used stones, glass and wood with pressure in absence of heat to iron clothes.

Different types of ironing methods:

a) Steam Iron

Before electric irons, steam irons are most popular. Coal has burn to convert water into steam, the steam with mechanical pressure is used for removing the wrinkles on clothes. This method is useful for soft water. If the water is hard, this method is not suitable since hard water form scales, and also white calcium powder which damage the life of clothes, moreover this method takes more time to start the ironing and it is costlier than electric iron.

b) Coal Iron

All commercial cloth iron works are coal base irons. This type of system produces heat by burning the chemical energy of coal. The generated heat energy is used for ironing. The production of byproducts such as Ash, CO₂ and SO₂ are drawbacks of these type systems. Ash changes the PH values of soil & ground water, it effects on plant growth and ecosystem. CO₂ causes for global warming. If a person is exposed to CO₂ to 30,000 ppm it effects slightly. If it is between 70,000-1,00,000 ppm the person becomes unconscious, SO₂ vapors more than 0.2ppm causes irritation, cough and shortness of breath and also effects lungs operation.

c) Electric Iron

It works on the principle that whenever current passes through the high resistance it generates heat energy (I^2Rt). The generated heat is used with mechanical pressure to remove the folds on clothes. This is simple and easy and also less time taken for ironing compared to steam iron.

3. PROPOSED SOLAR IRON

Domestic coal supply for cloth ironing in under developing smart cities is facing the issue of pollution and health hazards for last few years. Conventional cloth iron which runs by coal has faced the dearth. The proposed solar iron system is shown in Fig.1. In the proposed solar iron system, sun energy is converted into electric current using PV cells and this electric current passes through the heating element which generates heat. The generated heat energy with mechanical pressure is used to remove folds on clothes.

4. PARTS FOR SOLAR IRON BOX

The proposed system consists of the following parts and its function has explained in detailed along with its specifications.

4.1 Solar Panel

Sun radiate its energy in the form of electromagnetic waves and these electromagnetic waves are converted into electricity by means of solar cells. The number of cells is connected in series or parallel combinations to form a solar panel. The number of cells is connected in series or parallel to meet the supply requirement. Panels are connected in Series to increase the voltage and connected in Parallel connection to increase the current. Solar panel efficiency depends on type of material used in the PV cells. The efficiency value is in between the 15 to 19 %. Most of the Solar Panels have manufactured with crystalline silicon.

4.2 Charge Controller

Charge controller is used to charge the battery. These are of two types one is PWM base, and another one is MPPT method. In these two methods MPPT is more efficient method of charging. The battery does not efficiently charge without charging circuit. The charge controller protects the battery from over discharge and over charging. It also protect the battery from short-circuit.

Batteries are charged by two methods, one is constant current method, and another one is constant voltage method. Constant current method is best one compared to constant voltage. But it takes more time than constant voltage method. In constant voltage method initially the rated charging voltage has applied to the battery, but the battery temperature will increase.

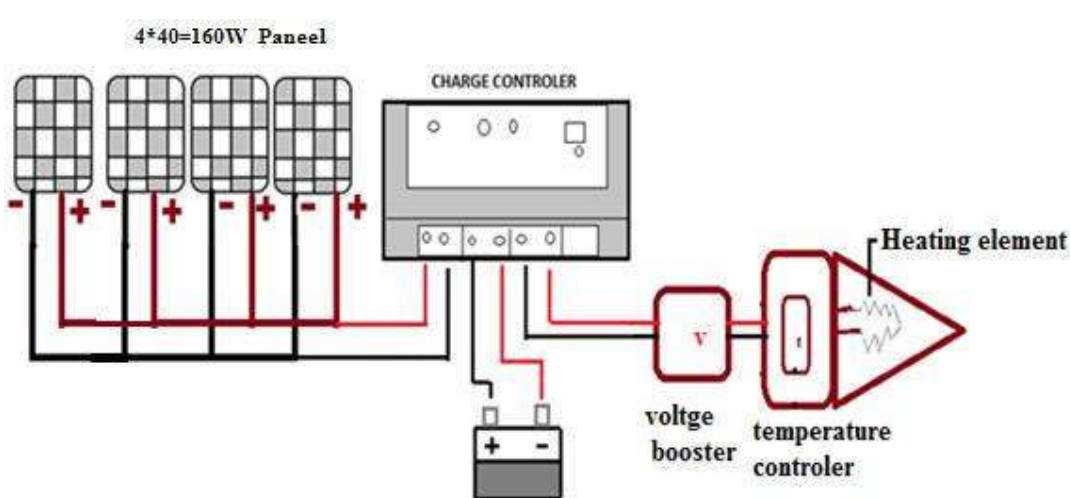


Fig. 1. Proposed system block diagram

Constant voltage method take less time to charge the battery compared to constant current method. The device factory default settings normally in open mode, if you need light control or light control plus timing mode, it need to open and close through set dip switch. When the key set ON is 1 normally close and the key set OFF is 0 normally open.

4.3 DC to DC Voltage Booster

Any normal battery gives 12V DC, to improve the voltage level of DC 12V to the desired value of voltage, convert 12V DC to AC using inverter, and this 12V AC is boost by a transformer or by DC-DC boost converter. For small ratings, usage of Inverters is costlier. So generally for small rating applications DC-DC boost converter are the most suitable. In this proposed system, **2x 150W, 12V - 35V DC-DC boost converter**, this voltage boosters increase the current flow in the heating element, due to this heat output value will increase. If we neglect power loss in the boosting circuit, input and output power is will be same.

The main advantage of DC-DC boost converter circuit is it maintains the output voltage constant from no load to full load. Without DC-DC boost converter the load voltage varies according to load due to drooping characteristics of solar cells. The output voltage of the DC-DC boost converter is set by using the potential divider. The output voltage can be varied according to resistance value of the potential divider.

4.4 Pilot Lamp

The pilot lamp in the proposed system is used for indication of ON state of heating element. If pilot lamp glows it means the heating element is generating heat and vice versa. The pilot lamp in the proposed system is 12V DC LED.

4.5 Heating Element

The heating element is one of the main parts of the proposed system, the heat output of the heating element depend on the current flow through that element and resistance of that element (I^2Rt). The rated heating capacity of the element depends on rated current carrying capacity and type of materials used in manufacturing of heating element. To decrease the resistance value of heating element, they are connected in parallel. To heating element coils are insulated with mica. The heating element wattage is reduced by removing some coils in the element.

4.6 Temperature Controller

Temperature controller controls the temperature of heating element by ON and OFF of the supply. Temperature controller contains the sensor, relay circuit, transducer. The sensor senses the temperature of the heating element and it converts heat into electric energy by transducer, this transducer give to electric signal to the comparator. The comparator compares the set point temperature to the actual value of heating

element. According to this, it will ON and OFF the element using relay to maintain the temperature as set point.

4.7 Sole Plate

Sole plate is a triangle shaped cast iron plate, which carries the heating element and temperature sensor, sole plate transfer the generated heat in the element to the cloth; bottom of sole plate is made-up of Brass for smooth operation and rust proof. The thickness of sole plate is 1.5cm, and its weight is 2kg.

4.8 Pressure Plate

Weight to wattage ratio is one of important factor for good iron, using pressure plate, good ironing can be done with low heat. Low heating element is sufficient with high weight pressure plate. Thickness of pressure plate used in proposed system is 3 cm, and 4kg weight.

4.9 Cover Plate

The cover plate is above the sole plate which covers the heating element. It is made up of stainless steel, 0.5 cm thickness and weight of 1 kg. It covers the heating element, and resists the heat dissipation of heating coil through surrounding air.

4.10 Handle

The handle is made with wood which is used for carry the whole iron box. Wood has good heat resistance, electric resistance. It is painted to increase its life time and handle is attached to the pressure plate.

4.11 Battery

Battery is electro chemical device which converts chemical energy into electrical energy and vice versa. Batteries are mainly of two types one is primary which are not rechargeable and another one are secondary batteries which are rechargeable. 90% batteries are lead acid batteries (secondary batteries). Battery capacity measured in Ah (Ampere Hours). Batteries are connected in series to increase its voltage and connect in parallel to increase current. In the proposed system 7.62 Ah battery (Lead-Acid) is used. Battery is used to back up supply when solar energy is less. In the proposed system batteries are charged using solar panel and charge controller circuit.

5. CALCULATIONS & TABULATION

In this paper the payback period calculations of a solar iron box with a simple mathematical equation has given below. The calculations of the payback period have done on basis of fuel saving cost for the proposed system.

5.1 Simple Pay Back

The payback period is the length of time required to recover the cost of an investment. The payback period of a given investment or project is an important determinant of whether to undertake the position or project and longer payback periods are typically not desirable for investment positions.

$$\text{Simple pay back} = \frac{\text{Initial Investment}}{\text{Net Annual saving per year}}$$

5.2 Internal Rate of Return (IRR)

The internal rate of return on an investment or project is the "annualized effective compounded return rate" or rate of return that sets the net present value of all cash flows (both positive and negative) from the investment equal to zero. Equivalently, it is the discount rate at which the net present value of future cash flows is equal to the initial investment, and it is also the discount rate at which the total present value of costs (negative cash flows) equals the total present value of the benefits.

$$\frac{\text{cash flow value}}{(1+IRR)^{\text{time}}} - \text{Initial Investment} = 0$$

5.3 Net Present Value (NPV)

$$\text{NPV} = (\text{PV Inflows}) - (\text{PV Outflows})$$

$$NPV = \sum_{t=1}^T \frac{C_t}{(1+r)} - C_o$$

Where C_t =Net cash inflow throughout the period

C_o =Total industrial costs

r = Number of time periods

The difference between the present value of the future cash flows from an investment and the amount of investment. Present value of the expected cash flows is computed by discounting them at the required rate of return.

The following case studies have done for cash flow of rupees 7,500 with discount of 21.406 and cash flow of rupees 6,300 with discount of 21.649 respectively.

Case-1: NPV for Cash flow in month for discount 21.406

Year	Cash flow in month (Rupees)	Discount	NPV
1	7500	21.406	6177.6
2	7500	21.406	5088.3
3	7500	21.406	4191.2
4	7500	21.406	3452.2
5	7500	21.406	2843.5
6	7500	21.406	2342.1
7	7500	21.406	1929.21
8	7500	21.406	1589.05
9	7500	21.406	1308.8
10	7500	21.406	1078.01
Total Net Present Value			30000.06

Case-2: NPV for Cash flow in month for discount for 21.649

Year	Cash flow in month (Rupees)	Discount	NPV
1	6300	21.649	5178.8
2	6300	21.649	4257.19
3	6300	21.649	3499.57
4	6300	21.649	2876.77
5	6300	21.649	2364.8
6	6300	21.649	1943.9
7	6300	21.649	1598.0
8	6300	21.649	1313.62
9	6300	21.649	1079.8
10	6300	21.649	887.6
Total Net Present Value			25000.05

6. EXPERIMENTAL RESULTS & DISCUSSION

The experiment has conducted with four solar panel of each rated with 40 W. The solar panel is connected through DC-DC boost converter to Iron press. The experimental set-up is shown in Fig. 2.



Fig. 2. Proposed system Experimental Setup

PRACTICAL TESTING RESULTS

The practical testing results have shown in the following table and observed the time taken to reach 100 degrees temperature for different load. The Heat time curve has shown in Fig. 3. The economic results have given in detail for better understanding.

S.No	Load Voltage(V)	Load Current(A)	Power (W)	Time taken to reach 100° temperature (Min)
1.	20.1	3.7	74.37	35
2.	25.3	4.7	118.91	30
3.	30.7	5.6	171.92	20

Battery Charging Results with Panel voltage of 19V

S.No	Charging Voltage (V)	Charging Current (A)	Time
1.	14.1	0.5	11:30 AM
2.	14.1	0.31	12:00 PM

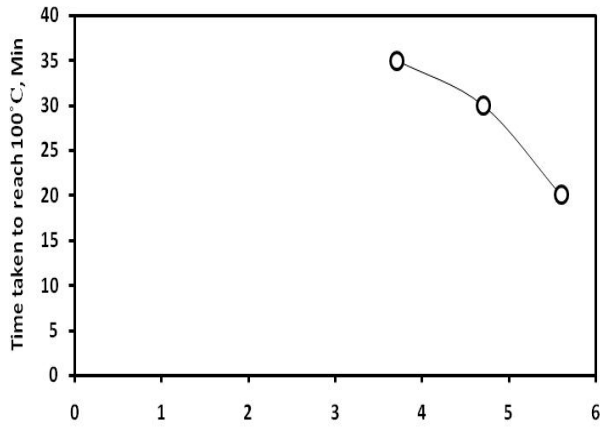


Fig.3. Heat Time Curve

ECONOMICAL RESULTS

IRR of Conventional System = **21.649**

% IRR of Proposed System = **21.406 %**

NPV of Conventional System = **Rs. 9185.196**

NPV of Proposed System = **Rs.10,696.676**

Simple payback period (in terms of fuel saving cost) = **0.6944 years**

With new solar ironing (in terms of fuel saving cost) = **2.0833 years**

7. CONCLUSION

The proposed system is solution for problems faced by domestic (commercial) coal based system. The proposed

system is beneficial to our life regarding economically, environmentally and socially. The proposed system has not any running cost and negligible maintains. It is new era for ironing environment which gives solutions of future troubles. Its pay back calculations explain the financial advantages. The Proposed system with battery backup gives continuous and uniform heating for ironing. Due to auto temperature control time taking for ironing is less compared to the conventional system. The proposed system is heavy weight, due to this low wattage heating element, that mean it consume less power than conventional domestic electric iron. A case study gives a great evidence for believing in implementation of the product in real life. Several tests are implemented sincerely to support the product.

REFERENCES

- [1] Mohibullah, Imdadullah and Ashraf; “Estimation of CO₂ Mitigation Potential through Renewable Energy Generation”; IEEE conference on Power and Energy, pp.24 – 29, 2006.
- [2] Sousa. J and Martins. A; “Optimal renewable generation mix of hydro, wind and photovoltaic for integration into the Portuguese power system”; pp.1 – 6, 2013
- [3] Sree. B., Ramaprabha. R. and Mathur. B. L.; “Modeling and controlling of standalone solar photovoltaic charge system”; Emerging Trends in Electrical and Computer Technology (ICETECT), pp.78 – 81, 2011.
- [4] Sanjeeva Reddy. B. R., Jambholkar. P., Badari Narayana and Srinivasa Reddy; “MPPT A logarithm Implementation for Solar Photovoltaic Module Using Microcontroller”, India Conference (INDICON); pp.1-3; 2011
- [5] Koutroulis. E., Blaabjerg. F.; “A new technique for tracking the global maximum power point of PV arrays operating under partial – shading conditions”, IEEE Photovoltaic’s, pp. 184 –190, 2012.
- [6] Gomes. M. A., Galotto Jr., L., Sampaio. L., Melo. A., Canesin. C. A.; “Evaluation of the main MPPT techniques for photovoltaic applications”, IEEE Transactions Industrial Electronics, pp.1156 – 1167, 2013.
- [7] Kashif. M. F., Sehwa Choi, Yongsoon Park, Seung – Ki Sul; “Maximum power point tracking for single stage grid-connected PV system under partial shading conditions”; 7th International Power Electronics and Motion Control Conference (IPEMC), Vol.2, pp.1377 – 1383, 2012.
- [8] Veerachary. M., Senju. T., and Uezato K.; “Neural network – based maximum – PowerPoint tracking of coupled – inductor interleaved boost converter supplied PV system using fuzzy controller”, Transactions Industrial Electronics, pp.749–758, 2003.
- [9] Syafaruddin, Karatepe. E., Hiyama. T., “Polar coordinated fuzzy controller based real-time maximum power point control of photovoltaic system”, Renewable Energy, pp. 2597–2606, 2009.
- [10] Jin C, Jiang W., “Design of a digital controlled solar water pump drive system for a nano-filtration system”, IEEE PEDS, Singapore, 2011.

Battery Management System for Solar PV Panel

Namani Rakesh^{1*}, T. Santosh², Udugula Malavya³ and D. Rishikesh⁴

Department of Electrical Engineering

¹Rajiv Gandhi University of Knowledge Technologies, Basar, Telangana, India

²National Institute of Technology, Tiruchirappalli, Tamilnadu, India

³Kamala Institute of Technology and Science, Singapur, Telangana, India

⁴Kakatiya Institute of Technology and Science, Warangal, Telangana, India

*e-mail: namanirakesh@rgukt.ac.in

Abstract – This paper deals the development of MPPT algorithm employing incremental conductance method with boost converter for stand-alone operation of PV system. The PV Panel have been modeled using MATLAB/Simulink and simulated results are furnished. Overcharging and deep discharging may damage the life of battery. It's essential to maintain the limits of battery charging. The charge control has been developed by a microcontroller. The prototype PV system consisting of PV panels, boost converter and battery has been built in the laboratory for experimental investigations. The successful hardware implementation shows the efficacy of the proposed system.

Keywords – Solar PV Array, Battery Management System,

I. INTRODUCTION

Now days, Energy is the major resource. The global primary energy demands are met from coal, oil, natural gas, nuclear etc. It is well known that utility of electricity has been drastically increased which led to power crisis problem. In order to overcome this problem additional generation is required. Coal, oil etc are playing a vital role in generation of electricity, in order to cope up with present day demand. Due to this drastic usage of conventional sources, there raising an enormous impact on environment. By burning of these fossil fuels leading to emission of harmful gases like CO₂ into the atmosphere, causing green house effect and exhaust of fuels [1]. As this is the burning issue today, it can be answered with the generation of power through renewable sources. In spite of advantages of the

renewable resources such as reliability, free of cost, requires less maintenance etc, the renewable generation mix technology with hydro, wind and solar energy has been integrated in the power system [2].

In spite of all advantages of renewable sources, the solar power generation is most preferable compared to other renewable sources because solar energy is widely available and it is free of cost. Solar energy can be converted into direct current electricity by photo voltaic effect. In view of the solar power generation, the utilization of solar energy has become popular in building solar wall system & stand-alone system [3-4].

Due to variation in light intensity and temperature from solar irradiations, there are various techniques has been adopted in order to track the maximum power. To maintain high efficiency, PV system should be operated optimally in all conditions including during partial shading. To obtain the maximum power, PV system is normally equipped with Maximum Power Point (MPP) tracker in their power converter control algorithm. In order to track the Global Peak (GP), many MPP tracking techniques have been proposed [5-7]. Recently artificial intelligence methods which include Fuzzy [8] and Neural Network [9] have been applied to track the MPP. In these methods, vast amount of training data is required for the system to be modelled accurately.

There are three basic types of dc-dc converter circuits, termed as buck, boost and buck-boost. In all of these circuits, a power device is used as a switch. DC – DC converters were called 'choppers'. The buck converter is called as 'step-down chopper', whereas boost converter is called as 'step-up

chopper'. The buck-boost converter can step-up and step down the input voltage. In this study of application the solar power generation is limited to day-time applications, so that the storage cost has been neglected which is the most considerable problem [10]. In this paper boost converter has been used. The high frequency pulses are generated and fed to the switch. The switch may be SCR, IGBT, and MOSFET etc [11]. In this paper, a simple MPPT based Boost converter has been interfaced between the PV module and battery to track the maximum available power from the PV module [12]-[13]. The paper deals with modelling of solar PV module, proposed system, results and conclusion.

II. MODELLING OF THE PV MODULE

A PV module is developed in MATLAB/SIMULINK platform. The modelled PV module characteristics are shown in Fig. 1. The module makes use of the Eqns. of a typical PV cell.

PV cell current given by

$$I_{PV} = I_{PH} - I_O \left(\exp\left(\frac{q(V + (R_{SE} \times I_{PV}))}{A \times K_B \times T}\right) - \frac{V + (R_{SE} \times I_{PV})}{R_{SH}} \right) \quad (1)$$

$$I_{PV} \cong I_{PH} - I_O \left(\exp\left(\frac{q(V + (R_{SE} \times I_{PV}))}{A \times K_B \times T}\right) \right) \quad (2)$$

When PV cell in open circuit condition

$$I_{PV} = 0$$

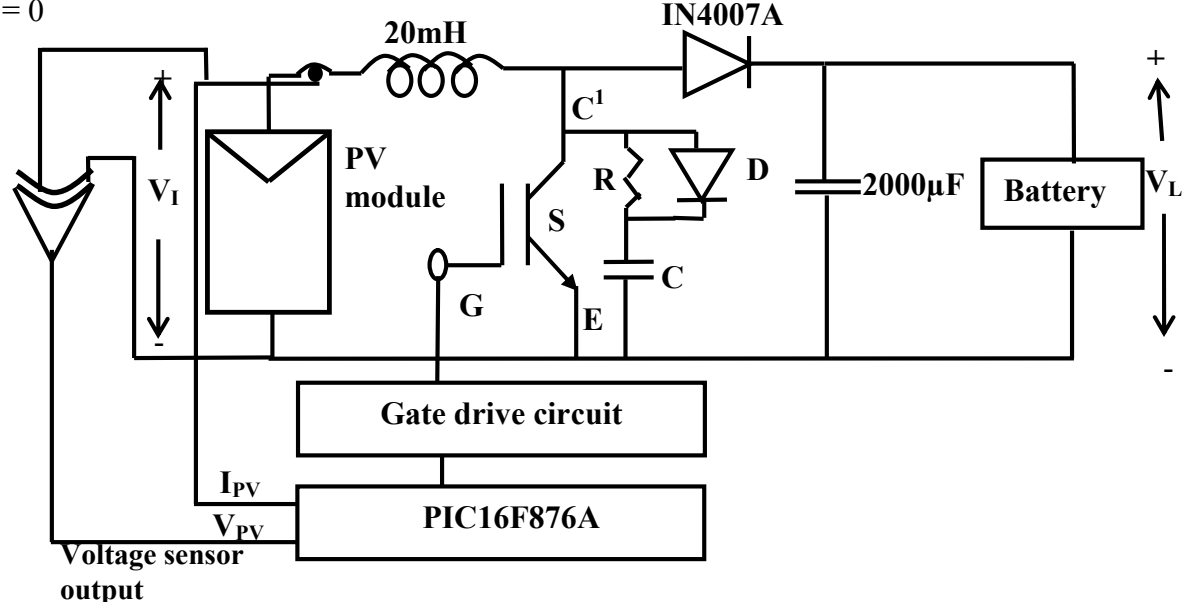


Fig. 2 Power circuit of the proposed stand-alone PV system

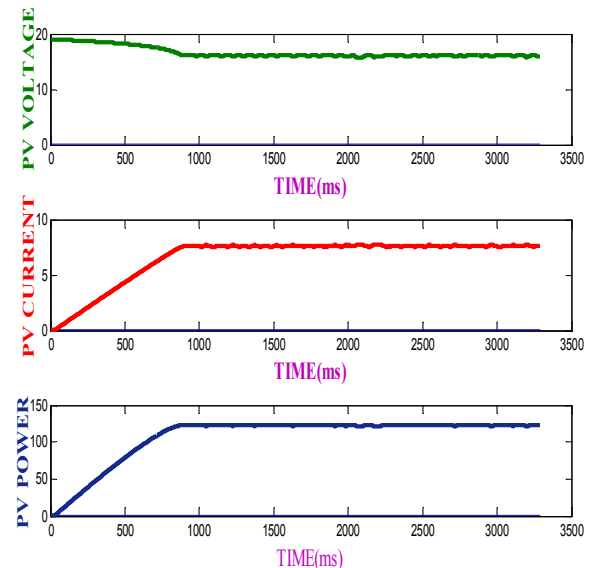


Fig. 1 PV module voltage, current and power vs time with MPPT

$$I_{PH} = I_O \left(\exp\left(\frac{q(V_{OC})}{A \times K_B \times T}\right) \right) \quad (3)$$

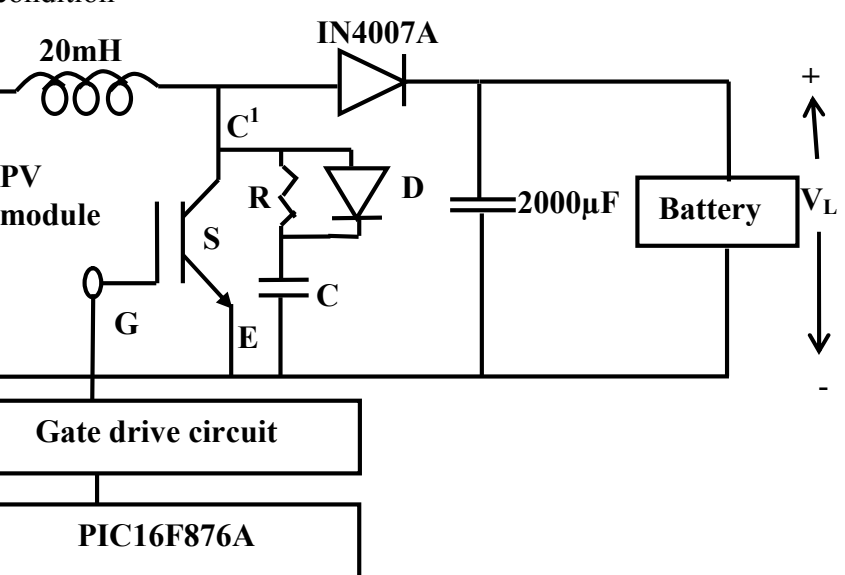
$$\text{Consider } \frac{I_O}{I_{PH}} = 10^{-9}$$

$$V_{OC} = \frac{A \times K_B \times T}{q} \times \ln\left(\frac{I_{PH}}{I_O}\right) \quad (4)$$

Substitute Equation 4 in Equation 3,

$$I_{PV} \cong I_{PH} - I_{PH} \times 10^{-9} \times \left(\exp\left(\frac{V + (R_{SE} \times I_{PV})}{V_{OC} / 20.723}\right) \right) \quad (5)$$

Here $I_{PH} \approx I_{SC}$



III. PROPOSED SYSTEM

The power circuit of the proposed stand-alone PV system is shown in Fig. 2 PV module is connected with the boost converter. In boost converter, IGBT is used as a switching device. For implementing the MPPT algorithm, the laboratory made PIC16F876A microcontroller has been used. The microcontroller has been connected with the boost converter through gate driver circuit (IDS12.12WSELOO). The maximum allowable switching frequency of gate driver is 100 KHz, and also provides the isolation between power and control circuit with IGBT switch protection. The RCD snubber circuit is employed for providing the dv/dt and di/dt protection to the switch. The designed value of the snubber components are $R=10K\Omega$, 10W, $C = 0.22\mu F$, 1000V dc. Then, the output of the boost converter is connected with the two number of 12V, 7AH batteries in series and a resistive load connected across batteries through switches. One microcontroller is used for MPPT and another microcontroller is used for battery charge control. Relay switches on both sides are automatically controlled by PIC16F876A (second). It will sense the battery voltage through voltage sensor. Whenever the voltage across batteries greater than 25.4V switch S1 will open similarly if batteries voltage is less than 23.2V switch S2 will open automatically by microcontroller. For driving the relays transistor based relay circuit is used. The complete hardware circuit setup is as shown in Fig. 3.

IV. HARDWARE RESULTS

Fig. 4 shows the variation of duty cycle during tracking of maximum power from PV system. Fig. 5 shows PV voltage, current and duty cycle at maximum power point at particular radiation. It is to be noted from the Fig. 4 that the duty cycle of the boost converter approximately 30%, The PV voltage and current are 16.8V and 6.08A. So obtained maximum power is in this condition 102 watts. Fig. 6 shows output current and battery current. Fig. 7 shows current through the load and battery voltage

at this particular irradiation. Boost converter output voltage and current at this point are 24.2V, 4.03A. Hence the output power of boost converter is 97.5 watts which has been used for charging the batteries. Fig. 8 shows the battery overvoltage and under voltage conditions.



Fig. 3 Hardware Setup

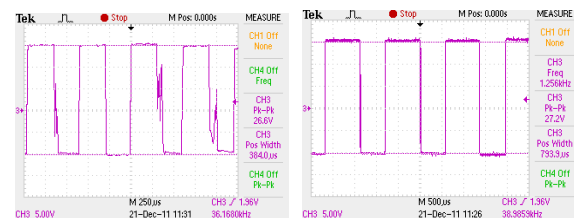


Fig. 4 Variation of duty cycle during maximum power tracking



Fig. 5 Gate pulse, PV voltage and current at maximum power point for a particular irradiation

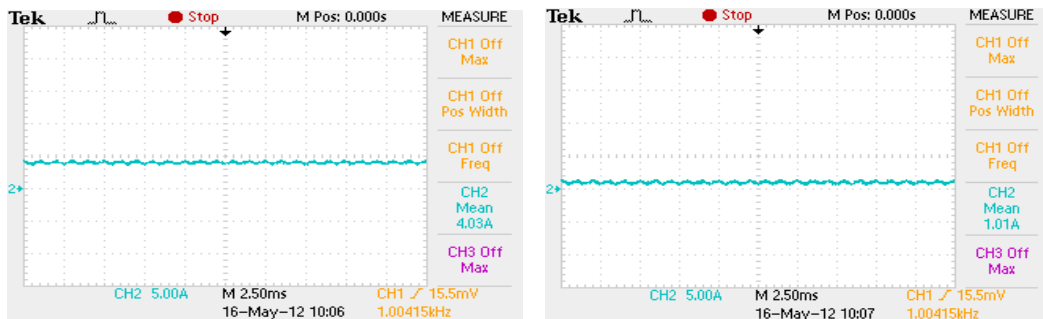


Fig. 6 Output current and battery current at maximum power point for a particular irradiation

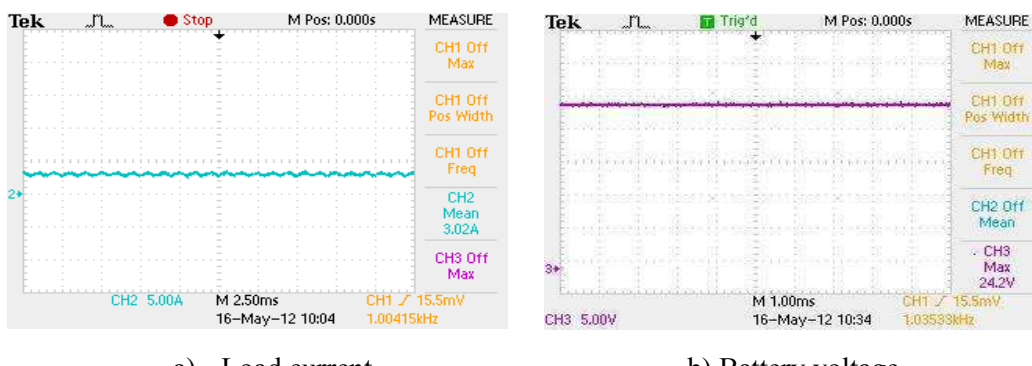


Fig. 7 Load current and battery voltage

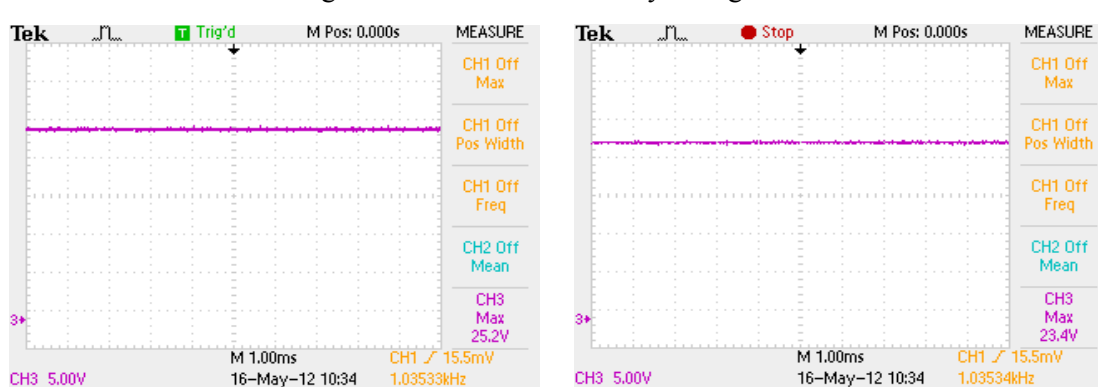


Fig. 8 Battery overvoltage and under voltage

CONCLUSIONS

The incremental conductance based MPPT algorithm employed with boost converter has been carried out to extract maximum power from solar panel in hardware. Since the proposed system is a stand-alone system with batteries. Design is made to optimize the batteries along with ratings. Further charge controller is also introduced to protect the battery from overcharging and deep discharging.

The incremental conductance MPPT algorithm incorporated in boost converter has been implemented using PIC16F876A controller. Battery charge controller also implemented using PIC16F876A controller. The experimental results show that the system has good dynamic response in all the aspects.

REFERENCES

- [1] Mohibullah, Imdadullah and Ashraf; "Estimation of CO₂ Mitigation Potential through Renewable Energy Generation"; IEEE conference on Power and Energy, pp.24 – 29, 2006.
- [2] Sousa. J and Martins. A; "Optimal renewable generation mix of hydro, wind and photovoltaic for integration into the Portuguese power system"; pp.1 – 6, 2013
- [3] Sree. B., Ramaprabha. R. and Mathur. B. L.; "Modeling and controlling of standalone solar photovoltaic charge system"; Emerging Trends in Electrical and Computer Technology (ICETECT), pp.78 – 81, 2011.
- [4] Sanjeeva Reddy. B. R., Jambholkar. P., Badari Narayana and Srinivasa Reddy; "MPPT A logarithm Implementation for Solar Photovoltaic Module Using Microcontroller"; India Conference (INDICON); pp.1-3; 2011.
- [5] Koutroulis. E., Blaabjerg. F.,; "A new technique for tracking the global maximum power point of PV arrays operating under partial – shading conditions", IEEE Photovoltaic's, pp. 184 –190, 2012.
- [6] Gomes. M. A., Galotto Jr., L., Sampaio. L., Melo. A., Canesin. C. A.; "Evaluation of the main MPPT techniques for photovoltaic applications", IEEE Transactions Industrial Electronics, pp.1156 – 1167, 2013.
- [7] Kashif. M. F., Sehwa Choi, Yongsoon Park, Seung – Ki Sul; "Maximum power point tracking for single stage grid-connected PV system under partial shading conditions"; 7th International Power Electronics and Motion Control Conference (IPEMC), Vol.2, pp.1377 – 1383, 2012.
- [8] Veerachary. M., Senju. T., and Uezato K.; "Neural network – based maximum – PowerPoint tracking of coupled – inductor interleaved boost converter supplied PV system using fuzzy controller"; Transactions Industrial Electronics, pp.749–758, 2003.
- [9] Syafaruddin, Karatepe. E., Hiyama. T., "Polar coordinated fuzzy controller based real-time maximum power point control of photovoltaic system", Renewable Energy, pp. 2597–2606, 2009.
- [10] Peter. P. K., Agarwal. V.; "A compact switched capacitor dc-dc converter based Global Peak Power Point tracker for partially shaded PV arrays of portable equipment", 37th IEEE Photovoltaic Specialists Conference (PVSC), pp. 194 – 199, 2011
- [11] Wouk, Victor; "VWP; A New Approach to Small, Light, Efficient, High Power Regulated Power Supplies"; I. E, IEEE Trans. Industrial Electronics, Vol.9, no.2, pp.84-96, 1962.
- [12] Shengyong Liu Xing Zhang., Haibin Guo.,Jun Xie., "Multiport DC/DC Converter for Stand-alone Photovoltaic Lighting System with Battery Storage," *Int.conf.on Electrical and Control Engineering*, vol.5, No.2, pp.3894-3897, June 2010.
- [13] Shayani, R.A., Oliveira, M.A.G, "Global Performance Measurement of a Stand-Alone Photovoltaic System," IEE trans. on Transmission & Distribution Conference and Exposition, vol.20, No.2, pp.1-6, Aug 2006.

A New technique to extract maximum power from wind turbine

Dingari Rishikesh¹, Namani Rakesh^{2*} and Udugula Malavya³

Department of Electrical and Electronics Engineering

¹Kakatiya Institute of Technology and Science, Warangal, Telangana, India

²Rajiv Gandhi University of Knowledge Technologies, Basar, Telangana, India

³Chaitanya Institute of Technology and Science, Warangal, Telangana, India

*namanirakesh@rgukt.ac.in

Abstract – To extract maximum power from the wind, this paper proposes a novel energy conversion technique. In this manuscript, a novel Energy Conversion Device-1(ECD-1) is proposed to convert the kinetic energy from wind to mechanical energy. The obtained mechanical energy is transmitted as a liquid through the pipes. The transmitted mechanical energy is used to rotate the self-excited induction generator shaft through Energy Conversion Device-2(ECD-2). The proposed technique gives better performance and results as compared to the conventional approaches and it overcomes the major hurdle of generator burden on the tower by placing the generator at ground level or near the load. The proposed technique allows high altitude towers to get the maximum swept area so that the power extracted from the wind can be increased. The obtained waveforms at different stages of the proposed technique are compared with the conventional method for better understanding and validation. The dynamic model of the proposed system is developed and simulated in MATLAB/SimMechanics.

Keywords - Wind Power, Maximum Power Extraction, Energy Conversion Device, Kinetic Energy and Self Excited Induction Generator

1. INTRODUCTION

There is a huge dependency on fossil fuels to meet the growing energy demand. As fossil fuels are depleting fast, the gap between the generation and energy demand is also widening. The generation of power from fossil fuel pollutes the environment and emission of harmful gasses which leads to a harmful impact on living beings and environment hazards like global warming and unbalanced food chain. To address above such problems, renewable energy sources such as wind energy are the best solution. Wind energy has the huge potential of energy among all other renewable energy sources [1].

Wind energy conversion system has undergone much advancement progressively towards more big and bulk turbine size, setting up of offshore wind parks which are situated far from load centers [2]. The wind power plants are situated relatively far from load & grid infrastructure so that the cost of grid reinforcement is reliant on the huge capital investment. Thus, maximum energy extraction from wind energy system has been implemented by using various maximum power point tracking methods in the literature [3-7].

Sea-crossing engineering over a few decades had shown many improvements, in which long span multitower suspension bridge has fascinated more attention. Long span multi-tower suspension

bridges(LSMTSB) like Taizhou Yangtze River Highway Bridge and Ma'anshan Yangtze has brought these bridges to engineering practice to a new period due to qualitative performance variation between traditional double tower suspension bridges & LSMTSB [8]. In theory and engineering structures, the knowledge of LSMTSB is very deficient. Research pays much attention to vertical load [9-12]. A typical wind turbine generator of 2.5MW features 80 m (262 ft) height of a rotor hub with a blade/rotor total width 89–99 m (292–325 ft) on an approximate. The nacelle consists of electrical power and control equipment's, generator and mechanical links like wind turbine blade to machine hub and generator [13]. For the operation of a wind turbine generator (WTG) in a stand-alone micro grid, technical challenges and major considerations are explained in [14]. The technological progression in wind turbine generation has encouraged the study and experimentation of large size machines. The major problem associated with large size wind electric generator causes a huge burden on wind tower is identified through this study. To address this problem, the authors have proposed novel energy conversion devices. This paper discusses the functional structure of wind turbine, proposed model, mathematical model of energy conversion devices, simulation of a system with and without proposed model, and mechanism for change in energy from in energy conversion devices.

The paper is as follows: Section-2 deals with Wind turbine functional structure. In Section-3, Proposed Wind turbine model has discussed. Later the Mathematical modelling, Simulation results and Conclusions have presented.

2. WIND TURBINE'S FUNCTIONAL STRUCTURE

The modern wind turbine principle components are the nacelle, gearbox, the rotor, shaft and the tower. The wind turbine captures the wind's kinetic energy, which consisting of two or more blades mechanically coupled to an electrical generator. Gear box is the major mechanical component which transforms wind turbines slower rotational speed to high rotational speed on the electrical generator. It is noted that the generator is located in the nacelle of the wind turbine. Hence, the mechanical stability of the turbine will be critical during gusty wind speed. Hence, in this paper, energy conversion devices (ECD's) are proposed, and it is placed between the turbine blade shaft and gearbox.

This helps in reducing the cost of material required for construction of wind turbine, and high altitudes can be reached to capture maximum available energy from the wind. A dynamic model of ECD is designed and simulated in Matlab/SimMechanics.

3. PROPOSED WIND TURBINE MODEL

The proposed model consists of energy conversion devices shown in Fig.1. The energy conversion device is mainly composed of cylinders at opened ends, piston, and revolute mechanism. When this model is linked to the wind turbine, wind energy is converted into mechanical energy, which is transmitted by the liquid to the other end of ECD-2 through ECD-1, which is available at the ground level connected to a generator.

The flywheels rotate clockwise and counter clockwise as piston base moves up and down respectively with pressure (A) and direction of liquid flow is given by (B) as shown in Fig.2. The MATLAB schematic models of the energy conversion devices are also shown in Fig.3.

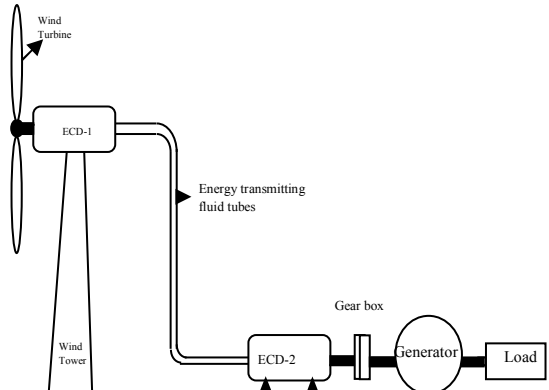


Fig.1. Proposed model wind turbine power conversion system
The flywheels rotate clockwise and counter clockwise as piston base moves up and down respectively with pressure (A) and direction of liquid flow is given by (B) as shown in Fig.3.

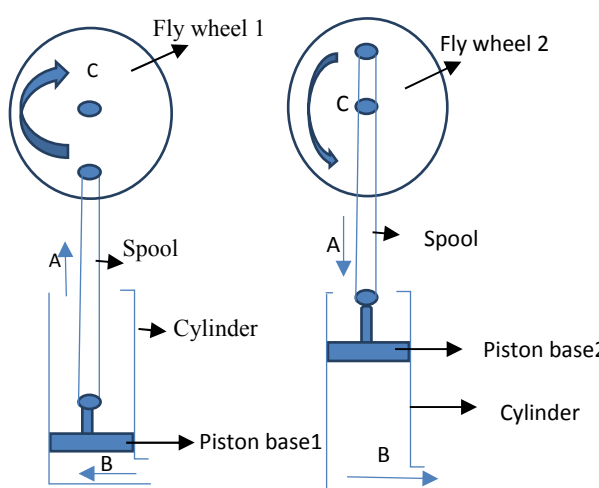


Fig. 2. Schematic diagram of ECD-1 and ECD-2

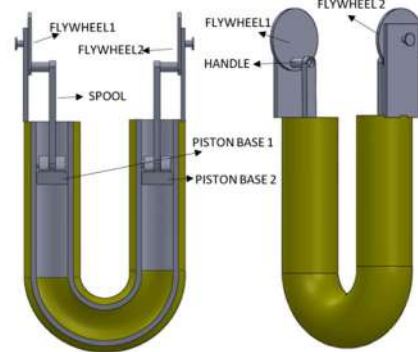


Fig. 3. Energy conversion devices schematic model

4. MATHEMATICAL MODELING OF ECD

The ECD consists of a liquid filled cylinder and piston with a narrow annular passage between them. Any relative motion between piston and cylinder is resisted by a liquid with a friction force (f_{v1}). Let the mass of piston be M_1 and M_2 . The elasticity of walls of cylinder and liquid is represented as spring (stiffness k_1) and dashpot (viscous friction coefficient f_{v2}).

Let us consider when force F_1 is applied to the piston of mass M_1 ; it moves by a distance of X_1 . The force is transmitted to the piston of mass M_2 using a spring and dashpot as shown in Fig. 4. Here, viscous frictions f_{v1}, f_{v4} and f_{v3}, f_{v5} are caused by forces acting on mass M_1 and M_2 respectively.

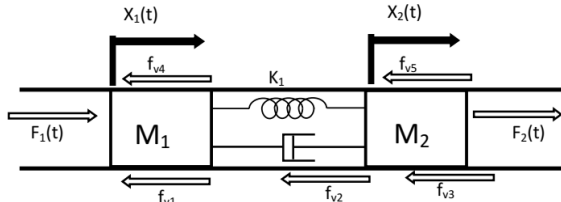


Fig.4. Block diagram representation of energy conversion device

Equation (1) and equation (2) are obtained by solving $\sum f_x = 0$.

$$(f_{v1} + f_{v2} + f_{v4}) \frac{dx_1}{dt} + M_1 \frac{d^2x_1}{dt^2} + k_1 x_1 = F_1(t) + k_1 x_2 + f_{v2} \frac{dx_2}{dt} \quad (1)$$

$$(f_{v2} + f_{v3} + f_{v5}) \frac{dx_2}{dt} + M_2 \frac{d^2x_2}{dt^2} + k_1 x_2 = F_2(t) + k_1 x_1 + f_{v2} \frac{dx_1}{dt} \quad (2)$$

Equation (3) and equation (4) are obtained by applying Laplace transformation to equation (1) and equation (2).

$$(f_{v1}S + f_{v2}S + f_{v4}S + M_1S^2 + k_1)X_1(S) = F_1(S) + (f_{v2}S + k_1)X_2(S) \quad (3)$$

$$(f_{v2}S + f_{v3}S + f_{v5}S + M_2S^2 + k_1)X_2(S) = F_2(S) + (f_{v2}S + k_1)X_1(S) \quad (4)$$

$$F_1(S) = (f_{v1}S + f_{v2}S + f_{v4}S + M_1S^2 + k_1)X_1(S) - (f_{v2}S + k_1)X_2(S) \quad (5)$$

$$F_2(S) = (f_{v2}S + f_{v3}S + f_{v5}S + M_2S^2 + k_1)X_2(S) - (f_{v2}S + k_1)X_1(S) \quad (6)$$

$$\begin{bmatrix} F_1(S) \\ F_2(S) \end{bmatrix} = \begin{bmatrix} (f_{v1}S + f_{v2}S + f_{v4}S + M_1S^2 + k_1) & -(f_{v2}S + k_1) \\ -(f_{v2}S + k_1) & (f_{v2}S + f_{v3}S + f_{v5}S + M_2S^2 + k_1) \end{bmatrix} \begin{bmatrix} X_1(S) \\ X_2(S) \end{bmatrix} \quad (7)$$

Fig.5 and Fig.6 show the angular displacement of shaft 1 and shaft 2 which are denoted by θ_1 and θ_2 respectively. The moment of inertia of wind turbine blades and flywheel 1 are denoted as J_1 and flywheel

2 and generator are denoted by J_2 . Here viscous friction is denoted as f_{v6} and f_{v7} on shaft 1 and shaft 2 respectively.

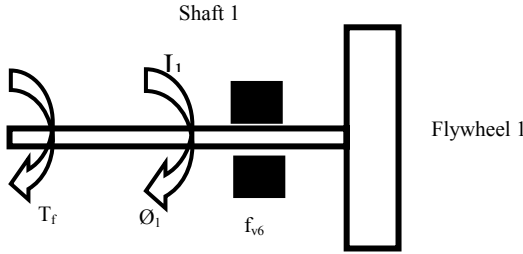


Fig. 5. Energy conversion devices fly wheel schematic model at wind turbine

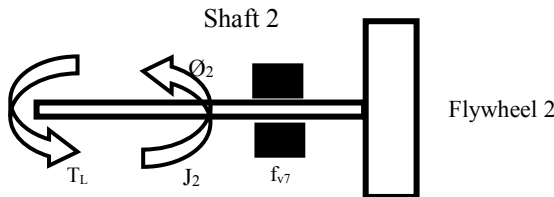


Fig. 6. Energy conversion device fly wheel schematic model at load

$$T_f = \text{L}^r \text{ distance} * f_1(t) \quad (8)$$

$$J_1 \frac{d^2\theta_1}{dt^2} + f_{v6} \frac{d\theta_1}{dt} + T_1 = T_f \quad (9)$$

Where T_f is torque developed by the wind turbine blades and T_1 is the load torque on the flywheel.

$$J_1 \frac{d^2\theta_1}{dt^2} + f_{v6} \frac{d\theta_1}{dt} + T_1 = \text{L}^r \text{ distance} * F_1(t) \quad (10)$$

$$J_2 \frac{d^2\theta_2}{dt^2} + f_{v7} \frac{d\theta_2}{dt} + T_2 = T_L \quad (11)$$

Where T_2 is the transmitted torque and T_L is the load torque.

$$J_2 \frac{d^2\theta_2}{dt^2} + f_{v7} \frac{d\theta_2}{dt} + (\text{L}^r \text{ distance} * F_2(t)) = T_2 \quad (12)$$

$$T_1 \approx T_2$$

$$J_1 \frac{d^2\theta_1}{dt^2} + J_2 \frac{d^2\theta_2}{dt^2} + f_{v6} \frac{d\theta_1}{dt} + f_{v7} \frac{d\theta_2}{dt} + T_L = T_f \quad (13)$$

$$J_1 \frac{d^2\theta_1}{dt^2} + J_2 \frac{d^2\theta_2}{dt^2} + f_{v6} \frac{d\theta_1}{dt} + f_{v7} \frac{d\theta_2}{dt} = \text{L}^r \text{ distance} * (F_1(t) - F_2(t)) \quad (14)$$

$$(J_1 S^2 + f_{v6} S) \theta_1(S) + (J_2 S^2 + f_{v7} S) \theta_2(S) = \text{L}^r \text{ distance} * (F_1(S) - F_2(S)) \quad (15)$$

5. SIMULATIONS AND RESULTS

The Simulation block diagram of proposed system consists of energy conversion device ECD-1 and turbine, ECD-2 along with transmitting tube and self-excited induction generator. The simulation study is carried out in MATLAB/SimMechanics. When the turbine starts to rotate, the turbine shaft rotates the flywheel, where the speed of turbine shaft and angular velocity of flywheel 1 are plotted and shown in Fig.7 and Fig.8 respectively. As the flywheel 1 rotates, it generates a certain force on piston base 2, which applies pressure P_1 on the liquid inside the cylinder.

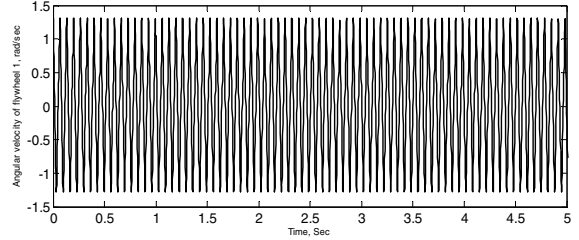


Fig. 7. Wind turbine shaft speed

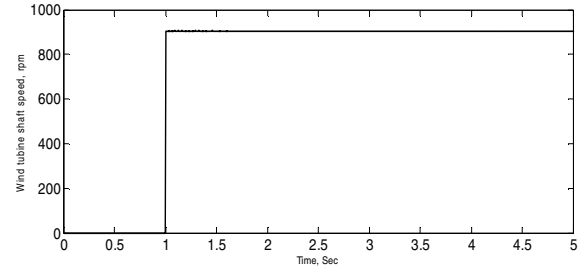


Fig. 8. Angular velocity of flywheel 1

When the force F_1 acted on the piston base 2, pressure P_1 will be generated and this pressure, in turn, helps in the development of force F_2 at piston base 1. The force F_2 helps in flywheel 2 to rotate in turn rotating the generator. The speed of generator shaft and angular velocity of Flywheel 2 are plotted and shown in Fig.9 and Fig.10 respectively.

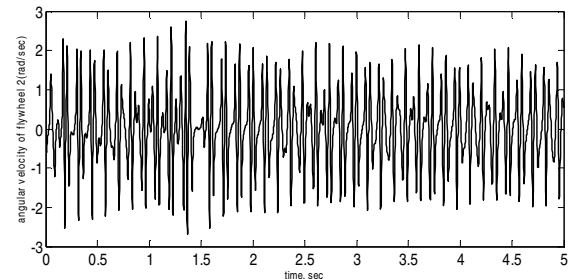


Fig. 9. Generator rotor speed

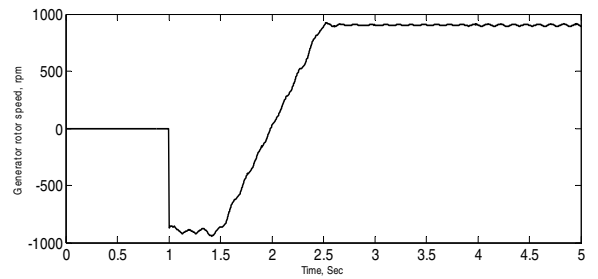


Fig. 10. Angular velocity of flywheel 2

5.1 THE MECHANISM FOR CHANGE IN ENERGY FORM

In this mechanism, the major role is played by pressurization of the liquid and vacuum force. When wind turbine starts to rotate, in the first half cycle of rotation ECD-1 applies high pressure on liquid thereby liquid moves to low pressure region making the ECD-2 rotate. In another half cycle of rotation, it creates a low pressure on liquid thereby liquid moves from high pressure to low pressure making the ECD-2 rotate.

In a closed container, the pressure difference x between two points in a liquid at rest depends only on the difference in the vertical height between the points,

$$x = \rho gh \quad (16)$$

X = pressure difference between particles

ρ = density of the liquid

g = acceleration due to gravity

z = difference in vertical height

If there is a change in pressure at a particular point, the change in pressure is transmitted to entire liquid without being diminished in magnitude as the pressure difference remains constant.

Bernoulli's equation relates the speed of fluid at one point, the pressure at that point and height of that point with a reference level. In this case, the tube is considered with the irrotational flow of an incompressible and no-viscous liquid. The liquid is contained between cross section A and B of the tube. The height of A and B are H_1 and H_2 respectively from a reference level. The liquid advances into the tube and after a time Δt are contained between the cross-section A' and B' as shown in Fig.11. Pressure acting at a part of liquid AA' and cross sectional area are P_1 and A_1 respectively. Pressure and cross-sectional area acting at a part of liquid BB' are P_2 and A_2 respectively.

(Δmg), the weight of the liquid considered. From the Bernoulli's equation, the speed of the liquids is determined v_1 and v_2 .

$$P_1 + \rho gh_1 + \frac{1}{2} \rho v_1^2 = P_2 + \rho gh_2 + \frac{1}{2} \rho v_2^2 \quad (17)$$

To show the usefulness of the proposed method, a three-phase, four-pole, 230 V, 50 Hz (1 p.u. frequency), 3.7 kW, delta-connected squirrel-cage induction machine with a three-phase star connected capacitor bank of 300 μF per phase was considered. The measured parameters of the generator are $R_1 = 1.30 \Omega$, $R_2 = 1.75 \Omega$, $X_1 = X_2 = 2.6 \Omega$, the rated stator phase current being 9.0 A. The simulation waveforms of stator line voltage, stator current, capacitor current and load current without proposed system and with the proposed system are shown in Fig. 12.

In the system without proposed model, the generation of stator line voltage and corresponding currents in stator, capacitor, and load are started after 0.5 Seconds onwards. In another case, the system with proposed model gives the respected voltage and currents after 2 seconds onwards. Because the system with proposed model takes some time for energy conversion through proposed Energy Conversion Devices. Even though, the system with proposed model generation starts with a delay of approximately 1.5 Sec compared to the system without proposed model. The efficiency of the system with proposed model is 61.075%; whereas the system without proposed model is 71.62%. The major advantages of the proposed system like reducing generator burden on the wind tower along with the comparable efficiencies give the necessity of the proposed system in real time applications.

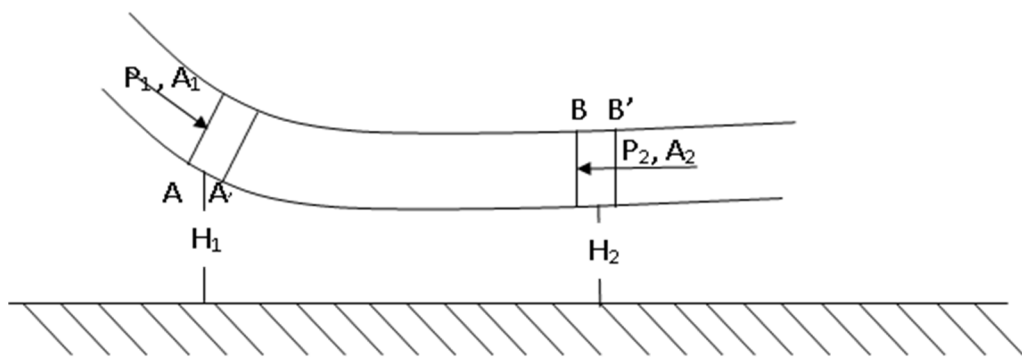


Fig.11. Mechanism of forces inside transmitting tubes

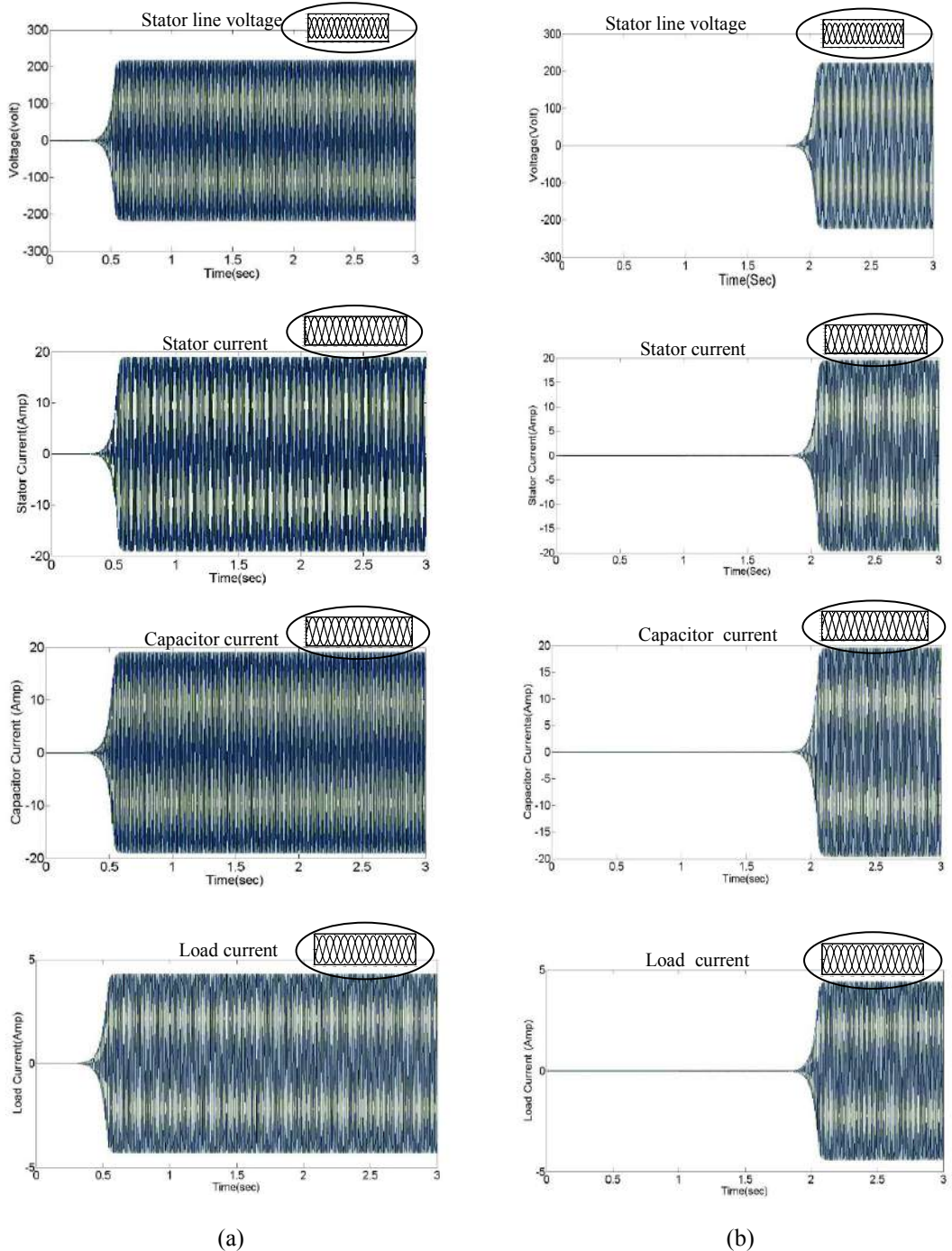


Fig. 12. Simulation waveforms of the system

- (a) *Without proposed system*
- (b) *With proposed system*

CONCLUSION

The proposed novel energy conversion technique to extract maximum power from the wind has successfully analyzed. The proposed technique overcomes the major hurdle of generator burden on wind tower by placing the generator at near the load. The better-achieved results as compared to the conventional approaches allow high altitude towers. So that the maximum power can be achieved from the wind, by allowing maximum swept area. The proposed technique has validated through mathematical analysis and MATLAB Simulations. The obtained waveforms of the conventional and the proposed technique clearly show the importance of the proposed technique in the present wind energy systems. The dynamic model of the proposed system is designed and simulated in MATLAB/SimMechanics.

REFERENCES

- [1] O. Wasynczuk, D. T. Man, and J. P. Sullivan, "Dynamic behavior of a class of wind turbine generators during random wind fluctuations," IEEE Power Engineering Review, pp. 47-48, 1981.
- [2] H. Polinder, J. A. Ferreira, B. B. Jensen, A. B. Abrahamsen, K. Atallah, and R. A. McMahon, "Trends in wind turbine generator systems," IEEE J. Emerg. Sel. Topics Power Electron., vol. 1, no. 3, pp. 174-185, 2013.
- [3] S. M. Muyeen, Ahmed. Al-Durra, and Hany. M. Hasani, "Modeling and control aspects of wind power systems," Intech, 2014.
- [4] M. R. Kazmi, H. Goto, H. J. Guo, and O. Ichinokura, "A novel algorithm for fast and efficient speed-sensorless maximum power point tracking in wind energy conversion systems," IEEE Trans. Ind. Electron., vol. 58, no. 1, pp. 29-36, 2011.
- [5] A. Koyanagi, *et al.*, "Study on maximum power point tracking of wind turbine generator using a flywheel," in Proc. Power Conversion Conference-Osaka, Japan, pp. 322-327, 2002.
- [6] B. Shen, B. Mwinyiwiwa, Y. Zhang, and B.T. Ooi, "Sensorless maximum power point tracking of wind by DFIG using rotor position phase lock loop (PLL)," IEEE Trans. Power Electron., vol. 24, no. 4, pp. 942-951, 2009.
- [7] A. Mirecki, X. Roboam, F. Richardeau, "Comparative study of maximum power strategy in wind turbines," International Symposium on Industrial Electronics, vol. 2, no. 1, pp. 993-998, 2004.
- [8] Zheng. Xiao-yan, and Xu. yue, "Factors study on structural characteristics of long-span multi-tower suspension bridge," Journal of Hefei University of Technology (Natural Science), vol.33, pp.1212-1217, 2010.
- [9] T. Fukuda, "Analysis of multi-span suspension bridges," Structural Division, ASCE, vol. 93, 1967.
- [10] C. P. Nazir, "Multispan balanced suspension bridge," Structural Engineering, vol. 112, pp. 2512-2527, 1986.
- [11] Fukuda. T, "Multispan suspension bridges under torsional loading," J. Jpn. Soc. Civ. Eng., 242, pp. 91-103, 1975.
- [12] Pugsley. A, "The Theory of suspension bridges," edward arnold publishing, London, England, 1957.
- [13] Robert. Hoerauf, "Considerations in wind farm grounding designs," IEEE Transaction on Industry Applications, vol. 50, no. 2, 2014.
- [14] Jaewoo. Kim, Dongmin. Kim, Seung-Mook Baek, Soo. Hyoung. Lee, Jung-Wook. Park, "A Survey on operation of wind turbine generators in stand-alone micro-grid," International conference on Power Electronics-ECCE Asia, pp.377- 384, 2015.

Proceedings of International Conference
on
Emerging Trends in Mechanical Engineering
(ICETiME-2016)

23rd -24th September, 2016

Organized by



Sponsored by



Indian Institution of Industrial Engineering

Department of Mechanical Engineering
Faculty of Science & Technology,
The ICFAI Foundation for Higher Education
(Deemed University under Section 3 of UGC Act. 1956)
Hyderabad- 501203

Contents

Foreword	iii
Acknowledgement	v

Theme-I: Design Engineering

1. Stress Analysis of a Plate with Two Circular Holes <i>SoniKumari, Sunil Kumar</i>	01-05
2. Energy Consumption Optimization of a Robot Manipulator <i>ChanakyaChervith .P.S.M, Abhilash. P Chandrasekhar. A</i>	6-11
3. Preparation and Characterization of Copper Metal Matrix Composites <i>G F Chakravarthi, Umed Singh</i>	12-14
4. Mechatronics Design and Development of Automated Surveillance System <i>J.Pavankumar, R.Uday Kumar</i>	15-18
5. Finite Element Analysis and Experimental Correlation of Piezoelectric Accelerometer Design <i>Veerabhadrareddy, Karthik A, Sampath Kumar, SaiKiran N. S. Karunanidhi, Y Giridhar</i>	19-24
6. Use of Nano Materials in the Construction on NPP's <i>Harika Devi Kotha, AvinashMalladi</i>	25-26
7. Engineering Characteristics and Applications of Cylindrical Shells of Functionally Graded Materials <i>R. K. Lalwani,</i>	27-34
8. Analysis of Ply Drops of Composite Materials <i>B. Venkat Sravan Kumar, Ch. Sridhar Reddy</i>	35-40
9. Effect of Thickness and Aging Time on Mechanical Properties and its Influence on Spring back of Al 6061 <i>P. Mahender, R. Pavan Kumar, Sohel, Uday, A.V.V. AnupamaSridevi, K. Mahesh ,J.NagaLakshmi</i>	41-43
10. Computation of Hardening Parameters and Finite Element Simulation of Monotonic Behavior of SS316 Steel <i>Anupam Sharma, Jagabandhu Shit</i>	44-48
11. Computation of stress intensity factor for dynamic load to predict failure of cracked geometry. <i>Saryjeet Roy, Jagabandhu Shit, Subhadip Chakraborty</i>	48-50
12. Material Characterization and Finite Element Simulation of Cyclic Plastic Behaviour of SS316 Steel <i>AvijitBhowmick, Jagabandhu Shit</i>	51-54

104.	Influence of Taper Cylindrical Tool Pin Profiles on Microstructure and Mechanical Properties of Friction Stir Welded Copper Weldments <i>L Suvarna Raju, G Santhanam, Dr C Srinivas</i>	530-533
105.	Effect of Friction Stir Welding Parameters and Aging on 2014-6061 Al Dissimilar Welding <i>T. Nagaraju, L. Sagar, A. Ashok Kumar, J. Nagalakshmi, A.V.V. AnupamaSridevi ,K. Mahesh</i>	534-537
106.	Closing Weld Bead Shape Manipulation through Temporal Plasma Quenching in Pulsed GTAW <i>Sushanta Kumar Sahu, Bikash RanjanMoharana, Susanta Kumar Sahoo</i>	538-541
107.	Study on the Influence of Process Parameters on Friction Surfaced AA5052 over AA2014 <i>K Vanitha, M Indira Rani, Y Jyothsna, K Anusha</i>	542-546
108.	Analysis of Friction Seam Welding of 3mm Thick AA6061 Plates <i>Y Jyothsna, M Indira Rani, K Anusha, K Vanitha</i>	547-550
109.	Parametric Optimization of Resistance Spot Welding of SS302 and Low Carbon Steel using Taguchi Method <i>SushreeSefali Mishra, Ajit Pattnaik , Debasish Mishra, Kamal Pal</i>	551-554
110.	Implementation of Genetic Algorithm in Flexible Job Shop Scheduling Problem for Minimizing Makespan <i>Manish Kumar Pandey, Sunil Agrawal</i>	555-560
111.	3D Bio-printing of Skin: An Overview <i>AvinashMalladi</i>	561-564
112.	Multi-Objective Optimization of Cutting Parameters using FIS in Turning Operation to Reduce Surface Roughness and Tool Vibration <i>K. Vivekananda, S. K. Sahoo , S. K. Dash</i>	565-569
113.	Prediction of machining parameters in Turning Operation to Reduce the Tool Vibration and Cutting Forces using GRA combined Taguchi <i>K. Vivekananda, S. K. Sahoo, Anshuman Kumar, R. A. Mohapatra</i>	570-574
114.	Improvements in Tensile Strength of Friction Stir Welded Parts by Parametric Control <i>Ankit Kumar Pandey, Suman Chatterjee, RavitejaBuddala, Swayam Bikash Mishra, Siba Sankar Mahapatra</i>	575-579
115.	Facility Location using Fuzzy TOPSIS: Indian Automotive Industry Case Missal.P, Sakhardande.M, Rajesh Prabhu Gaonkar	580-583
116.	Design and 3D printing of Mechanical Prosthetic Aortic Valve <i>L. Siva Rama Krishna, T. Rishi Narasimha satya Dev, D Swathi, Sriram Venkatesh</i>	584-588
117.	A Study on Cloud Manufacturing Systems <i>Sirisha Potluri, Sathya A.R</i>	589-592

118. An effective Jaya optimization for flexible job shop scheduling 593-598
*Raviteja Buddala, Siba Sankar Mahapatra, Ankit Kumar Pandey,
 Swayam Bikash Mishra*
119. Dimensional Analysis Based Model Development for Incremental Sheet Metal Forming 599-603
Manish Orao and Vinay Sharma
120. Scheduling of Flexible Manufacturing System by Particle Swarm Optimization 604-606
Parimita Panda, Prasant Ranjan Dhal
121. A Modified Close Neighbour Algorithm for Designing Cellular Manufacturing System 607-610
Amit Bhaskar, Rakesh Jain
122. Machinability Analysis of Aluminium Alloy 6061 in Electro-Discharge Machining: Effect of Tool Material 611-618
*Ankur Srivastava, Rahul, Kumar Abhishek, Ranjeet Kumar Sahu,
 Saurav Datta, Siba Sankar Mahapatra*
123. Optimization of Machining Parameters in Dry Drilling 619-624
Tapas Banerjee, Asish Bandyopadhyay, Pradip Kumar Pal
124. Effect of Aging and Dissimilar Welding of AA5083 and AA6082 on Mechanical Properties 625-629
*G.D.N. Sri Lakshmi, Y. Ashalatha, A. Ashok Kumar, J. Nagalakshmi,
 A.V.V. Anupama Sridevi and K.Mahesh*
125. Experimental Analysis of Friction Stir Processed AA7075 Plate Using 630-634
 Multiple Attribute Decision-Making Methods.
K Anusha, M Indira Rani, Y Jyothisna, K Vanitha
126. Optimization of Nd:YAG Laser Welding of Austenitic Stainless Steel Sheet using TLBO Approach 635-639
Nikhil Kumar, AsishBandyopadhyay

Theme-IV: Thermal Engineering

127. Simulation of Coal Gasification process for CO₂ capture using 2-D CFD Model in a Fluidized bed for Indian Coal 640-643
G.Suresh Kumar, AVSSKS Gupta, M.Viswanadham
128. Experimental Investigations on four stroke Diesel Engine by using Watermelon Seed Oil Methyl Ester as a Biodiesel 644-651
Prasad.D, Chandrika.V, Naga Raju K
129. Vapor Phase Drying; The Latest Technology for Moisture Removal From Transformer Coil Insulation 652-654
Mohd. Tareq Siddiqui, Jayant T. Pattiwar, Avinash P. Paranjape
130. Influence of Bending Process Parameters and Heat Treatment Methods on Springback of AISI 1026 Steel 655-659
S. Ramakrishna, C. Sravani, B. Ravinder, S. Srilakshmi, SK. Farzana, J. Naga Lakshmi, K. Mahesh ,A.V.V. AnupamaSridevi
131. Exergy Analysis of Thermal Power Plant 660-666
Gopikrishna.M, Dr. A.V.S.S.K.S.Gupta
132. Computational Fluid Dynamics Simulation of Circular Jet Burners to Investigate the Effect of Upstream Annular Cavities 667-670
Abhishek Kumar Dewangan, Dr. V.Raghavan, Akhilesh Kumar Sahu
133. Numerical Investigation of square arrayed multi-pinfin water block for microprocessor cooling 671-675
Mohammad Ayub Ansari, Harish Chandra Das
134. Performance Prediction of Capillary Tube for an Air Conditioning System using ANN 676-681
ChanakyaChervith.P.S.M, D.V. Raghunatha Reddy
135. Performance and Emission Evaluation of A Crude Pongamia Oil in A Low Heat Rejection Diesel Engine 682-691
ChirraKesavareddy
136. A Review on Performance of Vapour Compression Refrigeration System using Nano Additive Refrigerants 692-695
CH.Venugopal, D.V. Raghunatha Reddy
137. Experimental Investigation on Performance of Cooling Tower: Case Study 696-700
BanothHari Krishna, Tushar.N.Desai
138. Heat Transfer Enhancement through Perforated Fins 701-705
A.KalyanCharan, R.Uday Kumar, B. Balunaik
139. Performance Prediction of Vapor Compression Refrigeration System using Artificial Neural Network 706-711
D.V.Raghunatha Reddy, P.Bhramara, K.Govindarajulu

Effect of Thickness and Aging Time on Mechanical Properties and its Influence on Spring back of Al 6061

P. Mahender¹, R. Pavan Kumar², Sohel³, Uday⁴, A.V.V. Anupama Sridevi⁵, K. Mahesh⁶, J.NagaLakshmi⁷

^{1,2,3,4,7} Department of Metallurgical and Materials Engineering, RGUKT Basar, Adilabad – 504107, Telangana, India.

^{5,6} Department of Mechanical Engineering, RGUKT Basar, Adilabad – 504107, Telangana, India.

³sohelmohd155@gmail.com, ⁴balusangishetti420@gmail.com, ⁵anupamasridevi@gmail.com,

⁶mahesh.katakam@gmail.com, ⁷lakshmi.mme@gmail.com

Abstract— Spring back is one of the prominent defects that occur during bending process. Spring back significantly changes the final dimensions and geometry of the component there by it becomes important to reduce the spring back effect. The present paper focuses upon the influence of aging on the spring back effect of Al 6061 alloy. Aging conditions were optimized and it has been carried out on 1.6 mm and 2 mm thick sheets at 180°C for 16, 20 and 24 hours respectively. The presence of precipitates is identified by using XRD while the tensile tests were carried out to determine the mechanical properties of these specimens. Air bending of these samples at constant stroke distance and span length was carried out on UTM. The XRD peaks indicate the presence of Mg₂Si precipitates. Tensile strength and hardness of the material increased with the aging time up to 20hrs and later decreased. Sufficient decrease in spring back angles had been observed for this aging cycle. Interestingly, the spring back values of 2mm thick sheet was found to be higher than 1.6mm thick sheet which can be attributed to increased sample length. It was observed that 20 hrs of aging time at 180 °C is optimum for 6061 Al alloy with better mechanical properties and lower spring back values.

Keywords— Air bending, Aging, XRD, UTM, Springback.

1. INTRODUCTION

Stress analysis plays an important role in estimating the level of force required to deform any body without causing its failure. Elastic strain recovery in the formed part after deformation is called spring back effect. It is the geometric change made to a part at the end of the forming process when the part has been released from the forces of the forming tool. Spring back is mainly due to nonlinear plasticity with friction and heat loss in the material. Upon completion of sheet metal forming, deep-drawn and stretch-drawn parts spring back and thereby affect the dimensional accuracy of a finished part. The final form of a part is changed by spring back, which makes it difficult to produce the part.

There are two basic views as to why spring back occurs, one states that it is due to the displacement of molecules and the other considers spring back in terms of a

stress-strain diagram. One of the reasons for spring back is that as the material is bent the inner region of the bend is compressed while the outer region is stretched. This means that the molecular density is greater on the inside of the bend. Generally the compressive strength of material is greater than its tensile strength. This means that pressure will permanently deform the outer regions of the piece before it deforms the inner regions. The compressive stress is changed into spring back. The 6xxx-series aluminum alloys are widely used in many industries such as aerospace, automotive and food industry due to their high strength-to-mass ratio, good corrosion resistance, good mechanical properties or a combination of these properties [1]. So, spring back study on Al-6061 has been carried out. Al 6061 sheets of dimensions 100 mm x 17 mm x 1.6 mm and 100 mm x 17 mm x 2 mm subjected to solutionizing and ageing heat treatments followed by V-bending process. Since AA6061 alloy is a precipitation-hardenable material, its hardness, strength, work-hardening capability, formability and spring back are affected by the level of the solute in the solid-solution matrix and the amount, type, density, size and nature of the second-phase particles [2, 3]. The precipitation sequence for the 6xxx alloys, which has been widely accepted is [4]:

Super saturated solid solution → atomic clusters (Si clusters and Mg clusters) → dissolution of Mg clusters Mg, Si co-clusters → precipitates of an unknown structure (GP-I zones) → (GP-II zones) → B' → (stable Mg₂Si). Here GP stands for Guinier-Prestone zones which correspond to atomic clusters of solute atoms only a few atomic diameters in size.

2. Experimental Procedure

Al 6061 alloy have been chosen for the current study. Sheet Samples had been cut to dimensions of 100 mm x 17 mm x 1.6 mm and 100 mm x 17 mm x 2 mm. X-ray diffraction analysis were carried out on the base sample for 20 to 20-90°. The samples had been subjected to heat treatment i.e. solutionizing and age hardening in a muffle furnace. The temperature of the furnace had been raised to 540°C (heating rate of 10°C/min) and the samples were soaked for 2 h for solutionizing followed by water quenching to room temperature. Solutionizing causes the excess solute in the sample to be dissolved completely in

Effect of Friction Stir Welding Parameters and Aging on 2014-6061 Al Dissimilar Welding

T. Nagaraju¹, L. Sagar², A. Ashok Kumar³, J. Nagalakshmi⁴, A.V.V. Anupama Sridevi⁵, K. Mahesh⁶

^{1,2,3,4}Department of Metallurgical and Materials Engineering, RGUKT Basar, Adilabad, Telangana, India -

^{5,6}Department of Mechanical Engineering, RGUKT Basar, Adilabad, Telangana, India - 504017.

¹nagarajuthandrapally@gmail.com, ²sagar121843@gmail.com, ³ashokiiitbas@gmail.com,

⁴lakshmi.mme@gmail.com, ⁵anupamasridevi@gmail.com, ⁶mahesh.katakam@gmail.com

Abstract— Aluminium 2014 (Al-Cu alloy) series is best known for its mechanical properties like tensile strength and hardness but it has low corrosion properties while aluminium 6061(Al-Mg-Si alloy) series has good corrosion properties but low mechanical properties compared to the earlier. The present work examines the effect of friction stir welding parameters and aging on the dissimilar welding of Al 2014 and Al 6061 alloy. The welding is carried out for different combinations of as received and aged samples of 2014 and 6061 alloys with varying parameters such as rotational speed (600 RPM, 900 RPM) and transverse speed (45 mm/min, 90 mm/min). Aging was carried out at 180°C for 8 hours after it has been solution treated at 540°C for 90 minutes. Tensile results of as received and aged samples show no much difference in strength values but the %elongation of 2014 aged has decreased. The tensile test of dissimilar transverse weld samples showed that the strength values were lower than as received but interestingly the fracture has occurred at 6061 Al side and not at the weld zone. For as received dissimilar welding, the hardness of the weld zone was high for high rotational speed and low transverse speed where as for aged samples it is high for low rotational and transverse speeds.

Keywords— Aging, Rotational speed, Traverse speed, Friction Stir Welding and Dissimilar welding.

1. INTRODUCTION

Aluminum alloys, especially 6xxx and 2xxx are widely used in aerospace and marine industries in the construction of frames, pipelines and storage tanks. Variation in the chemical compositions and mechanical properties of the base materials offer a tough challenge in welding these dissimilar materials by a fusion welding process [1-3]. However, Friction stir welding is a solid state welding (metal is not melted) that uses a third body tool to join two facing surfaces. It is developed by The Welding Institute (TWI), UK, very much suitable for joining aluminium alloys. As no melting is involved during the process, the defects related to the presence of brittle interdendritic eutectic phases are eliminated, thus FSW would produce superior properties compared with fusion welds [4]. Many

researchers have studied that welding parameters such as rotational and welding speed, geometric parameters of the tool and the work piece, and initial material temperature influences the strength and microstructure of various aluminum friction stir welded joints. [5-8]. Hassan et al. [5] concluded that highest strength and ductility for the nugget zone is achieved for AA7010 for an optimum rotational rate and travel speed. In AA2014, weld speed is the main input parameter that has the highest influence on the tensile properties of the FSW joints while the peak temperature in the weld zone is primarily influenced by the rotational rate [6]. Sharma et al. [7] studied on AA7039 and reported that with the increasing rotation rate and decreasing welding speed the mechanical properties of FSW joints has improved. Contrary results were observed by Hao et al. [8] that increasing the tool rotation rate has reduced the ultimate tensile strength (UTS) while increasing the welding speed has increased the UTS of the Al-Mg-Er FSW joints. Da Silva et al. [9] have reported that intense onion ring like mixing pattern were observed at high rotation speeds in the stir zone while at low rotation speed, limited materials mixing has been observed. They also found minimum hardness value at the HAZ retreating side. Better mechanical properties are obtained when harder material is placed on the advancing side and softer material in retreating side [10]. The present work deals with welding of dissimilar materials (AA6061 and AA2014) using FSW by varying the welding parameters to understand its influence on material flow and its properties.

2. EXPERIMENTAL PROCEDURE

The aluminium plates of series AA6061 and AA2014 are taken for the experimental procedure of required dimensions (100mm x 60mm x 6mm). AA6061 and AA2014 alloys has been solutionized at 540°C for 90mins and then subjected to aging temperatures at 180°C for 8 hrs. FSW of various combinations of AA6061 and AA2014 has been performed at different rotational speed and traverse speeds as shown in table I.

Effect of Aging and Dissimilar Welding of AA5083 and AA6082 on Mechanical Properties

G.D.N. Sri Lakshmi¹, Y. Ashalatha², A. Ashok Kumar³, J. Nagalakshmi⁴, A.V.V. Anupama Sridevi⁵ and K.Mahesh⁶

^{1,2,3,4}Department of Metallurgical and Materials Engineering, RGUKT Basar, Adilabad, Telangana, India

^{5,6}Department of Mechanical Engineering, RGUKT Basar, Adilabad, Telangana, India – 504017

¹gdivya863@gmail.com, ²yerraashalatha@gmail.com, ³ashokiiitbas@gmail.com,

⁴lakshmi.mme@gmail.com, ⁵anupamasridevi@gmail.com, ⁶mahesh.katakam@gmail.com

Abstract— The aim of the present work is to investigate the effect of aging on the mechanical properties of dissimilar welded AA6082 and AA5083 plates by friction stir welding (FSW) process by varying the rotational speed and traverse speed. Dissimilar welding of AA5083 sample and AA6082 as received and aged (140°C and 180°C) samples were carried out with different rotational speeds (600 and 900 rpm) and traverse speeds (45 and 90 mm/min). Tensile test indicate that as the aging temperature of 6082 alloy is increasing, the properties of the material increase but these properties were inferior to the as received material. This might be due to the formation of fine precipitates of low amount. The ultimate tensile strength and % elongation of the dissimilar weld samples of as received material increases with increasing traverse speed. As the aging temperature increases, the weld strength increased even for a low traverse speed but the % elongation decreased drastically. The hardness values indicate that as the rotational speed and traverse speed increases, the hardness of the weld zone decreases for as received material while it increases for aged samples. The optimum rotational speed and traverse speed are found to be 900 rpm and 45 mm/min respectively for a dissimilar weld of AA5083 as received and AA6082 aged at 180°C.

Keywords— Aging, Rotational speed, Traverse speed, Friction Stir Welding and Dissimilar welding.

1. INTRODUCTION

Friction stir welding (FSW) is a welding process which uses a non-consumable rotating tool, invented mainly to avoid solidification related problems such as oxidation, shrinkage and porosity. Welding of aluminium by the arc welding methods would ultimately lead to inferior properties due to unavoidable defects [1]. A rotating tool is plunged into the work piece and translating it along the weld line generates the heat by friction at the tool surface. The microstructure and the mechanical properties of the welded joint primarily depends on material flow behaviour and the thermal cycle which are influenced by welding parameters such as welding speed, rotation rate and the pin/shoulder geometry [2,3]. AA5083 is a non heat treatable Al-Mg alloy with good corrosion resistance while AA6082 is an age hardening Al-Mg-Si alloy which forms Mg₂Si precipitates.

Both alloys exhibit higher strength to weight ratio, good ductility, and good corrosion resistance [4-6]. Dissimilar joining of these two materials leads to the combined properties of both materials, which makes this combination very much required in military applications such as light combat aircraft (LCA), light combat vehicle (LCV), future main battle tank(FMBT), bridge layer tank (BLT), armoured ambulance, submarine torpedo, etc [7].

Many researchers have studied the dissimilar welding of aluminium alloys, especially focusing on the evolution of microstructure and texture, tool pin profile and material flow during FSW [7-14]. Steuwer et al. [11] have investigated the effect of process parameters on residual stress in dissimilar FSW of AA5083–AA6082. It was reported that the residual stresses are predominately affected by rotational speed of the welding tool when compared with the traverse speed. The residual stress on the AA5083 side is larger when compared with the AA6082 side. Donatus et al. [14] studied the flow patterns in friction stir welds of AA5083 and AA6082 alloys. It was reported that slower traverse welding speeds when compared with higher traverse welding speed, provides a better mixture of materials in the weld zones. The material pull from the retreating side to advancing side is highest in the transition region between the tool shoulder domain and the tool pin domain. Threaded pin profiled tool shows superior performance when compared to tapered pin profiled tool due to the formation of finer and uniformly distributed precipitates, circular onion rings and smaller grain [7]. In the present work, an attempt has been made to join the heat treatable (AA6082) aged at different aging temperatures and non-heat treatable (AA5083) aluminium alloys by friction stir welding (FSW) to study the effect of welding parameters on its mechanical properties.

2. EXPERIMENTAL PROCEDURE

The aluminium plates of series AA6082 and AA5083 are taken for the experimental procedure of required dimensions (100mm x 60mm x 6mm). The schematic arrangement [15] of FSW process for dissimilar joints used in this study is presented in Fig.1.

AA6082 alloy has been solutionized at 540°C for 90mins and then subjected to aging temperatures at 140°C and 180°C for 8 hrs. FSW of various combinations of AA5083

Influence of Bending Process Parameters and Heat Treatment Methods on Springback of AISI 1026 Steel

S. Ramakrishna¹, C. Sravani², B. Ravinder³, S. Srilakshmi⁴, SK. Farzana⁵, J. Naga Lakshmi⁶, K. Mahesh⁷, A.V.V. Anupama Sridevi⁸

^{1,2,3,7,8}Department of Mechanical Engineering, RGUKT Basar, Adilabad, Telangana, India - 504017.

^{4,5,6}Department of Metallurgical and Materials Engineering, RGUKT Basar, Adilabad, Telangana, India - 504017.

¹ramakrishnasiluveru@gmail.com, ²sravani.chiluveri@gmail.com, ³madhuravi454@gmail.com,

⁴sadusrilikshmithirupathamma12@gmail.com, ⁵sk.farzana@gmail.com, ⁶lakshmi.mme@gmail.com,

⁷mahesh.katakam@gmail.com, ⁸anupamasridevi@gmail.com

Abstract— Spring-back is a common defect in sheet metal forming. In the present work, the spring back analysis is done on annealed and intercritical annealed (ICA) AISI 1026 steel samples by varying process parameters such as span length and stroke distance. As received samples are subjected to annealing at 925°C and subsequently ICA heat treatment process was carried out at 750°C and 780°C. Tensile tests were performed to determine the mechanical properties of all the samples. Numerical simulations were carried out on air bending to optimize the process parameters such as span length and stroke distance for annealed and ICA samples. Experimental analysis is also carried out based on the optimum results of simulations. The results indicate that as the stroke length is increasing, the final bend angles in the samples have decreased and came closer to punch angle. The optimum stroke length for annealed sample is found to be 50 mm with 50 mm span length while for ICA at 750°C sample is 50 mm for 110 mm span length and for 780°C sample is 40 mm for 50 mm span length in terms of thickness and stress distributions. The presence of hard and brittle martensite phase has increased the stress levels and decreased the springback in the ICA samples when compared to annealed samples. The amount of stresses developed is same in both the ICA samples while the thickness distribution is homogenous throughout the sheet in all the deformations except at the edges where thinning has occurred.

Keywords— Springback, Intercritical annealing(ICA), Span length, Stroke distance.

1. INTRODUCTION

Sheet metal forming is one of the most important manufacturing processes particularly valid for the automotive industry where it has an even more important key position. In the automotive industries, Dual Phase (DP) steels which are one of the types of advanced high strength steels (AHSS) have been widely used in various safety and structural parts of new vehicles with a good acceptance. However, one of the major problems of stamped parts made from AHSS sheets is the higher magnitude of springback

[1,2]. Spring-back is a common phenomenon in sheet metal forming, caused by the elastic recovery of the stresses during unloading which leads to some geometric changes in the product [3]. DP steels have been shown to possess high strength, high work-hardening rates and mild formability. DP steels are obtained by Intercritical annealing (ICA). ICA is done below upper critical temperature (A_3) and above lower critical temperature (A_1) lines transforming the austenite-ferrite phases to martensite-ferrite phases upon quenching which will improve the properties of the material [4].

An extensive study has been conducted by many researchers on understanding, prediction and control of springback on DP steels. Springback is related to many parameters like forming conditions, tool geometry, and other material properties such as sheet thickness, yield stress, work hardening, strain rate sensitivity and elasticity modulus [5-11]. Ozturk et al. [11] examined temperature effects as a forming condition on springback of the high strength steels and their results show that the springback decreases with increasing the temperature. Comparable study was also performed by Mori et al. [12]. Hani Aziz Ameen et al., [2] concluded that the hardness of the sheet increase the spring back back factor increase and spring back could be predicted effectively by sheet thickness. The present work studies the effect of heat treatment condition and bending parameters on carbon steel.

2. EXPERIMENTAL PROCEDURE

The material considered for the present investigation is AISI 1026 Steel sheets of 1.5mm thickness and length of 150mm and width of 60mm. these sheets were subjected to annealing process at 925°C with 1 hr soaking time. The annealed samples were then subjected to intercritical annealing process at two different temperatures i.e., 750°C and 780°C with a soaking time of 20 mins. After reaching the required temperature the samples were quenched in water to attain the required microstructures. Tensile specimens of ASTM E8 standard were cut using wire EDM machine and the test was carried out on Zwick/Roell Z100 UTM machine. Hardness values were determined using rockwell hardness machine.



One Day

2nd NATIONAL CONFERENCE



on

Nanoscience & Nanotechnology

29th March 2016

SOUVENIR



Sponsored by
UGC, NEW DELHI

Organized by

DEPARTMENT OF CHEMISTRY & PHARMACEUTICAL SCIENCES
UNIVERSITY COLLEGE OF SCIENCE, MAHATMA GANDHI UNIVERSITY
NALGONDA– 508 254

Dr. Y. Prashanthi
Convenor & Organizing Secretary
NCNN – 2016



SOUVENIR & ABSTRACTS

**ONE DAY
2nd NATIONAL CONFERENCE**

**ON
NANOSCIENCE & NANOTECHNOLOGY**

29th MARCH, 2016

**Sponsored by
UGC, NEW DELHI**



**ORGANIZED BY
DEPARTMENT OF CHEMISTRY &
PHARMACEUTICAL SCIENCES
MAHATMA GANDHI UNIVERSITY
NALGONDA**

SRI T. VIJAYA KUMAR, IAS
Vice-Chancellor I/C
MGU, Nalgonda



MESSAGE

I am delighted to know that, the Department of Chemistry & Pharmaceutical Sciences, Mahatma Gandhi University, Nalgonda is organizing a one day **2nd National Conference on Nanoscience& Nanotechnology** on 29th March, 2016. This topic assumes great significance in the modern context as it is an emerging field which is full of new ideas, innovation and applications.

Now a days, nanotechnology has been proved to be practical, relevant and achievable. This technology has now become an accepted filed of interdisciplinary research and is making great strides for its applicability in the areas of energy, science, technology, defence, space, agriculture and industry.

I am sure that the deliberations of this conference would accelerate interdisciplinary research and motivate the young researchers to seek path ways of mutual collaboration in tackling the problems of energy, environment, agriculture and health.

I appreciate the efforts made by the Convener, Organizing Committee, staff and students of the Department of Chemistry & Pharmaceutical Sciences for conducting this conference. I wish the program a grand success.

T. Vijay Kumar, IAS
Vice-Chancellor, I/c
MGU, NLG.

Prof. U. Umesh Kumar
Registrar, Mahatma Gandhi University
Nalgonda



MESSAGE

It is a pleasure to note that the Department of Chemistry & Pharmaceutical Sciences, Mahatma Gandhi University, Nalgonda is organizing 2nd National Conference on **Nanoscience and Nanotechnology (NCNN-2016)** on 29th March, 2016.

Nanomaterials play a key role in science and technology development. The field emerges with new findings day by day and forms interface with other areas such as chemistry, physics, materials, bio and medical. Hence, it is important for academicians, scientists, and young workers to meet to exchange and discuss their ideas for benefitting inter-disciplinary and multi- disciplinary researches. I am sure this Conference will form an effective platform to serve this very purpose.

I congratulate the Principal, Convener and organizing committee of NCNN-2016 and wish the conference a great success.

Prof. U. Umesh Kumar
Registrar, Mahatma Gandhi University
Nalgonda

CONTENTS

- 1. MESSEGES**
- 2. MAHATMA GANDHI UNVIERSITY PROFILE**
- 3. A PROFILE OF DEPARTMENT OF CHEMISTRY**
- 4. LIST OF FACULTY MEMBERS**
- 5. INVITED TALKS**
- 6. ABSTRACTS**



**2nd NATIONAL CONFERENCE ON
NANOSCIENCE & NANOTECHNOLOGY
NCNN - 2016**

**Dr. Y. Prashanthi
NCNN-2016**

**Mobile : 9010203857
Email : ncnn2016@gmail.com**

WELCOME MESSAGE

The Department of Chemistry & Pharmaceutical Sciences, Mahatma Gandhi University, Nalgonda is delighted to welcome you all to the **2nd National Conference on “Nanoscience & Nanotechnology”**. The goal of this conference is to encourage young scientists, researchers around the globe under the theme on the challenges in Nanoscience & Nano technology to focus on the expansion of collaborative research and ties among different countries. Now these fields have evolved into a great multi-disciplinary science encompassing activities and today's active scientists must take a note of growth and well being trends. The primary theme of the conference covers a broad range of topics on nanomaterials and applications including science, physics, biology, engineering and defense. The conference includes lectures by eminent scientists from various National Laboratories, Academic Institutions and Industries.

Research scholars and young faculty have different levels of skills and academic background and pursue their advanced chemical research. A foundation in primary skills of chemical methods would empower them and enhance their reach out into greater depths of chemical research.

I believe that we will have many more occasions to invite you to the Department of Chemistry and Pharmaceutical Sciences, Mahatma Gandhi University, Nalgonda.

In this context, the one day national conference on **“Nanoscience and Nanotechnology”** is organized to focus on in-depth knowledge for young scientists/faculty of chemistry.

Thank you once again for your participation and contribution for the success of the conference.

**Dr. Y. Prashanthi
Convener, NCNN-2016**

A BRIEF PROFILE OF MAHATMA GANDHI UNIVERSITY

Mahatma Gandhi University originally the PG Centre of Osmania University is established in the year 1987 to provide academic excellence to remote village students of the backward regions. The PG Centre is upgraded as Mahatma Gandhi University in the year 2007 and is one of the fast growing learning centers in India. Ever since its inception the University offering courses on inter-disciplinary approach and develop them on sustainable line.

The Main campus of the University is spread across in 240 acres and the off campus at Panagal in 10.3 acres of land. The University has four University colleges three in the main campus and one at Panagal campus; they are University College of Science and Informatics, University College of Arts and Social Sciences, University College of Commerce and Business Management and University College of Engineering and Technology. The University offers 18 regular courses like Integrated, UG and P.G programmes in the two campuses. The University has 213 affiliating colleges in which PG colleges are 33, Degree colleges are 119 and B.Ed colleges are 52. There are highly qualified regular teaching faculty - 36, Academic Consultants and Part time faculty -53.

The Emblem of the University is a round logo consisting of Dharma Chakra with peacock feathers on top and Nagarjuna Sagar Dam in the middle. It is skirted by a Wheel and Purnakumbham with two corns on the left and the right. The name of the University figures in four languages and also a Sanskrit inscription at the bottom, "**Saavidyaaya Vimukthaye**". At the top of the Logo is Ashoka's Dharma Chakra which stands for maintenance of Dharma implying cosmic order, moral principles and spiritual enlightenment. The Peacocks perched on either side of the wheel are a representation of the national bird. At the centre of the logo are cascades of water gushing out of the Nagarjuna Sagar reservoir located at Nandikonda hills of Nalgonda District. It is a symbol of national pride and a place of tourist importance for visitors from home and abroad.

The colourful Kalasham (Purnakumbham) in the logo has local relevance, historical significance and religious sanctity. At the bottom of the Kalasham is a book representing knowledge and learning, the very essence and soul of a University. At the bottom of the logo are two corns symbolizing greenery, granary and fertility.

The vision of University is committed to the cause and promotion of academic excellence. The University has an agenda of tapping and developing human resources in tune with the changing times. The University also has plans to reach out to the industrial sector in and around its jurisdictional area.

About the Department

The Department of Chemistry & Pharmaceutical Sciences, as the name suggests, is dedicated to the discovery, development and application of science in a wide range of academic and professional areas to create excellent quality of research work in a learning environment that promotes creativity, innovation and critical thinking amongst students.

The courses such as Chemistry & Pharmaceutical Chemistry are designed with keeping in mind their relation to science and their usefulness in different industry and government sectors. The Department has covered more than five years of its existence. Currently, the Department has full time faculty, Academic consultants and a number of distinguished guest faculties from India. The faculty of the Department has received research grants from various funding agencies.

The Department is actively collaborating with premier institutes and industries of both national and international repute. A good number of publications including research articles, reviews, books of national and international repute reveal its dedication to the field of Science. The scenario of placement is quite luminous. Our post-graduate students are the most sought-after in industry, academia, research and for varied professional including legal services.

Our primary object is to take the welfare of the students and train them into leaders rather than followers by monitoring their personality development besides sustaining their academic excellence.

LIST OF FACULTY MEMBERS

Department of Chemistry & Pharmaceutical Sciences
University College of Science & Informatics
Mahatma Gandhi University, Nalgonda

Dr. Annapoorna R.S. Butti

Head of the Department

Dr. M. Vasantha

Dr. D. Ramesh

Dr. M. Jyothi

Dr. A. Sridhar Rao

J. Shankara Chary

D. Ravinder Reddy

D. Abilasha

K. Mahathi

Kiran

Dr. Y. Prashanthi

Dr. R. Roopa

Dr. S. Kalyani

K. Geetanjali

K. Amarender

A. Thirupathi

G. Swetha

K. Narsimha

Naveen

One Day 2nd National Conference on Nanoscience & Nanotechnology

2nd National Conference on Nanoscience & Nanotechnology NCNN-2016

Chief Patron	: Sri T. vijay Kumar, IAS Vice-Chancellor I/c Mahatma Gandhi University, Nalgonda
Patron	: Prof. U. Umesh Kumar, Registrar, Mahatma Gandhi University, Nalgonda
Chairperson	: Dr. Annapoorna R.S. Butti Principal, UCSI Mahatma Gandhi University, Nalgonda
Convener & Organizing Secretay	: Dr. Y. Prashanthi Asst. Professor, MGU, Nalgonda

Organizing Committee

Dr. M. Vasantha	Dr. D. Ramesh
Dr. R. Roopa	Dr. M. Jyothi
Dr. S. Kalyani	Dr. A. Sridhar Rao
K. Geetanjali	K. Amarender
J. Shankara Chary	D. Ravinder Reddy
A. Thirupathi	D. Abilasha
G. Swetha	K. Mahathi
K. Narsimha	Naveen
Kiran	

Scientific Advisory Committee

Dr. S. Chandra Shekar, Director, IICT, Hyd.
Dr. Ch. Mohan Rao, Former Director, CCMB, Hyd.
Prof. S. Satyanarayana, Vice-Chancellor, IIIT, Hyderabad
Prof. G. Bhagyanarayana, Vice-Chancellor, PU, Mahaboobnagar
Prof. Shivaraj, Dept. of Chemistry, OU, Hyd.
Prof. Battu Satyanarayana, Dean of Sciences, MGU, Nalgonda
Prof. A. Ravindranath, Dean, UGC, OU, Hyd.
Dr. BV Subba Reddy, Principal Scientist, IICT, Hyd.
Prof. Kenneth J. Klabunde, Kansas State University, USA
Prof. Toyko Imae, Chair Professor, NTUST, Taipei, Taiwan
Prof. BVR Chowdary, Executive Director, NUS, Singapore
Prof. Asif, Riyaz, Saudi
Prof. J. Srikanth Babu, Univ. of Kwazulu-Natal, Durban, South Africa

PROGRAMME SCHEDULE

09:00 - 10:00	:	Registration
10:00- 11:00	:	Inaugural Session
11:00- 11:45	:	Key Note Address
11:45- 12:00	:	Tea Break
12:00- 12:45	:	Invited Talk -1
01:00- 2:00	:	Lunch
02:00- 2:45	:	Invited Talk -2
02:45- 3:30	:	Invited Talk -3
3:30-3:45	:	Tea Break
3:45-4:30	:	Invited Talk-4
4:30-5:00	:	Oral Presentation
5:00-5:30	:	Valedictory Session

INVITED TALKS / PLENARY SESSIONS

Applications of Nanomaterials in Energy, Health and Environment

Tata Narasinga Rao

International Advanced Research Center for Powder Metallurgy and New Materials (ARCI)
Balapur post, Hyderabad-500005, India
(E-mail: tata@arci.res.in)



The area of nanoscience and technology is growing rapidly around the world and the nanomaterials based products, especially in the consumer sector, are entering into the market very rapidly. India is competing, with some difficulty, with developed countries to make its position strong in this field. In other respect, several challenges have to be overcome in terms of production of nanomaterials at commercial scale, their processing, applications and their commercialization.

There are huge number of nano-based products already launched into the market especially in the areas of healthcare, cosmetics, textiles and household products. The engineering components have not picked up much, although some areas like composites are successful. While nanotechnology is advancing, the concerns about the toxicological issues are also increasing. Although formation of regulatory bodies is being proposed, it is difficult to monitor and control the products coming into market due to lack of standards made on the toxicology of nanomaterials.

In the present talk, application driven work done at ARCI in the area of nanomaterials will be presented in two parts, essentially to classify them as surface treated processes (e.g., textiles & water filters) and bulk embedded processes (e.g., composites & sintered products) with details on how the former class is processed to avoid toxic effects, while the second class is completely safe in terms of particle release and more practical from the commercial point of view.

Solid lipid nanoparticles of candesartan cilexetil and rosuvastatin calcium - pharmacokinetic and pharmacodynamic studies

Prof. Veerabrahma Kishan

Department of Pharmaceutics, University College of pharmaceutical sciences,
Kakatiya University, Warangal – 506009



Abstract

Nanotechnology is revolutionary in its impact on all fields, including drug delivery. Nanoparticles are studied as drug delivery systems. Among them, Solid lipid nanoparticles (SLNs) were introduced in 1991, and represent an alternative carrier system to traditional colloidal carriers, such as emulsions, liposomes and polymeric micro- and nanoparticles. SLN particles are made from solid lipids with a mean particle size ranging in between 50 - 1000 nm. A distinct advantage of SLNs when compared to polymeric nanoparticles is lack of cytotoxicity of polymers and the availability of a suitable large scale production method. This talk deals with the preparation technique and characterization of SLNs. Stability and solid state characterization of prepared SLNs. Further, special focus will be made on the pharmacokinetic and pharmacodynamic studies of two drugs, namely, candesartan cilexetil and rosuvastatin calcium when delivered by SLNs.

Energy and sensing applications of one-dimensional conducting polymer nanocomposites

Subhash B. Kondawar

*Department of Physics, Rashtrasant Tukadoji Maharaj Nagpur University, Nagpur - 440033,
India E-mail: sbkondawar@yahoo.co.in*

Conducting polymers are relatively new materials, extensively studied since the Nobel Prize in Chemistry in 2000 for the discovery of the first conducting polymer, polyacetylene. The research in the field of conducting polymers has been established and developed in an unexpectedly accelerated rate. Conducting polymers are unique functional materials owing to their high π -conjugated length, unusual conducting mechanism and reversible redox doping/de-doping process. To improve and extend their functions, the fabrication of multifunctionalized conducting polymer nanocomposites has attracted a great deal of attention because of the emergence of nanotechnology which has become an active field of research because of its tremendous potential for a variety of applications. When the size of many established, well-studied materials is reduced to the nanoscale, radically improved or new surprising properties often emerge. Conducting polymer nanocomposites emerged as a new field of research and development, directed to creation of new smart materials for use in modern and future technologies.

There are mainly four types of nanostructures: zero, one, two and three dimension structures. Among four types of nanostructures, one-dimensional nanostructures (fibers/tubes/wires) have been the focus of quite extensive studies worldwide because of their unique physical and chemical properties. Compared to the other three dimensions, one dimensional nanostructures have high aspect ratio, which could efficiently transport electrical carriers along one controllable direction, thus are highly suitable for moving charges in integrated nano-scale systems. Previous researcher emphasized the fabrication of one dimensional nanostructure of metal and inorganic semiconductors due to their novel electronic and optical properties. Recently, polymeric semiconductors have attracted increasing interest for their advantages of readily tunable bandgaps, rich redox chemistry, excellent flexibility and/or good processibility over conventional inorganic nanomaterials. One dimensional nanostructure conducting polymers have a deep impact on both fundamental research and potential applications in nanoelectronics, nanodevices, nanocomposite materials, bio-nanotechnology and medicine. Several novel methodologies have been developed for the preparation of nanostructure conducting polymers in the form of nanowires, nanofibers, and nanotubules. Conducting polymer nanofibers can be synthesized by several approaches, such as well-controlled solution synthesis, soft-template methods, hard-template methods and electrospinning technology. A powerful method of synthesising nanofibers of polymers and polymer composites is electrospinning, which utilises an applied electric stress to draw out a thin nanometer-dimension fiber from the tip of a sharp conical meniscus. To improve and extend the functions of these organic nanomaterials, one or more components are often incorporated to form multi-functionalized nanocomposites for various applications in the fields of electronics, sensors, catalysis, energy, electromagnetic interference (EMI) shielding, electrorheological (ER) fluids and biomedicine.

The talk on this topic is mainly focused on fabrication of polymer nanofibers by electrospinning, one-dimensional conducting polymer nanocomposites by in-situ chemical polymerization and their applications for supercapacitor and hydrogen gas sensor.

Ultrafast Exciton Dynamics in Alloy and Doped-Alloy Quantum Dot Materials: Implication in Solar Cell

Hirendra N. Ghosh

Radiation & Photochemistry Division, Bhabha Atomic Research Centre,

Mumbai – 400085, (India)

Email: hnghosh@barc.gov.in



Alloy and doped quantum dot (QD) materials have been the focus of material science research investigations due to their wide range of potential applications which includes third generation solar cell. For improving the efficiency of any devices made out of the above materials it's very important to monitor the charge carrier dynamics that includes carrier cooling, trapping and recombination dynamics. Till date not many reports are available on carrier cooling dynamics in doped, alloy and doped-alloy quantum dot materials. We have employed femto-second transient absorption studies on newly synthesized CdS_xSe_{1-x} alloy QDs, Mn-doped CdSe QD and CdSeTe alloy, and ternary CuInS₂ (CIS) alloy QD materials. Cooling dynamics of photoexcited charge carrier was found to be faster in doped QD as compared with that in the undoped QD. On the contrary in CdSeTe alloy material a new charge transfer state is produced where electron cooling dynamics drastically reduced in presence of Mn atom. Again electron cooling dynamics of the CdS_xSe_{1-x} alloy QDs are found to be much slower in contrast to pure CdS and CdSe QDs. Interestingly in CIS alloy defect induced donor sites found to play a major role in carrier cooling dynamics. Cascade of electron cooling dynamics was monitored after following the TA kinetics at different electronic states. Detail mechanism of the above processes involved in different QD materials and their implication in solar energy conversion efficiency will be discussed in the talk.

References:

1. T. Debnath, P. Maity, S. Maiti, and H. N. Ghosh, *J. Phys. Chem. Lett.* **2014**, 5, 2836.
2. P. Maity, T. Debnath, and H. N. Ghosh, *J. Phys. Chem. C*, **2015**, 119, 10785.
3. T. Debnath, S. Maiti, P. Maity, H. N. Ghosh, *J. Phys. Chem. Lett.* **2015**, 6, 3458.
4. P. Maity, T. Debnath, and H. N. Ghosh, *J. Phys. Chem. C*, **2015**, 119, 26202.
5. T. Debnath, S. Maiti, and H. N. Ghosh, *J. Phys. Chem. Lett.* **2016**, 7, (Just Accepted)

Photoluminescent Coatings and Paints

Goutam De

Nano-Structured Materials Division, CSIR-Central Glass and Ceramic Research Institute, 196, Raja S. C. Mullick Road, Jadavpur, Kolkata 700 032, India E-mail gde@cgcri.res.in



Efforts have been made to prepare photoluminescent nanodots (NDs) to cover the entire visible colour emission. Most of these NDs were synthesized in water or other suitable organic solvents in very low concentration, and are not convenient for practical uses. In major applications crucial demand is to confine high concentration NDs in a transparent film matrix. Fundamental hindrance behind this kind of incorporation is phase separation and agglomeration of NDs resulting in damage of their fundamental characteristics. Thus if attempted, severe photoluminescence (PL) quenching occurs due to such aggregation of NDs and of no use for device fabrication. So, quantum confinement of highly concentrated semiconductor or carbon dots in a transparent thin film matrix is a challenging issue. In our work this long demanding issue has been solved in a very cost effective way. We have used inorganic-organic hybrid approach to encapsulate high amount of micelle protected NDs in an organically modified silica (ORMOSIL) film [1] while maintaining their fundamental characteristics. In this lecture basics of PL, concepts of the ORMOSIL film [1] and three different examples [2-4] related to the incorporation of NDs in ORMOSIL will be highlighted. These are synthesis of full visible colour emitting durable high concentration Cd_{0.5}Zn_{0.5}S:Cu quantum dots (QDs) doped ORMOSIL films with high quantum yield on glass substrates [2], carbon nanodots (CNDs) incorporated ORMOSIL sols and films [3] and highly stable CdS:Cu QDs and its hybridization with carbon polymer dots (CPDs) as donor-acceptor pair to produce white light emitting composite NDs while embedding in the ORMOSIL sol and film matrix [4]. Sols can be useful to write or paint on different substrates as well. Such white light emitting durable ORMOSIL films and paints can be useful for device fabrication.

References:

- [1] S. K. Medda, G. De, *Ind. Eng. Chem. Res.*, **2009**, *48*, 4326.
- [2] M. K. Mishra, G. De, *J. Mater. Chem. C*, **2013**, *1*, 4816.
- [3] M. K. Mishra, A. Chakravarty, K. Bhowmik, G. De, *J. Mater. Chem. C*, **2015**, *3*, 714.
- [4] M. K. Mishra, S. Kundu, G. De, *J. Mater. Chem. C*, **2016**, *4*, 1665.

Nano-structures and thin films by pulsed laser deposition for engineering and technology applications

D.Ravinder

Department of Physics, Osmania University, Hyderabad-500007
E:mail: ravindergupta28@rediffmail.com



Abstract

Ferrite nano thin films were deposited from a target of Cu-Zn ferrite onto a sapphire substrate using XeCl excimer laser operating 308 nm with an energy of 225 mJ and a frequency of 30 Hz. Films were deposited from the target onto sapphire (001) substrates heated to 650⁰ C in an oxygen atmosphere of 100 m Torr. The laser beam was incident on the target face at an angle of 45⁰. Studies on crystal structure were done by X-ray diffractometry (XRD). The surface texture, cross-section morphology and grain size was observed by JEOL-JSM-6400 scanning electron microscopy, atomic force microscopy (AFM) and magnetic force microscopy (MFM). The observed results are useful in engineering, technological and potential applications. Potential applications such as (1) high density information storage in computers, (2) ferrofluid technology, magnetocaloric refrigeration, magnetic resonance imaging (MRI) enhancement, magnetic guided drug delivery, microwave devices and magnetic recording media and magnetic sensors.

ABSTRACTS

THE INFLUENCE OF SYNTHESIZED CU NANOPARTICLES ON GERMINATION AND GROWTH OF MUNGBEAN (*VIGNA RADIATA L.*) SEEDS EXPOSED TO CU NANOPARTICLES SUSPENSIONS

N.Jayarambabu^a, B. Siva Kumari^a, K.Venkateswara Rao^b, Y.T. Prabhu^b

^a Department of Botany, Andhra Loyola College, Vijayawada, Andhra Pradesh - India

^bCentre for Nano Science and Technology, Institute of Science and Technology,
Jawaharlal Nehru Technological University Hyderabad, Kukatpally, Hyderabad,
Telangana-500085, India

Abstract

The Cu nanoparticles were synthesized in an aqueous solution in the presence of PVP as stabilizer and CuSO₄ 5H₂O precursor. The synthesis proceed with addition of NaOH as pH adjustment, ascorbic acid as antioxidant and hydrazine hydrate as the reducing agent chemically synthesized copper nanoparticles and their characterization. In our work prepared different concentrations of Cu NPs suspensions (0.0, 50, 100 and 150mg) and seeds soaked in this suspension for 4hours. The examined the effects of Cu NPs on germination and growth of mungbean seeds and examined plant responses to Cu NPs treatment and for seeds planted in homogenized filed soils in a green house. Obtained the results 50mg Cu nanoparticles suspension shown enhanced germination and growth while 150mg significantly reduced the germination and growth. This experiment was conducted under greenhouse conditions.

Key word: Characterization,Cu nanoparticles, Mungbean Seeds, Germination, Growth measurements.

PRELIMINARY PHYTOCHEMICAL SCREENING AND ANTIBACTERIAL ACTIVITY OF *AEGLE MARMELOS*

Ch.Srinu,*¹ G.Sathish, G.Laxmi Prasanna, H. Ramana¹, and R. Vasanthi²

Venkateshwara Institute of Pharmaceutical Sciences, Charlapally, Nalgonda, Telangana State
Nalanda College of Pharmacy, Charlapally, Nalgonda, Telangana.State.

***For Correspondence**

Dr. H. Ramana, Principal, Venkateshwara Institute of Pharmaceutical Sciences, Charlapally,
Nalgonda, Telangana State Ph: +91-9848074857, E-mail: hechhu.ramana@gmail.com

Abstract

The use of traditional medicines holds a great promise as an easily available source as effective medicinal agents to cure a wide range of ailments among the people particularly in tropical developing countries like India. The present study investigates the phytochemical analysis of the major bioactive constituents of *Aegle marmelos* leaf extracts. Qualitative phytochemical analysis of aqueous, ethyl acetate and methanol extracts confirm the presence of Alkaloids, Saponins, Flavonoids and Phenolic compounds in all the three extracts. This indicates that the leaves can be useful for treating different diseases because the therapeutic activity of a plant is due to the presence of particular class of compounds and thus can serve as potential sources of useful drugs in future. The present investigations was undertaken to evaluate the

antimicrobial property of the flowers of *Aegle marmelos*. The studies revealed that methanol extract of *A. marmelos* possess significant antibacterial activity against these species *Bacillus subtilis*, *Staphylococcus aureus*, *Escherichia coli* and *Pseudomonas vulgaris*.

Keywords: *Aegle marmelos*, phytoconstituents and antibacterial

PHYTOCHEMICAL AND ANTIMICROBIAL ACTIVITY OF *OCCIMUM SANCTUM*

Abstract

The present study was carried out to evaluate the phytochemical and antimicrobial activity of *occimum sanctum*. It is an aromatic plant in the family Lamiaceae. The main chemical constituents of Tulsi are Oleanoid acid, Ursolic acid, Rosmarinic acid, Eugenol, Linalool and β caryophyllene. Extensively used in food products, perfumes, dental and oral products. Phytochemical screening of plant leaves reveals the presence of saponins, alkaloids, flavonoids cardiac glycosides, carbohydrates, terpenoids and tannins. Ethanol extract of leaves of *occimum sanctum* was prepared and antimicrobial activity was studied by disc diffusion method. Antimicrobial activity of ethanol extract of leaves in *Occimum sanctum* was carried in attempt to develop a new pharmaceutical drug from natural origin for prevention of pathogenic microbes.

Keywords: Antimicrobial activity, phytochemical analysis, IR studies, *Occimum sanctum*.

STUDIES OF RELAXATION MECHANISM AND ELECTRICAL PROPERTIES OF CE MODIFIED PB(ZR_{0.35}TI_{0.65})O₃ CERAMICS

Balgovind Tiwari^a, E. Siva Naga Vardhan^b

^aDepartment of Physics, RGUKT-RKValley, Idupulapaya, Vempalli, Kadapa 516330, A.P.

^bDepartment of MME, RGUKT-RKValley, Idupulapaya, Vempalli, Kadapa 516330, A.P.

sivanagavardhan.edara@gmail.com, 9493924976

Abstract

Cerium as a modifier has been used for first time to be substituted at B-site of PZT with Zr/Ti ratio of 35/65. For this purpose a high-temperature solid-state reaction technique was used to prepare the samples [i.e., Pb(Zr_{0.35-x}Ce_xTi_{0.65})O₃ (x = 0.00, 0.02, 0.06, 0.10)]. The Nyquist plots (complex impedance analysis) exhibits a significant effect of the grains (bulk) on the conduction mechanism on Ce substituted at Zr site of PZT systems. We did not observe any contribution of grain boundary and interface in the conductivity of these complex material systems. The results and observation of frequency dispersion of impedance also exhibits this similar behavior for both kinds of modifications. The occurrence of single arc in the complex modulus spectrum of all the compositions has shown the single-phase characteristics of modified PZT systems. The

spread and symmetric shape of modulus peaks suggests the existence of non-Debye type multiple relaxations.

Keywords: PZT, Cerium, Relaxation Mechanism, Impedance, Conductivity

PREPARATION OF RARE EARTH ORTHOBORATES, LaBO_3 , GdBO_3 , AND DyBO_3 BY SOL-GEL (GREEN CHEMISTRY) METHOD

Sreenu K*, P.V.B. Rao and Anno Kare

Department of Physics, CNCS Wollega University, Nekemte, Ethiopia.

Abstract

Rare earth Nano orthoborates of composition LaBO_3 , GdBO_3 and DyBO_3 have been prepared by Sol-gel method. This method provides a one of the convenient route for the synthesis of orthoborates at lower temperatures than its conventional solid state method. Powder X-ray diffraction for structural identifications and FTIR spectroscopy were used to vibrational modes evaluations these borates at different temperatures. These rare earth borates are isomorphism with different forms of CaCO_3 depending on the radius of rare earth ion. LaBO_3 crystallized in aragonite structure, GdBO_3 and DyBO_3 crystallized in vaterite structure. The morphology of these borates was obtained from Scanning electron microscopy(SEM).

Keywords: C. Infrared spectroscopy; C. X-ray diffraction; D. Optical properties.

DOPING EFFECT ON CRYSTAL STRUCTURE AND PHASE PROPERTIES OF CHROMIUM DOPED LITHIUM NANO-FERRITE

D.Ravinder Nayak, G.Aravind,B.Neheru,D.Ravinder

Department of Physics, Osmania University, Hyderabad-500007

Corresponding Author email id:ravindergupta28@rediffmail.com

Abstract

Lithium based ferrites are potential applications. Single phase soft ferrite nano crystallites could be synthesized by different methods. Out of various methods We have tried to synthesize Chromium doped Lithium Nano ferrites with a chemical formula $\text{Li}_{0.5}\text{Cr}_x\text{Fe}_{2.5-x}\text{O}_4$ (where $x=0.0, 0.2, 0.4, 0.6, 0.8$ and 1.0) using Citrate- Gel Auto Combustion Technique at low temperature (180°C) to improve their properties. It is a unique combination of the combustion and the chemical gelation processes. They are obtained as dried gel after the successful chemical reaction of these compositions of respective metal nitrate solutions in the midst of citric acid as catalyst. X-ray diffraction (XRD) analysis reveals that all the samples possess a single phase cubic spinel structure particle size of 17nm-26nm. The surface morphology and particle size of the samples was observed by Scanning electron microscopy (SEM) and ICPMS(Inductively coupled plasma mass spectroscopy).

Keywrds: Li-Crnano ferrites, Citrate- Gel Auto Combustion Technique, XRD, SEM, EDAX & ICPMS.

SYNTHESIS AND ANTIOXIDANT ACTIVITIES OF 3,5-DINITRO-4-[5(6)-NITRO-1H-BENZOIMIDAZOL-2-YLTHIO]-BENZENESULFON AMIDES

G. Mohan Rao, E. Ranjith, M. Vasudha and B. Vijaya Kumar

Research Centre, Department of Chemistry, C.K.M. College, Kakatiya University,
Warangal- 506 006 Telangana State, India
E-mail: mrgangula@gmail.com, vijayakumarbaru@gmail.com

Abstract

Benzimidazole is an aromatic heterocyclic compound. It is an important pharmacophore and a privileged structure in medicinal chemistry. 3,5-dinitro-4-(5-nitro-1*H*-benzimidazol-2-ylthio)benzenesulfonic acid has been prepared by the condensation of 4-chloro-3,5-dinitrobenzenesulphonic acid with 5-nitro-1*H*-benzimidazole-2-thiol using conventional and microwave induced methods. 3,5-dinitro-4-(5-nitro-1*H*-benzimidazol-2-ylthio)benzenesulfonic acid on treatment with thionyl chloride and followed by appropriate amines in tetrahydrofuran afford 3,5-dinitro-4-(5-nitro-1*H*-benzoimidazol-2-ylthio)-*N*-phenylbenzenesulfonamides. All the synthesized compounds were characterized by IR, ¹H NMR and Mass spectral data together with elemental analysis. These compounds were screened for antioxidant activity in three concentrations i.e. at 200, 400 and 600 µ g / ml and the activities are expressed in terms of % inhibition of 0.2 mM of DPPH. Their IC 50 values are also determined. Some compounds have shown significant antioxidant activity.

STRUCTURAL CHARACTERIZATION OF NANO CRYSTALLINE MNAl_x Fe_{2-x} O₄ FERRITES

Nehru boda^{1a}, D. Ravinder naik^{1b}, G. Aravind^{1c}, M. Srinivas^{1d},D. Ravinder^{1*}, Gopal boda², A. Panasa Reddy^{2*}

1. Department of physics, Osmania University, Hyderabad, 500007, Telangana, India.
2. Department of chemistry, college of Engineering, Osmania University, Hyderabad, 500007, Telangana, India.

*Correspondence Author; D. Ravinder; Email: ravindergupta28@rediffmail.com

Abstract

Nano crystalline aluminium doped Manganese ferrites having compositional formula MnAl_x Fe_{2-x} O₄ where (x=0.0, 0.2, 0.4, 0.6, 0.8and 1.0) were synthesized by the citrate –gel auto combustion method. Synthesized powders were sintered at 500°C for four hours in an air and characterized by XRD, SEM and EDS. X-ray diffraction analysis of the investigated samples showed cubic spinel structure of the ferrites without any impurity peak, the crystalline size was calculated using the Debye-scherrer formula and found in the range of 22-30nm and the values of lattice parameter (a) and X-ray density (d_x) decreases with the increases of Al³⁺content. Scanning electron microscope (SEM) studies revealed morphology of the Nano crystalline samples. An elemental

composition of the sample was studied by energy dispersive spectroscopy (EDS). The observed results can be explained on the basis of composition.

Key words: Mn-Al Nano ferrites, citrate gel auto combustion method, XRD, SEM and EDS.

STRUCTURAL AND DIELECTRIC PROPERTIES OF CHROMIUM SUBSTITUTED NICKEL NANO-FERRITES

R.Sridhar¹, D.Ravinder², K. Vijaya Kumar³

Vignan's Institute of Technology & Aeronautical Engineering College, Deshmukhi, Nalgonda.

Department of Physics, Osmania University, Hyderabad.

Department of Physics, Jawaharlal Nehru Technological University, Hyderabad, College of Engineering, Nachupally (Kondagattu), Karimnagar-Dist.,

²*Email Id: ravindergupta28@rediffmail.com*

Abstract

Mixed Ni-Cr Nano ferrites having the compositional formula $\text{NiCr}_x\text{Fe}_{2-x}\text{O}_4$ (where $x = 0.1, 0.3, 0.5, 0.7, 0.9$ and 1.0) were synthesized using Citrate-Gel auto combustion method. The materials were characterized by X-Ray Diffractometer (XRD) which confirmed the formation of single phase cubic spinel structure without any impurity peak and average crystallite size was in the range $9 - 11$ nm. The dielectric measurements were carried out at room temperature as a function of frequency and composition(X) in the range of $20\text{Hz} - 2\text{MHz}$. the dielectric constant (ϵ_r) shows a increasing trend with increase of Cr substitution in Ni nano-ferrites. The real part of dielectric constant (ϵ') and dielectric lose tangent ($\tan \delta$) showed a decreasing trend with increasing field frequency. The ac conductivity (σ_{ac}) is calculated from the dielectric measurements, it increases with the rise in frequency.

Keywords: Nano- Ferrites; Citrate-Gel Technique; X-Ray Diffraction; Dielectric Properties

SYNTHESIS, CHARACTERIZATION AND ELECTROCHEMICAL STUDY OF HYDROXY-FUNCTIONALIZED GRAPHENE

1Dipanwita Majumdar* and 2Sujata Pal

*1Department of Chemistry Barasat Govt. College, Barasat, Kokata-700124, WB

2Department of Chemistry, Habra SreeChaitanya College, Habra, WB.

Abstract

Hydroxy-Functionalized Graphene (hG) has been synthesized using one-pot sonochemical technique. The present exploration emphasizes on fabricating grapheme sheets with optimum oxygen functionalities which can help in establishing controlled electrical conductivity as well as appreciable electrochemical signature. Compared to other reported chemical procedures, we have adopted a simple, green, facile-one-pot sonochemical route for the synthesis of the material starting from pristine graphite

powder. The as-synthesized sample was characterized using FTIR, XPS, TGA and FESEM techniques. We further investigated the electrochemical performances using techniques such as cyclic voltammetry and chronopotentiometric charging/discharging cycles. The material shows potential applications as electrode material in energy storage devices.

Keywords: hydroxy-functionalized graphene, oxygen functionality, electrochemical performances.

References:

1. Yan Wang, Zhiqiang Shi, Yi Huang, Yanfeng Ma, Chengyang Wang,, Mingming Chen, and Yongsheng Chen, *J. Phys. Chem. C* **2009**, 113, 13103–13107.
2. Balasubramaniyan Rajagopalan and Jin Suk Chung *Nanoscale Research Letters* **2014**, 9, 535-544.
3. Prasanna Karthika, Natarajan Rajalakshmi, Kaveripatnam S. Dhathathreyan *Soft Nanoscience Letters*, **2012**, 2, 59-66.
4. Bin Xu, Shufang Yue, Zhuyin Sui, Xuetong Zhang, Shanshan Hou, Gaoping Cao, and Yusheng

A NARRATIVE SYNTHESIS AND CHARACTERIZATION OF CELLULOSE NAN FIBERS FROM JUTE FIBER

SNVS Murthy, Tentu Nageswara Raob, S Seshammac and K. Parameswarc

aDepartment of QAU, Vivo Bio Tech R&D Centre, Pragnapur, Medak, Telangana, India.

bDepartment of Chemistry, Krishna University, Machilipatnam, AP, India .

cDepartment of Analytical R&D, Vivo Bio Tech R&D Centre, Pragnapur, Medak, Telangana,

Email: murthychemist@gmail.com

Abstract

Cellulose can be obtained from fibers of plant tissues. Normally the natural fibers are composed through glucose and it's far insoluble in water due to its β (1-4) bonds and interactions of hydrogen bonds between the glucose chains. jute fiber is a wealthy source of fibers and it may be purified to achieve monocrystalline cellulose which might be used for the elaboration of natural nanoparticles. Amorphous areas of cellulose can be functionalized with different chemicals to improve some of its purposeful residences, which may be beneficial to broaden new nanomaterials. The goal of these paintings turned into to synthesis and characterizes cellulose nanofibers from jute fiber through chemical remedy the usage of mineral acids, alkaline and inorganic salts accompanied through mechanical remedy and disintegration techniques. To obtain and separate the cellulose nanofibers; the cellulose changed into purified and hydrolyzed through manner of warmth, sonication and ageing. Scanning electron microscope (SEM), transmission electron microscope (TEM) and x-ray diffraction (XRD) have been used to symbolize morphology, distribution and length. It became found to be distribution of length with maximum 45 ± 10 nm and fluctuated from five to 80 nm with a logarithmic distribution. XRD look at became evaluated for crystalline houses of jute fiber cellulose nanofibers on contrast with acknowledged well known cotton microcrystalline cellulose as reference. This paintings confirmed that it became viable to synthesize cellulose nanofibers from jute fiber, and its characterization

evidenced amorphous and crystalline areas in addition to nanofibers with triclinic structure.

ZNO THIN FILM: SYNTHESIS AND CHARACTERIZATION

T Narender Reddy, B Ramu, M D Vazeed and Ajay Kumar V*

Department of metallurgical and materials engineering,
Rajiv Gandhi University of Knowledge and Technologies-Basar
Basar, Adilabad, Telangana, India
Email: ajay@rgukt.ac.in

Abstract

The Zinc Oxide (ZnO) is a wide band gap n-type semiconductor, by adding impurities into ZnO junction will form and useful for the solar cell application. ZnO thin films were prepared by depositing ZnO solution on glass slide by spin coating, the solution was prepared by sol-gel technique. Zinc acetate dihydrate, 2-methoxy ethanol and monoethanolamine were used as a starting material, solvent and stabilizer respectively. The structural properties of ZnO thin films were characterized by Grazing incident X-Ray diffraction (GIXRD). The surface morphology and chemical composition of prepared zinc oxide thin films were observed by Field Emission Scanning Electron Microscope (FESEM) and Energy Dispersive Spectroscopy (EDS) attached to FESEM. The optical properties of ZnO thin films were studied using UV-Vis spectrophotometer for transmittance, absorption coefficient, energy band gap estimation. The mobility of the ZnO thin film was investigated by Hall Effect.

Keywords—*sol-gel; spin coatings; XRD; morphology*

SYNTHESIS, CHARACTERIZATION AND ELECTROCHEMICAL STUDY OF HYDROXY-FUNCTIONALIZED GRAPHENE

1Dipanwita Majumdar* and 2Sujata Pal

*1Department of Chemistry Barasat Govt. College, Barasat, Kokata-700124, WB
2Department of Chemistry, Habra SreeChaitanya College, Habra, WB.

Abstract

Hydroxy-Functionalized Graphene (hG) has been synthesized using one-pot sonochemical technique. The present exploration emphasizes on fabricating graphene sheets with optimum oxygen functionalities which can help in establishing controlled electrical charge storage revealing appreciable electrochemical signature. Compared to other reported chemical procedures, we have adopted a simple, facile-one-pot sonochemical route for the synthesis of the material starting from pristine graphite powder. The as-synthesized sample was characterized using FTIR, XPS, TGA and FESEM techniques which prompted formation of hydroxyl-functionalized graphene. We further investigated the electrochemical performances using techniques such as cyclic voltammetry and chrono-potentiometric charge/discharge cycles. The material shows potential applications in energy storage devices.

Keywords: hydroxy-functionalized graphene, oxygen functionality, electrochemical performances, specific capacitance, supercapacitor.

APPLICATIONS OF ZINC OXIDE NANOPARTICLES AS CATALYST IN DISSIPATION KINETICS OF QUIZALOFOP-ETHYL HERBICIDE IN DIFFERENT PH WATERS UNDER DIRECT SUN LIGHT

Tentu. Nageswara Rao^a, Tentu. Manohara Naidu^{b*}, T.B Patrudu^c, N. Krishna Rao^a and SNVS Murthy^d

^aResearch Scholar Department of Chemistry, Krishna University, Machilipatnam, AP, India.

^bResearch Scholar Department of Nuclear Physics, Andhra University, Visakhapatnam, AP,

^cDepartment of Chemistry, GITAM University, Hyderabad Campus, Telangana, India.

^dDepartment of QAU, Vivo Bio Tech R&D Centre, Pragnapur, Medak, Telangana, India.

Mobile No. : +91 8121277464, email Id: tentu6581@rediffmail.com.

Abstract

Studied the dissipation behavior of Quizalofop-ethyl under direct sunlight using Zinc oxide nanoparticles as catalyst. Zinc oxide nanoparticles are synthesized and characterized by scanning electron microscopy (SEM), X-ray diffraction (XRD), transmission electron microscope (TEM) and Fourier transform Infrared Spectroscopy (FT- IR). The experiment was conducted by spiking in three different aqueous buffer solutions having pH 4.0, 7.0 and 9.0 to give the uniform concentrations of T0 – Untreated Control, T1 – Quizalofop-ethyl 5.13 % w/v @ 0.2 mg/L of water and T2 – Quizalofop-ethyl 5.13 % w/v @ 0.4 mg/L of water. The spiked samples were kept under sunlight. The sampling occasions were 0.5, 2nd, 4th, 6th, 12th and 24th hour for acidic water (pH 4.0), neutral (pH 7.0) and basic water (pH 9.0). The collected samples were quantified using a validated high performance liquid chromatography with ultra Violet detector (HPLC-UV) at a wave length of 230 nm with flow rate of 1.0 mL/min, injection volume 5 μ L, column oven temperature being 30°C, with mobile phase as acetonitrile: HPLC Water (90:10 (v/v)) and Inertsil ODS, 250 mm x 4.6 mm, 5 μ m column was used. The method has the limit of detection 0.01 mg L⁻¹ and the limit of quantification (LOQ) 0.03 mg L⁻¹ based on signal to noise ratio 3:1 and 10:1 respectively for all the molecules investigated. The residues of Quizalofop-ethyl in aqueous buffer solutions dissipated to below the detectable level by 72nd hour. The DT50 (Half Life) of Quizalofop-ethyl was calculated by regression analysis from the dissipation data.

Key words: Zinc oxide Quizalofop-ethyl Scanning Electron Microscope (SEM) Transmission Electron Microscope (TEM) and High pressure liquid chromatography (HPLC)

**SYNTHESIS AND CHARACTERIZATION OF COPPER OXIDE
NANOPARTICLES USING *OCIMUM TENUIFLORUM* LEAF EXTRACT FOR
BIOMEDICAL APPLICATION.**

Dayakar. T, *K. Venkateswara Rao, CH. Shilpa Chakra.

Center for Nano Science and Technology,
Institute of Science and Technology, JNTUH, Hyderabad.
*Email: Kalagadda2003@gmail.com

Abstract

Anotechnology is one of the fastest developing sciences and Technology over the past few years. This is an emerging field of modern research dealing with synthesis, characterization and designing of biosynthesized nanoparticle structure ranging from approximately 1-100 nm. Copper Oxide (CuO nanoparticles) finds wide range of applications in agricultural, industrial engineering and technological fields. In this present study, we have synthesized CuO nanoparticles using nontoxic ecofriendly biological material namely *Ocimum tenuiflorum* leaf extract. The synthesized nanoparticles undergoes characterization techniques for the conformation of size, shape, structure, functional group, purity of nanoparticles using Scanning Electron Microscope (SEM), Fourier-transform infrared (FT-IR) spectroscopy, transmission electron microscopy (TEM), energy-dispersive X-ray spectroscopy (EDS), X-ray diffraction analysis (XRD), thermo gravimetric analysis (TGA) and differential thermal analysis (DTA). The antibacterial activity of these nanoparticles possess remarkable against human pathogenic bacteria. The antioxidant assay of these nanoparticles was estimated by using DPPH and Reducing power assay. From the obtained results it was suggested that in future, for biomedical concerns CuO nanoparticles could be effectively used.

Key words: Green synthesis, CuO nanoparticles, In-vitro antioxidant and antibacterial assay.

**EFFECT OF CERIUM MODIFICATION ON MORPHOLOGICAL AND
DIELECTRIC STUDIES OF PB(ZR_{0.35}TI_{0.65})O₃ ELECTROCERAMICS**

Balgovind Tiwari¹ and M. Vamsi Yadav²

¹Department of Physics, ²Department of Metallurgy and Materials Engineering,
APIIIT-RKValley, Rajiv Gandhi University of Knowledge Technologies, A.P., India-516330
balgovindtiwari@gmail.com

Abstract

We have used a high-temperature solid-state reaction technique to prepare polycrystalline samples of an electroceramic, lead zirconate titanate modified by cerium (Ce) with Zr/Ti ratio of 35/65 (i.e., Pb(Zr_{0.35-x}Ce_xTi_{0.65})O₃ (x = 0, 0.02, 0.06, 0.10)). The micro-structural analysis of the surface of the compounds by scanning electron microscopy (SEM) suggests that even by substitution of Ce at the Zr-site, the grains are uniformly and densely distributed over the entire surface of all the samples and are spherical in all the cases. Room temperature variation of relative dielectric constant (ϵ_r)

and dielectric loss ($\tan\delta$) as a function of frequency shows that ϵ_r and $\tan\delta$ decreases with rise in frequency, which is a general feature of normal ferroelectric material's dielectric properties, irrespective of composition of the specimens. The higher value of ϵ_r at lower frequencies is due to simultaneous presence of all types of polarizations (i.e., interfacial, ionic, dipolar, electronic, space charge, etc.) in the compounds. Detailed studies of the variation of dielectric properties with a temperature range of RT – 500°C reveal that the compounds showed (i) shift in T_c , and (ii) improvement in dielectric constant and loss.

Keywords: Polycrystalline; Scanning Electron microscopy (SEM); Dielectric constant; Dielectric loss and properties.

SYNTHESIS OF POLYMER BASED NANOCOMPOSITES AND THEIR ANTI BACTERIAL ACTIVITY

V. Sreedhar, Y. Prashanthi

Department of Chemistry, Mahatma Gandhi University, Nalgonda

Abstract

The silver nanoparticle embedded hyperbranched urethane alkyd nanocomposite based high solid antimicrobial coatings, which are useful as binder for protecting wide variety of substrates against corrosion as well as bacterial growth. Hyperbranched polyol (HBP) was synthesized using dipentaerythritol (DPE) as a core material and dimethylol propanoic acid (DMPA) as a chain extender. This was reacted with a varying concentration of linseed fatty acid to make hyperbranched alkyd (HBA) resins containing unreacted hydroxyl groups at outer periphery of the HBP. The resins were characterized by FTIR, ^{13}C NMR techniques. Using the resin with optimum properties, in-situ generation of silver nanoparticle was investigated. Formation of nano silver was confirmed by TEM, AFM, SEM-EDX, XRD and UV-Visible spectroscopic analysis. The surfaces coated with silver nanocomposite coating showed excellent antimicrobial activity against *serratia marcescens*.

Key words : Hyperbranched polymer, silver nanoparticle, antimicrobial activity.

ELECTRICAL AND TRANSPORT STUDIES OF PAN BASED GEL POLYMER ELECTROLYTES

N Krishna Jyothi^{1,2}, K Vijaya Kumar¹, G Sunita Sundari¹, P Narayana Murthy²

1-Dept. of Physics, K L University, Guntur Dt., A.P.

2-Dept. Of Physics, A N University, GunturDt. A.P.

mail: jyothinadella@kluniversity.in

Abstract

The gel polymer electrolyte films consisting of Polyacrylonitrile (PAN) as the host polymer, Sodium iodide (NaI) as dopant salt and Ethylene carbonate (EC) as plasticizer were prepared in different weight percent ratios of polymer and salt (polymer/salt=90/10;80/20;70/30;60/40) by the solution cast technique using DMF as

solvent. The PAN films were prepared without and with plasticizer as a reference. The electrical studies were performed using lab made conductivity setup. The complex formation between polymer and dissociated salt has been confirmed by Fourier transform infrared spectroscopy (FTIR). The pure PAN is thermally unstable. The addition of plasticizer EC increases thermal stability, mechanical strength and conductivity of gel polymer electrolyte. The variation of conductivity with salt concentrations from 10 wt.% to 60 wt.% was studied. The gel polymer electrolyte with composition 30 wt.% of NaI exhibited the highest conductivity of 5.99×10^{-4} S cm⁻¹ at 303K and 3×10^{-3} S cm⁻¹ at 373K. The conductivity temperature dependence of gel polymer electrolyte films obeys Arrhenius relationship which shows ionic hopping motion. The transport numbers both electronic (t_e) and ionic (t_i) were calculated using Wagner's polarization technique and it reveals the conducting species are predominantly due to ions. The ionic transport number for highest conducting film was found to be 0.991. It is found that the ionic conductivity and transport properties of the prepared gel polymer electrolytes are consistent with FTIR spectroscopic studies.

Key words: Gel polymer electrolytes, ionic conductivity, transport number, plasticizer, FTIR.

NANOEMULSION BASED HYDROGELS OF ITRACONAZOLE FOR TRANSDERMAL DRUG DELIVERY

Sunitha Sampathi^{1*}, Jitendra Wankar¹, Rakesh Achanta²

¹ Department of Pharmaceutics, National Institute of Pharmaceutical Education and Research (NIPER-HYD), Balanagar, Hyderabad, A.P. - 500037, INDIA.

Abstract

The present study aimed to formulate a nanoemulsion and nanoemulsion based hydrogel of itraconazole for transdermal delivery in the treatment of onchomycosis. The nanoemulsions were prepared using lecithin and sodium cholate as surfactant and co-surfactant. The prepared nanoemulsions were characterized for particle size and zeta potential. The optimized nanoemulsion was incorporated into 3% carbopol-934 solution to get a gel for improving convenience in superficial application. *In vitro* and *ex vivo* drug penetration studies of nanoemulsions and gels were determined using dialysis membrane and rat skin. FT-IR was performed to know the compatibility between the drug and excipients. The particle size was found around 223.9 nm to 154.3 nm. The viscosity of the nanoemulsions and nanoemulsion gel were found around 1964.89 mPa.S to 1644.82 mPa.S and 28.3 mPa.S to 8.58 mPa.S respectively. The polydispersibility value was found very low indicating uniformity of droplet size of the formulations. The drug content in gels was found in between 86.2% to 98.26%. The drug release was found to be 44.33 % to 73.6% after 24 h with permeation flux around 296.3 to 203.1 ($\mu\text{g}/\text{cm}^2/\text{hr}^1$). The results indicated that nanoemulsion based hydrogels

as promising vehicle for transdermal delivery of itraconazole. Further *in vivo* studies are to be performed to access its suitability for topical application.

Key Words: Itraconazole, nanoemulsion, nanoemulsion based hydrogel, lecithin, sodium cholate, carbopol.

NANO TECHNOLOGY PLAYS KEY ROLE TO REDUCE WATER POLLUTION

M. Rajendra Prasad, Y. Shalini, ^{\$}M. Jyothsna, V. Suresh, *G. Mahesh and N. Sumalatha

*Department of Plant pathology, ^{\$}Agronomy, *Entomology College of Agriculture, ANGRAU, Rajendranagar, Hyd-30
(E mail: yerukalashalini@yahoo.com)*

Abstract

Environmental nanotechnology is considered to play a key role in the shaping of current environmental engineering and science. Looking at the nano scale has stimulated the development and use of novel and cost-effective technologies for remediation, pollution detection, catalysis and others. However, there is also a wide debate about the safety of nano particles and their potential impact on environment and biota. New field of nano toxicology has received a lot of attention in recent years. There is the huge hope that nano technological applications and products will lead to a cleaner and healthier environment. Maintaining and re-improving the quality of water, air and soil, so that the Earth will be able to support human and other life sustainably, are one of the great challenges of our time. The scarcity of water, in terms of both quantity and quality, poses a significant threat to the well-being of people, especially in developing countries. The toxicity of some nanoparticles can be used for water disinfection where killing of microorganisms is intended, whereas the same property is unwanted when nanoparticles eventually enter the environment. The catalytic activity of a nanoparticle can be advantageous when used for the degradation of pollutants. The high absorption capacity of certain nanoparticles is exploited for the removal of organic and inorganic pollutants. Nanoparticles can increase the storage capacity of batteries and rechargeable batteries or used in flat screens where they reduce the amount of heavy metals.

MOLECULAR DIVERSITY STUDIES IN MUNGBEAN USING SSR MARKERS

**¹M. JYOTHSNA NAND; ²CH. ANURADHA; ³J. SATEESH BABU;KAMALA
⁴VENKATESWARAN; ⁵ K. ANITHA**

^{1,2}Institute of Biotechnology, ANGRAU, Hyderabad. ³ LAM Research station, Guntur

^{4,5} NBAGR, Hyderabad E-mail: jyothsna.cabm@gmail.com

Abstract

Estimation of genetic diversity in a crop species is prerequisite for its improvement. DNA markers provide an opportunity to characterize genotypes and to measure genetic

relationships precisely than other markers. Microsatellite markers are among the most popular genetic markers due to their characteristic features like high polymorphism, co-dominance, abundant informativeness, convenience of assay by PCR and distribution throughout the genome. In the present study, 50 SSR markers were used to analyze the genetic diversity of 54 mungbean genotypes, only 14 primers detected polymorphism while remaining 36 primers were monomorphic. The neighbour-joining tree developed based on weighted average for dissimilarity matrix using DARWIN, grouped the 54 genotypes into three clusters. Cluster-I contains 25 genotypes and the similarity coefficients ranged from 20-50% from similarity matrix, Cluster-II contains 15 genotypes and the similarity coefficients ranged from 22-62%, Cluster-III contains 14 genotypes and the similarity coefficients ranged from 16-45%.

POLYSACCHARIDE NANOPARTICLES AS DRUG CARRIERS IN CANCER TREATMENT

Murthy Chavali¹

¹ *Division of Chemistry, Department of Sciences and Humanities, Vignan University, Vadlamudi, Guntur 522 213 Andhra Pradesh, INDIA.*

Abstract

Nanoparticles owing to their small size, modified surface, improved solubility and multi-functionality, they have shown huge potential in biological, medical and pharmaceutical applications. Nanoparticle can pass through the smallest capillary vessels, restrict access of the drug to the chosen sites, and deliver the drug at a controlled and sustained rate to the site of action. They can penetrate cells and tissue gap, improve the pharmacokinetic and pharmacodynamics properties of drug, utility of drugs by reduce the toxic side effects. Drug delivery systems of nanoparticles have several advantages, such as high drug encapsulation efficiency, efficient drug protection against chemical or enzymatic degradation, unique ability to create a controlled release and cell internalization.

Polysaccharide based nanoparticles have received considerable attention in recent years as one of the most promising materials in the preparation of nanometric carriers. Polysaccharides have significant pharmacological Anti-tumour activity. Polysaccharides are highly stable, safe, non-toxic, hydrophilic and biodegradable. Polysaccharides have a large number of reactive groups, a wide range of molecular weight, varying chemical composition, which contributes to their diversity in structure and in property. One of the main advantages of polysaccharides as natural biomaterials, is their availability in natural resources and low cost in their processing, which make them very accessible materials to be used as drug carriers. In this work, we focus on

methods of preparation, characterisation of various polysaccharide nanoparticles and their physicochemical effects on Cancer cells have been discussed.

Keywords: *Polysaccharides, Nanoparticle, Drug delivery, Preparation, Characterization, Cancer cells.*

POLYSACCHARIDE NANOPARTICLES AS DRUG CARRIERS IN CANCER TREATMENT

Yugandhar Parepalli¹, Sudhakar Reddy Pamanji² and Murthy Chavali^{1*}

*1 Division of Chemistry, Department of Sciences and Humanities, Vignan University,
Vadlamudi, Guntur 522 213 Andhra Pradesh, INDIA.*

*2Department of Zoology, Vikrama Simhapuri University Post-Graduate Centre (P.G. Centre),
Kavali 524 201 Andhra Pradesh, INDIA.*

Abstract

Nanoparticles owing to their small size, modified surface, improved solubility and multi-functionality, they have shown huge potential in biological, medical and pharmaceutical applications. Nanoparticle can pass through the smallest capillary vessels, restrict access of the drug to the chosen sites, and deliver the drug at a controlled and sustained rate to the site of action. They can penetrate cells and tissue gap, improve the pharmacokinetic and pharmacodynamics properties of drug, utility of drugs by reduce the toxic side effects. Drug delivery systems of nanoparticles have several advantages, such as high drug encapsulation efficiency, efficient drug protection against chemical or enzymatic degradation, unique ability to create a controlled release and cell internalization.

Polysaccharide based nanoparticles have received considerable attention in recent years as one of the most promising materials in the preparation of nanometric carriers. Polysaccharides have significant pharmacological Anti-tumour activity. Polysaccharides are highly stable, safe, non-toxic, hydrophilic and biodegradable. Polysaccharides have a large number of reactive groups, a wide range of molecular weight, varying chemical composition, which contributes to their diversity in structure and in property. One of the main advantages of polysaccharides as natural biomaterials, is their availability in natural resources and low cost in their processing, which make them very accessible materials to be used as drug carriers. In this work, we focus on methods of preparation, characterisation of various polysaccharide nanoparticles and their physicochemical effects on Cancer cells have been discussed.

Keywords: *Polysaccharides, Nanoparticle, Drug delivery, Preparation, Characterization, Cancer cells.*

NANO MATERIALS FOR ELECTROCHEMICAL SENSORS

K. Chandrasekara Pillai

*Department of Physical Chemistry, University of Madras, Guindy Campus
Chennai- 600 025, INDIA*

Abstract

Nanomaterials constitute an emerging sub-discipline in the chemical and materials science. Nanomaterials have numerous commercial and technological applications including analytical chemistry, drug delivery, bioencapsulation, electronic, optical and mechanical devices. The enhanced surface area effects and increased electron transfer kinetic properties associated with the nanomaterials have been recognized to be of immense use in electrochemistry for developing them as molecular electrode materials for electrocatalysis and electroanalysis.

Design and development of inexpensive H₂O₂ sensor materials with high sensitivity, selectivity, and stability is of current interest for the development of biosensors based on the redox enzymes. Prussian blue (PB) is one such material with highly promising analytical properties towards H₂O₂ monitoring. However, its real-time performance is severely impeded due to its poor operational stability. Recently, we reported that nano clustered PB material (50 to 60 nm dia) prepared on a glassy carbon electrode by a simple one-pot electrochemical route could solve this instability problem to some extent [1,2]. It was further shown that PB sensor stability and its over-all analytical performance could be improved tremendously with still smaller sized PB nano-particles (10–20 nm dia) prepared from solutions of structure-directing soft-template surfactants like CTAB [1,2]. The utility of nano-structured CTAB-PB composite has also been extended for amperometric sensing and estimation of another biomolecule, namely, reduced glutathione [3].

Our other recent work on nano materials as amperometric sensors for H₂O₂ estimation in physiological conditions concerns with (i) nano copper species immobilized functionalized-multiwalled carbon nanotube + chitosan film [4], and (ii) PtM (where M = Pd, Ir) bimetallic nanoparticles [5]. All the details on preparation, characterization and utility will be presented and discussed.

IMPEDANCE STUDIES ON CHROMIUM SUBSTITUTED COBALT NANO FERRITES

M. Raghасudha^{1*}, D. Ravinder², P. Veerasomaiah¹, Shyamsunder goud¹, G. Satyanarayana Goud, B. Rambabu¹, N. Venkatesh¹

1. Department of Chemistry, University college of Science, Osmania University, Hyderabad-500007, Telangana, India 2. Department of Physics, University college of Science, Osmania University, Hyderabad-500007, Telangana, India 3. Department of Chemistry, M.V.S. Govt. Degree College, Mahabubnagar-509001, Telangana, India

*Corresponding author E Mail: raghasudha_m@yahoo.co.in

Abstract

Chromium substituted cobalt nano ferrites with the chemical composition $\text{CoCr}_x\text{Fe}_{2-x}\text{O}_4$ ($x=0.0, 0.5$ and 1.0) were synthesized by Citrate-gel auto-combustion method. X-ray diffraction analysis of all the chromium substituted cobalt ferrites confirmed the formation of a homogeneous single phased cubic spinel with a crystallite size of the particles in the range of 6-12nm. The impedance measurements were used to study the effect of grain and grain boundary on the electrical properties of the synthesized samples. The impedance measurements of the Co-Cr nano ferrites were carried out at room temperature in the frequency range of 100Hz to 1MHz. One semicircle observed in the Cole-Cole impedance plots of the ferrite compositions indicates that the conduction mechanism is solely due to the grain boundary.

Key words: Nano ferrites, Citrate gel method, Impedance study, Cole-Cole impedance plots

BIOSYNTHESIS OF NANOPARTICLES USING *DESMOSTACHYA BIPINNATA*

Swetha Garimella*

University College of Science and Informatics, Mahatma Gandhi University, Nalgonda

Abstract

Biosynthesis of silver nanoparticles using plant leaf extracts of *Desmostachya bipinnata* leaves extract was investigated in this study. Leaves extract prepared by using different Milli-Q-water were mixed with silver nitrate for synthesis of silver nanoparticles. Active photochemical present in the plant were responsible for the quick reduction of silver ion (Ag^+) to metallic silver nanoparticles (Ag^0). The reduced silver nanoparticles were characterized by UV-vis spectroscopy; FTIR and SEM. *Desmostachya bipinnata* plant materials mediated synthesis of silver nanoparticles is comparatively rapid and less expensive and could be applied in modern and ayurvedic medicine

Key words: *Desmostachya bipinnata*, Silver Nanoparticles, FTIR, SEM.

GREEN PREPARATION, CHARACTERIZATION OF PALLADIUM NANOPARTICLES BY GUM KARAYA AND THEIR FREE RADICAL SCAVENGING

Amrutham Santoshi Kumari, Maragoni Venkatesham, Dasari Ayodhya, Guttena Veerabhadram.

Department of Chemistry, University College of Science, Osmania University, Hyderabad-07.

Email: gvbhadr@gmail.com

Abstract

Synthesis of Palladium nanoparticles (PdNPs) by Gum Karaya (GK) in a single step reaction. GK acted as both the reducing as well as stabilising agent for the obtained nanoparticles. The uniqueness of this method is the high rate of synthesis using microwave irradiation method in Microwave oven at 320W for 10 mins. The formation and size of the PdNPs were characterized by UV-visible spectroscopy (UV-Vis), X-ray diffraction (XRD) and Fourier transform infrared spectroscopy (FTIR) and Transmission electron microscopic (TEM) techniques. The catalytic activity of PdNPs was examined spectrophotometrically through the free radical scavenging of DPPH. The PdNPs stabilized in GK exhibited very good catalytic activity and the kinetics of the reaction was found to be pseudo first order with respect to the DPPH.

Key words: Green synthesis, Radical scavenging, Gum Karaya, Microoven and DPPH.

BIOLOGICAL SYNTHESIS OF SILVER NANOPARTICLES USING COCONUT FRUIT GUM, STUDY OF ANTIBACTERIAL AND CYTOTOXIC ACTIVITY

Raju Nalvothula, Jahnavi Alwala, M.P.Pratap Rudra

Abstract

Silver nanoparticles were bio synthesized using aqueous extract of coconut fresh fruit gum. The synthesized nanoparticles were characterized by UV-Visible Spectrophotometer, Fourier Transform Infrared (FTIR) spectroscopy , Scanning Electron Microscope (SEM), Transmission Electron Microscopy (TEM) and EDAX analysis. The characterization results confirmed the formation silver nanoparticles. EDAX analysis confirmed the presence of an elemental silver signal without any peaks of impurities. The bio synthesized silver nanoparticles were studied for their antibacterial activity against *E.coli*, *B.subtillis*, *S.aureus*, *K.pneumonia* bacteria. It was observed from the results that synthesized Ag nanoparticles have mild antibacterial activity against the tested bacteria. Maximum zone of inhibition was observed for ***K.pneumoniae* bacteria followed by *B.subtillis* baceria**. Cytotoxic activities of synthesized Ag nanoparticles

were investigated in five different types of human cancer cells. It is evident from the results that the biosynthesized AgNPs showed strong anti-proliferative activity against U937 cell line (human histiocytic lymphoma).

Key words: Biological synthesis, antibacterial studies, cytotoxic studies, silver nano particles, coconut fruit gum.

GREEN SYNTHESIS OF GOLD AND SILVER NANOPARTICLES USING AVERRHOA BILIMBI FRUIT EXTRACT

R. S. Rimal Isaac, G. Sakthivel, and Ch. Murthy

Department of Nanotechnology, N.I. University, Kumaracoil, Tamil Nadu 629 180, India

Abstract

We report on rapid one-step green synthesis of gold and silver nanoparticles using fruit extract of *Averrhoa bilimbi* Linn. UV-Vis absorption spectroscopy was used to monitor the quantitative formation of gold and silver nanoparticles. The characteristics of the obtained gold and silver nanoparticles were studied using UV-Vis absorption spectroscopy (UV/Vis), Fourier transform infrared spectroscopy (FTIR), Scanning electron microscopy (SEM), and Energy-dispersive spectroscopy (EDX). UV/Vis spectrum showed Surface Plasmon Resonance (SPR) for both gold and silver nanoparticles at 540 and 420 nm. The EDX spectrum of the solution containing gold and silver nanoparticles confirmed the presence of elemental gold and silver signals. The average diameter of the prepared nanoparticles in solution was about 50–150 nm. Synthesized particles were either hexagonal or rhomboidal in shape. This synthesis approach of gold and silver nanoparticles is cost effective and can be widely used in biological systems. The effect of fruit extract and metal ion concentration was also studied.

IN VITRO SYNTHESIS, CHARACTERIZATION AND MEDICAL APPLICATION OF SILVER NANOPARTICLE BY USING A LOWER FUNGI

R. Nithya and R. Ragunathan

Department of Bioscience and Research Coimbatore-50, Tamilnadu

Abstract

Nanotechnology is a rapidly growing science of producing and utilizing nano sized particles that measure in nanometers. In this study we have reported the biological synthesis of silver nanoparticles using *Aspergillus niger* and its antimicrobial properties. The extracellular mechanism of silver nanoparticle creation was investigated

by UV-VIS spectroscopy, FTIR spectroscopy. The mechanism leading to nanoparticle formation was studied using nitrate reductase assay. The particles were further characterized using SEM with EDS, Particle size analysis. Obtained silver nanoparticles when tested for the antimicrobial action showed good results against the Gram positive and Gram negative bacteria.

Key words: Aspergillus niger Silver nanoparticle UV-VIS spectra SEM Particle size analysis Antimicrobial activity INTRODUCTION extracellularly by the fungus Aspergillus fumigatus

NANOFLUIDS WITH ENCAPSULATED TIN NANOPARTICLES FOR ADVANCED HEAT TRANSFER AND THERMAL ENERGY STORAGE

Sreeram Cingarapu¹, Dileep Singh¹, Elena V. Timofeeva² & Michael R. Moravek¹

Nuclear Engineering Division, Argonne National Laboratory, Argonne, IL 60439, USA

Abstract

Novel high-temperature heat transfer fluids (HTFs) with incorporated phase change nanomaterials were synthesized and tested for heat transfer and thermal energy storage. The advanced thermal properties were achieved by preparing a nanofluid consisting of core/shell silica encapsulated tin (Sn/SiO₂) nanoparticles dispersed in a synthetic HTF Therminol 66 (TH66) at loadings up to 5 vol%. Tin nanoparticles were synthesized by modified polyole reduction method followed by sol-gel silica encapsulation process. The measured increase in thermal conductivity of the nanofluid (~13% at 5 vol %) was in agreement with Maxwell's effective medium theory. Latent heat of phase change during melting of Sn core added ~11% increase to the volumetric thermal energy storage of the nanofluid when cycled in between 100 °C and 270 °C. The value could be further improved if thermal cycling is conducted in a narrower temperature range. The experimental results demonstrated dual functionality of the engineered nanofluids as desired for Concentrated Solar Power systems. Viscosity and stability of the nanofluids as well as thermal stability of core/shell nanomaterials) were investigated in a wide temperature range to obtain a perspective on any additional pumping power requirements for the nanofluid over the base fluid.

Key words : Thermal energy storage; heat transfer fluid; nanofluid; core-shell nanoparticles; phase change material; latent heat; thermal conductivity; tin nanoparticles

SYNTHESIS OF CHITOSAN / ZINCOXIDE NANOCOMPOSITES & THEIR ANTI BACTERIAL ACTIVITIES

J. Shankara Chari, K. Amarander

Department of Chemistry, Mahatma Gandhi University, Nalgonda

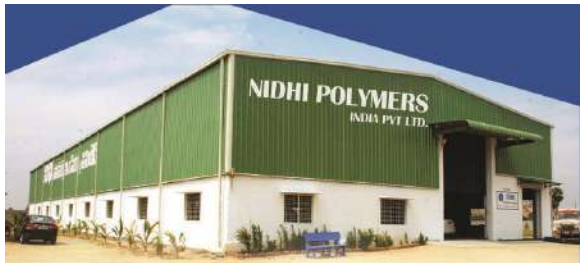
Abstract

Zinc Oxide nanoparticles (ZNPs) and CS/Zinc oxide nanocomposites (CS/ZnO NCs) were successfully synthesized by wet chemical method. Formation of ZNPs and the interaction of CS/ZnO NCs were characterized by X-ray diffraction (XRD), Zeta potential, and Transmission Electron Microscopy (TEM) techniques. Thermal stability of the prepared samples was characterized by Thermogravimetric Analysis (TGA). TEM images shows the interaction between the ZNPs and CS polymer and the particles has spherical like structure with average crystallite size of 22 nm and is in good agreement with XRD results. The aim of this study was to investigate the attachment of these nanoparticles with Escherichia coli (E. coli) bacterial outermost cell membrane and their mode of action against these bacterial strains by agar well diffusion method and resazurin dye reduction method. Both the test materials synthesized revealed resistivity against E. coli up to 6 mg/mL.

Keywords: Chitosan; Nanocomposites; Escherichia; Diffusion; Resazurin; Resistivity.







Nidhi PVC & HDPE Pipes is a fifteen year old enterprise, a pioneer in Designing, Developing and Manufacturing high quality uPVC and HDPE pipes for potable water supplies. Nidhi has carved a niche in this field of pipes and fittings for Water Management, Irrigation, Water Distribution and Sewage Disposal Systems. Backed by long experience, sophisticated infrastructural facilities & trained manpower Nidhi offer high quality products that are known for their superior performance, durability and negligible maintenance.

Nidhi's supreme quality has won the confidence of many Building Contractors, Govt. Departments and leading Architects & Consultants and thereby, included us in their projects.

We are engaged in manufacturing of all types of PVC & HDPE Pipes ranging from 20 mm to 315 mm diameter (20mm, 25mm, 32mm, 40mm, 50mm, 63mm, 75mm, 90mm, 110mm, 125mm, 140mm, 160mm, 180mm, 200mm, 225mm, 250mm, 280mm, 315mm) respectively.

We strive to remain at the forefront of technological innovation and product excellence through use of cutting edge technology and state-of-the-art systems and thus are committed to continuously offer new solutions that shall add value to all its stakeholders.



NIDHI
HDPE Pipes PVC Pipes

Nidhi Polymers India Pvt. Ltd. :
Arjalabai, Opp. Andhra Jyothi,
Addanki Bypass Road, NALGONDA.
Cell : 9948222119, 9948222115
web : www.nidhipipes.in; email : nidhipipesindustry@gmail.com

Nidhi PVC Industries :
Arjalabai, Opp. Sakshi News paper,
Addanki Bypass Road, NALGONDA.
Cell : 9948222114, 9948222118

RAJ Graphics, Agra, U.P., INDIA

నమ్మకమైనది..
దృఢమైనది...
మన్మికయినది....

రథ

ప.వి.సి. హైపులు

మీరు లసుకున్న
ప్రదేశానికి నాలో ప్రవేశంచే
నీదిని 100% సురక్షితంగా
నేపు తీసుకెళజా....



20mm to 315mm

NIDHI
HDPE Pipes PVC Pipes



NIDHI
PVC & HDPE PIPES
Reliable Time Bound
Quality Supply.

OUR PRODUCTS



PVC and uPVC Pipes

We are leading
Manufacturers and
Suppliers of
PVC Pipes...



Electrical Pipes

Nidhi's electrical
conduit pipes are
applied in
industries...

NIDHI'S QUALITY CONTROL AND TECHNOLOGY ADVANCEMENTS

Nidhi PVC, uPVC & HDPE pipes is ISO certified and are manufactured using system controlled and imported automatic machines that can give tremendous quality and performance to the pipes. Each product is prepared as per the BIS norms. We strive to remain at the forefront of technological innovation and product excellence through use of cutting edge technology and state-of-the-art systems and thus are committed to excellent quality and thereby, continuously offer new solutions that shall add value to all its stakeholders.



NIDHI PIPES
combines the state
of the art technology
with long standing
customer
relationships.



Casing Pipes

Casing pipes have
high impact and
compressive
strengths...



SWR Pipes

SWR Pipes
demanded by
the clients all
over the
country...



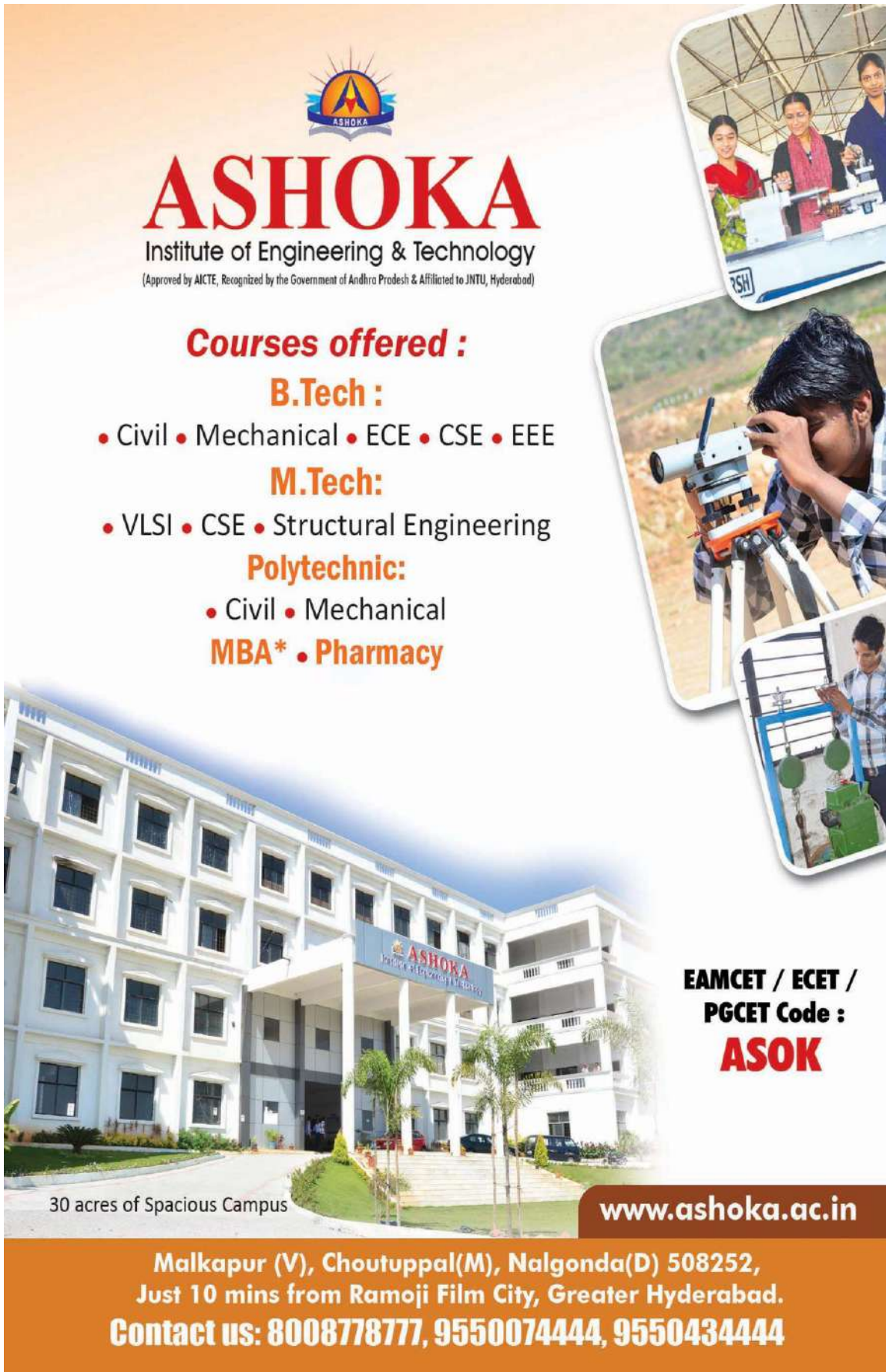
Blue Casing Pipes

We offer a comprehensive
range of blue casing
pipes...



HDPE Pipes

We are a highly
acclaimed
Manufacturer of
HDPE Pipes...



The image features the Ashoka Institute of Engineering & Technology logo at the top left. Below it, the word "ASHOKA" is written in large red letters, with "Institute of Engineering & Technology" in smaller black text underneath. A small note in parentheses states: "(Approved by AICTE, Recognized by the Government of Andhra Pradesh & Affiliated to JNTU, Hyderabad)". To the right of the text are three circular inset images: one showing two women working with lab equipment, another showing a student looking through a telescope, and a third showing a student working with a mechanical device.

Courses offered :

B.Tech :

- Civil • Mechanical • ECE • CSE • EEE

M.Tech:

- VLSI • CSE • Structural Engineering

Polytechnic:

- Civil • Mechanical

MBA* • Pharmacy

**EAMCET / ECET /
PGCET Code :
ASOK**

30 acres of Spacious Campus

www.ashoka.ac.in

**Malkapur (V), Choutappal(M), Nalgonda(D) 508252,
Just 10 mins from Ramoji Film City, Greater Hyderabad.**

Contact us: 8008778777, 9550074444, 9550434444



నాగార్జున కళాశాల

నాగార్జున నగర్, మిర్యాలగూడ, సెల్ : 9248022700/703.



B.Sc

Maths - Chemistry - Computer Science
Maths - Physics - Chemistry (TM & EM)
Micro Biology - Zoology - Chemistry
Micro Biology - Botany - Chemistry
Botany - Zoology - Chemistry (TM & EM)

B.Com

General
Computer Science

B.A.

History - Political Science - English (Litt.)
History - Political Science - Telugu (Litt.)
Economics - History - Political Science

MBA

MSc

Organic Chemistry

& B.Ed. D.Ed.

INTERMEDIATE

MPC | **BPC**
CEC + **HEC**

MLT, MPHW(F)

ప్రసిద్ధం : ఎ. మధుసూధన్ రెడ్డి M.Sc (Bio & Phy) B.Ed. M.Phil. (Ph.D)

కరసౌందర్య : ఎ. సఖింఛురెడ్డి

స్వాతంత్ర్య మొదటి పంచుకూరు నుండి అత్యుత్తమ ధనియలు సాధ్యమైన వీడ్యూల ట్రైక్ ట్రైగ్ కళాల పోతల ఫోన్ : 234742, మొబైల్ : 9989918825.



శ్రీ ఛాయితన్య

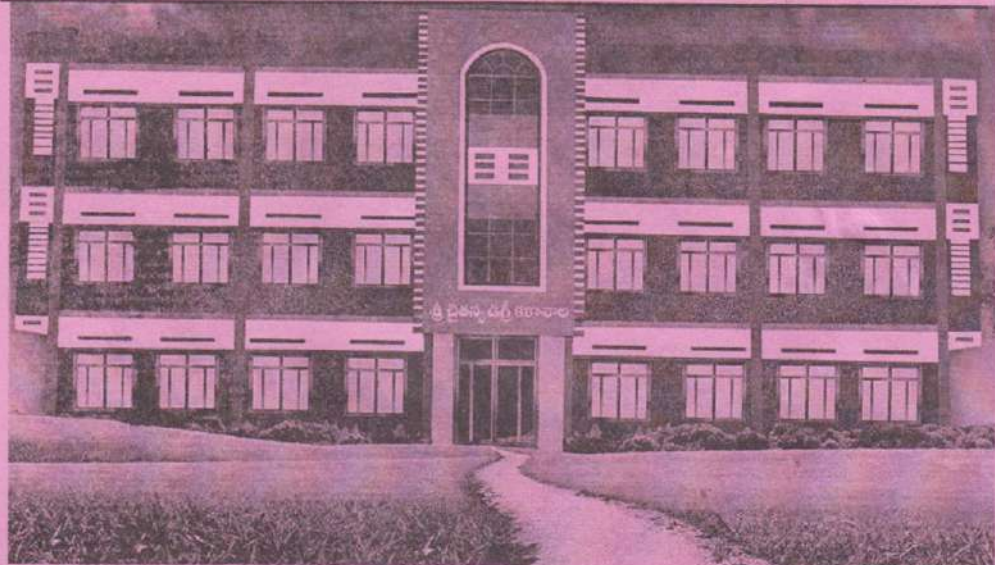
డిగ్రీ

కళాశాల

కో-ఎడ్యుకేషన్

బస్సిస్టాండ్ దగ్గర, విద్యార్థిమర్ స్కూల్ ప్రక్కన, అన్నార్ కాలసి, వల్లాదూర్.

(మహాత్మగాంధీ యూనివర్సిటీ అనుబంధం) (Regd. No. 3182H/512/2002-03/Acad/IV-2)



మా ప్రత్యేకతలు :

ఈ మంచి అనుభవం కలిగిన అధ్యాపకులచే విద్యార్థిదన.

ఈ ప్రశాంతమైన వాతావరణంలో అత్యంత విశాలమైన లాంతులు.

కళాల భవనం, అధ్యాపకుల లాల్ సాకర్యం.

ఈ దూరప్రాంతం నుండి విద్యార్థులకు బస్సిస్టాండ్ కు అది దగ్గరలో గల వీడ్యూల ట్రైక్ ట్రైగ్ కళాల.

ఈ మొదటి సంవత్సరము నుండి M.Sc., M.A., & B.Ed., తదితర కాంపిటీషన్ పరీక్షలకు తిక్షణ.

ఈ B.C., S.C., S.T. విద్యార్థులకు స్కూలర్సిప్ సికర్యం. NSS, Sports మరియు విషధ శ్రీపతిలలో తిక్షణ ఇవ్వబడును.



Courses Offered :

B.Sc.	M.P.Cs. M.P.C. B.Z.C.	B.A.	E.H.P. E.P.P. H.P.P. T.H.P.	B.Com.	Computers
--------------	-----------------------------	-------------	--------------------------------------	---------------	-----------

సెక్యూరిటీ

శ్రీ ఛాయితన్య డిగ్రీ కళాశాల, నెల్లగిండ.

గోక్కుర్ స్కూలర్స్, వి.టి.ఎస్, రామగౌరి, శ్రీకాండ, ఫోన్ : 223539, మొబైల్ : 9440102039.

With Best compliments from:-

Ashwini Chemicals & Instruments
SUPPLY OF
Laboratory Chemicals of Organic & Inorganic,
Physical Instruments of all types of equipments
Electronic Systems of Digital functions sets
Mechanical Engineering Lab. Works
Chemical Engineering Lab. setup
Glassware of all types of lab's &
Specific design glass Mouldings
Computer peripherals of all types of
Softwares like PRO-ENGG. autocad design
with mechanical instruments tools

Over 25 years experience

Lets See inside our Web site of
<http://www.ashwinichemicals.4mg.com>

On line Enquiry
(Send enquiry : Receive Quotations with full details of items price with photographs)
Watch the Web
with full multimedia Digital sound systems and animation of mechanical operations units with their specific explanations of different Voices with musical Instruments
U "DON'T MISS IT"

Contact for brouchers,pamphlets, ACI
Materials and further details :-

Ashwani Chemical & Instruments
Parsigutta,Hyderabad - 500 020 (**INDIA**),
Ph: 040-27630967, FAX :040-27630967
e-mail: ashwini_chem@yahoo.com
<http://www.ashwinichemicals.4mg.com>
Mobile: 9848240740

INSTRUMENTS :

- | | | |
|---------------------------|----------------------------|---------------------------------|
| 1. Autoclave | 21. Cooling centrifuge | 41. Microscope |
| 2. Water bath | 22. Micro centrifuge | 42. Cell counter |
| 3. Incubator | 23. Electrophoresis unit | 43. Ultra Cryostat |
| 4. Hotplate | 24. Power pack | 44. Ultra Bath |
| 5. Hotair oven | 25. Magnetic stirrer | 45. LCD Projectors |
| 6. Vacuum pump | 26. Orbital shaker | 46. OHP Projectors |
| 7. Anerobic culturejar | 27. Over Head Projector | 47. Laser Pointers |
| 8. Seiz filter | 28. Slide projector | 48. OHP -special coated Sheets |
| 9. Muffle furnace | 29. Heating mentle | 49. Computers -All Brands |
| 10. Digital balance | 30. Variable Auto pipette | 50. Lap Tops - All Brands |
| 11. Weighing balance | 31. Laminar flow | 51. Accessories- Any Parts |
| 12. Colony counter | 32. Hemocytometer | 52. Softwares - All Subjects |
| 13. Distilled water plant | 33. T L C kit | 53. Gas Cylinders -All Types |
| 14. U-V cabinet | 34. Paper chromatography | 54. Regulators - All Models |
| 15. pH meter | 35. Rotary shaker | 55. Fire Exhausters- All Models |
| 16. Calorimeter | 36. Cylinders, Nitrogen | 56. Lab. Glass wares |
| 17. Rotary shaker | 37. U-V spectrophoto meter | 57. Lab. Plasticwares |
| 18. Homogenizer | 38. Colorimeter 8 filters | 58. Lab. Misselenaeous |
| 19. Stirrer | 39. Fire Extinguisher | 59. Lab. Maintenance |
| 20. Vortex mixture | 40. Micro oven | 60. Lab. Insurance |



ನಾರ್ತ್ : ೯೮೪೯೭ ೦೬೦೫೮, ೯೮೪೯೮ ೮೬೮೬೨. ಫೋನ್ : ೦೮೬೬೨-೨೫೪೬೫೬
ಅಂತಿಮ ಸ್ವಿಲ್ಟ್ ವಿದ್ಯುತ್ ಲಸಿ ರಿಟೈಲರ್ ಶೆಕ್ಕಣಿಸ್ಟ್ ವಿಧ್ಯಾ ಸಿಂಧ್ಲಿಲ್

ಉರ್ಬನ್ ಕಾರ್ಬರ್ ಎಂಬ್

ಡಿ.ಆರ್. & ಎ.ಎ. ಕಿಶೋರ

SBH ಎಡುರುಗಾ, ನಕಿರೆಕಲ್, ಜಾ. ನಲ್ಹಿಗಳಂಡ.

B.Sc. : M.P.Cs. (ಕಂಪ್ಯೂಟರ್ ಸೈನ್ಸ್)
B.Sc. : M.C.CA. (ಕಂಪ್ಯೂಟರ್ ಅಷ್ಟಿಕೆಷನ್)
M.P.C, B.Z.C. (TM/EM)
B.Com (CA.) (ಕಂಪ್ಯೂಟರ್ ಅಷ್ಟಿಕೆಷನ್)
B.A. : T.H.P., E.H.P (TM) M.Sc (Organic Chemistry Regular Course)

ಎಜೆಲೆಕ್ಟ್ರಾನಿಕ್ಸ್, ಪ್ರೋಟೋ ಅವಾರ್ಡ್‌ಲ್ಯಾ
ಬಾನ್‌ಹಾರ್ಟ್, ವಾರ್ಚಾರ್ ಆಂಕಡ್‌ಲ್ಯಾ. ಅಂತಿಮ ಸ್ವಿಲ್ಟ್ ಲಸಿ ರಿಟೈಲರ್
ಅಷ್ಟಿಕೆಷನ್ CA, & T.P.I.T ಏಜ್ಯಾರ್ ಕಾರ್ಬರ್ ಎಂಬ್ ಕಾರ್ಬರ್ ಎಂಬ್ ಕಾರ್ಬರ್
ಅಂತಿಮ ಸ್ವಿಲ್ಟ್ ಲಸಿ ರಿಟೈಲರ್ ಕಾರ್ಬರ್ ಎಂಬ್ ಕಾರ್ಬರ್ ಎಂಬ್ ಕಾರ್ಬರ್

ಕರಣ್ಣಂಡಂಬ
M.Sc (Chemistry) B.Ed.
Sr. Lectl. In Chemistry

సంకల్పం!

సాధన !!

సాధువుం!!!

ప్రతి సం॥ తన ఫలితాల రికార్డులను తానే అధిగమిస్తూ, ఉన్నతానియా యూనివర్సిటీ పరిధిలో

అత్యధిక ఫలితాలు సాధిస్తూ విజయభేరి మౌరీస్టున్న ఎక్కువ విద్యాసంస్థ "జాగ్రుతి"

జాగ్రుతి

డిగ్రీ & పి.జి.
కళారాల

Established: 2003 O.P. ఆసుఖంధ సంస్థ

(LR No NDC-760/O.U. - 23/2003-2004)

Co-Education

Phone: 08685 - 246227

Cell: 9848970346, 9848350474

C.C. No! - 40161

JAAGRUTHI DEGREE & P.G. COLLEGE



Tuning Convolution Neural networks for Hand Written Digit Recognition

Laxmi Narayana Pondhu^{1*}, Govardhani Pondhu²

¹Dept. of CSE, Rajiv Gandhi University of Knowledge Technologies, Basar, India Govardhani Pondhu²

²Dept. of CSE Kodad Institute of Technology and Science, Kodad, India

*Corresponding Author: laxmi916@gmail.com

Available online at: www.ijcseonline.org

Accepted: 17/Aug/2018, Published: 31/Aug/2018

Abstract— Complex neural networks will take much time for training; we can achieve better accuracy with simpler models by tuning hyper-parameters of the model. Hyper parameter tuning is required for neural networks to improve the accuracy and to reduce the training time of neural networks. In this paper we used simple CNN model with four convolution layers, two pooling layers and two fully connected layers with hyper parameter tuning, batch normalization, learning rate decay, and normalization techniques to recognize hand written digit recognition. This model is giving 99.54% on test set.

Keywords— Convolution Neural Networks, CNN, Deep Learning, Parameter Tuning, Batch Normalization.

I. INTRODUCTION

Recently, Deep Neural Networks gained the much popularity because of its ability to solve complex problems. Deep Neural Networks are inspired by human brain, they are widely used in computer vision especially Convolution Neural Networks (CNN) [8] are playing vital role in computer vision applications.

In computer vision human hand writing recognition accurately is challenging task. Deep Neural Networks are used in this kind of complex problems it is difficult to solve complex problems by using shallow networks.

But all these Deep Neural Networks suffer from over fitting problem because of high variance; over fitting can be avoided by regularization techniques.

A. Convolution Neural Networks

In 1989 the new technique CNN was introduced by Yann LeCun for solving computer vision problems, Convolution Neural Network is multi layered feed forward neural network each layer consists of multiple neurons. When input is unstructured and very large then conventional neural networks can't perform well on that data, first we have to reduce dimensions of data without losing important information. In CNN convolution layers are used for extracting required features by applying convolution filters. Pooling layers are used for reducing the number of trainable parameters, pooling layers introduced between convolution layers. Flattening layer serialize the input features to feed

Neural Network. Fully connected layer is the neural network that will take the final decision this layer will return the probability for each decision variable.

B. Regularization of Neural Networks

There are various regularization techniques are there, most commonly used techniques are L2 Regularization, Dropout, Early Stopping, Data Augmentation. In L2 regularization cost function will be modified by adding regularization term. $J(w, b) = 1/m \sum_{i=1}^n (\text{target} - \text{predicted})^2 + \lambda/2m \sum \|w\|^2$

by adding regularization term to cost function it will restrict coefficients to fit perfectly to avoid over fitting. In Dropout technique randomly drop some nodes from neural network that will make network sparse, over fitted network so sensitive to small functions by dropping some nodes from network can be generalized then there will be no problem of over fitting. Early stopping is another technique that stops the training of neural network at point where more training increasing the error. Data Augmentation is another widely used technique to regularize neural network if more training data provided networks will perform better on unseen data, Data Augmentation generates data by image transformation techniques like rotating, horizontal flipping, vertical flipping etc.

C. Hyper parameter tuning

Hyper parameters tuning process finds best hyper parameters that are involved in building the Neural Network, if the network is deep we have to deal with number of hyper parameters like number of hidden layers, number of nodes in

each hidden layers, mini batch size, learning rate decay, optimization algorithms and momentum. By selecting appropriate hyper parameters we can get better performance.

D. Batch Normalization

Batch Normalization makes Neural Network robust; it makes training of deep neural networks much easier by converting activation values at hidden layers into specific range according to variance. If inputs of one hidden layers are in certain range training algorithms like gradient descent training will be much simpler and algorithm converge at faster rate

Rest of the paper is organized as follows, Section II contain the related work of Convolution Neural Networks tuning, Section III contain the methodology, which contains different techniques we used to tune CNN, Section IV describes results and discussion, Section V contains conclusion and future scope.

II. RELATED WORK

In There are numerous models proposed for image classification like handwritten digit recognition, deep learning models are performing better when compared with other models. Deep learning models accuracy further can be improved by tuning hyper parameters, batch normalization and regularization techniques.

In [1] James Bergstra and Yoshua Bengio proposed random search for hyper-parameter optimization. Y. Hou and H. Zhao [2] proposed depth neural networks to improve the hand written digit recognition. In [3] U. Meier, D. C. Ciresan, L. M. Gambardella and J. Schmidhuber proposed new technique Committee of Simple Neural Nets.

In [5] C. Laurent, G. Pereyra, P. Brakel, Y. Zhang and Y. Bengio, [6] Y. Xie, H. Jin and E. C. C. Tsang and in [7] D. Ito, T. Okamoto and S. Koakutsu, improved the performance of deep networks by batch using normalization. L. Chen, S. Wang, W. Fan, J. Sun and S. Naoi used new method [9] Cascading Training for Relaxation CNN on Handwritten Character Recognition, in [10] Tai-cong Chen, Da-jian Han, F. T. K. Au and L. G. Tham improved the neural networks performance by using learning rate decay and in [12] K. T. Islam, G. Mujtaba, R. G. Raj and H. F. Nweke improved the performance of handwritten digit recognition.

III. METHODOLOGY

A. Tuning of Convolution Neural Networks

To improve the accuracy of convolution neural network on MNIST handwritten digit dataset we applied parameter tuning, regularization and batch normalization. We created Convolution Neural Network (CNN) with four convolution layers with filter size 32 and kernel size 3 between each convolution layer we applied Batch normalization, in fully connected layer we have used 2 hidden layers with activation function relu, to avoid over fitting we introduced dropout between hidden layers with dropout rate 0.2, in the output layer we used softmax as activation function with ten nodes. We tried with two optimization algorithms RMSprop and Adam we are getting better results when adam optimizer used and we used categorical cross entropy as loss function and applied learning rate decay for better convergence of algorithm.

1) Parameter Tuning

Hyper parameter tuning is used to find the best hyper parameters; in this hyper parameter tuning we tested several combinations of hyper parameters. Grid Search is one hyper parameter tuning technique. GridSearchCV will train Artificial Neural Networks using k-fold cross validation to get relevant accuracy with different combination of the dictionary of hyper parameters and returns the best accuracy with best selection of these values.

In this paper we used random search instead of Grid Search because grid search will take much time in deep Neural Networks.

2) Normalization

Normalization will be used in neural networks to reduce over fitting. We applied dropout normalization between every hidden layer, we added dropout layer with rate 0.25 after each hidden layer.

We applied data augmentation by using keras library function. Data augmentation creates more training data by image transformation techniques, so neural networks trained with more data there will be no problem of over fitting.

3) Batch Normalization

Batch Normalization makes Neural Network training faster and also helpful in covariance shifting. We applied Batch normalization at every hidden layer of our model.

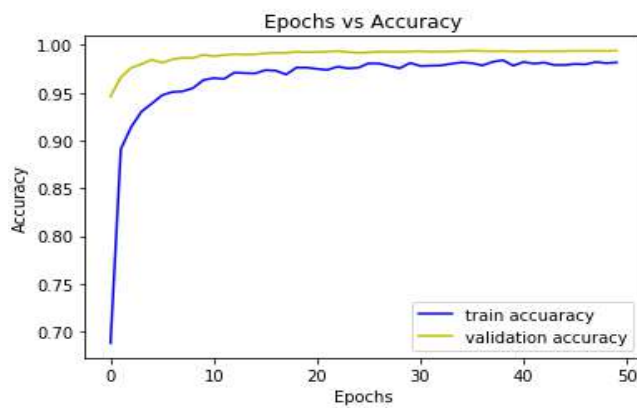


Figure 1. Accuracy train set vs test set

IV. RESULTS AND DISCUSSION

After applying all the above tuning techniques we got accuracy 98.04% for training set, on test set we got 99.54% accuracy. We have plotted the graph for accuracies of train, test for different number of epochs.

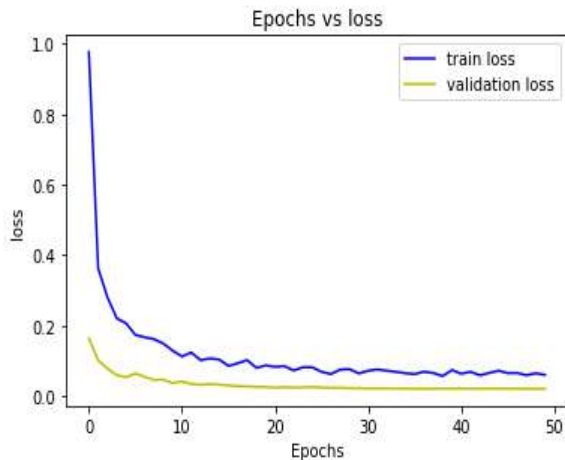


Figure 2. Loss train set vs test set

Table 1. Accuracy before tuning vs After Tuning

	Train	Test
CNN	97.42%	98.94%
CNN after Tuning	98.04%	99.54%

We are getting better Result after tuning process. Before tuning for the same model we got 98.94% accuracy on test set after tuning we got 99.54% accuracy.

V. CONCLUSION AND FUTURE SCOPE

From the above results we can conclude that we improved the CNN accuracy by applying parameter tuning, Batch normalization, Regularization and Normalization techniques without increasing model complexity. In future we have to try with bigger datasets like ImageNet and little modification to architecture.

REFERENCES

- [1] James Bergstra and Yoshua Bengio. 2012. Random search for hyper-parameter optimization. *J. Mach. Learn. Res.* 13 (February 2012), 281-305.
- [2] Y. Hou and H. Zhao, "Handwritten digit recognition based on depth neural network," *2017 International Conference on Intelligent Informatics and Biomedical Sciences (ICIBMS)*, Okinawa, 2017, pp. 35-38
- [3] U. Meier, D. C. Ciresan, L. M. Gambardella and J. Schmidhuber, "Better Digit Recognition with a Committee of Simple Neural Nets," *2011 International Conference on Document Analysis and Recognition*, Beijing, 2011, pp. 1250-1254.
- [4] L. Deng, "The MNIST Database of Handwritten Digit Images for Machine Learning Research [Best of the Web]," in *IEEE Signal Processing Magazine*, vol. 29, no. 6, pp. 141-142, Nov. 2012.
- [5] C. Laurent, G. Pereyra, P. Brakel, Y. Zhang and Y. Bengio, "Batch normalized recurrent neural networks," *2016 IEEE International Conference on Acoustics, Speech and Signal Processing (ICASSP)*, Shanghai, 2016, pp. 2657-2661.
- [6] Y. Xie, H. Jin and E. C. C. Tsang, "Improving the lenet with batch normalization and online hard example mining for digits recognition," *2017 International Conference on Wavelet Analysis and Pattern Recognition (ICWAPR)*, Ningbo, 2017, pp. 149-153.
- [7] D. Ito, T. Okamoto and S. Koakutsu, "A learning algorithm with a gradient normalization and a learning rate adaptation for the mini-batch type learning," *2017 56th Annual Conference of the Society of Instrument and Control Engineers of Japan (SICE)*, Kanazawa, 2017, pp. 811-816.
- [8] L. Lv, X. Cai, Y. Zeng and C. Chen, "Facial feature extraction method based on fast and effective convolutional neural network," *2017 IEEE 2nd Advanced Information Technology, Electronic and Automation Control Conference (IAEAC)*, Chongqing, 2017, pp. 2011-2015.
- [9] L. Chen, S. Wang, W. Fan, J. Sun and S. Naoi, "Cascading Training for Relaxation CNN on Handwritten Character Recognition," *2016 15th International Conference on Frontiers in Handwriting Recognition (ICFHR)*, Shenzhen, 2016, pp. 162-167.
- [10] Tai-cong Chen, Da-jian Han, F. T. K. Au and L. G. Tham, "Acceleration of Levenberg-Marquardt training of neural networks with variable decay rate," *Proceedings of the International Joint Conference on Neural Networks*, 2003., Portland, OR, 2003, pp. 1873-1878 vol.3.
- [11] T. Tanprasert and T. Kripriksawan, "An approach to control aging rate of neural networks under adaptation to gradually changing context," *Proceedings of the 9th International Conference on Neural Information Processing*, 2002. *ICONIP '02.*, Singapore, 2002, pp. 174-178 vol.1.
- [12] K. T. Islam, G. Mujtaba, R. G. Raj and H. F. Nweke, "Handwritten digits recognition with artificial neural network," *2017 International Conference on Engineering Technology and Technopreneurship (ICE2T)*, Kuala Lumpur, 2017, pp. 1-4.

Authors Profile

Mr. Laxmi Narayana Pondhu pursued Bachelor of Technology from University college of engineering, Kakatiya University, Kothagudem in 2010 and Master of Technology from National Institute of Technology Surathkal in year 2013. He is currently working as Assistant Professor in Department of Computer Science and Engineering, Rajiv Gandhi University of Knowledge Technologies, Basar, His research interests includes Data Analytics, Machine Learning, Deep Learning. He has 4 years of teaching experience.

Mrs Govardhani pursued Bachelor of Science and Master of Science from JNTUH, hyderabad. She is currently working as Assistant Professor in Department of Computer Science and engineering, KITS Kodad. Her main research work focuses on Machine Learning and Deep Learning. She has 3 years of teaching experience.

Email: Subscribe to Updat



International Journal of Computer Applications

Scholarly Peer-reviewed Research Publishing Journal

[Home](#)

[Archives](#)

[Special Issues](#)

[Proceedings](#)

[The Model](#)

[Topics](#)

[Editorial Board](#)

[Review Board](#)

[Journal Hardcopy](#)

[Peer Review](#)

[What is peer-review?](#)

[Join as Reviewer](#)

[Indexing](#)

[CrossRef](#)

[ISSN](#)

[Calls](#)

[Special Issue Proposals](#)

[Conference Proceedings](#)

[RDPD Program](#)

[Register as Volunteer](#)

[Webmaster Central](#)

[IJCA Statistical Data](#)

[FAQ](#)

[Contact Us](#)

[Article Correction Policy](#)

[Learn about the IJCA article correction policy and process](#)

[Copyright Infringement](#)

[Dealing with any form of infringement.](#)

[Peer Review Quote](#)

['Peer Review – A Critical Inquiry' by David Shatz](#)

[Print/ hard copy request](#)

[Directly place requests for print/ hard copies of IJCA via Google Docs](#)

Most Read Research Articles

- Novel Application of Multi-Layer Perceptrons (MLP) Neural Networks to Model HIV in South Africa using Seroprevalence Data from Antenatal Clinics
- An Effective Evolutionary Clustering Algorithm: Hepatitis C Case Study
- Adaptivity and Adaptability of Learning Object's Interface
- Enhanced TCP Westwood Congestion Avoidance Mechanism (TCP WestwoodNew)
- Migration of Legacy Information System based on Business Process Theory

[Home](#) > [Proceedings](#) > [ICCCMIT 2014](#) > [Number 3](#)

Call for Paper - April 2020 Edition

IJCA solicits original research papers for the April 2020 Edition. Last date of manuscript submission is **March 20, 2020**.

Number 3 (ISBN: 973-93-80885-90-2)

#	Article Title
1	Reusable Multi-Stage Multi-Secret Sharing Scheme based on Asmuth-Bloom Sequence Authors : Anjaneyulu Endurthi, Appala Naidu Tentu, V. Ch. Venkaiah
2	Automated Shopping Trolley for Super Market Billing System Authors : V. Vikram Arvind, S. Sainath, K. Surender, Thangakumar Jeyaprakash
3	Otsu based Multi-level Image Segmentation using Brownian Bat Algorithm Authors : B. Joyce Preethi, R. Angel Sujitha, V. Rajinikanth
4	An Optimized Circuit of 8:1 Multiplexer Circuit using Reversible Logic Gates Authors : O. P. Singh, Vandana Shukla, G. R. Mishra, R. K. Tiwari
5	A Comparative Study Of Different DOA Estimation Schemes and Adaptive Beam Forming Techniques for Target Detection and Tracking Authors : Susaritha U. S, Ganesh Madhan . M, Ragupathi. R, Ashita Priya Thomas
6	Performance Analysis of Asymmetric Cooperative Relaying Schemes for SISO Systems Authors : Mayuri. H
7	Comparative Analysis of Random Forest, REP Tree and J48 Classifiers for Credit Risk Prediction Authors : Lakshmi Devasena C
8	Comparitive Study on Various Cryptographic Techniques Authors : K. B. Priya Iyer, R. Anusha, R. Shakthi Priya
9	Enhancing Intrusion Detection System Performance using Firecol Protection Services based Honeypot System Authors : Rajalakshmi Selvaraj, Venu Madhav Kuthadi, Tshilidzi Marwala

© 2009-2020 International Journal of Computer Applications

FCS® (Foundation of Computer Science)

[Vision & Mission](#) | [Privacy Policy](#) | [Terms of Service](#)

Email:
Subscribe to Updat



International Journal of Computer Applications

Scholarly Peer-reviewed Research Publishing Journal

- [Home](#)
- [Archives](#)
- [Special Issues](#)
- [Proceedings](#)
- [The Model](#)
- [Topics](#)
- [Editorial Board](#)
- [Review Board](#)
- [Journal Hardcopy](#)
- [Peer Review](#)
- [What is peer-review?](#)
- [Join as Reviewer](#)
- [Indexing](#)
- [CrossRef](#)
- [ISSN](#)
- [Calls](#)
- [Special Issue Proposals](#)
- [Conference Proceedings](#)
- [RDPD Program](#)
- [Register as Volunteer](#)
- [Webmaster Central](#)
- [IJCA Statistical Data](#)
- [FAQ](#)
- [Contact Us](#)

- [Article Correction Policy](#)
Learn about the IJCA article correction policy and process
- [Copyright Infringement](#)
Dealing with any form of infringement.
- [Peer Review Quote](#)
'Peer Review – A Critical Inquiry' by David Shatz
- [Print/ hard copy request](#)
Directly place requests for print/ hard copies of IJCA via Google Docs

Most Read Research Articles

- Novel Application of Multi-Layer Perceptrons (MLP) Neural Networks to Model HIV in South Africa using Seroprevalence Data from Antenatal Clinics
- An Effective Evolutionary Clustering Algorithm: Hepatitis C Case Study
- Adaptivity and Adaptability of Learning Object's Interface
- Enhanced TCP Westwood Congestion Avoidance Mechanism (TCP WestwoodNew)
- Migration of Legacy Information System based on Business Process Theory

Home > Proceedings > ICCCIT 2014 > Number 3 > Reusable Multi-Stage Multi-Secret Sharing Scheme based on Asmuth-Bloom Sequence

Call for Paper - April 2020 Edition

IJCA solicits original research papers for the April 2020 Edition. Last date of manuscript submission is **March 20, 2020**.

[Read More](#)

Reusable Multi-Stage Multi-Secret Sharing Scheme based on Asmuth-Bloom Sequence

 Like 0
 Tweet
 Share
IJCA Social Web Research [\[LEARN MORE\]](#)



IJCA Proceedings on International Conference on Communication, Computing and Information Technology

© 2015 by IJCA Journal

ICCCIT 2014 - Number 3

Year of Publication: 2015

Authors: Anjaneyulu Endurthi Appala Naidu Tantu V. Ch. Venkaiah



Citation

Anjaneyulu Endurthi, Appala Naidu Tantu and Ch. V Venkaiah. Article: Reusable Multi-Stage Multi-Secret Sharing Scheme based on Asmuth-Bloom Sequence. *IJCA Proceedings on International Conference on Communication, Computing and Information Technology* ICCCIT 2014(3):1-6, March 2015. Full text available. [BibTeX](#)

Abstract

Two secret sharing schemes that use Asmuth-Bloom sequence and are based on Chinese Remainder Theorem (CRT) are proposed in this paper. The first scheme is designed for the case of a single secret and the second one is an extension of the first scheme to the case of multi-secrets. Novelty of the proposed schemes is that the shares of the participants are reusable i. e. same shares are applicable even with a new secret. Also only one share needs to be kept by each participant even for the multi-secret sharing scheme. Further, the schemes are capable of verifying the honesty of the participants including the dealer. Correctness of the schemes is also discussed.

References

1. M. Mignotte. How to share a secret. In T. Beth, editor, Cryptography-Proceedings of the Work-shop on Cryptography, Burg Feuerstein, 1982, volume 149 of Lecture Notes in Computer Science, pp. 371-375. Springer-Verlag, 1983
2. Asmuth, C. , Bloom, J. : A modular approach to key safeguarding. IEEE Transactions on Information Theory IT-29(2),pp. 208-210 (1983)
3. G. R. Blakley, Safeguarding cryptographic keys, AFIPS, Vol. 48 (1979), pp. 313-317.
4. Blakley, G. R. , Kabatianski, A. , Ideal perfect threshold schemes and MDS codes, ISIT95, p. 488, 1995.
5. Shamir, A. 1979. How to share a secret. Comm. ACM 22, 612-613.
6. G. J. Simmons. , How to (Really) Share a secret, Advances in Cryptology-CRYPTO'88,LNCS,403(1990),pp. 390-448.
7. Tompa, M. , Woll, H. How to share a secret with cheaters, J. Cryptology 1(2), pp. 133-138 (1988)
8. Cabello, S. , Padro, C. , Saez, G. Secret sharing schemes with detection of cheaters for a general access structure. In: Ciobanu, G. , P un, G. (eds.) FCT 1999. LNCS, vol. 1684, pp. 185-194. Springer, Heidelberg (1999)
9. Carpentieri, M. , De Santis, A. , Vaccaro, U. Size of shares and probability of cheating in threshold schemes. In: Helleseth, T.



Reusable Multi-Stage Multi-Secret Sharing Scheme Based on Asmuth-Bloom Sequence

Anjaneyulu Endurthi

School of Computer and Information Sciences, University of Hyderabad Hyderabad-500046, India

Appala Naidu Tenu

CR Rao Advanced Institute of Mathematics, Statistics, and Computer Science, Hyderabad-500046, India

V. Ch. Venkaiah

School of Computer and Information Sciences, University of Hyderabad Hyderabad-500046, India

ABSTRACT

Two secret sharing schemes that use Asmuth-Bloom sequence and are based on Chinese Remainder Theorem (CRT) are proposed in this paper. The first scheme is designed for the case of a single secret and the second one is an extension of the first scheme to the case of multi-secrets. Novelty of the proposed schemes is that the shares of the participants are reusable i.e. same shares are applicable even with a new secret. Also only one share needs to be kept by each participant even for the multi-secret sharing scheme. Further, the schemes are capable of verifying the honesty of the participants including the dealer. Correctness of the schemes is also discussed.

Keywords:

Multi-Secret, Mignotte's sequence, Asmuth-Bloom sequence, CRT, Secret sharing scheme.

1. INTRODUCTION

The requirement of the key being secret brings several problems. Storing a secret key with only one person or server or database reduces the security of the system to the security and credibility of that agent. Besides, not having a backup of the key introduces the problem of losing the key if a mischief occurs. On the other hand, if the key is held by more than one agent an adversary with a desire for the key has more flexibility of choosing the target. Hence the security is reduced to the security of the least secure or least credible of these agents. Secret sharing schemes are introduced to solve these problems of key management. The main idea of these schemes is to share a secret among a set of agents such that only the predefined coalitions can come together and reveal the secret, while no other coalition can obtain any information about the secret. Thus, the keys used in areas requiring vital secrecy like large-scale finance applications and command control mechanisms of nuclear systems, can be stored by using secret sharing schemes.

Secret sharing was first proposed by Blakley[3] and Shamir[5]. The scheme by Shamir relies on the standard Lagrange polynomial interpolation, whereas the scheme by Blakley[3] is based on the geometric idea that uses the concept of intersecting hyperplanes.

The family of authorized subsets is known as the access structure. An access structure is said to be monotone if a set is qualified then its superset must also be qualified. Several access structures are proposed in the literature. They include the (t, n) -threshold access structure, the Generalized access structure and the Multipartite ac-

cess structure. In the (t, n) -threshold access structure there are n shareholders. An authorized group consists of any t or more participants and any group of at most $t - 1$ participants is an unauthorized group. Let \mathbb{U} be a set of n participants and let $2^{\mathbb{U}}$ be its power set. Then the 'Generalized access structure' refers to situations where the collection of permissible subsets of \mathbb{U} may be any collection $\Gamma \subseteq 2^{\mathbb{U}}$ having the monotonicity property.

In multipartite access structures, the set of players \mathbb{U} is partitioned into m disjoint entities $\mathbb{U}_1, \mathbb{U}_2, \dots, \mathbb{U}_m$ called levels and all players in each level play exactly the same role inside the access structure.

In multi-secret sharing schemes the problem of sharing many secrets is addressed. A typical scenario wherein the multi-secret sharing problem occurs is as follows. In these schemes, every participant only needs to keep one shadow and many secrets can be shared independently without refreshing the shadow. In order to reconstruct a secret, each involved participant only needs to submit a pseudo shadow computed from the real shadow instead of the real shadow itself. The reconstruction of a secret cannot compromise the secrecy of the remaining secrets that haven't been reconstructed.

Suppose that a company has K secrets which are important for business functionalities. Each secret contains a key information needed to perform a business operation. The company does not trust any single employee to access any one of the secrets. The company decides that each secret be shared among employees/participants according to a specific threshold access structure. The company may use multiple secret sharing schemes to share these secrets. However each employee needs to keep multiple shadows to participate in each game of secret sharing corresponding to each secret. So, there will be a shadow/share management problem in this method. In a threshold multi-secret sharing scheme multiple secrets can be packed into one major secret such that each component secret is still controlled by a single shadow; whereas in CRT based threshold secret sharing schemes, each participant will have a separate shadow for each secret and reconstruction is done sequentially.

Detection of cheaters:

A verifiable secret-sharing scheme [18] provides its shareholders with an ability to verify that (a) the secret shadows obtained from the dealer are derived consistently from the same secret and (b) the secret shadows obtained from the other shareholder in the secret reconstruction process are genuine shadows. These abilities are very important. For example, a dishonest dealer can cheat some

shareholders by giving them fake shadows. Communication errors (i.e., noise) can also result in fake shadows. A shareholder may also cheat others in the secret reconstruction process by presenting a fake shadow to prevent others from obtaining the real secret. The following subsections defines Mignotte's and Asmuth-Bloom's schemes.

1.1 Overview of Mignotte's SSS

Mignotte's sequence: Let t and n be two integers such that $n \geq 2$ and $2 \leq t \leq n$. A (t, n) *Mignotte's sequence* is a sequence of pairwise co-prime positive integers $p_1 < p_2 < \dots < p_n$ such that

$$\prod_{i=0}^{t-2} p_{n-i} < \prod_{i=1}^t p_i$$

This can be seen to be equivalent to

$$\max_{1 \leq i_1 < \dots < i_{t-1} \leq n} (p_{i_1} * p_{i_2} * \dots * p_{i_{t-1}}) < \min_{1 \leq i_1 < \dots < i_t \leq n} (p_{i_1} * p_{i_2} * \dots * p_{i_t})$$

To share a secret S among a group of n users, the dealer does the following:

(1) Distribution:

- The secret S is chosen as a random integer such that $\beta < S < \alpha$
 $\text{where } \alpha = \prod_{i=1}^t p_i \text{ and } \beta = \prod_{i=0}^{t-2} p_{n-i}$
- Compute shares $I_i = S \bmod p_i$ for all $1 \leq i \leq n$.
- Distribute shares $I_i, 1 \leq i \leq n$, to n participants.

(2) Reconstruction:

- Given t distinct shares $I_{i_1}, I_{i_2}, \dots, I_{i_t}$ the secret S is reconstructed using the standard variant of Chinese Remainder Theorem, as the unique solution modulo $p_{i_1} \dots p_{i_t}$ of the system,

$$S \equiv I_{i_j} \bmod p_{i_j}, 1 \leq j \leq t$$

1.2 Overview of Asmuth-Bloom SSS

A sequence of pairwise coprime positive integers (can also be called as Asmuth-Bloom sequence) $p_0, p_1 < \dots < p_n$ is chosen such that

$$p_0 \prod_{i=0}^{t-2} P_{n-i} < \prod_{i=1}^t P_i$$

To share a secret S among a group of n users, the dealer does the following:

Distribution:

- The secret S is chosen as a random integer of the set Z_{p_0}
- Compute shares $I_i = (S + \gamma p_0) \bmod p_i$ for all $1 \leq i \leq n$
 $\text{Where } \gamma \text{ is an arbitrary integer such that } (S + \gamma p_0) \in Z_{p_1 \dots p_t}$
- Distribute share $I_i, 1 \leq i \leq n$ to n participants.

Reconstruction:

- Given t distinct shares $I_{i_1}, I_{i_2}, \dots, I_{i_t}$ the modified secret X is reconstructed using the standard variant of Chinese Remainder Theorem, as the unique solution modulo $p_{i_1} \dots p_{i_t}$ of the system

$$X \equiv I_{i_j} \bmod p_j, 1 \leq j \leq t$$

—The original secret can be reconstructed using $S = X \bmod p_0$

1.3 Two-variable one-way function

A two-variable one-way function $f(r, z)$ is a function that maps a random value r and a share z onto a bit string $f(r, z)$ of a fixed length. This function has the following properties.

- Given r and z , it is easy to compute $f(r, z)$;
- Given z and $f(r, z)$, it is hard to compute r ;
- Having no knowledge of z , it is hard to compute $f(r, z)$ for any r ;
- Given z , it is hard to find two different values r_1 and r_2 such that $f(r_1, z) = f(r_2, z)$;
- Given r and $f(r, z)$, it is hard to compute z ;
- Given pairs of r_i and $f(r_i, z)$, it is hard to compute $f(r', z)$ for $r' \neq r_i$.

2. RELATED WORK

Secret sharing scheme that uses Mignotte's sequence and is based on CRT is introduced in [1], and it is modified to result in another scheme by Asmuth-Bloom [2]. J. He, E. Dawson [14], proposed a multi-stage secret sharing scheme based on one way function in 1994 [16], [17] and [15]. They used Lagrange interpolation polynomial in order to perform secret sharing. Later in 2000, Chien et al. [20] proposed a new type of (t, n) multi-secret sharing scheme based on the systematic block codes. Subba Rao Y V and Chakravarthy Bhagvati [19] came up with a multi-stage secret sharing schemes based on CRT. In the later scheme multiple secrets are shared to different groups, such that each group receives share of the secret intended for it.

2.1 Motivation

Mignotte's and Asmuth-Bloom Schemes can be used whenever we have a single secret. They are not capable of handling multiple secrets. The proposed scheme can be extended to handle multiple secrets.

2.2 Our Results

Proposed a secret sharing scheme that uses Asmuth-Bloom sequence. It can be seen to be a variant of Asmuth-Bloom scheme. The proposed scheme is then extended to a multi-stage multi-secret sharing scheme. Correctness of both the schemes is discussed. A novel feature of our scheme, apart from being extendable to multi-stage multi-secret sharing scheme, is that the shares are reusable. That is the same set of shares can be used even with a different set of secrets.

3. PROPOSED SCHEME

In the previous schemes i.e Mignotte [1], Asmuth-Bloom [2], the shares are directly related to the secret. That is a new set of shares needs to be distributed whenever a new secret is to be shared. So, we hereby propose a scheme that overcomes this limitation; thereby allowing the shares to be reusable.

Overview of the scheme

Initially, the dealer comes up with the number of participants (n), threshold value (k), the secret (S) to be shared among the parti-

pants P_1, P_2, \dots, P_n , one way function (f), value γ and Asmuth-Bloom sequence $p_0, p_1, p_2, \dots, p_n$ to be used. Also the dealer chooses random values $y_i, 1 \leq i \leq n$ and distributes them one each to the participants (i.e y_i to P_i) as the pseudo shares of the participants. The dealer modifies the secret to X and then computes the (real) shares of the participants Z_i of $P_i, 1 \leq i \leq n$ from X . Now the dealer applies the chosen one-way function f to each of these random numbers (y_i), subtracts each of these resulting numbers $f(y_i)$ from the corresponding real shares ($Z_i, 1 \leq i \leq n$) of the participants and distribute the chosen random numbers y_i to the participants P_i . While reconstructing the secret, the participants first apply one-way function to the pseudo share, which they possess, adds the resulting value $f(y_i)$ to the corresponding public share and recovers the actual shares i.e Z_i . These shares are then used to recover X using CRT, from which actual secret S is reconstructed.

3.1 Distribution

- Let the chosen (k, n) Asmuth-Bloom sequence be $p_0, p_1, p_2, \dots, p_n$.
- Choose y_1, y_2, \dots, y_n such that $y_i \in Z_{p_i}$ as the pseudo shares.
- Choose the secret S such that $S \in Z_{p_0}$
- Modify secret S by computing $X = (S + \gamma p_0)$, Where γ is an arbitrary integer such that $(S + \gamma p_0) \in Z_{p_1 \dots p_k}$
- Compute shares $Z_i = X \bmod p_i, 1 \leq i \leq n$.
- Compute $d_i = (Z_i - f(y_i)) \bmod p_i$ as the shift values, where f is the chosen one way function.
- For every $i, 1 \leq i \leq n$, deliver y_i to the i^{th} participant through a secure channel and publish d_i

3.2 Reconstruction

- Each participant calculates his actual share by computing $Z_i = (d_i + f(y_i)) \bmod p_i$.
- The modified secret X is reconstructed from the shares Z_i of k participants using CRT.
- The original secret S can be reconstructed using $S = X \bmod p_0$

3.3 Example:

We hereby illustrate the proposed scheme with artificially small parameters.

3.3.1 Distribution

- Consider a publicly known $(3, 4)$ Asmuth-Bloom sequence. Let it be $3, 11, 13, 17, 19$.
- Let the random values be: $y_1 = 3, y_2 = 4, y_3 = 8, y_4 = 5, y_5 = 10$ and the chosen one-way function be the modulo exponentiation of 2 ($2^x \bmod 17$).
- Consider the secret as 2, as $2 \in Z_{p_3}$
- We need to consider γ such that $(S + \gamma p_0) \in Z_{p_1 \dots p_k}$. So choose $\gamma = 51$ which gives $X = (2 + 51 * 3) = 155 \in Z_{p_1 \dots p_k}$
- Computing $Z_i = X \bmod p_i$.
 $Z_{i_1} = 155 \bmod 11 = 1, Z_{i_2} = 155 \bmod 13 = 12, Z_{i_3} = 155 \bmod 17 = 2, Z_{i_4} = 155 \bmod 19 = 3$
- Computing shift values by $d_i = Z_i - f(y_i) \bmod p_i$.
 $d_1 = (1 - 8) \bmod 11 = 4, d_2 = (12 - 16) \bmod 13 = 9, d_3 = (2 - 1) \bmod 17 = 1, d_4 = (3 - 15) \bmod 19 = 7$.
 These values are made public and $y_i, i = 1, 2, \dots, n$ are privately delivered to the participants.

3.3.2 Reconstruction

—Any participant, say Z_1, Z_2, Z_3 wants to pool their shares and reconstruct the secret.

Hence they calculate their actual shares by $Z_i = (d_i + f(y_i)) \bmod p_i$.

$$Z_1 = (4 + 8) \bmod 11 = 1, Z_2 = (9 + 16) \bmod 13 = 12 \text{ and } Z_3 = (1 + 1) \bmod 17 = 2.$$

—The secret is reconstructed from the following equations using CRT.

$$S \equiv 1 \bmod 11, S \equiv 12 \bmod 13, S \equiv 2 \bmod 17$$

We have $M = 11 * 13 * 17 = 2431, M_1 = 2431/11 = 221, M_2 = 187, M_3 = 143$

$$\text{and } N_1 = 1, N_2 = 8, N_3 = 5$$

$$\text{Therefore, } X = [(1 * 221 * 1) + (12 * 187 * 8) + (2 * 143 * 5)] \bmod 2431 = 1586$$

and the secret $S = 1586 \bmod 3 = 2$, Hence the secret.

4. PROPOSED MULTI-STAGE MULTI-SECRET SHARING SCHEME

Overview of the scheme

In the initialization phase, dealer initializes Asmuth-Bloom sequence i.e $p_0, p_1, p_2, \dots, p_n$, number of participants n, threshold value k, and chooses the secrets $S_i, 1 \leq i \leq l$. The dealer also chooses secret shadows y_1, y_2, \dots, y_n , value γ , a one-way function f and a verification function F. In the distribution phase, the chosen secrets are modified by adding two consecutive secrets. Successful reconstruction of the secrets is possible only when the secrets lie between values of β and α . So as to bring the modified secrets (i.e $S'_i = S_i + S_{i+1}$) to this range, we divide the modified secrets by 2. The resulting values are the new modified secrets (S''). Again from these modified secrets X values are computed, from which the actual shares (Z_{ij}) of the participants are generated. From the actual shares $Z_{ij}, 1 \leq i \leq l, 1 \leq j \leq n$, and the pseudo shares y_1, y_2, \dots, y_n public values are computed. Verification values are also derived from the actual shares. Both the sets, i.e the set of the public and the the set of the verification values are made public. The random values (i.e. pseudo shares y_1, y_2, \dots, y_n) which were chosen by dealer are distributed privately to each participant. In the verification phase, any participant can compute the hash value by using verification function and check whether they are equal to the published verification values or not. In the reconstruction phase, participants can compute their actual shares by adding the images of one-way function of their secret shadows to the public values. CRT is used to reconstruct the X values, from which modified secrets are computed and if the flag bit corresponding to the modified secret is 1, then the modified secret is multiplied by 2 and 1 is added to it. Otherwise the modified secret is multiplied by 2. The actual secrets are then computed from these modified secrets.

4.1 Initialization

In this phase, all the variables are initialized and the secrets are chosen.

Algorithm 1 Initialization

- 1: Let $\{P_1, P_2, \dots, P_n\}$ be the n participants and k be the threshold value.
 - 2: Consider a publicly known (k, n) Asmuth-Bloom sequence, say $p_0, p_1, p_2, \dots, p_n$.
 - 3: Randomly choose n secret shadows y_1, y_2, \dots, y_n such that $y_i \in Z_{p_i}$ as the pseudo shares.
 - 4: Choose the secrets S_1, S_2, \dots, S_l such that $S_i \in Z_{p_0}, 1 \leq i \leq l$.
-

4.2 Distribution

In the distribution phase, actual secrets are modified except the l^{th} secret. Shares are computed from these modified secrets.

Algorithm 2 Distribution of Shares

- 1: Compute $S'_i = S_i + S_{i+1}$, for $i = 1, 2, \dots, l-1$
 - 2: If $(S'_i \bmod 2 == 1)$ then, $S''_i = (S'_i - 1)/2$ and $b_i = 1$, for $1 \leq i \leq l-1$
 Otherwise, $S''_i = S'_i/2$ and $b_i = 0$, for $1 \leq i \leq l-1$
 - 3: $S''_l = S'_l = S_l$
 - 4: $X_i = (S''_i + \gamma p_0)$, Where γ is an arbitrary integer such that $(S + \gamma p_0) \in Z_{p_1 \dots p_k}$
 For $i = 1, 2, \dots, l$ and $j = 1, 2, \dots, n$ do the following:
 - 5: Compute $Z_{ij} = X_i \bmod p_j$
 - 6: Compute $d_{ij} = (Z_{ij} - f^i(y_j)) \bmod p_j$, where f is a one way function and $f^i(x)$ denotes i successive applications of f to x . i.e $f^0(x) = x$ and $f^i(x) = f(f^{i-1}(x))$ for $i \geq 1$
 - 7: Compute $F(r, Z_{ij})$, where r is a random value
 - 8: Distribute y_j to each participant through a secure channel and publish all $d_{ij}, F(r, Z_{ij})$ values, r and two-variable one-way function $F(r, z)$.
-

4.3 Verification

In this phase, each participant can verify the allocated shares. Reconstructor also can verify the shares provided by the participants.

Algorithm 3 Verification of shares

- 1: Participants can verify their shares by calculating $F(r, Z_{ij})$, where Z_{ij} itself can be computed by using pseudo shares and the corresponding public values.
 - 2: Similarly, reconstructor also can verify honesty of the other participants by computing $F(r, Z_{ij})$.
-

4.4 Reconstruction

Secrets are reconstructed in sequential order starting from the last, i.e the l^{th} secret. Any k participants can pool their shares and reconstruct these secrets.

Algorithm 4 Reconstruction of secrets

- 1: Each participant $j, 1 \leq j \leq n$, willing to take part in the reconstruction, calculates $Z_{ij} = (d_{ij} + f^i(y_j)) \bmod p_j, 1 \leq i \leq l$
 - Case 1: If $i = l$**
 2: Construct X_l value from corresponding shares Z_{lj} using CRT.
 - 3: From X_l value, $S_l = S'_l = S''_l = (X_l \bmod p_0)$ is constructed and hence the secret S_l
 - Case 2: For $i = l-1, l-2, \dots, 1$ do the following:**
 - 4: Construct X_i using CRT from the shares Z_{ij}
 - 5: Construct $S''_i = X_i \bmod p_0$
 - 6: $S'_i = S''_i * 2$
 - 7: If $b_i = 1, S'_i = S''_i + 1$
 - 8: Compute the i^{th} secret as $S_i = S'_i - S'_{i+1}$
-

4.5 Example

We hereby illustrate the proposed scheme with artificially small parameters.

4.5.1 Initialization

—Consider a group of 5 participants $\{P_1, P_2, P_3, P_4, P_5\}$ wherein 3 participants are sufficient to reconstruct the secret. That is the number of participants, n , is 5 and the threshold, k , is 3.

—Consider the Asmuth-Bloom sequence as 8,17,23,29,31,37 (where $p_0 = 8$)

—Let the random values be: $y_1 = 6, y_2 = 13, y_3 = 24, y_4 = 29, y_5 = 35$ and one-way function $f(x) = 2^x \bmod 43$

—Consider the secrets to be $S_1 = 2, S_2 = 3, S_3 = 5, S_4 = 7$ which lie in Z_{p_8} .

4.5.2 Distribution

—Computes $S'_i = S_i + S_{i+1}$ for $i = 1, 2, 3$.

$$S'_1 = S_1 + S_2 = 2 + 3 = 5$$

$$S'_2 = S_2 + S_3 = 3 + 5 = 8$$

$$S'_3 = S_3 + S_4 = 5 + 7 = 12$$

$$S'_4 = S_4 = 7$$

—Check the condition $(S'_i \bmod 2 == 1)$ and correspondingly compute S''_i ,

$$S''_1 = (5 - 1)/2 = 2 \text{ and } b_1 = 1$$

$$S''_2 = 8/2 = 4 \text{ and } b_2 = 0$$

$$S''_3 = 12/2 = 6 \text{ and } b_3 = 0$$

$$S''_4 = S'_4 = 7.$$

—Compute $X_i = (S''_i + \gamma p_0)$, consider $\gamma = 89$ as $(S''_i + \gamma p_0)$ should lie in Z_{p_1, p_2, \dots, p_k} . Therefore, $X_1 = 714, X_2 = 716, X_3 = 718, X_4 = 719$

—Compute $Z_{ij} = X_i \bmod p_j$, for $i = 1, 2, 3, 4$ and $j = 1, 2, 3, 4, 5$. This gives

$$Z_{11} = 0, Z_{12} = 1, Z_{13} = 18, Z_{14} = 1, Z_{15} = 11$$

$$Z_{21} = 2, Z_{22} = 3, Z_{23} = 20, Z_{24} = 3, Z_{25} = 13$$

$$Z_{31} = 4, Z_{32} = 5, Z_{33} = 22, Z_{34} = 5, Z_{35} = 15$$

$$Z_{41} = 5, Z_{42} = 6, Z_{43} = 23, Z_{44} = 6, Z_{45} = 16$$

—Compute public values $d_{ij} = (Z_{ij} - F^i(y_j)) \bmod p_j, 1 \leq i \leq 4, 1 \leq j \leq 5$

$$d_{11} = 13, d_{12} = 2, d_{13} = 12, d_{14} = 30, d_{15} = 6$$

$$d_{21} = 11, d_{22} = 8, d_{23} = 7, d_{24} = 30, d_{25} = 12$$

$$d_{31} = 3, d_{32} = 6, d_{33} = 21, d_{34} = 20, d_{35} = 13$$

$$d_{41} = 3, d_{42} = 11, d_{43} = 21, d_{44} = 2, d_{45} = 12$$

— $y_j, 1 \leq j \leq 5$ values are delivered to each participant through a secure channel and $d_{ij}, 1 \leq i \leq 4, 1 \leq j \leq 5$ values are published.

4.5.3 Reconstruction. Since the threshold is 3, let us assume that the participants P_1, P_2 and P_5 cooperate in the reconstruction procedure. So, they perform the following operations to reconstruct the secret.

—Each participant calculates his actual share for secret S_i i.e. the j^{th} participant calculates $Z_{ij} = (d_{ij} + f^i(y_j)) \bmod p_j$. Also they know public values b_1, b_2 and b_3 i.e. 1, 0 and 0 respectively.

—Construct the value X_4 by pooling shares Z_{41}, Z_{42}, Z_{45} and using CRT as follows:

We have $M = 17 * 23 * 37 = 14467, m_1 = 851, m_2 = 629, m_3 = 391$
 and $N_1 = 1, N_2 = 3, N_3 = 30$

Therefore, $S_4 = ((5 * 851 * 1) + (6 * 629 * 3) + (16 * 391 * 30)) \bmod 14467 = 719$.

—Now calculate secret S_4 by $S_4 = X_4 \bmod p_0$ implies $S_4 = 719 \bmod 89 = 7$, Hence the secret S_4

—Compute X_3, X_2, X_1 by pooling shares $(Z_{31}, Z_{32}, Z_{35}), (Z_{21}, Z_{22}, Z_{25}), (Z_{11}, Z_{12}, Z_{15})$ respectively. Therefore,

$X_3 = ((4 * 851 * 1) + (5 * 629 * 3) + (15 * 391 * 30)) \bmod 14467 = 718$

$X_2 = ((2 * 851 * 1) + (3 * 629 * 3) + (13 * 391 * 30)) \bmod 14467 = 716$

$X_1 = ((0 * 851 * 1) + (1 * 629 * 3) + (11 * 391 * 30)) \bmod 14467 = 714$

—Compute S''_3, S''_2, S''_1 Therefore,

$S''_3 = X_3 \bmod p_0 = 718 \bmod 8 = 6$

$S''_2 = X_2 \bmod p_0 = 716 \bmod 8 = 4$

$S''_1 = X_1 \bmod p_0 = 714 \bmod 8 = 2$

—Since $b_3 = 0$, we have $S'_3 = S''_3 * 2 = 12$

and $b_2 = 0$, we have $S'_2 = (S''_2 * 2) = 8$

also since $b_1 = 1$, we have $S'_1 = (S''_1 * 2) + 1 = 5$

—Construct secrets S_3, S_2, S_1 sequentially by evaluating the expression $S_i = S'_i - S_{i+1}$ as follows:

$S_3 = S'_3 - S_4 = 12 - 7 = 5$

$S_2 = S'_2 - S_3 = 8 - 5 = 3$

$S_1 = S'_1 - S_2 = 5 - 3 = 2$

Hence the required secrets.

5. SECURITY ANALYSIS

In this section, correctness of the proposed multi-stage multi-secret scheme is discussed.

5.1 Correctness

Theorem The secrets can be reconstructed if and only if the set of participants reconstructing the secrets is an authorized set.

Proof

—Case 1: S_l reconstruction

As explained in the reconstruction, each participant $P_j, 1 \leq j \leq n$ can compute the actual share Z_{lj} corresponding to the value

X_l . Note that X_l is such that $X_l \in Z_{p_1, p_2, \dots, p_k}$. From the principle of CRT, any k or more participants will be able to reconstruct X_l where as any set of atmost $(k - 1)$ participants will not be able to reconstruct the same. Further, from the obtained X_l , the required secret $S_l = S'_l = S''_l$ is reconstructed.

—Case 2: Reconstruction of remaining secrets

Following the same procedure explained in case 1, one can reconstruct X_{l-1} and hence S''_{l-1} and $S'_{l-1} = 2S''_{l-1} + b_{l-1}$ from which $S_{l-1} = S'_{l-1} - S_{l+1}$ can be computed. Similarly the other secrets can be recovered. Note that all this is possible by an authorized set and not by an unauthorized set. This is because the modified secrets X_i lies in Z_{p_1, p_2, \dots, p_k}

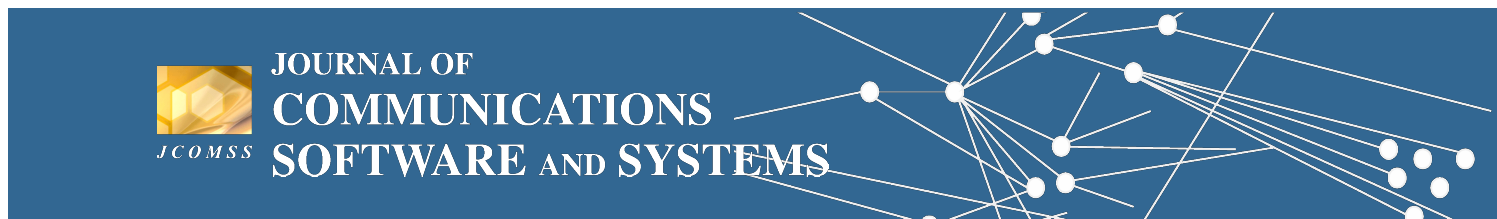
6. CONCLUSIONS

In this paper, we have proposed a secret sharing scheme that uses Asmuth-Bloom sequence and it is based on the Chinese Remainder Theorem. This scheme is then extended to multi-stage multi-secret sharing scheme. A novel feature of our schemes is that the shares of the participants are reusable, i.e. same shares can be used even with a new set of secrets. It also checks the dealer participant's honesty. This feature finds its use if the dealer distributes fake shares to the participants or a participant may provide a fake share to other participants in reconstruction. Correctness of the scheme is also discussed.

7. REFERENCES

- [1] M. Mignotte. How to share a secret. In T. Beth, editor, Cryptography-Proceedings of the Work-shop on Cryptography, Burg Feuerstein, 1982, volume 149 of Lecture Notes in Computer Science, pp. 371-375. Springer-Verlag, 1983
- [2] Asmuth, C., Bloom, J.: A modular approach to key safeguarding. IEEE Transactions on Information Theory IT-29(2), pp. 208-210 (1983)
- [3] G. R. Blakley, Safeguarding cryptographic keys, AFIPS, Vol. 48 (1979), pp. 313-317.
- [4] Blakley, G. R., Kabatianski, A., Ideal perfect threshold schemes and MDS codes, ISIT95, p. 488, 1995.
- [5] Shamir, A. 1979. How to share a secret. Comm. ACM 22, 612-613.
- [6] G.J.Simmons., How to (Really) Share a secret, Advances in Cryptology-CRYPTO'88,LNCS,403(1990),pp.390-448.
- [7] Tompa, M., Woll, H. How to share a secret with cheaters, J. Cryptology 1(2), pp. 133-138 (1988)
- [8] Cabello, S., Padro, C., Saez, G. Secret sharing schemes with detection of cheaters for a general access structure. In: Ciobanu, G., Pun, G. (eds.) FCT 1999. LNCS, vol. 1684, pp. 185-194. Springer, Heidelberg (1999)
- [9] Carpentieri, M., De Santis, A., Vaccaro, U. Size of shares and probability of cheating in threshold schemes. In: Helleseth, T. (ed.) EUROCRYPT 1993. LNCS, vol. 765, pp. 118-125. Springer, Heidelberg (1994)
- [10] Ogata, W., Kurosawa, K., Stinson, D.R. Optimum secret sharing scheme secure against cheating. SIAM J. Discrete Math. 20(1), pp. 79-95 (2006)
- [11] Goldreich, O., Ron, D., Sudan, M. Chinese remainder with errors. IEEE Trans. Inform. Theory, 2000, IT-46, pp. 1330-1338.

- [12] D. Pasaila, V. Alexa, and S. Iftene, Cheating detection and cheater identification in crt-based secret sharing schemes. IACR Cryptology ePrint Archive, vol. 2009, p. 426, 2009.
- [13] C. Ding, D. Pei, and A. Salomaa, Chinese Remainder Theorem. Applications in Computing, Coding, Cryptography. Singapore: World Scientific, 1996.
- [14] J. He, E. Dawson, Multistage secret sharing based on one-way function. Electronics Letters 30 (19) (1994) 1591-1592.
- [15] J. He, E. Dawson, Multisecret-sharing scheme based on one-way function. Electronics Letters 31 (2) (1995) 93-95.
- [16] L. Harn, Comment: Multistage secret sharing based on one-way function. Electronics Letters 31 (4) (1995) 262.
- [17] L. Harn, Efficient sharing (broadcasting) of multiple secrets. IEEE Proceedings-Computers and Digital Techniques 142 (3) (1995) 237-240.
- [18] M. Stadler, Publicly verifiable secret sharing. Advances in Cryptology, EUROCRYPT-96, Lecture Notes in Computer Science, vol.1070, Springer-Verlag, 1996, pp.190-199.
- [19] Subba Rao Y V and C. Bhagvati, CRT based threshold multi secret sharing scheme. International Journal of Network Security, vol. 16, no. 3, pp. 194-200, 2014.
- [20] H.Y. Chien, J.K. Jan, Y.M. Tseng, A practical (t, n) multi-secret sharing scheme. IEICE Transactions on Fundamentals E83-A (12) (2000) 2762-2765.



HOME ABOUT LOGIN REGISTER SEARCH CURRENT ISSUE JOURNAL ARCHIVES
ANNOUNCEMENTS CALL FOR PAPERS HOTTEST TOPICS IN ICT

Home > Archives > Vol 11, No 1 (2015)

TECHNICAL CO-SPONSORSHIP



PUBLISHED BY:



Croatian Communications and Information Society in cooperation with the University of Split, FESB, Croatia

JOURNAL INDEXING



Vol 11, No 1 (2015)

Special Issue on Network Security and Data Mining

Table of Contents

Editorial

Network Security and Data Mining PDF
Priya Iyer K B i-ii

Open Call Articles

[Efficient Routing in Mobile Adhoc Networks Emphasizing Quality of Service by Trust & Energy based AODV](#) PDF
S. Sridhar, R. Baskaran 1-7

[Single Sign-on Mechanism for Secure Web Service Access through ISSO](#) PDF
Ramamurthi Deeptha, Rajeswari Mukesh 8-14

[Reusable Multi-Stage Multi-Secret Sharing Schemes Based on CRT](#) PDF
Anjaneyulu Endurthi, Oinam B. Chanu, Appala N. Tenu, V. Ch. Venkaiah 15-24

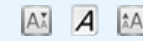
[Effectiveness of Support Vector Machines in Medical Data mining](#) PDF
Padmavathi Janardhanan, Heena L., Fathima Sabika 25-30

[Mining Software Repositories for Defect Categorization](#) PDF
Sakthi Kumaresan, Ramachandran Baskaran 31-36

[Towards Effective Control of P2P Traffic Aggregates in Network Infrastructures](#) PDF
Pedro Sousa 37-47

[OPEN JOURNAL SYSTEMS](#)

FONT SIZE



USER

Username

Password

Remember me

[Login](#)

JOURNAL CONTENT

Search

Search Scope

All

[Search](#)

Browse

[By Issue](#)

[By Author](#)

[By Title](#)

INFORMATION

[For Readers](#)

[For Authors](#)

[For Reviewers](#)

[For Section Editors](#)

[For Librarians](#)

MEMBERSHIP

Crossref
Similarity Check
Powered by iThenticate

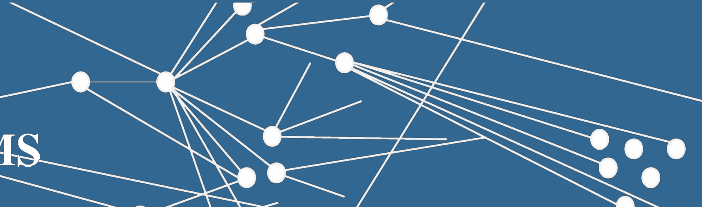
[Journal Help](#)

Journal of Communications Software and Systems (JCOMSS) ISSN 1845-6421 (Print), ISSN 1846-6079 (Online), DOI: <https://doi.org/10.24138/jcomss>. This work is licensed under a: 





JOURNAL OF COMMUNICATIONS SOFTWARE AND SYSTEMS



[HOME](#)
[ABOUT](#)
[LOGIN](#)
[REGISTER](#)
[SEARCH](#)
[CURRENT ISSUE](#)
[JOURNAL ARCHIVES](#)

[ANNOUNCEMENTS](#)
[CALL FOR PAPERS](#)
[HOTTEST TOPICS IN ICT](#)

[Home](#) > Vol 11, No 1 (2015) > Endurthi

TECHNICAL CO-SPONSORSHIP



PUBLISHED BY:



Croatian Communications and Information Society in cooperation with the University of Split, FESB, Croatia

JOURNAL INDEXING















Reusable Multi-Stage Multi-Secret Sharing Schemes Based on CRT

Anjaneyulu Endurthi, Oinam B. Chanu, Appala N. Tantu, V. Ch. Venkaiah

Abstract

Three secret sharing schemes that use the Mignotte's sequence and two secret sharing schemes that use the Asmuth-Bloom sequence are proposed in this paper. All these five secret sharing schemes are based on Chinese Remainder Theorem (CRT) [8]. The first scheme that uses the Mignotte's sequence is a single secret scheme; the second one is an extension of the first one to Multi-secret sharing scheme. The third scheme is again for the case of multi-secrets but it is an improvement over the second scheme in the sense that it reduces the number of publicvalues. The first scheme that uses the Asmuth-Bloom sequence is designed for the case of a single secret and the second one is an extension of the first scheme to the case of multi-secrets. Novelty of the proposed schemes is that the shares of the participants are reusable i.e. same shares are applicable even with a new secret. Also only one share needs to be kept by each participant even for the multi-secret sharing scheme. Further, the schemes are capable of verifying the honesty of the participants including the dealer. Correctness of the proposed schemes is discussed and show that the proposed schemes are computationally secure.

Keywords

Multi-Secret, Mignotte's sequence, Asmuth- Bloom sequence, CRT, Secret sharing scheme

Full Text:

[PDF](#)

DOI: <http://dx.doi.org/10.24138/jcomss.v11i1.113>

SHARE

This work is licensed under a [Creative Commons Attribution-NonCommercial 4.0 International License](#).

[OPEN JOURNAL SYSTEMS](#)

FONT SIZE

A A A

USER

Username

Password

Remember me

[Login](#)

JOURNAL CONTENT

Search

Search Scope

[Search](#)

Browse

[By Issue](#)

[By Author](#)

[By Title](#)

INFORMATION

[For Readers](#)

[For Authors](#)

[For Reviewers](#)

[For Section Editors](#)

[For Librarians](#)

MEMBERSHIP

 Similarity Check
Powered by iThenticate

[Journal Help](#)

1 of 2

ARTICLE TOOLS

-  [Print this article](#)
-  [Indexing metadata](#)
-  [How to cite item](#)
-  [Finding References](#)
-  Email this article (Login required)
-  Email the author (Login required)

Journal of Communications Software and Systems (JCOMSS) ISSN 1845-6421 (Print), ISSN 1846-6079 (Online), DOI: <https://doi.org/10.24138/jcomss>. This work is licensed under a: 



Reusable Multi-Stage Multi-Secret Sharing Schemes Based on CRT

Anjaneyulu Endurthi, Oinam Bidyapati Chanu, Appala Naidu Tentu, and V. Ch. Venkaiah

Abstract—Three secret sharing schemes that use the Mignotte's sequence and two secret sharing schemes that use the Asmuth-Bloom sequence are proposed in this paper. All these five secret sharing schemes are based on Chinese Remainder Theorem (CRT) [8]. The first scheme that uses the Mignotte's sequence is a single secret scheme; the second one is an extension of the first one to Multi-secret sharing scheme. The third scheme is again for the case of multi-secrets but it is an improvement over the second scheme in the sense that it reduces the number of public values. The first scheme that uses the Asmuth-Bloom sequence is designed for the case of a single secret and the second one is an extension of the first scheme to the case of multi-secrets.

Novelty of the proposed schemes is that the shares of the participants are reusable i.e. same shares are applicable even with a new secret. Also only one share needs to be kept by each participant even for the multi-secret sharing scheme. Further, the schemes are capable of verifying the honesty of the participants including the dealer. Correctness of the proposed schemes is discussed and show that the proposed schemes are computationally secure.

Index Terms—Multi-Secret, Mignotte's sequence, Asmuth-Bloom sequence, CRT, Secret sharing scheme

I. INTRODUCTION

The requirement of the key being secret brings several problems. Storing a secret key with only one person or server or database reduces the security of the system to the security and credibility of that agent. Besides, not having a backup of the key introduces the problem of losing the key if a mischief occurs. On the other hand, if the key is held by more than one agent an adversary with a desire for the key has more flexibility of choosing the target. Hence the security is reduced to the security of the least secure or least credible of these agents. Secret sharing schemes are introduced to solve these problems of key management. The main idea of these schemes is to share a secret among a set of agents such that only the predefined coalitions can come together and reveal the secret, while no other coalition can obtain any information about the secret. Thus, the keys used in areas requiring vital secrecy like large-scale finance applications and command control mechanisms

of nuclear systems, can be stored by using secret sharing schemes.

Secret sharing was first proposed by Blakley[3] and Shamir[4]. The scheme by Shamir relies on the standard Lagrange polynomial interpolation, whereas the scheme by Blakley[3] is based on the geometric idea that uses the concept of intersecting hyperplanes.

The family of authorized subsets is known as the access structure. An access structure is said to be monotone if a set is qualified then its superset must also be qualified. Several access structures are proposed in the literature. They include the (t, n) -threshold access structure, the Generalized access structure and the Multipartite access structure. In the (t, n) -threshold access structure there are n shareholders. An authorized group consists of any t or more participants and any group of at most $t - 1$ participants is an unauthorized group. Let \mathbb{U} be a set of n participants and let $2^{\mathbb{U}}$ be its power set. Then the 'Generalized access structure' refers to situations where the collection of permissible subsets of \mathbb{U} may be any collection $\Gamma \subseteq 2^{\mathbb{U}}$ having the monotonicity property.

In multipartite access structures, the set of players \mathbb{U} is partitioned into m disjoint entities $\mathbb{U}_1, \mathbb{U}_2, \dots, \mathbb{U}_m$ called levels and all players in each level play exactly the same role inside the access structure.

In multi-secret sharing schemes the problem of sharing many secrets is addressed. In these schemes, every participant needs to keep only one shadow and many secrets can be shared independently without refreshing the shadow. In order to reconstruct a secret, each involved participant only needs to submit a pseudo shadow computed from the real shadow instead of the real shadow itself. The reconstruction of a secret cannot compromise the secrecy of the remaining secrets that haven't been reconstructed. A typical scenario wherein the multi-secret sharing problem occurs is as follows.

Suppose that a company has l secrets which are important for business functionalities. Each secret contains a key information needed to perform a business operation. The company does not trust any single employee to access any one of the secrets. The company decides that each secret be shared among a set of employees/participants according to a specific threshold access structure. The company may use multiple secret sharing schemes to share these secrets. However each employee needs to keep multiple shadows to participate in each game of secret sharing corresponding to each secret. So, there will be a shadow/share management problem in this method. Hence the need for multi-secret sharing schemes.

Manuscript received February 25, 2015; revised April 12, 2015.

A. Endurthi is with the Computer Science and Engineering Department, RGUKT - IIIT Basar, Telangana State, 504107, India (e-mail: anjaneyuluendurthi@gmail.com)

O. B. Chanu and V. Ch. Venkaiah are with the School of Computer and Information Sciences, University of Hyderabad, 500046, India (e-mail: obidypatichanu@gmail.com, venkaiah@hotmail.com)

A. N. Tentu is with the CR Rao Advanced Institute of Mathematics, Statistics, and Computer Science, Hyderabad, 500046, India (e-mail: naidunit@gmail.com)

A. Detection of cheaters

A verifiable secret-sharing scheme [13] provides its shareholders with an ability to verify that (a) the secret shadows obtained from the dealer are derived consistently from the same secret and (b) the secret shadows obtained from the other shareholder in the secret reconstruction process are genuine shadows. This ability is important because a dishonest dealer can cheat share holders by giving them fake shadows. Also communication errors can result in fake shadows. A shareholder may also cheat others in the secret reconstruction process by presenting a fake shadow to prevent others from obtaining the real secret. Secret sharing schemes involving cheaters is discussed in [5] and Cheating detection and identification in CRT based schemes was presented by pasaila [7].

B. Related Work

Secret sharing scheme that uses Mignotte's sequence and is based on Chinese Remainder Theorem [8] is introduced in [1], and it is modified to result in another scheme by Asmuth-Bloom [2]. J. He, E. Dawson [9], proposed a multi-stage secret sharing scheme based on one way function in 1994 [10], [11], [12]. They used Lagrange interpolation polynomial in order to perform secret sharing. Later in 2000, Chien et al. [15] proposed a new type of (t, n) multi-secret sharing scheme based on the systematic block codes. Subba Rao Y V and Chakravarthy Bhagvati [14] came up with a multi-stage secret sharing scheme based on CRT. In the later scheme multiple secrets are shared to different groups, such that each group receives a share of the secret intended for it.

C. Motivation

Mignotte's and Asmuth-Bloom Secret Sharing Schemes are based on CRT. They are designed to handle single secret only and hence they are not capable of handling multiple secrets. So, to share multiple secrets, one needs to initiate multiple (one for each secret) secret sharing schemes. Also the shares distributed in connection with (corresponding to) one secret cannot be reused for a different secret. That is shares need to be distributed whenever a new secret is to be shared. This results in receiving a participant to keep multiple shares corresponding to each secret. So, there will be a share management problem. This paper addresses this aspect of the secret sharing schemes and proposes several schemes that overcome this issue.

The paper is organised as follows: The following subsections gives an overview of Mignotte and Asmuth-Bloom schemes. Section 2 gives an overview of the Mignotte's and Asmuth-Bloom Schemes. Section 3 and 4 propose Mignotte's sequence based reusable secret sharing schemes designed for single and multiple secrets respectively. Section 5 improves on the multi-secret Sharing Scheme given in Section 4 by reducing the number of public values required. Sections 6 and 7 propose Asmuth-Bloom sequence based reusable secret sharing schemes designed for single and multiple secrets respectively. Our results are shown in section 8 and Concluding remarks are in section 9.

II. EXISTING SCHEMES

A. Overview of Mignotte's SSS

Mignotte's sequence: Let t and n be two integers such that $n \geq 2$ and $2 \leq t \leq n$. A (t, n) *Mignotte's sequence* is a sequence of pairwise co-prime positive integers $p_1 < p_2 < \dots < p_n$ such that

$$\prod_{i=0}^{t-2} p_{n-i} < \prod_{i=1}^t p_i$$

This can be seen to be equivalent to

$$\max_{1 \leq i_1 < \dots < i_{t-1} \leq n} (p_{i_1} * p_{i_2} * \dots * p_{i_{t-1}}) < \min_{1 \leq i_1 < \dots < i_t \leq n} (p_{i_1} * p_{i_2} * \dots * p_{i_t})$$

To share a secret S among a group of n users, the dealer does the following:

1) Distribution:

- The secret S is chosen as a random integer such that $\beta < S < \alpha$
where $\alpha = \prod_{i=1}^t p_i$ and $\beta = \prod_{i=0}^{t-2} p_{n-i}$.
- Compute shares $I_i = S \bmod p_i$ for all $1 \leq i \leq n$.
- Distribute shares $I_i, 1 \leq i \leq n$, to n participants.

2) Reconstruction:

- Given t distinct shares $I_{i_1} I_{i_2}, \dots, I_{i_t}$ the secret S is reconstructed using the standard variant of Chinese Remainder Theorem, as the unique solution modulo $p_{i_1} \dots p_{i_t}$ of the system,

$$S \equiv I_{i_j} \bmod p_{i_j}, 1 \leq j \leq t$$

B. Overview of Asmuth-Bloom SSS

A sequence of pairwise coprime positive integers (can also be called as Asmuth-Bloom sequence) $p_0, p_1 < \dots < p_n$ is chosen such that

$$p_0 \prod_{i=0}^{t-2} P_{n-i} < \prod_{i=1}^t P_i$$

To share a secret S among a group of n users, the dealer does the following:

Distribution:

- The secret S is chosen as a random integer of the set Z_{p_0} .
- Compute shares $I_i = X = (S + \gamma p_0) \bmod p_i$ for all $1 \leq i \leq n$ where γ is an arbitrary integer such that

$$p_0 \prod_{i=0}^{t-2} P_{n-i} < (S + \gamma p_0) < \prod_{i=1}^t P_i$$

- Distribute shares $I_i, 1 \leq i \leq n$, to participants.

Reconstruction:

- Given t distinct shares $I_{i_1} I_{i_2}, \dots, I_{i_t}$ the modified secret X is reconstructed using the standard variant of Chinese Remainder Theorem, as the unique solution modulo $p_{i_1} \dots p_{i_t}$ of the system

$$X \equiv I_{ij} \pmod{p_{ij}}, 1 \leq j \leq t$$

- The original secret can be reconstructed using $S = X \pmod{p_0}$

C. Two-variable one-way function

A two-variable one-way function $F(r, z)$ is a function that maps a random value r and a share z onto a bit string $F(r, z)$ of a fixed length. This function has the following properties.

- Given r and z , it is easy to compute $F(r, z)$;
- Given z and $F(r, z)$, it is hard to compute r ;
- Having no knowledge of z , it is hard to compute $F(r, z)$ for any r ;
- Given z , it is hard to find two different values r_1 and r_2 such that $F(r_1, z) = F(r_2, z)$;
- Given r and $F(r, z)$, it is hard to compute z ;
- Given pairs of r_i and $F(r_i, z)$, it is hard to compute $F(r', z)$ for $r' \neq r_i$.

III. REUSABLE SINGLE SECRET SCHEME BASED ON MIGNOTTE'S SEQUENCE

In the previous schemes i.e Mignotte [1], Asmuth-Bloom [2], the shares are directly related to the secret. That is a new set of shares needs to be distributed whenever a new secret is to be shared. So, we hereby propose a scheme [6] that overcomes this limitation; thereby allowing the shares to be reusable.

Overview of the scheme

Initially, the dealer comes up with the number of participants, (n), threshold value, (k), the secret (S) to be shared among the participants P_1, P_2, \dots, P_n , one way function, (f) and the Mignotte's sequence p_1, p_2, \dots, p_n to be used. Also the dealer chooses random values $y_i, 1 \leq i \leq n$, and distributes them one each to the participants (i.e y_i to P_i) as the pseudo shares of the participants. The dealer then computes the (real) shares (Z_i) of the participants $P_i, 1 \leq i \leq n$, from the secret. Now the dealer applies the chosen one-way function f to each of these random numbers (y_i), subtracts each of these resulting numbers $f(y_i)$ from the corresponding real shares $Z_i, 1 \leq i \leq n$, of the participants. These values are made public. While reconstructing the secret, the participants first apply one-way function to the pseudo share, which they possess, adds the resulting value $f(y_i)$ to the corresponding public share and recovers the actual share Z_i . These shares are then used to recover the secret using CRT.

A. Distribution

- Dealer chooses a publicly known (k, n) Mignotte's sequence p_1, p_2, \dots, p_n
- Chooses randomly y_1, y_2, \dots, y_n such that $y_i \in Z_{p_i}$ as the pseudo share of the i^{th} participant.
- Chooses the secret S such that $\beta < S < \alpha$, where $\alpha = \prod_{i=1}^k p_i$ and $\beta = \prod_{i=0}^{k-2} p_{n-i}$.

- Computes $Z_i = S \pmod{p_i}, 1 \leq i \leq n$.
- Computes $d_i = (Z_i - f(y_i)) \pmod{p_i}, 1 \leq i \leq n$, as the shift values, where f is the chosen one way function.
- For every $i, 1 \leq i \leq n$, deliver y_i to the i^{th} participant through a secure channel and publish d_i

B. Reconstruction

- Each participant calculates his actual share by computing $Z_i = (d_i + f(y_i)) \pmod{p_i}$.
- The secret is reconstructed from the shares Z_i of k or more participants using CRT.

C. Example:

1) Distribution:

- Consider a publicly known $(3, 5)$ Mignotte's sequence to be $5, 7, 11, 13, 17$.
- Let the random values be $y_1 = 3, y_2 = 4, y_3 = 8, y_4 = 5, y_5 = 10$ and the chosen one-way function be the exponentiation of 2 modulo 17.
- Consider the secret as 297 which lies between β and α , where $\beta = 221$ and $\alpha = 385$.
- Compute $Z_i = S \pmod{p_i}, 1 \leq i \leq 5$.
 $Z_1 = 297 \pmod{5} = 2, Z_2 = 297 \pmod{7} = 3, Z_3 = 297 \pmod{11} = 0, Z_4 = 297 \pmod{13} = 11, Z_5 = 297 \pmod{17} = 8$.
- Compute shift values $d_i = Z_i - f(y_i) \pmod{p_i}, 1 \leq i \leq 5$.
 $d_1 = (2 - 8) \pmod{5} = 4, d_2 = (3 - 16) \pmod{7} = 1, d_3 = (0 - 1) \pmod{11} = 10, d_4 = (11 - 15) \pmod{13} = 9, d_5 = (8 - 4) \pmod{17} = 4$.

These values are made public and $y_i, 1 \leq i \leq 5$, are privately delivered to the participants.

2) Reconstruction:

- Three participants, say Z_1, Z_2, Z_5 , want to pool their shares and reconstruct the secret. So they calculate their actual shares by computing $Z_i = (d_i + f(y_i)) \pmod{p_i}$ for $i = 1, 2$ and 5 . That is
 $Z_1 = (4 + 8) \pmod{5} = 2, Z_2 = (1 + 16) \pmod{7} = 3$, and $Z_5 = (4 + 4) \pmod{17} = 8$.
- The secret is reconstructed from the following equations using CRT.

$$\begin{aligned} S &\equiv 2 \pmod{5} \\ S &\equiv 3 \pmod{7} \\ S &\equiv 8 \pmod{17} \end{aligned}$$

We have $M = 5 * 7 * 17 = 595, m_1 = \frac{M}{5} = 119, m_2 = \frac{M}{7} = 85, m_3 = \frac{M}{17} = 35$ and $N_1 = 4, N_2 = 1, N_3 = 1$ where $N_i, 1 \leq i \leq 3$ are such $m_1 N_1 = 1 \pmod{5}, m_2 N_2 = 1 \pmod{7}, m_3 N_3 = 1 \pmod{17}$

Therefore, $S = ((2*119*4)+(3*85*1)+(8*35*1)) \pmod{595} = 297$

Hence the secret.

IV. PROPOSED MULTI-STAGE MULTI-SECRET SHARING SCHEME BASED ON MIGNOTTE'S SEQUENCE

Overview of the scheme

As in the previous single secret scheme, here also the dealer initializes all the required parameters. The only difference is

that the dealer chooses multiple, say l , secrets S_i , $1 \leq i \leq l$, instead of a single secret. The chosen secrets S_i , $1 \leq i \leq l$, are then modified to $S'_i = S_i + S_{i+1}$, $1 \leq i \leq l-1$, except the last secret S_l , which remains as it is. Successful reconstruction of the secrets is possible only when the secrets lie between the values of β and α . So as to bring the modified secrets (i.e. $S'_i = S_i + S_{i+1}$) to this range, we divide each of the modified secret by 2. While doing so, we modify the secrets S'_i by subtracting 1 from the odd secrets and record this by setting a flag bit b_i . The resulting values are the final modified secrets (S''_i), from which the actual shares (Z_{ij}) of the participants are generated. From the actual shares Z_{ij} , $1 \leq i \leq l$, $1 \leq j \leq n$, and the pseudo shares y_1, y_2, \dots, y_n public values d_{ij} are computed. Verification values are also derived from the actual shares. Both the sets, i.e the set of the public (d_i values) and the set of verification values are made public. The random values (i.e pseudo shares y_1, y_2, \dots, y_n) which were chosen by the dealer are distributed privately to each participant. In the verification phase, any participant can compute the hash value by using verification function and check whether they are equal to the published verification values.

In the reconstruction phase, participants compute their actual shares by adding the images of the one-way function of their secret shadows to the public values. CRT is used to reconstruct the modified secrets, which are then multiplied by 2. S_{i-1} is then recovered by subtracting the previously reconstructed secret S_i .

A. Initialization

In this phase, all the variables are initialized and the secrets are chosen.

Algorithm 1 Initialization

- 1: Let $\{P_1, P_2, \dots, P_n\}$ be the n participants and k be the threshold value.
 - 2: Consider a publicly known (k, n) Mignotte's sequence, say $p_1 < p_2 < \dots < p_n$.
 - 3: Randomly choose n secret shadows y_1, y_2, \dots, y_n such that $y_i \in Z_{p_i}$ as the pseudo shares.
 - 4: Choose the secrets S_1, S_2, \dots, S_l such that $\beta < S_i < \alpha$, $1 \leq i \leq l$, where $\alpha = \prod_{i=1}^k P_i$ and $\beta = \prod_{i=0}^{k-2} P_{n-i}$.
-

B. Distribution

In the distribution phase, actual secret is modified except the l^{th} secret. Shares are computed from these modified secrets.

Algorithm 2 Distribution of Shares

- 1: Compute $S'_i = S_i + S_{i+1}$, for $i = 1, 2, \dots, l-1$
 - 2: For $i = 1, 2, \dots, l-1$
 - Begin
 - 3: If $(S'_i \bmod 2 == 1)$ then $S''_i = (S'_i - 1)/2$ and set $b_i = 1$
 - 4: Else $S''_i = S'_i/2$ and set $b_i = 0$.
 - End.
 - 5: $S''_l = S'_l = S_l$
 - For $i = 1, 2, \dots, l$ and $j = 1, 2, \dots, n$ do
 - Begin
 - 6: Compute $Z_{ij} = S''_i \bmod p_j$
 - 7: Compute $d_{ij} = (Z_{ij} - f^i(y_j)) \bmod p_j$, where f is a one way function and $f^i(x)$ denotes i successive applications of f to x . i.e $f^0(x) = x$ and $f^i(x) = f(f^{i-1}(x))$ for $i \geq 1$
 - 8: Compute $F(r, Z_{ij})$, where r is a random value
 - End.
 - 9: Distribute y_j to each participant through a secure channel and publish all d_{ij} , $F(r, Z_{ij})$ values, r and two-variable one-way function $F(r, z)$.
-

C. Verification

In this phase, each participant can verify the allocated share. Reconstructor also can verify the shares provided by the participants.

Algorithm 3 Verification of shares

- 1: Participants can verify their shares by calculating $F(r, Z_{ij})$, where Z_{ij} itself can be computed by using pseudo shares y_j and the corresponding public values d_{ij} .
 - 2: Similarly, reconstructor also can verify honesty of the other participants by computing $F(r, Z_{ij})$.
-

D. Reconstruction

Secrets are reconstructed in sequential order starting from the last, i.e, the l^{th} , secret. Any k or more participants can pool their shares and reconstruct these secrets.

Algorithm 4 Reconstruction of secrets

- 1: Each participant j , $1 \leq j \leq n$, willing to take part in the reconstruction calculates $Z_{ij} = (d_{ij} + f^i(y_j)) \bmod p_j$, $1 \leq i \leq l$
 - 2: Any k participants can pool their shares and reconstruct the secrets S_l, S_{l-1}, \dots, S_1 in a sequential order as follows
 - 3: If $i = l$, then construct $S''_l = S'_l$ and hence the secret S_l using CRT from the shares Z_{lj}
 - For $i = l-1, l-2, \dots, 1$ do the following:
 - 4: Construct S''_i using CRT from the shares Z_{ij}
 - 5: $S'_i = S''_i * 2$
 - 6: If $b_i = 1$, $S'_i = S'_i + 1$
 - 7: Compute the i^{th} secret as $S_i = S'_i - S'_{i+1}$
-

E. Example

We hereby illustrate the proposed scheme with artificially small parameters.

1) Initialization:

- Consider a group of 5 participants $\{P_1, P_2, P_3, P_4, P_5\}$ wherein 3 participants are sufficient to reconstruct the secret. That is the number of participants, n , is 5 and the threshold, t , is 3.
- Consider the Mignotte's sequence as 5,7,11,13,17 in which $\beta = 221$ and $\alpha = 385$.
- Let the random values be: $y_1 = 3, y_2 = 4, y_3 = 8, y_4 = 5, y_5 = 10$.
- Consider the secrets to be $S_1 = 251, S_2 = 282, S_3 = 323, S_4 = 317$ which lie between β and α .

Let the chosen one way function be exponentiation of 2 modulo

2) Distribution:

- Compute $S'_i = S_i + S_{i+1}$ for $i = 1, 2, 3$. That is
 $S'_1 = S_1 + S_2 = 251 + 282 = 533$
 $S'_2 = S_2 + S_3 = 282 + 323 = 605$
 $S'_3 = S_3 + S_4 = 323 + 317 = 640$
 $S'_4 = S_4 = 317$.
- Check the condition $(S'_i \bmod 2 == 1)$ and correspondingly compute S''_i ,
 $S''_1 = (533 - 1)/2 = 266$ and $b_1 = 1$
 $S''_2 = (605 - 1)/2 = 302$ and $b_2 = 1$
 $S''_3 = 640/2 = 320$ and $b_3 = 0$
 $S''_4 = S'_4 = 317$.
- Compute $Z_{ij} = S''_i \bmod p_j$, for $i = 1, 2, 3, 4$ and $j = 1, 2, 3, 4, 5$. This gives
 $Z_{11} = 1, Z_{12} = 0, Z_{13} = 2, Z_{14} = 6, Z_{15} = 11$
 $Z_{21} = 2, Z_{22} = 1, Z_{23} = 5, Z_{24} = 3, Z_{25} = 13$
 $Z_{31} = 0, Z_{32} = 5, Z_{33} = 1, Z_{34} = 8, Z_{35} = 14$
 $Z_{41} = 2, Z_{42} = 2, Z_{43} = 9, Z_{44} = 5, Z_{45} = 11$

- Compute public values $d_{ij} = (Z_{ij} - f^i(y_j)) \bmod p_j$, $1 \leq i \leq 4, 1 \leq j \leq 5$
 $d_{11} = 3, d_{12} = 5, d_{13} = 1, d_{14} = 4, d_{15} = 7$
 $d_{21} = 1, d_{22} = 0, d_{23} = 3, d_{24} = 7, d_{25} = 14$
 $d_{31} = 3, d_{32} = 3, d_{33} = 8, d_{34} = 6, d_{35} = 13$
 $d_{41} = 3, d_{42} = 5, d_{43} = 4, d_{44} = 1, d_{45} = 9$
- $y_j, 1 \leq j \leq 5$ values are delivered to each participant through a secure channel and $d_{ij}, 1 \leq i \leq 4, 1 \leq j \leq 5$ values are published.

3) Reconstruction: Since the threshold is 3, let us assume that the participants P_1, P_2 and P_5 cooperate in the reconstruction procedure. So, they perform the following operations to reconstruct the secret.

- Each participant calculates his actual share for secret S_i i.e., the j^{th} participant calculates $Z_{ij} = (d_{ij} + f^i(y_j)) \bmod p_j$. Also they know from the public values that b_1, b_2 and b_3 are 1,2, and 0 respectively.
- Construct the secret S_4 by pooling shares Z_{41}, Z_{42}, Z_{45} and using CRT as follows:
We have $M = 5 * 7 * 17 = 595, m_1 = 119, m_2 =$

$$85, m_3 = 35 \text{ and } N_1 = 4, N_2 = 1, N_3 = 1$$

$$\text{Therefore, } S_4 = ((2 * 119 * 4) + (2 * 85 * 1) + (11 * 35 * 1)) \bmod 595 = 317.$$

- Computing S''_3, S''_2, S''_1 by pooling shares $(Z_{31}, Z_{32}, Z_{35}), (Z_{21}, Z_{22}, Z_{25}), (Z_{11}, Z_{12}, Z_{15})$ respectively, we have,
 $S''_3 = ((0 * 119 * 4) + (5 * 85 * 1) + (14 * 35 * 1)) \bmod 595 = 320;$
 $S''_2 = ((2 * 119 * 4) + (1 * 85 * 1) + (13 * 35 * 1)) \bmod 595 = 302; \text{ and}$
 $S''_1 = ((1 * 119 * 4) + (0 * 85 * 1) + (11 * 35 * 1)) \bmod 595 = 266$
- Since $b_3 = 0$, we have $S'_3 = S''_3 * 2 = 640$.
Similarly $b_2 = 1$ implies that $S'_2 = (S''_2 * 2) + 1 = 605$ and $b_1 = 1$ implies that $S'_1 = (S''_1 * 2) + 1 = 533$.
- Construct secrets S_3, S_2, S_1 sequentially by evaluating the expression $S_i = S'_i - S_{i+1}$ as follows:
 $S_3 = S'_3 - S_4 = 640 - 317 = 323$
 $S_2 = S'_2 - S_3 = 605 - 323 = 282$
 $S_1 = S'_1 - S_2 = 533 - 282 = 251$
Hence the required secrets.

F. Correctness

In the following correctness of the proposed multi-stage multi-secret scheme is discussed.

Theorem The secrets can be reconstructed if and only if the set of participants reconstructing the secrets is an authorized set.

Proof

• Case 1: S_l reconstruction

As explained in the reconstruction, each participant P_j , $1 \leq j \leq n$ can compute the actual share Z_{lj} corresponding to the secret $S_l = S'_l = S''_l$ from d_{lj} . Note that S''_l is such that $\beta < S''_l < \alpha$. This is because $S''_l = S'_l = S_l$ and $\beta < S_l < \alpha$. Since $\alpha = \prod_{i=1}^k P_i$ and $\beta = \prod_{i=0}^{k-2} P_{n-i}$, from the principle of CRT, any k or more participants will be able to reconstruct $S''_l = S_l$ where as any set of atmost $(k-1)$ participants will not be able to reconstruct the same.

• Case 2: Reconstruction of remaining secrets

Following the same procedure explained in case 1, one can reconstruct S''_{l-1} and hence $S'_{l-1} = 2S''_{l-1} + b_{l-1}$ from which $S_{l-1} = S'_{l-1} - S_l$ can be computed. Similarly the other secrets can be recovered. Note that all this is possible by an authorized set and not by an unauthorized set. This is because the product of any $k-1$ primes is less than or equal to β ; whereas the secrets $S_i, 1 \leq i \leq l-1$ and hence S''_i lie in the interval (β, α) .

V. IMPROVED MULTI-STAGE MULTI-SECRET SHARING SCHEME BASED ON MIGNOTTE'S SEQUENCE

Note that the previous scheme uses flag bits, which are made public, to keep track of whether the modified secrets are even

or odd. This increases the number of public values by $l - 1$, where l is the number of secrets. But the number of public values is one of the parameters that determine the goodness of a scheme; that is, lesser the number of public values of a scheme better it is. Motivated by this observation, we hereby propose an improved scheme for multi-secrets. Overview and correctness of this scheme is similar to the previous one.

A. Distribution Phase

Algorithm 5 Distribution of Shares

- 1: For $i = 1, 2, \dots, l$ and $j = 1, 2, \dots, n$ do the following:
 - (i) Calculate $Z_{ij} = S_i \bmod p_j$.
 - 2: For $i = l$ and $j = 1, 2, \dots, n$ do the following:
 - (i) Compute $d_{lj} = (Z_{lj} - f^l(y_j)) \bmod p_j$
 - 3: For $i = 1, 2, \dots, l - 1$ and $j = 1, 2, \dots, n$ do the following:
 - (i) Compute $d_{ij} = Z_{ij} \oplus f^i(y_j) \oplus (S_{i+1} \bmod p_j)$. That is convert $Z_{ij}, f^i(y_j)$ and $(S_{i+1} \bmod p_j)$ to binary, exor these binary values, and assign the resulting value to d_{ij} .
 - 4: Compute $F(r, Z_{ij})$, where r is a random value
 - 5: Distribute y_j to each participant through a secure channel and publish all $d_{ij}, F(r, Z_{ij})$ values, r and two-variable one-way function $F(r, z)$.
-

B. Reconstruction

Secrets are reconstructed in sequential order starting from the l^{th} , secret. Any k participants can pool their shares and reconstruct these secrets.

Algorithm 6 Reconstruction of secrets

- 1: For $i = l$ and $j = 1, 2, \dots, n$ do the following
 - 2: calculate $Z_{lj} = (d_{lj} + f^l(y_j)) \bmod p_j$.
 - 3: For $i = l - 1, l - 2, \dots, 1$ and $j = 1, 2, \dots, n$ do the following :
 - 4: calculate $Z_{ij} = (d_{ij} \oplus f^i(y_j) \oplus (S_{i+1} \bmod p_j))$.
 - 5: Any k participants can pool their shares and reconstruct the secrets S_l, S_{l-1}, \dots, S_1 in a sequential order using CRT from the shares Z_{ij} .
-

Note: Verification is same as in the previous schemes.

C. Example

Let the values of the parameters be as in the example of the previous section.

1) *Distribution:* Only those steps that differ from the previous one are given. The difference is only in the calculation of the true and public values of the secrets.

- Compute $Z_{ij} = S_i \bmod P_j$ for $i = 1, 2, 3, 4$ and $j = 1, 2, \dots, 5$. This gives

$$\begin{aligned} Z_{11} &= 1, Z_{12} = 6, Z_{13} = 9, Z_{14} = 4, Z_{15} = 13 \\ Z_{21} &= 2, Z_{22} = 2, Z_{23} = 7, Z_{24} = 9, Z_{25} = 10 \\ Z_{31} &= 3, Z_{32} = 1, Z_{33} = 4, Z_{34} = 11, Z_{35} = 0 \\ Z_{41} &= 2, Z_{42} = 2, Z_{43} = 9, Z_{44} = 5, Z_{45} = 11 \end{aligned}$$

- Compute public values $d_{ij} = (Z_{ij} \oplus f^i(y_j) \oplus (S_{i+1} \bmod P_j)), 1 \leq i \leq 3, 1 \leq j \leq 5$

$$\begin{aligned} d_{11} &= 11, d_{12} = 20, d_{13} = 15, d_{14} = 2, d_{15} = 3 \\ d_{21} &= 0, d_{22} = 2, d_{23} = 1, d_{24} = 11, d_{25} = 25 \\ d_{31} &= 3, d_{32} = 1, d_{33} = 9, d_{34} = 12, d_{35} = 10 \end{aligned}$$
 - Calculate $d_{4j} = (Z_{4j} - f^4(y_j)) \bmod p_j, 1 \leq j \leq 5$

$$\begin{aligned} d_{41} &= 3, d_{42} = 5, d_{43} = 4, d_{44} = 1, d_{45} = 9 \end{aligned}$$
 - $y_j, 1 \leq j \leq 5$ are given to each participant through a secure channel and $d_{ij}, 1 \leq i \leq 4, 1 \leq j \leq 5$ values are published.
- 2) *Reconstruction:* Assume that the participants P_1, P_2 and P_5 cooperate to reconstruct the secrets.
- Compute $Z_{4j} = (d_{4j} + f^4(y_j)) \bmod p_j$ for $j = 1, 2$, and 5
 - Construct the secret S_4 as 317 by pooling shares $Z_{41} = 2, Z_{42} = 2, Z_{45} = 11$ and using CRT
Compute $Z_{ij} = (d_{ij} \oplus f^i(y_j) \oplus (S_{i+1} \bmod p_j))$ for $i = 3, 2, 1$ and $j = 1, 2, \dots, 5$
Compute S_3 as 323, S_2 as 282, S_1 as 251 by pooling shares $(Z_{31}, Z_{32}, Z_{35}), (Z_{21}, Z_{22}, Z_{25}), (Z_{11}, Z_{12}, Z_{15})$ respectively.

D. Comparison

The comparison between the previous Multi-Stage Secret sharing scheme and Improved Scheme is shown below.

VI. PROPOSED SINGLE SECRET SHARING SCHEME BASED ON ASMUTH-BLOOM SEQUENCE

Overview of the scheme

Initially, the dealer comes up with the number of participants (n), threshold value (k), the secret (S) to be shared among the participants P_1, P_2, \dots, P_n , one way function (f), value γ and Asmuth-Bloom sequence $p_0, p_1, p_2, \dots, p_n$ to be used. Also the dealer chooses random values $y_i, 1 \leq i \leq n$, and distributes them one each to the participants (i.e y_i to P_i) as the pseudo shares of the participants. The dealer modifies the secret to $X = S + \gamma p_0$ and then computes the (real) shares of the participants $P_i, 1 \leq i \leq n$, from X . Now the dealer applies the chosen one-way function f to each of these random numbers (y_i), subtracts each of these resulting numbers $f(y_i)$ from the corresponding real shares $Z_i, 1 \leq i \leq n$ of the participants and distribute the chosen random numbers y_i to the participants P_i . While reconstructing the secret, the participants first apply one-way function to the pseudo share, which they possess, adds the resulting value $f(y_i)$ to the corresponding public share and recovers the actual shares, Z_i . These shares are then used to recover X using CRT, from which the actual secret S is reconstructed.

A. Distribution

- Let the chosen (k, n) Asmuth-Bloom sequence be $p_0, p_1, p_2, \dots, p_n$.

TABLE I
COMPARISON

S.No	Property	Previous Scheme	Improved Scheme
1	No. of Public values	$ln + (l - 1)$	(ln)
2	Information Leak	Leak information to intruders	No information is leaked
3	Computationally Security	Less secure	More secure

- Choose y_1, y_2, \dots, y_n such that $y_i \in Z_{p_i}$ as the pseudo shares.
- Choose the secret S such that $S \in Z_{p_0}$
- Modify secret S to $X = (S + \gamma p_0)$, where γ is an arbitrary integer such that $\beta < (S + \gamma p_0) < \alpha$ where $\beta = p_0 \prod_{i=0}^{k-2} P_{n-i}$ and $\alpha = \prod_{i=1}^k P_i$.
- Compute shares $Z_i = X \bmod p_i, 1 \leq i \leq n$.
- Compute $d_i = (Z_i - f(y_i)) \bmod p_i$ as the shift values, where f is the chosen one way function.
- For every $i, 1 \leq i \leq n$, deliver y_i to the i^{th} participant through a secure channel and publish d_i

B. Reconstruction

- Each participant calculates his actual share by computing $Z_i = (d_i + f(y_i)) \bmod p_i$.
- The modified secret X is reconstructed from the shares Z_i of k participants using CRT.
- The original secret S is then reconstructed using $S = X \bmod p_0$

C. Example:

The proposed scheme is hereby illustrated with artificially small parameters.

1) Distribution:

- Consider a publicly known $(3, 4)$ Asmuth-Bloom sequence. Let it be $3, 11, 13, 17, 19$.
- Let the random values be: $y_1 = 3, y_2 = 4, y_3 = 8, y_4 = 5$ and the chosen one-way function be the exponentiation of 2 modulo 17.
- Consider the secret as 2, as $2 \in Z_{p_0}$
- We need to consider γ such that $\beta < (S + \gamma p_0) < \alpha$ where $\beta = p_0 \prod_{i=0}^{k-2} P_{n-i}$ and $\alpha = \prod_{i=1}^k P_i$. So choose $\gamma = 431$ which gives $X = (2 + 431 * 3) = 1295$
- Computing $Z_i = X \bmod p_i$.
 $Z_{i_1} = 1295 \bmod 11 = 8, Z_{i_2} = 1295 \bmod 13 = 8, Z_{i_3} = 1295 \bmod 17 = 3, Z_{i_4} = 1295 \bmod 19 = 3$
- Computing shift values by $d_i = [Z_i - f(y_i)] \bmod p_i$.
 $d_1 = (8 - 8) \bmod 11 = 0, d_2 = (8 - 16) \bmod 13 = 5, d_3 = (3 - 1) \bmod 17 = 2, d_4 = (3 - 15) \bmod 19 = 7$.

These values are made public and $y_i, i = 1, 2, \dots, n$ are privately delivered to the participants.

2) Reconstruction:

- Any participant, say Z_1, Z_2, Z_3 wants to pool their shares and reconstruct the secret.
Hence they calculate their actual shares by $Z_i = (d_i + f(y_i)) \bmod p_i$.
 $Z_1 = (0 + 8) \bmod 11 = 8, Z_2 = (5 + 16) \bmod 13 = 8$, and
 $Z_3 = (2 + 1) \bmod 17 = 3$.
- The secret is reconstructed from the following equations using CRT.

$$\begin{aligned} S &\equiv 1 \bmod 11, \\ S &\equiv 12 \bmod 13, \\ S &\equiv 2 \bmod 17 \end{aligned}$$

We have $M = 11 * 13 * 17 = 2431, M_1 = 2431 / 11 = 221, M_2 = 187, M_3 = 143$ and $N_1 = 1, N_2 = 8, N_3 = 5$
Therefore, $X = [(8 * 221 * 1) + (8 * 187 * 8) + (3 * 143 * 5)] \bmod 2431 = 1295$
and the secret $S = 1295 \bmod 3 = 2$,
Hence the secret.

VII. PROPOSED MULTI-STAGE MULTI-SECRET SHARING SCHEME BASED ON ASMUTH-BLOOM SEQUENCE

Overview of the scheme

The dealer initializes all the parameters and chooses the required multiple secrets $S_i, 1 \leq i \leq l$, as against the single secret of the previous scheme. In the distribution phase, the chosen secrets except the last are modified to S'_i by adding two consecutive secrets, i.e. $S'_i = S_i + S_{i+1}$. Successful reconstruction of the secrets is possible only when $(S_i + \gamma p_0)$ lies between $p_0 \prod_{i=0}^{k-2} P_{n-i}$ and $\prod_{i=1}^t P_i$. So as to bring the modified secrets (i.e $S'_i = S_i + S_{i+1}$) to this range, we divide the modified secrets by 2. The resulting values are the new modified secrets (S''_i). Again from these modified secrets X values are computed, from which the actual shares (Z_{ij}) of the participants are generated. From the actual shares $Z_{ij}, 1 \leq i \leq l, 1 \leq j \leq n$, and the pseudo shares y_1, y_2, \dots, y_n public values are computed. Verification values are also derived from the actual shares. Both the sets, i.e the set of the public and the the set of the verification values are made public. The random values (i.e. pseudo shares y_1, y_2, \dots, y_n) which were chosen by the dealer are distributed privately to each participant. In the verification phase, any participant can compute the hash value by using the verification function and check whether they are equal to the published verification values or not.

In the reconstruction phase, participants can compute their actual shares by adding the images of the one-way function

of their secret shadows to the public values. CRT is used to reconstruct the X values, from which modified secrets are computed and if the flag bit corresponding to the modified secret is 1, then the modified secret is multiplied by 2 and 1 is added to it. Otherwise the modified secret is just multiplied by 2. The actual secrets are then computed from these modified secrets.

A. Initialization

In this phase, all the variables are initialized and the secrets are chosen.

Algorithm 7 Initialization

- 1: Let $\{P_1, P_2, \dots, P_n\}$ be the n participants and k be the threshold value.
 - 2: Consider a publicly known (k, n) Asmuth-Bloom sequence, say $p_0, p_1, p_2, \dots, p_n$.
 - 3: Randomly choose n secret shadows y_1, y_2, \dots, y_n such that $y_i \in Z_{p_i}$ as the pseudo shares.
 - 4: Choose the secrets S_1, S_2, \dots, S_l such that $S_i \in Z_{p_0}, 1 \leq i \leq l$.
-

B. Distribution

In the distribution phase, actual secrets are modified except the last. Shares are computed from these modified secrets.

Algorithm 8 Distribution of Shares

- 1: Compute $S'_i = S_i + S_{i+1}$, for $i = 1, 2, \dots, l-1$
 - 2: If $(S'_i \bmod 2 == 1)$ then, $S''_i = (S'_i - 1)/2$ and $b_i = 1$, for $1 \leq i \leq l-1$
Otherwise, $S''_i = S'_i/2$ and $b_i = 0$, for $1 \leq i \leq l-1$
 - 3: $S''_l = S'_l = S_l$
 - 4: $X_i = (S''_i + \gamma p_0)$, where γ is an arbitrary integer such that $(S_i + \gamma p_0)$ lies between $p_0 \prod_{i=0}^{t-2} P_{n-i}$ and $\prod_{i=1}^t P_i$.
 - 5: For $i = 1, 2, \dots, l$ and $j = 1, 2, \dots, n$ do
Begin
 - 6: Compute $Z_{ij} = X_i \bmod p_j$
 - 7: Compute $d_{ij} = (Z_{ij} - f^i(y_j)) \bmod p_j$, where f is a one way function and $f^i(x)$ denotes i successive applications of f to x .
 - 8: Compute $F(r, Z_{ij})$, where r is a random value
End
 - 9: Distribute y_j to each participant through a secure channel and publish all $d_{ij}, F(r, Z_{ij})$ values, r and two-variable one-way function $F(r, z)$.
-

C. Verification

In this phase, each participant can verify the allocated shares. Reconstructor also can verify the shares provided by the participants.

Algorithm 9 Verification of shares

- 1: Participants can verify their shares by calculating $F(r, Z_{ij})$, where Z_{ij} itself can be computed by using pseudo shares and the corresponding public values.
 - 2: Similarly, reconstructor also can verify honesty of the other participants by computing $F(r, Z_{ij})$.
-

D. Reconstruction

Secrets are reconstructed in sequential order starting from the last, i.e the t^{th} secret. Any k participants can pool their shares and reconstruct these secrets.

Algorithm 10 Reconstruction of secrets

- 1: Each participant $j, 1 \leq j \leq n$, willing to take part in the reconstruction, calculates $Z_{ij} = (d_{ij} + f^i(y_j)) \bmod p_j, 1 \leq i \leq l$
Case 1: If $i = l$
 - 2: Construct X_l value from corresponding shares Z_{lj} using CRT.
 - 3: Compute $S_l = S'_l = S''_l = (X_l \bmod p_0)$
Case 2: For $i = l-1, l-2, \dots, 1$ do the following:
 - 4: Construct X_i using CRT from the shares Z_{ij}
 - 5: Construct $S''_i = X_i \bmod p_0$
 - 6: $S'_i = S''_i * 2$
 - 7: If $b_i = 1$, $S'_i = S'_i + 1$
 - 8: Compute the i^{th} secret as $S_i = S'_i - S'_{i+1}$
-

E. Example

We hereby illustrate the proposed scheme with artificially small parameters.

1) Initialization:

- Consider a group of 5 participants $\{P_1, P_2, P_3, P_4, P_5\}$ wherein 3 participants are sufficient to reconstruct the secret. That is the number of participants, n , is 5 and the threshold, k , is 3.
- Consider the Asmuth-Bloom sequence as 8,17,23,29,31,37 (where $p_0 = 8$)
- Let the random values be: $y_1 = 6, y_2 = 13, y_3 = 24, y_4 = 29, y_5 = 35$ and one-way function $f(x) = 2^x \bmod 43$
- Consider the secrets to be $S_1 = 2, S_2 = 3, S_3 = 5, S_4 = 7$ which lie in Z_{p_0} .

2) Distribution:

- Compute $S'_i = S_i + S_{i+1}$ for $i = 1, 2, 3$ so that we have S'_1, S'_2, S'_3 and S'_4 as 5, 8, 12 and 7 respectively.
- Check the condition $(S'_i \bmod 2 == 1)$ and correspondingly compute S''_i ,
 $S''_1 = (5 - 1)/2 = 2$ and $b_1 = 1$
 $S''_2 = 8/2 = 4$ and $b_2 = 0$
 $S''_3 = 12/2 = 6$ and $b_3 = 0$
 $S''_4 = S'_4 = 7$
- Compute $X_i = (S''_i + \gamma p_0)$, consider $\gamma = 1200$ as $(S''_i + \gamma p_0)$ should lie between $p_0 \prod_{i=0}^{t-2} P_{n-i}$ and $\prod_{i=1}^t P_i$. Therefore, $X_1 = 9602, X_2 = 9604, X_3 = 9606, X_4 = 9607$

TABLE II
COMPARISON OF EXISTING AND PROPOSED SCHEMES

S.No	Scheme	Multi-Secret	Reusable	No.of public values	Sequence used
1	Mignotte Scheme(existing)	Single	No	No public values	Mignotte Sequence
2	Asmuth-Bloom Scheme(existing)	Single	No	No public values	Asmuth-Bloom Sequence
3	Reusable Single Secret Sharing Scheme I	Single	No	No public values	Mignotte Sequence
4	Proposed Multi-Stage Multi-Secret Sharing Scheme I	Multi	Yes	$\ln + (l-1)$	Mignotte Sequence
5	Improved Multi-Stage Multi-Secret Sharing Scheme	Multi	Yes	\ln	Mignotte Sequence
6	Reusable Single Secret Sharing Scheme II	Single	Yes	No public values	Asmuth-Bloom Sequence
7	Proposed Multi-Stage Multi-Secret Sharing Scheme II	Multi	Yes	$\ln + (l-1)$	Asmuth-Bloom Sequence

- Compute $Z_{ij} = X_i \bmod p_j$, for $i = 1, 2, 3, 4$ and $j = 1, 2, 3, 4, 5$. This gives
 $Z_{11} = 14, Z_{12} = 11, Z_{13} = 3, Z_{14} = 23, Z_{15} = 19$
 $Z_{21} = 16, Z_{22} = 13, Z_{23} = 5, Z_{24} = 25, Z_{25} = 21$
 $Z_{31} = 1, Z_{32} = 15, Z_{33} = 7, Z_{34} = 27, Z_{35} = 23$
 $Z_{41} = 2, Z_{42} = 16, Z_{43} = 8, Z_{44} = 28, Z_{45} = 24$
- Compute public values $d_{ij} = (Z_{ij} - F^i(y_j)) \bmod p_j$, $1 \leq i \leq 4, 1 \leq j \leq 5$
 $d_{11} = 10, d_{12} = 12, d_{13} = 26, d_{14} = 21, d_{15} = 14$
 $d_{21} = 8, d_{22} = 18, d_{23} = 21, d_{24} = 21, d_{25} = 20$
 $d_{31} = 0, d_{32} = 16, d_{33} = 6, d_{34} = 11, d_{35} = 21$
 $d_{41} = 0, d_{42} = 21, d_{43} = 6, d_{44} = 4, d_{45} = 20$
- $y_j, 1 \leq j \leq 5$ values are delivered to each participant through a secure channel and $d_{ij}, 1 \leq i \leq 4, 1 \leq j \leq 5$ values are published.

3) *Reconstruction:* Since the threshold is 3, let us assume that the participants P_1, P_2 and P_5 cooperate in the reconstruction procedure. So, they perform the following operations to reconstruct the secret.

- Each participant calculates his actual share for secret S_i i.e. the j^{th} participant calculates $Z_{ij} = (d_{ij} + f^i(y_j)) \bmod p_j$. Also they know public values b_1, b_2 and b_3 i.e. 1, 0 and 0 respectively.
- Construct the value X_4 by pooling shares Z_{41}, Z_{42}, Z_{45} and using CRT as follows:

We have $M = 17 * 23 * 37 = 14467$,
 $m_1 = \frac{M}{17} = 851, m_2 = \frac{M}{23} = 629, m_3 = \frac{M}{37} = 391$
and $N_1 = 1, N_2 = 3, N_3 = 30$

Therefore, $S_4 = ((2 * 851 * 1) + (16 * 629 * 3) + (24 * 391 * 30)) \bmod 14467 = 9607$.

- Now calculate secret S_4 as $S_4 = X_4 \bmod p_0$ so that $S_4 = 9607 \bmod 8 = 7$, Hence the secret S_4
- Compute X_3, X_2, X_1 by pooling shares $(Z_{31}, Z_{32}, Z_{35}), (Z_{21}, Z_{22}, Z_{25}), (Z_{11}, Z_{12}, Z_{15})$ respectively. Therefore,
 $X_3 = ((1 * 851 * 1) + (15 * 629 * 3) + (29 * 391 * 30)) \bmod 14467 = 9606$
 $X_2 = ((16 * 851 * 1) + (13 * 629 * 3) + (21 * 391 * 30)) \bmod 14467 = 9604$
 $X_1 = ((14 * 851 * 1) + (11 * 629 * 3) + (19 * 391 * 30)) \bmod 14467 = 9602$

- Compute S''_3, S''_2, S''_1 Therefore,
 $S''_3 = X_3 \bmod p_0 = 9606 \bmod 8 = 6$
 $S''_2 = X_2 \bmod p_0 = 9604 \bmod 8 = 4$
 $S''_1 = X_1 \bmod p_0 = 9602 \bmod 8 = 2$
- Since $b_3 = 0$, we have $S'_3 = S''_3 * 2 = 12$
and $b_2 = 0$, we have $S'_2 = (S''_2 * 2) = 8$
also since $b_1 = 1$, we have $S'_1 = (S''_1 * 2) + 1 = 5$
- Construct secrets S_3, S_2, S_1 sequentially using the expression $S_i = S'_i - S'_{i+1}$ and arrive at
 $S_3 = S'_3 - S'_4 = 12 - 7 = 5$
 $S_2 = S'_2 - S'_3 = 8 - 5 = 3$
 $S_1 = S'_1 - S'_2 = 5 - 3 = 2$
Hence the required secrets.

F. Correctness

Correctness of the scheme is same as the one given in section 4 except that X values replace S'' values and that $S_i = X_i \bmod p_0$ for $1 \leq i \leq l$.

VIII. OUR RESULTS

Three Schemes that use the Mignotte's Sequence and then two Schemes that use the Asmuth-Bloom Sequence proposed by this paper. The first and the fourth Schemes are designed for single secret; whereas the remaining three Schemes are designed for multiple secrets. Among the proposed Schemes, third Scheme is an improvement over the Second one in the sense that it reduces the number of required public values. Also discussed in the paper is the correctness of the schemes. Novelty of our schemes, in contrast to the existing schemes is that the shares are reusable. Table II represents the comparative analysis of existing schemes (Mignotte and Asmuth-Bloom) and proposed schemes.

IX. CONCLUSIONS

In this paper, we have proposed three secret sharing schemes that use the Mignotte's sequence and two secret sharing schemes that use the Asmuth-Bloom sequence. All these five secret sharing schemes are based on Chinese Remainder Theorem (CRT). The first scheme that uses the Mignotte's sequence is a single secret scheme. It is extended to the multi-stage multi-secrets in the second scheme, which is later improved to result in a third scheme. The first scheme that uses the Asmuth-Bloom sequence is designed for the case of

a single secret and the second one is an extension of the first scheme to the case of multi-secrets. A novel feature of our schemes is that the shares of the participants are reusable, i.e., same shares can be used even with a new set of secrets. It also checks the dealer participant's honesty. This feature finds its use if the dealer distributes fake shares to the participants or a participant may provide a fake share to other participants in reconstruction. Correctness of the scheme is also discussed.



Anjaneyulu Endurthi Currently serving as Lecturer in Rajiv Gandhi University of Knowledge Technologies (IIT), Basar, India. He obtained his Master of Technology (MTech) in Computer Science from University of Hyderabad, in 2014 and Bachelor of Technology (BTech) in Computer Science & Engineering from Jawaharlal Nehru Technological University, Hyderabad in 2008. His research interests includes Cryptography and Cyber Security.

REFERENCES

- [1] M. Mignotte. *How to share a secret*. In T. Beth, editor, Cryptography- Proceedings of the Work-shop on Cryptography, Burg Feuerstein, 1982, volume 149 of Lecture Notes in Computer Science, pp. 371-375. Springer-Verlag, 1983
- [2] Asmuth, C., Bloom, J.: *A modular approach to key safeguarding*. IEEE Transactions on Information Theory IT-29(2), pp. 208-210 (1983)
- [3] G. R. Blakley, *Safeguarding cryptographic keys*, AFIPS, Vol. 48 (1979), pp. 313-317.
- [4] Shamir, A. 1979. How to share a secret. Comm. ACM 22, 612-613.
- [5] Tompa, M., Woll, H. *How to share a secret with cheaters*, J. Cryptology 1(2), pp. 133-138 (1988)
- [6] "Anjaneyulu Endurthi, Appala Naidu Tentu, V.Ch.Venkaiah. *Reusable Multi-stage Multi-secret Sharing Scheme Based on Asmuth-Bloom Sequence*. Proceedings of International Conference on Communication Computing and Information Technology, Department of Computer Science, M.O.P. Vaishnav College for Women (Autonomous), Chennai, Tamil Nadu, India. 12 th and 13 th December 2014."
- [7] D. Pasaila, V. Alexa, and S. Iftene, *Cheating detection and cheater identification in crt-based secret sharing schemes*. IACR Cryptology ePrint Archive, vol. 2009, p. 426, 2009.
- [8] C. Ding, D. Pei, and A. Salomaa, *Chinese Remainder Theorem*. Applications in Computing, Coding, Cryptography. Singapore: World Scientific, 1996.
- [9] J. He, E. Dawson, *Multistage secret sharing based on one-way function*, Electronics Letters 30 (19) (1994) 1591-1592.
- [10] J. He, E. Dawson, *Multisecret-sharing scheme based on one-way function*, Electronics Letters 31 (2) (1995) 93-95.
- [11] L. Harn, *Comment: Multistage secret sharing based on one-way function*, Electronics Letters 31 (4) (1995) 262.
- [12] L. Harn, *Efficient sharing (broadcasting) of multiple secrets*, IEEE Proceedings-Computers and Digital Techniques 142 (3) (1995) 237-240.
- [13] M. Stadler, *Publicly verifiable secret sharing*, Advances in Cryptology, EUROCRYPT-96, Lecture Notes in Computer Science, vol.1070, Springer-Verlag, 1996, pp.190-199.
- [14] Subba Rao Y V and C. Bhagvati, *CRT based threshold multi secret sharing scheme*, International Journal of Network Security, vol. 16, no. 3, pp. 194-200, 2014.
- [15] H.Y. Chien, J.K. Jan, Y.M. Tseng, *A practical (t, n) multi-secret sharing scheme*, IEICE Transactions on Fundamentals E83-A (12) (2000) 2762-2765.



Oinam Bidyapati Chanu Currently persuing her Master of Technology in Computer Science from University of Hyderabad, India. She has obtained her Bachelor of Technology from National Institute Of Technology, Durgapur(NIT D), India in 2011.



Appala Naidu Tentu is a Research Scientist at CR Rao Advanced Institute of Mathematics, Statistics, and Computer Science (AIMSCS), University of Hyderabad Campus. He obtained his Master of Technology (MTech) in Computer Science from National Institute of Technology, Suratkal (NITK) in 2010 and Master of Science (M.Sc) from Andhra University, in 2007. Currently, he is pursuing his PhD in Computer Science from JNTU Hyderabad. His research interests are in the areas of cryptography, cryptanalysis and design of security protocols.



V. Ch. Venkaiah obtained his Ph.D. in 1988 from the Indian Institute of Science (IISc), Bangalore, India, in the area of Scientific Computing. He worked for several organizations including the Central Research Laboratory of Bharat Electronics, Tata Elxsi India Pvt. Ltd., Motorola India Electronics Limited, all in Bangalore. He then moved onto academics and served IIT Delhi, IIIT Hyderabad, and C R Rao Advanced Institute of Mathematics, Statistics, and Computer Science. He is currently serving the University of Hyderabad, India.

Performance Analysis of Machine Learning Algorithms for Gender Classification

Laxmi Narayana Pondhu

Department of Computer Science and Engineering
 Rajiv Gandhi University of Knowledge Technologies
 Basar, India
 laxmi916@gmail.com

Govardhani Kummari

Department of Computer Science and Engineering
 Kodada Institute of Technology and Science for Women
 Kodada, India
 k.govardhani@gmail.com

Abstract—We have various machine algorithms for gender classification but choosing best one is important task. For selecting best algorithm we conducted experimental study on machine learning algorithms for gender classification. In this experimental study of machine learning algorithms, we analyzed performance of various algorithms for gender classification using voice dataset. From this study we concluded that SVM and ANN are giving best results. After tuning parameters ANN outperforms SVM giving accuracy 99.87% on test data.

Keywords—Machine learning; Deep learning; SVM; Artificial Neural Networks;

I. INTRODUCTION

Gender prediction is important in applications like targeted advertisements, interactive systems and mobile based health care systems. Based on the gender of a person interactive systems respond accordingly. If marketing firms know the the gender of the person then they can target respective people who potentially buy the products. Classifying the gender of a person accurately based on their voice is a challenging problem in machine learning.

Deep learning models are more suitable for unstructured data like audio, video and images. Deep learning models perform better results when the data is large.

In this paper we used the voice dataset consists of 3168 male and female voice acoustic features to train different machine learning algorithms. From this research we compared the accuracy of different algorithms.

II. RELATED WORK

There are numerous machine learning, deep learning models to classify the person is male or female based on speech. In [1] with Support Vector Machines attained 95% accuracy for the gender classification system. In [2], pitch was used for the gender classification with Multi Layer Perception Neural networks chived the accuracy of 96%. In [3] Support Vector Machines, Classification and Regression Tree (CART) [4] models were used. In [5] Lee and Lang used Support Vector Machine(SVM). In [6] Silovsky and Nouza used

Gaussian Mixture Models(GMM). In [7] by using Multilayer Perceptron (MLP) networks achived 96.74% accuracy.

III. SPEECH DATASET

The speech dataset [10] has 3168 voice samples of male and female. Each sample consists acoustic properties of voice.

Dataset file contains the following fields [9]:

meanfreq, mode, sd, centroid, Q25, Q75, skew, IQR, kurt, sp.ent, meanfun, minfun,maxfu, mindom, meandom, maxdom, dfrange, modindex,label.

“label” two values for male or female classification.

The remaining fields are acoustic properties of voice dataset described in TABLE I.

TABLE I. ACOUSTIC PROPERTIES OF EACH VOICE SAMPLE

Acoustic Properties	
Properties	Description
meanfreq	mean frequency (in kHz)
sd	standard deviation of frequency
median	median frequency (in kHz)
Q25	first quantile (in kHz)
Q75	third quantile (in kHz)
IQR	interquartile range (in kHz)
skew	skewness (see note in specprop description)
kurt	kurtosis (see note in specprop description)
sp.ent	spectral entropy
sfm	spectral flatness
mode	mode frequency
centroid	frequency centroid
peakf	peak frequency (frequency with highest energy)
meanfun	average of fundamental frequency measured across acoustic signal
minfun	minimum fundamental frequency measured across acoustic signal

maxfun	maximum fundamental frequency measured across acoustic signal
meandom	average of dominant frequency measured across acoustic signal
mindom	minimum of dominant frequency measured across acoustic signal
maxdom	maximum of dominant frequency measured across acoustic signal
dfrange	range of dominant frequency measured across acoustic signal
modindx	modulation index. Calculated as the accumulated absolute difference between adjacent measurements of fundamental frequencies divided by the frequency range
label	male or female

IV. PERFORMANCE ANALYSYS OF ALGORITHMS

Classification algorithms are used for solving problems like identification of person gender, intruder detection and Spam detection etc. In this research paper we compared classification algorithms using voice dataset.

We did conduct experiment with machine learning classification algorithms on voice dataset and observed the train and test set accuracies for seven classification algorithms.

We used sklearn preprocessing library for data preprocessing. In voice dataset no missing values present in the dataset, label-encoder used for converting string values into int values and applied standard scalar for standardization of values . We used pandas, numpy packages to load the dataset, to perform numerical calculations respectively and sklearn package used for modeling the machine learning algorithm. In all the experiments test set size is 0.25. Keras and Tensorflow used in Artificial Nural Networks(ANN). We used 10 fold cross validation to train the models. The accuracies are shown in the Table II.

Both the SVM and ANN are giving better results compared with other machine learning algorithms. SVM is giving 97% accuracy on both train, test sets with linear kernel. Artificial Neural Network with three hidden dense layer of each contains 1000 nodes and relu as activation function, one input layer with 20 features and one output layer consists two nodes. In the output layer softmax is used as activation function and adam optimizer used then ANN is giving 98% accuracy.

From the TABLE II we can conclude SVM and ANN have better accuracies. Parameters influences the machine learning algorithm performance. We can further improve these algorithms by parameter tuning.

TABLE II. ACCURACY OF MACHINE LEARNING MODELS

Accuracy(%)		
Model	Training set	Test set
Logistic Regression	97.264	97.727
KNN	98.527	97.727
Naive Bayes	89.352	89.394
Decision Tree	100	96.717
Random Forest	99.832	97.601
SVM	97.432	97.97
ANN	100	98.358

V. PRAPOSED WORK

Parameter tuning [11] is used to find the best hyper parameters. GridSearch technique is used to find best hyper parameters. GridSearch will test several combinations of hyper parameters and returns the best selection that gives best accuracy.

We created dictionary with hyper parameters and applied on GridSearchCV of keras library. GridSeachCV will train Artificial Neural Networks using k-fold cross validation to get relevant accuracy with different combinations of the dictionary of hyper parameters and returns best accuracy with best selection of these values.

We tried with several hyper parameter on ANN algorithm with different batch sizes 10,20,32, different number of epochs 50,100,200 and with different optimizers are adam, rmsprop. Best parameter values are batch size 32, epochs 100 and optimizer rmsprop.

We applied parameter tuning on SVM using GridSeachCV with different kernels linear, rbf, poly, different gamma and C vales. Best parameter values are C 0.6, gamma 0.04 and kernal rbf. After applying parameter tuning SVM, ANN are giving improved results. We applied 0.1 dropout between hidden layer to avoid over fitting machine learning model.

VI. RESULT ANALYSIS

The improved accuracies of SVM, ANN are shown in the Table III.

TABLE III. ACCURACY OF MODELS AFTER PARAMETER TUNING

Accuracy(%)		
Model	Training set	Test set
SVM(kernel='rbf')	98.274411	98.611111
ANN	99.789562	99.873737

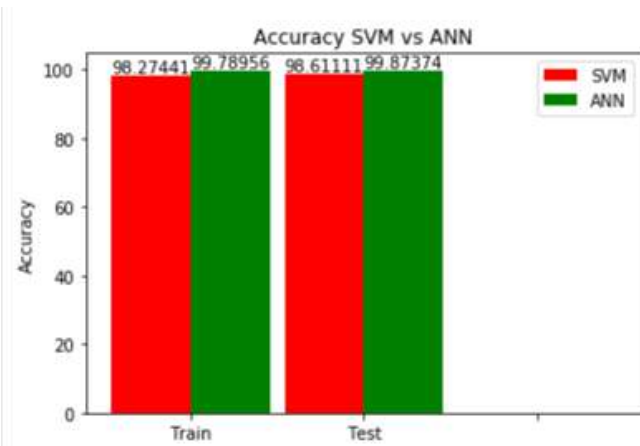


Fig. 1. Accuracy SVM vs ANN.

Results of algorithms are shown in the Fig. 1. X-axis shows algorithms and Y-axis shows Accuracy of the algorithm.

VII. CONCLUSION

Support-vector machines and Deep neural networks are performing better on voice dataset. Parameter Tuning is giving the 98.6% accuracy with SVM and 99.87% with ANN. From the above results we can conclude that deep neural networks are performing better compared with all machine learning algorithms to classify gender of a person using acoustic properties of voice.

REFERENCES

- [1] S. Gaikwad, B. Gawali, and S. C. Mehrotra, "Gender identification using SVM with combination of MFCC," *Advances in Computational Research*, vol. 4, no. 1, pp. 69–73, 2012.
- [2] S. M. R. Azghadi, M. R. Bonyadi, and H. Sliahosseini, "Gender classification based on feedforward backpropagation neural network," in *Artificial Intelligence and Innovations 2007: From Theory to Applications: Proceedings of the 4th IFIP International Conference on Artificial Intelligence Applications and Innovations (AIAI 2007)*, C. Boukis, L. Pnevmatikakis, and L. Polymenakos, Eds., vol. 247 of *IFIP The International Federation for Information Processing*, pp. 299–304, Springer, Berlin, Germany, 2007.
- [3] Cortes, Corinna & Vapnik, VN. (1995). Support Vector Networks. *Machine Learning*. 20. 273-297. 10.1023/A:1022627411411.
- [4] L. Breiman, J.H. Friedman, R.A. Olshen, C.J. Stone, *Classification and Regression Trees*, CRC Press, 1984.
- [5] K.-H. Lee, S.-I. Kang, D.-H. Kim et al., "A Support Vector Machine-Based Gender Identification Using Speech Signal," *IEICE Transactions on Communications*, pp. 3326-3329, 2008.
- [6] J. Silovsky, and J. Nouza, "Speech, Speaker and Speaker's Gender Identification in Automatically Processed Broadcast Stream,"
- [7] Büyükyılmaz, Mücahit & Çıbıkḍiken, Ali. (2016). Voice Gender Recognition Using Deep Learning. 10.2991/msota-16.2016.90.
- [8] <https://github.com/primaryobjects/voice-gender>
- [9] M. Araya-Salas, G. Smith-Vidaurre, warbleR: an R package to streamline analysis of animal acoustic signals. *Methods Ecol Evolution*, 2016, doi:10.1111/2041-210X.12624.
- [10] dataset, <https://github.com/primaryobjects/voice-gender/blob/master/voice.csv>
- [11] http://neupy.com/2016/12/17/hyperparameter_optimization_for_neural_networks.html
- [12] G. S. Archana and M. Malleswari, "Gender identification and performance analysis of speech signals," *2015 Global Conference on Communication Technologies (GCCT)*, Thuckalay, 2015, pp. 483-489.
- [13] M. A. Keyvanrad and M. M. Homayounpour, "Improvement on automatic speaker gender identification using classifier fusion," *2010 18th Iranian Conference on Electrical Engineering*, Isfahan, Iran, 2010, pp. 538-541.